



This work is protected by copyright and other intellectual property rights and duplication or sale of all or part is not permitted, except that material may be duplicated by you for research, private study, criticism/review or educational purposes. Electronic or print copies are for your own personal, non-commercial use and shall not be passed to any other individual. No quotation may be published without proper acknowledgement. For any other use, or to quote extensively from the work, permission must be obtained from the copyright holder/s.

Pennsylvanian carbonate mud mounds from the
sub-aerial to sub-marine transition along a tilted
foreland basin, Cantabrian Mountains, Spain.

Steven Leslie Rogers

Ph.D

October 2015

Keele University

Abstract

Carbonate mud mounds from the Pennsylvanian aged San Emiliano Formation (Cantabrian Mountains, Spain) are commonly well exposed. The mounds range from 2 to 50 m in height and were observed to be primary geological features. Microfacies, ultrafacies, palaeontological and geochemical studies have revealed the composition of the mounds and surrounding carbonates. The factors and controls of mound nucleation, growth and demise have been established. The mounds are skeletal-microbial/pack-wackestones. Peloidal, homogenous and clotted micrites are the main sedimentological constituents of the mounds. Microfossils are dominant with *Donezella*, *Claracrusta*, *Rothpletzella* and *Girvanella* being common. Small foraminifera, bryozoans, corals and algae are all present within the mounds, but are more common within off-mound carbonates. The mounds show evidence of deposition within shallow water environments. The formation of the mounds was controlled by a dynamic relationship between Donezellacean algae, and microscopic encrusters. Fluctuating environmental conditions lead to the alternate dominance between the two groups, resulting in accretion and stabilisation of carbonate muds. Off-mound carbonate sediments generally show more evidence for deeper, and in some cases, higher energy environment of deposition. These carbonates are generally packstones, and two distinct types occur: a *Donezella* dominated carbonate with oncoids, and a cyclical micrite-marl sequence which is dominated by 'phylloid' algae, bryozoans and corals. Comparable mounds from the Lois-Cigüera Formation, of the local Bernesga Valley, were deposited in a deeper environment. A relationship between *Donezella*, *Claracrusta*, *Rothpletzella* and *Girvanella* was not observed within the mounds of the Lois-Cigüera Formation. These mounds are compositionally different to their San Emiliano counter-parts. The San Emiliano Fm. was deposited on the sub-aerial to sub-marine transition on a tilted foreland basin. Carbonate and mound deposition took place within a basin during periods of heightened tectonic activity. Carbonates of the San Emiliano Fm. were originally aragonitic. Three new fossil morphotypes are presented.

Contents

List of Figures	v-viii
List of Tables	viii
List of Abbreviations	viii-ix
1. Introduction	1
1.1 Research Aims and Objectives	2
1.2 Geological Setting and Sedimentology of the San Emiliano Formation	2
1.3 Palaeogeography	11
1.4 Palaeoenvironment.....	13
1.5 Summary	14
1.6 Chapter Outlines	14
2. Literature Review	17
2.1 Carbonate Mud Mounds.....	17
2.1.2 Stromatactis, Cavities and Carbonate Mud Mounds	21
2.2 Microbial Vs Biodepositional Mounds	23
2.2.1 Microbial Mud Mounds	23
2.2.2 Biodepositional Mud Mounds.....	24
2.3 Depositional Environment	25
2.3.2 The Micrite Problem	28
2.4 Palaeoecology	31
2.4.1 Dominant Biota	31
2.5 General Initiation Mechanisms and Growth	36
2.5.1 Hydrothermal Venting and Hydrocarbon Seepage	37
2.5.2 Topographic and Bathymetric Controls	38
2.5.3 Shallow Water Atoll Model	39
2.5.4 Geosphere Biosphere Coupling (humification– biodepositional phenomena)	39
2.6 Geological Setting.....	40
2.6.1 Structural Controls	41
2.7 Industrial Implications	41
2.7.1 Hydrocarbons	42
2.7.2 Metallogenic Mineral Deposits	42
3. Methods and Materials	43
3.1 Field methods.....	43
3.2 Sample Preparation	44
3.3 Thin Section Microscopy	46
3.4 Scanning Electron Microscopy and Energy Dispersive X-ray Spectrometry	47

3.4.1 Framboidal Pyrite.....	48
3.5 Isotope analysis.....	49
3.6 X-Ray Fluorescence.....	50
3.6.1 Continuous wavelet transform	51
3.7 Database Generation	52
4. Microfacies Analysis	53
4.1 Candemuela Mound	54
4.1.1 Basal Facies	55
4.1.2 Mound Facies.....	62
4.1.3 Capping Facies.....	79
4.1.4 Interpretation.....	86
4.2 Unit 8	91
4.2.1 Interpretation.....	96
4.3 Pinos Hairpin Limestone.....	96
4.3.1 Interpretation.....	115
4.4 Pinos Pylon Mound.....	117
4.4.1 Basal Facies	118
4.4.2 Mound Facies.....	123
4.4.3 Interpretation.....	126
4.5 Pinos East Mound	129
4.5.1 Mound Facies.....	131
4.5.2 Interpretation.....	145
4.6 Sena de Luna Mound	147
4.6.1 Basal and Flank Facies.....	148
4.6.2 Mound Facies.....	151
4.6.3 Interpretation.....	154
4.7 Cármenes South Mound.....	156
4.7.1 Basal Facies	157
4.7.2 Mound Facies.....	160
4.7.3 Interpretation.....	165
4.8 San Martín Mound	167
4.8.1 Basal Facies	168
4.8.2 Mound Facies.....	171
4.8.3 Interpretation.....	174
4.9 Chapter Summary	176
5. Ultrafacies Analysis	178
5.1 Candemuela Section.....	179
5.1.1 Basal Limestone Facies.....	180
5.1.2 Mound Facies.....	185

5.1.3 Capping Facies.....	199
5.1.4 Interpretation.....	205
5.2 Other mounds.....	206
5.3 Framboidal Pyrite.....	214
5.4 Chapter Summary	217
6. Palaeontology.....	218
6.1 Algae	219
6.1.1 <i>Donezella</i>	220
6.1.2.1 <i>Donezella</i> Ultrastructure	224
6.1.2 <i>Beresella</i>	226
6.1.3 <i>Dvinella</i>	227
6.1.4 <i>Komia</i> and <i>Ungdarella</i>	228
6.1.5 <i>Claracrusta</i>	229
6.1.6 <i>Wetheredella</i>	232
6.1.7 <i>Archaeolithophyllum</i>	233
6.1.8 <i>Petschoria</i>	235
6.1.9 <i>Fourstonella</i>	236
6.1.10 Solenoporacean Red Algae	236
6.1.11 Dasyclad algae	237
6.2 Cyanobacteria, Calcimicrobes and Microproblematica	238
6.2.1 <i>Girvanella</i>	240
6.2.2 <i>Rothpletzella</i>	241
6.2.3 <i>Renalcis</i> and <i>Epiphyton</i>	243
6.2.4 <i>Shamovella</i> (= <i>Tubiphytes</i>)	243
6.2.5 <i>Archaeolithoporella</i>	244
6.3 Foraminifera.....	244
6.3.1 <i>Tetrataxis</i>	245
6.3.2 <i>Lasiodiscus</i>	246
6.3.3 Fusulinids.....	247
6.3.4 Miliolinids.....	249
6.4 Bryozoans	250
6.5 Other Fossils	252
6.5.1 Corals	253
6.5.2 Shelly Fauna.....	253
6.5.3 Tuberitinidae	254
6.5.4 Others.....	257
6.6 Systematic Palaeontology	257
6.7 Chapter summary	267
7. Siliciclastic Units	269

7.1 Log - Unit 3.....	274
7.2 Log - Unit 4.....	274
7.3 Log - Unit 8.....	275
7.4 Interpretation.....	277
7.5 Chapter Summary	278
8. Geochemistry	280
8.1 Stable Isotope Geochemistry	281
8.2 X-Ray Fluorescence Geochemistry	282
8.3 Chapter Summary	295
9. Discussion	296
9.1 Mound description	296
9.2 Palaeoecology: interpretation.....	300
9.2.1 The Role of <i>Donezella</i> and its Associated Biota.....	301
9.3 Origin of Micrite	303
9.3.1 Does the Carbonate have an Aragonitic Origin?.....	304
9.4 Water Depth	306
9.5 Salinity	311
9.6 Depositional Environment	311
9.7 Initiation, Growth and Demise.....	315
9.8 Comparison with Other Mounds.....	316
9.9 The Distribution of Carbonate Mud Mounds Through Space and Time	318
9.10 Chapter Summary	328
10. Conclusion	330
10.1 Future Work	333
References	334
Acknowledgements	363
 Appendix 1. Point Count	
Appendix 2. EDS Maps	
Appendix 3. Sedimentary Logs	
Appendix 4. XRF Data	
Appendix 5. Distribution Database	

List of Figures

FIGURE 1.1 - Location map of the study area	4
FIGURE 1.2 - Geological map of the study area.....	6
FIGURE 1.3 - Litho- and biostratigraphy of the study area	10
FIGURE 1.4 - Palaeogeographic reconstruction of the studied time interval.....	12
FIGURE 2.1 - Basic features of mud mound	19
FIGURE 2.2 - Waulsortian phases	21
FIGURE 2.3 - Carbonate factories	26
FIGURE 2.4 - Diagenetic path of aragonite to calcite	30
FIGURE 2.5 - Ranges of deep water mound biota	32
FIGURE 2.6 - Mound control - topographic highs	39
FIGURE 2.7 - Humic substance based model of marine CaCO ₃ precipitation	40
FIGURE 2.8 - Mound control - faulting	41
FIGURE 4.1 - The Candemuela Mound	55
FIGURE 4.2 - Photomicrographs Candemuela <i>basal facies</i> (caption pg. 58)	57
FIGURE 4.3 - Photomicrographs Candemuela <i>basal facies</i> (caption pg. 61)	60
FIGURE 4.4 - Photomicrographs Candemuela <i>mound facies</i> (caption pg. 64).....	63
FIGURE 4.5 - Photomicrographs Candemuela <i>mound facies</i> (caption pg. 67).....	66
FIGURE 4.6 - Photomicrographs Candemuela <i>mound facies</i> (caption pg. 70).....	69
FIGURE 4.7 - Photomicrographs Candemuela <i>mound facies</i> (caption pg. 72).....	71
FIGURE 4.8 - Photomicrographs Candemuela <i>mound facies</i> (caption pg. 75).....	74
FIGURE 4.9 - Photomicrographs Candemuela <i>mound facies</i> (caption pg. 78).....	77
FIGURE 4.10 - Photomicrographs Candemuela <i>capping facies</i>	80
FIGURE 4.11 - Photomicrographs Candemuela <i>capping facies</i> (caption pg. 83).....	82
FIGURE 4.12 - Photomicrographs Candemuela <i>capping facies</i>	85
FIGURE 4.13 - Unit 8 traverse	93
FIGURE 4.14 - Unit 8 traverse	94
FIGURE 4.15 - Unit 8 traverse	95
FIGURE 4.16 - The Pinos Hairpin Limestone.....	98
FIGURE 4.17 - Photomicrographs Pinos Hairpin <i>sub-facies 1</i> (caption pg. 101).....	100
FIGURE 4.18 - Photomicrographs Pinos Hairpin <i>sub-facies 2</i> (caption pg. 104).....	103
FIGURE 4.19 - Photomicrographs Pinos Hairpin <i>sub-facies 2</i> (caption pg. 106).....	105
FIGURE 4.20 - Photomicrographs Pinos Hairpin <i>sub-facies 3</i> (caption pg. 108/9).....	108
FIGURE 4.21 - Photomicrographs Pinos Hairpin <i>sub-facies 3</i> (caption pg. 111).....	110
FIGURE 4.22 - Photomicrographs Pinos Hairpin <i>sub-facies 4</i>	112
FIGURE 4.23 - Photomicrographs Pinos Hairpin <i>sub-facies 2</i> (caption pg. 115).....	114
FIGURE 4.24 - Pinos Pylon Mound.....	118

FIGURE 4.25 - Photomicrographs Pinos Pylon <i>basal facies</i> (caption pg. 121)	120
FIGURE 4.26 - Photomicrographs Pinos Pylon <i>basal facies</i> (caption pg. 123)	122
FIGURE 4.27 - Photomicrographs Pinos Pylon <i>mound facies</i> (caption pg. 126)	125
FIGURE 4.28 - Pinos East Mound	130
FIGURE 4.29 - Photomicrographs Pinos East <i>sub-facies 1</i> (caption pg. 134)	133
FIGURE 4.30 - Photomicrographs Pinos East <i>sub-facies 1</i> (caption pg. 136)	135
FIGURE 4.31 - Photomicrographs Pinos East <i>sub-facies 1</i> (caption pg. 138)	137
FIGURE 4.32 - Photomicrographs Pinos East <i>sub-facies 2</i> (caption pg. 141)	140
FIGURE 4.33 - Photomicrographs Pinos East <i>sub-facies 2</i> (caption pg. 143)	142
FIGURE 4.34 - Photomicrographs Pinos East <i>sub-facies 3</i> (caption pg. 145)	144
FIGURE 4.35 - Sena de Luna Mound	148
FIGURE 4.36 - Photomicrographs Sena <i>basal/flank facies</i> (caption pg. 151)	150
FIGURE 4.37 - Photomicrographs Sena <i>mound facies</i> (caption pg. 154)	153
FIGURE 4.38 - Cármenes South Mound	157
FIGURE 4.39 - Photomicrographs Cármenes <i>basal facies</i> (caption pg. 160)	159
FIGURE 4.40 - Photomicrographs Cármenes <i>mound facies</i> (caption pg. 163)	162
FIGURE 4.41 - Photomicrographs Cármenes <i>mound facies</i> (caption pg. 165)	164
FIGURE 4.42 - San Martín Mound	168
FIGURE 4.43 - Photomicrographs San Martín <i>basal facies</i> (caption pg. 170/71)	170
FIGURE 4.44 - Photomicrographs Cármenes <i>mound facies</i> (caption pg. 174)	173
FIGURE 5.1 - Ultrafacies - Candemuela <i>basal facies</i> (caption pg. 182)	181
FIGURE 5.2 - Ultrafacies - Candemuela <i>basal facies</i> (caption pg. 184)	183
FIGURE 5.3 - Ultrafacies - Candemuela <i>mound facies</i> (caption pg. 187)	186
FIGURE 5.4 - Ultrafacies - Candemuela <i>mound facies</i> (caption pg. 189)	188
FIGURE 5.5 - Ultrafacies - Candemuela <i>mound facies</i>	190
FIGURE 5.6 - Ultrafacies - Candemuela <i>mound facies</i> (caption pg. 192)	191
FIGURE 5.7 - Ultrafacies - Candemuela <i>mound facies</i>	193
FIGURE 5.8 - Ultrafacies - Candemuela <i>mound facies</i> (caption pg. 195)	194
FIGURE 5.9 - Ultrafacies - Candemuela <i>mound facies</i> (caption pg. 197)	196
FIGURE 5.10 - Ultrafacies - Candemuela <i>mound facies</i> (caption pg. 199)	198
FIGURE 5.11 - Ultrafacies - Candemuela <i>capping facies</i> (caption pg. 201)	200
FIGURE 5.12 - Ultrafacies - Candemuela <i>capping facies</i> (caption pg. 203)	202
FIGURE 5.13 - Ultrafacies - Candemuela <i>capping facies</i> (caption pg. 205)	204
FIGURE 5.14 - Ultrafacies - Other mounds (caption pg. 209)	208
FIGURE 5.15 - Ultrafacies - Other mounds (caption pg. 211)	210
FIGURE 5.16 - Ultrafacies - Other mounds (caption pg. 213)	212
FIGURE 5.17 - Framboidal pyrite	215
FIGURE 5.18 - Framboidal pyrite - size frequency graphs	216
FIGURE 6.1 - <i>Donezella</i>	223

FIGURE 6.2 - <i>Donezella</i> ultrastructure (caption pg. 225/226).....	225
FIGURE 6.3 - <i>Beresella</i>	227
FIGURE 6.4 - <i>Dvinella</i>	228
FIGURE 6.5 - Ungdarellacean algae	229
FIGURE 6.6 - <i>Claracrusta</i>	231
FIGURE 6.7 - <i>Wetheredella</i> (caption pg. 233).....	232
FIGURE 6.8 - <i>Archaeolithophyllum</i>	235
FIGURE 6.9 - Solenoporacean algae.....	237
FIGURE 6.10 - Dasyclad algae	238
FIGURE 6.11 - <i>Girvanella</i>	241
FIGURE 6.12 - <i>Rothpletzella</i>	243
FIGURE 6.13 - <i>Tetrataxis</i>	246
FIGURE 6.14 - Fusulinid foraminifera.....	249
FIGURE 6.15 - Miliolinid foraminifera.....	250
FIGURE 6.16 - Bryozoans.....	252
FIGURE 6.17 - Tuberitinidae	256
FIGURE 6.18 - <i>Donezella</i> sp. 1	260
FIGURE 6.19 - Schematic sketches of <i>Donezella</i>	261
FIGURE 6.20 - Photomicrographs of Lasiodiscidae	265
FIGURE 6.21 - Schematic sketches of Lasiodiscidae	266
FIGURE 7.1 - Idealised foreland basin models.....	270
FIGURE 7.2 - location map of log locations	271
FIGURE 7.3 - Photomicrographs of clastics	272
FIGURE 7.4 - Log - Unit 3.....	273
FIGURE 7.5 - Log - Unit 4.....	275
FIGURE 7.6 - Log - Unit 8.....	276
FIGURE 8.1 - Isotope scatter graph	282
FIGURE 8.2 - Correlation panel of major elements	284
FIGURE 8.3 - Comparison between CaO and SiO ₂	285
FIGURE 8.4 - Correlation panel of trace elements.....	286
FIGURE 8.5 - Cross-plots for important elements	289
FIGURE 8.6 - Interpretation of chemostratigraphic log.	290
FIGURE 8.7 - Continuous Wavelet (Morelet) Transform analysis.	293
FIGURE 8.8 - ‘Berger’ periodicity correction for astronomical time scale.	294
FIGURE 9.1 - Sea-level compared to deposition, Candemuela mound	297
FIGURE 9.2 - Discrepancy between San Emiliano and Bernesga Valley mounds.....	299
FIGURE 9.3 - Representation of mound formation.....	303
FIGURE 9.4 - Diagenetic pathway of San Emiliano mounds	306
FIGURE 9.5 - Sea-level reconstruction	310

FIGURE 9.6 - Reconstruction of the depositional environment/setting	314
FIGURE 9.7 - Mounds in space and time - Cambrian	321
FIGURE 9.8 - Mounds in space and time - Ordovician and Silurian	322
FIGURE 9.9 - Mounds in space and time - Devonian	323
FIGURE 9.10 - Mounds in space and time - Carboniferous.....	324
FIGURE 9.11 - Mounds in space and time - Permian and Triassic.....	325
FIGURE 9.12 - Mounds in space and time - Jurassic and Cretaceous	326
FIGURE 9.13 - Mounds in space and time - Cenozoic	327

List of Tables

TABLE 1.1 Stratigraphy of lithologies local to study area.....	5/6
TABLE 2.1 - Waulsortian phases	21
TABLE 2.2 - Overview of mound biota	32-35
TABLE 4.1 - Summary of SMF for the Candemuela Mound	89-90
TABLE 4.2 - Summary of SMF for the Pinos Pylon Mound	128
TABLE 4.3 - Summary of SMF for the Pinos East Mound	146-147
TABLE 4.4 - Summary of SMF for the Sena de Luna Mound	155
TABLE 4.5 - Summary of SMF for the Cármenes Mound	166
TABLE 4.6 - Summary of SMF for the San Martín Mound	175
TABLE 8.1 - Isotope analysis	282
TABLE 9.1 - Summary of <i>Donezella</i> related buildups	317-318

List of Abbreviations (in order of use)

FNP - Fold and Nappe Province
 CAC - Central Central Asturian Coalfield Province
 PNP - Ponga Nappe Province
 PDEP - Picos de Europa Province
 PCP - Pisuerga-Carrión Province
 SEM - Scanning Electron Microscope
 XRF - X-Ray Fluorescence
 PVP - Polyvinylpyrrolidone
 SMF - Standard Microfacies Type
 FE-SEM - Field Emission Scanning Electron Microscope
 EDX - Energy Dispersive X-ray Spectrometer
 NERC - Natural Environment Research Council
 NIGL - NERC Isotope Geosciences Laboratory
 PDB - Pee Dee Belemnite
 CWT - Continuous Wavelet (Morelet) Transformation
 UTM - Universal Transverse Mercator
 CAN - Candemuela Mound
 PHL - Pinos Hairpin Limestone
 PPM - Pinos Pylon Mound
 PEM - Pinos East Mound
 SDL - Sena de Luna Mound

CSM - Cármenes South Mound
SMM - San Martín Mound
TOC - Total Organic Carbon
PMS - Pitted Microspar
LPM - Less-Pitted Microspar
NPM - Non-Pitted Microspar
SS - Smooth Spar
PM - Pitted Micrite
NPM - Non-Pitted Micrite
PD - Pitted Dolomite
DOL - Dolomite
CC - Clastic Component
FP - Framboidal Pyrite
PY - Pyrite
IO - Iron Oxide
SP - Spicule
PPM - Parts Per Million

1. Introduction

Carbonate mud mounds are a type of marine buildup which originate by the successive vertical and lateral accretion of carbonate muds (Monty, 1995). This type of buildup became increasingly recognised during the 1970s and 1980s when it was found that various mound types, and their associated structures, microfacies and biotas extended a diverse geological range and often included features which were poorly understood or unknown at the time (Wilson, 1975; James, 1980, Longman, 1981, James, 1983; Lees, 1988; Monty *et al.*, 1988 and Swennen, 1988). Mud mounds are complex structures which respond to facies changes and have been found to record shifts in lithofacies and biofacies (Monty, 1995).

This study focuses on the nucleation and formation, and subsequent growth and demise, of carbonate mud mounds of the Pennsylvanian aged La Majúa Member of the San Emiliano Formation, Cantabrian Mountains, Spain. Some aspects of the sedimentology and palaeontology of the formation have been previously investigated (e.g. Rácz, 1964; Brouwer and van Ginkel, 1964; van Ginkel, 1965; Winkler Prins, 1968; Moore *et al.*, 1971; Martínez Chacón, 1977; Cachán Santos, 1978; Bowman, 1979; Martínez Chacón, 1979, Bowman 1982; Wagner and Bowman, 1983; Martínez Chacón and Winkler Prins, 1984; Bowman, 1985; Carballeira *et al.*, 1985; Wagner and Winkler Prins, 1985; Kullmann and Rodríguez, 1986; Martínez Chacón, 1986; Fernández Lopez and Sánchez de Posada, 1987; Gandl, 1987; Villa *et al.*, 1988; Dingle *et al.*, 1993; Fernández, 1993; Hensen *et al.*, 1995; van Ginkel and Villa, 1996; Samankassou, 2001; Bahamonde *et al.* 2002; García-Bellido & Rigby, 2004 & Martínez Chacón and Winkler Prins, 2010) and the presence of carbonate mud mounds recognised. Carbonate mud mounds provide a unique window into the geological and environmental setting in which they were formed. The investigation of such structures can be used to investigate facies shifts and provide insight to the conditions operating at time of deposition.

1.1 Research Aims and Objectives

The main purpose of this study is to conduct a detailed investigation on the carbonate mud mounds within the San Emiliano Formation and surrounding lithologies, with a purpose of characterising the mounds and establishing the mode of nucleation and growth. This study has a multidisciplinary approach and combines several sedimentological, palaeontological and geochemical aspects and techniques. The aims of this project are to provide a microfacies, palaeontological and geochemical analysis of carbonate mud mounds and associated sediments from the San Emiliano Formation (Pennsylvanian age) and coevally deposited sediments from the Bernesga Valley, Cantabrian Mountains, Spain. This research aims to forward our knowledge on the nucleation and formation mechanisms of carbonate mud mounds during localised sedimentation and basin development. The mounds associated with this research will be compared to other mounds reported both spatially and temporally. To achieve these aims the following objectives of this research are:

- *To characterise the sedimentary nature of the La Majúa Member of the San Emiliano Formation with emphasis on the carbonate units*
- *Constrain the palaeontological community associated with the carbonate mud mounds present*
- *Identify external and internal controls on sedimentary deposition of the carbonate mud mounds present*
- *Identify processes (physical, biological or chemical) responsible for mound nucleation and growth*

1.2 Geological Setting and Sedimentology of the San Emiliano Formation

The study area is mostly confined to outcrops in the San Emiliano Formation, which are located within the Cantabrian Mountains, León Province, Northern Spain, around the small rural town from which it takes its name (Fig. 1.1). The area sits within (and formed as a result of the formation of) the Variscan Belt (often referred to as the Iberian Massif for the area of the belt in Western Europe, Spain and Portugal), which formed as a result of the Variscan Orogeny

(Bahamonde *et al.*, 2002). The orogeny occurred during the Late Palaeozoic as a consequence of Gondwana (in the south) and Laurussia (toward the north) converging (Matte, 2001). The convergence of these continental blocks resulted in the closure of the Rheic and Proto-Tethys oceans (Matte, 2001).

The Iberian Massif has been informally arranged into six tectonostratigraphic units, these units were based upon differences in facies associations, structural styles, metamorphism and magmatism (Lotze, 1945). The northern most of these units is where the study area is located and is called the Cantabrian zone (Lotze, 1945 & Pérez-Estaún *et al.*, 1988). The Cantabrian zone consists of an incomplete Cambrian-Ordovician sedimentary sequence, a Silurian and Devonian sequence which is complete toward the west but is missing elsewhere and several thousand metres of strata spanning the Tournaisian to the Gzhelian Stages (Carboniferous) which represent sediments deposited within the foreland basins associated with the Variscan Orogeny (Bahamonde *et al.*, 2002). Table 1.1 shows a summary of the major lithostratigraphical formations found within the Cantabrian zone, focussing specifically around the San Emiliano area, Figure 1.2 shows a geological map of the main area of study.

The Cantabrian zone (Lotze, 1945 & Pérez-Estaún *et al.*, 1988) is further subdivided into five tectonic units: the Fold and Nappe (FNP), Central Asturian Coalfield (CAC), Ponga Nappe (PNP), Picos de Europa (PDEP) and Pisuerga-Carrión (PCP) provinces. The San Emiliano Formation belongs to the La Sobia-Bodón/Aramo units of the Fold and Nappe Province (Pérez-Estaún *et al.*, 1988 & Bahamonde *et al.*, 2002).

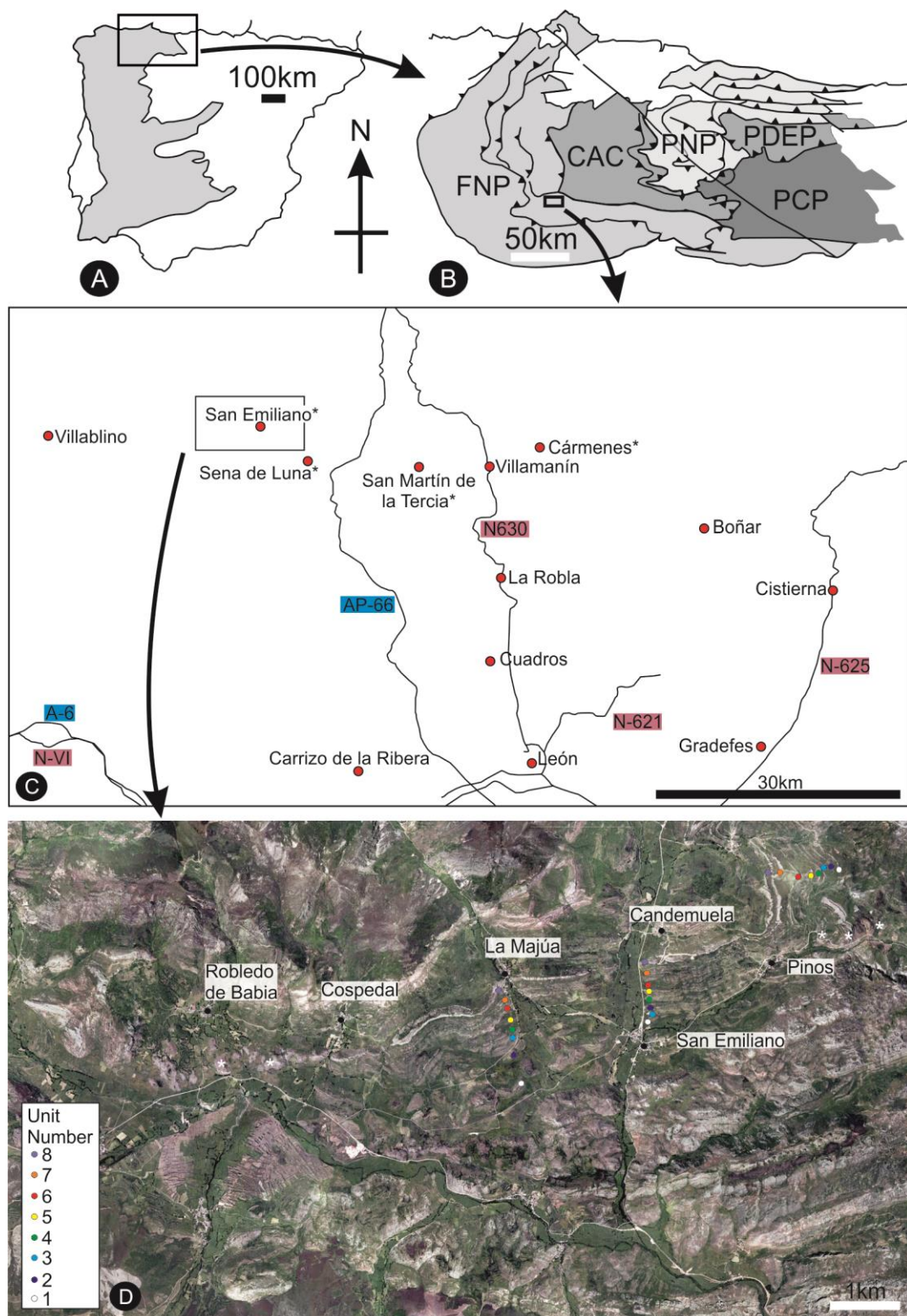


FIGURE - 1.1 Location of San Emiliano and sample locations. A, Outline of the Iberian Massif highlighted in grey. B, The Cantabrian zone divided into tectonostratigraphic provinces; FNP – Fold and Nappe Province, CAC – Central Asturian Coalfield, PNP – Ponga Nappe Province, PDEP – Picos De Europa Province, PCP – Pisuerga-Carrión Province. C, Major

roads and settlements in the vicinity of the study area, locations with a * indicate areas of sampling. D, The San Emiliano valley with settlements indicated. Coloured dots refer to limestone units within the San Emiliano Formation. Samples were obtained from locations indicated by a * and a traverse along the northern most limestone unit (unit 8, purple dot). A and B after Bahamonde *et al.*, 2002. C and D based on Google Earth 2013.

Age	Formation
Cambrian	<p>The Herrería Formation (900-1700m thick) is of lower Cambrian age and consists of a siliciclastic dominated succession with feldspathic quartzites, sandstones, conglomerates and rare dolomitic levels (Liñán <i>et al.</i>, 2002 and Álvaro <i>et al.</i>, 2003).</p> <p>The formation has been interpreted to have been deposited as part of a braid-plain delta (Wotte, 2009). The Herrería Fm. is overlain by the Láncara Formation (150-225m thick) which represents upper lower - lower mid Cambrian ages and consists of shallow water carbonates which are stromatolitic dolomites in their lower half becoming a nodular, red limestone (referred to as a griotte) in the upper half. The lower-middle Cambrian boundary is placed at the lithological boundary within the Láncara Fm. The Oville Formation (80-800m thick) is middle Cambrian to Tremadocian in age and comprises siliciclastics, which are generally glauconitic sandstones and green shales. A quartzite with a few intercalated shales called the Barrios Formation (80-1020m thick) is of the same age as the Oville Fm. The lower parts of the formation likely representing a lateral facies shift (Liñán <i>et al.</i>, 2002).</p>
Ordovician	<p>The Barrios Formation mentioned in the previous section is often the only Ordovician lithology found in most of the Cantabrian zone, there is evidence that they reach upper Lower Ordovician in age (Gutiérrez-Marco <i>et al.</i>, 2002). Gutiérrez-Alonso <i>et al.</i> (2007) provide a U-Pb depositional age for the upper Barrios Fm. at 477.47 ± 0.93 Ma, during the Floian (Tremadocian). The Barrios Fm. is often found overlain by Silurian, Devonian or Carboniferous lithologies.</p>
Silurian	<p>Often found overlying the Barrios Fm. is the Formigoso Formation (100-300m thick), this succession consists of black and grey siltstones and shales with some thin sandstone intercalations and spans from the Aeronian to Sheinwoodian stages. The Formigoso Fm. is overlain by the San Pedro Formation (80-200m thick) which is grey and reddish ferruginous sandstones with some limestone lenses. The San Pedro Fm. is accepted to represent upper Wenlock to Lower Devonian deposits (Truyols <i>et al.</i>, 1974; Rodríguez González, 1983; Aramburu <i>et al.</i>, 1992; Richardson <i>et al.</i>, 2000, 2001 & Robardet and Gutiérrez-Marco, 2002). Priewalder (1997) indicates that part of the formation reaches the Přídolí, further to this, the work of Richardson <i>et al.</i>, (2000 & 2001) confirms the formations upper boundary is within the Lochovian.</p>
Devonian	<p>The San Pedro Fm. ends in the Lochkovian and is overlain by a dominantly calcareous succession known as the La Vid Group (400-600m thick) which reaches the upper Emsian in age (García-Alcalde <i>et al.</i>, 2002). The Santa Lucía Formation consists of shallow marine</p>

	limestones of Upper Emsian to Lower Eifelian age (Herrmann and Hubmann, 1994). Reefal facies are common (Fernández-Martínez <i>et al.</i> , 2003). Overlying the predominantly carbonate Santa Lucía Fm. is the Eifelian to Givetian age Huergas Formation (Wagner and Fernandez-Garcia, 1971); a dark shaly and marly lithology with a sharp boundary with the underlying Santa Lucía Fm. (García-López and Bastida, 2002).
Carboniferous	The Barcaliente Formation (300-350m thick) is a sequence of shelf carbonates deposited within the shallower parts of the Variscan foreland (i.e. the northern and eastern parts) and was deposited during the Serpukhovian. During the Bashkirian a thick carbonate platform was deposited upon raised platforms, these carbonates are known as the Valdeteja Formation (up to 1000m thick). Towards the southern and western parts of the foreland, orogen derived clastics interfingered with carbonate units filling the foredeep, these units are collectively known as the San Emiliano Formation (1800m thick) this formation was deposited from the Bashkirian to Moscovian (Bowman, 1979, 1982 and 1985).

TABLE 1.1- Summary of the major formations found within the study area, their age and their major characteristics.

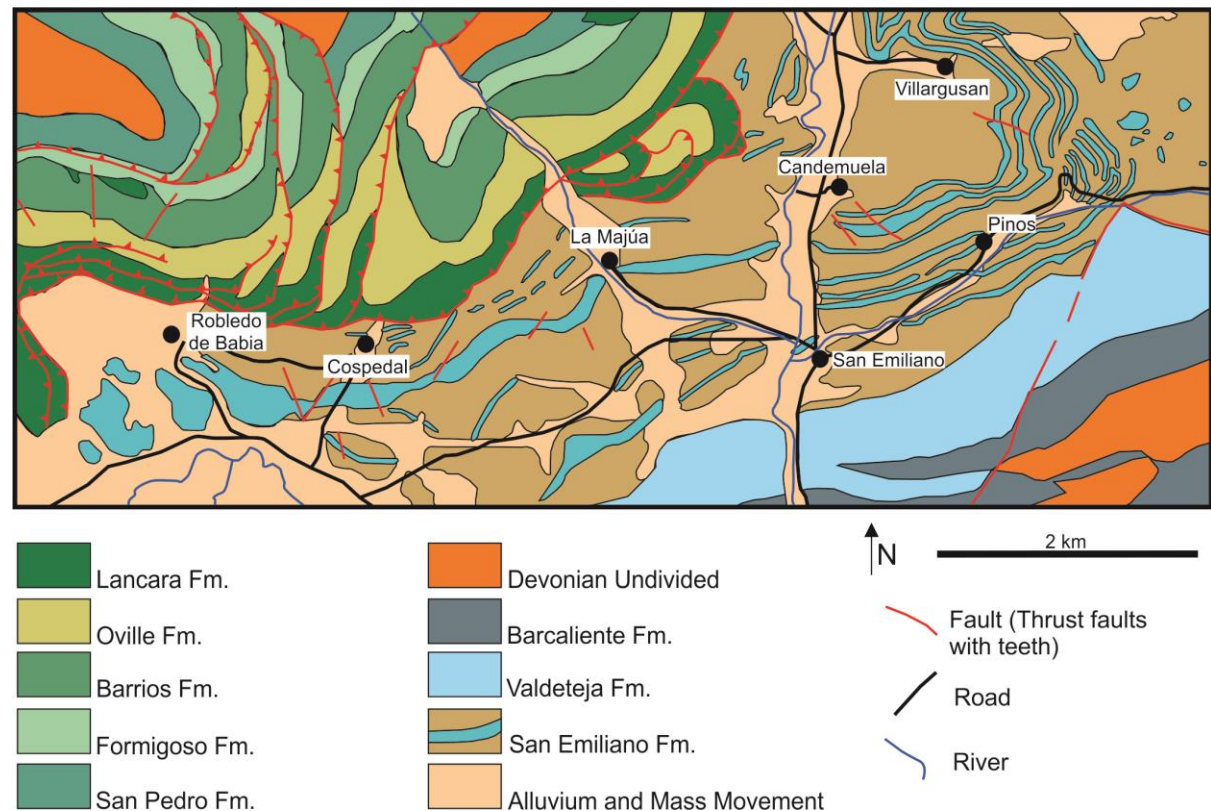


FIGURE 1.2 - A geological map showing the main area of study. For more information on the given stratigraphic formations see Table 1.1. (Modified after Suárez *et al.*, 1991)

The San Emiliano Formation, first introduced by Brouwer and van Ginkel (1964), was formally described by Bowman (1982). Carboniferous sediments from the San Emiliano area were first

mentioned by Monreal (1879) and Barrois (1882). The first simplified maps of the San Emiliano area were produced by Gómez de Llarena and Rodríguez Arango (1948) and García-Fuente (1952). The lithologies, stratigraphy and various palaeontological aspects of the San Emiliano Formation have been documented and discussed in a number of publications (Rácz, 1964; Brouwer and van Ginkel, 1964; van Ginkel, 1965; Winkler Prins, 1968; Moore *et al.*, 1971; Martínez Chacón, 1977; Cachán Santos, 1978; Bowman, 1979; Martínez Chacón, 1979, Bowman 1982; Wagner and Bowman, 1983; Martínez Chacón and Winkler Prins, 1984; Bowman, 1985; Carballeira *et al.*, 1985; Wagner and Winkler Prins, 1985; Kullmann and Rodríguez, 1986; Martínez Chacón, 1986; Fernández Lopez and Sánchez de Posada, 1987; Villa *et al.*, 1988; Dingle *et al.*, 1993; Fernández, 1993; Hensen *et al.*, 1995; van Ginkel and Villa, 1996; Samankassou, 2001; Bahamonde *et al.* 2002 & Martínez Chacón and Winkler Prins, 2010).

The San Emiliano Formation consists of at least 1800 m (Bowman, 1982) of Pennsylvanian aged (Bashkirian to Moscovian), alternating deltaic clastics and shallow marine carbonates, with rare thin coal bands (Bowman, 1979). Some authors have suggested that the formation may be up to 2000 m (Fernández, 1993) or 2400 m (Martínez Chacón and Winkler Prins, 1984) in thickness. At the San Emiliano type locality (i.e. the San Emiliano valley, as shown in Fig. 1.1 and 1.2) Bowman (1982) subdivided the formation into three constituent members, based upon the proportions of clastic and carbonate sediments. These are the [1] Pinos, [2] La Majúa and [3] Candemuela Members. The [1] Pinos Member consists of black shales passing into siltstones with thin sandstone interbeds; the member is approximately 250 m thick. The [2] La Majúa Member consists of alternating regressive deltaic and shallow marine clastics (with occasional, thin coal bands) separated by eight major transgressive limestone units (Bowman, 1979); the member is approximately 1050 m in thickness. Fusulinid Foraminifera collected from the upper part of the La Majúa Member have indicated a late Bashkirian age (van Ginkel and Villa, 1996). The [3] Candemuela Member consists of deltaic and shallow marine clastics with coal beds and seatearths; the member is approximately 500 m thick. Figure 1.3 shows the stratigraphic range of the San

Emiliano Fm. at the type locality. The formation is thought to have been deposited within the foredeep of a foreland basin ahead of the advancing Variscan orogenic front (Bahamonde *et al.*, 2002), although several authors have argued for an extensional to strike slip setting (Bowman, 1985 & Wagner and Winkler Prins, 1985). The foreland basin was limited to the north by the Valdeteja Formation, a carbonate platform which formed before, and in places lies conformably beneath, the San Emiliano Formation (Bowman, 1979, 1982 and 1985). Fernández (1993) explained the diachronous boundary between the formations in relation to the shape and evolution of the sedimentary basin. The basin was filled by orogenically derived material from the advancing Variscan front to the south (Ernst *et al.*, 2005). The tectonic effects of the Variscan Orogenesis would have resulted in unstable, mobile basins in which a rapid temporal and spatial variation in the deposition of sediments occurred (Bahamonde *et al.*, 2002). The top of the formation is either cut off by thrust faulting or is unconformably overlain by upper Stephanian (= Gzhelian) sediments (Wagner, 1965).

30 km east of the San Emiliano Valley, in the Bernesga Valley, a Moscovian aged succession, comprising mainly turbidites, carbonate debris flows and shallow water siltstones can be found exposed in the northern flank of the Cármenes (see Fig. 1.2 C) syncline (Bowman, 1982 & van Ginkel and Villa, 1996). This sedimentary succession is commonly known as the Lois-Cigüera Formation (Rácz, 1964; Brouwer and van Ginkel, 1964; de Meijer, 1971; Van De Graff, 1971 & Bowman, 1982, 1985), and is a stratigraphic equivalent to the San Emiliano Fm. The Lois-Cigüera Fm. consists of the basal Villanueva Beds, the middle “Caliza masiva” unit and the top Villamanín Beds. Brouwer and van Ginkel (1964) erected the Lois-Cigüera Fm. (as well as two other similar formations; the Pongo and Prioro Fm’s.) on the basis that the sediments were mostly detrital (turbiditic and debris flow). According to Wagner and Fernández-García (1971) it was doubtful that a distinction between the correlative formations could be maintained. Moore *et al.* (1971) reported the San Emiliano Formation as missing or reduced along the northern limb of the Cármenes syncline, and reported that the “rhythmic units” of the San Emiliano Fm. (as observed

in the vicinity of San Emiliano) are not found in the Villamanín area and are absent (or reduced) as a result of uplift and erosion, the responsible uplift believed to be associated with the Cantabrian Block (as defined by Radig, 1962). Bowman (1982) reports several lithologies (turbidites, shallow water siltstones and carbonate debris) which are recognised as being the same age as the San Emiliano Fm. Due to the sufficiently distinct facies and distribution the Lois-Cigüera Fm. is separated from their San Emiliano valley counterparts (Bowman, 1982 & van Ginkel and Villa, 1996). The San Emiliano Formation was often mistakenly reported from the Villamanín area previous to Moore *et al.* (1971) and Bowman (1982). The distinction is still not recognised by some authors (Riding, 1979 & Samankassou, 2001).

Carbonate units within the San Emiliano Formation are generally confined to the La Majúa Member. These units are laterally persistent limestones. Bowman (1979) recognised five lithofacies (following the classification scheme established by Dunham, 1962 with modifications by Embry and Klovan, 1971) within the second lowest stratigraphically exposed limestone unit. The lithofacies he recognised were: [1] *Donezella* bafflestone, [2] bioclastic wackestone, [3] bioclastic packstone, [4] oncolithic, whole fossil wackestone and [5] sparsely fossiliferous wackestone. Carbonate mud mounds can be frequently observed within the limestone units of the San Emiliano Formation at the type locality (Bowman 1979) and within the Lois-Cigüera Formation of the Cármenes syncline (Hensen *et al.*, 1995 and Samankassou, 2001). Bowman (1979) refers to “mound limestone (bafflestone)”, these features are described as “...lenticular to hump-shaped mounds, 2.40-6.10 m high and up to 30m wide.” (Bowman 1979, p. 30). These mounds are described as being formed by *in situ* growths of *Donezella* which act as a baffler for carbonate muds, with formation ceasing due to a change in water depth or energy levels. From the Lois-Cigüera Formation of the Cármenes syncline Samankassou (2001) reported mounds 6-12m thick, characterised by a skeletal-microbial boundstone controlled by sea level and siliciclastic flux. Hensen *et al.* (1995) recognised carbonate mud mounds of both primary and diagenetic origin from the Lois-Cigüera Formation. The Lois-Cigüera mounds are a good comparison for the

mounds of the San Emiliano Formation due to their similarities in stratigraphic age and temporal distribution. Where discussed in this thesis the “San Emiliano Valley mounds” refers to: the Candemuela Mound (29T 744467.52 4763114.34), mounds along Unit 8 (29T 737976.62 4761190.87 to 29T 744167.29 4763054.05), the Pinos Pylon Mound (30T 258176.93 4763445.24) and the Pinos East Mound (30T 258465.30 4763828.33); the Pinos Hairpin Limestones (30T 257750.58 4763450.38) are also from the San Emiliano Valley but contain no mounds. “Bernesga Valley mounds” refer to: the Sena de Luna Mound (30T 258869.07 4756321.56), the Cármenez South Mound (30T 291652.20 4758406.30) and the San Martín Mound (30T 279070.51 4758646.38).

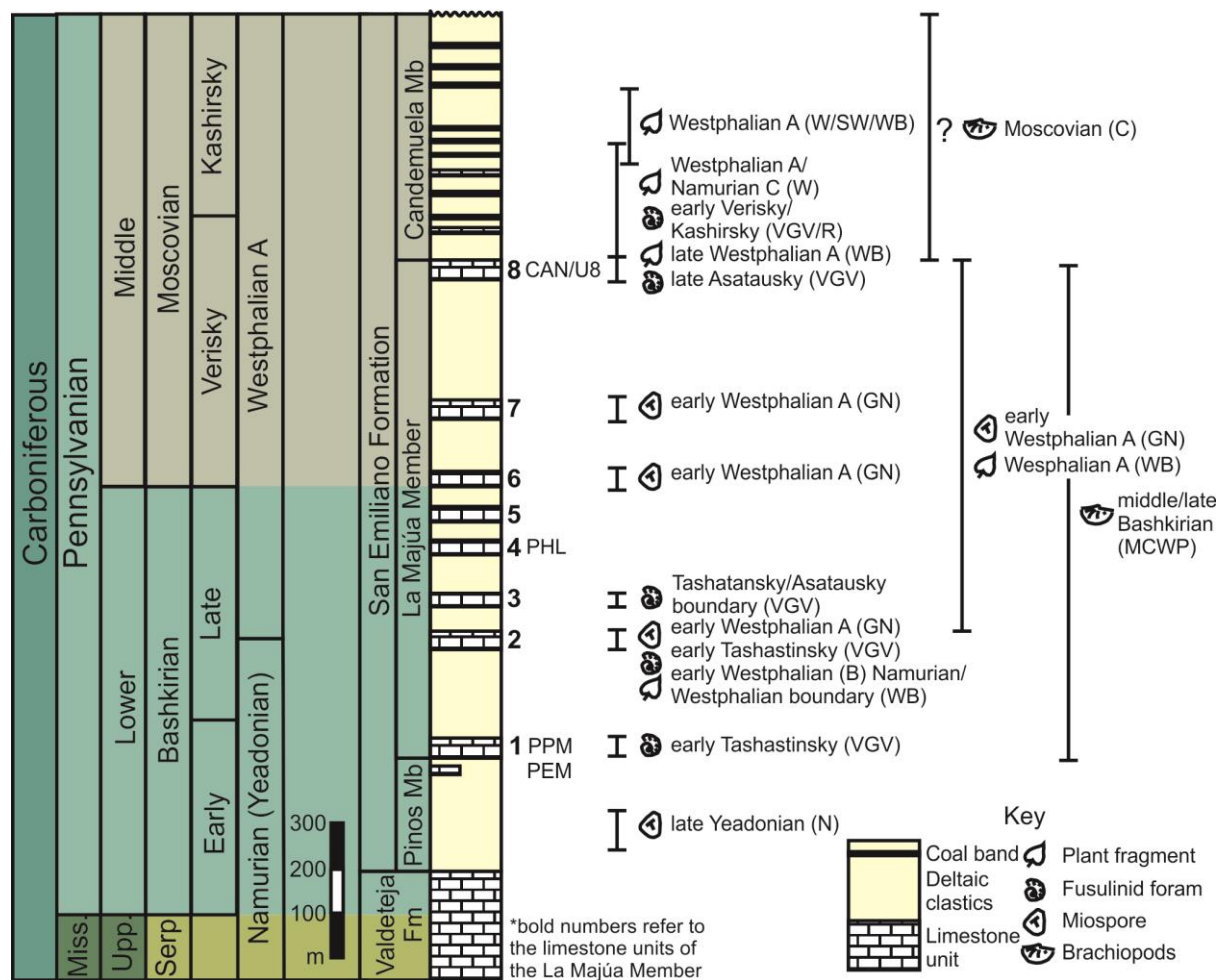


FIGURE - 1.3 Litho- and biostratigraphy of the San Emiliano Formation at the type point, San Emiliano. Age of the Formation based upon various authors stratigraphic studies are provided,

alluding to a Bashkirian to early Moscovian age for the La Majúa Member. Specimen bearing limestone units are labelled 1-8. B = Bowman, 1982; C = Carballeira *et al.*, 1985; GN = Gueinn and Neves *in* Bowman, 1982; MCWP = Martínez-Chaçon and Winkler Prins, 1979; N = Neves *in* Bowman, 1982; R = Rumjantseva *in* Wagner and Bowman, 1983; SW = Stockmans and Williére, 1965; VGV = Van Ginkel and Villa, 1996; W = Wagner, 1959; WB = Wagner and Bowman, 1983. Modified after Van Ginkel and Villa (1996). Miss. = Mississippian, Upp. = Upper, Serp. = Serpukhovian, Fm = Formation, Mb = Member. PEM = Pinos East Mound, PPM = Pinos Pylon Mound, PHL = Pinos Hairpin Limestone, CAN = Candemuela Mound, U8 = Unit 8.

1.3 Palaeogeography

During the Pennsylvanian series, Spain was positioned on the eastern flank of Pangea, west of the coast of the Palaeo-Tethys Ocean (Fig. 1.4). Throughout the Carboniferous, northern Spain was under the influence of crustal shortening, associated with the Variscan Orogeny (Julivert, 1978; Marcos & Pulgar, 1982; Pérez-Estaún *et al.*, 1988; Rodríguez Fernández, 1993 and Keller *et al.* 2008). Large epicontinental seas were present in the Russian platform, much of northern Europe and in northern Africa (Vai, 2003). The basin into which the San Emiliano Fm. was deposited is one of several en echelon, continental basin seaways which opened toward the southeast and closed to the northwest (Vai, 2003). Vai (2003) produced bathymetric curves (inferred from environmental reconstructions) for the intracratonic basins of the upper Carboniferous, indicating that the Cantabrian basins had a continental/marine transitional bathymetric profile during the Moscovian before becoming dominantly lowland terrestrial in profile in the Kasimovian. The Carboniferous sedimentology of northern Spain is dominated by foreland basin deposition.

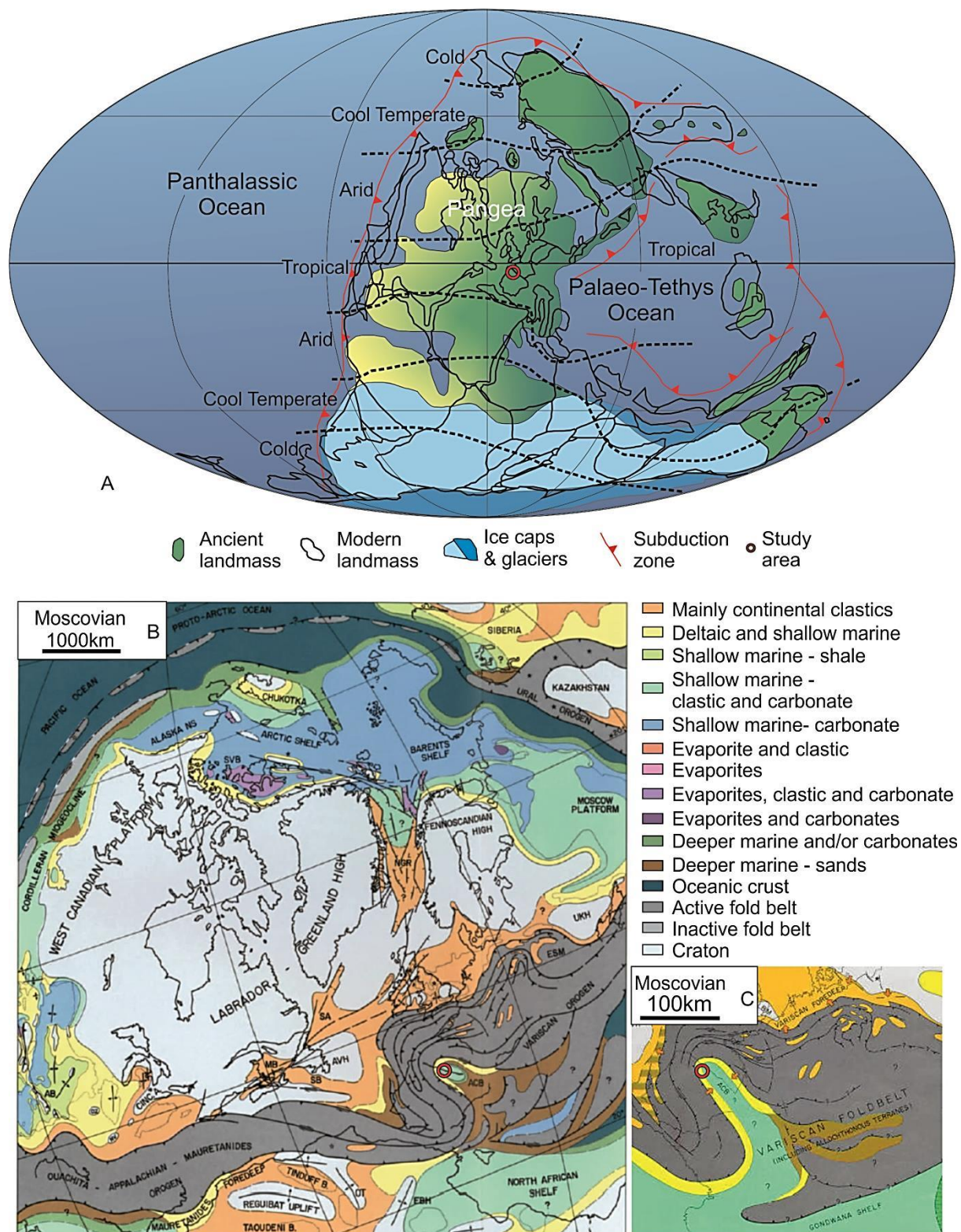


FIGURE - 1.4 A. The palaeogeography of the Bashkirian to Moscovian (315Ma). The study area can be seen just south of the equator on the eastern board of the Pangean supercontinent (as indicated by the yellow dot). The extent of glaciation and regional climates are based upon the extent of climatologically sensitive lithologies. B and C. Structural, lithological and environmental

reconstructions for central Europe in Moscovian times, the Cantabrian basin can be seen as a narrow sea-way connecting with the Palaeo-Tethys Ocean to the south west. AB - Anadarko Basin, ACB - Aquitaine-Cantabria Basin, Alaska NS - Alaska North Slope, AVH - Avalion High, CINC A - Cincinnati Arch, EBH - El Bjot High, ESM - East Salesman Massif, MB - Magdalen Basin, NGR - Norwegian-Greenland Sea Rift, NV - Nashville Dome, OT - Ougarta Trough, OZ - Ozark Uplift, SA - Saint Anthony Basin, SB - Sidney Basin, SVB - Sverdrup Basin, UKH - Ukranian High. A, based on figures from the Paleomap Project, Scotese (2003). B, after Ziegler (1989). C, after Ziegler (1990)..

1.4 Palaeoenvironment

During the Carboniferous the Earth was under “ice house” conditions as a result of the glaciation of the continents positioned adjacent to the South Pole (Tabor and Montañez, 2004 & Tabor and Poulsen, 2008). This included present day Antarctica, Australia, South America, South Africa and India (Fig. 1.4). The glacially dominated climate was subject to rapid and continued cyclical climate change (e.g. Crowell, 1978; Veevers and Powell, 1987; Crowley and Baum, 1991 & 1992 & Scheffler *et al.*, 2003). “Ice house” conditions are generally thought to have first stabilised during the Serpukhovian (e.g. Stephenson *et al.*, 2010 & Barham *et al.*, 2012). The timing for the onset of global cooling has been indicated to have been during the Viséan (Barham *et al.*, 2012) reaching a glacial maximum during the Moscovian. Previous studies of Pennsylvanian sedimentary deposits suggest that the glaciers were subject to cyclic waxing and waning, resulting in high-frequency sea-level variations (Wanless and Sheppard, 1936; Crowell, 1987; Veevers and Powell, 1987; Crowley and Baum, 1992; Scheffler *et al.*, 2003 & Joachimski *et al.*, 2006). As a result of these sea level fluctuations many Upper Mississippian to Upper Pennsylvanian sediments display cyclic lithological and depositional patterns. Late Carboniferous deposits of Spain are dominated by sedimentation coeval with the Variscan Orogeny within foreland basins that were both mobile, and unstable. As a result of this units and formations are temporally and spatially varied, often correlating across a small geographical area. Aragonite is believed to have been the dominant precipitation state for calcium carbonate, and the term ‘aragonitic sea’ is often applied to Late Carboniferous oceans (Ries, 2010).

1.5 Summary

This is a multidisciplinary study which ultimately aims to critically analyse various carbonate mud mounds from the Pennsylvanian age deposits of the area local to San Emiliano. Several campaigns in the area resulted in the collection of detailed field data. This includes 254 samples, three sedimentary logs (recording approximately 100 m of sediments), numerous sketches and descriptions from 59 locations, as well as a 600 data-point chemostratigraphic log. Following from the collection of field data and sampling, preparations were made to conduct a microfacies and ultrafacies analysis of the mounds studied. 201 thin sections were prepared from selected samples, 177 of these were used within the microfacies analysis, the remaining 24 were used to investigate various biotas or sedimentary features. 31 blocks were prepared for ultrafacies analysis. Geochemical analysis was carried out in the form of elemental composition and carbon and oxygen isotope data. Elemental composition data was collected in the field whilst 6 (whole rock) samples were crushed for isotope analysis. Palaeontological data were studied both in the field and with thin section analysis and SEM observations.

1.6 Chapter Outlines

Below is a brief description of the major themes and outcomes contained within each of the chapters of this thesis. A literature Review and Methods and Materials chapters are also presented but are not summarised here.

4. Microfacies Analysis

A distinct microfacies is observed between mounds from the San Emiliano Valley and those of the Bernesga Valley. The San Emiliano Mounds are bioclastic and fenestral pack- and floatstones, characterised by homogenous, peloidal and clotted micrite sediments and a *Donezella*/encruster biological assemblage. The mounds are the result of biological construction of *Donezella* thickets,

which are baffled, bound and stabilised by microscopic encrusters including the genera *Rothpletzella*, *Girvanella* and *Claracrusta*. The San Emiliano Valley mound counterparts, from the Bernesga Valley, contain a higher biological diversity and often show more evidence for transported grains. The mounds were formed in a shallow, warm environment within both the euphotic zone and normal wave base. The San Emiliano Mounds were deposited in a restricted environment which was probably hypersaline.

5. Ultrafacies Analysis

Micrite, microspar and spar crystals with subordinate dolomites and clastics were observed. Evidence for an aragonitic precursor to the calcite, now present is given. Aragonite needle relics and a pitted crystal surface of most microspars were found. Framboidal pyrite found within the samples indicated that they formed in sediments below an oxygenated water column, however, localised anoxia existed.

6. Palaeontology

Donezelliaceans were major components of nearly all of the mounds studied. A relationship between *Donezella*, *Rothpletzella*, *Claracrusta*, *Girvanella* and occasionally *Wetheredella* is evident and is responsible for the nucleation and growth of the carbonate mud mounds from the San Emiliano Valley. The palaeoecological assemblage observed indicates a restricted environment. The group of organisms responsible for mound nucleation and growth quite probably represent a colonial assemblage. Three new species are recognised and presented.

7. Clastic Intervals

The sediments of the San Emiliano Formation consist of cyclothems representing deposition within the foredeep of a foreland basin. Carbonate deposition occurs at a time of clastic input quiescence and transgression. The depositional environments of the San Emiliano Valley sediments and the Bernesga Valley sediments are distinct. The San Emiliano Valley sediments

represent a shallower environment dominated by deltaic deposition whereas the Bernesga Valley sediments are related to gravity flows into a deeper environment.

8. Geochemistry

Hydrocarbon seepage and hydrothermal venting are dismissed as initiation mechanisms. Cyclicality is recognised within the elemental composition data, probably indicating Milankovitch scale cycles with tectonic activity juxtaposed over it. The major carbonate units of the La Majúa Member are thought to have formed during a tectonically driven transgression overprinted on a sea-level low stand.

9. Discussion

The culmination of the multidisciplinary elements of this study are presented. Interpretations made in previous chapters are summarised and integrated into models. The relationship of carbonate mounds spatially and temporally is investigated in an attempt to reveal any global scale trends that may be conducive to mound formation. The feasibility of interpretations and their implications are visited and possibilities for future work are considered.

2. Literature Review

A literature review regarding carbonate mud mounds of varying compositions and origins and several associated topics is presented here. Mounds have been described from various geological settings and environments and have been recorded from the late Proterozoic, up to, and including, modern times. The abundant variations of mound type appear to change throughout time, with various types being dominant in some time periods but completely absent from others. Several formation mechanisms have been proposed for carbonate mud mounds, some mechanisms pertain to particular mound types, and other, more general mechanisms have also been suggested. Carbonate mud mounds, their nucleation, growth and structure is examined here and nomenclature associated with carbonate mud mounds is explored.

2.1 Carbonate Mud Mounds

Carbonate mud mounds are a type of marine build-up consisting mostly of carbonate muds - mostly micrite or biomicrite (Pratt, 1995) containing various metazoans and algae (Monty, 1995) (Fig. 2.1). The term ‘mud-mound’ was first used extensively to describe buildups of carbonate muds by Wilson (1975). Wilson (1975) provided a comprehensive review of carbonate buildups which highlighted the polygenetic nature of mud mounds. He also considered mud mounds to be distinct from organic framework reefs, and indicated that they form in a variety of environments throughout the Phanerozoic. James (1980 & 1983) introduced the term ‘reef mound’ for lenticular occurrences of carbonate muds with some organic bindstone that formed in a range of environments (from deep basins to shallow/lagoonal). At a similar time, Longman (1981) suggested that mud mounds and reefs were part of a continuum, where a mud mounds framework was provided by seagrass and algae, and reefs by larger, more ridged walled organisms. Various authors refer to mounds as reefs due to topographic relief and the relationship to ‘ecological’ reefs. The term ‘reef mound’ was used extensively by authors (e.g. West, 1988; Brunton and Dixon, 1994; Lehrmann, 1999), until James and Bourque (1992) introduced three ‘mound’ types

(microbial, skeletal and mud), all of which, they suggested, graded into reefs. Subsequently, Monty *et al.* (1995) edited a Special Publication of the International Association of Sedimentologists as the result of an earlier symposium on ‘Carbonate mud-mounds’, thereafter the term ‘carbonate mud mound’ has been commonly used when describing buildups of carbonate mud. The term ‘carbonate mud mound’ was formally defined by Riding (2002). The majority of work published around the time, and since Monty *et al.* (1995), refer to the buildups as ‘mounds’ (e.g. Samankassou, 2001), ‘mud mounds’ (e.g. Wendt *et al.*, 1993; Wood, 2001 & Sager *et al.*, 2003 etc.) or, most commonly, ‘carbonate mud mounds’ (e.g. Neuweiler *et al.* 2001; Krause *et al.*, 2004 & Floquet *et al.*, 2012 etc.), often using the terms interchangeably. The earlier term ‘reef mound’ has become less popular, assumedly due to its evocation of organic reefs, though it is still occasionally used (e.g. Koch *et al.* 2002). Within this thesis, the term “carbonate mud mound” (with “mounds”, and “mud mounds” used as interchangeable terms) is used as suggested by Riding (2002), and refers to mound shaped deposits which are composed of carbonate muds with grains no larger than 62 µm.

Carbonate mud mounds have been reported from various environments (see 2.3 *Depositional Environments* below), from the Proterozoic (these are microbial lenses interpreted as the ‘forerunners’ to true carbonate mud mounds) to modern times. These build-ups occur throughout the Palaeozoic, Mesozoic and Cenozoic and are found at a variety of latitudes and water depths (Bosence and Bridges, 1995; Monty, 1995; Pratt, 1995; Flajs *et al.*, 1995; Wood, 2001; Riding, 2002 & Krause, *et al.* 2004) Throughout geological time mounds have somewhat of an episodic history. Mounds appear to have formed prolifically in the early Cambrian, late Devonian and early Carboniferous with the last significant number of mounds forming in the early Cretaceous (Wood, 2001 & James and Wood, 2010).

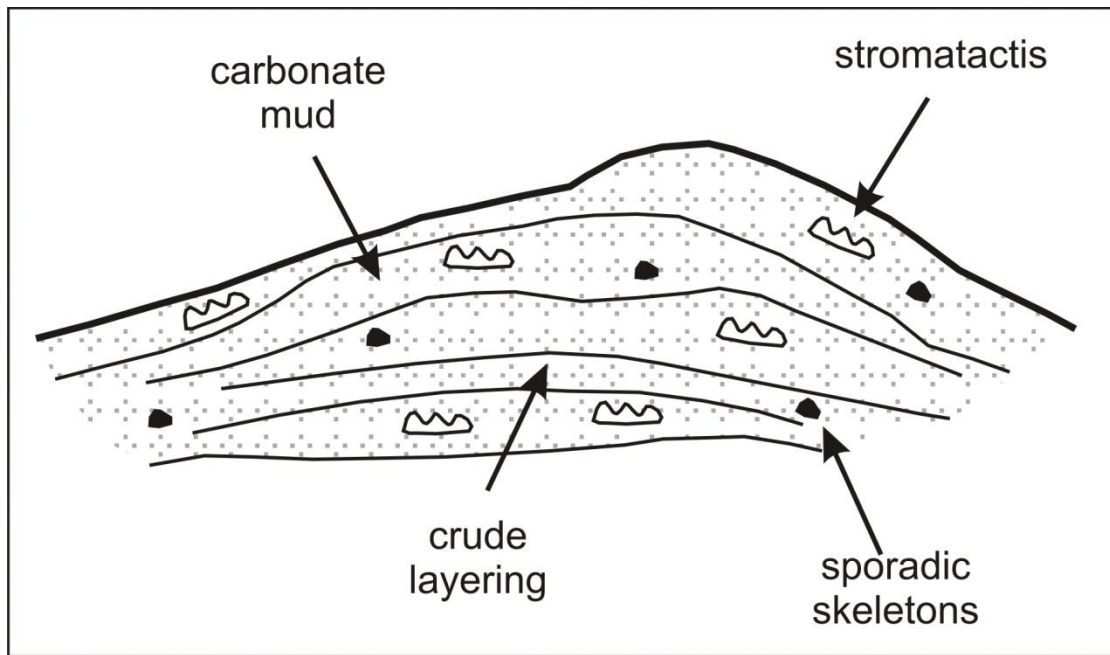


FIGURE 2.1 - The commonly occurring, basic features of mud mounds according to Riding (2002).

Various ‘sub-groups’ and naming’s have been used to describe mud mounds. Many Palaeozoic mounds are referred to as ‘Waulsortian-like’ mounds. These are mounds which bear similarities to the original Waulsortian mounds from the Dinantian age strata of the Waulsort area, Belgium (Dehantschutter and Lees, 1996). They are found across many parts of the world including northern Europe, North America, central Asia and north Africa. Lees and Miller (1995) defined Waulsortian mounds as “...dominated by an association of polymuds with at least one of the grain-type assemblages A-D and the accompanying macrofaunas and lying in the upper Tournaisian or lower most Viséan.” The term ‘Waulsortian-type mound’ is reserved for mounds with convincing similarities. As seen in Table 2.1 Waulsortian-type mounds contain up to four stages of growth (Lees and Miller, 1985). These phases of growth are characterised by various biotic assemblages and sedimentary features and have been interpreted to form at varying depths (Fig. 2.2). Other examples of attempts to classify and group mud mounds include Monty (1995) and Pratt (1995). Monty (1995) suggested a fourfold division consisting of:

1. Stromolitic mud mounds with rhythmic layers of microbial growth and sedimentation.
2. Non-laminated microbial mud mounds with mottled, thrombolitic or bioturbated fabrics.

3. Metazoan framework and framework reefs.
4. Stromatactoid mud mounds with mudstones, boundstones and common spicules.

Pratt (1995) suggested three main divisions of mounds:

1. Microbial, comprising of tufa-like structures of calcified fillements or fenestrate bryozoans.
2. Thromboid, thromboidal structures associated with metazoans.
3. Biomicritic, stromatactis bearing biomicrites.

Unlike more commonly known ‘ecological’ or ‘organic’ reefs (i.e. shallow water tropical coral reefs) mud mounds are not supported by a large, rigid framework. They are, however, regarded as being part of an overlap in composition, primary physical characteristics and modes of diagenesis with those of ‘ecological reefs’ (Longman, 1981; James and Bourque, 1992; Bosence and Bridges, 1995; Kopaska-Merkel and Haywick, 2001a; Wood, 2001 & Riding, 2002). Mound size ranges from under 1 meter to several hundreds of meters thick (Pratt, 1995). The occurrence of deep sea mounds provides important geological information: palaeo-oceanographic conditions, sea level dynamics and the structural fabric of the underlying crust (Pratt, 1995).

The majority of mounds discovered are microbial in nature and include phototrophic and hetrotrophic bacteria, which are believed to degrade sponges and mucilages resulting in the local precipitation of carbonates (Monty, 1995). The single organism group that has continuously played the role of primary micro-frame builders are cyanobacteria. This is due to the induction of passive calcification of organic secretions and degraded products (Pratt, 1995). In some cases cyanobacteria may behave more as bafflers than as micro-framework builders, and may even act as both. Although mounds are rarely devoid of fossils their presence are generally too scarce to unequivocally account for mound formation. Riding (2002) has suggested that establishing the degree of organic involvement is problematic; exemplified by the differing views upon what stromatactis is (see 2.1.2 *Stromatactis, Cavities and Carbonate Mud Mounds* below).

Phase A (1)	The basal zone. Characterised by a low diversity assemblage with abundant fenestellid bryozoans and crinoid debris. Shelly material and stromatactoid cavities are common. This represents the ‘classic’ Waulsortian facies (Tucker and Wright, 1990)
Phase B (2)	Dominant siliceous sponges with dense micrite muds which often contain possible evidence of cyanobacteria
Phase C (3)	More diverse than A and B with the appearance of gastropods, trilobites and echinoids. Porostromate tubes (<i>Girvanella</i> , <i>Rothpletzella</i> etc.) appear. Peloids are a common component.
Phase D (4)	Algaly coated and micritized grains are common. Calcareous algae including dasycladaceans occur, ooids can be found along with fenestellid bryozoans.

TABLE 2.1 Summary of the main characteristics of Waulsortian phases A-D as defined by Lees and Miller (1985)

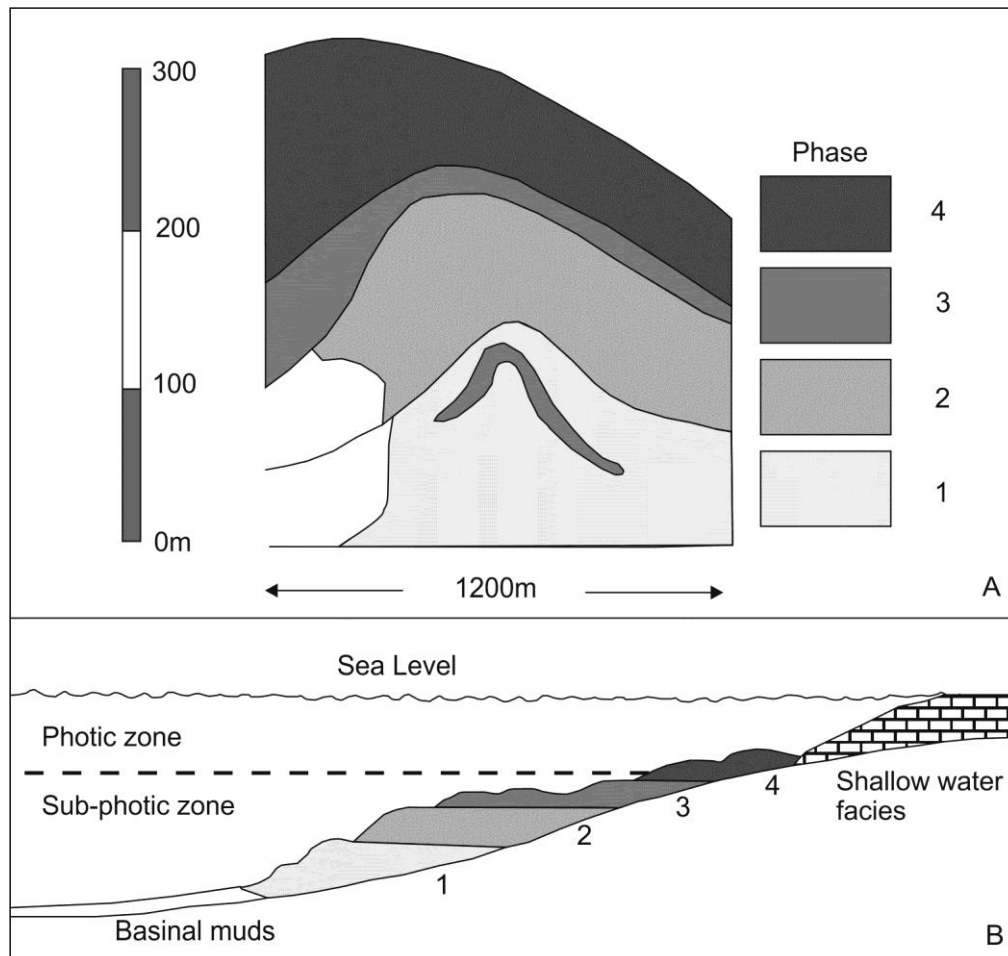


FIGURE -2.2 A. A cartoon schematic of the Furfooz Waulsortian mound in Belgium. The various Waulsortian phases are shown. B. Possible depth zonation for Waulsortian and Waulsortian-type mounds on a carbonate ramp. After Tucker and Wright (1990).

2.1.2 Stromatactis, Cavities and Carbonate Mud Mounds

Cavities, including fenestral, birdseye and stromatactis fabrics are commonly observed and associated with mud mounds (e.g. Bathurst, 1980; Bourque and Raymond, 1994; Monty, 1995;

Bosence and Bridges, 1995; Lees and Miller, 1995; Stenzel and James, 1995; Neuweiler *et al.*, 2001; Riding, 2002; Aubrecht *et al.*, 2002; DiFilippo *et al.*, 2003; Krause *et al.*, 2004; Hladil, 2005; Hladil *et al.*, 2006; Aubrecht *et al.*, 2009 & Pas *et al.*, 2011). Stromatactis was first termed and distinguished as a distinct type of cavity by Dupont (1881). It is a spar body common within Palaeozoic mud mounds (Neuweiler *et al.*, 2001), but only sporadically observed within Mesozoic mounds (Bathurst, 1982 & James and Bourque, 1992). Stromatactis cavities are characterised by a flat base and an undulating upper surface, filled partially with internal sediments with geopetal cements above. The cavity filling cements consist of an outer fibrous marine cement with a late blocky spar interior (Neuweiler, *et al.*, 2001). The size and shape of stromatactis has been observed to differ within individual mounds (Stenzel and James, 1995), as well as spatially and temporally (Hladil, 2005). The origin of the stromatactis fabric has been attributed to several factors including a fossil (Dupont, 1881), permineralised unfossilisable organism (Lecompte, 1937), as the result of rapid, uninterrupted sedimentation (Hladil, 2005) or the most commonly accepted origin, as the result of centripetal cementation in a cavity system (Neuweiler *et al.*, 2001). It should be noted that the origin of the cavity system itself is also attributed to several factors, the most common factor being sponge networks which undergo early diagenesis and cementation (e.g. Bourque and Gignac 1983 & Bourque and Raymond, 1994). Stromatactis cavity networks form in shallow subsurface environments within the subfloor sediments (Bathurst, 1982 & Lees and Miller, 1995). Fenestral and birdseye cavities generally lack the internal sediment and fibrous marine cement fill of stromatactis and are filled by spary calcite. Fenestral cavities are characterised by an undulose upper surfaces whereas birdseye cavities are often lens-like in shape (Flügel, 2004). Both stromatactis and fenestral cavities represent 3D spar networks (Bathurst, 1982; Flügel, 2004 & Neuweiler *et al.*, 2001), whilst birdseye cavities are isolated cavities (Flügel, 2004). Stenzel and James (1995) inferred a change in size and morphology of observed stromatactis upwards throughout a mound (the cavities are observed to increase in size and complexity) to be the result of increased water movement and related erosion through cavity systems as the mound formed.

2.2 Microbial Vs Biodetritral Mounds

Carbonate mud mounds are generally seen to have formed within a spectrum with two end members (Bosence and Bridges, 1995); either as a result of microbially precipitated carbonate muds, or the result of accumulated transported muds and bio-detritus. The two end members and their characteristic features are discussed below.

2.2.1 Microbial Mud Mounds

Microbial mud mounds are mounds which are interpreted to have had an *in situ* microbial origin (e.g. James and Bourque, 1992; Pickard, 1992; Flajs and Hüssner, 1993; Flajs *et al.*, 1995; Monty, 1995; Pickard, 1996; Russo *et al.*, 1997; Neuweiler *et al.*, 1999; Belka, 1998; Neuweiler *et al.*, 2000 Pratt, 2000; Riding, 2000 & Rodríguez- Martínez *et al.*, 2003). Microbial aided precipitation of micrite consists of precipitation around microbial filaments and coccoids as microbial mud (Taberner and Bosence, 1995). Other mechanisms which may assist with *in situ* precipitation might involve stabilization and lithification (Riding, 2002). The attribution of a microbial origin ultimately means that mounds can form in a self-sufficient way (Riding, 2002), without the need of imported sediments or baffling organisms. Microbial mounds are closely associated with stromatactis and early marine/microbial cements (Bosence, 1995).

The idea of ‘in house’ production of microbial micrites is strongly supported by the occurrence of carbonate mud mounds enclosed in siliciclastic environments and high angles of accumulation (Riding, 2002). However, microbial micrites from ancient examples are not easily recognised. This is due to our fairly poor knowledge of Palaeozoic microbial micritic grains and their related fabrics (Monty, 1995). The main sites for carbonate precipitation are generally found in decaying aggregates of bacteria, which, usually leave no detectable cell structures (Monty, 1995). Evidence has been found for fossilised bacteria in micritic crystals, this is frequently observed with cyanobacteria, which are believed to be an important factor for microbial mound formation due to the evolution of a sheath (glycocalyx), able to condense carbonates on its surface. This step in evolution took place at roughly the same time that mud mounds are first observed, some 800-

700Ma (Monty, 1995). Folk (1993) found evidence (SEM images) of bacteria and nannobacteria in abundance in recent carbonate sediments (hot spring deposits from Viberto, Italy). After recognising nannobacteria in the Italian hot springs Folk (1993) reported that finding them in less extreme environments was easier; bacteria and nannobacteria from Bahaman (Joulters Cay) ooids and hardgrounds and in Great Salt Lake aragonite ooids and cements were shown. He also reported nannobacteria from Palaeozoic and Mesozoic rocks and concluded that due to their great abundance they are likely to play a prominent role in catalysing the precipitation of carbonates. Other examples of fossilised bacteria in micritic crystals include: Maurin and Noël (1977) who found “banana-shaped” bacteria and abundant spheroids and bumps in Mississippian age micrites (although Folk (1993) dismisses the spheroids and bumps as artefacts of the polishing process); Camoin and Maurin (1988) reported images of fossilised bacteria from Turonian mud mounds in Tunisia.

However, fossilised bacteria in mud mounds very rarely occur, this leads to a fundamental problem whilst defining mounds as microbial in origin (Riding 2002). Many authors offer only circumstantial evidence and often fall back upon assumptions when establishing an origin or find it difficult to distinguish between microbial or biotrital mounds (Lees and miller, 1995; Taberner and Bosence, 1995 & Kopaska-Merkel and Haywick, 2001a). Mounds formed by chemosynthetic microbes, often with associated polychaete tubes and bivalves (e.g. Beauchamp and Savard, 1992; Peckmann *et al.*, 1999 & Cavalazzi *et al.*, 2007) are regarded as a subset of microbial mounds (Bosence and Bridges, 1995). Neuweiler *et al.* (2003) stated that deep water mounds should not be designated a microbial origin unless a site-specific microbial community has been demonstrated.

2.2.2 Biotrital Mud Mounds

Biotrital mud mounds are mounds which are interpreted to be composed dominantly of broken and transported skeletal debris (Bosence, 1995; Bosence and Bridges, 1995; Taberner and Bosence, 1995 & Kopaska-Merkel and Haywick, 2001b). Muds from these mounds may be locally

generated or transported. Biodeutral mounds form due to an inorganic accumulation of muds (which may have a microbial origin). Bioclastic grains may consist of coral, foraminifera, mollusc, bryozoan and coralline algal debris (Taberner and Bosence, 1995).

Negative evidence for the identification of biodeutral mounds is the lack of stromatolites or other cavity systems and a lack of early marine cementation (Bosence, 1995 & Taberner and Bosence, 1995).

2.3 Depositional Environment

In general, carbonate sediments originate as skeletal grains or precipitates within the depositional environment (Flügel, 2004). Modern carbonate architecture is controlled by a number of factors: relative changes in sea level, bathymetric profile, shelf width, leeward or windward position, currents, storms and climates (Bosellini, 1989). Because of the multitude of depositional environments – from the tropics to the poles and from non-marine settings to over 500 m depth – certain ‘models’ have been suggested applying to the precipitation and accumulation of carbonates (Flügel, 2004). However, carbonate environments generally have a dominant biological control, due to the continued evolution of organisms throughout time and due to spatial fluxes (light, chemical energy, gases, sediments etc.) any such models are only general in nature (Insalaco *et al.*, 2000). Carbonate mud mounds have been reported from a wide variety of depositional settings. Carbonate mud mounds *nomen est omen* are composed of carbonate muds, the formation of which, especially in ancient examples, are somewhat problematic. The depositional environment is discussed below whilst the specific “micrite problem” is discussed in section 2.3.2 *The Micrite Problem* below.

A carbonate factory is the concept of a zone of high carbonate production that is sensitive to environmental conditions and is spatially restricted (Wright and Burgess, 2005), typically due to photic and turbiditic regulation. This concept varies greatly from that of siliciclastic sedimentation systems which rely upon physically complex delivery systems from source to final deposition site.

Schlager (2000 and 2003) has proposed the existence of three main carbonate ‘factory’ types: Tropical shallow water (dominated by light dependent organisms), cool-water (associated with heterotrophic skeletal producers) and mud mound (microbial and abiotic precipitate dominated) ‘factories’ (Fig. 2.3). These factory classifications were based upon observations of marine carbonate precipitation modes. Varying marine carbonate grains or precipitates are viewed as part of a continuum between the differing depositional environments or ‘factories’ (Pedley and Carannante, 2006).

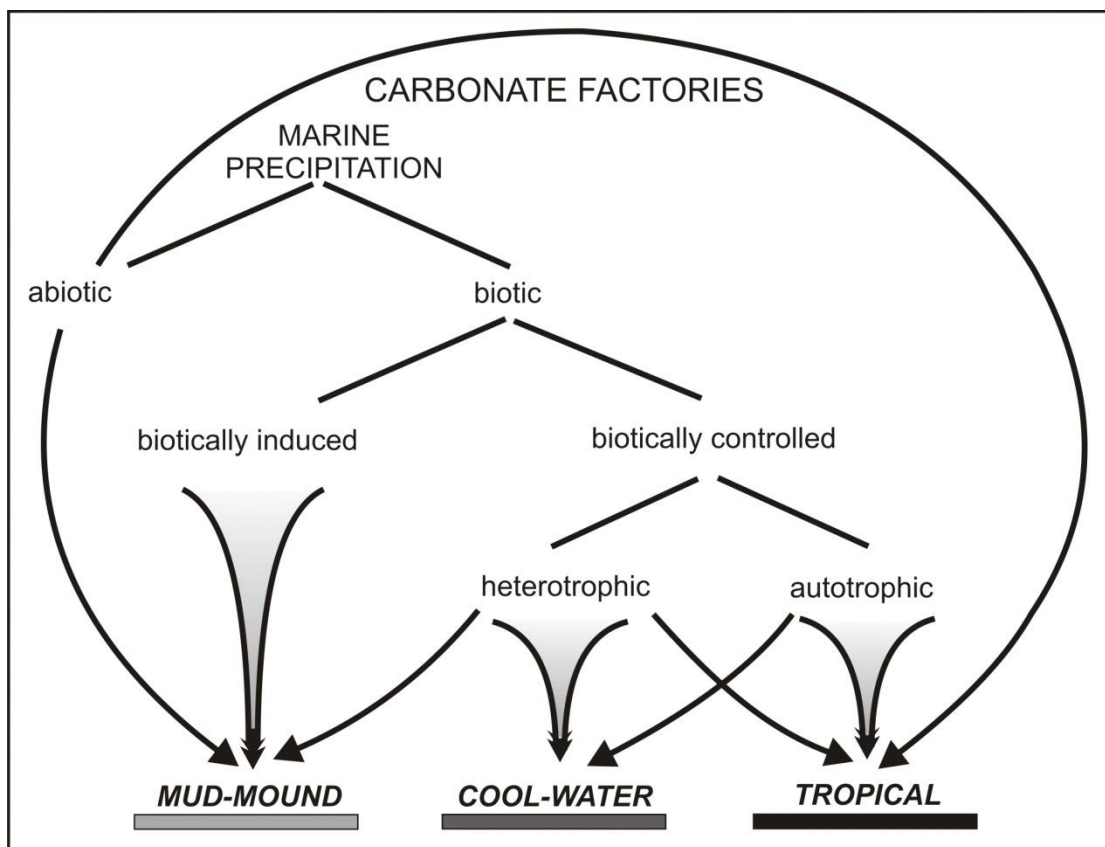


FIGURE - 2.3 The pathways of carbonate precipitation in aquatic environments, governed by the degree of biotic influence, combine in characteristic ways to form carbonate factories: the mud-mound factory is dominated by biotically induced precipitates (mostly micrite); the cool-water factory is dominated by heterotrophic organisms; the tropical factory is dominated by heterotrophic organisms with autotrophic symbionts or biotically controlled precipitates from autotrophic organisms. From Schlager (2003).

However, these ‘factories’ do not occur in pure form, that is to say, no carbonate rock will be purely autotroph dominated or purely biotically induced (Schlager, 2003). Carbonate rocks will

consist of mixtures of these basic categories, the ‘factories’ represent three commonly occurring modes of marine precipitation.

Pomar and Hallock (2008) have explained temporal and chronological differences in carbonate precipitation as a response to shifts in partial $p\text{CO}_2$ and $p\text{O}_2$ and the concentrations of Ca^{2+} and Mg^{2+} . In addition to adjustments imposed by biological extinctions.

Wright and Burgess (2005) have argued that current interpretations of carbonates using microfacies analyses are limited, and that the use of microfacies analyses, is therefore, limited. Dissolution is capable of skewing sediment compositions, suggesting that ancient carbonates are unrepresentative of their original sediments. Schlager (2003) and Dodd and Nelson (1998) reported that tropical [shoal-water] systems (of the Great Barrier Reef, as studied by the oil industry as a modern analogue to exploration targets in Palaeozoic and Mesozoic of North America and Mesozoic and Cenozoic of Asia) are inadequate models for many ancient examples. Insalaco *et al.* (2000) have questioned the viability of Schlager’s (2000) tripartite classification, which is based upon modern deposits and express concerns over the legitimacy of application for ancient examples.

In terms of carbonate mud mound deposition, depositional environments for individual/groups of mounds are generally given as a result of a microfacies analysis of the mound in question. The surrounding lithologies are also often used to help reconstruct the depositional environment. Depositional environments interpreted for mud mound formation commonly include: extensional basins and related passive margins (e.g. Barnaby and Read, 1990; Fernandez *et al.*, 2006; de Hass *et al.*, 2009 & Shen and Hairou, 2010), foreland basins (e.g. Gutteridge, 1995; Weller, 1995; Peckmann *et al.*, 2001 & Antoshkina, 2006), inverted basins (e.g. Chafiki *et al.*, 2004), shallow water atolls (e.g. Dronov, 1993), tidal flats (Schmidt *et al.*, 2001) and from both regressive (e.g. Dehantschutter and Lees, 1996; Lees, 1997 & Calner *et al.*, 2010) and transgressive (e.g. King, 1986; Jeffrey and Stanton, 1996 & Devuyst and Lees, 2001) sequences. For a full list of mounds

and their environmental setting, age and location, refer to 9.9 *The distribution of Carbonate Mud Mounds through Space and Time* in chapter 9. *Discussion* as well as Appendix 5. *Distribution*.

2.3.2 The Micrite Problem

As suggested above ancient carbonates are often unrepresentative of their original sediment, the *Micrite Problem* exemplifies this and should be taken into account whilst dealing with fine grained carbonates. As carbonate mud mounds are, by definition fine grained, the origin of fine grained carbonates is explored here. The formation of lime muds - and therefore the origin of fine-grained carbonates - is a key issue within carbonate sedimentology (e.g. Folk, 1965 and 1974; Fischer *et al.*, 1967, Flügel, 1967; Honjo, 1969; Bathurst, 1970 and 1975; Tucker and Wright, 1990; Kaźmierczak *et al.*, 1996; Munnecke and Samtleben, 1996; Pratt, 2001 and Flügel, 2004). Micrites, microspars and associated peloids are common in Phanerozoic age rocks, however their origins are often difficult to determine due to a lack of diagnostic features (Berkyová and Munnecke, 2010), this is often referred to as the *Micrite Problem*. The terms ‘micrite’ and ‘microspar’ were first coined by Folk (1959) and are essentially portmanteaus of ‘microcrystalline calcite’ and ‘microcrystalline sparite’. Micrite is defined as calcite crystals with a size of around 2 µm (or anything 4 µm or lower) with microspars accounting for those crystals between 5-15 µm. Most studies (including this study) which deal with micrites and microspars refer to the works of Folk (1959, 1965 and 1974) and use the terms as defined above. The origin of fine-grained carbonates comes from the lithification of lime muds, this is problematic since micrites are polygenetic, meaning in ancient carbonates it can be difficult (or impossible) to ascertain the origin of the sediments. The origin of fine-grained carbonate sediments has been attributed to various processes, namely: the breakdown of calcareous skeletal grains, the disaggregation of peloids (origins of which include faecal pellets and the breakdown of calcareous algae, micritised grains or mudclasts) and chemical or biochemical precipitation (e.g. Lowenstam and Epstein, 1957; Stockman *et al.*, 1967; Neumann and Land, 1975; Tucker and Wright, 1990; Hillis, 1999 Flügel, 2004; see Berkyová and Munnecke, 2010 and references therein). Due to the nature of the size of grains it is necessary to investigate fine grained carbonates using Scanning Electron

Microscopy (SEM). The SEM study of recent lime mud sediments and some ancient examples has indicated that the difference in sizes between micrite and microspar could be controlled by the precursor sediments of a lithified carbonate (e.g., Steinen, 1982; Lasemi and Sandberg, 1984 & Munnecke *et al.*, 1997). Both high-Mg calcite and aragonite are meta-stable and under normal diagenetic conditions are replaced by stable, low-Mg calcite (Tucker and Wright, 1990). Aragonite and high-Mg calcite crystals grow as elongate or needle-like crystals with widths generally a few microns across, this is because Mg ‘poisons’ the sideward growth of calcite, forcing the precipitation of either aragonite or fibrous calcite (Folk, 1974). When these sediments undergo diagenesis the aragonite and fibrous high-Mg calcite are replaced by low-Mg calcite, which because of the lower Mg/Ca ratio, is not restricted in sideward growth, resulting in the engulfment and replacement of aragonite needles and high-Mg calcites (Folk, 1974; Tucker and Wright, 1990 & Munnecke and Samtleben, 1996). This ‘aggrading neomorphism’ results in crystal sizes relative to the original length of the aragonitic or high-Mg calcite sediment (Fig. 2.4). Micrite is thought to be the result of low-Mg precursor muds (which are not replaced), with microspar forming due to the aggrading neomorphism of high-Mg and aragonitic precursor muds. Aragonitic precursors are characterised by [1] their grain size (microspar), [2] a higher strontium content, [3] pitted crystal surfaces, and locally [4] primary aragonite needles in their original orientation. Both primary aragonite and pitted textures of microspar crystals are regarded as indications of an aragonitic precursor sediment composition (Steinen, 1982; Lasemi and Sandberg, 1984; Munnecke and Samtleben, 1996 & Munnecke *et al.*, 1997).

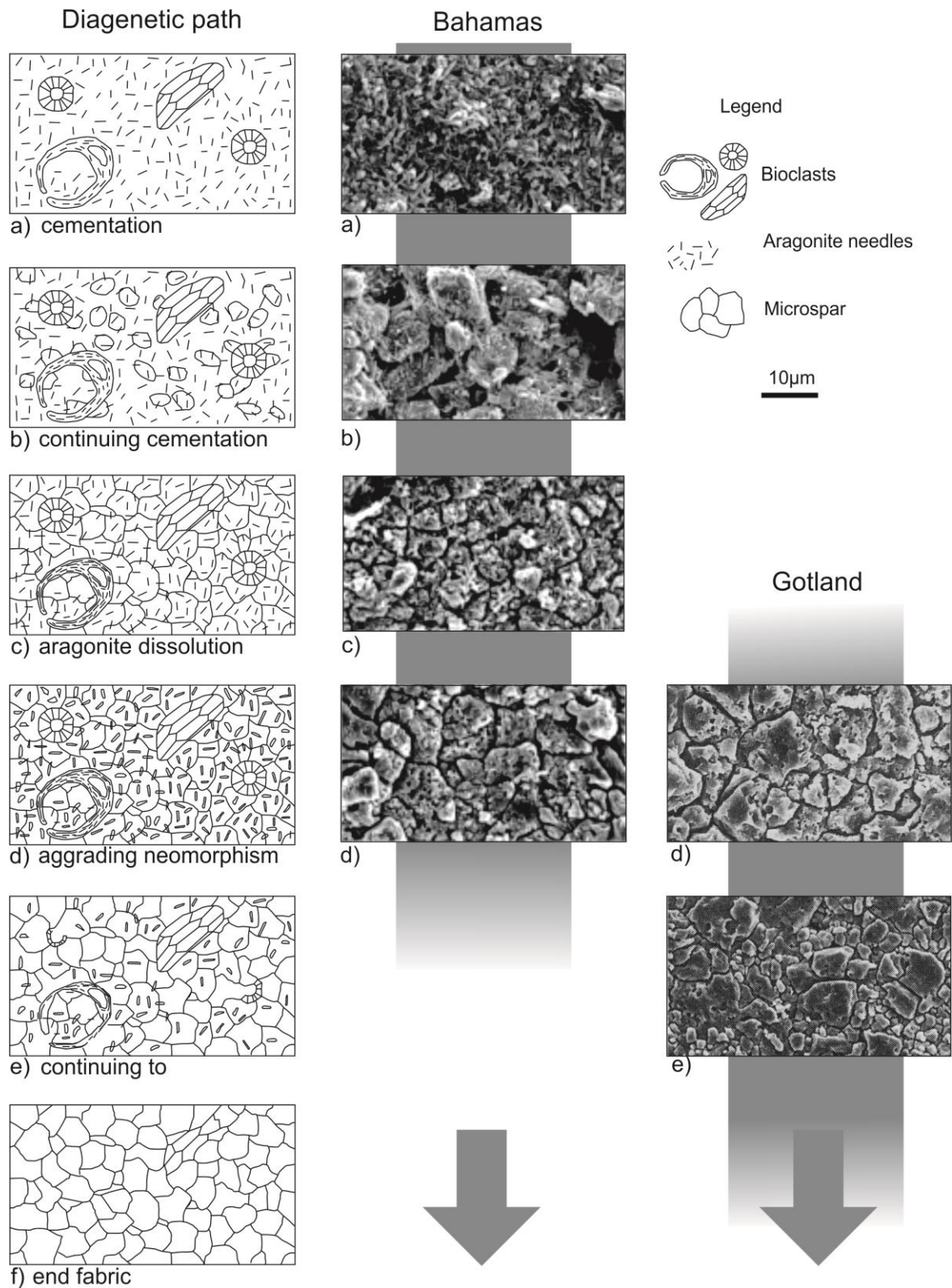


FIGURE - 2.4 Reconstruction of the diagenetic path from unconsolidated aragonite-dominated mud to lithified limestone with comparisons from carbonates from the Pliocene of the Bahamas and the upper Silurian of Gotland. a) Unlithified aragonite needle mud. b) Beginning of precipitation of microspar. c) Completely cemented sediment. d) Pitted texture as a result of dissolution of aragonite needles. e) Microspar as a result of continued aggrading neomorphism. f) Equigranular microspar with no pitted textures. From Munnecke *et al.* (1997).

2.4 Palaeoecology

The biota of mounds is discussed by various authors, Pratt (1995) summarised the range of invertebrate groups and microbial microfossils. (Fig. 2.5 – Note that the Proterozoic ‘deep-water reefs’ indicated by Pratt (1995) refer to low relief mounds and columnar stromatoids and are therefore not true reefs). Table 2.2 records the major groups of biota reported from carbonate mud mounds throughout the Phanerozoic. As emphasised by the table, mound communities are often associated by cyanobacteria, microscopic encrusting forms and microporobionts.

2.4.1 Dominant Biota

A wide range of biota are found within carbonate mud mounds, with certain communities becoming dominant at different time intervals and within different environmental settings. Mounds often exhibit a dominance of one particular biota or the dominance of a small group of biota. Examples of specific biota dominated mounds include: ‘Phylloid’ algal mounds (e.g. Mazzullo and Cys, 1979; Samankassou and West, 2002; Doherty *et al.*, 2002 & Grammer and Ritter, 2009) and *Donezella* mounds (e.g. Bowman, 1979; Samankassou, 2001 & Cook *et al.*, 2007).

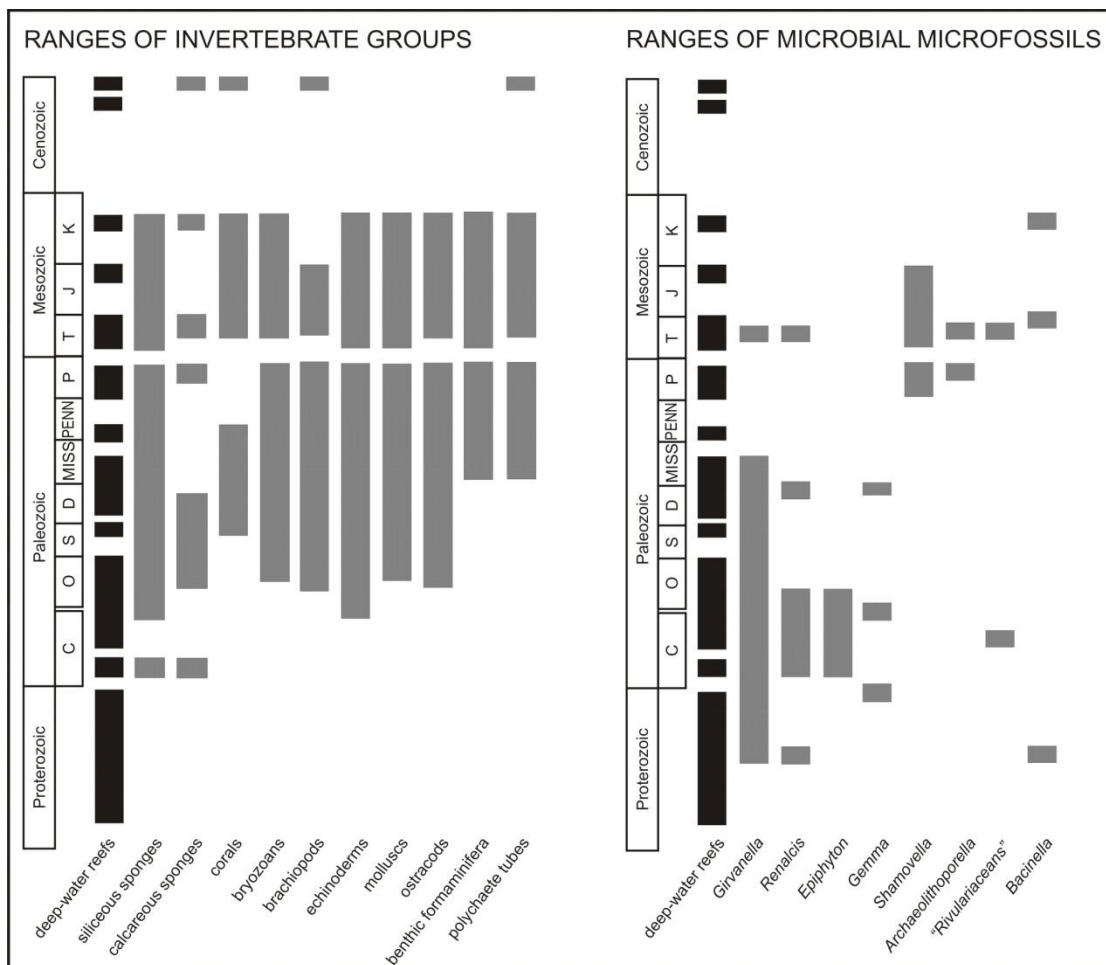


FIGURE - 2.5 Ranges of invertebrate groups and microbial microfossils from deep water mounds. ‘Calcareous sponges’ refers to archaeocyaths, stromatoporids, sphinctozoans etc. ‘Rivulariaceans’ refers to structures such as *Ortonella*, *Bevocastria*, *Hedstromia*, *Macrotubus* and *Garwoodia*. ‘*Renalcis*’ refers to grape like micrite objects in Neoproterozoic to Middle Triassic biolithites. ‘Gemma’ refers to micrite walled spheroids including calcispheres in the late Devonian. After Pratt (1995), modern deep water mound data from Kenyon *et al.*, (2003).

Ecological composition of mounds

Cambrian

During the lower Cambrian of the Flinders ranges, two major types of carbonate buildups formed; (1) low-energy, archaeocyath-sponge-spicule mud mounds and, (2) high-energy, archaeocyath-calcimicrobe bioherms (James and Gravestock, 1990). These mounds formed in a shallow water environment. Archaeocyaths are not associated with photosynthetic symbionts. Calcified microbial microfossils observed in these mounds were *Epiphyton*, *Renalcis*, *Girvanella* and *Botomaella*. Mounds may contain brachiopods and trilobites. Stromatactis is found in many of the buildups. These biota were the major components of metazoan bioherms in the early Cambrian (Rees *et al.*, 1989). Middle Cambrian mounds from House Range, Utah, USA, show evidence of calcified filaments and tubes, and although not directly observed evidence points towards a microbial origin. Stromatactis is evident in the mounds (Elrick and Snider, 2002). Upper Cambrian mounds contain *Girvaella*, *Renalcis*, *Epiphyton* and

Tharama, *Gemma* is also thought to have been present (Pratt, 1995).

The majority of Cambrian mud mounds are observed from the North American continent. The growth of carbonate platforms and carbonate buildups from the Lower, Middle and Late Cambrian may be due to a variety of reasons; global warming after late Precambrian glaciation, the migration of the North American continent towards the equator, a semi-arid climate limiting clastic influx and possibly a decrease in clastic-sediment during sea level rise (Barnaby and Read, 1990).

Cambrian aged mounds have been described from the Lánacara Formation of the Cantabrian Mountains as calcimicrobial-archaeocyathan bioconstructions (Perejón *et al.*, 2012).

Ordovician

Lower to Middle Ordovician shallow water examples comprise of *Girvanella* and *Epiphyton*, crinoid holdfasts, bryozoans, corals, stromatoporoids, lithistid sponges and the calcareous red algae, *Solenopora*. Ramp examples exhibit bioclasts of sponge spicules, trilobites, brachiopods, nautiloids, cystoid ossicles and *Nuia* (possibly calcareous green algae) and *Halysis* (calcareous green algae). Deep shelf examples contain *Girvanella*, bioclasts are dominated by cystoid ossicles, trilobites, siliceous sponge spicules, gastropods, brachiopods, nautiloids and *Nuia* (Pratt, 1995). The macrofaunas of Upper Ordovician mounds are bryozoan dominated with pelmatozoans, stromatoporoids, cephalopods, ostracods and some coral subordinates (Crow *et al.*, 2001).

Silurian

Silurian shallow water buildups are composed of stromatoporoids with auxiliary tabulate corals, bryozoans, *Solenopora*, probable calcified cyanobacteria (*Hedstroemia*, *Wetheredella*(?) and *Rothpletzella*), lithistid sponges and cavity dwelling *Renalcis*. Many deeper water mounds display abundant stromatactis (Texoris and Carozzi, 1964; McGovney, 1988 & Pratt, 1995). Upper Silurian (Ludlovian) buildups from Gaspé (Quebec, Canada) are stromatactis rich, with siliceous sponge spicules, crinoid ossicles, favostid corals, stromatoporoids, dasycladacean green algae (*Rhabdoporella*), brachiopods, ostracods and fenestrate bryozoans. *Girvanella* can be observed in stromatactis (Borque and Gignac, 1983; Bourque *et al.* 1986; Bourque and Aymot, 1988 & Pratt, 1995). Shallow and deep water mounds from Alaska were found to contain calcareous algae, cyanobacteria and microproblematica (Soja and Riding, 1993). Mound associates described were: *Solenopora* association – *Solenopora*, *S. filiformis*, *S. gotlandica*, *Rothpletzella*; *Renalcis* association – *Renalcis*, *Rothpletzella*, stromatoporoids, halystids, solenopores and brachiopods; *Girvanella*-*Tuxekanella* association – *Girvanella*, *Tuxekanella*, *Rothpletzella*, *Headstromia*, *Wetherdella*, stromatoporoids, tabulate and rugose corals, *Atrypa* brachiopods, gastropods and amphipods; *Epiphyton*-*Sphaerina* association – *Epiphyton*, *Sphaerina* small *Hecetaphyton*, aphrosalpingoids and poorly laminated stromatolites.

Devonian

Devonian shallow water mounds are associated with *Renalcis*, *Rothpletzella* and *Girvanella*. Associated biota is typically diverse, including brachiopods, crinoids, trilobites, gastropods and ostracods. Ramp buildups contain the calcimicrobes *Renalcis*, *Rothpletzella*, *Girvanella* and *Wetheredella*. Associated biota included tabulate and rugose corals, fenestrate bryozoans, gastropods, brachiopods, crinoids, echinoids, ostracodes, trilobites, foraminifers (*Sorosphaera*), dacryoconarids, conodonts, tentaculitoids, bivalves and rare shark teeth (Kaufmann, 1998a, 1998b & Pratt, 1995). Deep water buildups were much the same as their ramp counter parts, stromatactis was common throughout

Devonian examples (Pratt, 1995).

The growth of the Moroccan ‘kess-kess’ mounds also occurred within the Devonian, the ecology of these mounds consists of auloporids, thamnoporids, favostids and accessory fauna of crinoids, trilobites, tentaculids, goniatites, nautiloids, conodonts, rare placoderms and brachiopods. No evidence was found for microbes or sponges (Belka, 1998 & Mounji *et al.*, 1998).

A series of mass extinction events towards the end of the Devonian led to the loss of skeletal reef-building organisms from the Upper Devonian and lower Carboniferous marine ecosystems, mud mounds are, however, abundant at this time (Pickard, 1996).

Carboniferous

Lower Carboniferous (Mississippian) shallow/ramp mounds are the most abundant known mound, most are of the characteristic ‘Waulsortian’ type. Bryozoans, encrusting foraminifera (including *Aphralysia*), rugose and tabulate corals, thromboids, stromatoids, *Girvanella*, *Solenpora*, *Shamovella* (often called *Tubiphytes* – see chapter 6. *Palaeontology*), *Renacelis*, siliceous sponges, bivalves, gastropods, nautiloids, moravimminids (calcareous green algae?), calcispheres, aoujgaliids (calcareous red algae?), echinoids and trilobites are associated with Mississippian Waulsortian type mounds. Deep shelf mounds are associated with fenestrate bryozoans, brachiopods, sponges, corals, trilobites, ostracods, gastropods and dasycladalean algae. Stromatactis is common throughout Mississippian mounds (Pratt, 1995; Dehantschutter and Lees 1996 & Pickard, 1996). Possible fish remains were recorded by Brown and Dodd (1990).

Upper Carboniferous (Pennsylvanian) shallow water mounds from Alabama are associated with bryozoans, echinoderms, gastropods, brachiopods, bivalves, ostracods, foraminifers, rugose corals and rare trilobites (Kopaska-Merkel and Haywick, 2001b). Deeper marine (below wave base) mounds from the San Emiliano Formation (north Spain) as described by Samankassou (2001) are dominated by the algae *Donezella* (other algae and related problematica present are: *Rectangulina*, *Anthracoporella*, *Archaeolithophyllum*, *Epimastopora*, *Komia*, *Eflugelia* (= *Fourstonella*) and *Shamovella*), agglutinated worm tubes and calcisponges, with accessory fossils of foraminifers (*Climmacamina* and *Paleotextularia*). Mounds dominated by ‘phylloid’ algae have been described from Kansas (Samankassou and West, 2002).

Permian

Permian mounds were stromatactis bearing mounds dominated by fenestrate bryozoans and lithistid sponges. Associated accessory fossils include crinoids, *Shamovella*, gastropods, ammonites, brachiopods, ostracods, trilobites and foraminifers (Pratt, 1995 & Blendinger *et al.*, 1997). Fenestrate bryozoan and crinoidal facies disappear by the end of the Permian. Late Permian – early Triassic mud mounds produce a characteristic framework similar to those of earlier times. This framework is composed mostly of thromboids or microbial crusts, newly evolved calcisponges and sessile foraminifera coated by microbial encrustations (Pratt, 1995).

Triassic

Early Triassic mud mounds are microbial in nature (Pruss and Bottjer, 2004). Middle Triassic biostromes are dominated by brachiopods and crinoids. Gastropods along with rare bryozoans and possible corals also occupied the biostromes (Zonneveld, 2001). Mud mounds from the middle Triassic contain very few skeletal organisms, among those that do occur

	are <i>Shamovella</i> , skeletal cyanobacteria and sphinctozoan sponges (Russo <i>et al.</i> , 1997).
Jurassic	Early Jurassic mound are associated with <i>Tubiphytes</i> , thrombolites and algae with auxiliary sponges, annelids, bryozoans, brachiopods, bivalves and corals. Foraminifers, ostracods, gastropods and echinoderms are rarer associated biotas (Pratt, 1995 & Chafiki <i>et al.</i> , 2004). Sponges are the dominant mound building biota in Moroccan Jurassic mounds (Neuweiler, 2001). Stromatactis is observed in mounds from the Lower and Upper series of the system, these are the youngest of known true stromatactis mounds, free of supporting sponges, <i>Shamovella</i> or corals, these mounds are not widespread and are far less common than sponge mud mounds (Aubrecht <i>et al.</i> , 2002; Aubrecht <i>et al.</i> ; 2009). Upper Jurassic siliceous sponge – microbial mounds are abundant in what was the Neo-Tethys (e.g. southern Germany and the Alps). Two major types of mounds formed in these times, coral-sponge-microbial mounds which represented a transition from shallow water coral facies to a deep water siliceous sponge facies. Microbial elements associated included <i>Shamovella</i> . Microbial mounds are the other major mound variety; these were relatively common within the late Jurassic. Metazoan remains consist of rare siliceous sponges. Microencrusters comprise of low diversity <i>Terebella-Shamovella</i> (Schmid <i>et al.</i> , 2001).
Cretaceous	Cretaceous mounds (that are not associated with methane seeping) are dominated by cyanobacteria, microbes and siliceous sponges. Accessory biota consisted of serpulid worms, bryozoans, foraminifers, pelecypods, ostracods, echinoderms and possible brachiopods. Some examples contained red algae. Stromatactis was present (Murillo- Muñetón and Dorobek, 2003). Seep related mounds are common throughout the Cretaceous, dominantly located in the southwestern U.S.A. (Birgel <i>et al.</i> , 2006; Kaufmann <i>et al.</i> , 1996 & Shapiro and Fricke, 2002). Cold seep related mounds are reported from the Canadian Arctic (Beauchamp and Savard, 1992). Tepee Buttes (mounds associated with methane vents) are associated with diverse molluscs, foraminifers and radiolarian species (Kaufmann <i>et al.</i> , 1996). Cool seep related mounds from the Canadian Arctic have been interpreted as chemosynthetic carbonate mounds, seep biota consists of abundant bivalves and serpulid worm tubes with accessory ammonites, gastropods, foraminifers and fish teeth (Beauchamp and Savard, 1992). Biota from these seep mounds is higher in abundance and diversity than the surrounding area, although this evidence alone is not sufficient enough to designate seeping as the origin (Beauchamp and Savard, 1992 & Kaufmann <i>et al.</i> , 1996).
Cenozoic	Many Cenozoic mounds have recently been found due to increased interest in possible links with hydrocarbons and the ability to collect seismics on such structures. Biotic studies upon recent mounds are lacking. Corals, sponges, tube worms and brachiopods have, however, been viewed on the surface of mounds (de Haas <i>et al.</i> , 2009; Foubert <i>et al.</i> , 2008; Kenyon <i>et al.</i> , 2003; Roberts <i>et al.</i> , 2008; van Weering <i>et al.</i> , 2003 & Wienberg <i>et al.</i> , 2008).

TABLE 2.2 - A brief overview of ecological associations and palaeoecological evolution within the context of mud-mound related biota

2.5 General Initiation Mechanisms and Growth

The initiation and nucleation of mud mounds generally remains unclear. The presence or absence of mud mounds from areas of the globe (both today and in the past) suggests that formation is related to a tangible triggering process. Formation mechanisms for various mounds have been suggested, but as of yet, an all-encompassing generic model for the initiation of mud mounds has not been created. Because the term “carbonate mud mound” is used to describe carbonate buildups of various compositions and origins, it is only logical that mechanisms of initiation, growth and demise are also varied. Generic modes of formation such as the local accumulation of carbonates due to the role of various bafflers, binders and framework builders (as introduced above in 2.1 and 2.2) are commonly cited as formation mechanisms for carbonate mud mounds (James and Bourque, 1992). Several specific mechanisms and controls on nucleation are also currently advocated include local topography and bathymetry (Stenzel and James, 1995), halokenesis, argilokinesis, faults, hydrothermal vents (Monty, 1995; Beachamp, 1992 & Belka, 1998) hydrocarbon seeps/accumulations (Peterson, 1966a, 1966b, 1966c; Murillo-Muñetón and Dorobek, 2003; Sager, *et al.*, 2003 & Naeth *et al.*, 2007) and bacterial methanogenesis in organic matter (Wu and Chafetz, 2002). Due to the episodic nature of mound formation (i.e. peaks in abundance for the early Cambrian, late Devonian and early Carboniferous) several authors have proposed links between oscillating oceanic conditions and mound formation (Wood, 2001). Global sea-level change, including large transgressive events which resulted in the stratification of basins creating zones which were conducive to mound formation was proposed by Brunton and Dixon (1994). Kirkby (1997) suggested a link between Waulsortian-type mounds and the formation of abundant ooid production, mounds are proposed to form in constrained periods where considerable amounts of autochthonous micrite was produced. Webb (1996) has suggested that mound formation is possibly driven by changes in the sea water saturation state of partial $p\text{CO}_2$ and Ca/Mg ratios with global temperature distribution as a possible control. Below, several mechanisms that are site specific are discussed. Individual mounds/complexes have been linked to

local environmental changes, e.g. Harper *et al.* (2014) report Ordovician mounds from Greenland which formed as the result of deterioration of local environmental conditions.

2.5.1 Hydrothermal Venting and Hydrocarbon Seepage

Venting is a popular theory for mound initiation and growth, both seeps and vents are known to be common at continental margins (Campbell, 2006) as are mud-mounds from the Phanerozoic, seeps commonly occur in siliciclastic environments (Rollet *et al.*, 2006). Carbonate produced at hydrocarbon seeps are relatively depleted in ^{13}C , and generally occur where faulting, diapirism, sediment compaction, or underwater landslides tap organic-rich pore waters (Campbell, 2006). It is therefore sensible to assume there may be a link between seeps and vents and mud-mound initiation/growth (Hovland, 1990).

Chemosynthetic communities have been observed to thrive around hydrothermal vents and cold hydrocarbon seeps and are thought to depend or greatly benefit from the substances being vented or seeping (Hovland, 1990; Campbell, 2006 & Hovland and Thomsen, 1989). Biota from such communities are generally more diverse, larger and of higher numbers than the biota of surrounding areas, a trait often observed in ancient mud-mounds (Pratt, 1995 & Kaufmann *et al.*, 1996). This evidence alone is not sufficient enough to designate seeping as the origin (Beauchamp and Savard, 1992 & Kauffman *et al.*, 1996).

Chemosynthetic based life is dependent upon CH_4 and H_2S , which is usually found as a result of seeping oil and gas or as the result of the disassociation of gas hydrates. Biota associated with vents have also been found in association with dead whale falls, sunken wood, in reduced sediments and in the rotting organic cargo of a shipwreck (Campbell, 2006). Chemosynthesis (chemoautotrophic symbiosis) is likely to be an ancient adaptation (Fortey, 2000). Seeping oil and gas are usually associated with an active petroleum system and has been reported from around the world at varying depths (10 to 3000 m). Shallow seepage can be related to a variety of origins – groundwater, biogenic or thermogenic and can range from micro to macro-seepage (Rollet *et al.*, 2006). Methane seeps are often associated with bacterial mats (Hovland, 2007). The formation of

the early Devonian ‘Kess-Kess’ carbonate mud mounds of the Anti-Atlas mountains (Morocco) have been linked to submarine hydrothermal venting (Belka, 1998). These mounds were found to be situated upon a series of radial faults which acted as a conduit for hydrothermal fluid flow which was driven by the ballooning of an underlying intrusive body (Belka, 1998).

Gas hydrates are crystalline compounds of gases and water that are fairly stable under high pressure and low temperature and are typical of deep water sediments worldwide (Egorov *et al.*, 1999). Gas hydrates main component is methane. A hydrate typically dissociates over several months, however most observed hydrates are associated with active fluid discharge sites suggesting that hydrates can be re-supplied (Egorov *et al.*, 1999). The Håkon Mosby mud volcano and related carbonate mounds (SW Barents Sea) are modern day examples of structures associated with the submarine release of methane - as a result of venting and hydrate disassociation (Prasolov *et al.*, 1999; Beyer, 2006 & Kaul *et al.*, 2006). Similarly, Sager *et al.* (2003) and MacDonald *et al.* (2003) report hydrocarbon seep related, chemosynthetic biota within a mounded bathymetry from the Gulf of Mexico.

2.5.2 Topographic and Bathymetric Controls

Topographic and bathymetric theories of initiation and growth are based upon areas of increased photic energy (Fig. 2.6), those with decreased photic energy or areas protected against currents. The large majority of mounds, including numerous Waulsortian and Waulsortian-like mounds, are reported to be deep-sea mounds (Monty, 1995). Examples of mounds interpreted to have formed within the photic zone include the mounds from a Mid Ordovician foreland basin (Stenzel and James, 1995), the Devonian Rocky Camp mound of Tosolini *et al.* (2012) and Holocene aged shallow water mounds of Mazzullo *et al.* (2003). Samankassou *et al.* (2013) concluded that Pennsylvanian mounds from the Puebla De Lillo area of the Cantabrian Mountains nucleated upon palaeohighs. Local bathymetric highs have also been championed as controls for the lower Carboniferous mounds of the Midland Valley of Scotland (Pickard, 1992). These mounds formed

on a topographic high (related to localised, reduced subsidence) due to reduced clastic influence and clear waters (Pickard, 1992).

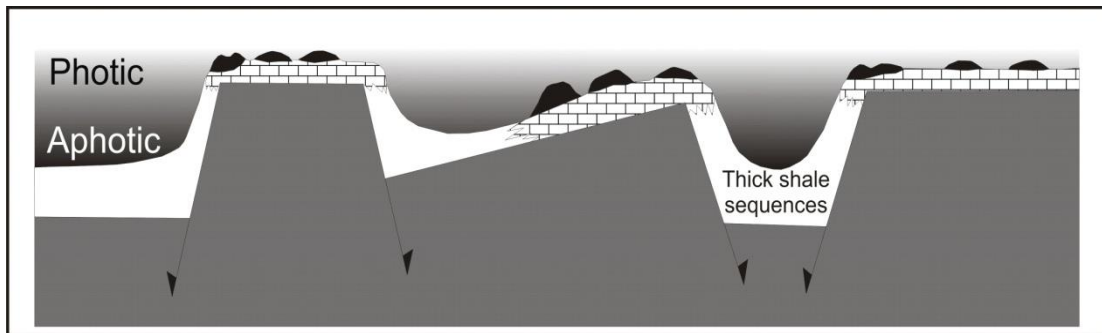


FIGURE - 2.6 Example of mounds controlled by highs, here the mounds are restricted to highs within an extensional regime, black lenses represent carbonate mounds. On these topographic highs the mounds may be subject to increased photic levels, lower clastic influence, lower turbidity and clearer waters than surrounding areas. After Pickard (1996).

2.5.3 Shallow Water Atoll Model

The shallow water atoll model has been proposed by Dronov (1993) as an explanation to the formation of Waulsortian-type mounds from southern Tien-Shan. The model is based upon that of a modern atoll, the flanks of this ‘atoll’ are made up of crinoid accumulations which are wave resistant. A lagoon forms inside the crinoid accumulations and is protected from wave action and bottom currents, lime mud accumulates in the protected lagoon especially on the lee-side of the crinoidal accumulations.

2.5.4 Geosphere Biosphere Coupling (humification– biodiagenetic phenomena)

Neuweiler *et al.* (2003) suggest that humification is more important for calcite authogenesis than any site-specific microbialism metabolism (although benthic biomass is required). The work of Neuweiler *et al.* (2000) and Neuweiler *et al.* (2003) indicates that mounds are biodiagenetic phenomena involving invertebrate biomass conversion (i.e. humification), suboxia and a related stage of calcite mineral precipitation (Fig. 2.7). Carbonate precipitation and cementation reflect the chemistry of their precipitating and presently surrounding waters (Harris *et al.*, 1985; Kharaka *et al.*, 1986; Walter, 1986 & Wood, 1986). This hypothesis suggests that mound nucleation,

formation and growth will only occur in environments where abundant humic substances and dissolved organic matter is present.

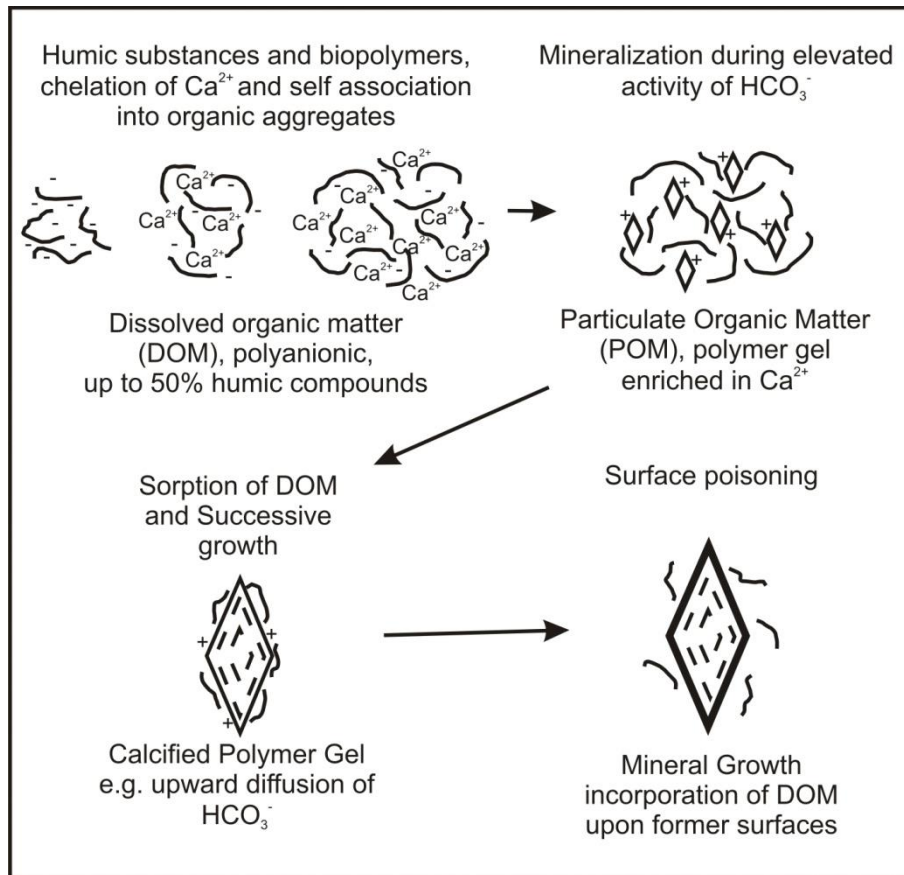


FIGURE - 2.7 Humic substance based model of marine, authigenic calcium-carbonate precipitation and succeeding inhibition of mineral growth. After Neuweiler *et al.* (2000).

2.6 Geological Setting

Geological setting appears to be an important factor in mound formation, a preference for continental/passive margins and foreland basins appears to be present. Geological features associated with mound formations include structurally controlled highs and lows (e.g. horst and graben associations in extensional regimes), faulting (as a conduit for fluid dispersion sites) and sites of depositional centres and fluid pumping.

2.6.1 Structural Controls

Mounds that have been found linked to fluid dispersion sites have their nucleation points controlled by local faulting (Fig. 2.8). At convergent margins the consolidation of the upper plate and dewatering of the subducting plate can produce seep sites as fluids rise. Mud mounds have been found at the Central American forearc controlled by fluid seep (Kutterolf *et al.*, 2008), these mounds have been found to have a ‘lifetime’ reaching into the hundreds of thousands of years.

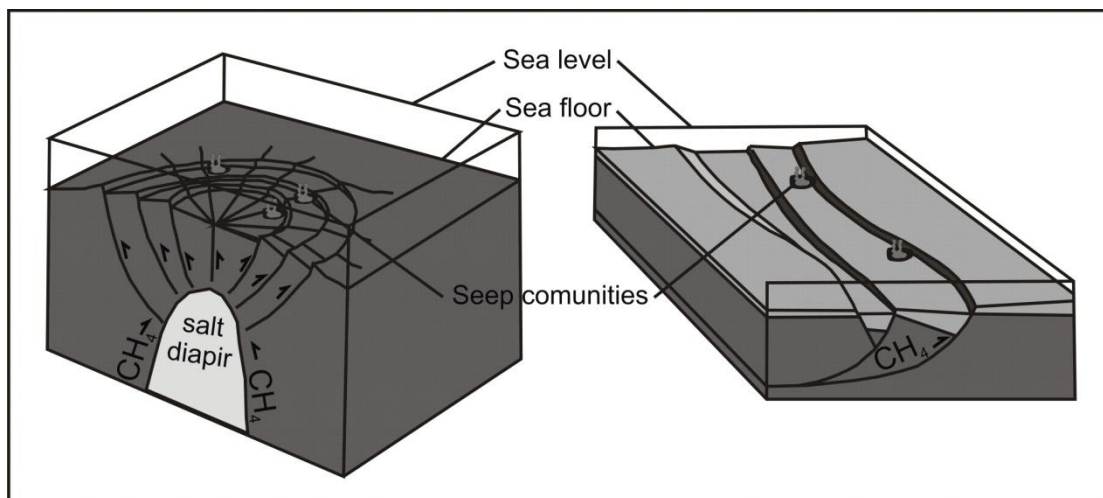


FIGURE - 2.8 Two possible scenarios for mound formation linked to faulting; the left hand diagram shows extensional faulting associated to salt piercing, methane gas seeping along conduits provided by faulting (indicated by arrows). The right hand diagram shows methane seeping along a listric fault forming a half graben. After Beauchamp and Savard (1992).

2.7 Industrial Implications

Carbonate mud mounds along with carbonate deposits in general have become increasingly common exploration and extraction targets for economically viable resources. The contemporary association of mud mounds with hydrocarbons and the advancement of multibeam bathymetry and side scanning sonar imagery and continued use of 2D seismics on shelf areas has led to the increased study of modern mound structures (van Weering *et al.*, 2003 & Foubert *et al.*, 2008). This increased recognition of the industrial (and scientific) potential of mud mounds (along with cold water carbonates) led to the European Union funded Atlantic Coral Ecosystem Study (ACES), Environmental Controls on Mound Formation Along the European Margin

(ECOMOUND) (both 2000 to 2003) and The Internal Mound Factory (GEOMOUND) (2004-2007) research programmes and later the 2005-2009 Hotspot Ecosystem Research on Europe's Deep-Ocean Margins (HERMES) (see Beyer, 2001; van Gaever *et al.*, 2004; Kirikoulakis *et al.*, 2004; Roberts and Freiwald, 2005; Kirikoulakis *et al.*, 2005; Beyer, 2006; Beyer *et al.*, 2007 & Kirikoulakis *et al.*, 2007).

2.7.1 Hydrocarbons

In recent years carbonate mud mounds have been linked to the migration and accumulation of hydrocarbons. Pennsylvanian age oil and gas production from Arizona, New Mexico, Utah and Colorado (the Paradox Basin) is from mounds which have provided a reservoir and trap (Peterson, 1966a, 1966b, 1966c & Chidsey *et al.*, 1996). Mounds found throughout the central Baltic Sea (outcropping on the isle of Gotland) have been characterised and were successfully drilled (Sivhed *et al.*, 2004). Buried carbonates are favoured hydrocarbon prospecting sites due mainly to their high porosity and potential for containing large quantities of petroleum (Hovland, 1990). Reservoir scale mounds have been studied to establish reservoir characteristics (Doherty *et al.*, 2002 & Li *et al.*, 2013), though mounds have been found to form difficult hydrocarbon systems to exploit (Doherty *et al.*, 2002). Buried mounds have been discovered from the analysis of their geochemical and geophysical signals at surface levels. In Texas (Stephens county) a C₂ – C₄ halo was discovered from soil samples, drilling the centre of this halo encountered a Mississippian age mud mound (80m high) with a rich supply of oil (Hovland, 1990). Garland *et al.* (2012) report that advances in geophysical equipment and techniques has resulted in the increased recognition of carbonate mounds as exploration targets.

2.7.2 Metallogenic Mineral Deposits

Metallogenic deposits are often found in carbonate bodies, Waulsortian mud mounds in Ireland have been found to contain amounts of zinc ore which are economically viable to mine (De Vos *et al.*, 2005).

3. Methods and Materials

This study has taken a multidisciplinary approach, in an attempt to reach solutions unattainable by a single a discipline alone. The main methodologies implemented here are: carbonate and clastic sedimentology, palaeontology, chemostratigraphical and geochemical analysis and database generation.

3.1 Field methods

To establish both the spatial distribution and internal composition of the carbonate mud mounds within the study area, samples were obtained from both lateral sections and from well-exposed mounds. 254, fist sized samples were collected from a total of 59 locations. The majority of samples (227) came from the San Emiliano Valley, the others (27) samples came from the Bernesga Valley toward the east of San Emiliano. To investigate the spatial distribution of mounds, samples were obtained from the laterally extensive, uppermost carbonate unit within the La Majúa Member of the San Emiliano Formation (see Fig. 1.1). For the purpose of detailed microfacies investigations, a well-exposed mound, ‘typical’ of the San Emiliano Valley mounds, was sampled to include extensive coverage across basal, mound and capping facies (within this study the mound is referred to as the Candemuela Mound). Other mounds were sampled in a similar fashion, where possible, but it was generally found that mounds were not as well exposed as the Candemuela Mound. In some cases, very few samples could be obtained due to local fauna and flora (e.g. the Pinos Pylon Mound), the mounds from the Bernesga Valley have been previously studied (e.g. Hensen *et al.*, 1995 & Samankassou, 2001) so a bias toward the San Emiliano Valley mounds was implemented. The mounds of the Bernesga Valley were sampled to provide a direct comparison to those of the San Emiliano Valley and the data presented in previous studies. Carbonate units which are part of the San Emiliano Formation but are barren of carbonate mud mounds were also sampled to allow for correlations and comparisons. Three logs of cyclic clastic-carbonate sequences from the Sam Emiliano Formation were measured, recording approximately 100 m of sediments. All samples were clearly labelled and described in the field,

photographs were taken of outcrops and full notes, sketches and measurements were taken at each location. A chemostratigraphic log analysis was obtained in the field consisting of 600 data points at 10 cm intervals through a sedimentary succession of mixed clastics and carbonates (see section 3.6 *X-Ray Fluorescence* below).

3.2 Sample Preparation

To complete a microfacies analysis, it was required to make a thin-section (occasionally more than one) for each sample. Thin sections were mounted on 3.8 by 7.6 cm slides (where possible) and were ground to a thickness of around 50 µm. In total 201 thin sections were produced from 254 samples. The majority of slides were half-stained with an Alizarin Red Solution and Potassium Ferricyanide Staining Solution. When stained, ferroan calcites and dolomite react with the solution and show a characteristic blue colour, whilst non-ferroan calcites show a red colour.

For analysis under a Scanning Electron Microscope, 31 polished blocks were made from selected samples. These were chosen as either a representative sample of a facies identified during microfacies analysis or because they contained a high number of well-preserved biota. The blocks were cut perpendicular to the bedding and so that they fit onto a 2.5 cm SEM stub. Surfaces were polished and subsequently scanned at a high resolution to provide a “map” of the stub when under the SEM. Once polished and documented (with areas of interest marked on the “maps”) the surface was etched. Etching was conducted in a fashion similar to that used by Munnecke *et al.* (2000) where the stubs were cleaned in distilled water and then etched in 0.1M hydrochloric acid for 10 seconds +/- 3 seconds. 8 of these samples were then mounted upon a stub with a carbon tab and sputter coated with gold. Later, samples which were made were not sputter coated and were simply mounted onto stubs with a carbon tab (see 3.4 *Scanning Electron Microscopy and Energy Dispersive X-ray Spectrometer* below). Several loose specimens were obtained from a decalcified bed. These were simply picked from the crumbled samples and mounted on a stub with a carbon tab.

During fieldwork several well-preserved fossils were found (including algae, brachiopods and corals) and collected from several marl beds. These samples were taken to the laboratory with the aim of removing all clastic material from them and leaving the calcareous specimens clean. Once clean, the specimens were observed below a low power microscope (see below) and in some cases with an SEM. The samples were first washed in distilled, slightly warmed water to remove any attached soil or dirt. To remove any clastic material still attached to the specimens, potassium hydroxide (KOH) pellets were placed upon them with a little water and left for over 24 hours. KOH creates an exothermic reaction with water resulting in soluble potassium silicates. Any residue was washed off in warm water with the aid of a fine bristled brush. Once clean of all clastic material two of the specimens (a pair of excellently preserved *Archaeolithophyllum* thalli with encrusting aulopodid corals) were used to make a silicon mould and a cast before the specimen was thin sectioned and cut for SEM investigation. A silicon rubber kit was used to create the mould and EasyFlow™ series polyurethane liquid plastic was used to make casts. The results were a set of very high quality casts and moulds which showed excellent representation of the original specimens.

For X-Ray Fluorescence (XRF) data to be obtained in the laboratory pressed powdered tablets were made for analysis, these tablets are made from a proportion (8 g, see below) taken from approximately 200 g of a whole rock sample. Rock tablets were made in several steps. Firstly, rock samples which were representative of several mounds/locations were chosen, washed and dried. Weathered material was removed using a rock splitter. The resulting fresh samples were crushed using a jaw crusher to create a pea-sized gravel. Around 40 g of this gravel was transferred to an Agate ring mill and set upon a shaking platform for 3 minutes. After each sample went through this process, the resulting powder was bagged and labelled to be pressed at a later time and all the machines were thoroughly cleaned before the next cycle began. Pressed powder tablets were made by mixing powdered rock with a polyvinylpyrrolidone – methylcellulose binder (PVP solution) and compressing into tablets, following the method of Watson (1996). Firstly, an agate pestle and mortar was cleaned with an alcohol-soaked tissue and approximately 8 g of rock

powder was weighed and transferred to the mortar. Up to 1 ml of PVP solution was added and mixed in using the pestle. The platens and die were cleaned with an alcohol-soaked tissue and the powder transferred to the die and pressed to 10 tons for 20 seconds. The pressure was released and the pellet removed by inverting the die, removing the base-plate, inserting the aluminium spacer cap and pushing out the pellet using the press. At this point, if the surface of the disc was cracked, the disc was ground to a powder and returned to the mortar, adding a few more drops of PVP solution. The pellets were placed on a wire support and dried in an oven at 110 °C overnight. Pellets were stored in a labelled polythene bag and kept in a cool dry place.

3.3 Thin Section Microscopy

All 201 thin sections were first investigated with a Brunel Microscopes 'Z' series Trinocular Stereomicroscope. Thin sections were subsequently investigated with a Prior Binocular PX032POL. Measurements were taken using a graticule with a precision of $\pm 2.5 \mu\text{m}$. Photomicrographs were taken on a Canon Powershot G5 attached to a Zeiss Max ERB microscope.

A microfacies analysis was conducted on 177 of the thin sections. Methods used generally followed the procedures set out by Flügel (2004) and terminology set out therein was used, plus that coined by Folk (1959, 1965 and 1974), Dunham (1962) and Tucker and Wright (1990). Specific terminology referring to different taxa introduced by various authors has also been used. A detailed study on the microfacies and depositional environments was undertaken. Standard Microfacies Types (SMF Types) were used to group facies recognised in thin section into groups with similar compositional aspects which reflect depositional environmental controls. These include texture, sedimentological features and biological assemblages and preservation. Standard Facies Types were first introduced by Flügel (1972) and were subsequently defined and expanded upon by Wilson (1975) who recognised 24 SMF types which were used to differentiate different facies belts of an idealized rimmed platform. The rimmed platform model was used here as it is a good fit to the geometry of a foreland basin. The remaining thin sections (24) were used in the investigation of various palaeontological specimens and sedimentological features.

3.4 Scanning Electron Microscopy and Energy Dispersive X-ray Spectrometry

Prepared stubs were investigated using two separate Scanning Electron Microscopes. The 8 gold sputtered blocks were first investigated using a Hitachi S45000 FE-SEM at the Electron Microscope Unit of Keele University, UK. This SEM was used to obtain the first ultrafacies images and to investigate the wall structure of several organisms, namely of the family Tuberitinidae. In August 2012 a Hitachi Tabletop TM3000, with attached Bruker Energy Dispersive X-ray Spectrometer (Quantax 70) (EDX) analytical system, was installed within the William Smith Building, Keele University, UK. The TM3000 was subsequently used for all SEM investigation as it provided high-magnification and high-resolution images for samples which required little preparation (i.e. stubs only require polishing and etching to be viewed under the SEM, no coating is required).

The SEM was mainly required to create topographic, three-dimensional images to investigate the crystal textures within both organisms (i.e. wall structure) and within cements. The procedures and terminology set out by Krinsley *et al.* (1998) and Reed (2005), and more specifically those of Lasemi and Sandberg, (1984) Munnecke *et al.* (1997) and Flügel (2004) are used here (see 5. *Ultrafacies Analysis* below for more detail). The TM3000 uses mainly backscatter electrons to image specimens, rather than secondary electrons. This is because secondary electron detection requires a better vacuum. Hitachi have introduced a “Charge-up reduction mode” which reduces the amount of charging in a “lesser” vacuum by tolerating contaminants to a higher degree than other, larger SEMs. The tilting of samples is not required as the SEM makes use of a 4-quadrant backscatter detector - these detectors can be switched on and off to create shadow effects. Backscatter electrons originate from the electron beam and are reflected when they interact with the specimen atoms. The use of the TM3000 meant preparation and usage time were reduced, increasing data output. To investigate the elemental composition of samples the Bruker EDX analytical system was used (the EDX system operates in a fashion described below for XRF analysis, see 3.6 *X-Ray Fluorescence*). The EDX is capable of light element detection from Boron upwards and can perform linescans, mapping and multiple point analysis. The EDX was used on

the samples for no shorter period than 3 minutes, the optimal time being 5 to 6 minutes. Using the Bruker Quantax 70 software package, the characteristic lines superimposed upon the continuum (X-ray spectrum) produced by incident electrons could be investigated, allowing the presence of individual elements to be scrutinised. Maps were made of most specimens whilst linescans were particularly useful when looking at the wall structure of several palaeontological specimens.

Minor problems were encountered with specimen charging whilst investigating un-coated samples with the TM3000, this tended to occur when the machine had been used for prolonged periods of time. This could be negated by using the “Charge-up reduction” mode and by ensuring the samples were completely dust free, and by taking adequate breaks from using the machine. Occasionally, the consequences of the “edge-effect” (e.g. Reed, 2005) could be observed whilst element mapping. This results in the edges (often raised edges) of crystals and grains appearing brighter (or more enriched with a certain element). The samples within the TM3000 cannot be tilted (as there is no need to tilt samples to create 3D images) so this phenomenon is difficult to reduce whilst using a TM3000. However, being aware of the “edge-effect” means that it can be explained logically when it occurs.

3.4.1 Framboidal Pyrite

The size distribution of pyrite framboids are a useful tool in the analysis of ancient redox levels (Wignall and Newton, 1998). Polished blocks were analysed under an SEM (see above) and pyrite framboids were observed. Framboids were easily identified by their characteristic morphology and brightness in SEM images. Images of framboids were taken where they were found and measured on screen. Wignall *et al.* (2005) report that this method of measurement underestimates the true diameter of the framboids (as not all cuts will be through the median diameter) but this underestimation does not exceed 10% (Wilkin *et al.*, 1996). Pyrite framboids form in dysoxic conditions near to the redox boundary (Wignall *et al.*, 2005). When the redox boundary is located close to the sediment surface, framboids form within the sediments with a size range of between 4 and 50 μm (Wilkin *et al.*, 1996 & Wignall *et al.*, 2005). Where oxygen-restriction increases the

redox boundary moves up into the water column, resulting in framboids forming within the water column (Wignall *et al.*, 2005). The framboids which form in the anoxic water column have a very short period of formation time as they soon drop out of the water column, as a result these framboids are small (<6 µm), have a narrow range of size distribution and are found in abundance (Wilkin *et al.*, 1997). Bond and Wignall (2010) suggest that weakly oxygenated bottom waters are characterised by common framboids that are slightly larger than those formed in anoxic conditions (6 to 10 µm). In environments with partial oxygen restriction, framboids are rarely found and are relatively larger (>10 µm). This method has been used successfully to predict levels of oxygen-deficiency within ancient silts (Wilkin *et al.*, 1996, 1997, Wignall and Newton, 1998, Wignall *et al.*, 2005 & Bond and Wignall, 2010) and Liao *et al.* (2010) used this method to assess palaeo-redox conditions within shallow water microbialites.

3.5 Isotope analysis

Carbon and Oxygen isotope analysis was carried out on 6 carbonate (whole rock calcite/micrite) samples at the NERC Isotope Geosciences Laboratory (NIGL), Nottingham, UK. A VG Optima Mass Spectrometer with manifold was used. Isotopes are variants of a particular element (e.g. isotope data obtained within this study - $^{13}\text{C}/^{12}\text{C}$ and $^{18}\text{O}/^{16}\text{O}$). Isotopes have the same number of protons and electrons as their equivalent chemical element but have a different number of neutrons - $^{13}\text{C}/^{12}\text{C}$ both have 6 protons, however, ^{13}C has 7 neutrons whilst ^{12}C has 6. These disparities result in a difference in the mass and energy of each isotope. Due to these physical differences isotopes of the same element will react differently to certain events (light isotopes are more reactive than heavier isotopes). This results in the ratios of isotopes shifting as a result of kinetic properties, the ratios can then be interpreted to divulge information (in the case of carbonate samples) about depositional proxies such as temperature, salinity and the presence of hydrocarbons. (Hoefs, 1997, Allègre, 2008 & Valley and Cole, 2001). Data obtained was calibrated against the Pee Dee Belemnite (PDB). In this study carbon isotopes were used to investigate if a relationship between fluid flows (e.g. hydrocarbon seepage) and mound nucleation

and growth existed for the studied mounds. Carbonates which form during hydrocarbon seepage have characteristically low $\delta^{13}\text{C}$ values as they inherit the signature from their carbon source (Peckmann and Thiel, 2004). It can therefore, be assumed, that if the mud mounds of the San Emiliano Formation have low $\delta^{13}\text{C}$ values, they were formed around a hydrocarbon seep.

3.6 X-Ray Fluorescence

X-ray Fluorescence (XRF) techniques were utilised to investigate the bulk composition of the lithologies studied. Analysis was carried out using a NITON XL3t 900Analyzer with GOLDD Technology, Keele University, UK. This handheld XRF was used both as a static device in the laboratory and as a portable device in the field to collect a chemostratigraphic log.

When bombarded with gamma rays (high energy X-rays) a material will emit secondary (or fluorescent) X-rays. Gamma rays are energetic enough to expel or “push” electrons from their tightly held orbit around an atom, causing their electronic structure to become unstable. Due to this instability an electron from a higher orbit (or shell) will “jump” into the orbit (or shell) of the electron which was expelled. This “jump” causes a release of energy which corresponds directly with the distance between the two orbits involved. The energy released is therefore specific to different elements and the subsequent energy levels detected fit into specific “lines” superimposed upon the continuum or X-ray spectrum (Jenkins and De Vries, 1969 & Beckhoff *et al.*, 2006).

In the laboratory, prepared tablets are placed on the XRF apparatus and analysed for three minutes. The resulting data was transferred to a spreadsheet where it was analysed. The XRF used is a portable device and therefore applicable for use in the field. A chemostratigraphic profile was taken along a road section with a point taken every 10 cm. The working surface had to be flat and as fresh as possible.

XRF data are used to investigate the elemental composition of the selected lithologies in order to assess cyclicity within the strata and to show any enrichment for elements which may be related to hydrothermal venting (e.g. Belka, 1998). The data may also suggest a provenance for the

sediments and can primarily be used to investigate whether cyclicity can be recognised within the sediments.

The XRF collected data utilised within this study consists of a chemostratigraphic log taken in the field. The resulting data is subject to an internal machine calibration and is not calibrated against international standards. The data is presented as parts per million (ppm) for trace elements and as weight percentage (wt%) for major elements. The conversion of counts per second to ppm and wt% is done internally by the XRF, and via a macro within Excel respectively. The use of these data is justified as it was collected in the field, where calibration material is not available. The data is used to identify general trends and patterns (e.g. Friedrich *et al.*, 2011), absolute values are not of interest or use within the remit of this study. As absolute values are not utilised a moving average with a period of 10 was formatted for those elements which were used to infer trends or patterns.

3.6.1 Continuous wavelet transform

Continuous Wavelet (Morlet) Transformation (CWT) analysis was undertaken using the PAST software (Hammer *et al.*, 2001). The CWT is an analysis method where data can be inspected at a variety of different scales, it is best suited to data with evenly spaced points (Hammer *et al.*, 2005).

This method was used in order to investigate whether any periodicities were detectable within the chemostratigraphic log obtained. A Wavelet (Morelet) Transform was used for this time-series analysis in order to inspect any cyclicity detected at different wavelengths. Unlike a Fourier Transform, the Wavelet Transform highlights any non-stationary signals (i.e. changes in the frequency of a signal through time). The data used for this analysis were chosen from the XRF data obtained as a chemostratigraphic log. The elements used for this analysis were Si, K, Ca, Ti and Zr (common rock forming elements that were within detection limit). This method has been used by others as a tool for illustrating

various cycles, including: diversity curves in planktonic foraminifera (Prokoph *et al.*, 2000) and for highlighting orbital cyclostratigraphy (De Vleeschouwer *et al.*, 2013).

3.7 Database Generation

A database which incorporates the locations, age and geological setting (plus information on the source of the material, i.e., journal article title and author etc.) of known carbonate mud mounds and associated buildups was created, using the PostgreSQL software. This database was used to make palaeogeographic reconstructions for known mounds temporally and spatially. These reconstructions were created to investigate any relationships between mound formation and their abundance through time and space.

4. Microfacies Analysis

In this section the findings from a microfacies analysis of thin sections made from samples taken during field work are set out, as well as an interpretation of the finding at the end of each segment. A microfacies analysis is regarded as “...the total of all sedimentological and palaeontological data which can be described and classified from thin sections...” (Flügel, 2004 pg. 1). A microfacies analysis of carbonates from the San Emiliano district focusses on several areas. The “Candemuela Mound” is the subject of a high resolution analysis and is used as a case study for the mounds found within the carbonate units of San Emiliano Formation at the type locality. A traverse across one of these carbonate units (“Unit 8”) has been analysed to investigate the lateral variation across the carbonate deposit. Microfacies types established from the Candemuela Mound have been used as a basis for this lateral traverse. Several other carbonate mud mounds from within the San Emiliano Formation (local to the type locality) were analysed and compared to the Candemuela Mound, these are: the Pinos Pylon Mound and the Pinos East Mound. Several mounds from south of San Emiliano and the Bernesga Valley (the Lois-Cigüera Formation of the Cármenes syncline), these being: the Sena de Luna Mound, the Cármenes South Mound, the San Martín Mound and the mounds described by Samankassou (2001) from the Cármenes Syncline. Whilst the formation and nucleation of mud mounds is of most interest in this project it is also important to investigate the carbonate units which are devoid of build-ups, the ‘phylloid’ algal dominated “Pinos Hairpin” carbonates have been analysed to provide data for these units. The results from each location were then compared to show if any trigger or nucleation events for mound nucleation and growth can be recognised. In addition, a point count of several samples was undertaken. 513 points per slide were recorded (see Appendix 1. *Point Count*). All thin section were cut perpendicular to bedding where possible and were cut 50-60 µm thick. Most slides were half stained (see chapter 3. *Methods and Materials*). Within this chapter, microfacies analysis are reported first for the localities from the San Emiliano Valley (the Candemuela Section, Unit 8, Pinos Hairpin Limestone, Pinos Pylon Mound and the Pinos East Mound) followed by those localities sampled from south of San

Emiliano (Sena de Luna Mound) and from the Bernesga Valley (Cármenes South Mound and the San Martín Mound). For more information on individual taxa described see chapter 6. *Palaeontology* below. UTM coordinates are provided for each location. Sample numbers are given for corresponding photomicrographs in the description.

Abbreviations used in text: CAN (Candemuela Mound), PHL (Pinos Hairpin Limestone), PPM (Pinos Pylon Mound), PEM (Pinos East Mound), SDL (Sena de Luna Mound), CSM (Cármenes South Mound), SMM (San Martín Mound).

4.1 Candemuela Mound

29T 744467.52 4763114.34

The Candemuela road cutting section (Fig. 4.1) is an exposure of the upper-most (8th) major limestone unit of the La Majúa Member, consisting of 13 m of micritic limestone above a 43 m thick succession of alternating silts and sands. A sharp boundary exists between the siliciclastic and limestone units. The base of the limestone section consists of bedded limestone (1 m) which passes into mounded limestone (4 m). Bedded limestone overlies the mound before siliciclastics become, once again, dominant. This mound is typical of those observed within the La Majúa Member, and due to the excellent exposure of both the underlying clastic succession and the presence of both basal and capping bedded carbonates has been used for a detailed microfacies investigation.

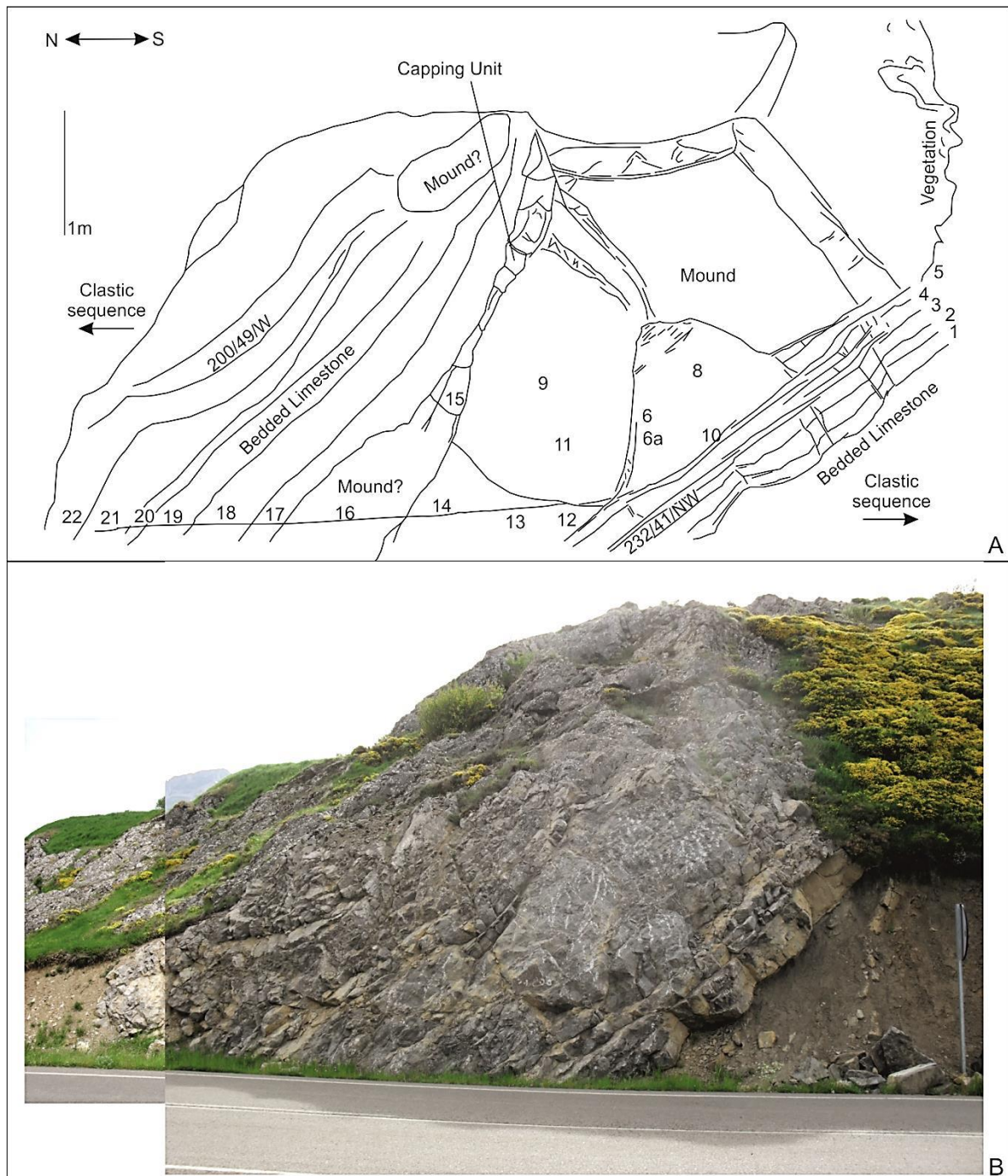


FIGURE – 4.1 A. An annotated field sketch of the Candemuella Mound, showing sample locations. B. Field photo, from right to left lithology changes from clastics to bedded limestone, mounded limestone and returns to bedded limestone. Road sign for scale (140 cm).

4.1.1 Basal Facies

The basal limestone (samples 1 to 4, fig. 1) consist of 1 m of bedded limestones which range from 13 to 32 cm thick. In hand specimen the bottom most bed appears a darker blue-grey than the subsequent beds. Numerous fossils are visible, with shelly fauna and algae identified. The limestones are micritic and exhibit a porcelaneous fracture.

The bottom most bed (**CAN sample 1**) has a distinct microfacies to that of the subsequent beds beneath the mound (samples 2-4), and is therefore described separately. The basal bed is a skeletal-microbial bafflestone consisting of intertwining (often bio-cemented) thickets of branching *Donezella* (with some *Beresella*) thalli, which enclose cavities with internal evidence of calcimicrobes and some poorly developed primary cavities filled with sparite. Microbial cavities occur as clumps of calcimicrobial sheaths within a homogenous and peloidal micrite whilst the primary cavities appear to be part of an irregular, porous network within the *Donezella* thickets. The lower part of the sample is dominated by bodies of encrusting *Claracrusta*, *Donezella*, *Girvanella* and probably foraminifera. The encrusting appears non-selective and coats algae, foraminifera, *Girvanella* and mudchips. *Donezella* thalli are mostly well preserved can be observed as either: *in situ* as a three dimensional “shrub” like framework with abundant baffled micritic sediment and free floating microfossils, or as broken fragments, these fragments show little sign of wear. The micrite-walled calcimicrobe *Girvanella* is commonly well preserved as small tangled clumps within thin layers of microspar which acts as a bio-cement between algal thalli, a micritic envelope is present on most bioclasts. Other than the dominant Donezellaceans and associated encrusting calcimicrobes (*Girvanella* and *Rothpletzella*), red algae (*Archaeolithophyllum*), Beresellids, Tuberitinidae and rare, small foraminiferas and ostracods are found. The ostracods are white in colour. **SMF 7-Bafflestone.** An *Algal bafflestone* characterised by *in situ* growth of algae (framebuilders – Donezellaceans and encrusters – *Komia*) with associated baffled sediments, free floating biota and several cyanoliths.

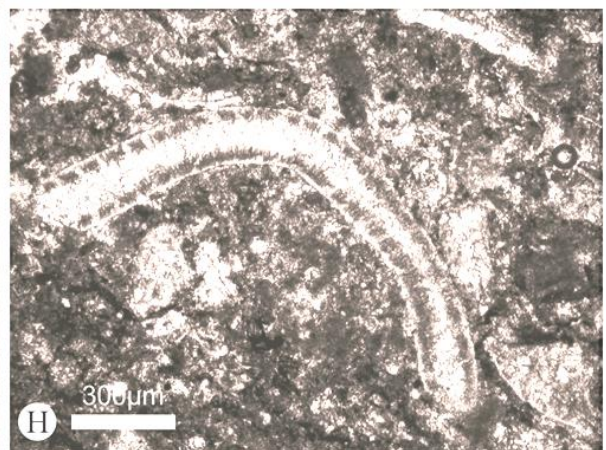
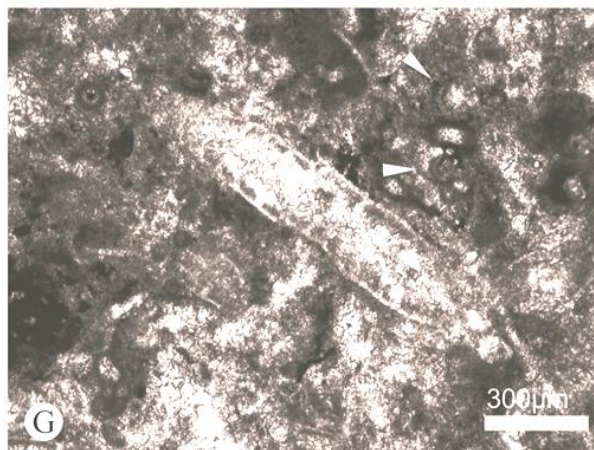
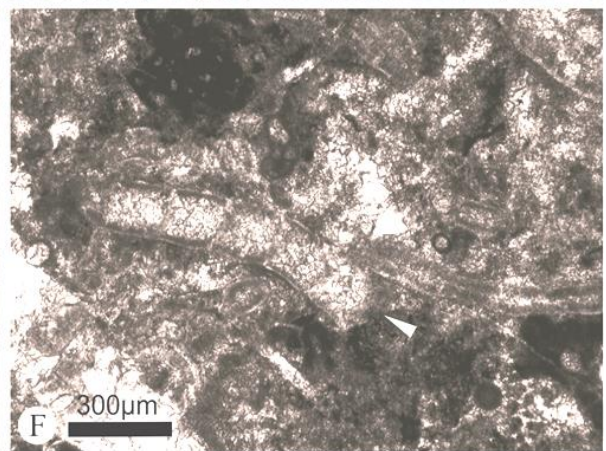
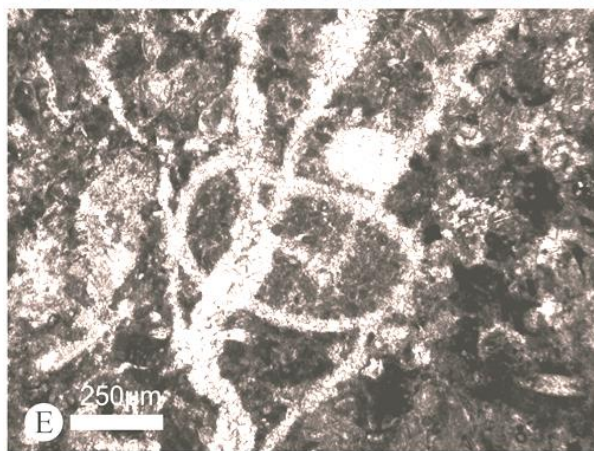
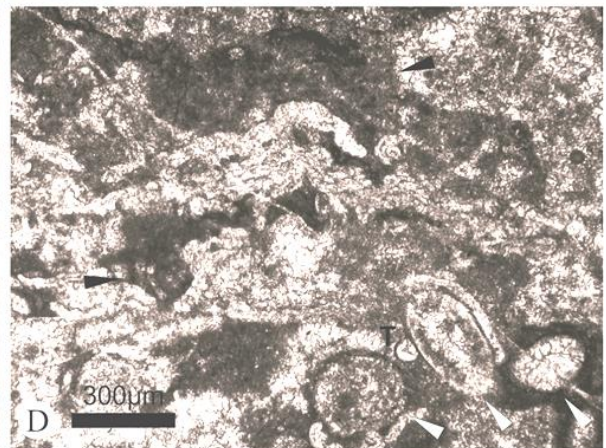
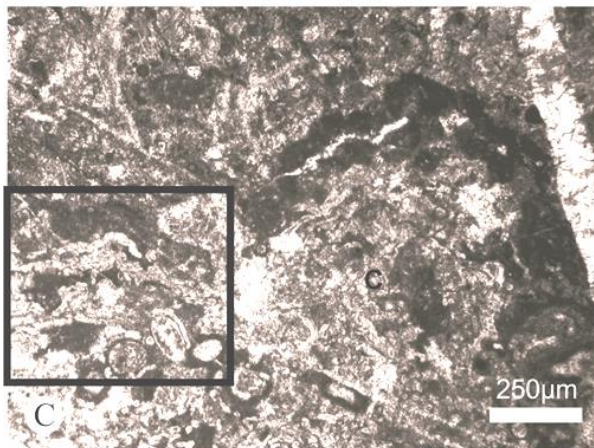
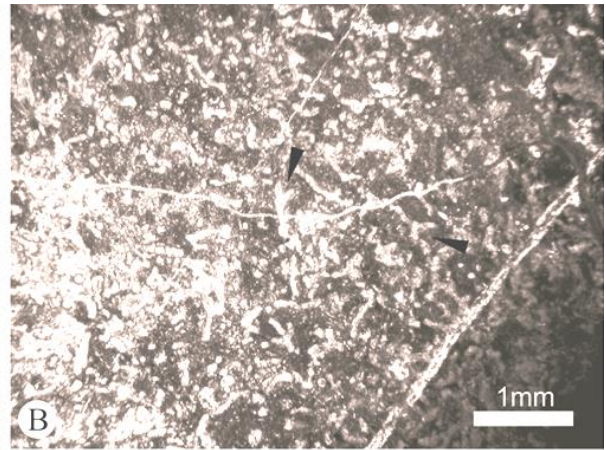
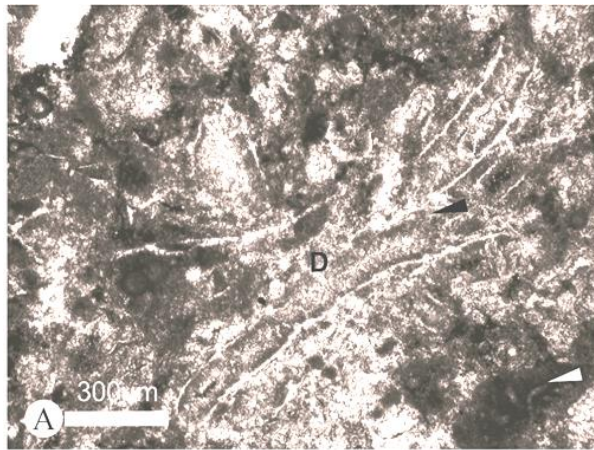


FIGURE - 4.2

A. (CAN 1) Bafflestone of the Basal Limestone Facies showing longitudinal sections through several entwined *Donezella* thalli (D). Dark encrustations can be observed, some *Girvanella* tubes (white arrow) are well preserved in both “enrolled” and “dispersed” habits as outlined by Pratt (2001). A peloidal micritic sediment framework is observed between thalli in association with a microsparitic bio-cement around the algae (black arrow).

B. (CAN 1) *Donezella* specimens as a three dimensional framework embedded within a poorly defined peloidal micrite with some calcimicrobe and probably foraminifera encrustation, several free floating mobile organisms are baffled (white arrows). Some poorly developed primary constructed cavities are supported by the branching Donezellaceans (black arrow).

C. (CAN 1) A photomicrograph showing “cyanolith” like growths (C) toward the base of the sample. *Claracrusta* specimens creating encrusting sheets of tubes which can be seen to branch, the sheets encrust several substrates showing no preference. The specimen exhibits the characteristic growth form of *Claracrusta*, the first few crusts are flat with few undulations, with subsequent crusts becoming increasingly convoluted. Encrusted substrates include mud chips, Donezellacean “shrub” like growths (individual thalli are rarely encrusted), round bodied, recrystallised specimens (classified as *Petschoria* – a red ungdarellid algae) and *Girvanella* (which also play an encrusting role in the formation of the *Girvanella*-like growths).

D. (CAN 1) A close-up of the area highlighted in C. The *Petschoria* like specimens can be clearly seen toward the bottom right (white arrows), note the attached *Tuberitina* (T). *Girvanella* (white arrow) specimens seen in an “encrusting” habit (Pratt, 2001) can be observed using sheets of *Claracrusta* (black arrow) as a substrate.

E. (CAN 1) Peloidal sedimentary fabric within a round bioclast (possibly algal in origin) surrounded by baffling *Donezella* and calcimicrobes (darker patches) – some specimens are observed as broken but with little reworking. Calcimicrobial and encrusting growths are often surrounded by sparite in primary chambers.

F. (CAN 1) Longitudinal section of a specimen of *Donezella lunaensis* Rácz (arrow). The thallus is rounded and tube like. The tubes are segmented with partitions which generally occur perpendicularly to the wall. The thallus is generally constricted where partitions are present, resulting in a barrel like appearance of each partitioned section. The wall consists of two parts, a thin, outer calcite wall and a thicker inner wall. The inner wall is generally dark in colour, the tubes are filled with a calcite cement, specimens occasionally have a yellowish hyaline colour.

G. (CAN 1) A specimen of *Beresella* in association with calcimicrobial growths (*Girvanella*, arrows) with homogenous and peloidal micrites.

H. (CAN 1) A longitudinal section through a specimen of *Beresella hermineae* Rácz. The specimen has a cylindrical body with no branching. The central cavity is filled with a calcite cement. The wall is composed of a thin outer wall and a darker inner wall, which is perforated with pores which are perpendicular to the wall and in a spiral arrangement (see *Beresella* in chapter 6. *Palaeontology* below).

Within **samples 2, 3 and 4** an increased dominance of *Donezellaceans* and *Beresellids* is observed; the entwined thalli of the alga averaging 49% volume of the Basal Limestone facies. Micritic envelopes on bioclasts are common along with microsparitic cementation between algal thalli. Evidence for microbial activity is present within cavities formed by algal entwinement. A clotted micritic fabric and clumped *Girvanella* tubes, are observed. Mud-support occurs in association with clotted fabrics. Several cortoids are present, showing micritised rims with evidence of encrusting calcimicrobes and microboring. Some dark material may represent bituminous material. Small foraminiferas (including *Tetrataxis*), gastropods, Tuberitinidae and red algae are present in minor abundance. *Tetrataxis* appears in its attached form, generally attached to algal matter. **SMF 18-Dasy.** *Dasyclad grainstone* characterised by a high abundance of intertwined algal thalli (dasyclad) with a peloidal sedimentary framework and low species diversity (Fig. 4.3).

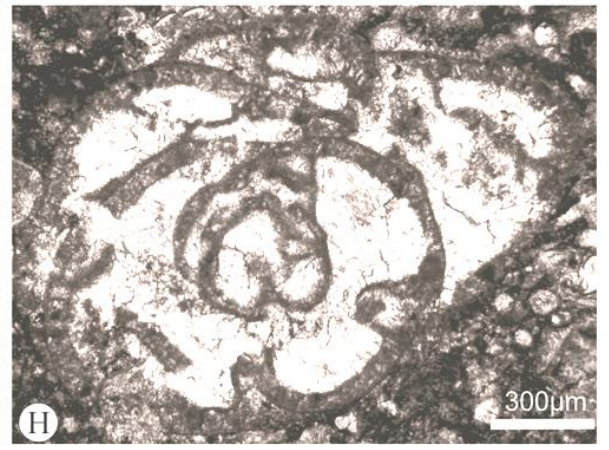
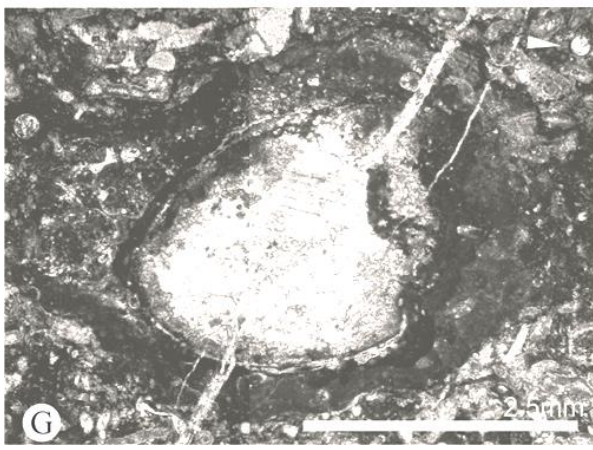
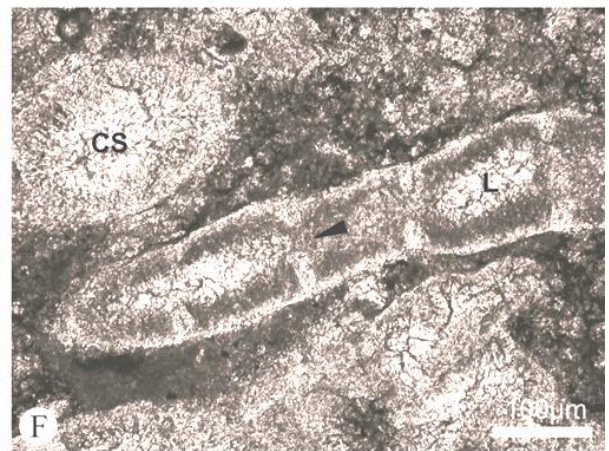
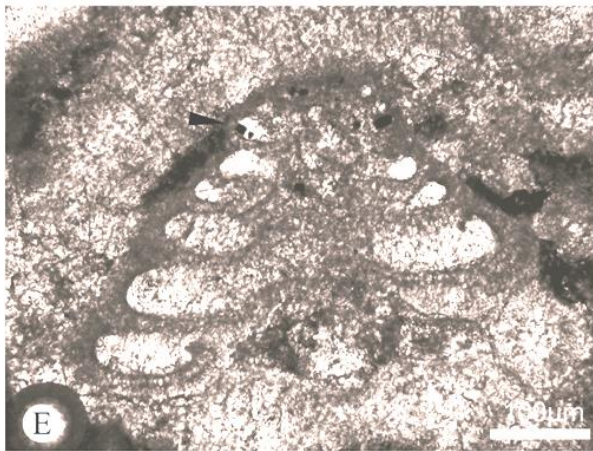
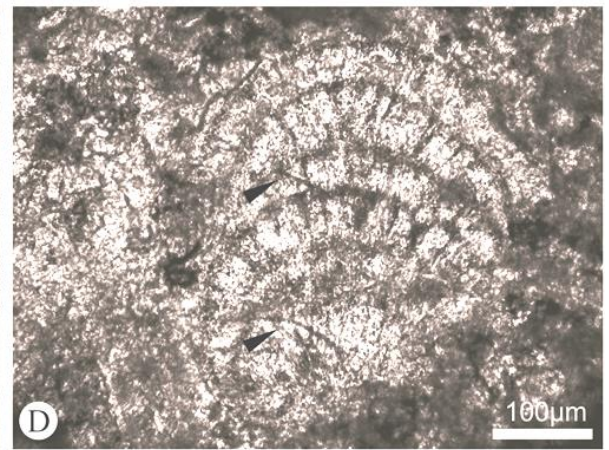
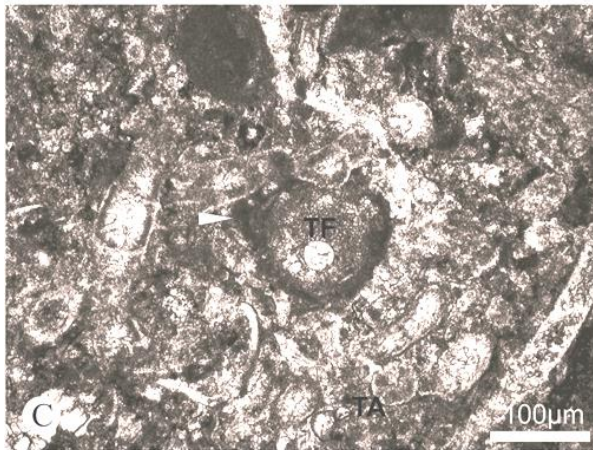
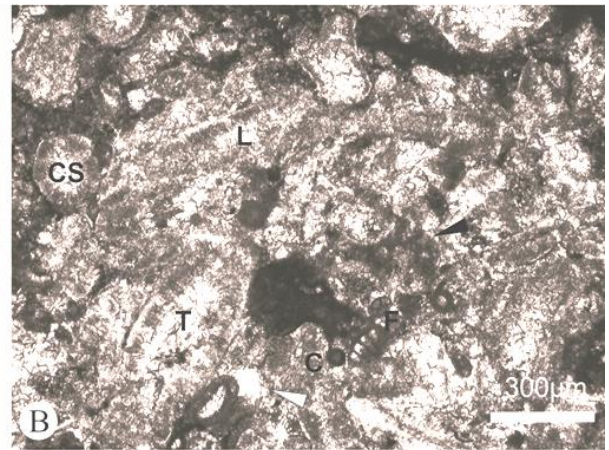


FIGURE - 4.3

A. (CAN 3) Photomicrograph showing a large cortoid (central clast) which may be a recrystallised 'phylloid' algal thalli with typical micritic rim and micro borings. Some encrusting foraminifera and calcimicrobes are present as white laminae and tube-like forms within the micritic envelope. The high dominance of Donezellanid algal thalli, with associated foraminifera and Tuberitinidae can be observed.

B. (CAN 2) Cross section (CS), longitudinal (L), and tangential (T) sections of *Donezella* specimens encased in cement surrounded with clotted and peloidal sediment and encrustations (black arrow). Foraminifera (F) and calcispheres (C) can be observed baffled between thalli. Several small, primary cavities filled with a sparitic cement (arrow) these are constructed cavities and formed due to the configuration of juxtaposed biotic forms.

C. (CAN 3) Photomicrograph showing entwining nature of the Donezellanid algae, several thalli are cemented together with clotted micrite and bio-cement. A cortoid (centre) exhibiting a characteristically uneven surface with microborings and encrusters (white arrow). Several Tuberitinidae are present in various forms – both attached (TA) and free (TF).

D. (CAN 4) Solenoporacean red algae. Thalli consist of crescent shaped threads of vertically divergent cells; the cells becoming wider toward the top. Some boring is evident (arrows) Recrystallisation of the originally aragonitic algae has damaged much of the original algal structure. Calcite crystals mimicking a precursor polymorphic aragonite crystal habit resulting in a straight extinction under cross polars.

E. (CAN 4) *Tetrataxis*. Conical test consisting of several whorls, which overlap. Wall is composed of a dark microgranular outer layer and a lighter, fibrous inner layer. Specimens are often seen to be attached. Below the test of this specimen a calcite 'pod' and what appears to be an algal thalli can be observed. Note the occurrence of pyrite within several of the chambers and crusted to the outer side (arrow).

F. (CAN 2) Longitudinal (L) and cross sections (CS) through a specimen of *Donezella lutugini* Maslov. Note that the internal partitions do not meet in the middle, resulting in perforations between each "barrel" throughout the central cavity (arrow).

G. (CAN 2) A large cortoid consisting of a recrystallised and partially dolomitised bio-clast (possibly a brachiopod) with undulating encrusted layers of red algae (*Archaeolithoporella*) and foraminifera. Some boring is evident. Note the free floating *Tuberitina* baffled by Donezellanid algae (arrow).

H. (CAN 2) An example of a rare foraminifera found within the samples, most likely of the genus *Bradyina*.

4.1.2 Mound Facies

The mound facies (**samples CAN 5 to 14 and CAN 16 to 18**, fig. 4.1) consists of a 4 m thick limestone mound, with discernible palaeo-topographic relief, it appears lighter in colour than the surrounding bedded limestones. The mound is a homogenous micritic feature with typical porcelaineous fracture, few fossils are visible in hand samples. What appears to be a brecciated ‘vent’ is evident through the centre of the mound, however, no filling cement is present and it is unclear if this feature is primary in origin. The ‘vent’ could be related to the compaction and compression of the mound sediments or may even be related to the blasting of the outcrop when the neighbouring road was laid. The boundary between mound and bedded limestones is sharply defined with some onlap evident.

Samples 5, 7 and 10 represent the first of several sub-microfacies which are united under the ‘Mound Facies’ heading. They are fenestral packstones characterised by non-laminated peloidal and clotted micrite associated with variously sized fenestral cavities and bioclasts. Cavities are spar-filled and range from small ‘birdseye’ to larger, irregular voids. Several cavities have a stromatactoid fabric; flat based voids with undulating roofs, often with fine sediment fill at the bottom – providing an excellent way-up indicator for the samples. Isolated clasts of sedimentary framework can be found within some of the larger cavities, as can an occasional, sparse, coating of pyrite. Sedimentary framework consists of both sparitic and micritic peloids, the latter associated with a relative abundance of encrusted *Donezella* thalli, peloids are often thromboidal or aligned.. Encrusters appear microbial in nature with some *Girvanella* tubes preserved. Donezellaceans and related Beresellids are well preserved and relatively large, and are often seen to form a three dimensional framework (often the algal framework appears to directly control the occurrence of cavities), and exhibit a yellow colour – possibly a hyaline structure. **SMF 10. Bioclastic Packstone.** Characterised by broken and worn algal (dasyclad) thalli, pelmicritic sedimentary framework with fenestral and stromatactoid cavities (Fig. 4.4).

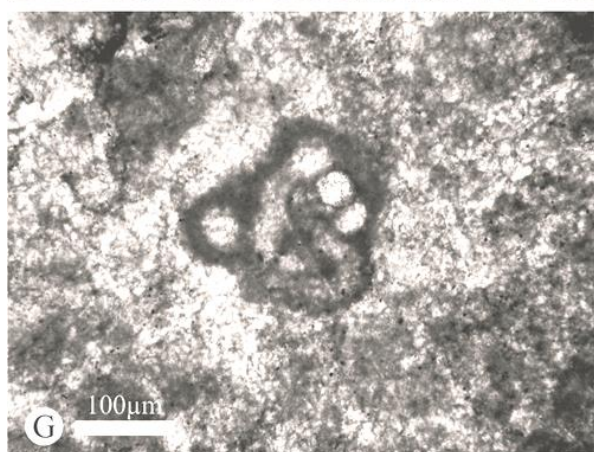
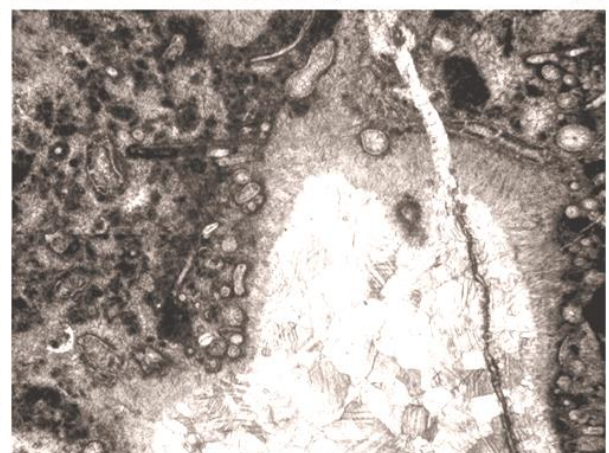
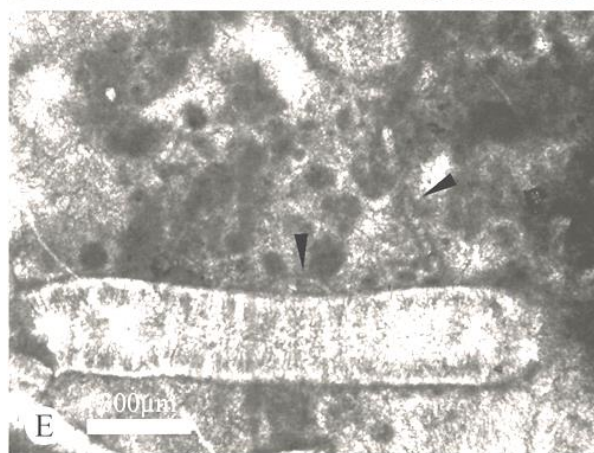
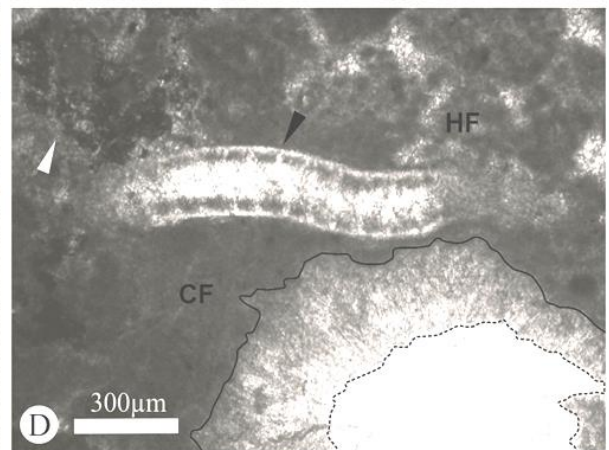
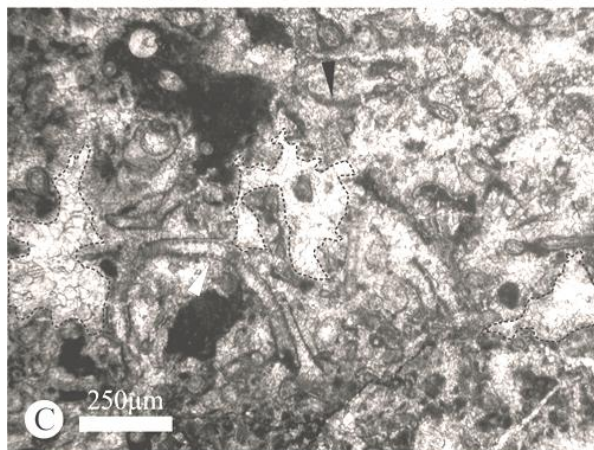
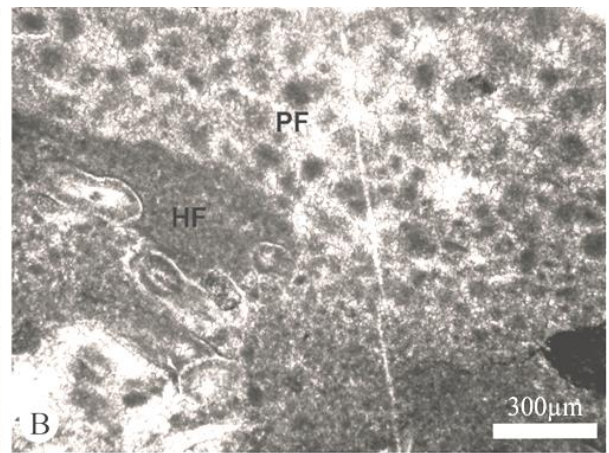
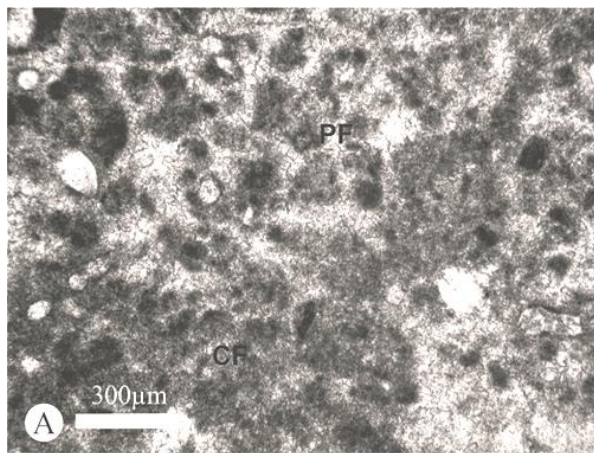


FIGURE - 4.4

A. (CAN 7) A photomicrograph showing the nature of the sedimentary framework - sub-rounded micritic grains (peloidoidal fabric - PF). Some areas consist of poorly sorted grains with distinct size differences, indicating that the peloids were formed by the reworking of a poorly lithified carbonate mud. Other micrite deposits appear well sorted and of the same/similar size, often homogenous although generally appearing as a clotted fabric (CF) – possibly representing microbial peloids or the diagenetic alteration of a biological structure.

B. (CAN 10) Mud peloids (PF) exhibiting some poorly developed layering overlying finer peloids and homogenous micrite which is in close association with entwined algal thalli. It is possible that the homogenous to slightly clotted micrite (HF) has been baffled by the algae and then a higher energy event occurs eroding and reworking some weakly lithified muds into peloids. Which are in turn deposited as the poorly laminated specimens observed here.

C. (CAN 10) Large specimens of *Beresella* (white arrow) and associated *Donezella* (black arrow) forming a framework with primary constructed cavities cemented by a blocky sparitic calcite (dashed lines outline a few of these cavities).

D. (CAN 7) *Dvinella*. The thalli are rounded and tube like, without branching. Like *Beresellids* the thalli show no “constrictions” where partitions occur along the inner walls of the thallus (black arrow). Two distinct walls can be noted, a light outer wall and a darker, microgranular, inner wall which is segmented by partitions that occur perpendicular to the outer wall. The partitions appear to have slight perforations forming a conduit between segments. A fenestral cavity can be observed toward the bottom of the photomicrograph, note the rim of fibrous cement (full line) the calcite crystals are divergent from the substrate, with an undulose extinction and central fill of blocky calcite cement (dashed line). The sedimentary matrix is micrite with homogenous (HF) and clotted (CF) fabrics. A possible growth form (erect, clotted, irregular growth of micritic bodies) similar to that of the calcimicrobial group *Renalcis* or *Epiphyton* (Flügel, 2004) is marked by a white arrow.

E. (CAN 7) *Dvinella*. Note the thin micritic envelope surrounding the bioclast and the peloids that appear to be stacked vertically from the flat, upper surface of the specimen. Several of the peloids appear thrombotic or aligned in nature and resemble the calcified bacteria *Renalcis*. The arrows points at two faint, but discernible filaments, which are calcimicrobial sheaths. The evidence from this photomicrograph suggests that the clotted peloidal material may well be micritised remains of cyanobacterial colonies.

F. (CAN 5) A stromatactoid cavity showing a characteristic flat base and undulating roof, internal sediment, marine cement and late blocky cement. The marine cement (radial cement) exhibits some needle like crystals as well as the more common fibrous crystals. This example of stromatactis appears surrounded by *Donezellacean* algae, many examples of cavity fabrics from this study show the same relationship, with the algae directly responsible for the construction of the cavity framework.

G. (CAN 10) A tight clump of tubes. enclosed within a micritic envelope within a sparitic cement. This is possibly a foraminifera and resembles *Calcitornella*.

Sample 6A represents the next sub-group from the Mound Facies. Similar to samples 5, 7 and 10 it is a fenestral packstone characterised by well-defined birdseye, fenestral and stromatactid cavities. The major difference is the much higher definition of cavities and a reduction in the size of Donezellacean thalli diameter. Homogenous micrite and peloidal micrite fabrics account for the majority of sediments. Pelmicritic fabrics occur baffled between Donezellacean thalli or rarely as a cavity fill. Homogenous micrite occurs exhibiting no obvious fossil content and little in the way of sedimentary fabrics, slight clotting can occasionally be observed, several cyanolith like growths and encrusting sheets are observed, individual algae thalli are rarely encrusted, although colonies are. Encrusting sheets occur in a repetitive manor in association with alternating Donezellacean growths. Biodiversity observed within this sample is low, associated with the highly dominant Donezellaceans are rare Tuberitinidae and foraminiferas, plus encrusting *Claracrusta*, *Komia*, *Rothpletzella* and *Archaeolithoporella*. Some selective dolomitisation has occurred, often as contact or floating equigranular rhombic to non-rhombic crystals within the blocky cement filling the fenestral cavities. **SMF 21-Fen.** *Fenestral packstone*. This is characterised by fenestral cavities, peloidal sedimentary fabrics and a dasyclad algal framework (Fig. 4.5).

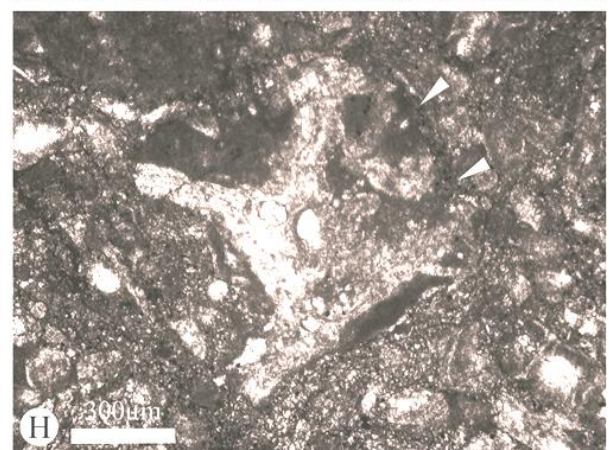
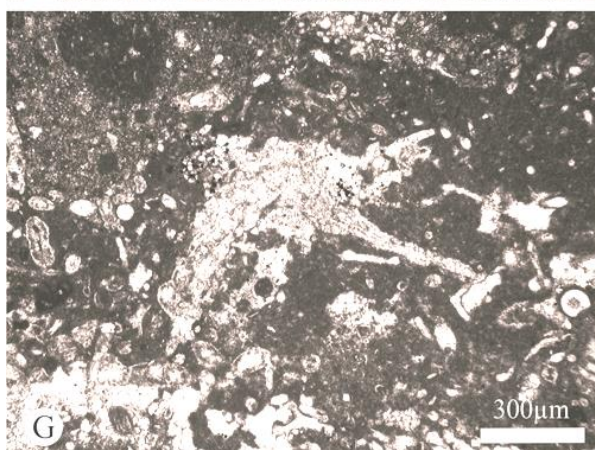
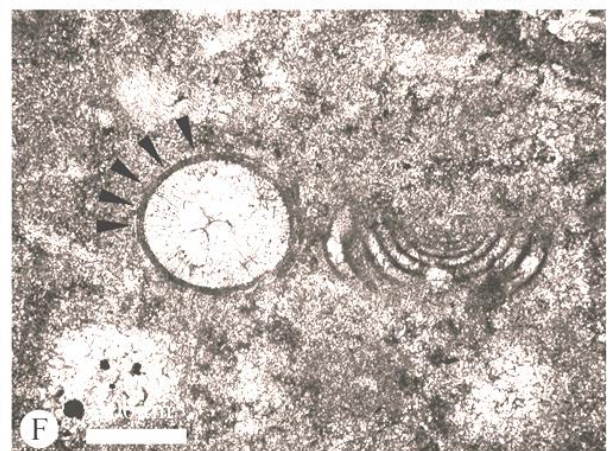
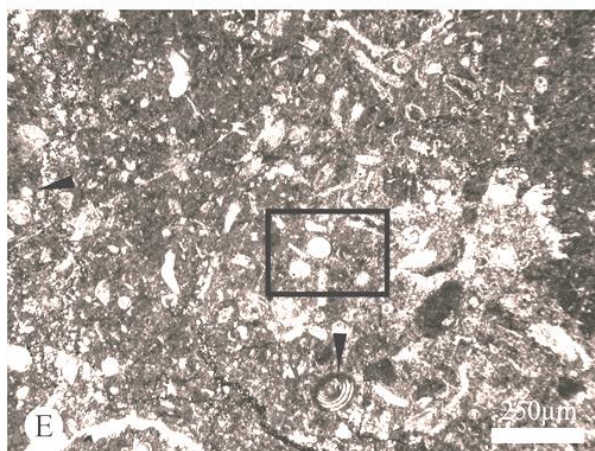
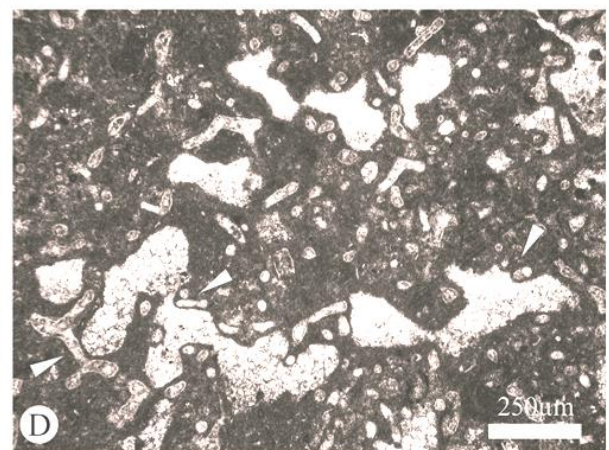
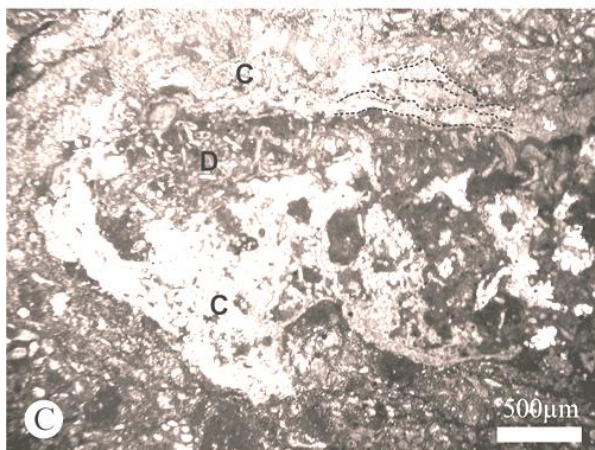
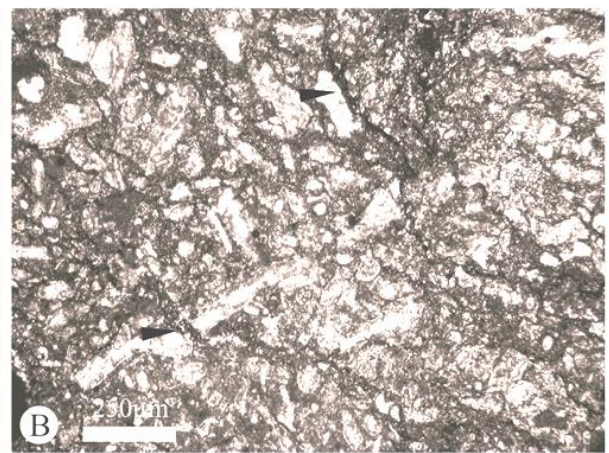
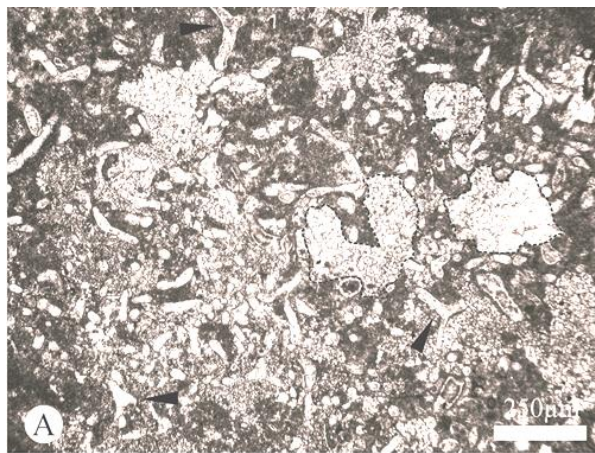


FIGURE - 4.5

A. (CAN 6A) Fenestral packstone fabric showing well preserved *Donezella lutugini* Maslov (arrows), several of the tube like thalli show various branching angles. A non-laminated peloidal and clotted micritic sedimentary fabric, along with several (selectively dolomitised) fenestral cavities (dashed line marks several of these cavities) can be observed within the framework created by the *Donezella* colony.

B. (CAN 6A) Packstone consisting of broken (and in some cases worn) algal thalli and cementing micrite. This particular fabric is host to several stylolites (arrows). The stylolites are seen to anastomose around the mechanically stronger bioclasts and compact the micritic sedimentary matrix.

C. (CAN 6A) A relatively large cortoid consisting of a nucleus of a *Donezella* colony (D) strongly encrusted by *Claracrusta* (C), which consists of rows of irregular, braid like cells. *Claracrusta* regularly grows with a flat base with undulating rows towards the top, see the dashed lines toward the top-right corner for an example (see Fig. G below); this growth geometry can be observed in several directions for this cortoid, suggesting that the photomicrograph may be recording the transect through a bulbous floret of *Donezella* which has been encrusted. *Donezella* can be observed growing on the upper surface of the encrusting sheet

D. (CAN 6A) Photomicrograph showing well defined fenestral cavities, which are controlled by the position of the algal thalli. Homogenous micrite is the dominant sediment with some peloidal and clotted micrite. The cavities have a sparitic fill with no evidence of a stromatactoid fabric. The geometry of the cavities (flat base, undulating roofs) in the bottom half of the figure may suggest some sort of hard ground or surface on which the base of the cavity network has formed, with the roof being defined by algal growth (arrows).

E. (CAN 6A) Peloidal and clotted micrite. Many algal remains are broken and worn, note the inclusion of several mobile organisms (free-floating *Tuberitina* and foraminifera, as marked by arrows). The reworked nature of many bioclasts and the inclusion of several free floating organisms may indicate a period of increased energy activity

F. (CAN 6A) Close-up of the *Tuberitina* specimen in the centre of Fig. E., indicators of an aragonitic precursor can be seen perpendicular to the dark micritic wall (see arrows) of the spherical chamber. An oblique section through a foraminifera, probably *Lasiodiscus* (see samples 13, 14 and 16 below), is also shown.

G. (CAN 6A) Specimen of the encruster *Claracrusta*. A smooth basal row with subsequent rows becoming increasingly wavy. This specimen exhibits several cells showing the irregular nature associated with them. They often appear to be “bean” shaped in longitudinal section and “dish” shaped in tangential section.

H. (CAN 6A) Evidence of reworking. A rounded and transported specimen of *Komia*, note the sharp boundary between the *Komia* containing clast and the surrounding packstone (marked by arrows). The characteristic cell alignment of *Komia* is particularly well preserved for much of this specimen.

Samples 6, 8 and 11 consist of entwined and partially broken Donezellacean thalli within a mostly homogenous micritic sedimentary fabric. However, the very base of the samples consists of a non-laminated peloidal micrite with evidence of several possible hardgrounds (Fig. 4.6 C). Cavities are mostly absent (samples 6 and 11 = 1%, sample 8 = 5% sparitic cavity fill). Bioclasts are encrusted by a uniform dark micrite with some bifurcation and tubes preserved. From the preserved tubes it is most likely that the crusts consisted of *Girvanella* or some other similar calcimicrobe. The enveloping darker micrites contain the majority of bioclasts and have an undulating, sharp boundary with a second, lighter micrite (also homogenous) which was most likely baffled into cavities formed between encrusted Donezellacean colonies. The baffled micrite is less homogenous than the micrite forming the crusts. In places, isolated sparite crystals can be observed as can several bifurcated fabrics. Some rare rhodoids consisting of isolated Donezellacean ‘nodules’ are present as are several laminar structures consisting of *Claracrusta*, *Shamovella*, *Rothpletzella* and some *Girvanella*. Several specimens of a newly discovered species - *Donezella robusta* spec. nov., are present in these samples (see chapter 6. *Palaeontology* below). Rare, isolated bryozoa fronds, Tuberitinidae and several foraminiferas are observed within the homogenous micritic fabric. Biodiversity observed within these samples is low. Columnar stylolites are present throughout samples. **SMF-23.** *Non-laminated, fine grained peloidal micrite.*

SMF 8. *Bioclastic floatstone.* These are characterised by whole fossil algal thalli (*Donezella*) framed in micrite with rare mobile organisms (i.e. free floating *Tuberitina*) (Fig. 4.6).

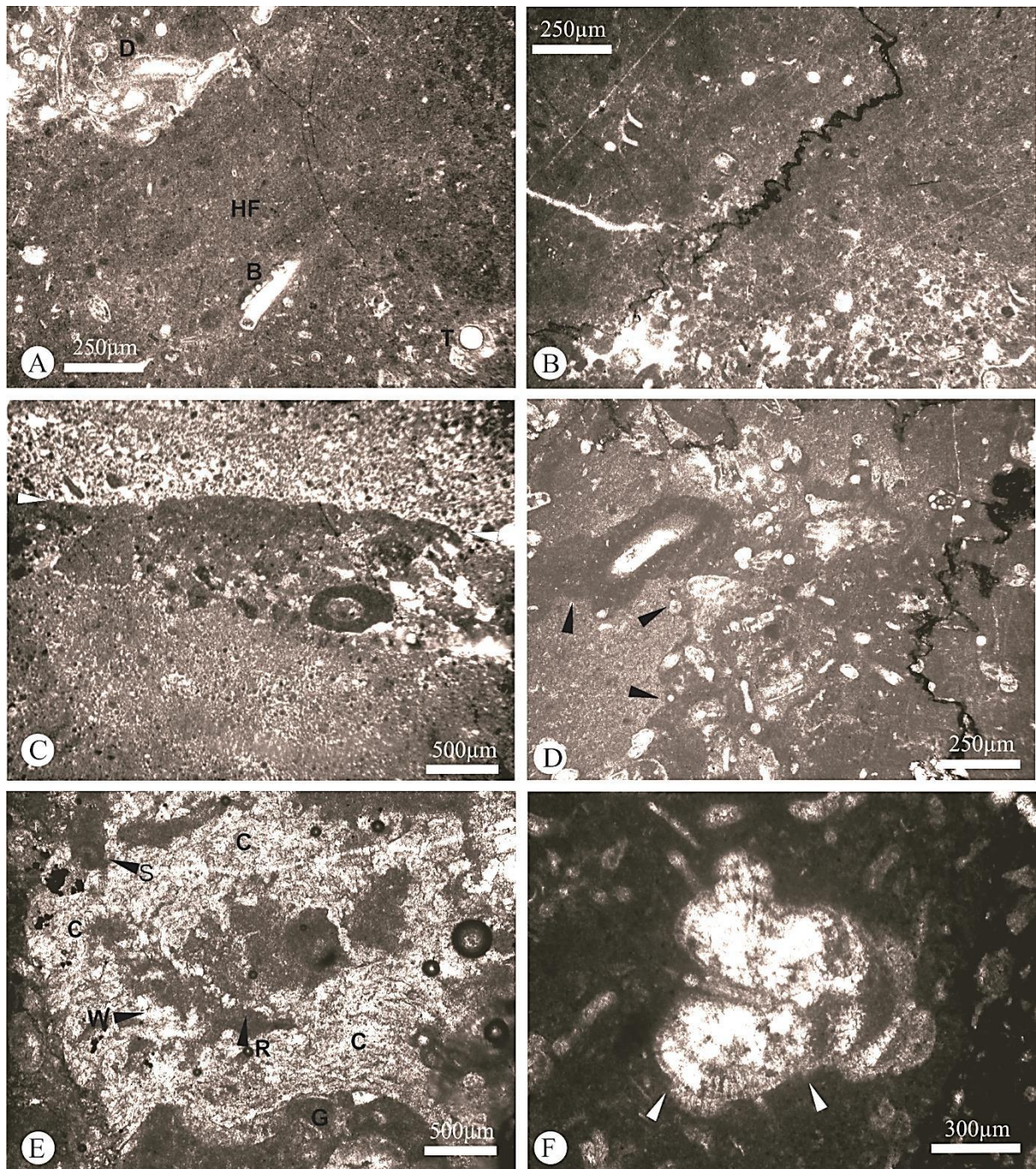


FIGURE - 4.6

A. (CAN 11) A photomicrograph showing patches of entwined *Donezella* thalli (marked by D), plus broken *Donezella* thalli, bryozoan fronds (B) and free floating organisms (e.g. *Tuberitina*, marked by T) within a sedimentary framework of a dominant homogenous micritic fabric, with several pellets of darker homogenous micrite. Bioclasts generally have a micritic envelope.

B. (CAN 11) Non-laminated peloidal and homogenous micrite showing a spar filled cavity network towards the bottom. Peloidal fabrics are rare for these samples. Fossil content is low with very few algal fragments and some rare *Tuberitinoids*. A non-bedding parallel, crenulated stylolite is present through the centre of the photomicrograph

C. (CAN 11) Some lamination and possible imbrication of rare peloids is observable in this figure. A possible hardground forms a boundary between a darker, finer peloidal micrite with few pore spaces and a lighter slightly laminar peloidal micrite. The upper surface here (arrows) appears filamentous.

D. (CAN 6) A bioclastic floatstone of whole *Donezella* thalli framed in a dark, homogenous micritic envelope, surrounded by a lighter, slightly coarser homogenous micrite with very little bioclast content. Arrows mark the clear boundary between the darker, bioclastic micrite and the lighter, coarser micrite. Crenulated stylolites are again present in this figure.

E. (CAN 6) A community of microscopic encrusters consisting of *Wetheredella* (W), *Girvanella* (G), *Rothpletzella* (R) and *Shamovella* (S) in association with the dominant encruster, the algae *incertae sedis*, *Clara crusta* (C). The dark micritic patches at the centre of the calcimicrobial dome exhibits some “shrub” like features and several components that most resemble micritised cyanobacterial/calcimicrobial tubes.

F. (CAN 11) A rare specimen of calcareous red algae. Evidence of an aragonitic precursor can be seen in the form of needle shaped crystals (arrows) and a sweeping extinction.

Samples 9, 12 and 18 are dominantly entwined broken and whole algal thalli (Donezellaceans) with microbial encrusters and a dark homogeneous micritic sedimentary matrix. These samples are similar to samples 6, 8 and 11 but consist of a much higher abundance of algal fossils and less micritic sediments. Algal thalli in sample 9 are generally smaller than those of 12 and 18, and are often more worn/broken, some algae appears yellow/orange – possibly a hyaline structure. Algal thalli are often entangled and entwined with microspar and micrite acting as a bio-cement between branches. The micritic sedimentary fabrics present are a homogenous and a fine peloidal fabric with furcated tubes and ‘clumps’ of *Girvanella*

Some circular features of dark homogenous micrite appear to resemble bioclasts which have most likely undergone micritisation. Other than microbial organisms, *Tuberitina* appear to be the only encrusters of the Donezellacean cohort. Some mobile fossil forms are present including free floating Tuberitinidae and fusulinid foraminiferas, these are generally baffled between algal thalli and are often encrusted. Fossil cavities are occasionally filled with an opaque, angular/cubic mineral which is most probably pyrite (see *Chapter 5 Ultrafacies*). Several thin bedding parallel, irregular, anastomosing stylolites can be observed. Sample 9 contains some echinoid fragments.

SMF 10. Bioclastic packstone. This is characterised by an abundance of whole fossil and broken algal thalli with a homogenous micritic bio-cement (Fig. 4.7).

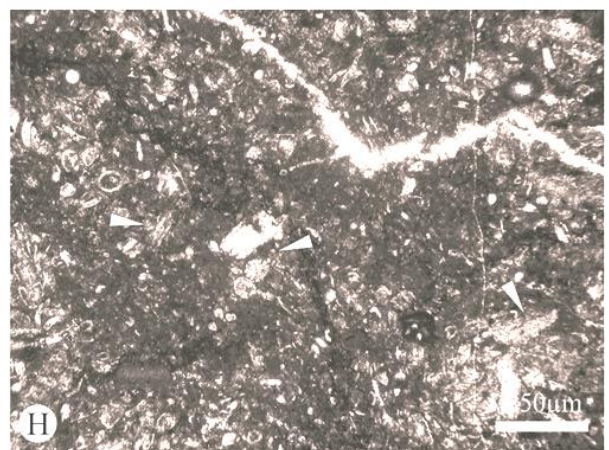
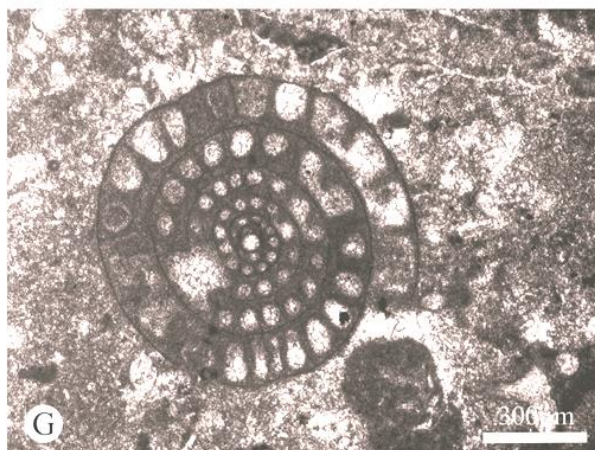
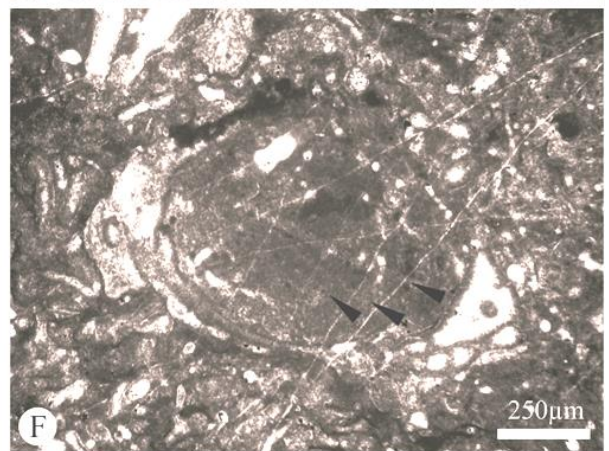
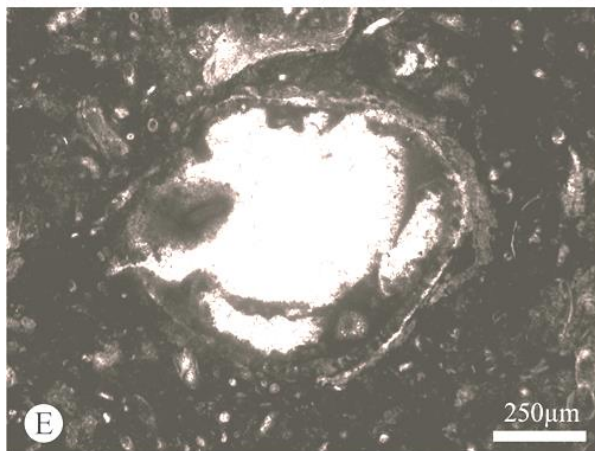
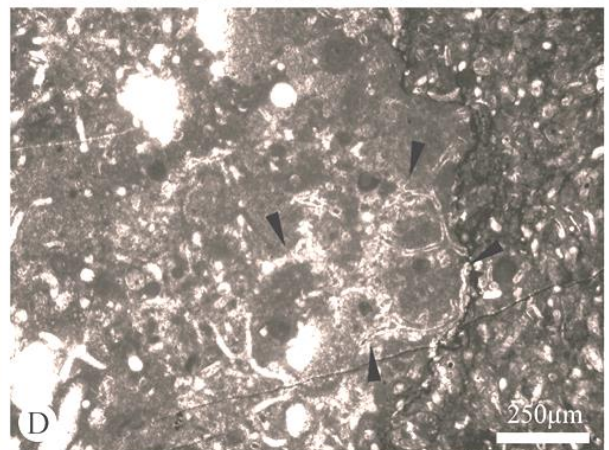
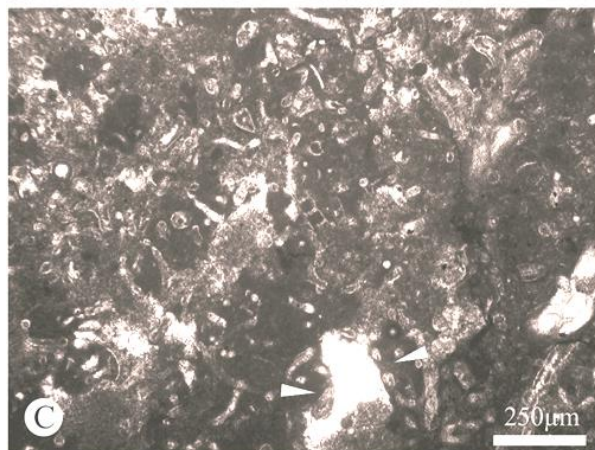
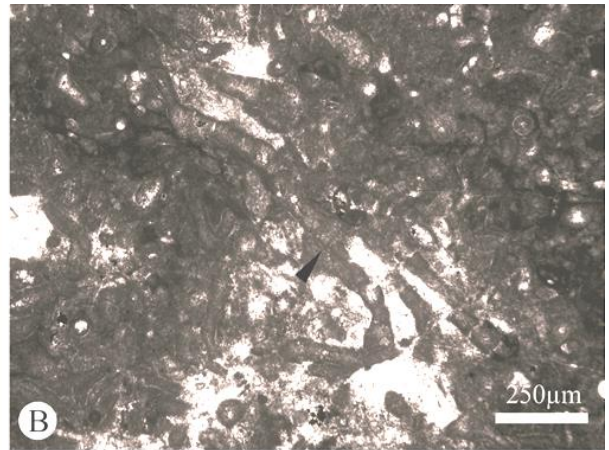
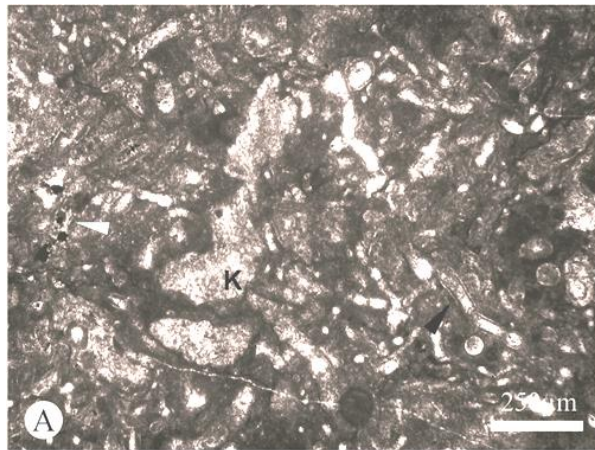


FIGURE – 4.7

A. (CAN 12) Photomicrograph showing the entwined, branching nature of the algal growth in these samples, the encrusting red algae *Komia* (K) is present, as are several free floating organisms (fusulinid foraminifera and Tuberitinidae). Bioclasts are enveloped in a dark homogenous micrite which partially acts as a bio-cement between algal thalli. The Donezella-like thalli generally consist of a calcitic, microgranular wall filled with sparry calcite (black arrow), however, several specimens here can be observed with an opaque, cubic fill – most likely to be pyrite (white arrow).

B. (CAN 12) A large specimen of *Donezella lutugini* Maslov, exhibiting branching (arrow) with sparry bio-cementation between thalli. A dark homogenous micrite forms the bio-cement between most entwined algal thalli.

C. (CAN 18) Another photomicrograph showing entwined algal thalli forming a three dimensional framework into which homogenous micrite is supported (either as bio-cement, or as baffled sediment). Note the occurrence of a rare constructed cavity, which like others from this study, appears to be supported directly by the surrounding algal thalli (arrows).

D. (CAN 18) This photomicrograph shows both whole algal thalli in a shrub like growth and broken thalli forming a packstone. *Donezella lunaensis* Rácz, with characteristic perpendicular branching of thalli. Here the *Donezella* shows a structure, consisting of square like growths of thalli (black arrows). To the right of the figure is the more dominant packstone fabric consisting of partially broken *Donezella* thalli.

E. (CAN 18) An encrusted, partially micritised bioclast. Encrustation is dominant to the top side of the bioclast suggesting possible *in situ* encrusting. The dominant encruster is *Claracrusta*, which has grown with a distinctive flat base layer with increasingly wavy subsequent layers.

F. (CAN 12) A spherical cortoid within an entwined Donezella-like framework. Several filamentous tubes can be observed within the spherical micrite ‘body’ of the cortoid (arrows). This branching cluster of tube like features are reminiscent of the calcified cyanobacteria *Ortonella*, of the “*Hedstromia Group*” (Flügel, 2004). Clumps of this globular growth form may indicate a high energy event within an inner carbonate ramp. Micro-boring is not prominent on this micritised grain and the micritic coating is quite regular, this is most likely an example of a constructive micrite envelope.

G. (CAN 18) Sagittal section of a fusulinid foraminifera. Note that the ultra-structure of the wall has been destroyed.

H. (CAN 19) Echinoid fragments present in a small lens of bioclastic packstone. The fragments appear as broken and worn clasts in association with broken and worn algal thalli, small fusulinid foraminifera and rare free floating Tuberitinidae. The assemblage observed here is indicative of a higher energy event, possibly an isolated event due to the minimal abundance of the deposit.

Samples 13, 14 and 16 are dominantly peloidal and non-laminated homogenous micrites with few microfossils and spar-filled intragranular pores with some cavities. Microfossils consist of broken and worn Donezellacean fragments, occasional free floating *Tuberitina* and rare *Girvanella* tubes. Peloids (pelmicrite) are of differing sizes, forming irregular laminations. Homogenous micrite accounts for roughly half of the samples, several faint thromboidal textures can be observed. The shape and orientation of some peloids suggests that they may originate from the micritisation of bioclasts, the internal fossil structure being destroyed leaving a micrite peloid which has a reminiscent shape, and relationship with surrounding peloids similar to that of the original bioclast (Flügel, 2004 & Samankassou *et al.*, 2005). Although some fossil remains are present they are relatively uncommon (when compared to other samples in this study) within the homogenous micrites. Algal remains (Donezellaceans) account for the majority of preserved microfossils, no framework is apparent and the sections of tube like thalli observed are often broken and rounded. Cavities range from ‘birdseye’ to fenestrae with several showing a stromatactoid fabric. A fibrous marine cement with a later blocky sparite fill is common in these cavities. In other samples algal thalli have been seen to play a role in the formation of cavities, however, in these samples several cavities appear without algal “scaffolding” (although the majority can still be seen to have an element of biological construction). **SMF 23. Non-laminated homogenous micrite with very rare fossils** characterised by homogenous micrite with some thromboidal textures, a lack of fossiliferous material and some micritised clasts. And, **SMF 16-Laminated. Fine-grained peloidal packstone.** This is characterised by poorly laminated peloids of various sizes and spar filled intragranular pores, some broken algal thalli (Fig. 4.8).

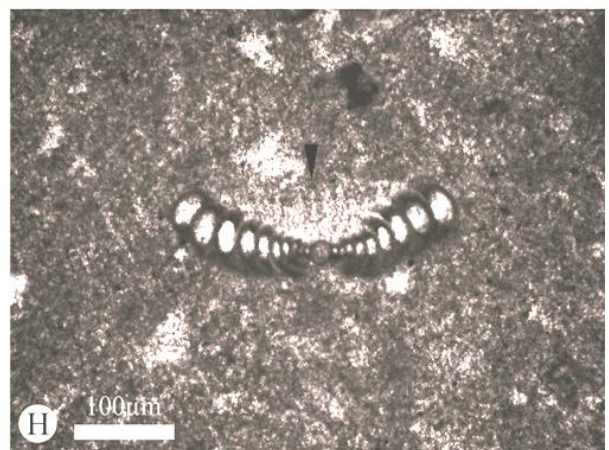
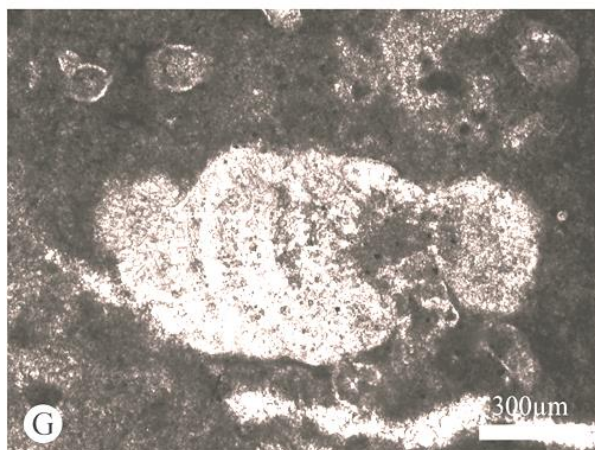
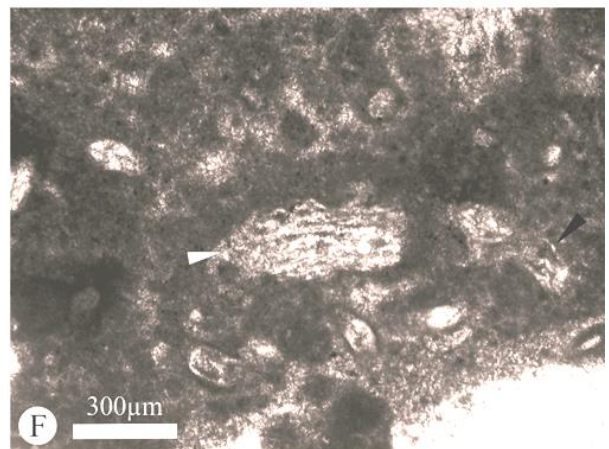
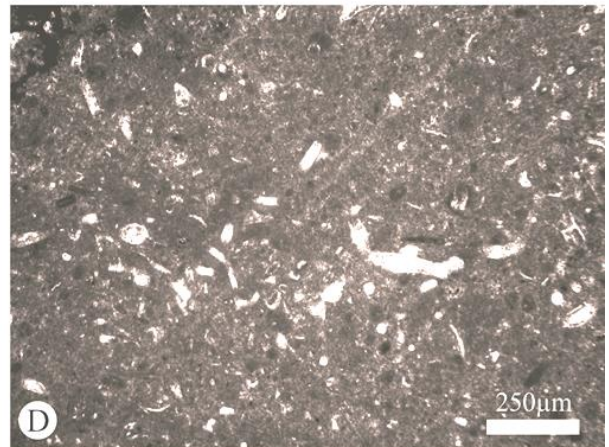
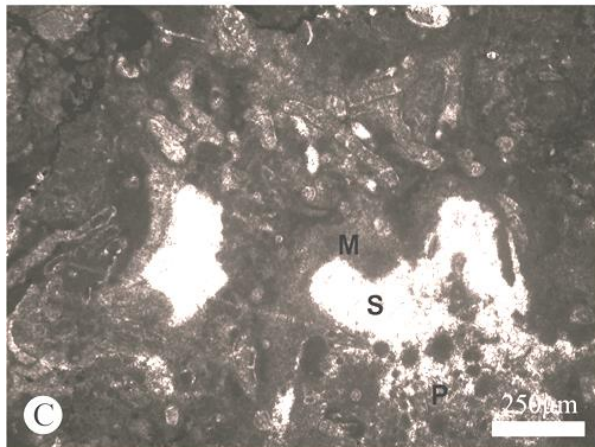
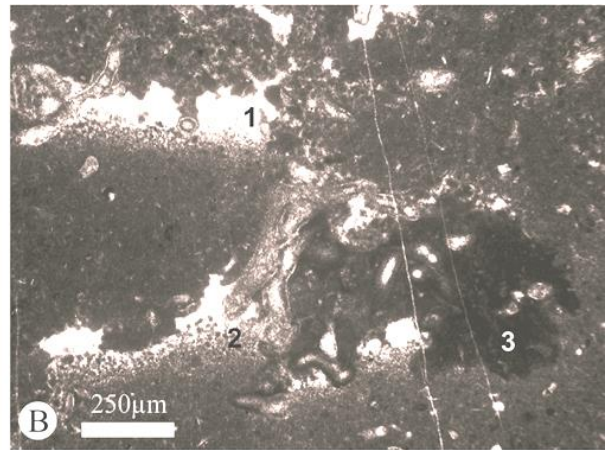
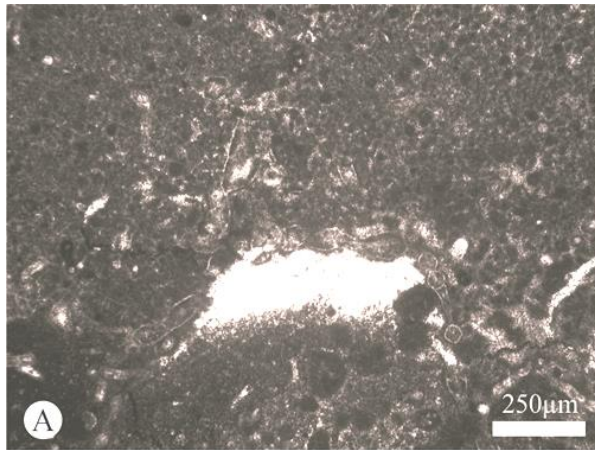


FIGURE - 4.8

A. (CAN 13) A photomicrograph showing a predominantly non-laminated peloidal texture with a constructed cavity. The cavity is fenestral and was formed by the algal thalli observed directly surrounding it, the cavity is filled with layered internal sediments and a blocky sparitic cement. Algal thalli can be seen as both smaller, broken fragments and as part of a larger, branching organism.

B. (CAN 14) Several fenestral cavities are present within a non-laminated peloidal and homogenous micritic sedimentary framework. Cavities 1 (1), 2 (2) and 3 (3) are all fenestral in geometry and are filled with internally deposited, poorly layered peloids with a clear, blocky spar calcite. Cavity 3 appears to be supported by algal thalli and is filled by homogenous micrite with evidence of borings and calcimicrobial tubes, this cavity shows a cryptic habitat which was inhabited by calcimicrobes and burrowing organisms.

C. (CAN 16) Stromatactoid cavities with characteristic flat bottoms and undulating roofs with layered internal sediment fill (micritic peloids (P)), marine (M) and late sparry (S) cements. The stromatactoid cavities are surrounded by a homogenous micrite dominated by *Donezella* thalli.

D. (CAN 16) Homogenous micrite with some randomly distributed peloids and broken algal remains. Most bioclasts exhibit a micritic envelope. The micrite envelopes are generally concordant to the surface of the clast and range from several to 30 µm in thickness.

E. (CAN 16) Several examples of fenestral and stromatactoid cavities within a dark homogenous micrite. Several free floating Tuberitinidae are present. Bioclasts in this photomicrograph are surrounded by a micritic envelope.

F. (CAN 16) A laminated stromatolithic growth of tubular encrusting forms – most likely *Rothpletzella* (white arrow) and *Girvanella* (black arrow). The encrusting growth is supported by a clotted and peloidal micritic sedimentary framework. Some small fragments of algae thalli are present, the specimen is void of any other biota.

G. (CAN 16) Calcareous red algae exhibiting layered growth. The specimen was previously aragonitic as exhibited by the needle like crystals which form perpendicular to wall surfaces, a sweeping extinction and the off-yellow colour of the polymorphic calcite crystals. A micritised rim can be observed around the edge of the specimen.

H. (CAN 14) A foraminifera showing a differentiated test. An axial section of *Lasiodiscuss sellieri* Dessauvage and Dağ. Note the spherical initial chamber and microgranular wall. The last volution of the secondary chamber is not quite in the general plane of coiling. The arrow points to a hyaline cover (consisting of columns) on the dorsal side of the foraminifera.

Samples 17 and 19 are poorly laminated, bioclastic algal packstones composed of fragments of broken algal thalli with associated foraminiferas, mobile Tuberitinidae, gastropod shells and mud chips. The occurrence of mud chips and micrite infill of several interstices between algal thalli shows grain support. The micritic envelope around bioclasts, which is a common feature of many of the other samples is not present in this microfacies, nor are any peloids. Donezelloids are broken and often rounded. Specimens are often small and consist of only one or two “barrels” of the tube like thallus. Several of the algal specimens have been recrystallised, resulting in wall structure obliteration. In addition the broken nature of the specimens makes a distinction between *Donezella*, *Beresella* and *Dvinella* impossible. Several of the mud chips consist of entwined algal thalli with homogenous micrite sediment framework – much like the microfacies observed for samples 9, 12 and 18. These mud chips are often angular. Micrite which fills gaps between bioclasts often exhibits evidence of calcimicrobial tubes. Poor lamination can be observed throughout the sediments, many bioclasts are aligned parallel to bedding, as are several stylolitic bands. Stylolites occur as irregular anastomosing, non-sutured seam swarms, and appear to be made of clays and/or organic material (insoluble matter). The non-sutured seams occur due to the more ridged bioclasts surrounded by more soluble cements. **SMF 18-Dasy. Bioclastic packstone.** These samples are characterised by an abundance of whole and broken Donezelloids with homogenous and mud chips with calcimicrobes and micritic cements (Fig. 4.9).

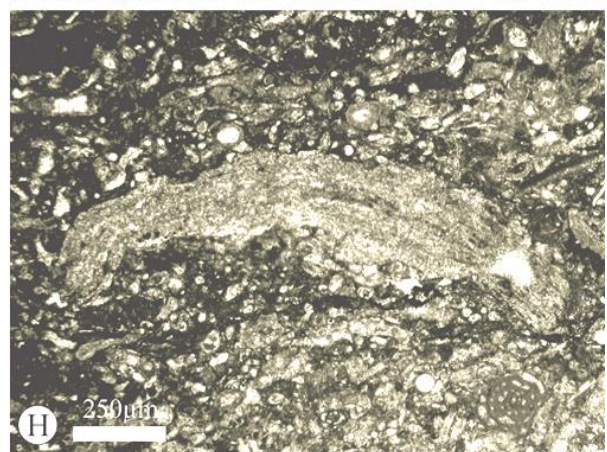
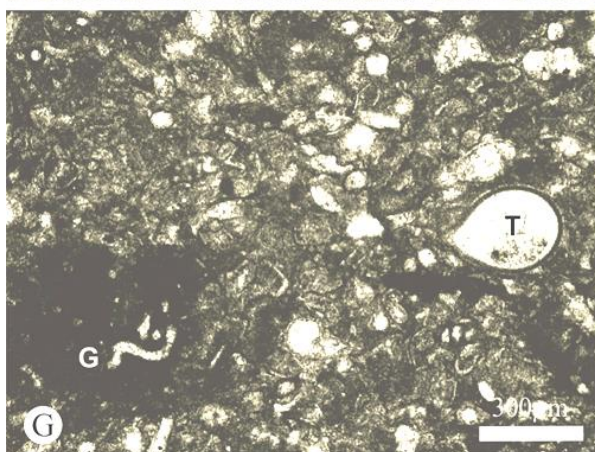
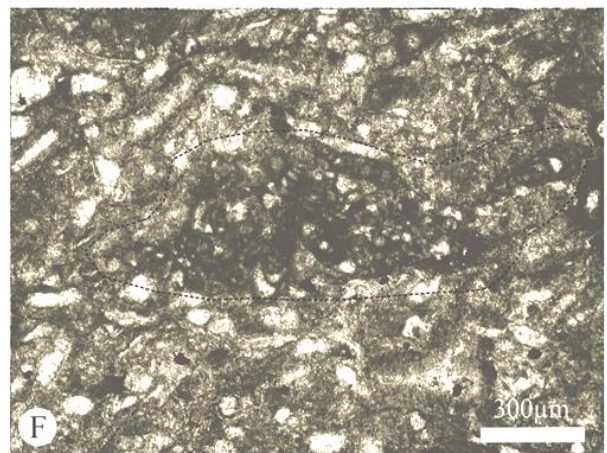
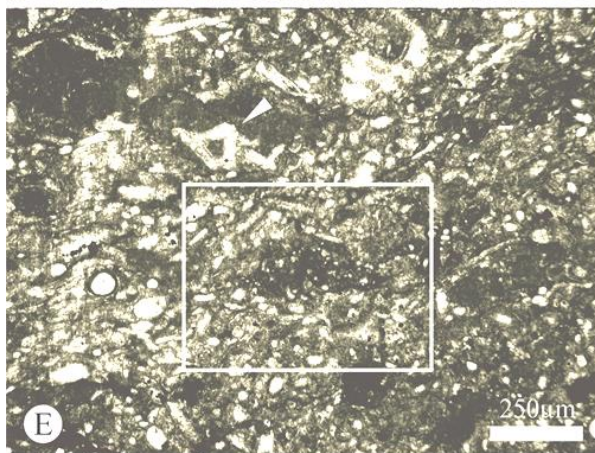
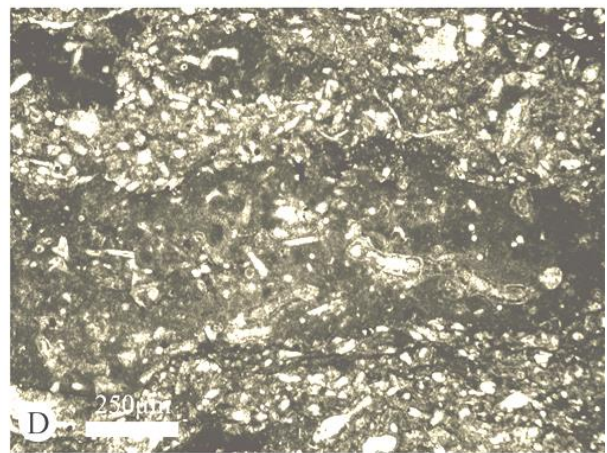
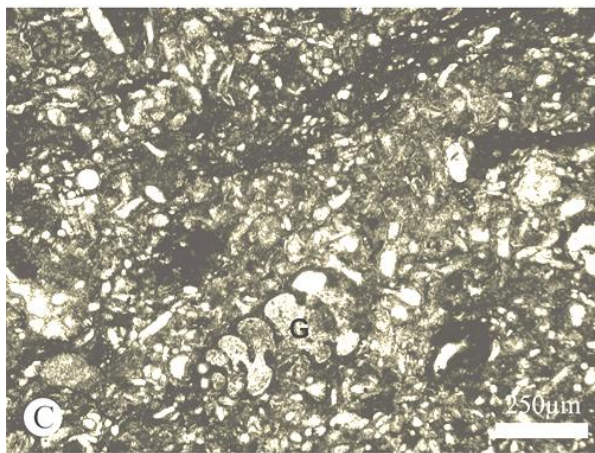
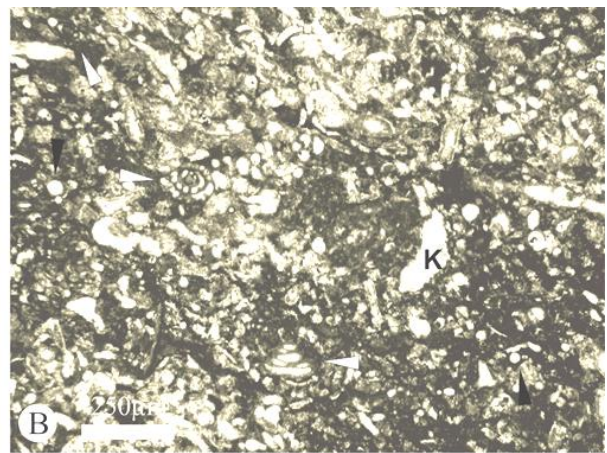
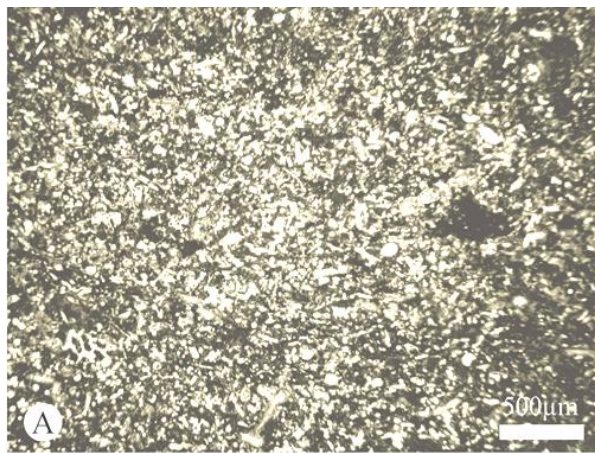


FIGURE - 4.9

A. (CAN 17) A photomicrograph showing mostly broken algal thalli forming a weakly laminated packstone. Several Tuberitinidae are present. Mud chips occur as grain supported clasts.

B. (CAN 17) Fusulinid foraminifera including *Tetrataxis* (white arrows) and the encrusting red algae, *Komia* (K) are present along with Tuberitinidae (black arrows) and broken algae. This figure shows a higher micrite content than that of Fig. A. a common feature which is typical of this microfacies.

C. (CAN 19) The difference in cement between the broken algae dominated layers and the microbially dominated lenses can be seen in the figure. The micrite has a slightly larger crystal size and consequently a brighter appearance when forming a bio-cement between bioclasts, which are dominantly algal thalli. Where the micrite is the major constituent (mud chips and areas of mud supported rock) the colour is much darker and bioclasts are scarcer. Note the occurrence of a large foraminifera, this is the largest bioclast observed in the microfacies analysis of the Candemuela Mound.

D. (CAN 19) An example of the heterolithic nature of this microfacies, the central band of the photomicrograph is dominated by a micritic wackestone, which contains far fewer – but much better preserved algal thalli (arrow) than the surrounding packstone.

E. (CAN 19) Several examples of algal thalli which have been broken, worn and in some cases, recrystallised so any internal structures have been obliterated (arrow).

F. (CAN 19) An enlargement of the area marked out in Fig. E. A cluster of small, assumedly, encrusting foraminifera (within the dashed line). These specimens are quite possibly miliolinid foraminifera. Assemblages similar to this are not seen in any previously described microfacies, and foraminifera of this size are rarely observed as individuals. Only axial sections are apparent in this example. The foraminifera appear to have a spherical initial chamber with several volutions arranged with no deviation from the growth axis. This assemblage may represent bioclastic shoaling?

G. (CAN 19) A relatively large specimen of *Tuberitina* (T), in its stretched and free stage. Also note the mud chip with a clump of *Girvanella* (G).

H. (CAN 17) A specimen of the encruster *Rothpletzella*, note how the laminations are unlike the increasingly divergent sheets of *Clara crusta* seen in this study, these sheets are mostly concordant with the first encrusting sheet.

4.1.3 Capping Facies

The capping facies sees a return to bedded carbonates and begins with a bed with a high clastic component, which is onlapping on to the mound. The contact between the capping bed and the mound is sharp. **Sample CAN 15** is a grain supported packstone consisting of broken and transported fossil fragments, sparry calcite crystals and an insoluble clastic/organic material sedimentary framework. Calcite crystals occur interspersed within a poorly laminated very fine quartz and insoluble organic framework. Bioclasts are dominantly broken Donezellacean fragments, the orientation of which is slightly imbricated, indicating a current direction. Donezellaceans are again the most dominant type of fossil, free floating *Tuberitina* are observed as well as some encrusting *Komia* and large fragments of bryozoan fronds, which exhibit the typical “brick like” wall structure. Several flattened, opaque lenses occur, these are possibly plant fragments which have been compacted by further sedimentation, several shell fragments also appear flattened. **SMF 4. Bioclastic-lithoclastic packstone.** This is characterised by grains of differing origins including locally derived bioclasts and imported shallow marine material (quartz grains and plant (as observed in hand specimens) fragments) (Fig. 4.10).

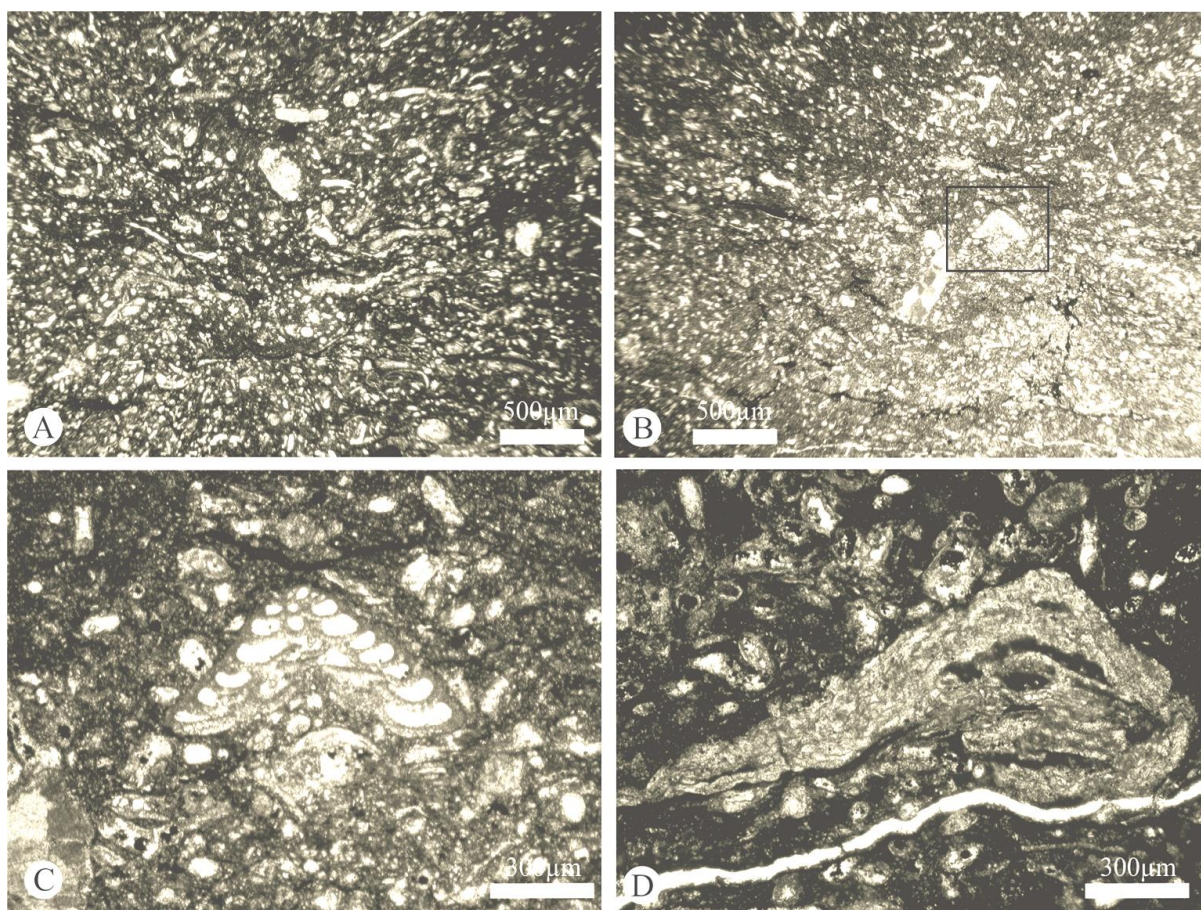


FIGURE - 4.10

A. (CAN 15) Packstone exhibiting imbricated clasts which are supported by a mixture of micrite, sparite and small quartz clasts. Several bioclasts are flattened, indicating rapid deposition or only partial lithification before an increased load was applied. Bioclasts include algal fragments, bryozoan fragments, shell fragments and reworked encrusters. Note that the darker matrix material is dominantly quartz grains.

B. (CAN 15) A photomicrograph showing an area where calcitic bio-cementation between algal thalli is dominant over clastic matrix mass.

C. (CAN 15) Enlarged area from B. A specimen of the foraminifera *Tetrataxis* with several whorls, the inclusion of this foraminifera with bio-cemented algal thalli may indicate that this specimen was attached within the algal clump or grazing the thalli for food, and not a free floating specimen.

D. (CAN 15) Calcified sheets of the encruster *Claracrusta*, which is seen with the characteristic growth pattern. Note that many of the fragments of algal thalli within the surrounding micrite matrix are in filled with matrix material and not sparry cement like other examples in this study. This indicates that the fragments are thoroughly broken and the walls of the “barrel” like thalli compromised.

Samples 20 and 21 are classified between a wacke- and a packstone. This sub-microfacies is characterised by a homogenous to slightly peloidal micrite sedimentary framework, partially baffled by branching *Donezella* and partly supporting large bioclasts (over 1 mm in size) and cortoids. Bioclasts are densely packed and consist mainly of *Donezella* and *Beresella* thalli. *Donezella* occurs as both a branching three dimensional network and as broken fragments. Some algal thalli are micritised with wall structures destroyed, leaving only outlines of the thalli. Bryozoans are relatively common in these samples and are often the largest bioclasts found. Bioclasts are frequently enveloped by a micritic rim. Foraminifera and calcimicrobes are well preserved and appear with relatively high biodiversity, both mobile and attached forms of the *incertae sedis* family Tuberitinidae are also well preserved and relatively abundant. A few rare echinoid plates are present. Calcimicrobial assemblages range from small isolated clumps, to larger encrustations involving several organisms. The cortoids in these samples are spherical in nature and resemble ooids but for the lack of any laminae, they generally consist of a recrystallised spherical nucleus with a micritic rim exhibiting calcimicrobial growth. These samples show a biodiversity higher than the other samples from the Candemuela Mound, the microfossils present within these samples also show some excellent preservation. **SMF 5- reef derived bioclastic wacke-/packstone.** This is characterised by densely packed whole and broken bioclasts with a homogenous to clotted micrite framework (Fig. 4.11).

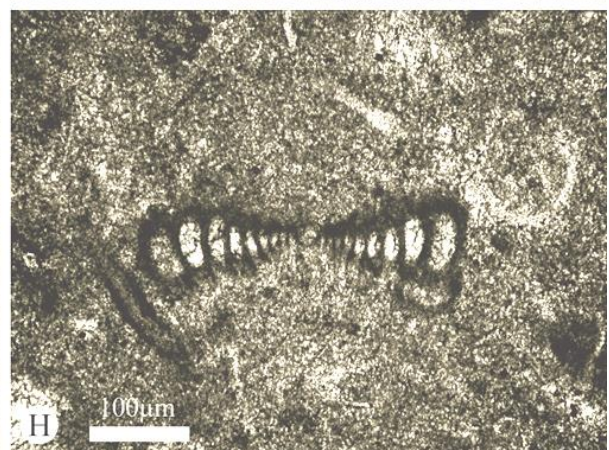
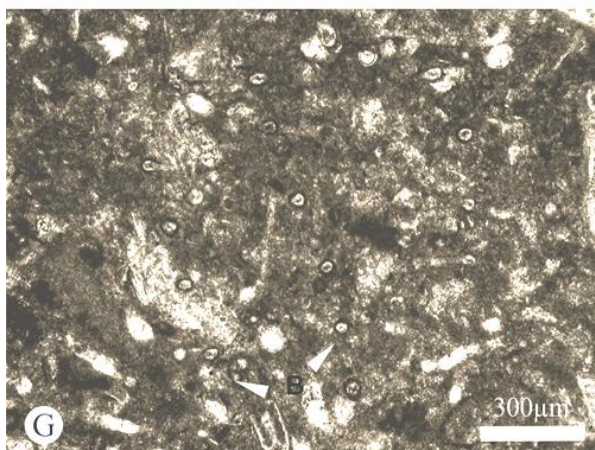
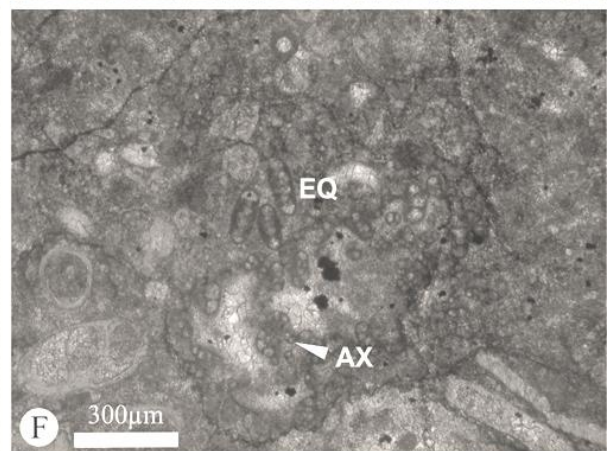
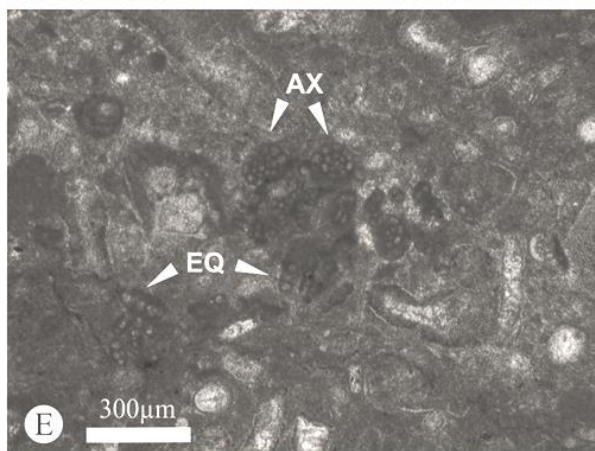
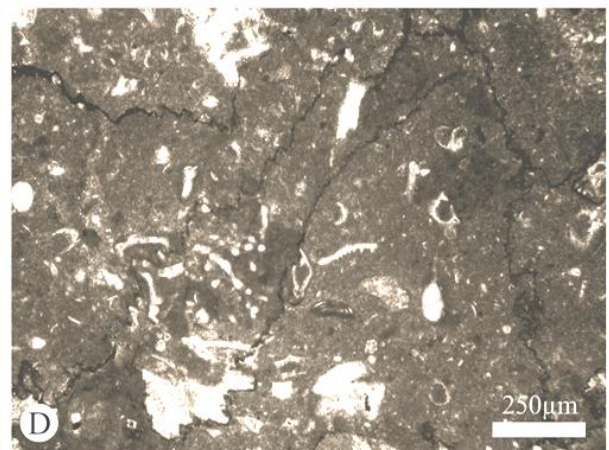
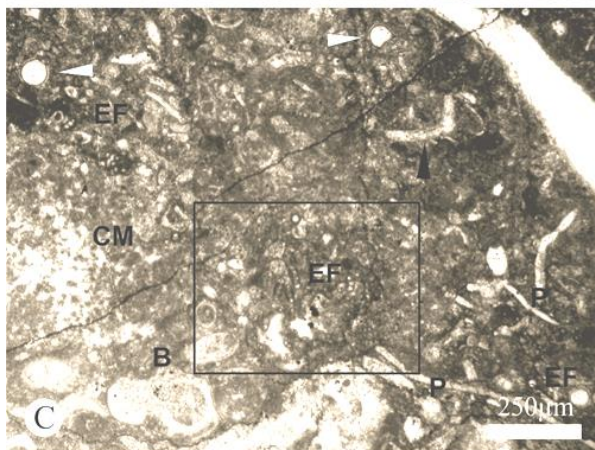
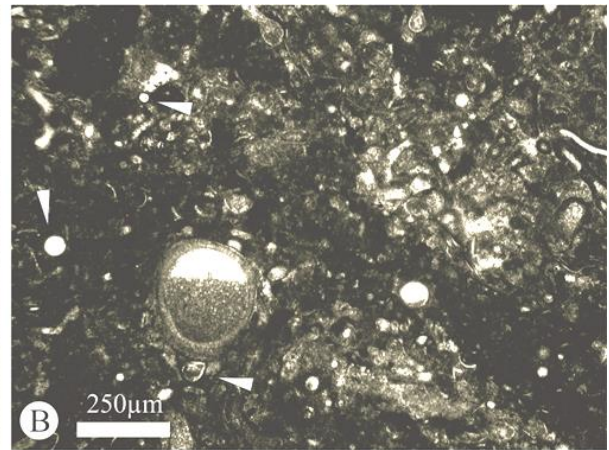
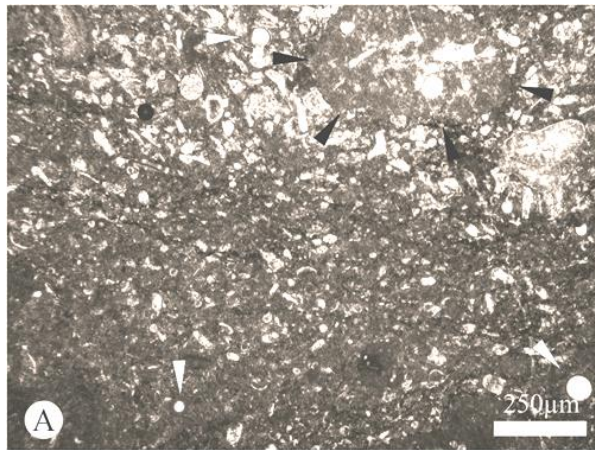


FIGURE - 4.11

A. (CAN 21) Closely packed, broken algal thalli, several free floating Tuberitinidae (white arrows) and a rounded wackestone mud chip, marked by black arrows.

B. (CAN 20) Several algal thalli broken and cemented by both micritic bio-cement and encrusting calcimicrobes. The supporting matrix is dominantly homogenous micrite. Tuberitinidae are present in both attached and free forms (white arrow). Note the geopetal fill of the large dasyclad algae specimen.

C. (CAN 20) A photomicrograph showing a reasonably high biodiversity in comparison to most other microfacies described from the Candemuela Mound. In addition to the common Tuberitinidae (white arrows) and Donezellaceans (black arrow) are 'phylloid' algal blades (P), bryozoan fragments (B), clotted micrite (CM) fabric which resembles several "bush" like bodies and several clusters of encrusting foraminiferas (EF) are also present.

D. (CAN 21) A photomicrograph of the wackestone component of this microfacies, mostly homogenous micrite supporting several algal thalli, which are broken and rounded. Foraminiferas and poorly preserved bryozoans are also present. Several fenestral cavities are present and stylolites run through the entire sample.

E. (CAN 20) Poorly preserved algal thalli, most of their internal structure is destroyed. A clump of small encrusting, multi-chambered planispiral foraminiferas are observable toward the centre. Both axial (AX) and equatorial (EQ) sections are observable. These small clusters of presumably encrusting foraminiferas only occur within these specimens and only within the parts of the assemblage that are more pack- than wackestones. These are interpreted to be miliolinid foraminifera.

F. (CAN 20) Close-up of the area outlined in C. Another clump of miliolinid foraminifera, again both axial (AX) and equatorial (EQ) sections are observable.

G. In this microphotograph several bryozoan fronds (B) are observable.

H. (CAN 21) A reasonably well preserved example of a moderately common foraminifera from the family Lasiodiscidae. The characteristic hyaline columns are missing from the dorsal side and the wall has undergone some micritisation. Small tubular appendages which diverge toward the proloculum are still preserved, these appendages suggest that this is a specimen of the species *Lasiodiscus sellieri* Dessauvage and Dağar.

Sample 22 represents the last carbonate unit before a return to siliciclastic lithologies. A peloidal grainstone with abundant bioclast fragments and some evidence of microbial encrustation. Micritic peloidal grains are sub-rounded, poorly sorted and non-laminated. Bioclasts consist of broken algal thalli with some small foraminifera and Tuberitinidae. Calcimicrobial tubes are present as small sheets, clumps and as encrusting envelopes upon bioclasts. Very fine grained sparitic cement is present in pores between micrite peloids and bioclasts, a small amount of fibrous marine cement is present in the few larger cavities. A fragment of the red algae *Fourstonella* (= *Eflugelia*) is found within these samples. The foraminifera *Tetrataxis* is observed attached to a reworked mud chip, it is likely that the foraminifera was attached previous to reworking, the fact it was attached has likely helped to preserve the clast to which it is attached to. These samples have a relatively high biodiversity and preservation is good. **SMF 16-Non-Laminated.** *Fine-grained, bioclastic, peloidal grainstone.* This sample is characterised by non-laminated peloidal micrite and broken bioclasts (Fig. 4.15).

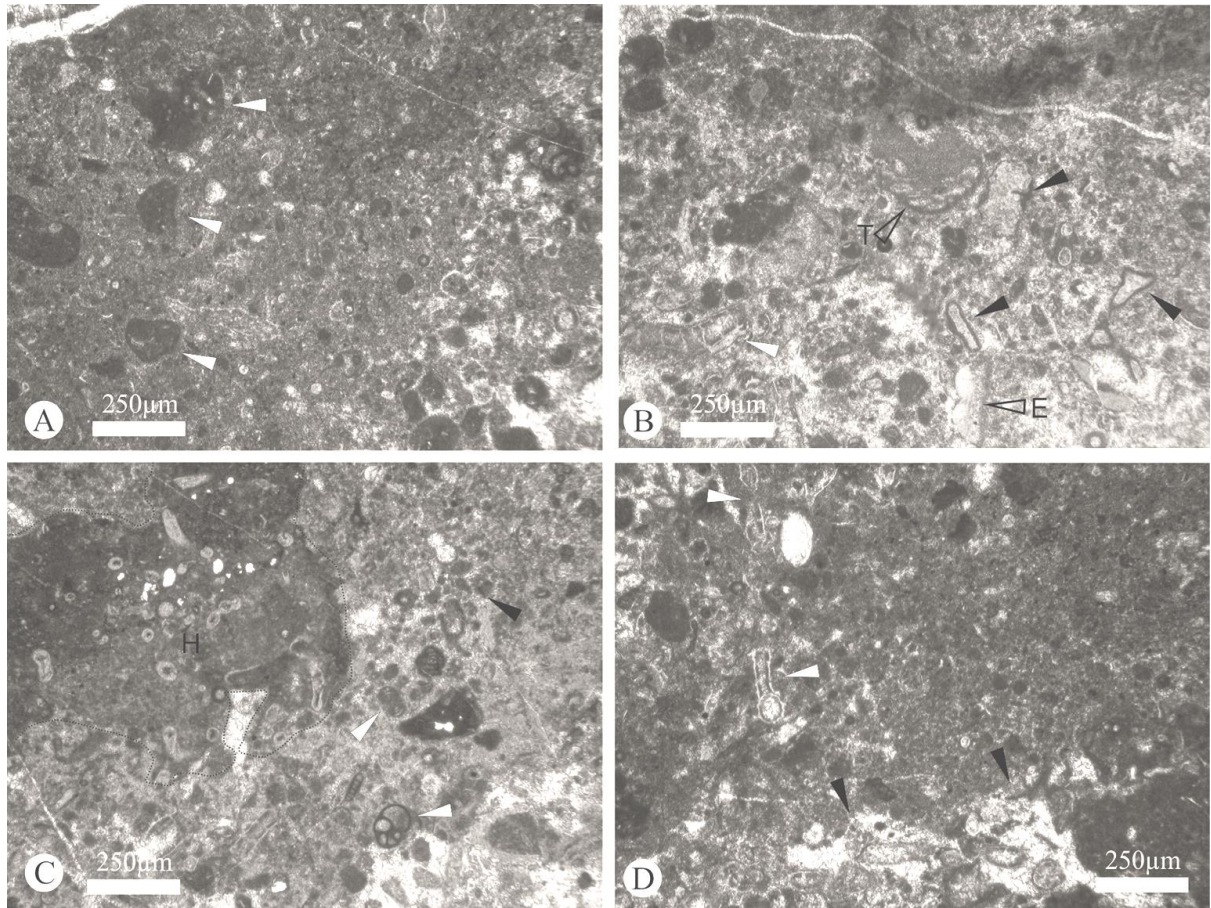


FIGURE - 4.12

A. (CAN 22) Non-laminated, variously sized peloids and rounded mud chips (white arrows). Several mud chips include tubular features which may be calcimicrobial in origin, see the chip indicated by the top arrow. Peloids are generally surrounded by homogenous micrite, note the sparry cement toward the bottom right corner.

B. (CAN 22) A photomicrograph showing peloids and bioclasts within a sparry cement. The micrite has a more clotted texture toward the top of the image. Bioclasts consist of worn and broken fragments of Donezella (white arrows), foraminifera including *Tetrataxis* (T), several recrystallised bioclasts with micritic envelopes which morphologically resemble algae (black arrows) and the red algae *Fourstonella johnsoni* (E) with the characteristic thin rows of quadratic cells.

C. (CAN 22) Homogenous micrite can be seen concentrated around algal thalli which most resemble *Petschornia*. (H and dotted outline). Several foraminifera are found (white arrows) associated with peloidal sediment (P) and sparry cement.

D. (CAN 22) Broken Donezella thalli (white arrows) with a peloidal sediment. Black arrows indicate a small fenestral cavity, some sparry cement can be observed within the peloidal sediments.

4.1.4 Interpretation

The basal facies is characterised by well-preserved, dense thickets of *Donezella* and *Beresella*, which were common in Bashkirian and Moscovian age carbonates. These carbonates typically occur as low-relief mounds or banks within marine lagoonal settings (Flügel, 2004). Cortoids and cyanoliths suggest a shallow subtidal back-reef environment - in the geological setting of these sediments (i.e. a foreland basin) it is envisaged that a tectonic structure (e.g. a blind thrust or the forebulge) may act as a barrier in the place of a 'traditional' reef. The Barcalienta and Valdeteja Formations (which were deposited to the north of the San Emiliano Fm.) may also have acted as a barrier. Behind these a lagoonal (or lagoon-like) environment is interpreted to have formed. The low-diversity of the microfacies would suggest a relatively stressed environment, the high number of algae and little else may suggest either a high saline or brackish environment. Although rare, the occurrence of attached *Tetrataxis* is further evidence for a stressed environment (Cossey and Mundy, 1990). The low diversity and simple nature of the taxa observed may indicate a pioneer community. The biological niche the organisms have filled is certainly newly opened – as evident in the shift in lithology (from clastic dominated to carbonate dominated). The standard microfacies interpretation (SMF – 7 for sample 1 and SMF – 18 for samples 2 – 4) indicate a change in environmental conditions, most likely a shift from mid/inner ramp to a restricted inner ramp/platform position (relative sea level fall).

The light colour of the mound (when compared to the darker basal beds) may indicate a lower TOC value, perhaps alluding to a shorter formation period. The shape of the mound doesn't suggest any asymmetry and the boundary between mound and bedded units is sharp, with some overlapping beds - this may also indicate that the mound accumulated faster than the surrounding capping and basal facies. The mound facies is dominated by various packstones, containing mostly Donezelliaceans. Throughout the mound facies, fenestral cavities are observed as well as several stromatolite cavity networks. Peloidal micrite and homogenous micrite are more common than in the basal beds, and in some cases are the major constituents. Much of the peloidal micrite is non-laminated and appears as clotted growths and other "shrub" like forms. The presence of what is

quite possibly a calcified filamentous cyanobacterial sheath suggests that peloids are possibly micritised remains of these and of the calcareous algae. Homogenous micrite is often in association with faint thrombolytic textures, perhaps hinting at a microbial or algal origin. The heterolithic nature of this facies indicates a considerable variation in current flow, energy conditions and sea levels during the deposition of the mud mounds. The biota associated with this facies remains mostly the same and is dominated by non-complex alga and encrusting cyanobacterial forms. This association of biota suggest a restricted, shallow, low energy environment, which, although showing evidence for changing conditions and some higher energy events remains restricted, shallow and dominantly low energy throughout the deposition of the mounds.

The capping facies consists of three distinct lithologies, a packstone characterised by its lithoclastic component in addition to its bioclastic component which is found 'draped' over the Candemuela Mound. Above that is a wacke- packstone with accessory bioclasts which include taxa typical of metazoan dominated carbonates. The last distinct lithology is a peloidal grainstone. This microfacies is similar to that observed for samples 13, 14 and 16 within the mound facies. This sequence is interpreted to represent a relative change in sea level and energy. The relatively large, reworked and broken bioclasts within the unit draped over the mound, plus the presence of increased clastics indicate a higher energy depositional environment than that of the mound. Some imbrication of bioclasts and lamination is evident, suggesting stronger current activity. The second unit sees a return to dominant carbonate deposition with peloidal and homogenous micrite, transported bioclasts are present and several foraminifera not observed in other samples are apparent, as are some poorly developed laminae. This is interpreted to represent lower energy conditions but still relatively deep (compared to the mounds depositional environment). The occurrence of several different foraminifera, bryozoans and more *Tuberitina* may indicate the environment is becoming less restricted and more open. The final carbonate unit consists of non-laminated peloids with a similar biota to the previous unit, rounded mud chips and peloids are common which suggests the reworking of the carbonate sediments and implies a shallow depth.

Within all three of these capping units *Donezelloids* are absent or found as broken and transported clasts. With the occurrence of a similar biological community with the presence of mud chips it is envisaged that the depositional depth of the last unit was similar to the depth of mound formation or slightly deeper, but with a higher energy level. The higher energy may be a result of the environment becoming more open, making it difficult for the algae to establish and grow into shrub like thickets. The mound is thought to have been smothered by the draping unit as a result of an increase of clastic material to the basin as a result of thrust propagation. The bedded units on top of the mound indicate a relative sea-level rise; this is interpreted to be flexure related basin subsidence.

The changes in microfacies throughout the mound suggest a steady sea level rise throughout deposition. The basal mound samples (5, 7, 6a and 10) commonly have well preserved algal thickets and stromatolite cavities possibly indicating a very shallow environment (although stromatolite cavities are known to have formed from a wide variety of depths (e.g. Bathurst 1980 and 1982)). The dominance of *Donezelloids* then decreases with more homogenous and peloidal sediments being observed within samples 6, 8, 9, 11, 12 and 18 (sample 18 represents sea level fluctuation post mound smothering). These samples indicate a slightly deeper environment. Finally the mound (samples 13, 14, 16, 17 and 19) shows increased evidence of deepening, including re-worked bioclasts, mud chips and some imbricated material and poorly developed laminae suggesting transportation. The presence of stromatolite and fenestral cavities with internal early marine cement implies that there was constant movement of water through the carbonates when they were partially lithified, which would suggest the presence of a current or wave activity.. The peloids, bioclasts, microfossils and cavities show little sign of compression, which may indicate an early lithification which occurred before younger sediments were deposited on top and could compress the sediments. Miliolinid foraminifers observed may indicate a saline environment. Table 4.1 summarises the microfacies analysis of the Candemuela Mound.

Samples	SMF	Characteristics	Interpretation
1 (basal)	7-Bafflestone	Algal bafflestone. <i>In situ</i> growth of <i>Donezellaceans</i> with baffled sediments and cyanoliths.	Shallow depth, restricted environment. Below wave base.
2, 3 and 4 (basal)	18-Dasy	Dasyclad grainstone. Intertwined algal thalli with peloidal sediments.	Shallow depth, restricted environment. Below wave base.
5, 7 and 10 (mound)	10	Bioclastic packstone. Worn and broken thalli. Peloidal sediments and stromatactoid cavities.	Very shallow depth, restricted environment, within wave base. Low - moderate energy, lagoonal environment.
6a (mound)	21-Fen	Fenestral packstone. Fenestral cavities, pelmicritic sediments and dasyclad bafflers.	Very shallow depth, restricted environment, within wave base – Low - moderate energy, lagoonal environment.
6, 8 and 11 (mound)	23 intercalated with 8	Non-laminated, fine-grained peloidal micrite. Bioclastic floatstone. Whole fossil algal thalli framed in micrite.	Shallow depth, restricted, protected environment. Below wave base.
9, 12 and 18 (mound)	10	Bioclastic packstone characterised by an abundance of whole fossil and broken algal thalli with homogenous micritic sediment.	Shallow depth, restricted, protected environment, within wave base. Low - moderate energy, lagoonal environment.
13, 14 and 16 (mound)	23 intercalated with 16-	Non-laminated homogenous micrite with few bioclasts. Fine-	Heterolithic unit representing energy

	laminated	grained peloidal packstone.	fluctuations within a moderate depth, restricted, protected environment. Below wave base.
17 and 19 (mound)	18-Dasy	Bioclastic packstone. Whole and broken Donezellacea with homogenous micrite including mud chips.	Shallow depth, restricted, protected environment. Below wave base.
15 (capping)	4	Bioclastic-lithoclastic packstone. Transported bioclasts, organic fragments and quartz grains.	Moderate depth, moderate energy. Influx of sediment from hinterland. Below wave base.
20 and 21 (capping)	5	Reef derived bioclastic wacke-/packstone.	Moderate/low depth, low energy, non-restricted environment. Below wave base.
22 (capping)	16-non-laminated	Fine-grained, bioclastic, peloidal grainstone. Bioclasts are worn. High biodiversity.	Moderate/low depth, open, low energy environment. Below wave base.

TABLE - 4.1 Summary of the main standard microfacies, characteristics and interpretations for the Candemuela Mound.

4.2 Unit 8

29T 737976.62 4761190.87 to 29T 744167.29 4763054.05

Unit 8 is the top most carbonate unit within the La Majúa Member. It can be traced from just south of the village of Robledo de Babia (Fig. 1.1), where it appears as isolated mounds with a clastic inter-mound fill, rare conglomerate lenses can be observed within the mounds to the west of the outcrop. The conglomerates are para-polymictic with clasts consisting of well rounded quartz and lithic cobbles. As one traces the unit towards the east, mound bearing limestones become more predominant than bedded limestones. The unit is mostly formed of the latter association of a bedded facies with mounds. Carbonate mud mounds appear as “featureless” structures and can be observed across the entire unit. Mounds range from two to several tens of metres in thickness. Mounds are lens and mound shaped and occur both as isolated buildups and as superimposed complexes. Using the standard microfacies observed within the Candemuela section to indicate the facies a sample belongs to, combined with field observations, data from Unit 8 can be used to show mound distribution laterally across the exposed strata. Generally two types of limestone were observed in the field, these consisted of bedded, blue/grey lime mudstone with some macrofossils visible. These often exhibited a gassy odour. The second type consisted of a lighter, creamy grey micrite which often had no observable features and could be seen to have a domal geometry at outcrop. From Figures 4.13, 4.14 and 4.15 it is possible to see the relationship between bedded and mound carbonates across a section of Unit 8. Figure 4.13 is a sketch of the beginning of the laterally persistent unit with several isolated mounds in the foreground. Figures 4.14 and 4.15 show 850 m of the best exposed section of the unit from west to east. The mounds have microfacies the same as those described for the Candemuela Mound whereas the bedded material shows similarities to off mound (basal and capping) facies described from the Candemuela Mound and those from elsewhere. Across the Unit a basal, mound and capping facies can be observed within field sketches taken. The basal facies consists of planar beds with mounds sat conformably above. The capping facies also consists of bedded carbonates but these can often

be seen lapping onto mounds. Mound carbonates are generally bioclastic packstones consisting of low biologically diverse (microscopic) assemblages with *Donezella*, laminar encrusting forams, cyanobacteria and calcimicrobes being the dominant biotas. Peloidal and homogenous micrites are common within mounds and often form non-laminated accumulations. Cavities are present and are mostly of the 'constructed' variety - the cavities being directly formed by biota, however, some well-developed stromatactis cavities are also present in some samples. The bedded material contains a more diverse biological assemblage, with larger bioclasts present (e.g. gastropods which are over 1 mm in size). Bioclasts often show evidence of transportation and are often abraded or broken. A micritic envelope covering the grains is often present.

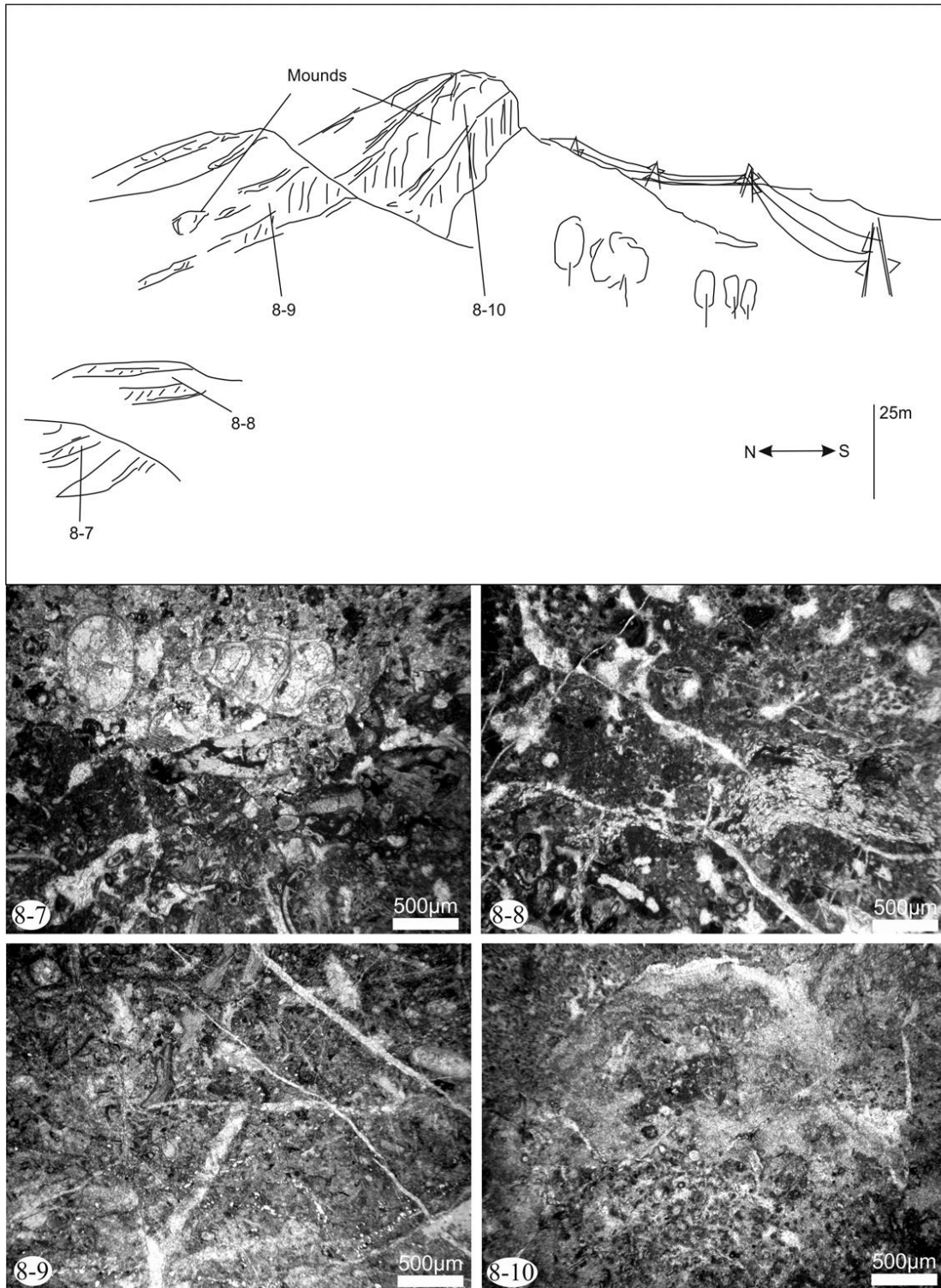


FIGURE - 4.13 A field sketch with sample locations annotated, photomicrographs correspond to the numbers indicated. 8-8 and 8-10 represent mound facies whilst 8-7 and 8-10 represent bedded carbonates. Within 8-8 and 8-10 a biological component is recognisable, notable are the domal cyanobacterial/calcimicrobe growths which along with *Donezella* form packstones with some bind/bafflestone qualities.

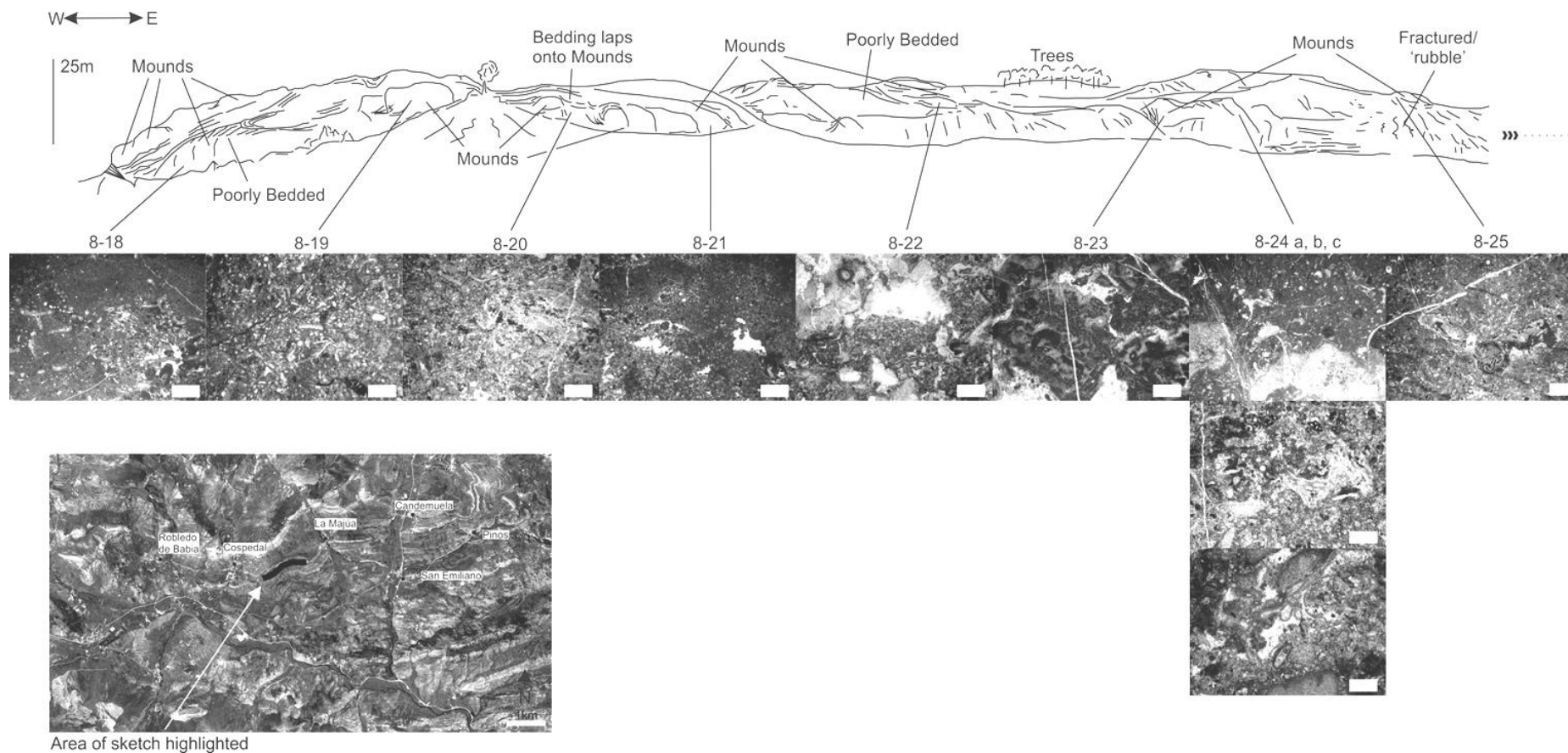


FIGURE - 4.14

The first half of a field sketch along a well exposed section of the eighth carbonate unit (unit 8). Photomicrographs correspond to indicated sample locations, from photomicrographs facies which correspond to the mound and off mound facies identified for the Candemuela Mound. The mounds are of the same composition and can be seen to have formed across the unit. Generally the mounds are found with around a metre of bedded limestones below and often several metres above (similar to the Candemuela mound).

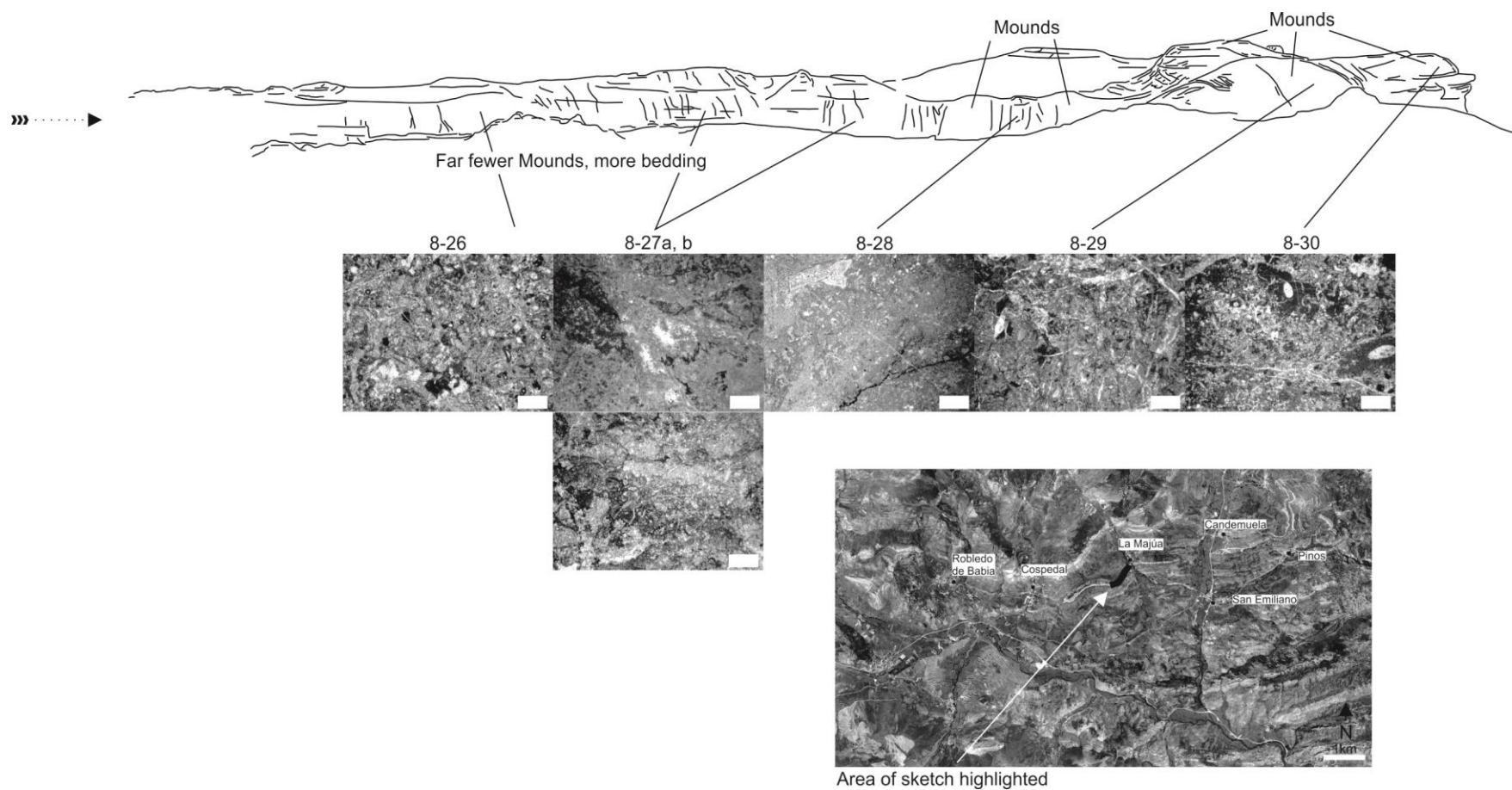


FIGURE - 4.15

The second half of a field sketch along Unit 8 (slightly northeast of Fig. 14.14), the unit shows slightly more bedded carbonates and fewer mounds which suggests that mound formation was not uniform across the unit.

4.2.1 Interpretation

Across Unit 8 it is evident that features which resemble mounds in the field (i.e. mound geometry and lacking of primary geological features such as bedding) are indeed carbonate mud mounds which are primary mounds and not diagenetic in origin. The variation of distribution across the Unit suggests that local conditions across the unit changed, with a probable change in water depth, the more bedded carbonates representing a shallower depth than that which the mounds were formed in. It is interesting to note that sections which contain mounds have a similar vertical profile to that of the well exposed Candemuela Mound, the profile being a mound (of various thicknesses, ranging from a few to 50 m) sitting atop of around a metre of bedded carbonates and being capped by bedded carbonates which lap onto and cover the mounds. This suggests that across the basin, mounds began to nucleate and grow at a similar time, the various thickness of mounds may suggest varying success rates of individual mounds which then get capped by bedded carbonates at the same time across the basin. This is interpreted to represent basin wide sea level variation, the mounds representing a transgressive event. Individual mounds do not show any evidence of asymmetry, preferred orientation or thickness changes. This may suggest that currents were not a strong control on the geometry of the mounds.

4.3 Pinos Hairpin Limestone

30T 257750.58 4763450.38

The Pinos Hairpin Limestone (Fig. 4.16) is located on a hairpin bend on the track out east of Pinos (Fig. 1.1). The limestones form part of the fourth major limestone unit within the La Majúa Member. Although no mounds are present in this section and no mounds have been observed along this horizon in this study it is an important lithology. A comparison is made with those units which do exhibit mounds as the carbonates observed here represent a different environment of deposition than those with mounds. The outcrop is 5 m thick and consists of cyclic beds of 'phylloid' dominated floatstones and marls (Fig 4.16). The contact between the limestone and the

marl beds is general sharp, however, in places the contact appears transitional. The samples are dark grey to black in colour and have a gassy smell when broken open, both indicative of high organic carbon concentration. 'Phylloid' algae appear as laminar sheet, to cup and bowl like structures, often in association with tube like structures growing perpendicularly to their upper surface. Solitary rugose corals can be observed, several specimens are observed to be overgrown by the 'phylloid' algae. Brachiopods and gastropods are also present. Within the Pinos Hairpin Limestone five sub-facies have been identified each of which represents a different biological community, clastic component and most likely, relative sea level. The five sub-facies identified are based mainly upon the dominance of one or more biota, the matrix material is quite homogenous throughout the facies. The sub-facies identified are: 1] bioclastic packstone (high diversity), 2] microbial and algal baffle/boundstone, 3a] *Donezella* boundstone, 3b] *Donezella* bafflestone, 4] *Petschoria* and 'phylloid' algal bafflestone and 5] Whole fossil wackestone (with dominant 'phylloid' algae).

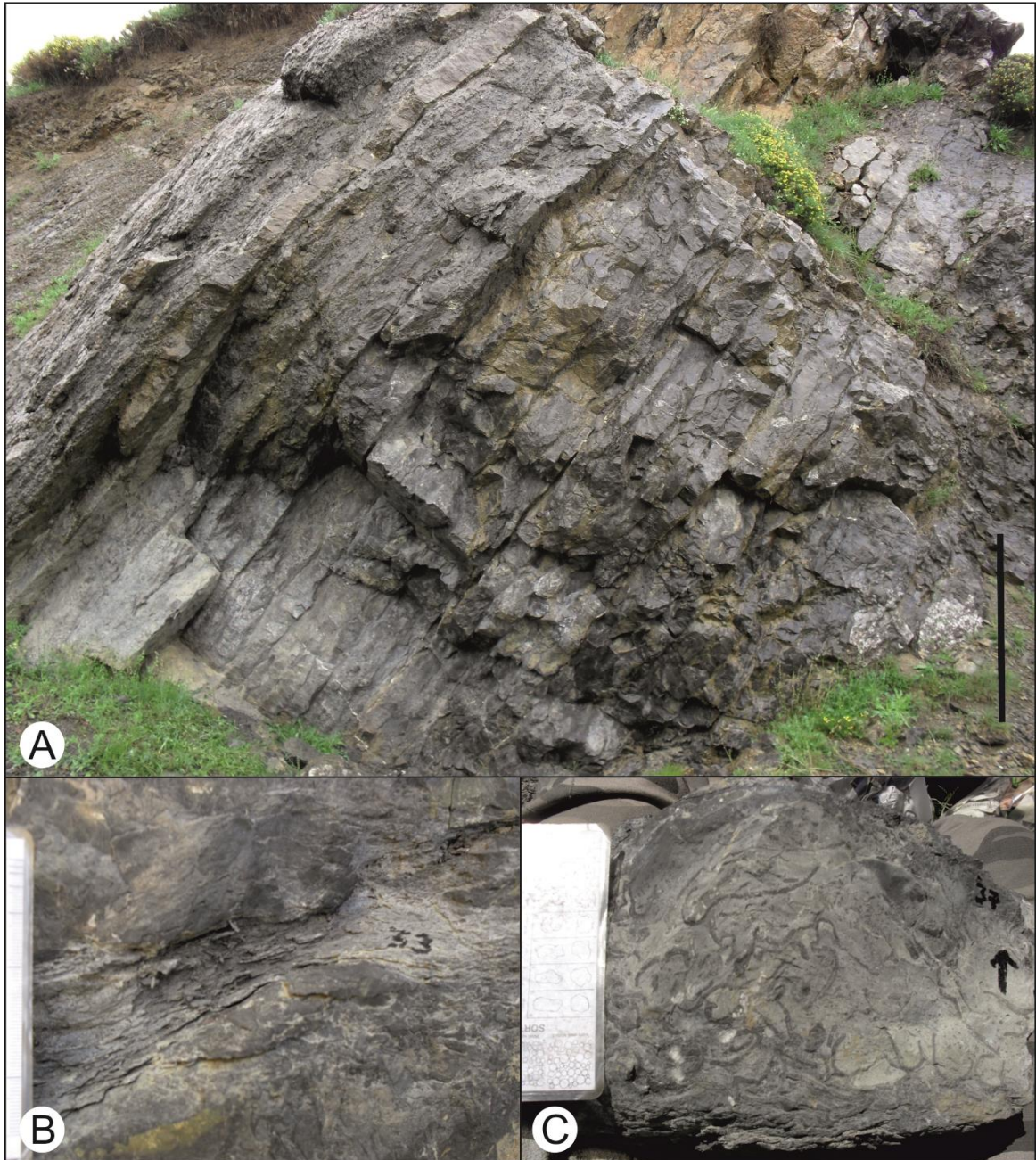


Figure 4.16. A. A photo of the outcrop sampled at the Pinos Hairpin. Scale bar = 1 m. B. and C. Examples of typical beds found, B. shows a marl interbedded with limestone, the contact between the marls and corresponding limestone is usually sharp. C. Within the limestone beds well preserved 'phylloid' algae are commonly cyathiform (cup-shaped) or leaf-like in shape. Grainsize chart = 10 cm.

Sub-facies one is representative of **samples PHL 1, 10, 11, 12, 19, 21, 24, 25, 26, 34, 35, 37, 39, 42, 48, 50 and 58**. The sub-facies consists of well-preserved whole and broken fossils of both sessile and mobile biota with a mostly homogenous micrite and microcrystalline quartz matrix. Cavity networks are rare but can be found in association with some of the encrusting and baffling elements. The diversity within this sub-facies is relatively high with foraminifera, gastropods,

Tuberitina and various algae and encrusting microbial forms present. Identifiable algae include the algae *Ungdarella*, *Donezella* (see chapter 6. *Palaeontology* below for details of the classification of *Donezella* within the red algae) and *Archaeolithophyllum* which is well-preserved in these samples. Other, probably Dasycladacean algae are also present. Encrusting forms are observed as both laminar sheets and undulose growths often associated with a substrate including the surfaces of other biota. The majority of bioclasts are found as whole fossils and show evidence of *in situ* growth, however a small amount of bioclasts appear broken, especially *Donezella* thalli. Broken clasts do not show evidence of abrasion or of any micritic envelopes or other encrustations. The matrix is generally a homogenous micrite with occasional lenses and laminations of microcrystalline quartz, this quartz fraction can be clearly seen to be more abundant in association with the growth of laminar ‘phylloid’ algae thalli. Cavities, where present, are birds-eye to fenestral in geometry with a clear, blocky calcite fill. The cavities appear to be directly linked to the biota surrounding them, several cavities have an internal sedimentary fill consisting of peloidal micrite. **SMF 8.** *Whole fossil wackestone with bioclastic packstones.* This is characterised by predominantly sessile organisms within a homogenous micrite with some small mobile forms and a minor detrital quartz component (Fig. 4.17).

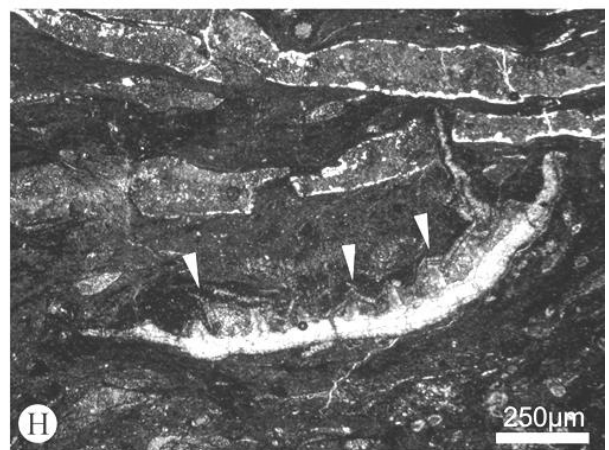
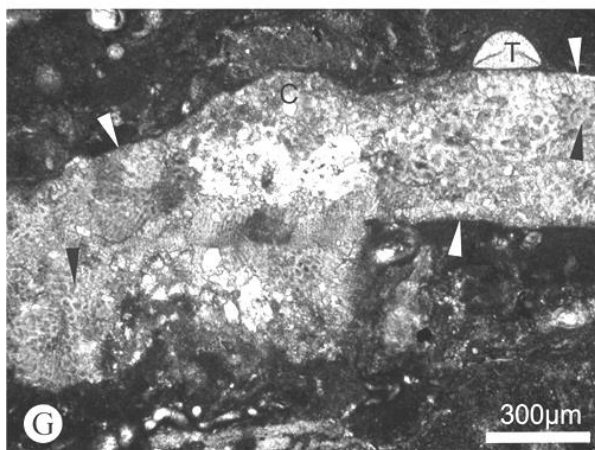
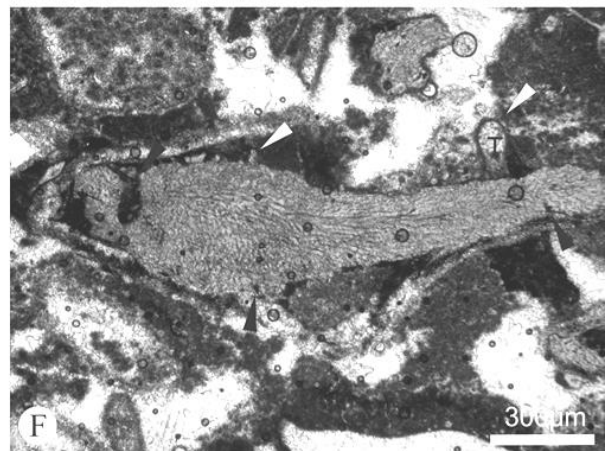
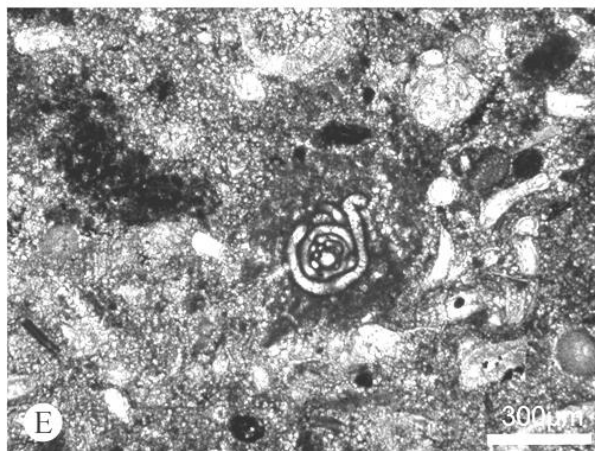
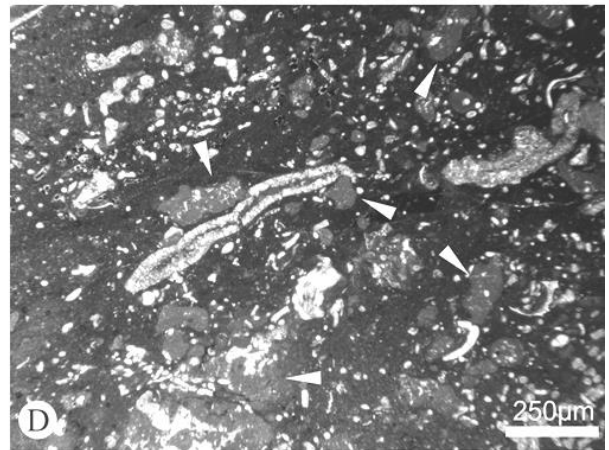
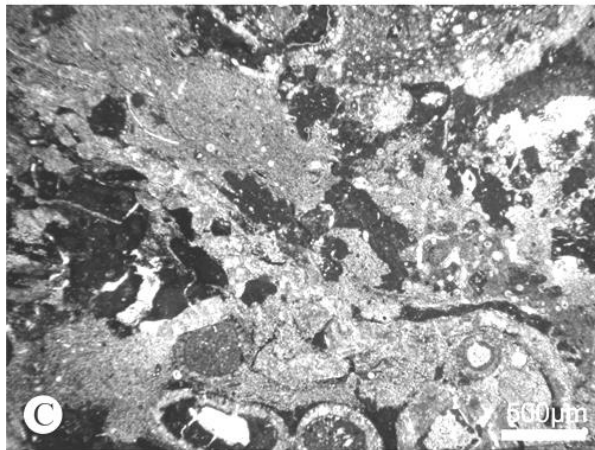
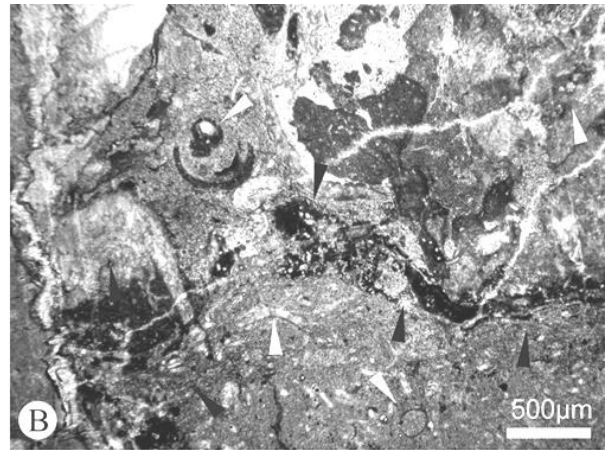
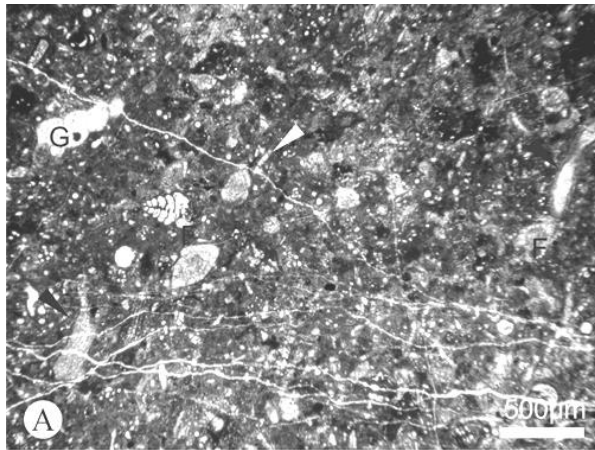


FIGURE - 4.17

A. (PHL 1) An overview image of various biota observed within sub-facies 1 including foraminifera (F), gastropods (G), red algae (black arrow) and *Donezella* (white arrows). The bioclasts are observed 'suspended' within a framework of sessile algae and homogenous micritic sediments.

B. (PHL 37) A photomicrograph of the encrusting component of this facies. Laminations of encrusting biota can be clearly seen (black arrows). Homogenous micrite can be seen baffled by the encrusters whilst a matrix dominated by microspar and microcrystalline quartz dominates the rest of the image. Several bioclasts can be observed (white arrows). An upwards growing feature which shows branching with a thrombotic texture is observable and may be the result of calcimicrobial growth (CM).

C. (PHL 39) Here the relationship between the biotas seen in A and B can be observed.

D. (PHL 58) Parts of this sub-facies contain a more sparse distribution of bioclasts and a higher sediment component. Here the nature of the homogenous micrite can be observed as well as several irregular inclusions of microspar (white arrows), which are rounded and may represent mud chips reworked and transported from elsewhere.

E. (PHL 19) A foraminifera consisting of small spherical proloculus with a tubular, coiled outer chamber. Possibly *Calcitornella*.

F. (PHL 24) A well preserved specimen of the *Ungdarella* algae. The characteristic long thin rows of quadratic to rectangular cells can be observed. This specimen has been encrusted by various forms (white arrows) including a *Tuberitina* (T). The specimen also shows evidence of boring and possibly a very thin micritic envelope (black arrows). Several fenestral cavities with either a clear, blocky cement or peloidal micrite surround the *Ungdarella* thallus.

G. (PHL 42) Cross-section through a specimen of *Archaeolithophyllum*. A distinct hypothallus (HT) and perithallus (white arrows) can be observed, the bioclast is a honey colour. The hypothallus consists of polygonal cells (black arrow) forming crustose multi-foliate sheets of differentiated cells. The perithallus is mostly recrystallised but preserved sections of wall perpendicular laminae can be observed (black arrows). A conceptacle may be present (C). Note the attached *Tuberitina* (T). The matrix is homogenous micrite with *Donezella thalli* present.

H. (PHL 50) Cross-section through *Archaeolithophyllum* with some polygonal hypothallus cells preserved. The white bioclast is a thick walled encrusting bryozoan with upward growing zooecia (white arrows)

Samples **2, 6, 9, 13, 14, 15, 16, 17, 25, 27, 29** and **38** are representative of sub-facies two, a microbial and algal baffle/boundstone. The major components of this sub-facies are encrusting calcimicrobes and encrusters in association with gregarious sessile organisms. The sedimentary matrix consists of homogenous micrite and some microspars. Homogenous micrite is more commonly found where baffling organisms are present. Encrusters are abundant and are usually found in consecutive laminar and undulose layers of organisms and dark homogenous micrite

which contort to conform to the subjacent hard ground, which is usually in the form of a bioclast or lens of bioclastic/microspar grainstone. Stromatoporoids are observed and appear to be overgrown by chaetetid sponges. The calcimicrobe *Rothpletzella* and algae *incertae sedis* *Claracrusta* are dominant, some *Girvanella* is present as are small communities of *Archaeolithoporella* and *Wetheredella*. The microscopic encrusting communities are found as either a direct encruster of bioclasts or as cavity fills within what were presumably cryptic cavities. The red alga *Ungdarella* is found as whole, branching growths. Thick walled encrusting auloporid corals are also present. *Donezella* occurs in small isolated growths and is found with baffled homogenous micrite and bird-eye and fenestral cavities between the entwined, barrel like thalli. The sedimentary matrix is a homogenous micrite where organic baffling takes place. This sub-facies has a high diversity of encrusting and baffling organisms, with an apparent absence of mobile and free floating biota. The upright and columnar growth of several biota provided a biological framework in which encrusters have baffled sediments. Preservation of microscopic calcitic tubes is high and most likely related to the homogenous micrite matrix. A problematic structure consisting of brown to honey coloured spheres (10-50 µm) with internally radial crystals is found within a cryptic cavity with some internal cavity fill of peloidal micrite, it is possible that this is spherulitic precipitated carbonate (Fig. 4.19 C). **SMF 7-Framestone/Bafflestone. Organic boundstone.** These samples are characterised by the coupled upward growth of an organic framework and the baffling of homogenous sediment within a framework of encrusting forms (Fig. 4.18 and Fig. 4.19).

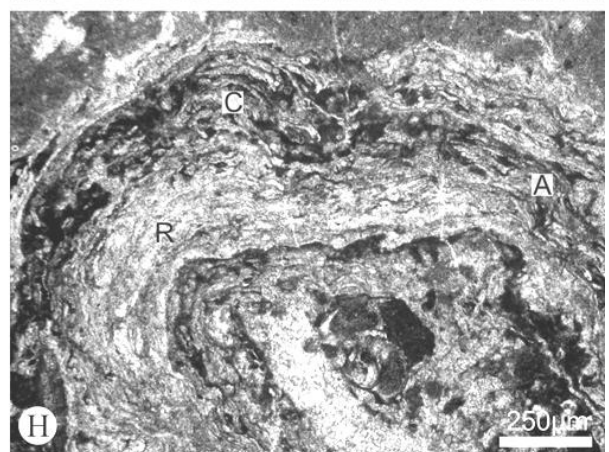
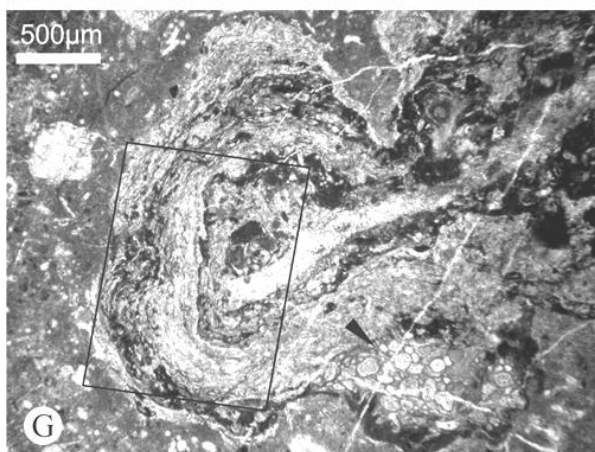
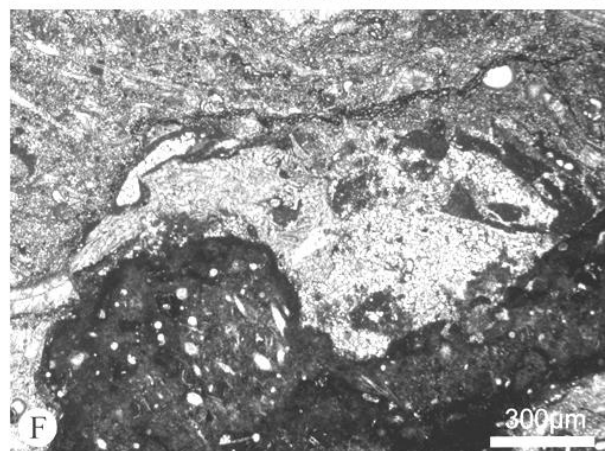
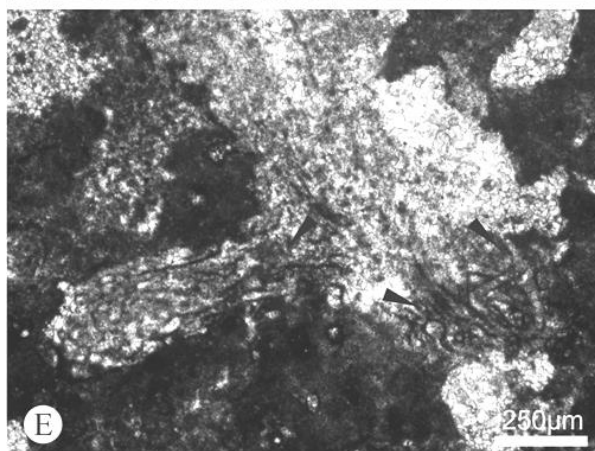
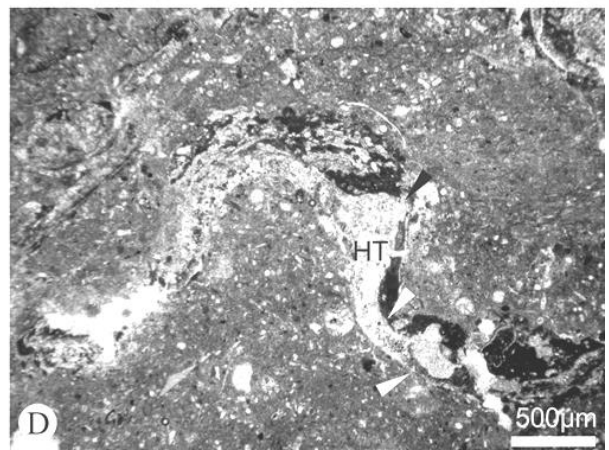
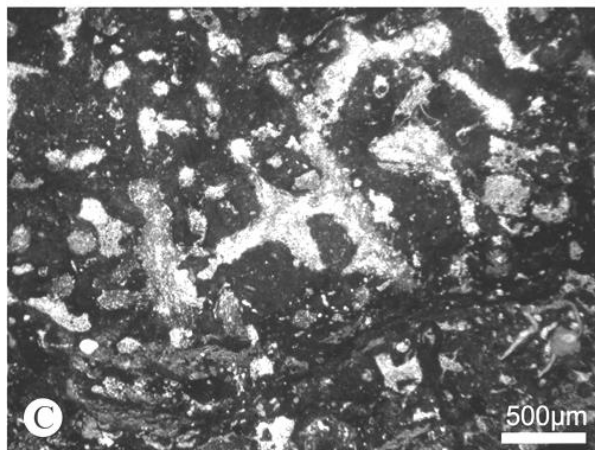
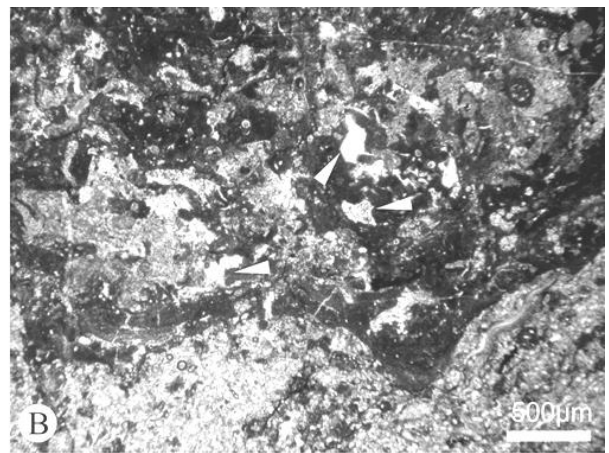
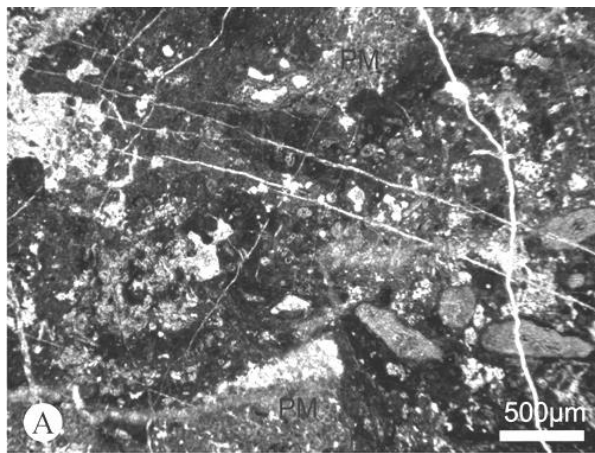


FIGURE 4.18

A. (PHL 2) *Ungdarella* and *Donezella* are the major frame builders present in this image. A homogenous micrite with some rare peloidal micrite (PM) can be observed to make up the sedimentary matrix.

B. (PHL 9) A large number of encrusting forms can be seen in this image, often baffling homogenous micrite. Evidence for encrusters is generally laminations of light coloured sheets of rounded and tube like laminae often with a morphology which generally reflects the shape of the subjacent material to which it is attached. Several small birds-eye cavities can be observed (white arrows).

C. (PHL 14) A curious quadratic framework with a homogenous micrite sedimentary matrix. This structure is likely to be the cast of a sponge, where the soft organic material has decayed but the morphology of the pore structure has been preserved by *Girvanella*, which occupied the cavity.

D. (PHL 27) A specimen of *Archaeolithophyllum* which has been extensively encrusted, polygonal cells of the hypothallus (HT) and the perithallus (white arrows) can still be recognised. Note the steep sided conceptacle on the upper side of the thallus (black arrow).

E. (PHL 17) A close-up of the area highlighted in C. here the internal structure of the quadratic growth form can be observed and it consists of contorted and entwined tubes (black arrows) with some evidence for branching. The structure greatly resembles *Girvanella*. Due to the quadratic growth form this may represent a cavity left as the result of the decay of a soft bodied organism (possibly a sponge) with *Girvanella* then proceeding to colonise the cryptic cavity.

F. (PHL 14) In this photomicrograph a clear distinction between the darker homogenous micrite and matrix containing microcrystalline quartz and some microspar is evident. The homogenous micrite contains several tubular and spherical bioclasts which probably acted as bafflers or producers for the micrite. The quartz containing section shows some extent of laminar deposition.

G. (PHL 29) A calcimicrobial community encrusting a 'phylloid' algae thallus. The encrusters comprise of chain-like and branching laminar sheets of bean and sausage shaped cells of *Rothpletzella*, and *Claracrusta*; which grows in sheets that become more undulose with each successive layer. Some *Archaeolithoporella* which is characterised by couples of dark and light laminae is present as are globular, cystose growths which resemble *Wetheredella* (black arrow). Note the dark homogenous micrite which is baffled by the encrusters and compare to the micrite found elsewhere in this specimen.

H. (PHL 29) A close-up of the area highlighted in G. Here the relationship between *Rothpletzella* (R) and *Claracrusta* (C) with the subordinate *Archaeolithoporella* (A) can be seen. *Rothpletzella* has 'chains' of rounded cells which form uniform layers whilst *Claracrusta* can be seen as 'chains' of sausage and bean shaped cells which begin to deviate from the subsurface and become contorted. *Archaeolithoporella* occurs as thin white laminae with a 'coupled' laminar homogenous micrite before the occurrence of the next white laminae.

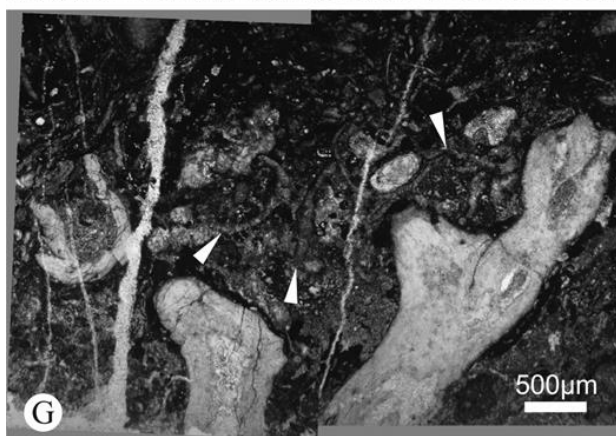
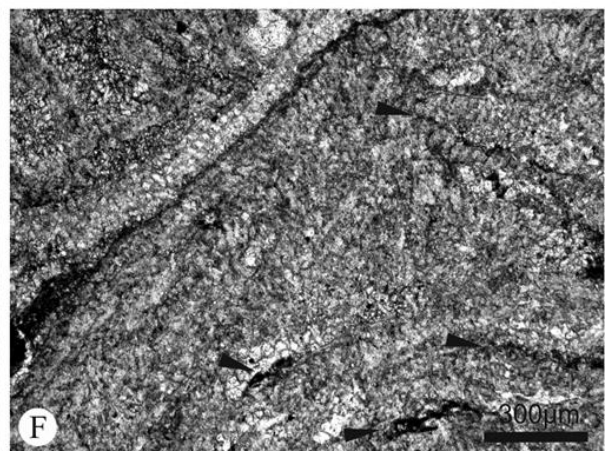
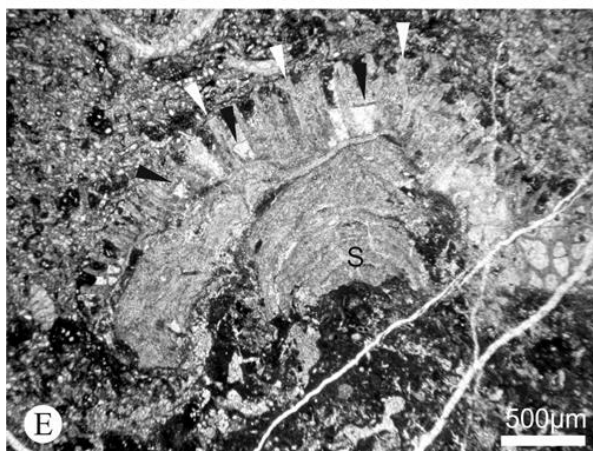
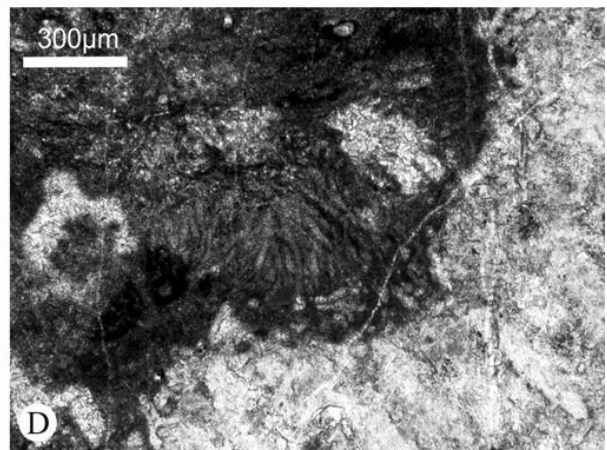
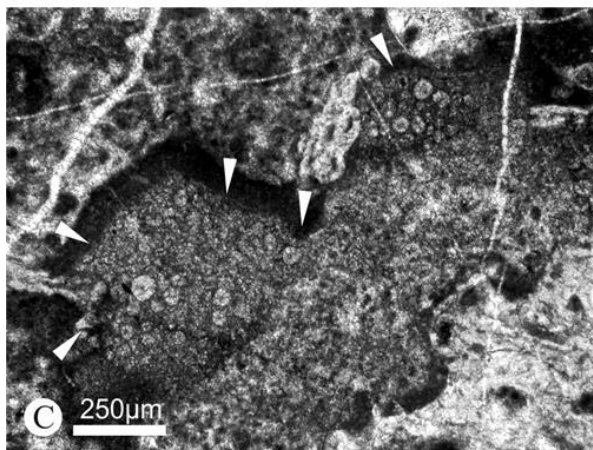
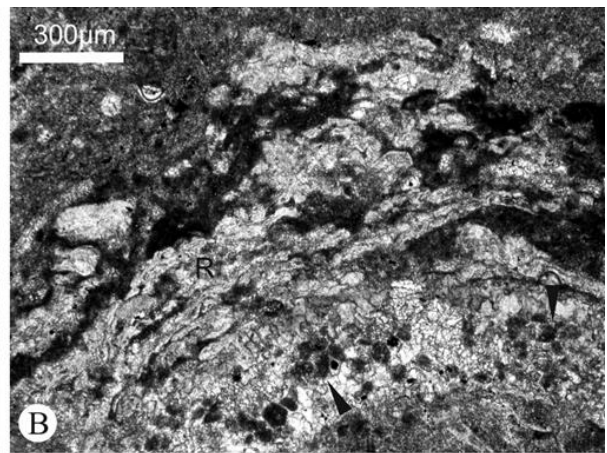
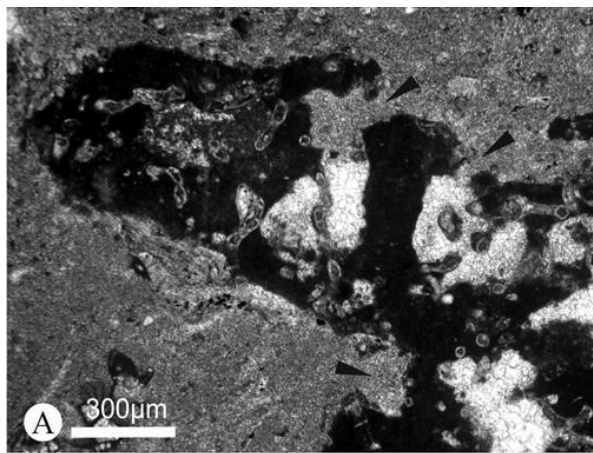


FIGURE - 4.19

A. (PHL 6) *Donezella* forming a framework and baffling, or binding dark homogenous micrite between the thalli. Several cavities can be seen within the *Donezella*/homogenous micrite fraction. These cavities are fenestral and have a clear, blocky cement fill, though microspar can be seen to infiltrate into some of the cavities (black arrows). The other sediment observable here is a microspar with some broken bioclasts.

B. (PHL 27) An excellent example of the encruster *Rothpletzella* (R), sheets of bean like cells laminated on an *Archaeolithophyllum* thallus. The polygonal cells are well preserved in this specimen (black arrows).

C. (PHL 9) An unknown structure, honey coloured spherical growths (10 to 50 μm in diameter) with an internal radial crystal pattern (white arrows). These clumps of spheres are surrounded by a homogenous micrite rim and sit atop of a peloidal micrite. These spheres are reminiscent of bacterially precipitated carbonates, though the size is far too large. These may be carbonate spherulites?

D. (PHL 6) Well preserved *Girvanella* tubes, growing on a coral. The tubes are around 20 μm thick and up to half a millimetre long. The *Girvanella* appears to be growing perpendicular to the substrate.

E. (PHL 9) A stromatoporoid (S) (see F.) which has grown as a columnar stack of horizontally uniform layers each with internal vertical structures. The stromatoporoid is encrusted and overgrown by a chaetetid sponge showing basal budding, the tabula (black arrows) and spicules (white arrows) are clearly visible

F. (PHL 9) A close-up of the area highlighted in E. here the vertical internal structure of the horizontally laminar layers can be seen. The stromatoporoid is a yellow colour. Thin bands of homogenous micrite can be observed between the stacked layers (black arrows).

G. (PHL 13) Thick walled, encrusting auloporid corals. The corals have an upward growth profile. Between the corals thin tube like forms can be observed (white arrows) which appear to branch and baffle the micritic sediments.

Sub-facies three is dominated by Donezellaceans and is further subdivided into sub-facies A (samples 3, 4 and 5) and sub-facies B (samples 7, 8, 18, 36, 40, 41, 43, 44, 45, 46, 53, 54, 55 and 57) due to the distribution of the Donezellaceans. The diversity of both sub-facies is very low with just a few examples of other biota present (rare foraminifera). Sub-facies A is a skeletal-microbial bafflestone consisting of entwined thickets of branching Donezellacean. The algal thalli consist of the characteristic branching, tube like thalli with barrel like segments which are tightly spaced, often with homogenous micrite between them. The preservation of the thalli is not particularly good, though external walls with periodically spaced internal growths perpendicular to the wall forming barrel like segments are identifiable. In some cases the shrub like growth form of the

Donezelleaceans can be seen to form nodular calcite growths where thalli are bio-cemented to each other. Evidence for reworking and abrasion of bioclasts is very rare. Cavities are absent. Sub-facies B is again dominated by the presence of Donezelleaceans, here they form more of a framework where homogenous micrite is baffled between the branching thalli. Birds-eye and fenestral cavities are occasionally present between branching thalli, the geometry of the cavities appears directly controlled by the growth position of the algae. Unlike sub-facies A, sub-facies B contains a component of microcrystalline quartz, this occurs as laminar accumulations as well as lenticular accumulations which have been baffled by the *Donezella*. A sub-quadratic growth pattern can often be observed for Donezelleaceans. Evidence of abrasion and reworking is, like in sub-facies A, low. **SMF 7-Bafflestone.** *Algal bafflestone*. This sub-facies is characterised by the in-situ growth of algae with associated baffled sediments. Note that sub-facies B also has a framework component (sub-facies A, Fig. 4.20, sub-facies B, Fig. 4.21).

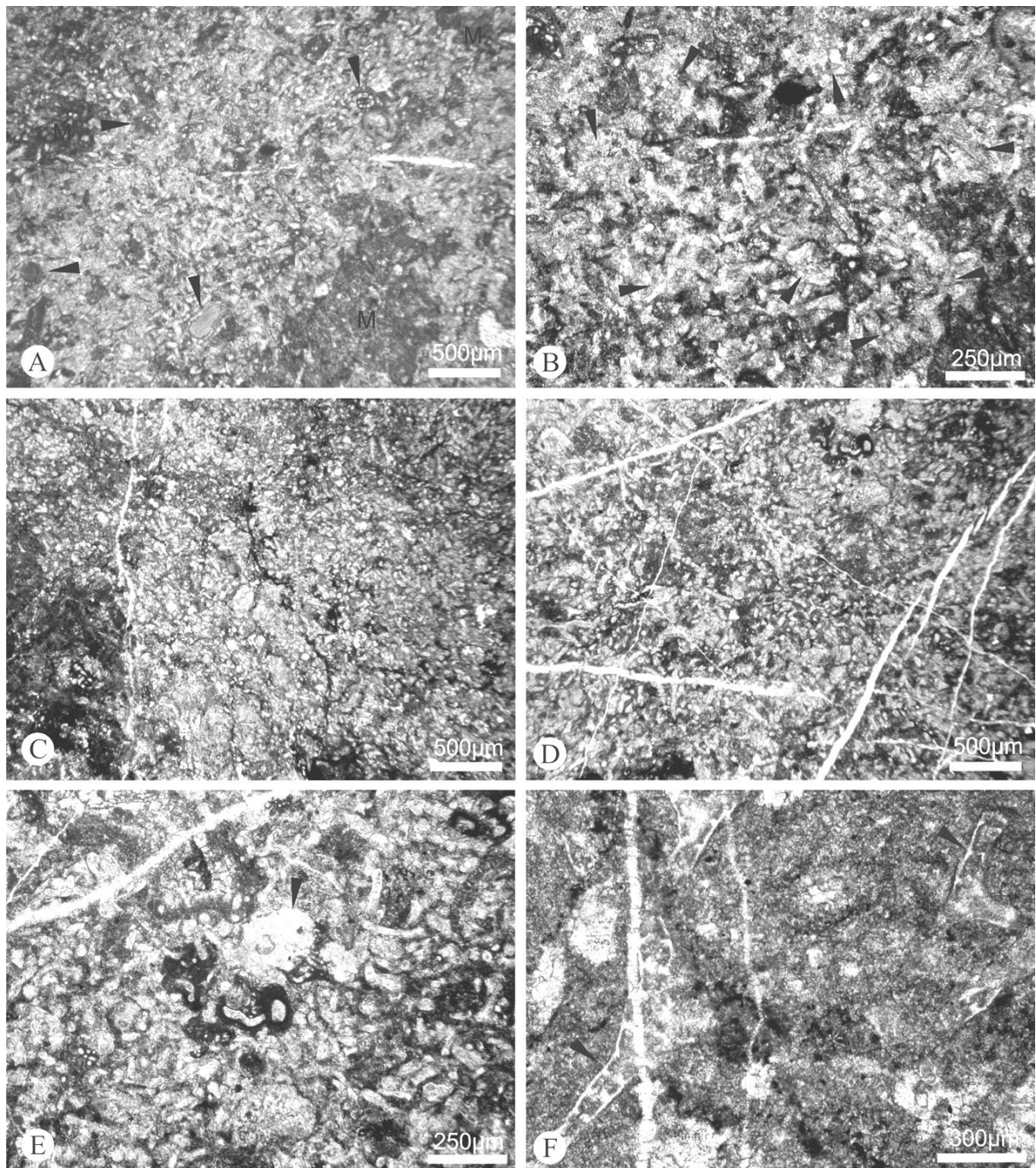


FIGURE - 4.20

A. (PHL 3) Sub-facies A is dominated by entwined and bio-cemented Dorezellaceans. In this overview the dominance of the algae can be observed, some patches of micrite (M) and several mobile organisms can be seen (black arrows) within the mesh of algal thalli. Preservation of the Dorezellaceans varies from completely recrystallised to well preserved thalli. Most of the tube like algal thalli have a thin micritic envelope and any space between thalli is filled with a dark homogenous micrite. Other bioclasts observed include foraminifera, these have been micritised.

B. (PHL 3) Close-up of the area highlighted in A. the relationship between the entwined *Dorezella* and the micritic sediment can be seen more clearly. Around some thalli, particularly ones which are entwined around others, a microspar coating can be observed (black arrows) this may be the

result of bio-cementation of the algal thalli, with the dark homogenous micrite being baffled by the branching and bush like *Donezella* growths.

C. (PHL 4) A photomicrograph showing the slightly nodular effect found within some of the larger *Donezella* thickets. The 'nodules' are formed of *Donezella* thalli with microspar cements and are possibly the result of greater carbonate precipitation occurring around the entwined *Donezella*.

D. (PHL 5) An overview of branching Donezellaceans with baffled dark homogenous micrite, again the dominance of the *Donezella* can be seen.

E. (PHL 5) A fragment of what is probably ancestral coralline red algae (black arrow) can be observed in this image. Note the micritic coating around several of the bioclasts where a cavity between algal thalli occurs.

F. (PHL 4) Here the wall structure and segmentation of the algae can be seen (black arrows), these particular specimens show the characteristic construction of *Donezella lutugini* Maslov.

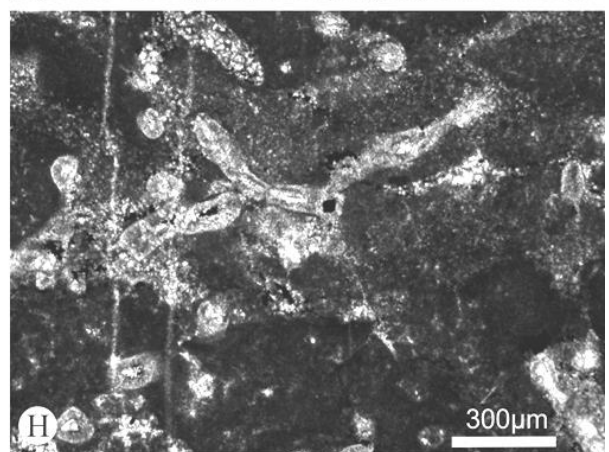
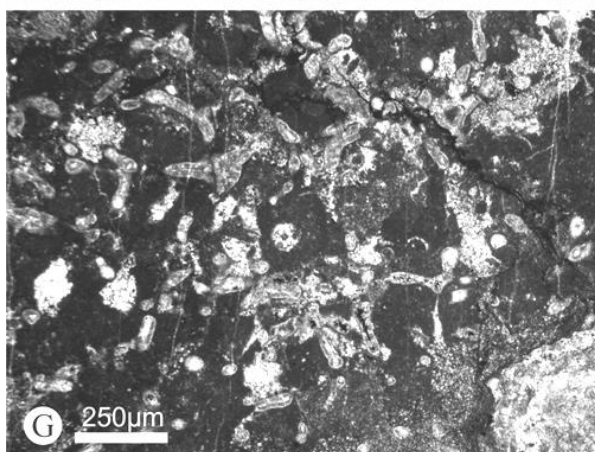
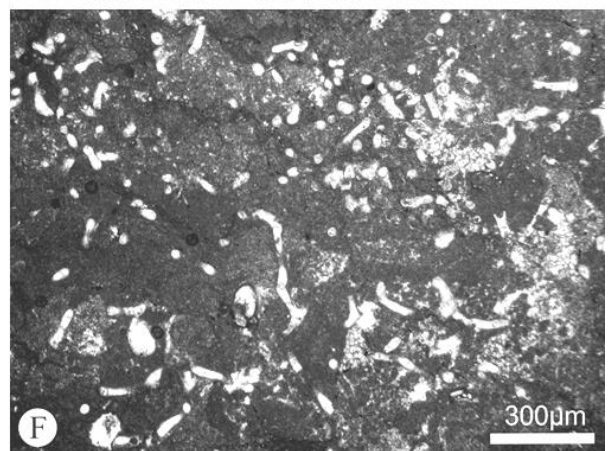
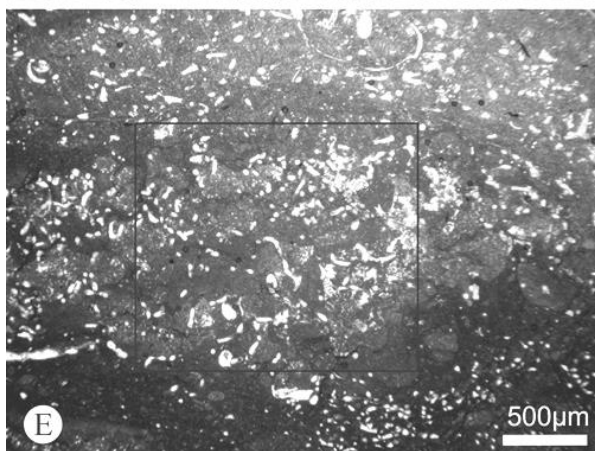
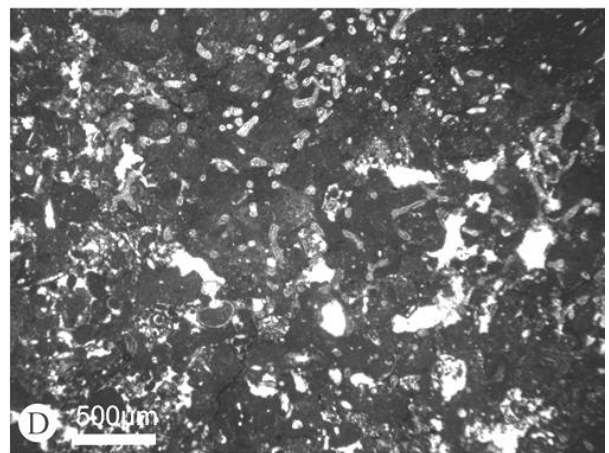
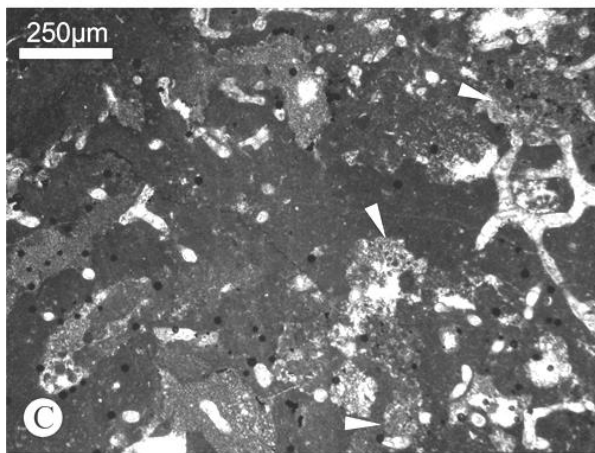
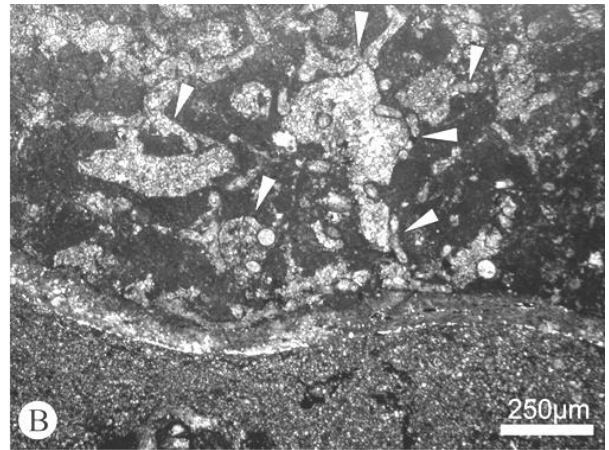
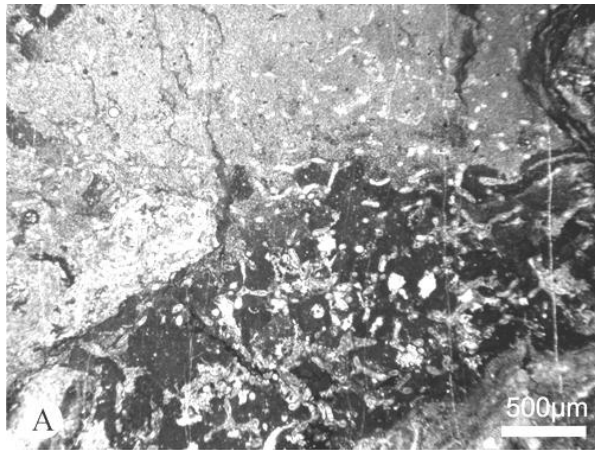


FIGURE - 4.21

A. (PHL 40) An overview showing both a *Donezella* dominated area with baffled homogeneous micrite and a lighter area consisting of microspar and some microcrystalline quartz with sparse *Donezella* bioclasts. The *Donezella* dominant area shows framework formed by the *Donezella*, note the difference between this framework and the previously described entwined thickets from sub-facies A. Several cavities are found within some of the pore spaces of the framework, the rest is filled with a dark homogenous micrite.

B. (PHL 41) The relationship between cavities and the *Donezella* framework can be observed well in this image (white arrows). Note how the edges of the cavities are often in conjunction with *Donezella* thalli - suggesting that the cavities are a direct result of parts of the *Donezella* framework being left unfilled, this would create many small, unconnected cavities. The isolation of the cavities may explain why no fibrous marine cement is observed within them.

C. (PHL 53) *Donezella* thalli with good preservation of wall structure can be observed in a branching manner with baffled micrite and cavities which are partially filled with peloidal micrite in some cases (white arrows).

D. (PHL 54) An overview of the *Donezella* framework with various, irregular cavities and a uniform, homogenous micrite matrix.

E. (PHL 55) A photomicrograph showing an area of the sub-facies where a greater quartz component can be found in association with microcrystalline spar. The quartz and microspar component is found baffled by the *Donezella* before becoming the dominant sediment toward the top.

F. (PHL 55) A close-up of the area highlighted in E. note that the microspar and quartz is baffled around the *Donezella* thalli.

G. and H. (PHL 40) these images show the branching and framework building nature of the *Donezella* observed in this sub-facies.

Sub-facies four represents just three of the samples: **20**, **22** and **23**. This sub-facies sees a framework formed of the red algae *Archaeolithophyllum*, *Ungdarella* and *Petschoria* with some probable ‘phylloid’ algae and some upright and branching bryozoans. The biota are dominantly concentrated into laminar accumulations with a homogenous micrite matrix. *Donezella* is found in several areas. Bioclasts make up the majority of this facies **SMF 8. Whole fossil wackestone**. This microfacies is characterised by predominantly sessile organisms within a homogenous micrite (Fig. 4.22).

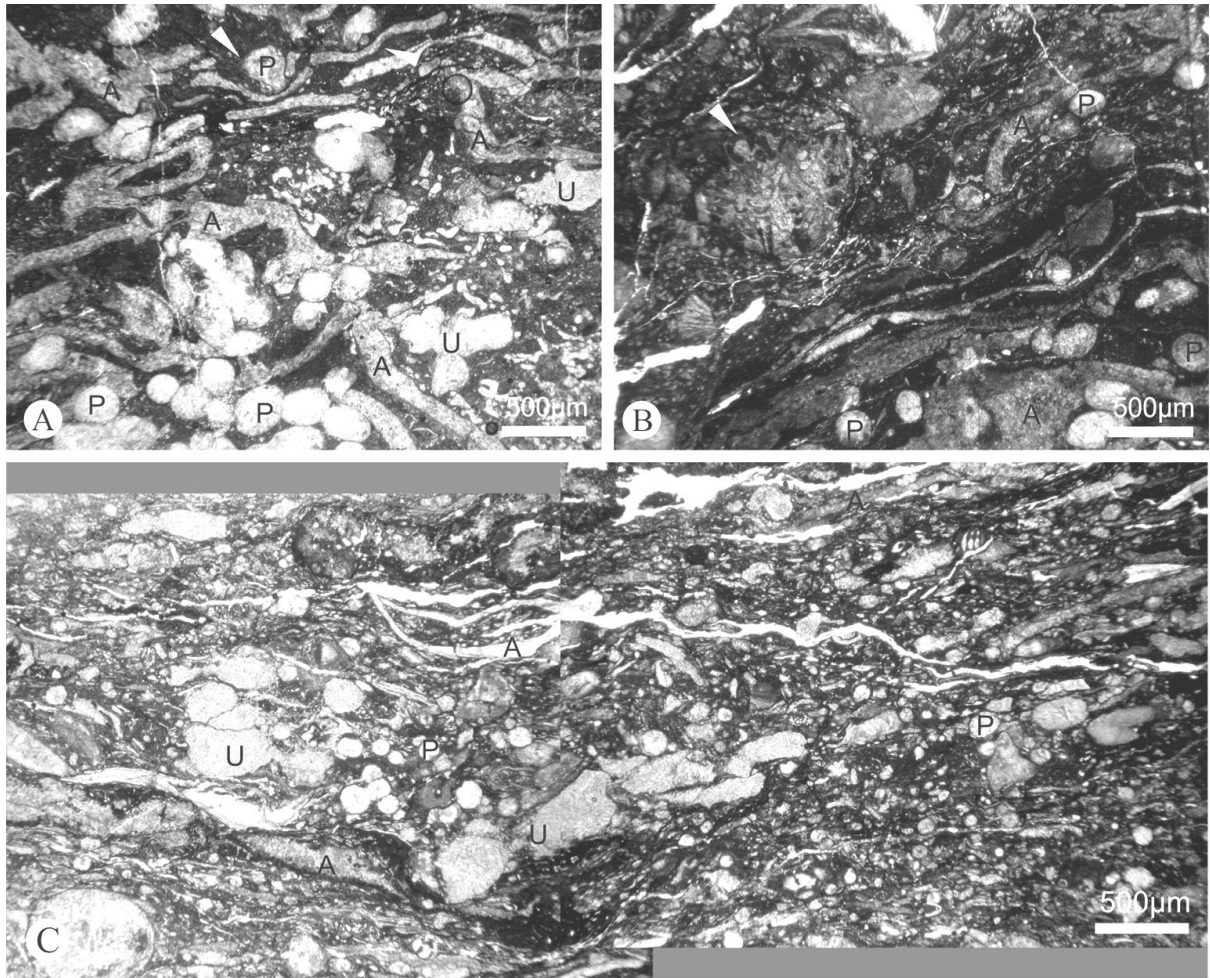


FIGURE - 4.22

A. (PHL 22) A photomicrograph showing several whole fossils within a homogenous micrite. The red algae *Archaeolithophyllum* (A), *Ungdarella* (U) and *Petschoria* (P) can all be observed in life position, all showing framework and sediment trapping capability. In this image a rare growth of entwined *Donezella* can be observed growing in association with the other organisms. *Petschoria* appears to use *Archaeolithophyllum* as a substrate in several examples here, forcing the latter to grow around it (white arrows).

B. (PHL 22) The laminar growth habit of *Archaeolithophyllum* (A) can be seen here, again it appears to provide a substrate for other organisms, in this case both *Petschoria* (P) and an upward growing, branching bryozoan (white arrow).

C. (PHL 20) A photomicrograph showing multiple thin specimens of *Archaeolithophyllum* (A) with large branching *Ungdarella* (U) and the relatively rare *Petschoria* (P).

Sub-facies five represents samples **28, 30, 31, 32, 33, 47, 49, 51** and **52**. A floatstone consisting of sessile organisms, including dominant ‘phylloid’ algae, with a homogenous micrite matrix with some microcrystalline quartz. The ‘phylloid’ algae consists of laminar, often dish shaped growths

several millimetres to centimetres long and millimetres thick. The thalli are generally recrystallised which may suggest an aragonitic precursor mineral phase. Even with this recrystallisation a cortical and medulla can often be recognised. Several juvenile sponge forms are present. The sedimentary matrix is mostly homogenous micrite, often with a microcrystalline quartz component. Within the sedimentary matrix small broken and transported bioclasts consisting of *Donezella* thalli and rare bryozoan fronds are found. Shell fragments are a rare component and appear to act as a substrate for encrusting calcimicrobes, which are not observed to encrust algal thalli within these samples. **SMF 8.** *Whole fossil wackestone with bioclastic packstones.* These are characterised by predominantly sessile organisms within a homogenous micrite (Fig. 4.23).

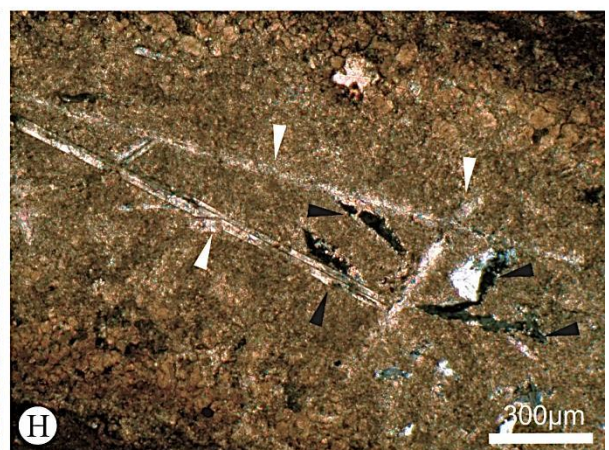
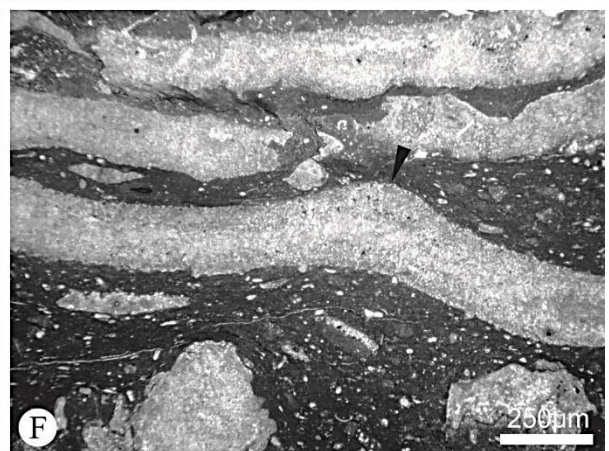
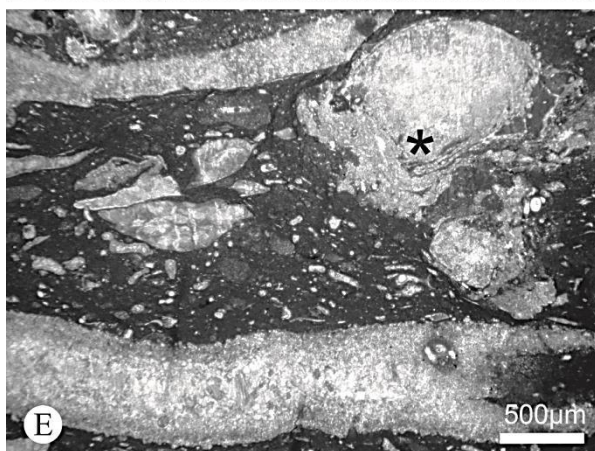
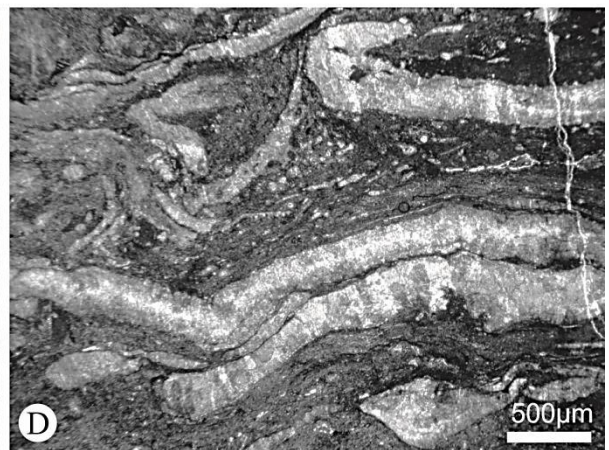
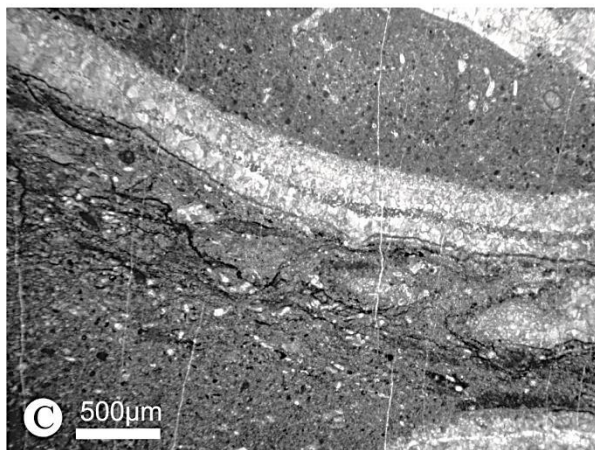
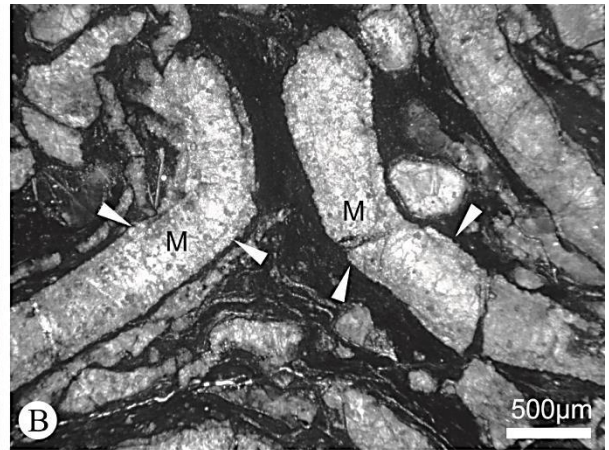
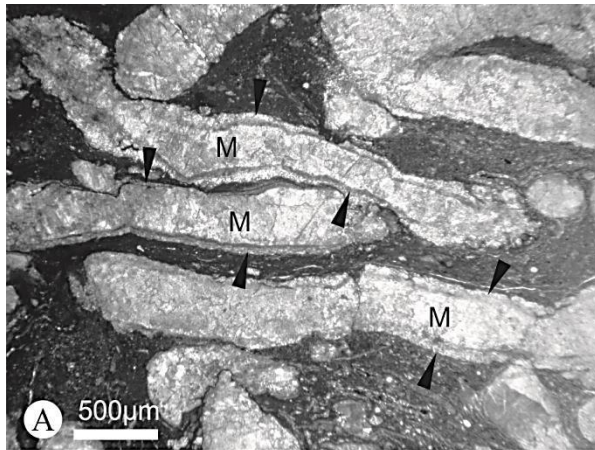


FIGURE - 4.23

A. (PHL 30) 'Phylloid' algae wackestone showing whole fossils. The thalli are often recrystallised like those seen in this image, though evidence for cortical (arrows) and medulla zonation can still be recognised. Note the low diversity observable and the apparent lack of encrusting forms.

B. (PHL 30) The 'phylloid' algae are generally observed as laminar, dish to bowl like growths, here two thalli can be seen to be growing upwards, perhaps as a result of competition for growth space laterally, or as a way of obtaining a greater surface area - making it more successful at photosynthesis. Again a cortical (arrows) and medulla zone (M) is recognisable. The sedimentary framework is homogenous micrite.

C. (PHL 32), D. (PHL 47), E. (PHL 51) and F. (PHL 51) More examples of the 'phylloid' wackestone. In E. a shell fragment can be observed that has been colonised by encrusters (*). This might suggest that during life the 'phylloid' algae did not provide a sufficient hard ground for encrusters. A conceptacle can be observed in F. (arrow).

G. and H. (xpl) (PHL 49) within several specimens elongated calcite crystals with quartz grains (black arrows) can be observed.

4.3.1 Interpretation

The carbonate unit found at the Pinos Hairpin has an overall high bio-productivity with each sub-facies showing a high component of bioclasts. Each sub-facies has a dominant biota with the exception of sub-facies 1 which appears to have elements from all of the other sub-facies. The sedimentary matrix for the unit as a whole is a dark homogenous micrite with some more microspar and quartz rich components. Bioclasts rarely show any evidence of abrasion, breakage or transportation so the entire section is interpreted to have been deposited within a low energy environment. The high bio-productivity, but general dominance of one (or a few) biota suggests a restricted environment, the different communities established changing accordingly to environmental shifts. This could be a shift controlled by fluctuating sediment input, salinity, water depth, a combination of more than one on these, or a different factor altogether. 'Phylloid' algae may suggest a shallow, warm water environment. The depositional setting is likely to represent less of a restricted environmental setting than that of the mound bearing carbonates (due to a greater biological diversity) and most likely represents the platform margin or a slope environment. The occurrence of whole, uncrushed fossils indicates that burial and compaction is not responsible for the cyclic carbonate and marls observed and it is a primary, sedimentological feature. The diagenetic model for such deposits proposes that aragonite dissolution from (what

becomes) the marl layers is precipitated as low-Mg micrite in (what becomes) the under- or overlying limestone layer (Munnecke and Samtleben, 1996).

4.4 Pinos Pylon Mound

30T 258176.93 4763445.24

The Pinos Pylon Mound (PPM) is found just to the east on the track out of the village of Pinos. The mound sits within the first major limestone unit of the La Majúa Member and is atop of a sequence of ‘phylloid’ pack- to floatstone and marl dominated beds several meters thick (similar to the Pinos Hairpin Limestone). The major limestone unit to which the PPM belongs is the thickest of the eight units in the La Majúa Member and is the only mound in this study to be found atop a significant sequence of ‘phylloid’ algal pack- to floatstones and marls. The mound is 50 m high and is exposed for several hundred metres, although only the base of the mound is accessible; this access is restricted by local fauna. The ‘phylloid’ pack- to floatstone consists of 21 beds of around 15 cm in thickness, each consisting of a cyclical bed of ‘phylloid’ pack- to floatstone with a small clastic component up to a marl dominated layer barren of large bioclasts (these limestone to marl beds are similar to those of the Pinos Hairpin Limestone). The ‘phylloid’ algae appears as cup and bowl like structures and are commonly associated with tubular structures interpreted to be aulopodid corals. Several whole brachiopod shells and gastropod shells have been found. The PPM is micritic and appears to be devoid of primary features (i.e. bedding), the micrite is a light grey/blue colour and exhibits a conchoidal fracture. The mound appear fossil free in hand specimen. The basal facies for the PPM consists of the ‘phylloid’ algal pack- to floatstones and marls. The mound facies is only represented by a handful of samples (due to access reasons) and the capping facies is not present, although it could be that the clastics between unit 1 and 2 are effectively the capping facies of the PPM. Several three dimensional specimens of the algae were recovered from this site - see chapter 6. *Palaeontology* below.

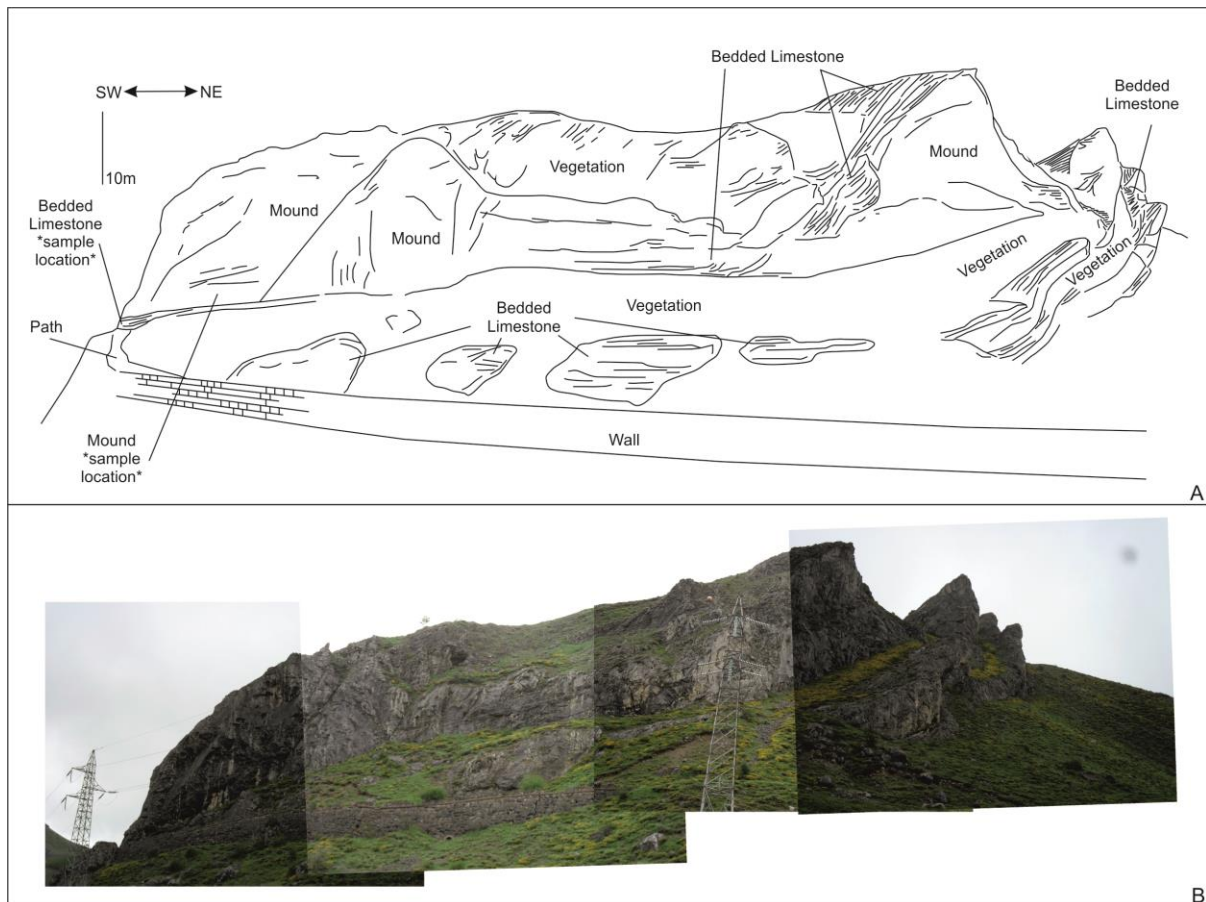


FIGURE – 4.24 A. An annotated field sketch of the Pinos Pylon Mound, showing sample locations. B. Field photos.

4.4.1 Basal Facies

The basal facies consists of 21 beds of carbonate (**samples PPM 1 to 21**), bioclastic pack- to floatstone to marly wackestone cycles. The carbonate dominated parts of the cyclic beds (sub-facies one) are associated with mostly sessile organisms rooted in a homogenous micrite. What is most likely to be ‘phylloid’ algae, due to its geometry and angular to flared terminations is common. Although the majority of specimens are recrystallised there are several which demonstrate a monostromatic form. Encrusting forms are also very common and well preserved in this sub-facies generally comprising tubular calcitic forms (*Rothpletzella* and *Claracrusta*). Encrusting bryozoans are locally found in association with both the ‘phylloid’ algae and calcimicrobial encrusters as are several sponges. Several upright, tubular forms are present, they have a honey coloured calcitic wall which consists of laminae of crystals toward the outside and radial crystals toward a central cavity. The tube like forms appear to consist of several growth

stages each arranged like a bowl one atop another, these are interpreted to be aulopodid corals. Dasyclad algae are present in small numbers as are trilobite fragments and rare gastropod shells. The sedimentary matrix is a homogenous micrite with some lenses and patches of micrite with microgranular quartz grains. The algae and other encrusters form laminar surfaces parallel to bedding, and act as substrate themselves, often for other encrusters, more homogenous micrites are usually baffled by these laminar features. Sub-facies two is mostly devoid of the bioclasts found in sub-facies one and represents the more marly component of the beds. Broken bioclasts consisting of echinoderm plates, shell fragments (ornamented gastropods are identifiable), trilobite fragments, sponge spicules and various algae and calcisphere-like forms are present. The shelly fragments, sponge spicules and echinoid plates have rare, thin coatings, of micrite whereas the algal fragments generally have a thick micritic envelope and in some cases they are found as cortoids. The cortoids appear as rounded accumulations of homogenous micrite, with evidence of microbial encrustations in the form of tubes and cauliflower like textures. The bioclasts are fragmented and often sub-angular, whereas the cortoids are more rounded. Neither clasts show any strong depositional fabrics, some weak laminae can be inferred in places. The sedimentary framework is mostly a wackestone consisting of homogenous micrite with microcrystalline quartz grains supporting the various bioclasts. Some bioclasts are found in association with peloids, which are rounded and of the same size. Stylolites are more common in this sub-facies than in sub-facies one. Cavity networks are not observed in either sub-facies, blocky calcite is uncommon and occurs only as cement between some of the larger bioclasts and within recrystallised bioclasts.

SMF 8 with SMF 10. *Whole fossil wackestone with bioclastic packstones.* This is characterised by predominantly sessile organisms within a homogenous micrite with some small mobile forms, with worn and coated bioclasts within a micritic and microcrystalline quartz matrix (Fig. 4.25 and Fig. 4.26).

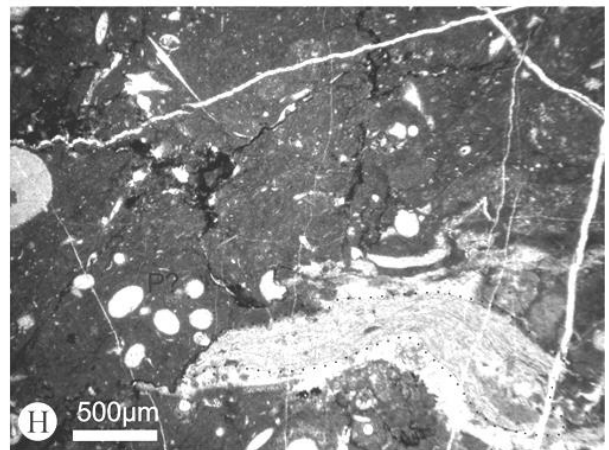
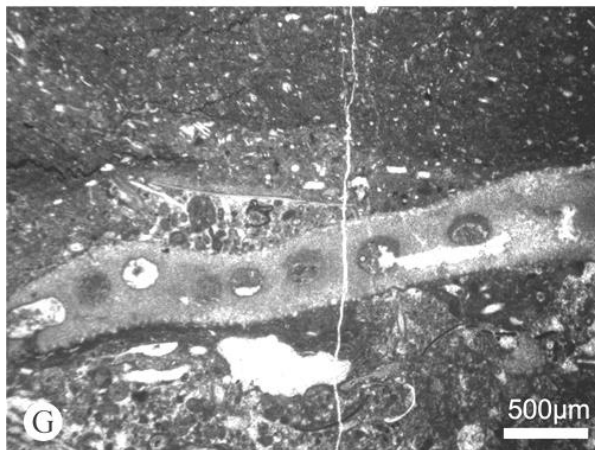
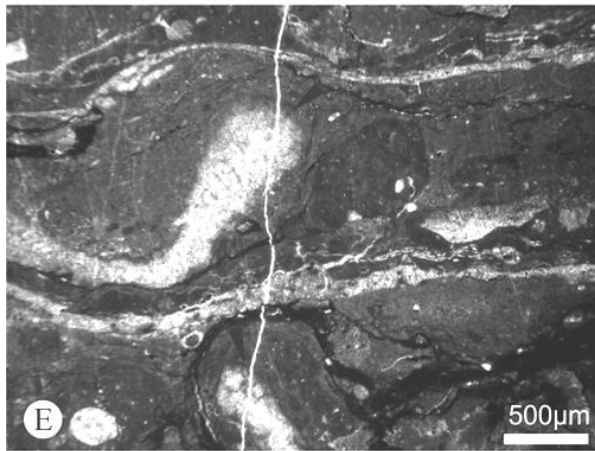
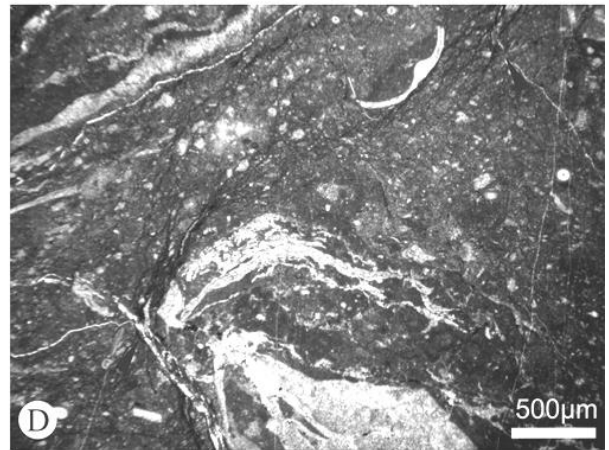
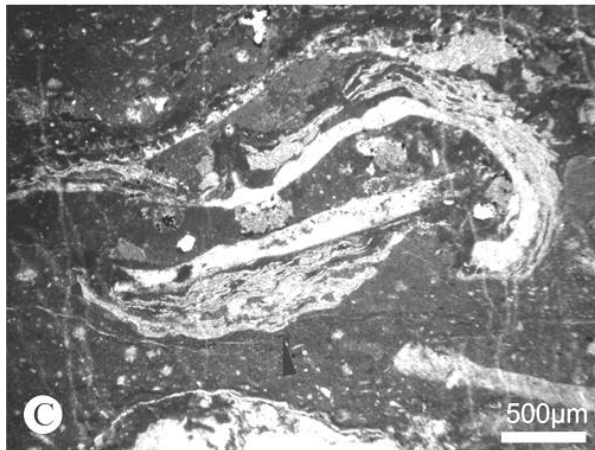
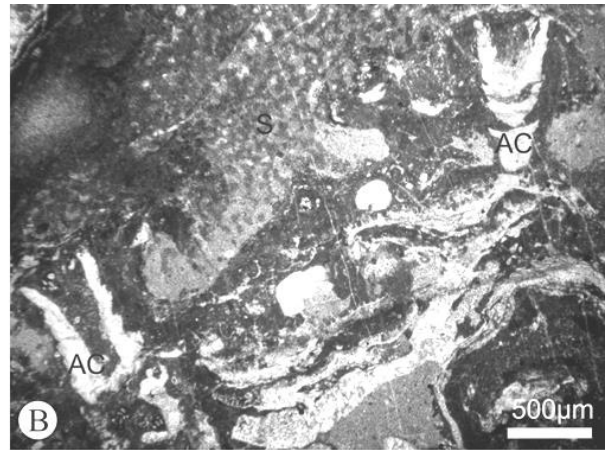
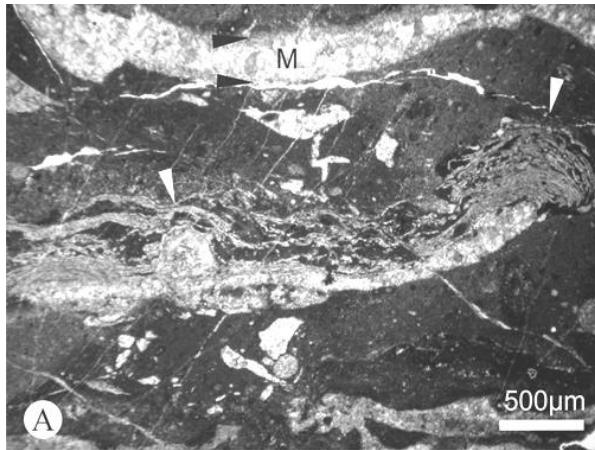


FIGURE - 4.25

A. (PPM 3) A photomicrograph showing the major textural features observed within sub-facies one. The sedimentary matrix is predominantly homogenous micrite, with a component of homogenous micrite with microcrystalline quartz. These two sediments can be distinguished in the image due to the micrite which contains quartz appearing lighter. 'Phylloid' algae which has been recrystallised can be observed in its laminar, "corn-flake" like growth position. The specimen toward the top of the image shows evidence of a distinct cortical (black arrow) zone which is recrystallised by much finer calcite crystals than the central medulla (M). Another major laminar feature within this sub-facies are cyanobacterial encrusters, which are often, as seen here, observed in association with 'phylloid' algal fragments. The encruster seen here is *Claracrusta* (white arrows), identified by its bean and sausage shaped cells, growing in lamination which become more undulose away from the laminations attached to the hardground.

B. (PPM 5) Here a relatively high diversity of encrusting forms can be observed. Aulopodid corals (AC), encrusting bryozoans, 'phylloid' algae, encrusting calcimicrobes and an encrusting sponge (S) can be observed. 'Phylloid' algae and encrusting *Rothpletzella* are at the base of this succession of encrusters. Encrusting bryozoans can be seen forming several sheet like bodies separated by homogenous micrite. Above this, two upstanding, thick walled aulopodid corals are found and finally a sponge. The sponge occurs on top of, and between the aulopodids, which are relatively short compared to other examples observed which suggests the sponge smothered and stopped the growth of the corals.

C. (PPM 9) Thick encrustations of sheet like calcimicrobial tubes (black arrows). The encrusters are growing on a hardground provided by 'phylloid' algae (possibly *Archaeolithophyllum*). Above these encrusting bryozoans can be observed. Several cavities which have been selectively filled by dolomite are found between the two 'phylloid' algae thalli. Within these cavities an angular opaque mineral, most likely pyrite is present.

D. (PPM 10) A bioclastic wackestone comprising of small, rounded bioclasts and homogenous micrite with *Rothpletzella* forming in small crescent shaped tubules. Several splayed stylolites can be observed within the sediment matrix. The stylolites are quite flat and are generally parallel to bedding, except when associated with bioclasts, where they meander around - exploiting the weaker sedimentary matrix. 'Horse tail' structures where the stylolite seams diverge laterally are indicated (arrows)

E. (PPM 11) A recrystallised algal thalli exhibiting a somewhat characteristically thickened end (arrows). The laminations of encrusters can be seen to undulate due to the growth position of the 'phylloid' algae, providing evidence that the 'phylloid' algae is *in situ* and grew as flattened laminar sheets with upturned edges. The heterogeneous sedimentary matrix can be seen with lighter micrite and microcrystalline quartz and darker homogenous micrite.

F. (PPM 12) Three specimens of the thick, calcite walled aulopodid corals. The corals are upright and a distinct central cavity is observable. The corals appear to grow in stages which resemble stacked cups. Homogenous micrite can be seen below the corals and the encrusters which are providing a hard ground, whilst micrite with microcrystalline quartz is baffled by the corals (lighter coloured sediment).

G. (PPM 15) A specimen of 'phylloid' algae which clearly shows a simple, undifferentiated, monostromatic form.

H. (PPM 16) A thick encrustation of *Rothpletzella* (outlined). The sedimentary micrite consists of small rounded bioclasts within a homogenous micrite with microcrystalline quartz grains. Toward the bottom left corner a possible specimen of the algae *Petschiria* can be observed, supposedly, it is using the *Rothpletzella* encrustation as a hardground for its growth.

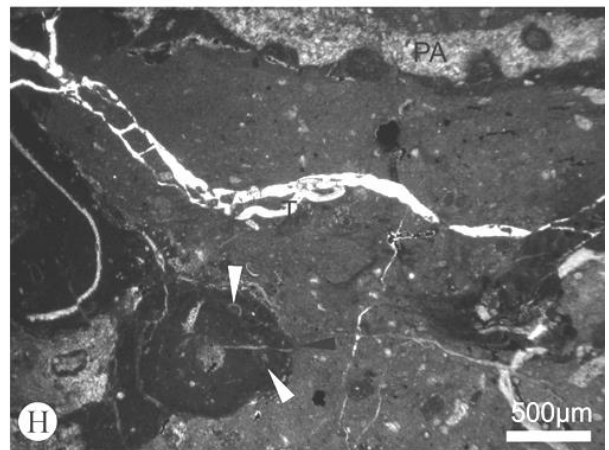
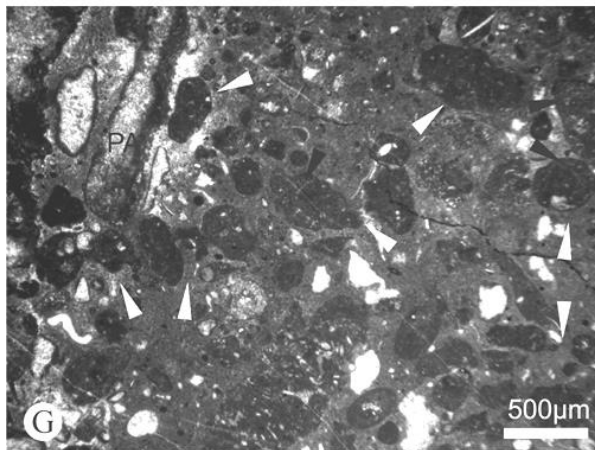
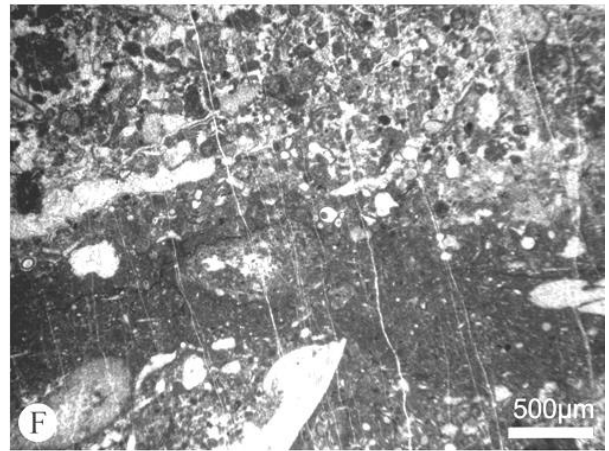
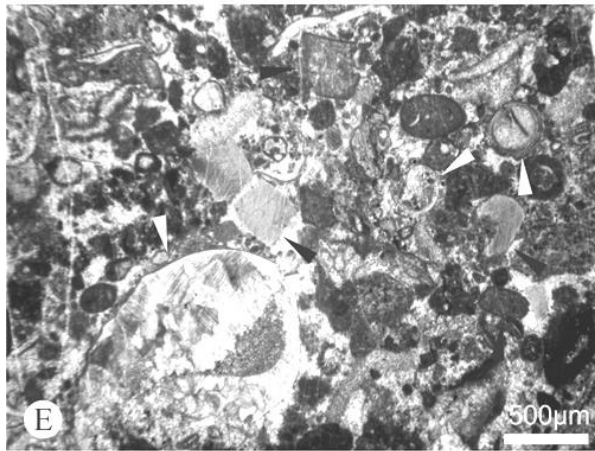
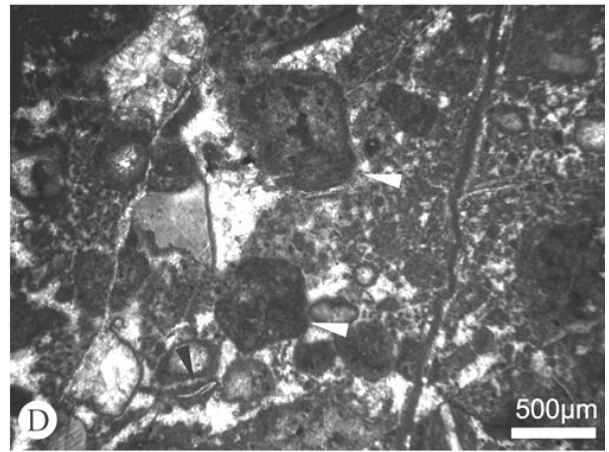
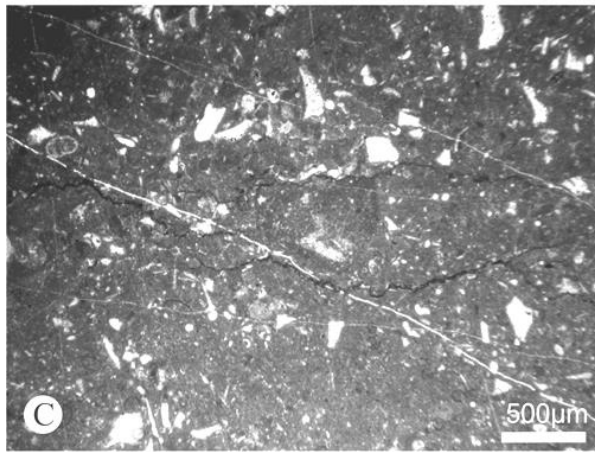
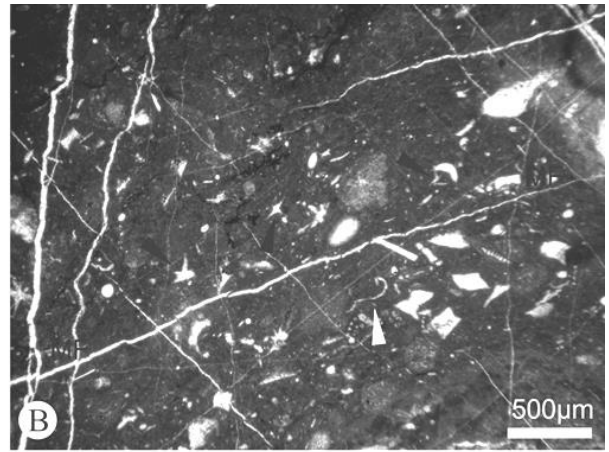
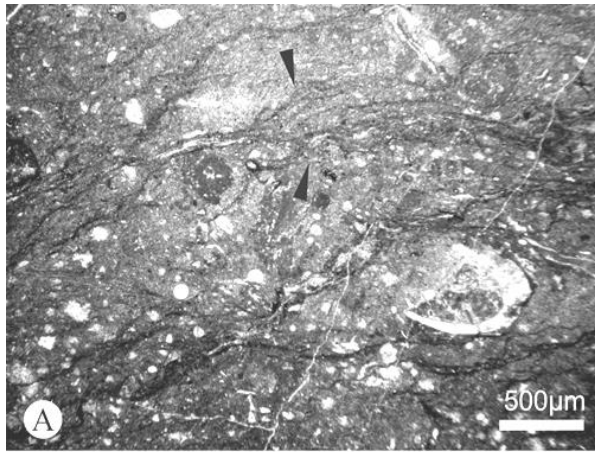


FIGURE 4.26

A. (PPM 6) The major sedimentary feature of sub-facies two is shown in this photomicrograph. A highly stylotised wackestone of small bioclasts within a homogenous micrite, with microcrystalline quartz grains. Bioclasts are often broken and include echinoderm plates, shell fragments and small mobile forms, including *Tuberitina*. Stylolites are bedding parallel, irregular and anastomosing, a 'horse tail' feature characterised by the lateral splaying of the pressure solution seam can be observed (arrows). Several oncoids consisting of consecutive layers of dark, homogenous micrite around a small nucleus of a fragmented bioclast are present.

B. (PPM 16) Homogenous micrite wackestone which contains less quartz than the previous example (A.) Several bioclasts are identifiable including trilobite fragments (white arrow) and sponge spicules (black arrows). Several angular clasts which have been recrystallised are present, some have evidence of a wall structure and the geometry of them suggests a bioclastic origin. Several sets of conjugate micro-fractures (MF) are present; these are filled with blocky calcite.

C. (PPM17) In this photomicrograph the wackestone texture can again be observed. Bioclasts are again broken and recrystallised and stylolites are present. The sediments toward the top left appear darker than the more central sediments, this is due to the quartz content of the unit, where the matrix contains more quartz it appears lighter.

D. (PPM 2) Several parts of this sub-facies are dominated by a bioclastic packstone, often with a pelmicritic matrix. Here the bioclasts consist of echinoderm fragments and other angular clasts which exhibit a thin micrite envelope. Other clasts observable here may be mud chips (white arrows), made of reworked peloidal sediments. These clasts have micrite envelopes and appear more homogenous than the peloidal component of the sample and have a texture reminiscent of clotted micrite, this may indicate a microbial role in the formation, or preservation of the clasts. Note the trilobite fragment indicated (black arrow).

E. (PPM 13) A packstone consisting of relatively large bioclasts including echinoderm fragments (black arrows) and a gastropod shell (white arrow) with a geopetal fill. Most of the bioclasts exhibit a thin micritic rim, however most of the echinoderm fragments do not. Peloidal micrite is commonly associated with a spary matrix fill.

F. (PPM 19) A photomicrograph displaying the heterolithic nature of sub-facies two. A band of mostly homogenous micrite wackestone is observable toward the centre and is bounded by a bioclastic packstone to the top and bottom. Several micro-fractures run through this sample.

G. (PPM 4) Cortoids (white arrows) of consecutive layers of dark, homogenous micrite with calcified tubes. Some layers can be seen to have a shrub-like growth form (black arrows). The cortoids are associated with other bioclasts, note the recrystallised 'phylloid' algal clast (PA). The sedimentary matrix consists of a homogenous micrite.

H. (PPM 1) Homogenous micrite, a 'phylloid' algal fragment (PA) and a cortoid (black arrow). The algal fragment shows some preserved evidence for a monostromatic form. The cortoid has a small round nucleus and has distinct layers of lighter material, which consists of calcimicrobial tubes and growths (white arrows). Trilobite fragments are indicated (T).

4.4.2 Mound Facies

The mound facies (**samples PPM 22 to 24**) consists of a mudstone to wackestone with homogenous and peloidal micrite, with a low diversity assemblage consisting of 'phylloid' algal

thalli and encrusting forms. The very base of the mound facies is a bioclastic grainstone with shelly fragments and a homogenous micrite. The majority of the facies appears to be peloidal, clotted and homogenous micrites with some rare stromatactoid cavity networks. The peloids are of a dark homogenous micrite and are rounded in shape and of various sizes, no laminae are apparent. The peloids are generally found within a homogenous micrite matrix, and occasionally a clear, blocky spar. Cavity networks are uncommon, they are typical stromatactoid cavities with flattened bases, undulose roofs and have an internal sedimentary fill, followed by fibrous cement and a final, clear, blocky cement. Bioclasts are relatively rare, they consist of laminar algal thalli which show evidence of differentiated forms, with a cortical layer obvious from the medullary layer. There are two different evidences for this differentiated form, the first is different sized crystals for both the cortical and medullary layers - the cortical layer is crystalised by small, blocky crystals with uniformly spaced inclusions of an opaque mineral (black arrows), the medulla is crystalised by elongate crystals which have grown perpendicular to the cortical layer. The second evidence is an algal thalli which has indented structures along its walls which are filled with micrite, this is probably a secondary infilling of primary tubules. Encrusting forms present include auloporid corals, *Rothpletzella* and the coralline red algae *Ungdarella*. *Rothpletzella* is found as characteristic sheets of calcitic tubes which are concordant with the subjacent substrate. The specimens of *Ungdarella* have ramous thalli and typical rows of quadratic cells. The auloporid corals are found as small encrustations which fail to grow to any substantial height. The facies has a low biodiversity and is dominated by laminar and encrusting growth forms. **SMF 8.** *Wackestone with whole fossils*. This facies is characterised by whole sessile organisms rooted in mostly homogenous and peloidal micrite (Fig. 4.27).

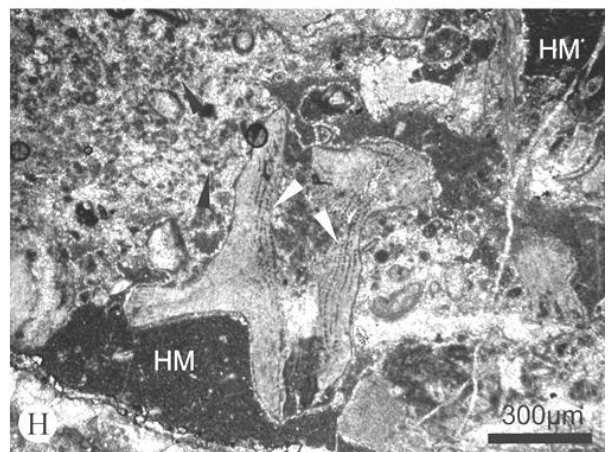
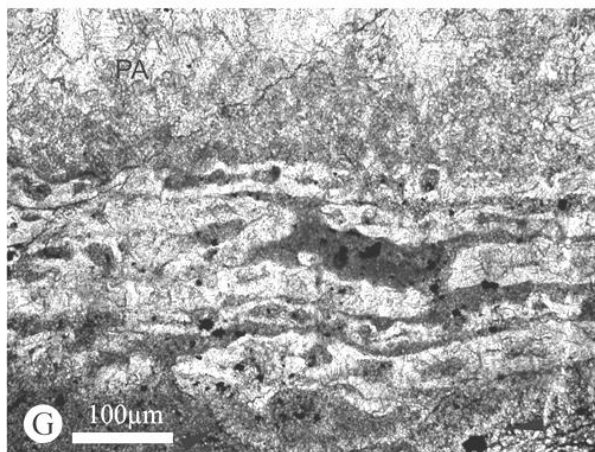
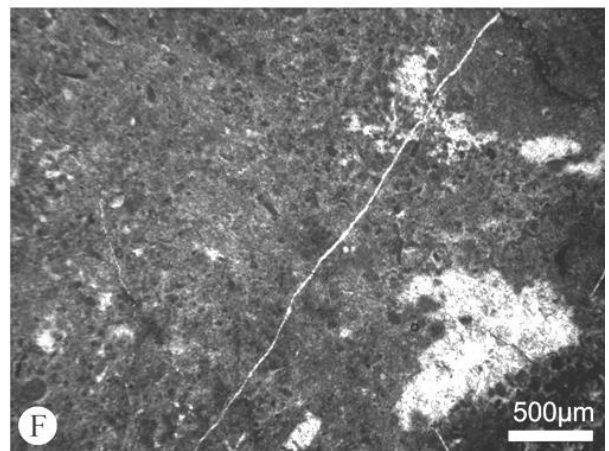
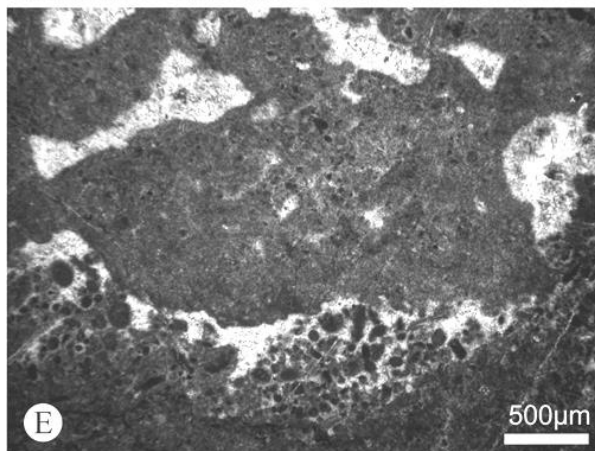
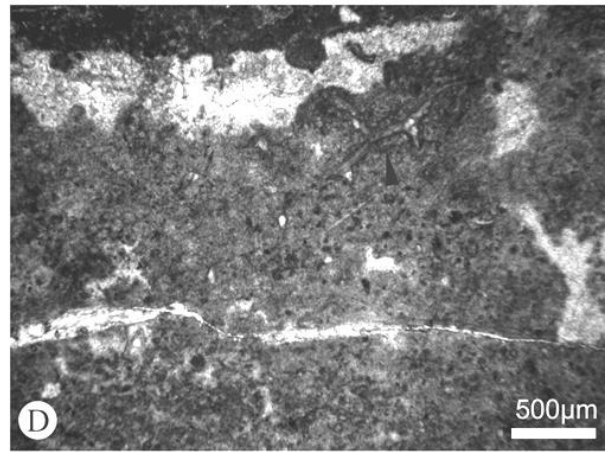
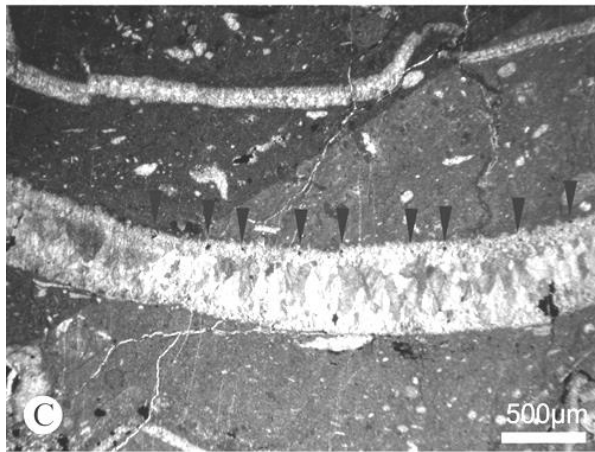
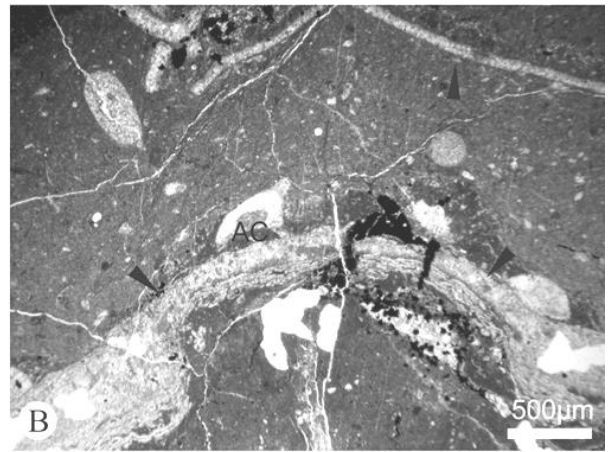
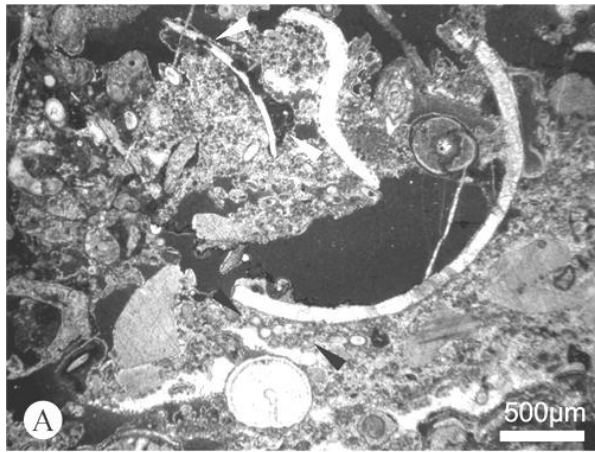


FIGURE - 4.27

A. (PPM 22) A photomicrograph of the very base of the mound facies. A bioclastic grainstone with a relatively high diversity and a homogenous micrite matrix is shown. Bioclasts include large shell fragments including gastropods. Several foraminifera are present including what may be a specimen of *Saccaminopsis* (black arrows). Several of the grains are encrusted and show evidence of boring. Encrustations appear as hemispherical to tubular growths (white arrows).

B. (PPM 23) A laminar algal thalli with associated encrusting biota. The ‘phylloid’ algae (black arrows) are poorly preserved and show no internal structure. Encrusters are dominantly calcimicrobial *Rothpletzella*. This biota is usually seen encrusting the upper surface of a hardground but in this example is seen growing in a cryptic habitat. An aulopodid coral (AC) can be observed on the upper surface of the algae and appears to have failed to grow to any significant height. An opaque, mostly cubic mineral can be observed in association with the biota in this image. This mineral is most likely to be pyrite.

C. (PPM 23) A rare ‘phylloid’ algal thalli showing a differentiated cortical and medulla. The cortical zone has been crystalised by small blocky, generally equigranular calcite crystals whilst the medulla has larger more elongate crystals which have grown perpendicular to the cortical surface. Note the inclusion of small opaque crystals at almost uniform spacing along the upper cortical surface (black arrows).

D. (PPM 24) Toward the top a ‘phylloid’ algae with evidence of primary tubules (now filled with micrite). The majority of the photomicrograph shows the dominant sedimentary texture for the mound facies; a homogenous and peloidal micrite. Peloids are rounded and of differing sizes and are not laminated. A thrombolytic texture can often be observed for the peloids. What is probably a bryozoan frond can be observed (arrow).

E. (PPM 24) Homogenous and peloidal micrite, with several cavities showing a clear, blocky spar fill. The peloids observed in the bottom half of the image vary in size and shape, but are always rounded. No bioclasts are observable.

F. (PPM 24) Homogenous and peloidal micrite with a distinctive stromatactoid cavity. The cavity has a flat base and a sediment infill, with undulose roof and an isopachous fibrous cement and a blocky spar.

G. (PPM 23) An example of the encruster, *Rothpletzella*. The specimens are found as sheets of rounded chambers and often look like strings of sausages or a necklace of beads. The walls are often a yellow/brown colour with chambers sometimes appearing to branch perpendicular to the cutting direction. In this image the *Rothpletzella* is found on the underside of a recrystallised algal thalli (PA), and several botryoidal-like growths can be found attached to them (black arrows). Several angular/cubic opaque crystals are present concentrated around the *Rothpletzella* sheets, these are most likely to be pyrite. Also note the fan like growths encrusting the base of the bottom row of filaments.

H. (PPM 22) An example of *Ungdarella*. The characteristic rows of quadratic cells are clearly visible (white arrows). Note the homogenous micrite (HM) and the more peloidal micrite with some thromboidal textural qualities (black arrows).

4.4.3 Interpretation

The mound facies of the Pinos Pylon Mound is seen as a distinct change in lithology at outcrop scale, passing from bedded ‘phylloid’ dominated marls to a homogenous, massive micrite mound.

The basal beds are dominated by laminar layers of 'phylloid' algae and various encrusting forms, the sedimentary matrix is of micrite and quartz, the ratio of which begins with low quartz at the base of a bed to high quartz toward the top. This results in cyclical beds of whole fossil wackestones into marls. The presence of continuous laminar growths of 'phylloid' algae, encrusting cyanobacteria and auloporid corals (which are found as upstanding tubes) within the carbonate dominant section of the beds but not the marl section indicates that accumulation rates are faster for the latter. The faster accumulation results in less time for the organisms to establish themselves successfully. 'Phylloid' algae which grow as large laminar sheets and cup like structures in close proximity to one another may suggest a wave induced dominated environment, where the algal blades are juxtaposed and stacked to reduce wave destruction. The very base of the mound sees the inclusion of several features which are found in abundance in the subjacent, bedded material. Individual 'phylloid' algal plates with encrusters and small auloporid corals which fail to reach any significant height are observed, which may suggest that the environmental conditions were suitable for them to grow in. The rarity of these biota and their smothered appearance (especially of the short auloporid corals) suggests carbonate precipitation and accumulation was faster for mound material than for the bedded material. Quartz grains disappear within the mound and a dominant micrite component is found, and micrite is often peloidal or homogenous sometimes with a clotted texture. Thrombolitic structures can be observed in some micrites and it is likely that a cyanobacterial growth was responsible for this. Within the mound several small cavities are found within the micritic matrix, these cavities are bird's eye or fenestral cavities, often found in laminar arrangements, the undulose roofs and flat bases.. Very few, small and rare Dorellaceans were found at this location. The basal sediments are interpreted to represent cyclical sea level changes where the carbonate dominant portion is deposited in shallow, warm, wave dominated water where the precipitation of carbonate is coeval with background sedimentation of fine clastics. The marl component is representative of transgressive events where the water depth increases resulting in lower light and warmth levels. The dominant biota within the carbonates struggle to survive and carbonate production is greatly reduced, leading to the

accumulation of greater ratios of marl. Alternatively the marl may be representative of cyclical pulses of increased clastic input into the basin or as a result of dissolution and precipitation of the carbonate minerals during diagenesis (Munnecke and Samtleben, 1996). The mound facies is interpreted to have been deposited after a transgressive sea level rise in shallow, warm, calm and restricted waters. Carbonate production is thought to have been high, with the environmental conditions similar to that of the carbonates within the basal beds. The mound may have resulted from increased calcimicrobial and cyanobacterial growth within a restricted and shallow (with occasional sub-aerial episodes) environment where waters were supersaturated in regards to carbonates and production was increased. Within a foreland basin this mound is interpreted to have nucleated and grown on the fore bulge, whilst the basal beds were deposited on the flanks of the forebulge or similar environment. Table 4.2 summarised the microfacies analysis of the Pinos Pylon Mound.

Samples	SMF	Characteristics	Interpretation
1-21 (basal)	8 with 10	Predominantly sessile organisms within a homogenous micrite. With worn and coated bioclasts within a micritic and microcrystalline quartz matrix.	Very shallow depth, restricted environment. Low - moderate energy, lagoonal environment.
1-3 (mound)	8	Whole sessile organisms rooted in mostly homogenous and peloidal micrite.	Shallow depth, restricted environment.

TABLE - 4.2 Summary of the main standard microfacies, characteristics and interpretations of the Pinos Pylon Mound.

4.5 Pinos East Mound

30T 258465.30 4763828.33

The Pinos East Mound (PEM) is a conspicuous mound found below the first major limestone unit of the La Majúa Member and above a zone of silicified calcareous, fissile silts. The outcrop is domal in geometry measuring 30 m in height 90 m in width (Fig.4.23). Hand specimens are light, creamy grey lime mudstone often with visible fenestral cavity structures which range from millimetres to decimetres in size. Cavity fills are sparitic and look to be formed of radial crystals. Some black, carbonaceous material can be found within some cavities, this is likely to be pyrobitumen. Several macro fossils can be observed in hand specimen and solitary branching corals, gastropods and brachiopods can be found in several samples. This mound is different from the others described as it is not found as part of a wider carbonate deposit and is solitary, confined within calcareous siltstones; these mounds are similar to those mounds observed at the furthest west extent of Unit 8. Several smaller outcrops of carbonate material are found in the vicinity of the mound and are most likely olistoliths, indeed the PEM was originally mapped as an olistolith (by the Geological Survey of Spain), however the size, geometry and lack of primary bedding or frameworks indicate that this outcrop is a carbonate mud mound. Due to the nature of the outcropped material no basal or capping materials are present (other than calcareous silts). As such just the mound facies can be investigated instead of the basal-, capping- and mound facies. Five distinct standard microfacies are recognised as contributing to the mound facies of the Pinos East Mound, these are grouped into three sub-facies.

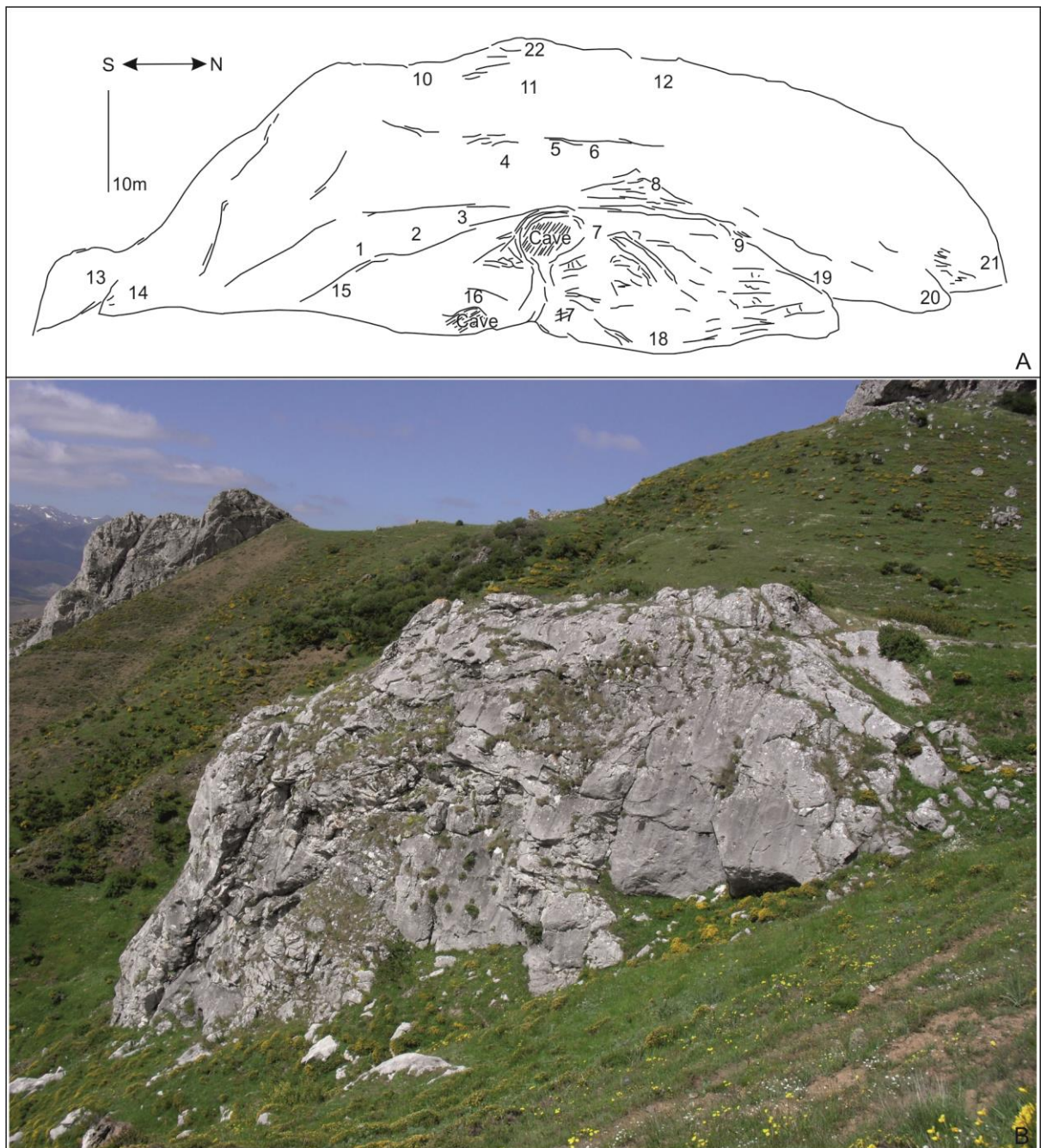


FIGURE - 4.28. A. An annotated field sketch of the Pinos East Mound with sample locations highlighted. B. Field photos.

4.5.1 Mound Facies

Sub-facies one represents the majority of samples taken from the mound: **samples PEM 3, 5, 6, 8, 9, 10, 12, 13, 14, 20, 21 and 22**. This sub-facies is a fenestral packstone with spar filled voids in a pelmicritic framework. The framework consists of non-laminated peloids of varying sizes, most of which are rounded. The peloids are entirely micritic and often sit within a slightly coarser micro-spar matrix. Some micritised and abraded bioclasts can be recognised as well as some well-preserved foraminifera, white ostracods and Tuberitinae. Both destructive (micrite envelopes associated with the microboring into, and abrasion of, the bioclast) and constructive (layers of microcrystalline calcite with varying thickness, which do not alter the bioclast it surrounds) micrite envelopes are observable. Bioclasts often show no evidence of microboring, however, several bioclasts are heavily abraded and microboring and recrystallisation is evident. These heavily abraded and microbored clasts are likely to have had an originally aragonitic skeleton. Some echinoid plates are present; these are enveloped within micrite and show no evidence of overgrowth. Calcimicrobial sheaths and other problematic encrusting forms can be observed within homogenous micrite which is often surrounded by cavities. What appear to be solitary, branching corals are observed 'floating' within a fibrous marine cement in one sample. The cavities are often several millimetres to decimetres in size and most exhibit a fenestral geometry and can often be found forming bioclastic floatstones. The majority of cavities are orientated such that their bases are parallel with the base of the mound; the base is generally flat with the roof being undulating. Several cavities are stromatolite cavities and exhibit the characteristic flat base, undulating roof with internal sediments and marine cements. Cementation within the cavities consists of cloudy light honey coloured, isopachous crusts of fibrous to bladed crystals which are often up to a millimetre in length and grow perpendicular to the substrate. Often fringes of silty/micritic material can be observed before another crust of fibrous cement is found. The majority of the cavities can be found with clear, blocky spar crystals at the centre. This final, late cement has a sharp, distinct boundary with the fibrous/bladed cement. Both isopachous fibrous and radial cements can be commonly recognised. Fibrous cements are characterised by tightly

packed fibrous crystal radiating from the substrate and into the cavities and radial fibrous cement is recognised by curved twins, an extinction which follows the direction of the viewing platform of the microscope and sub crystals which are increasingly divergent from the substrate within single crystals. Evidence of substrates are apparent as are clasts derived from a possible sub-aerial origin. These clasts consist of couplets of dark and light laminated layers which show no evidence of fossils and contain desiccation/dewatering related fractures. Stylolites and other evidence of compression is rare. Selective dolomitisation occurs within a few cavity networks.

SMF- 21 and 16. *Fenestral packstone with a peloidal grainstone framework.* Characterised by a fenestral and stromatolite cavity networks within a framework of peloidal grainstone. Bioclasts are sparse and consist mostly of foraminifera, micritised grains and small mobile organisms (calcspheres and Tuberitidae) (Fig. 4.29, Fig. 4.30 and Fig. 4.31).

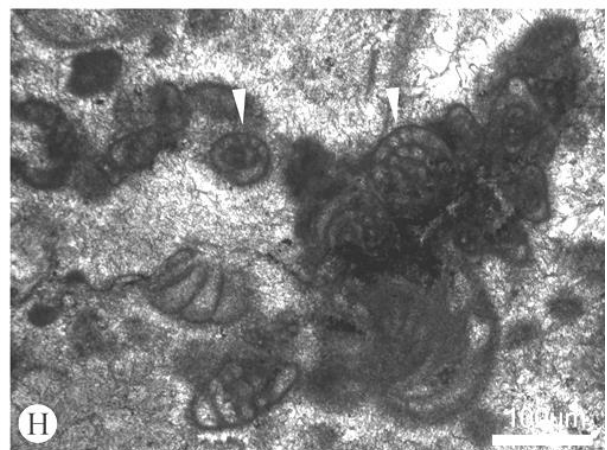
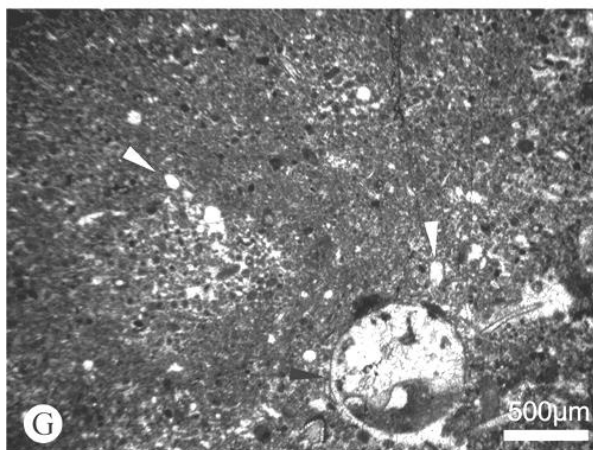
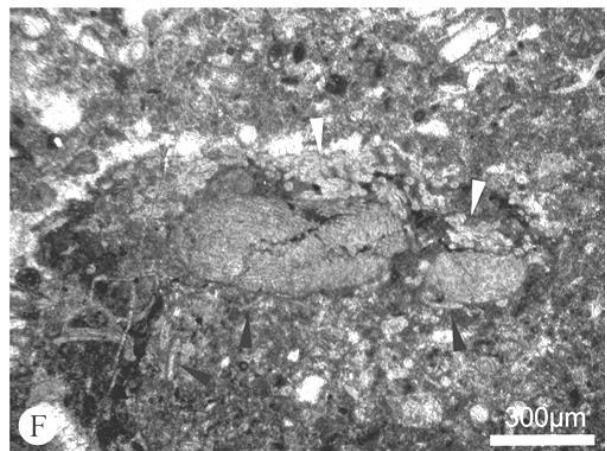
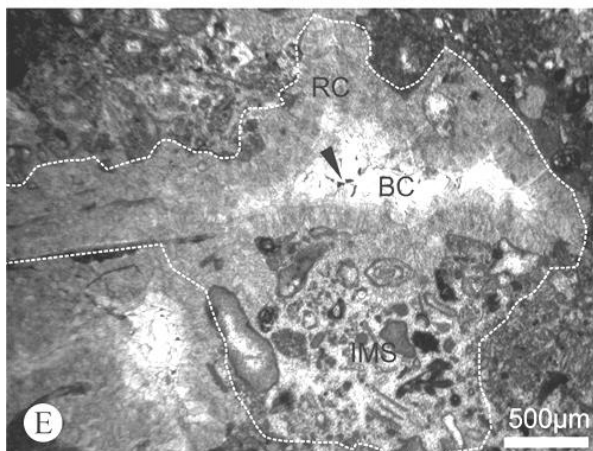
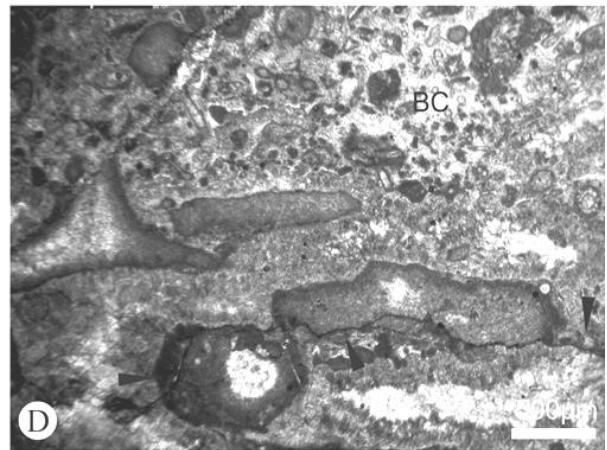
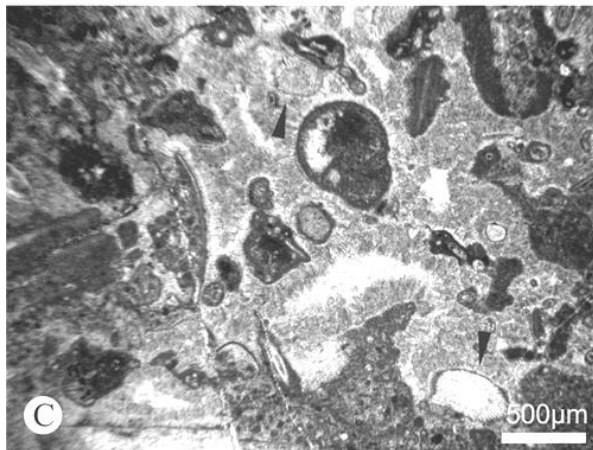
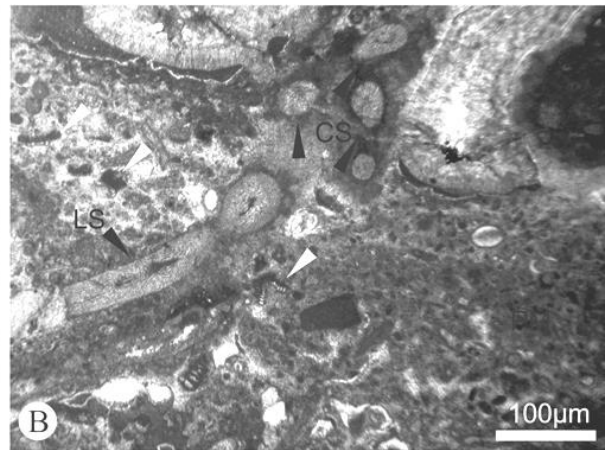
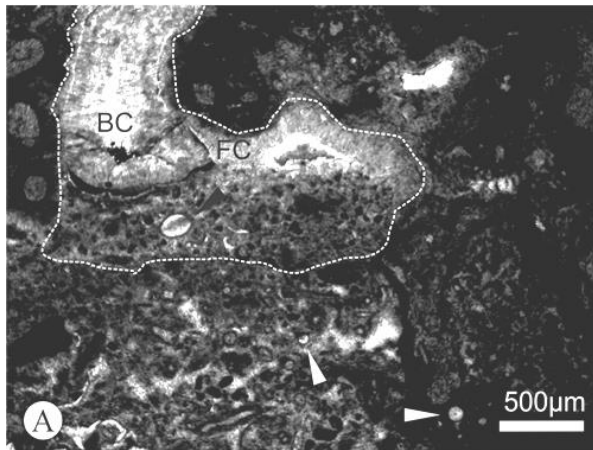


FIGURE - 4.29

A. (PEM 3) The characteristic peloidal sedimentary framework can be observed. Peloids are often rounded and consist of micrite. The peloids are of varying sizes ranging from 10 to 60 μm in diameter and are generally not laminated. Several bioclasts are identifiable including Tuberitinidae (white arrow) and an ostracod (black arrow) which has had micritisation of the shell. The cavity in this photomicrograph exhibits a stromatactoid texture (outlined). A marine sedimentary fill is evident in the flat based cavity as is a crust of fibrous marine cement (FC) and some clear, blocky cement (BC). The cavity also exhibits the characteristic undulating roof. To the right of this image an area of clotted micrite is observable; this texture is a rarity within these samples.

B. (PEM 3) This image is of the area to the right of A. Several bioclasts are present in the image. An 'ancestral red algae' of the ungdarellacea (probably *Ungdarella*) is seen in both cross- (black arrow, CS) and longitudinal section (black arrow LS). The algae display the typical ramified thallus with perithallium consisting of long thin rows of quadratic cells. Several foraminifera's belonging to the genus *Lasiodiscus* are present (white arrows).

C. (PEM 6a) Bioclasts which have been abraded and have a micrite envelope can be seen 'floating' within a fibrous crust of isopachous cement. Two echinoid fragments can be observed (black arrow), both have a micritic envelope and show no sign of syntaxial overgrowth.

D. (PEM 6b) In this photomicrograph a rare stylolite (arrow) can be observed apparently anastomosing around two recrystallised and abraded bioclasts. Many peloids in this image can be seen to have originated from a bioclast of some sort (BC), and so, are probably the products of biological degradation or micritisation. Clear blocky cement is present as the cement within which some peloids are found.

E. (PEM 8) A stromatactoid cavity with an undulose roof and flat base (outlined), with internal marine sedimentary (IMS) fill and a fibrous isopachous crust of cement (FC) with later blocky cement (BC) which has several opaque inclusions (arrow). The internal sediment fill of the cavity can be seen to be different to the sediment which forms the framework of the samples. The internal sediment is essentially a bioclastic grainstone, whereas the surrounding sediments are a bioclastic/peloidal packstone.

F. (PEM 8) Another specimen of an ungdarellacea, this time most likely to be *Komia*. Several encrusted forms can be seen around the ancestral red algae including *Rothpletzella* (white arrows) and small, apparently branching, calcareous tubes which may be either small specimens of *Donezella* or more likely clumps of entwined *Girvanella* (black arrows).

G. (PEM 9) The peloidal nature of the sediments observed within this sub-facies. Peloids are of various sizes and are non-laminated, the sediment is grain supported and has a blocky spar fill wherever micrite is not present between peloids. The black arrow indicates a bioclast (possibly an algae?) which has a geopetal fill, sediment at the base of the body cavity and blocky cement at the top. Ostracods are present in this section (white arrows).

H. (PEM 6a) An accumulation of multi-chambered planispiral miliolinid foraminifera within a homogenous micrite 'clump'. The majority of foraminifera are seen cut along an equatorial section (arrows). These foraminifera are probably encrusters. These are similar to several clumps of foraminifera observed within the Candemuela Mound.

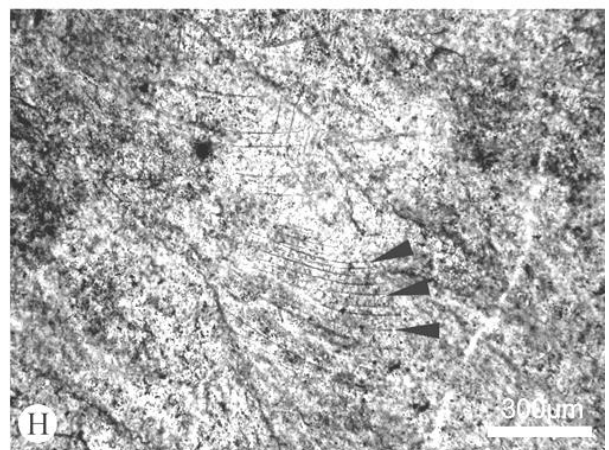
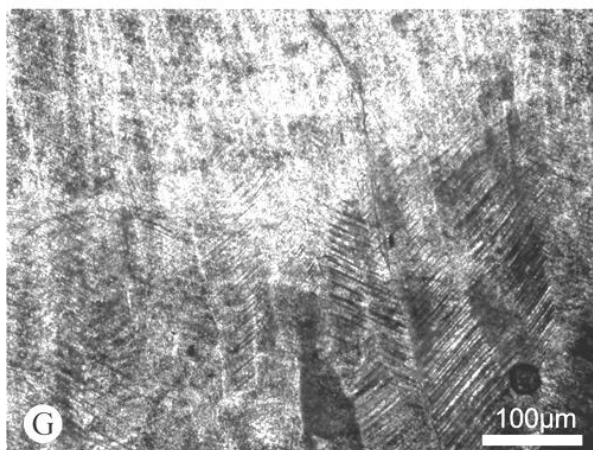
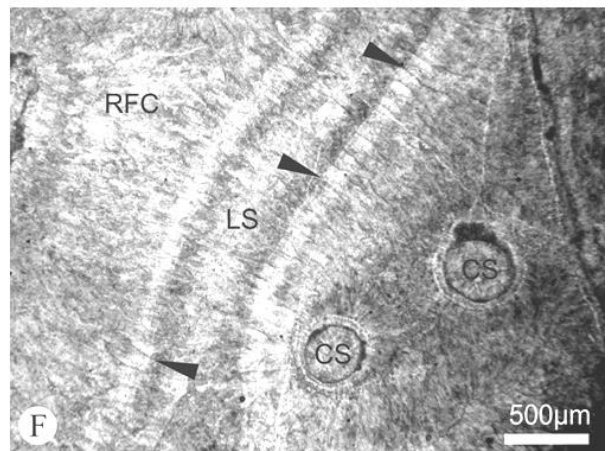
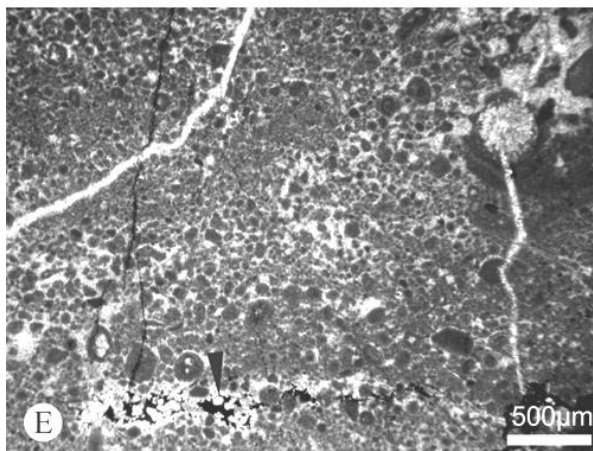
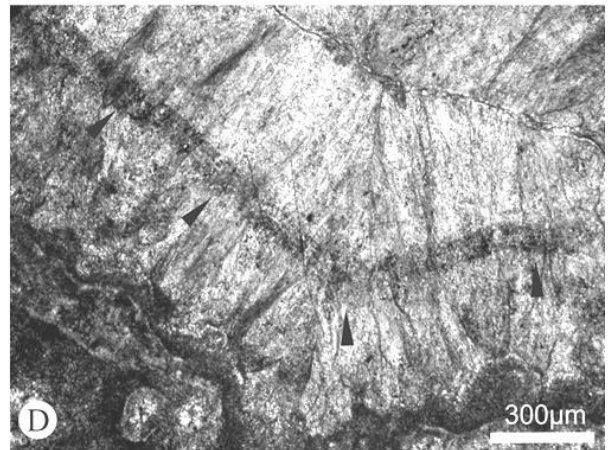
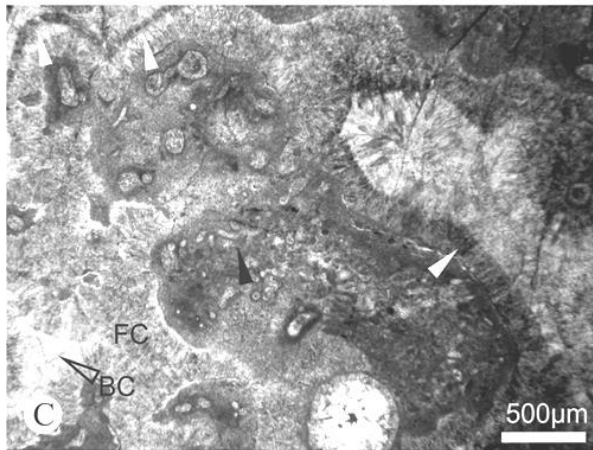
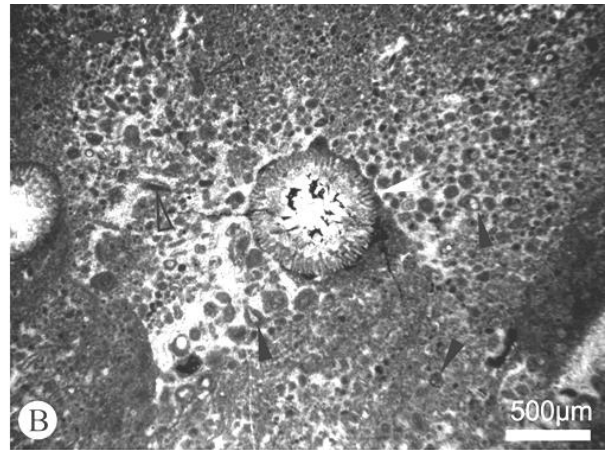
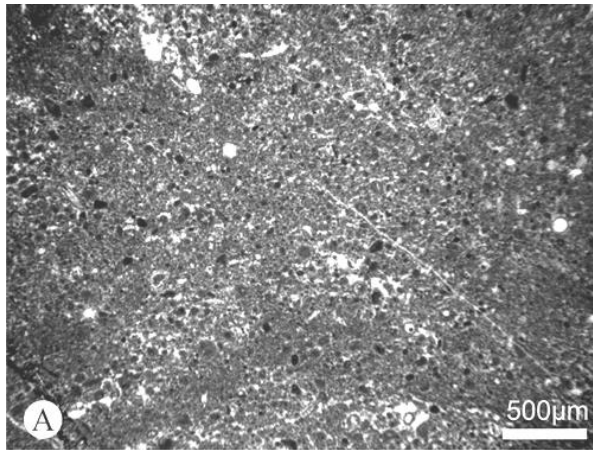


FIGURE - 4.30

A (PEM 9). Pelmicritic grainstone with varying sizes of non-laminated peloids, some small bird's eye and fenestral cavities are present and filled with blocky spar.

B. (PEM 9) A rugose coral (white arrow) with a thin micritic envelope within the peloidal grainstone, many peloids appear rounded and some display evidence of a bioclastic origin, heavily micritised walls can be seen in several examples (black arrows). A few peloids exhibit a tube like geometry (open arrows). Note the opaque crystals within the cavity of the coral.

C. (PEM 10) Cavities with crusts of fibrous, isopachous cements (FC) surrounding homogenous micrite (HM) with calcareous tubes. The tube like structures (black arrow) are bean like shapes and are arranged in a rudimental layer, these tubes may well represent *Girvanella*. Some of the fibrous crusts are cloudier than others (white arrows).

D. (PEM 10) Radial fibrous cement, seen as isopachous crusts within cavities. Crystals grow perpendicular from the substrate and subcrystals can be seen to diverge from the substrate within single crystals. A fine layer of micritic material can be seen running uniformly through the cavity (arrows), suggesting several episodes of crystal growth with gaps between allowing for the deposition of the micrite bands.

E. (PEM 12) Some slight lamination of the peloids may be present in this photomicrograph, several layers of finer/coarser peloids can be seen. Toward the bottom of the image a cavity filled with opaque material with 'floating' spar crystals can be seen (black arrows).

F. (PEM 14) Cross sections (CS) and a longitudinal section (LS) through a solitary, branching fossil that is most likely to be a rugose coral (as seen in hand specimen). The corals are found within fibrous and radiaxial fibrous cement, the fibrous nature of the crystals appears to penetrate the coral walls, suggesting the neomorphism and overgrowth of the fibrous cement over the coral (arrows).

G. (PEM 14) Radial fibrous cement. Crystals grow perpendicular to substrate becoming more and more divergent. Straight twin planes observable, crystals have uniform extinction.

H. (PEM 14) Radiaxial fibrous cement. Subcrystals are divergent within a single crystal. Curved twin planes (arrows). Undulose extinction in the same direction in which the viewing platform is rotated under crossed polars. Dark inclusions may be micro-dolomites.

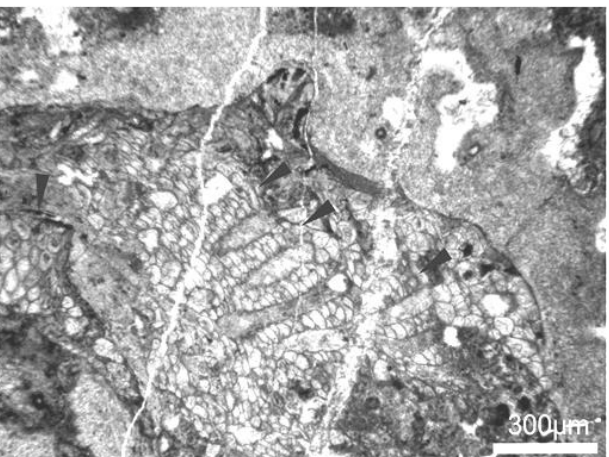
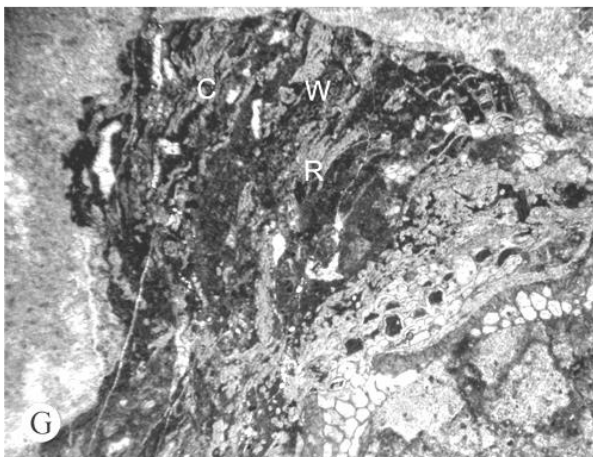
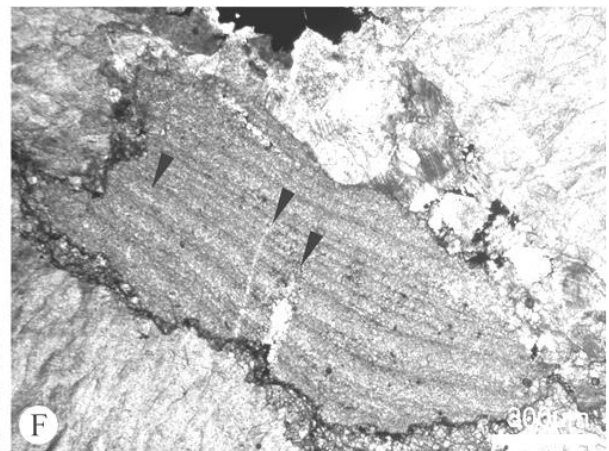
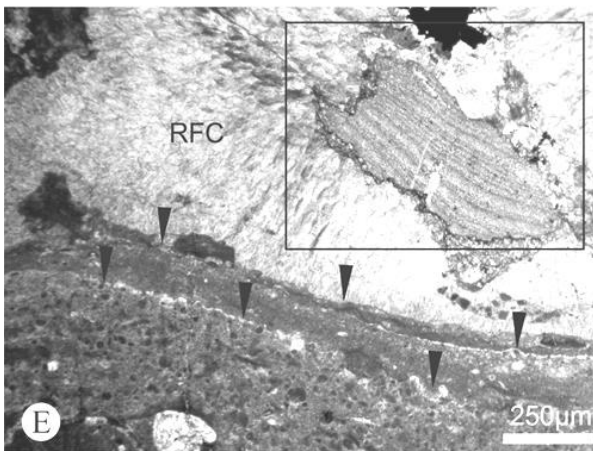
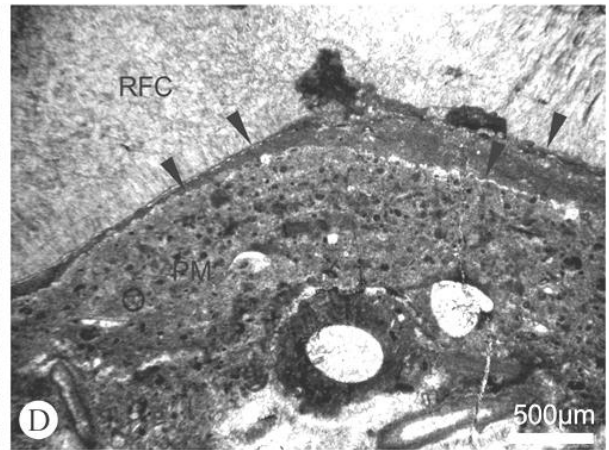
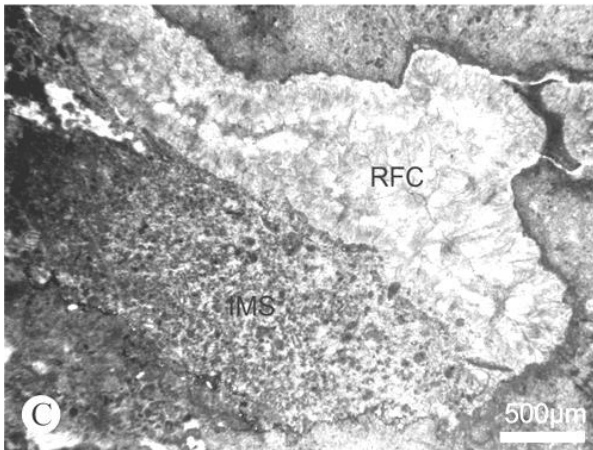
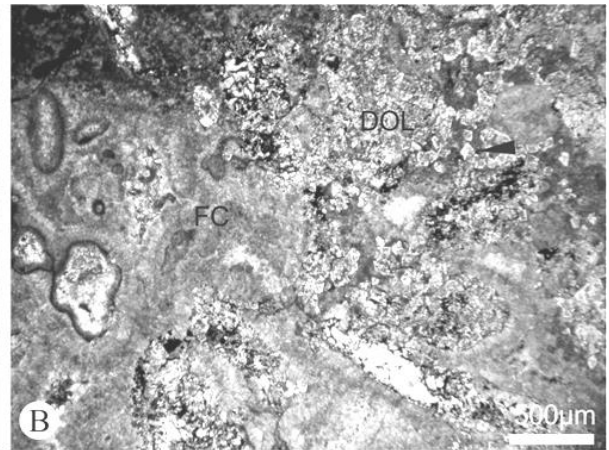
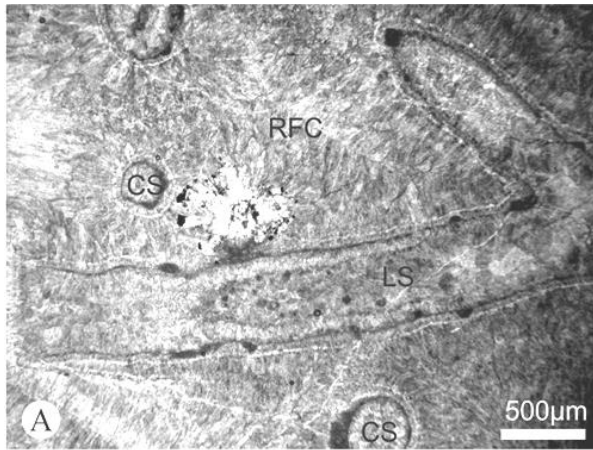


FIGURE - 4.31

A. (PEM 14) Longitudinal (LS) and cross sections (CS) through a solitary and branching rugose coral. Radial fibrous cement surrounds the bioclasts.

B. (PEM 14) Within the samples investigated for this sub-facies very little dolomite is observable, however there are several cavities which have a selective dolomitic fill. In this photomicrograph dolomite rhombs can be seen confined to a cavity with a sharp boundary with fibrous cement (FC) and peloidal micrite (PM).

C. (PEM 21) A Stromatolite cavity exhibiting the characteristic internal marine sedimentary fill (IMS) and radial fibrous cement (RFC). This cavity is lacking the common block spar fill commonly observed within the centre of the fibrous cement fill. The internal sediment fill has a larger proportion of micro-spar crystals as matrix fill between the peloids.

D. (PEM 20) Peloidal micrite (PM) in a homogenous micrite matrix can be observed below a thin layer of homogenous micrite (HM) and finally radial fibrous cement (RFC). Within the peloidal grainstone several larger bioclasts can be seen, possible laminations can be seen within the peloids. Two possible hardgrounds, colonised by encrusting foraminifera are interpreted (arrows).

E. (PEM 20) The same hardgrounds as seen in D. can be seen in this photomicrograph, here several more specimens of encrusting foraminifera can be seen. Note the clast within the radial fibrous cement.

F. (PEM 20) A close-up of the area highlighted in E. A clast consisting of alternating laminae of finer (darker) material and coarser (lighter) material (white arrows). The clast shows no evidence of fossils and laminations appear as if they follow a palaeo-topography. Several vertical fractures are observable (black arrows), these fractures probably represent dewatering fractures. This clast is interpreted to have originated in an extremely shallow, possibly sub-aerial environment and could possibly be a clast of caliche. The angular nature, finely laminated layers and vertical microcracks of the clast, as well as the proximity to two hardgrounds may indicate sub-aerial exposure and possibly a period of non-deposition.

G. (PEM 21) A hemispherical mound of bryozoa, formed by several generations of encrusting bryozoans. The pore structure (arrows) of these bryozoans looks typical of the fistuliporoids. To the left of the image several other encrusting forms are evident; these are the calcimicrobes *Wetheredella* (W), *Rothpletzella* (R) and *Claracrusta* (C). *Wetheredella* appears as layers of hemispherical or bean shaped chambers, *Rothpletzella* are flat to curved sheets of tubes and *Claracrusta* consists of layers of sausage like shape chambers which begin as flat laminations and become increasingly undulose.

Sub-facies two is representative of **samples PEM 1, 2, 11, 15, 16, 17, 18 and 19**. These samples are bioclastic packstones and wackestones of coated and abraded skeletal grains, some pelmicritic material is evident but not in the quantities observed for sub-facies one. Bioclasts consist of shell and bryozoan fragments with whole fossil gastropods, foraminifera, ostracods, calcispheres and algae in various states of preservation. *Donezella* like tubes are present and are found as a branching network, forming framework support for shrub like structures which are often several

millimetres in height and width. Some uncommon, encrusting forms are present although these are found attached to transported, broken bioclasts and are not *in situ*. All bioclasts show some degree of coating by micrite, in some examples the bioclasts can be seen to be completely micritised, micritic envelopes are selective and are more prominent in bioclasts which lack a rigid outer shell (e.g. crustaceans, brachiopods etc.) and are more likely to have had a primary aragonite skeleton (i.e. some 'phylloid' algae). Constructive micrite envelopes are observed on the majority of bioclasts whilst destructive micrite envelopes associated with microborings are observed on clasts which resemble 'phylloid' algae in geometry. The packstones and wackestones are mostly mud supported, with some examples being supported by a sparry calcite. Bioclasts appear to have been transported. Cavity networks are present but are much smaller in size than those observed in sub-facies one and are much less common. Cavity fill consists of honey coloured fibrous cement, found in isopachous layers, often with clear blocky cement toward the centre. The crystals of the fibrous cement have grown perpendicular to the substrate and often terminate in a jagged fashion. Evidence for radial fibrous cement can be observed in several of the larger cavities. Where peloidal micrite is abundant it is a grainstone with no obvious laminations consisting of micrite peloids of varying sizes, peloids are generally rounded in shape. **SMF 10 and 16.** *Bioclastic packstone/wackestone with worn and micritised grains and non-laminated peloidal grainstone.* This sub-facies is characterised by abraded, transported and coated bioclasts forming a pack/wackestone with some substantial accumulations of peloidal grainstones (Fig. 4.32 and Fig. 4.33).

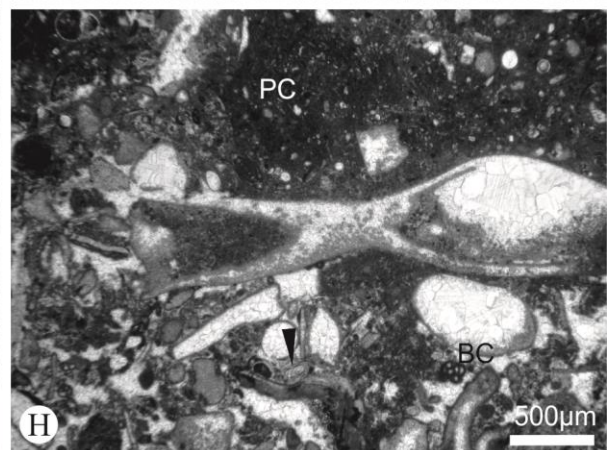
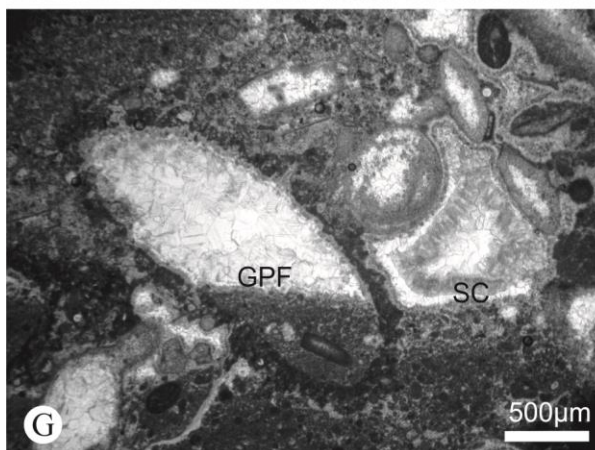
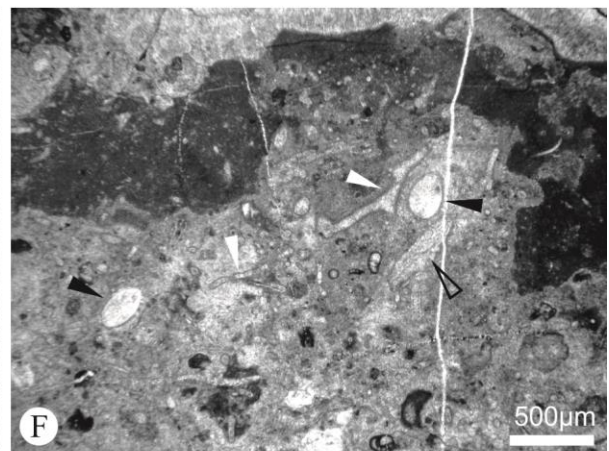
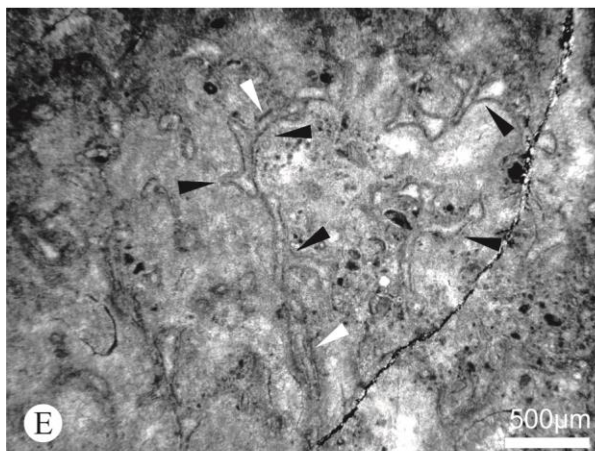
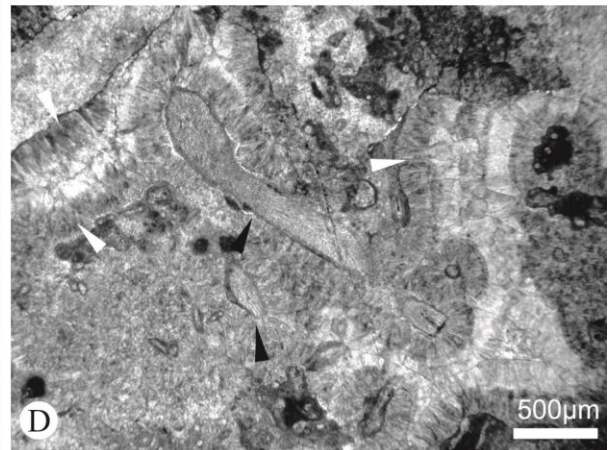
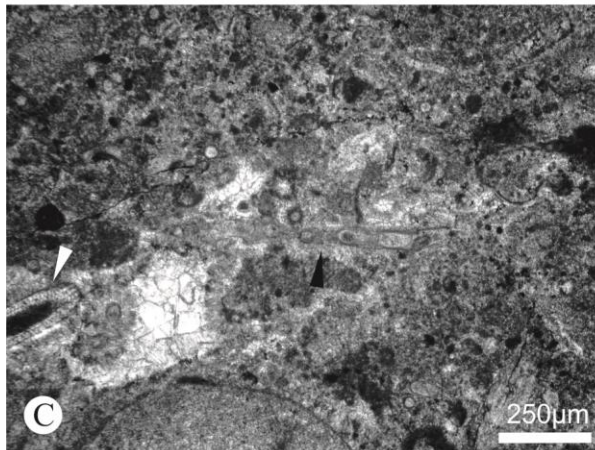
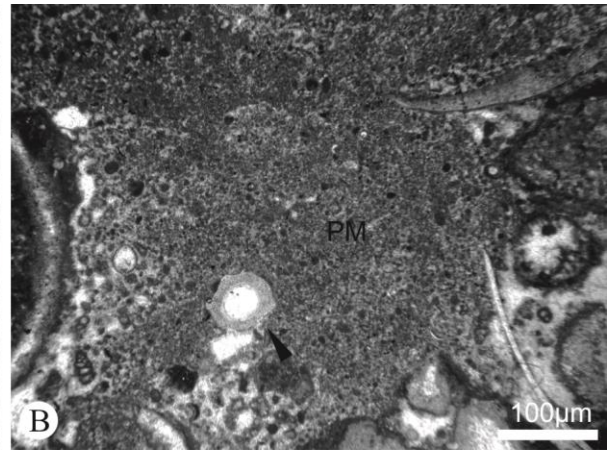
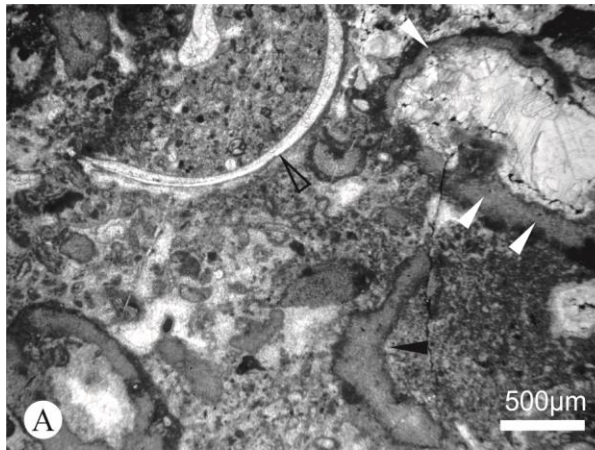


FIGURE - 4.32

A. (PEM 1) Various bioclasts displaying a varying degree of micritisation. A shell fragment (open arrow) with a thin micrite envelope, the shell is possibly a section through a gastropod. The white arrow indicates a grain that has a relatively thick micrite envelope and has been subjected to some boring, as evident by the small hole like structures (the white arrows also indicate these). The clast is filled with blocky spar and a small amount of opaque material. Black arrows indicate some highly degraded and micritised remains, the wall and internal structure is completely micritised and identification is difficult, the elongated, somewhat rectangular shape of the clast may indicate an algal origin. Note the various sized peloids acting as the sedimentary framework, these peloids are exclusively micritic and are all rounded.

B. (PEM 1) A photomicrograph of the peloidal grainstone facies. Several bioclasts are present including a rare echinoid plate (black arrow). The peloids are micritic in nature and are of various sizes, ranging from roughly 1 μm up to 20 μm . Some micritised bioclasts are even larger, the breakdown of these micritised bioclasts is most likely the origin of the peloids.

C. (PEM 2) Various sized peloids and bioclasts. Note the elongate bioclast which appears to be several bulb like chambers stacked one atop another (black arrow). The wall structure looks similar to that of *Donezella*, this specimen may possibly be a reproductive organ of *Donezella*, or of an odd cutting effect through a branching section?

D. (PEM 11) Fibrous cement and blocky spar fill of cavities, which are rare in these samples in comparison to sub-facies one. Isopachous crusts of fibrous cement (white arrows) can be seen growing perpendicular to the substrate with a clear blocky spar at the centre of the cavities. An 'ancestral red algae' most probably *Ungdarella* can be observed acting as the scaffold of these cavities (black arrows). *Ungdarella* is characterised by a ramified thallus with rows of long, thin quadratic cells.

E. (PEM 11) *Donezella lunaensis* Rác is abundant in this image and is characterised by a tube like structure consisting of 'barrels' of wall (white arrow) and its perpendicular branching. The framework created by the specimen observed here is shrub-like and consists of a quadratic pattern created by the branching of several long tubes (black arrows). The top most section of image shows the dark micrite which covers the shrub like *Donezella* growth.

F. (PEM 11) Branching *Donezella* thalli can again be observed (white arrows), capped with a dark, homogenous micrite (HM). Two white ostracods (black arrows) and a specimen of *Komia* can be seen (open arrow).

G. (PEM 15) A micritised grain with a geopetal fill (GPF) juxtaposed next to a stromatactoid cavity (SC) with several generations of cement. The micritised grain has a light micrite wall with a darker micrite envelope, the bioclast has a geopetal fill consisting of internal sediments at the base and blocky spar at the top. The stromatactoid cavity has the characteristic sedimentary fill at the base with fibrous cement and blocky spar fill. The cavity appears to be geometrically related to the bioclasts surrounding it.

H. (PEM 16) Bioclastic grainstone (BG) with a peloidal grainstone (PG). Black arrow indicates broken *Donezella* thallus.

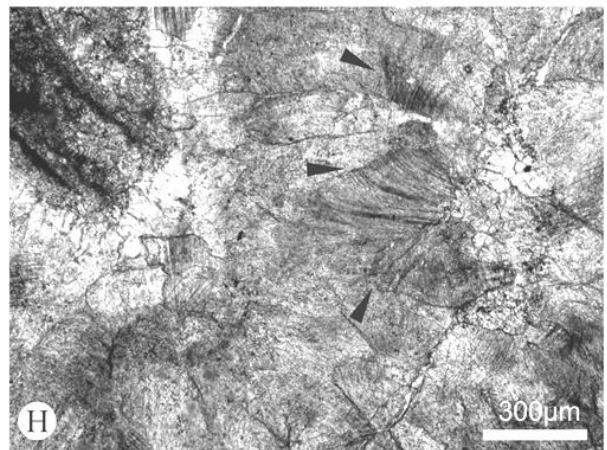
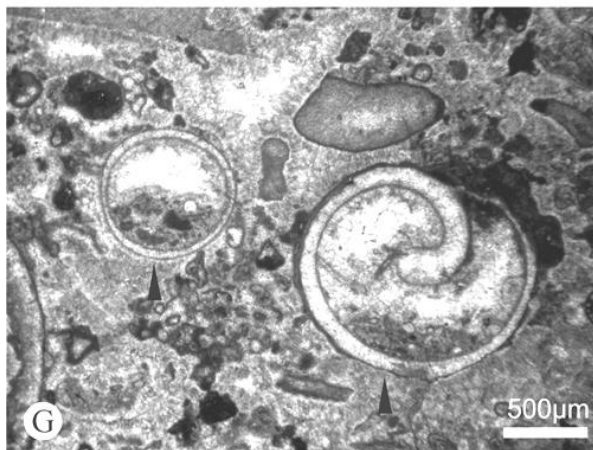
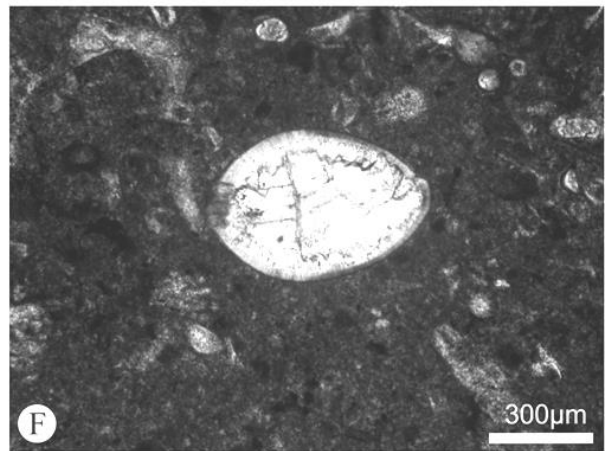
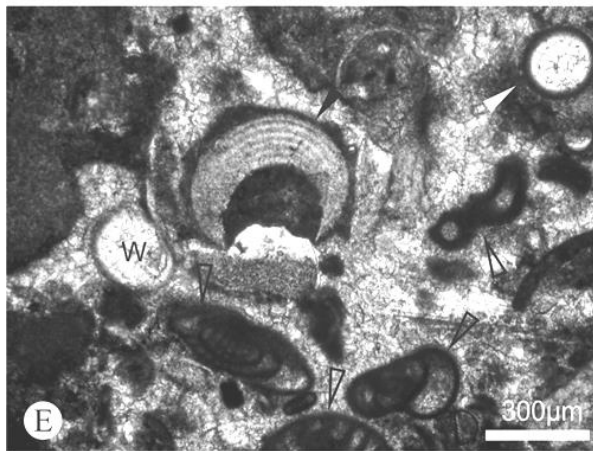
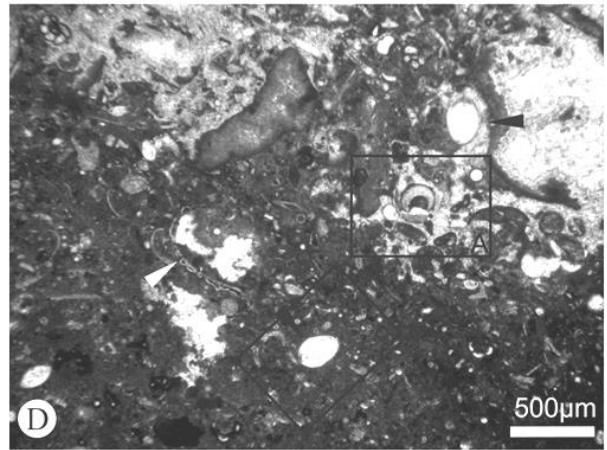
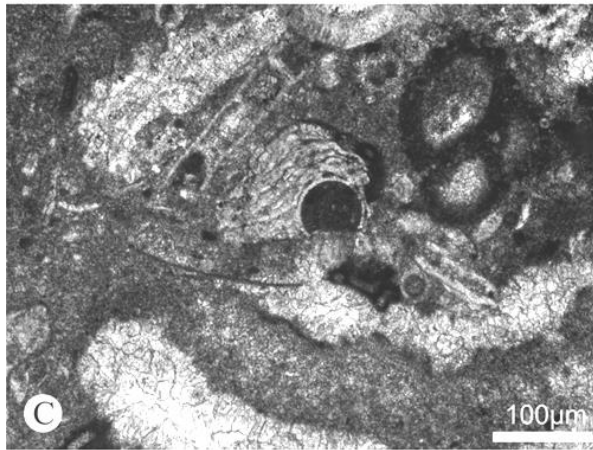
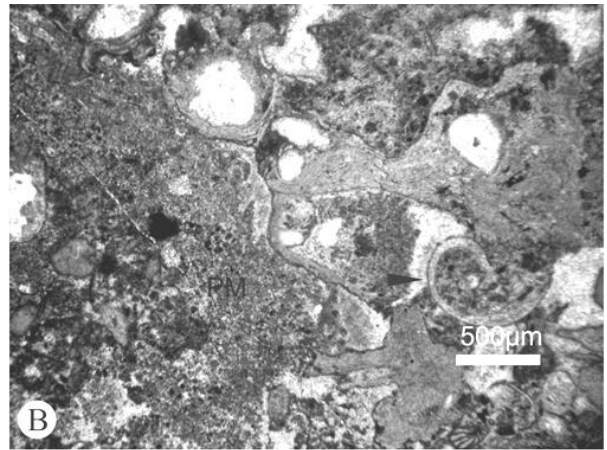
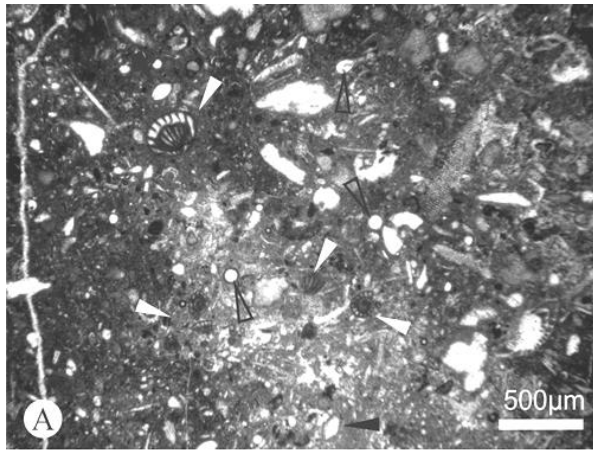


FIGURE - 4.33

A. (PEM 16) Bioclastic packstone consisting of coated and partially abraded skeletal grains, here several multi-chambered planispiral foraminifera can be seen (white arrows) in association with ostracods (black arrows) and Tuberitinae (open arrows).

B. (PEM 16) The calcimicrobe *Rothpletzella* binding several algal thalli together. *Rothpletzella* (arrows) is characterised by flat to curved encrusting sheets of tubes. A gastropod shell is present as is peloidal micrite (PM).

C. (PEM 18) Broken and micritised bioclasts with some laminar cavity structures which are filled with a thin crust of fibrous cement and blocky spar. A broken *Donezella* thalli and encrusting *Rothpletzella* are notable bioclasts.

D. (PEM 18) Various sized peloids and bioclasts forming a bioclastic packstone. The larger grains tend to be bioclasts, here ostracods (black arrows) and encrusting foraminifera (white arrow) can be identified. A fenestral cavity with a fibrous isopachous crust and blocks spar fill can be seen toward the top right corner.

E. (PEM 18) Close-up of area 'A' highlighted in D. A solenoporacean red algae, probably *Solenopora*, a nodular thalli with distinct growth zonation and some micro-boring (black arrow). Other bioclasts include a *Tuberitina* (white arrow) a solitary *Wetheredella* (W) chamber and several multi chambered foraminifera (open arrows).

F. (PEM 18) Close-up of area 'B' highlighted in D. An ostracod clearly displaying two valves with obvious overlap, the thick wall is relatively well preserved. The ostracods in these samples are all white, suggesting a shallow burial depth.

G. (PEM 19) Gastropod shells with geopetal fills (arrows), both display a thin micritic envelope.

H. (PEM 17) Radial fibrous cement. Curved twins (arrows) and sub-crystals which become divergent within a single crystal.

Sub-facies three represents samples **PEM 4** and **7**. This sub-facies is by far the least common sub-facies observed within the Pinos East Mound. These samples are coated bioclastic packstone/grainstone, the diversity of bioclastic material is high and the size of the bioclasts is larger than in the other two sub-facies. All bioclasts have a micrite envelope, most are destructive with clasts bored and strongly micritised/recrystallised indicating a possibly originally aragonitic skeleton. Dasyclad algae are common as are small foraminifera. Large algal clasts (500 µm wide and well over 500 µm long) are commonly observed. Some bioclasts have evidence of micro-borings and biogenic encrustations and are therefore cortoids. There are still some micrite peloids which act as a sedimentary framework and in some cases are found as a cavity fill. Cavity networks are small compared to sub-facies one and two and are rare. Fenestral cavities are often

filled with blocky spar but in some cases the isopachous fringe of fibrous cement is present. **SMF**

11. Coated bioclastic grainstone. These samples are characterised by oncoids and bioclasts which are abraded and coated with micrite (Fig. 4.34).

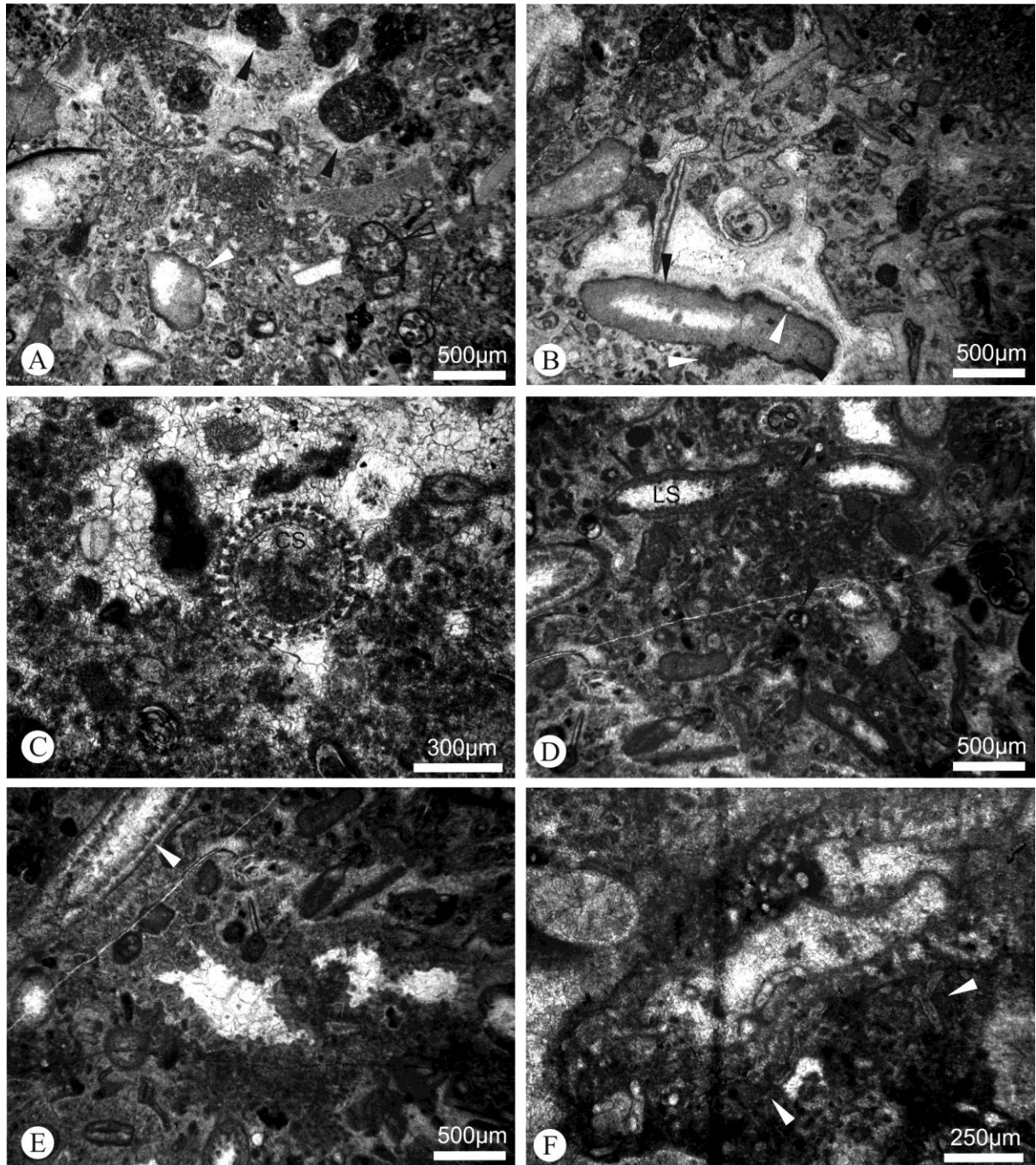


FIGURE - 4.34

A. (PEM 4) Bioclasts and oncoids ranging from $<10\ \mu\text{m}$ to $>500\ \mu\text{m}$, many of the grains which appear to be peloids are small (or fragments of) bioclasts. Two types of oncoids can be observed,

dark thrombolitic oncoids (black arrows) and lighter oncoids with a darker outer layer and often blocky spar toward the centre (white arrows). The darker oncoids may have been formed by calcimicrobes, their thrombolitic nature is evidence of this. Foraminifera are also present (open arrows).

B. (PEM 4) Oncoids and coated bioclasts are here surrounded by radial, fibrous cement. One of the few fenestral cavities found in this sub-facies can be observed with a fill consisting of a thin, honey coloured isopachous fringe of fibrous cement with a clear blocky spar fill. Oncoids show evidence of micro-boring (black arrows) and bio-encrustation (white arrows).

C. (PEM 4) and D (PEM 7) Cross section (CS) and longitudinal section (LS) through a dasyclad algae with a thick, perforated wall. In D other bioclasts include foraminifera (black arrows) and a gastropod (white arrows)

E. (PEM 7) The dasyclad algae (arrow) in this section has a peripheral zone consisting of thin cortical branches separated by a clear infill. The wall is a continuous calcite layer in a thin micrite envelope. This specimen is probably *Beresella*. The cavity at the centre of the photomicrograph is fenestral and doesn't have any fibrous fringe of cement and is just blocky spar.

F. (PEM 7) A clump of *Donezella* (arrows) forming a small cortoid. The *Donezella* appear to have grown around a bioclast which has been bored and micritised. *Donezella* thickets possibly suggest a shallow water environment.

4.5.2 Interpretation

The mound facies of the Pinos East Mound has been subdivided into three sub-facies, each of these facies represents different microfacies types and therefore a different environment of deposition. Sub-facies one is characterised by micritic peloids and common fenestral and stromatactoid cavities, the specimens were deposited within a restricted environment which is interpreted to have been very shallow, with some evidence of sub-aerial exposure. The biotic assemblage is similar to that observed for much of the Candemuela Mound, however, Donezelliaceans and Beresellids are not present and larger bioclasts, including corals, gastropods and bryozoans, appear more often. Bioclasts often show some degree of abrasion and constructive micritic envelopment. It is suggested that the depositional environment for sub-facies one was within shallow, warm water which had relatively normal salinity (as indicated by the varied biological assemblage). Sub-facies two has a higher abundance of 'larger' bioclasts (>300 µm) than sub-facies one. Most bioclasts show evidence of transport, for example broken *Donezella* thalli. Micrite envelopes of both a destructive and constructive nature are again observed. Cavities are smaller and rarer and the occurrences of *Donezella* acting as a frame builder are the greatest

differences between sub-facies one and two. Sub-facies two is interpreted to have been deposited at wave base, in a slightly deeper environment than sub-facies one. The biological assemblage is once again quite diverse suggesting that the environment is not hyper-saline or brackish. Sub-facies three contains the highest amount of bioclasts and cortoids measuring >500 µm. Once again micritic envelopes are present which would suggest that sub-facies three, like one and two, was deposited in shallow warm water. The destructive micritisation of several bioclasts is extensive resulting in rounded clasts of dark, homogenous micrite, with associated micro-borings - this advanced micritisation (in comparison with specimens from sub-facies one and two) would suggest a shallower and warmer environment where micritizing calcimicrobes are more prolific. The higher abundance of algae may also suggest a shallow environment.

The abundance of rounded peloids and bioclasts/cortoids would suggest constant water action for all three sub-facies indicating a position at, or above wave base. Flügel (2004) notes that grainstones with cortoids can often be associated with patch reefs scattered across a shelf or in a leeward position behind reef belts. Sub-facies one is interpreted to have been deposited within a restricted setting with occasional sub-aerial exposure, sub-facies two had a restricted to slightly open marine setting whilst sub-facies three is interpreted to have been deposited on the leeward flank of a platform margin or equivalent setting, in the case of foreland basin deposition this most likely corresponds to the forebulge or topographic high related to piggy back basins.

Pyrobitumen observed within this mound may indicate that the structure has acted as a hydrocarbon reservoir in the past. Table 4.3 summarises the microfacies analysis of the Pinos East Mound

Samples	SMF	Characteristics	Interpretation
3, 5, 6, 8, 9, 10, 12, 13, 14, 20, 21 and 22 (sub- facies 1)	21 with 16	Fenestral packstone of spar filled cavities within a peloidal grainstone/packstone (non-laminated).	Shallow depth, at, or within wave base. Occasional sub-aerial exposure.

1, 2, 11, 15, 16, 17, 18 and 19 (sub- facies 2)	10 with 17	Bioclastic packstone with worn and abraded skeletal grains, with a grainstone of peloidal micrite.	Shallow depth, at wave base, slightly deeper than sub-facies one.
4 and 7 (sub- facies3)	11	Coated bioclastic grainstone.	Shallow depth, leeward flank of forebulge.

TABLE - 4.3 Summary of the main standard microfacies, characteristics and interpretations of the Pinos East mound.

4.6 Sena de Luna Mound

30T 258869.07 4756321.56

This mound is situated just to the south of Sena de Luna, directly adjacent to the campsite Rio Luna. The mound forms part of a carbonate ridge with clastic sediments to either side. Several ‘featureless’ mounds can be observed within what is mostly bedded limestones in the area. The mound is a light blue/grey micrite lacking in primary geological features with bedded and slightly nodular, darker micrites below. Several shelly fragments and some echinoid fragments were found in the bedded material. The area appears quite tectonised and the outcrops are fractured, as a result samples 1 and 9 are not useful for the microfacies analysis. Sample 11 was taken from a fractured area which has been dolomitised and is also of no use for the microfacies analysis. The mound has a recognisable basal/flank facies and a mound facies which have some cross overs.

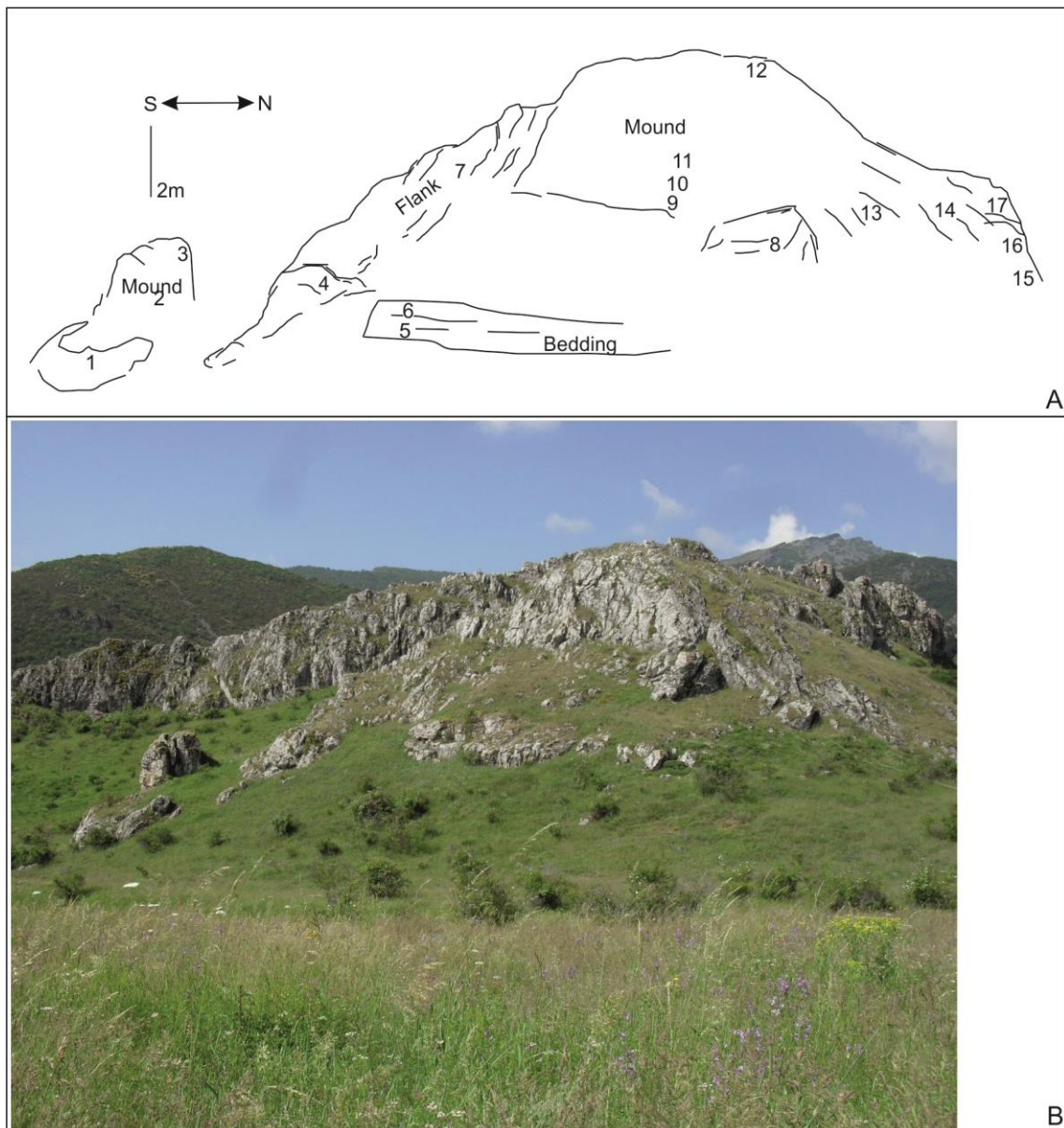


FIGURE - 4.35 A. An annotated sketch of the Sena de Luna mound, with sample locations numbered. B. Field photos.

4.6.1 Basal and Flank Facies

The basal and flank facies (**samples SDL 4, 5, 6, 7 and 8**) are found as bedded units beneath the mound, samples 4 and 7 are taken from beds which appear to truncate onto and onlap the mound structure. The major textures observed are coated and abraded bioclasts and cortoids sometimes associated with cavities. Bioclasts include foraminifera, broken algal thalli and shelly fragments. A micritic envelope enclosing all bioclasts is observable, ranging from a thin lamination to a thick agglutinated coating of calcified tubes and dark homogenous to slightly peloidal micrite. Evidence

of micro-boring of the bioclasts is absent, the micrite envelopes are constructive and several clasts are better classified as oncoids. Non-laminated peloidal sediment accounts for the majority of sediment in the facies, peloids are rounded, of various sizes and occasionally have a sausage or bean like geometry and can often be seen in clumps and bush like structures. Where the peloidal micrite texture is absent a fibrous or blocky spar is present. The fibrous cement is found as isopachous fringes between clasts (coated bioclasts or cortoids), it has a yellow or honey colour and is sometimes seen as a partial cavity fill. **SMF-11** and **SMF-16-Non-Laminated**. *Coated Bioclastic grainstone* and *Non-Laminated Peloidal boundstone*. This facies is characterised by bioclasts with a constructive micritic envelope within a peloidal and sparry sedimentary fabric (Fig. 4.36).

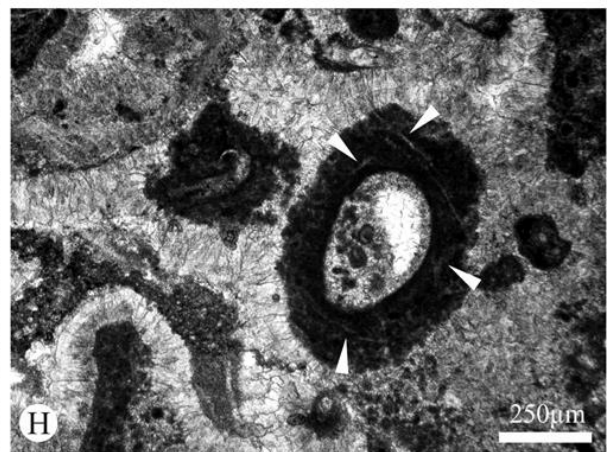
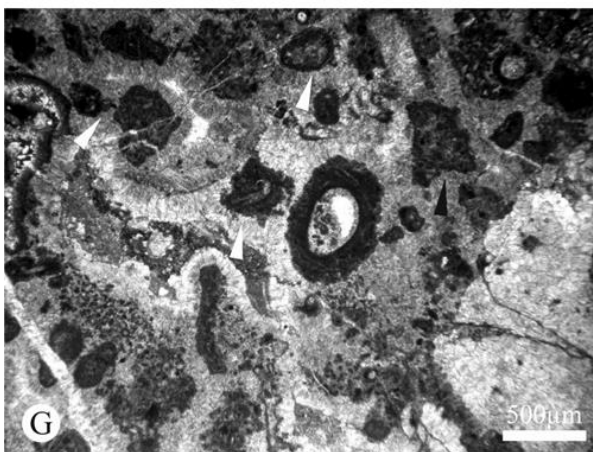
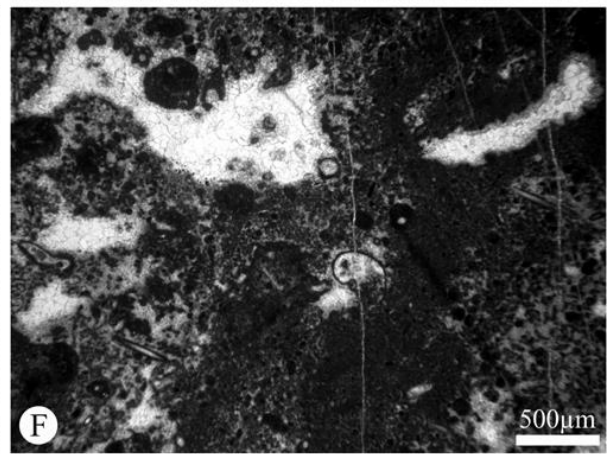
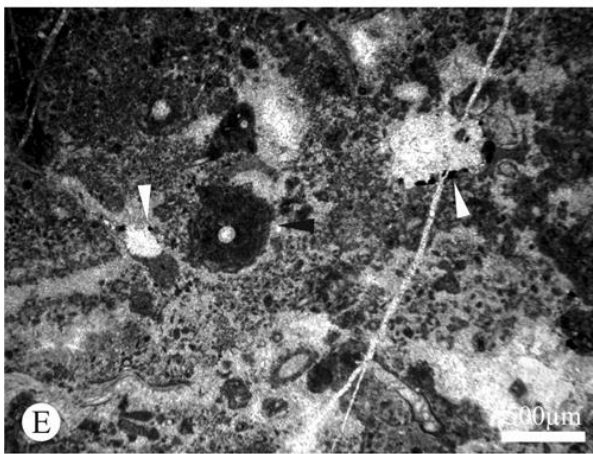
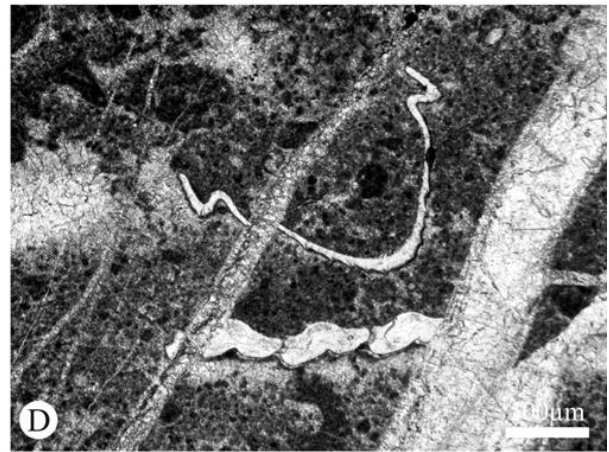
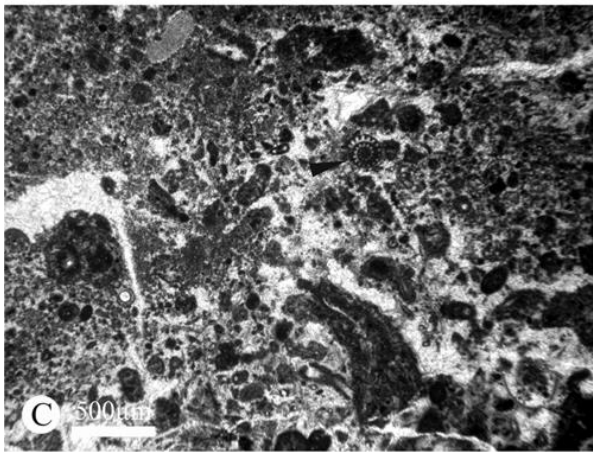
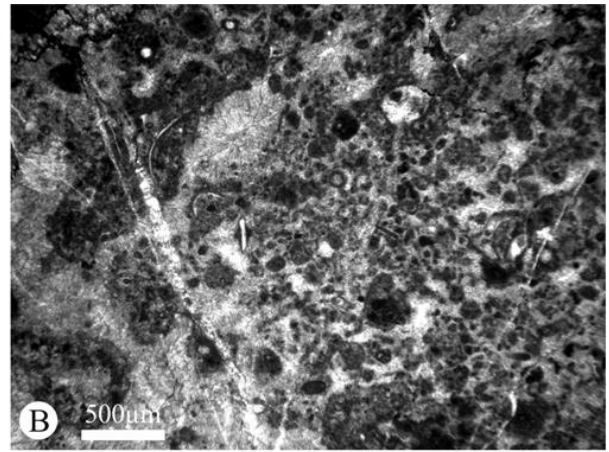
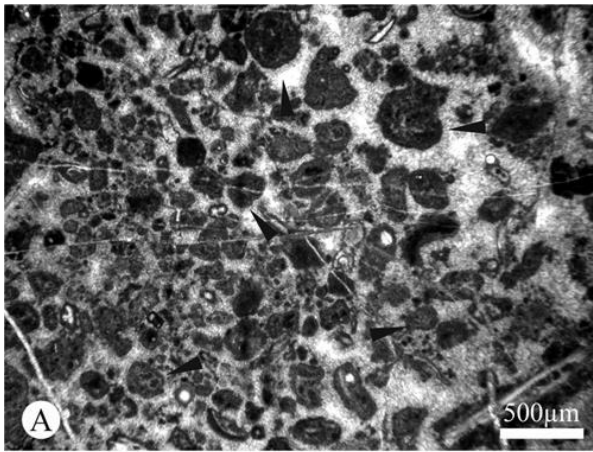


FIGURE - 4.36

A. (SDL 6) A photomicrograph of coated bioclasts within a spar cement. The majority of the clasts are oncoids (arrows) which consist of laminations of dark and light micrite. The coating on the bioclasts is a thin micrite of constant thickness. The spar cement which fills the space between clasts consists of both a honey coloured fibrous spar and a clear blocky spar.

B. (SDL 8) Coated bioclasts and peloidal grains of varying sizes and shapes, though all are rounded. A variation in the density of micrite forming the peloids is also clear, lighter peloids are less closely packed micrites which occasionally have some microspars. The darker, almost opaque peloids are composed of densely packed homogenous micrite. The darker micrite can often be seen enveloping bioclasts.

C. (SDL 4) Coated bioclasts and peloids, here a rare Fusulinid foraminifera can be identified (arrow)

D. (SDL 5) Shelly fragments with a very fine micrite envelope

E. (SDL 5) A conspicuous oncoid (black arrow) within a peloidal sedimentary framework with several thin laminar fenestral cavities. The oncoid has a spherical bioclastic nucleus which may have a porous wall structure? The coating of the bioclast consists of alternating dark micritic clumps and lighter micritic layers. Several cavities are present in this photomicrograph, within these cavities a cubic, opaque mineral is present (white arrows), most likely pyrite.

F. (SDL 6) Peloidal micrite closely spaced forming an almost homogenous micrite. Toward the centre a gastropod shell can be observed.

G. (SDL 7) Several oncoids (white arrows) are observable in this image they reside within a fibrous spar cement with some peloidal micrite. An angular clast of peloidal micrite is also indicated (black arrow), this suggests some form of reworking of the peloidal sediments.

H. (SDL 7) A close-up of the area highlighted in G. Here the coating of an oncoid can be seen clearly. The coating can be seen as dark peloids with thin layers of a lighter micrite. Several calcareous tubes can also be observed, these are likely to be encrusting *Girvanella* tubes (arrows)

4.6.2 Mound Facies

The mound facies (**Samples SDL 2, 3, 10, 12, 13, 14, 15, 16 and 17**) mainly consists of homogenous and peloidal micrite. Several stromatactoid cavities are present and oncoids are a common constituent. Micrite is often homogenous but also occurs as peloids in poorly laminated layers or columns and clumps. Peloids are rounded and of various size and most appear to be formed of homogenous micrite but others can be seen to include bioclastic fragments and calcareous tubes. Oncoids are rounded and consist of a nucleus (generally a bioclast) which is enveloped in consecutive layers of dark, peloidal and tube like micrite and a lighter micrite. Oncoids are deposited apparently randomly throughout a peloidal framework. Stromatactis cavity networks occur in laminar sheets and consist of flat bottomed, undulose roofed cavities with a

lower filling of internal sediments (mostly peloidal micrite) and a spar filling consisting of an isopachous fringe of honey coloured fibrous cement, and a clear, blocky spar. Biodiversity is low, bioclasts make up less than 5% of the constituent parts and those present include shell fragments and some foraminifera. **SMF 16-Non-Laminated** and **21-Fen.** *Non-laminated peloidal grainstone* and *fenestral wackestone*. These are characterised by non-laminated micritic peloids with oncoids and laminar fenestral and stromatactoid cavity networks (Fig. 4.37).

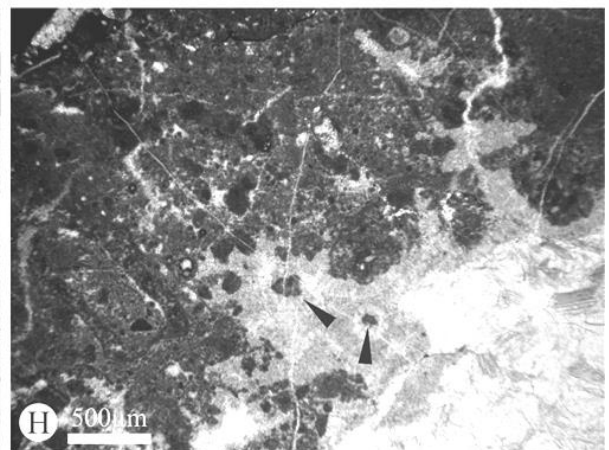
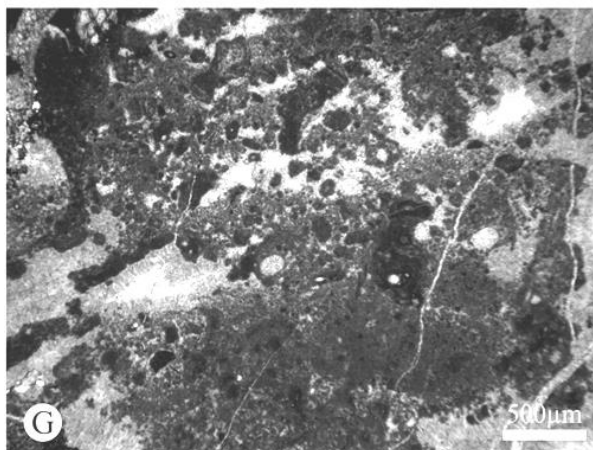
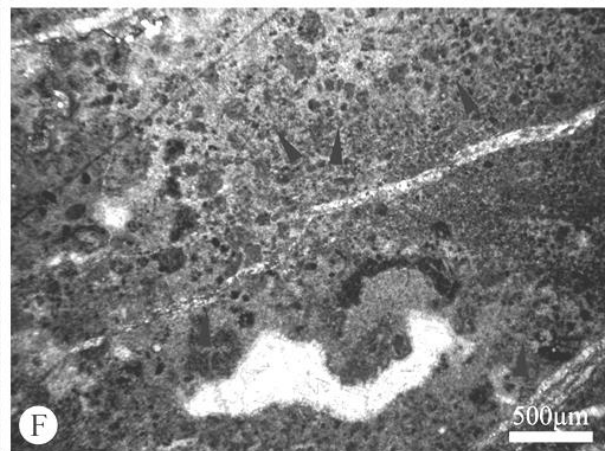
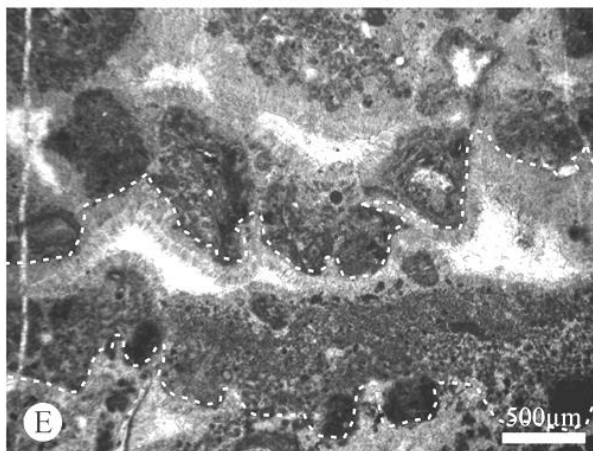
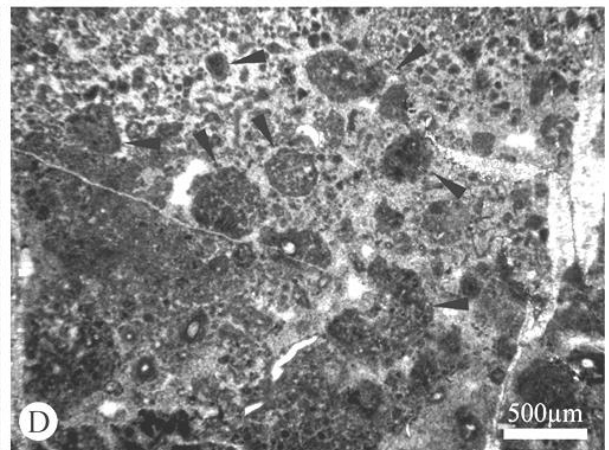
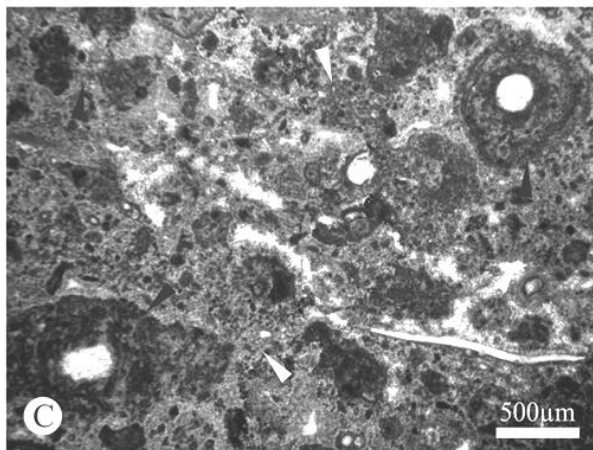
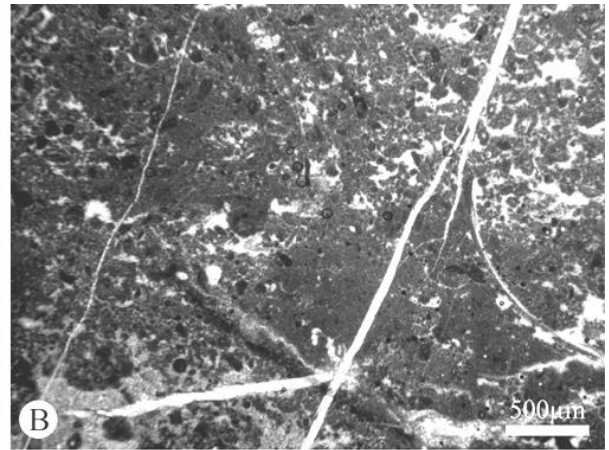
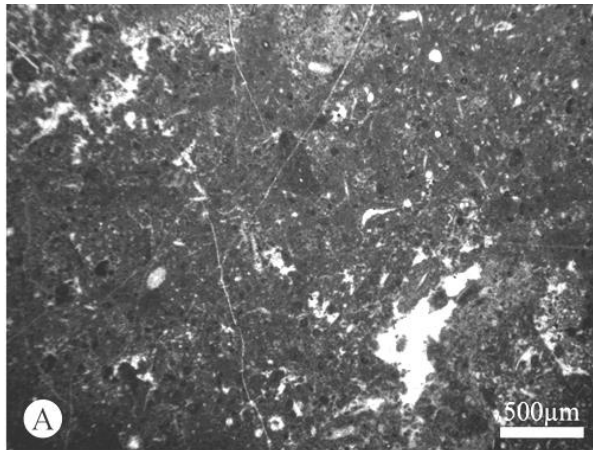


FIGURE - 4.37

A. (SDL 2) Peloidal and homogenous micrite with very few bioclasts and several small laminar fenestral cavities.

B. (SDL 14) Laminar fenestral cavities are quite dominant in this image, they are filled with a clear, blocky spar. The micrite is mostly homogenous with a few peloids and very few bioclasts. Peloids have various sizes and are often darker in appearance than the surrounding homogenous micrite.

C. (SDL 15) Here the micrite component of the sample has become more peloidal and also exhibits some oncoids. Peloids (white arrows) are of various sizes and are not laminated, they have been deposited in association with the larger oncoids (black arrows). The oncoids generally have an obvious nucleus with subsequent layers of clotted micrite layers and layers of more homogenous micrite. Several of the oncoids appear to have a very thin micritic envelope.

D. (SDL 17) Oncoids (arrows) form an important sedimentary role in some areas. Here multiple oncoids can be observed in association with peloids and some homogenous micrite. Where micrite isn't present as a cement between oncoids and peloids, a fibrous, honey coloured spar is found in isopachous fringes. The oncoids often have a conspicuous nucleus with clotted micrite layers surrounding it. Often the clotted micritic laminations appear as layers of 'sausage' or 'bean' shaped clumps of micrite with alternating homogenous layers of micrite.

E. (SDL 13) Several excellent examples of laminar stromatactis cavities (one layer is outlined), with characteristic flat bases, undulose roofs, internal sedimentary fill and both fibrous and blocky calcite cements. The sedimentary fill consists of fine peloids with very rare bioclasts. Spar fill consists of a fibrous calcite which is honey coloured and contains inclusions which make it appear drusy, this cement forms as a fringe of elongate crystals growing perpendicular to the substrate. This fibrous layer is in filled with a clear blocky spar. In this example the cavities are very closely spaced, with the top of one set of cavities forming the base of the next.

F. (SDL 10) Peloidal micrite exhibiting a thromboidal texture in several places (arrows), although the majority appears as non-laminated peloids of various sizes. The fenestral cavity toward the bottom has the characteristic flat bottom and undulose roof.

G. (SDL 3) Oncoids, peloidal micrite and stromatactoid cavities, again the amount of bioclasts observable is low as is overall biodiversity. The sedimentary framework consists of a pelmicritic to homogenous micritic texture. In this example oncoids seem to be more abundant within the sedimentary infill of the stromatactoid cavities than they are in the matrix material.

H. (SDL 3) In this photomicrograph a large stromatactoid cavity can be observed with mud chips included within the fibrous calcite cement, this suggests that the sediment wasn't fully lithified when the fibrous cement was precipitated.

4.6.3 Interpretation

The Sena de Luna Mound has a relatively similar basal/flank facies and mound facies, both are partially characterised by SMF 16-Non-Laminated. The major differences between the facies are the presence of bioclasts in the flank and cavity networks within the mound. The coated grains consist of both bioclasts with a thin micritic envelope and also oncoids consisting of coatings of

various thicknesses with evidence of calcimicrobial sheaths. The coated bioclasts in the flank and basal material suggests that they were probably deposited in a marginal setting, the bioclasts which form the nucleus of these coated grains show no sign of boring or other abrasion and therefore the micritic envelopes are likely to be constructive in origin, indicating a low energy environment. Although not completely missing from the mound facies, coated grains are almost totally confined to those consisting of a spherical nucleus with a clotted micrite and calcitic tube coating. Clasts consisting of shell and bryozoan fragments of foraminifera with a thin micritic coating are missing. There are a large number of laminar fenestral and stromatoloid cavity networks within the mound facies. Evidence for cyanobacteria is in the form of thrombolitic textures within the peloidal micrites, which indicate a bifurcated origin, possibly a calcimicrobe like *Renalcis*, and calcitic tubes preserved within the coatings of oncoids and within several peloids. The mound is interpreted to have formed due to increased restriction and shallowing of the depositional environment. Very few *Donezella* were observed at this location. Table 4.4 summarises the microfacies analysis of the Sena de Luna Mound.

Samples	SMF	Characteristics	Interpretation
4, 5, 6, 7 and 8 (base and flank)	11 and 16-Non-laminated	Bioclasts with a constructive micritic envelope within a peloidal and sparry sedimentary fabric.	Moderate/low depth, open, low energy environment. Below wave base.
2, 3, 10, 12, 13, 14, 15, 16 and 17 (mound)	21-Fen and 16-Non-laminate	Non-laminated micritic peloids with oncoids and laminar fenestral and stromatoloid cavity networks.	Very shallow depth, restricted environment, within wave base – low - moderate energy, lagoon-like environment.

TABLE - 4.4 Summary of the main standard microfacies, characteristics and interpretations of the Sena de Luna mound.

4.7 Cármenes South Mound

30T 291652.20 4758406.30

This Mound is found in the Bernesga Valley, to the South of Cármenes near to the village of Almazura and forms part of a thin limestone ridge, along which numerous mound features can be observed. The mound is a light, creamy grey in colour and is micritic and lacking in any observable primary geological features (Fig. 4.33). A few rare shell fragments were found in the flank material in hand specimen and veins of calcite are common through some areas of the mound. Both a mound and a basal facies were identified for this mound, with the mound being separated into three sub-facies.

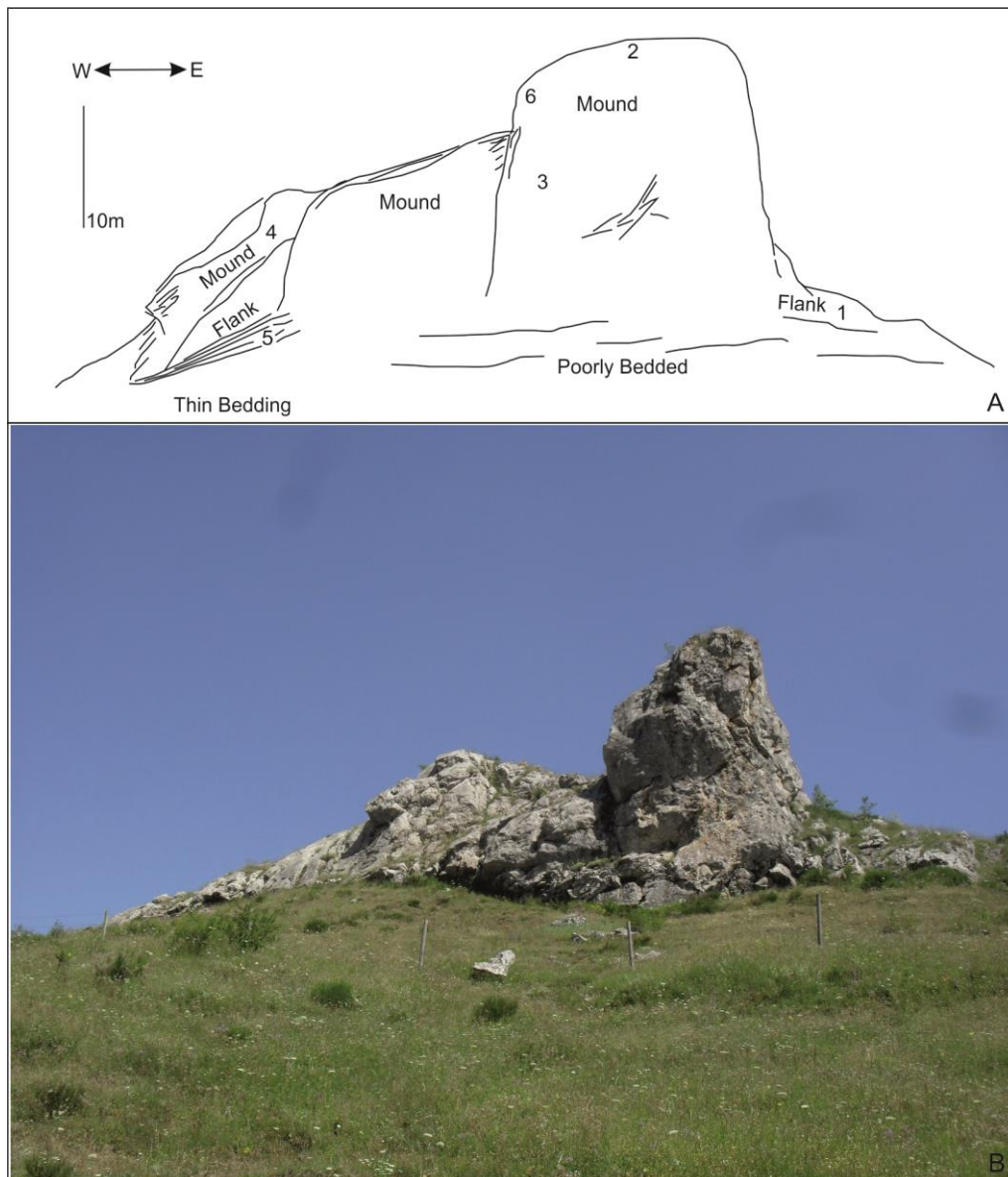


FIGURE - 4.38 A. An annotated field sketch of the Cármenes South Mound, sample points are highlighted. B. Field photo.

4.7.1 Basal Facies

The basal facies (**samples CSM 1 and 3**) is relatively heavily fractured and as such many calcite veins run through the samples, as do many stylolites. The abundance of veins has helped identify some stages of diagenesis for this mound. Although the samples are highly fractured and stylolitised the basal facies can still be recognised as being a skeletal-microbial bafflestone, consisting of branching and entwining *Donezella* thalli with thrombolytic, clotted and peloidal micrite in between. The *Donezella* has the characteristic barrelled, tube like thalli. Dark

homogenous micrite as well as peloids which are clotted or thrombolytic in nature can be seen occupying the gaps between each thalli. Some areas between thalli are filled with a clear blocky cement, which may act as a bio-cement in some cases. Several cavities in the basal facies have been selectively dolomitised and several of these cavities also appear to have opaque minerals concentrated within them. Several veins show evidence of early burial cementation, most veins in the sections studied have exhibited a pink/red colour when stained. Several veins here show a blue colour where stained, indicating a ferroan calcite as opposed to the non-ferroan pink/red colour staining. Some zoning within individual crystals can be observed. **SMF 7-Bafflestone.** *Algal bafflestone*. Characterised by branching and entwined *Donezella* with associated baffled sediments consisting of peloidal, clotted and thrombolytic micrite (Fig. 4.38).

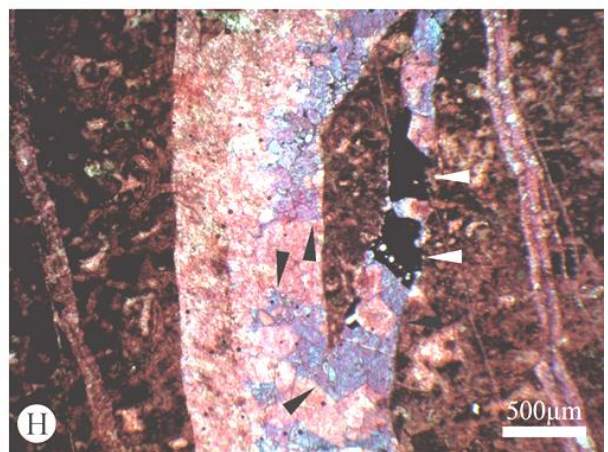
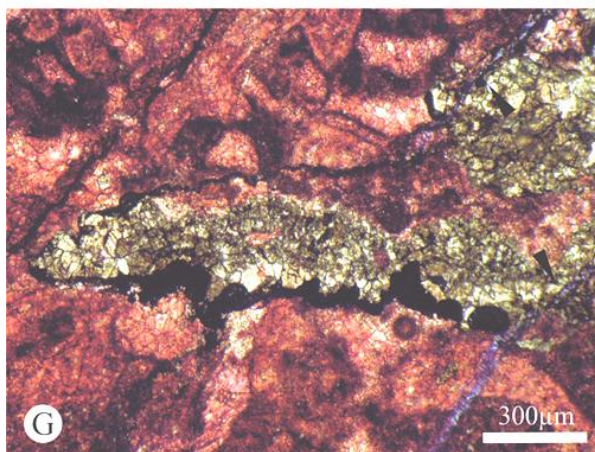
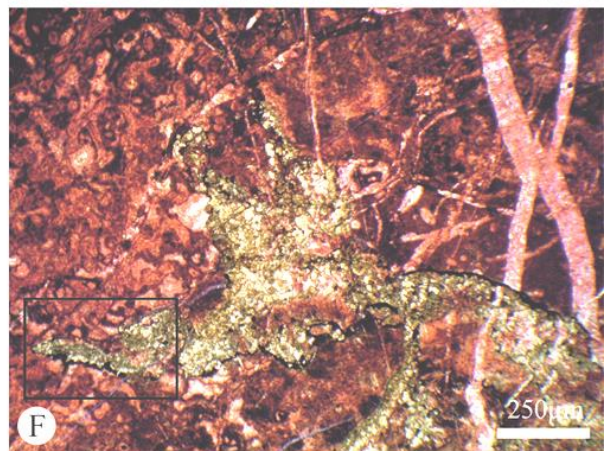
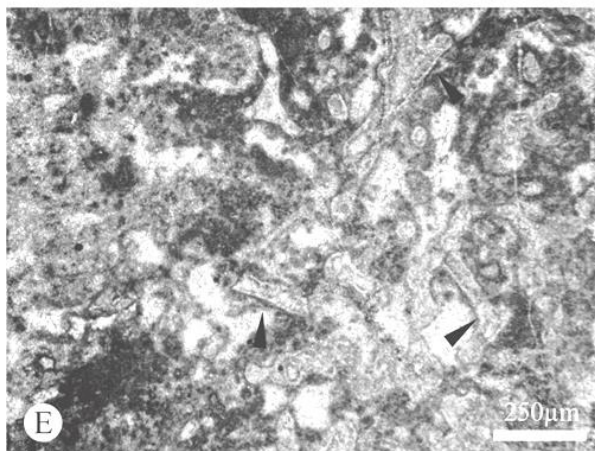
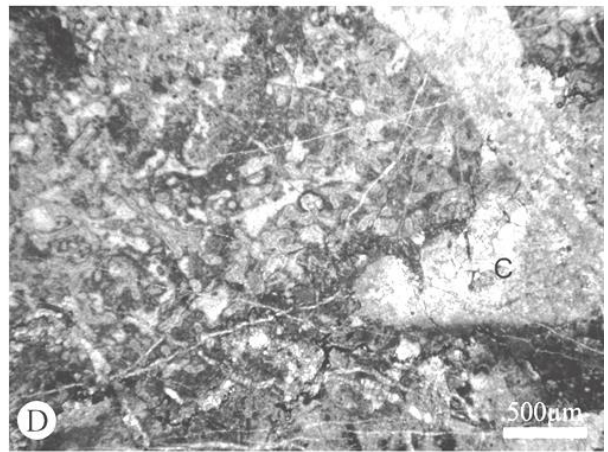
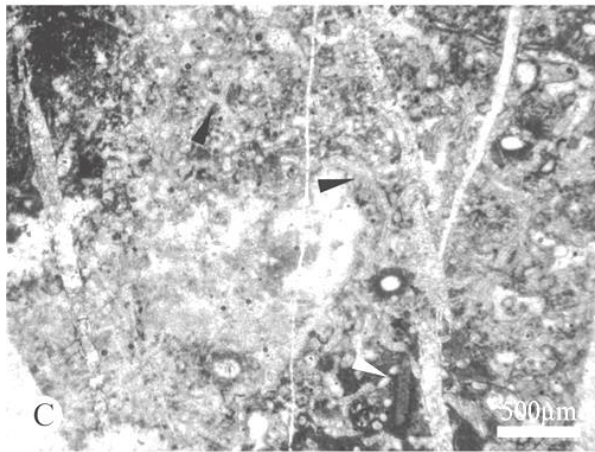
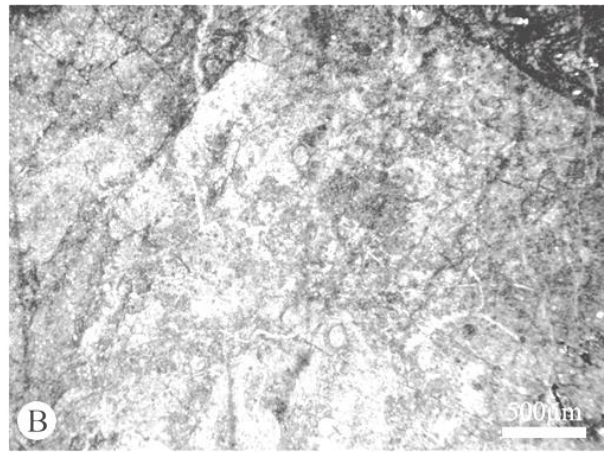
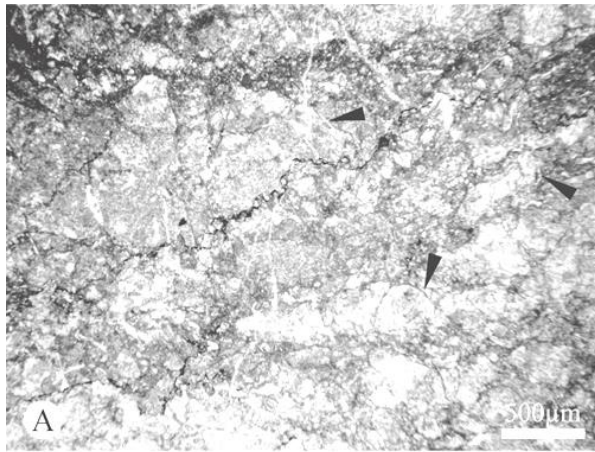


FIGURE - 4.39

A. (CSM 1) A stylobreccia consisting of packed carbonate clasts. Pressure solution has removed much of the original micrite with clasts being mainly composed of spar. The rounding of the clasts (arrows) is likely to be due to pressure solution itself and not as a product of transportation of the clasts.

B. (CSM 1) Here veins and some stylolites can be observed along with some probable recrystallisation of a peloidal sedimentary framework. This part of the sample, like the section shown in A. represents an area which can be clearly identified as fractured in hand samples.

C. (CSM 3) Branching tube like thalli of *Donezella* can be seen (black arrows) with a peloidal to homogenous sedimentary framework. Some rare worm burrows with associated micritic rims can be seen in this image (white arrow).

D. (CSM 3) A cavity (C) with a flat base and undulose roof can be seen to be cross cut by a vein plus many other small micro-fractures/veins can be seen traversing this photomicrograph. The majority of the image is dominated by *Donezella* thalli with a clotted and peloidal sedimentary matrix. Most bioclasts can be seen with a thin micrite envelope. Biodiversity is very low.

E. (CSM 3) A close-up of the area highlighted in D. here the typical characteristics of *Donezella* can be seen; branching, tube like thalli, with 'barrel' segmentation (arrows). A thin clear outer wall and a thicker, darker inner wall can be recognised.

F. (CSM 3) Dolomite can be seen here as the yellow/brown material which is characteristically unstained. The dolomitisation appears to have only affected selective cavities. Distinct veins of non-ferrous (pink/red) calcite can be seen to be cross cut by the dolomite (arrows) indicating dolomitisation occurred after the formation and cementation of these veins occurred. The rest of the image consists of a similar fabric as that seen in D. *Donezella* with a clotted, homogenous and peloidal sedimentary framework. Note the very thin ferroan calcite veins on the left side of the cavity.

G. (CSM 3) A close-up of the area highlighted in F. here the small ferroan calcite veins can be seen more clearly, they can be seen to cut across the dolomite (arrows) indicating that the precipitation of ferroan calcite was the last cement to occur.

H. (CSM 3) A relatively large vein with both ferroan (blue) and non-ferroan calcite. The presence of both, with zoning (black arrows) present within single crystals suggests that the fluid from which they were precipitating was not stable and its composition fluctuated. This vein cross cuts everything else in the sample and therefore was the last feature to form. Note the angular opaque minerals formed in the right branch of the vein (white arrows).

4.7.2 Mound Facies

The mound facies (**samples CSM 2, 4, 5 and 6**) of the Cármenes South Mound can be seen as a transition from a *Donezella* and bioclastic wackestone to a laminoid fenestral packstone and a thrombolitic peloidal bindstone. The wackestone is formed of *Donezella* thalli, and coated and encrusted bioclasts of echinoderm plates and some foraminifera, the sedimentary framework is a homogenous micrite with some spar filled cavities. *Donezella* is observed as entwining thalli

within a homogenous micrite. Bioclasts are enveloped in a smooth coating of homogenous micrite which is distinguishable to the micrite of the sedimentary frame work as it is darker and contains absolutely no spar crystals. These micrite envelopes are constructive and no evidence of destructive boring is observed. Dark homogenous micrite also occurs as patches of nearly opaque micrite which form tube like and rounded structures with patches of spar or lighter micrite toward the centre, these bounding forms are closely spaced and are interpreted to be the agglutinated worm tube *Thartharella*. Encrustation occurs as single, hemispherical growths which are most likely to be encrusting foraminifera, but are reminiscent of the calcimicrobe *Wetheredella*. There appears to be no layering of the bioclasts but they do seem to be confined to patches and clumps. The fenestral and peloidal packstone component of the mound consists of fenestral, spar and internal sediment filled cavities with a homogenous micrite framework, biodiversity is low with some foraminifera and encrusting forms. The peloidal constituent is formed of peloidal micrite of various sizes and colour, some lamination is apparent and a thrombolytic texture is common. Several rounded mud chips (or possibly oncoids) are present and a meniscus cement can be observed between some specimens. Some patches of bioclastic wackestones can be found within the fenestral and peloidal dominated facies. **SMF 21** with **SMF 16-Laminated** and **SMF 11. Fenestral packstone** with *Peloidal bindstone* and *Coated Bioclastic grainstone*. These are characterised by laminar fenestral cavities and thrombolytic and laminated peloidal micrite with low biodiversity, and bioclasts with micritic envelopes (Fig. 4.40 and Fig. 4.41).

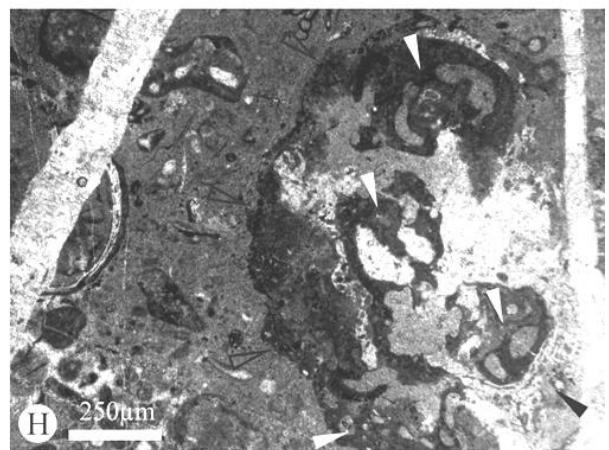
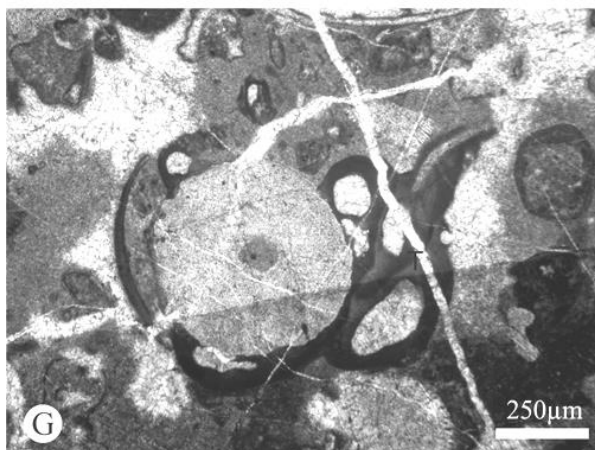
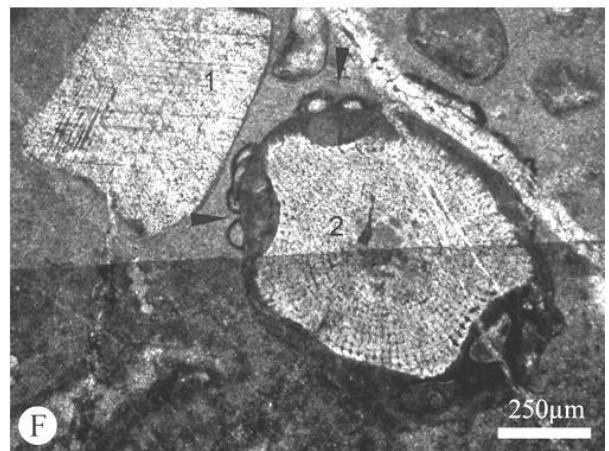
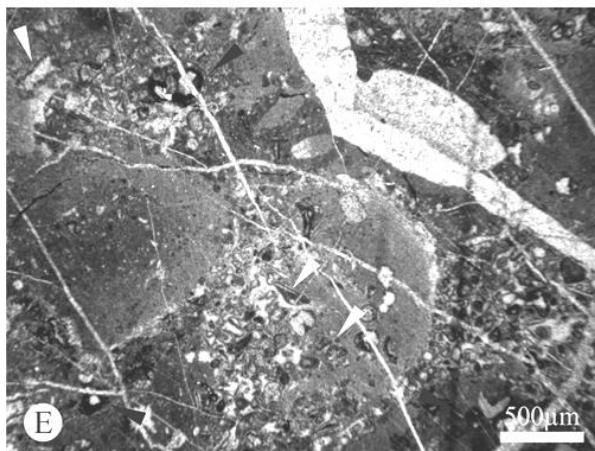
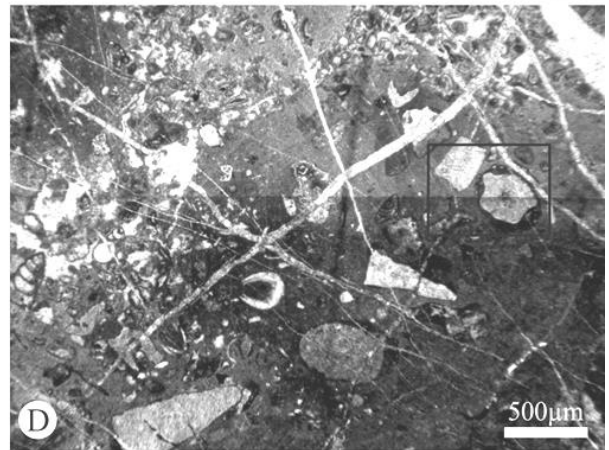
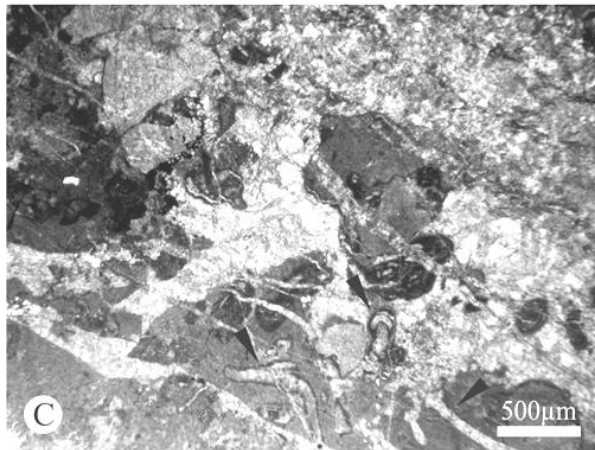
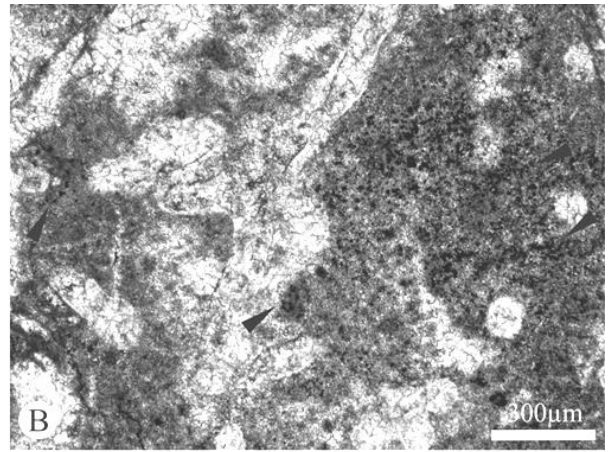
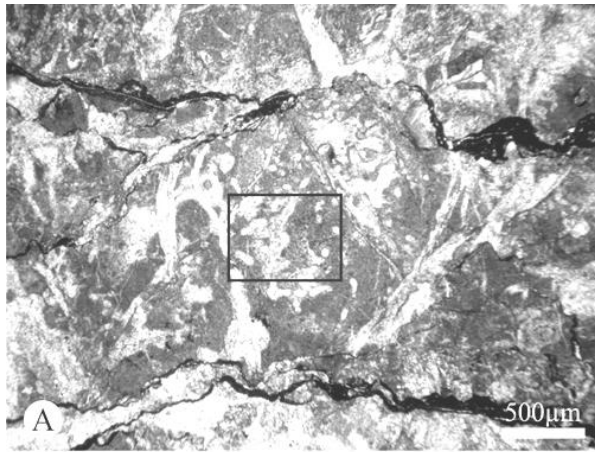


FIGURE - 4.40

A. (CSM 5) Branching and entwining *Donezella* thalli with homogenous micrite baffled between thalli. *Donezella* is the only biota observed in this image. Note the large stylolites with areas of styloaccumulate, which consists of clays and organic material. The stylolites have formed parallel to bedding and have an irregular anastomosing character.

B. (CSM 5) A close-up of the area highlighted in A. *Donezella* (white arrows) with the characteristic barrel like segmentation and branching. The specimens of *Donezella* are not particularly well preserved in this sample. The micritic sedimentary framework can be seen to have many inclusions of equigranular dark patches, in places these inclusions have a layered texture (black arrows) around bioclasts - possibly hinting at biological mechanism of deposition.

C. (CSM 6) Homogenous micrite with *Thartharella*, seen as tubes with an agglutinated sheath formed of micrite (arrows)

D. (CSM 6) Coated, lightly abraded bioclasts consisting of mostly echinoid fragments and foraminifera, biodiversity is low. Micrite envelopes are generally the same thickness around the clast and range from a fine coating to a reasonably thick coating in association with encrusters (see F.)

E. (CSM 6) Patches of coated bioclasts within a micritic framework. Some micrite envelopes are far darker (black arrows) than others (white arrows). Note the *Thartharella* like structures (T).

F. (CSM 6) A close-up of the area highlighted in D. An example of the various micritic envelopes. The echinoderm fragment at the top, left corner (1), has a very thin micritic envelope which is of constant thickness. The central echinoid plate (2), which shows typical uniform pore spacing, has an envelope of varying thickness which terminates at the same level, resulting in a rounded clast. This may suggest some reworking post-enveloping. The micritic envelope on the second bioclast is in association with encrusting forms (arrows). The encrusters on the upper half of the central bioclast are individual, hemispherical encrusters reminiscent of both *Wetheredella* and *Tuberitina*.

G. (CSM 6) An echinoderm plate which appears to have been baffled by *Thartharella*. The *Thartharella* consists of closely spaced tubes of agglutinated micrite (T).

H. (CSM 6) An encrusted clump consisting of *Claracrusta* (black arrow), *Thartharella* (white arrow) and speckled clumps of dark micrite. The dark micrite occurs in aggregated shapes with several microspar filled cavities and may represent a laminar *Shamovella* growth (open arrow).

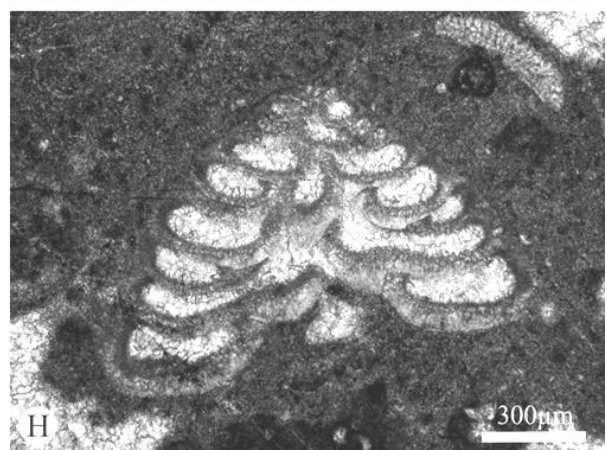
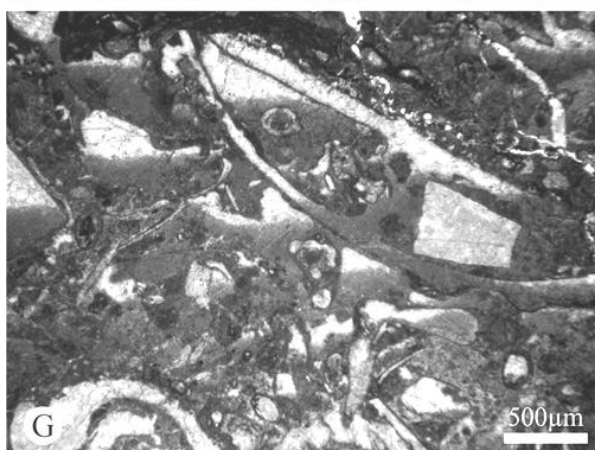
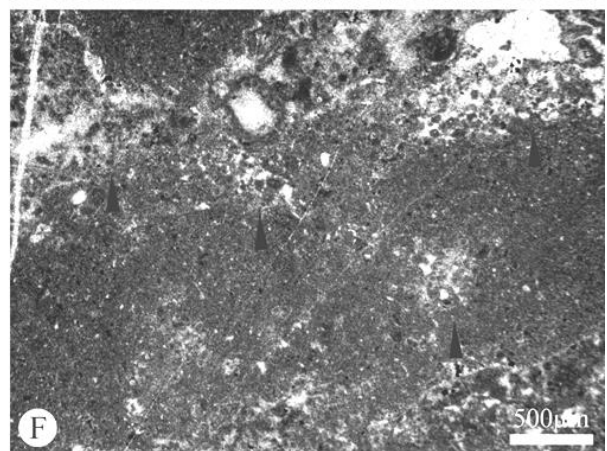
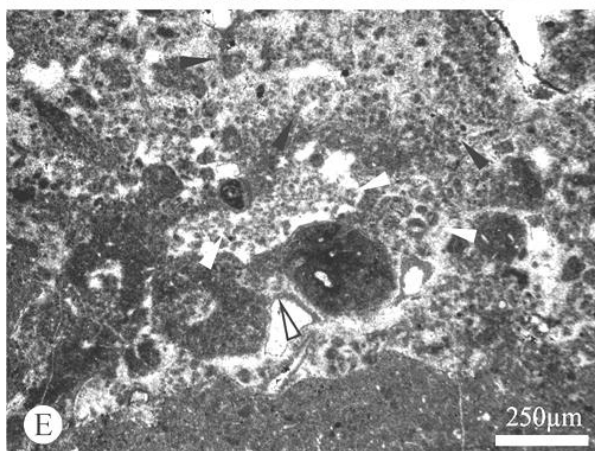
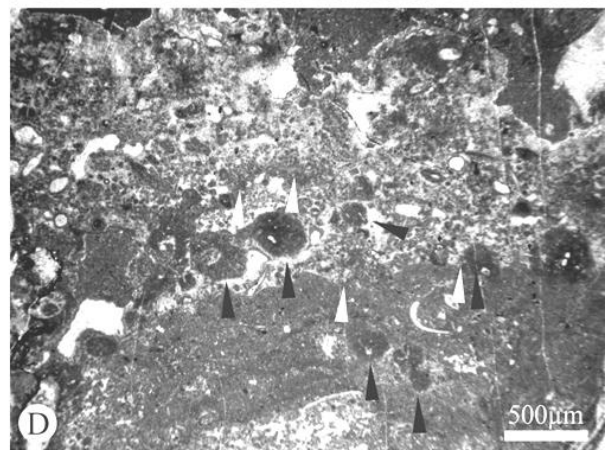
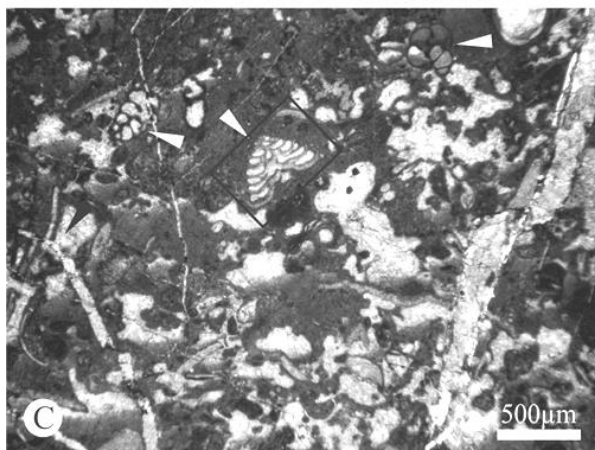
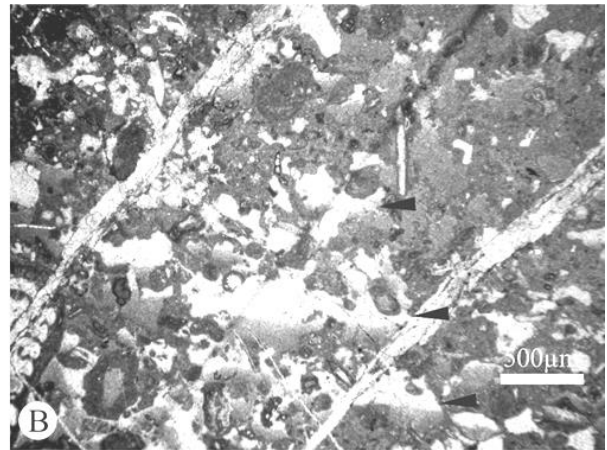
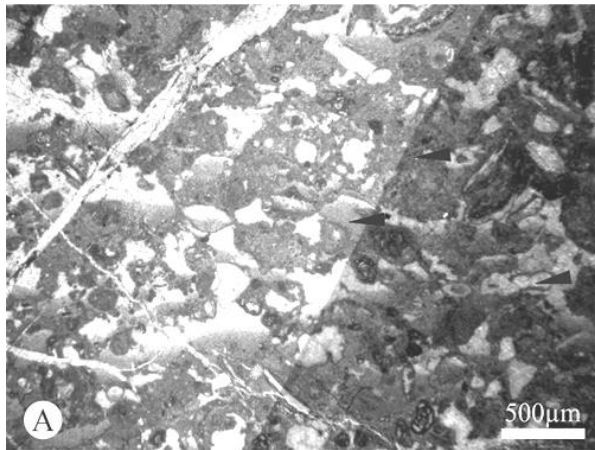


FIGURE 4.41

A. (CSM 2) and B. (CSM 2) Laminar fenestral cavities (arrows) with an internal sedimentary fill of homogenous micrite with some peloids at the base and clear spar toward the top. Cavities generally have a flattened base and an undulose roof. The cavities resemble stromatactis, but for the lack of any radial marine cement within their upper section. These cavities are probably aborted stromatactis, where there is rapid sedimentation of the cavities which plugs the cavity network.

C. (CSM 2) Fenestral cavities similar to those in A. and B. Here the sedimentary framework is better observed. It is a homogenous micrite with very few bioclasts, in this image several foraminifera (including one of the genus *Tetrataxis*) can be observed (white arrows). A rare patch of the problematic algae *Rectangulina* can be observed in a characteristic bundle of straight, non-segmented tubes (black arrow).

D. (CSM 4) A photomicrograph showing the thrombolytic to laminar nature of the peloidal micrite observed within the samples, the laminations appear to consist of peloids of different sizes and include some possible oncoids or rounded mud chips (black arrows). The thrombolytic texture occurs as pillar like and bush like clumps of laminated peloids (white arrows). This sample suggests a high amount of microbial control over the deposition of the peloids

E. (CSM 4) A close-up of the area highlighted in D. Some of the peloids which make up the thrombolytic textures exhibit a 'sausage' or 'bean' like geometry (white arrows) others are seen to be formed into lines or branches (black arrows) and resemble *Renalcis*. A meniscus cement can be observed between the two larger oncoid like bodies (open arrow).

F. (CSM 4) Peloidal micrites which show few signs of lamination or thrombolytic textures, the arrows point to several 'patches' of thrombolytic micrite, this might suggest that the more homogenous sections of micrite may originally have had a thrombolytic texture, but, due to primary compression this texture was lost, resulting in the homogenous micrite texture.

G. (CSM 2) An example of some of the larger bioclasts which can be occasionally observed in lenses within the fenestral and peloidal textures. Bioclasts are in a homogenous micrite framework.

H. (CSM 2) A close-up of the *Tetrataxis* highlighted in C. The *Tetrataxis* can be seen with its characteristic conical test, with several whorls. The walls ultrastructure is not well preserved.

4.7.3 Interpretation

The Cármenes South Mounds basal assemblage consists of a high dominance of *Donezella*. These algae form branching and entwined growths with a micritic sedimentary framework often baffled between the thalli. The basal unit is likely to have been deposited in a restricted, shallow and warm environment. *Donezella* thickets are a relatively common occurrence in lower Pennsylvanian age carbonates and probably formed in a lagoonal environment. The facies shift within the mound facies from a *Donezella* dominated wackestone and coated bioclastic grainstone to a fenestral cavity and thrombolytic peloidal dominated packstone/bindstone indicated a sea

level fall from a relatively shallow, restricted environment such as a platform-margin or foreland equivalent (forebulge) to an extremely shallow and restricted environment. This interpretation is justified by the existence of coated and abraded bioclasts, as well as the existence of *Donezella* thickets, both indicating warm, shallow waters, which pass into clotted and fenestral cavity dominated textures. The thrombolytic nature of the peloids indicates a subtidal environment, several of the column like thrombolites resemble stromatolites. Laminoid fenestral fabrics and meniscus cement tend to indicate a supratidal environment and may have formed due to the wetting and drying of carbonate muds, or the drying out and puckering of cyanobacterial mats from the subjacent carbonate muds. Carbonate production was halted when clastic deposition was ‘turned back on’. This mound indicates deposition within a regressive sea level. The variation of ferroan (stains blue) and non-ferroan calcite (stains pink) as a cavity fill indicates fluctuating pore water compositions (with varying redox conditions) and may suggest that the fracture system was highly permeable. This mound closely resembles those described from the area by Samankassou (2001). Table 4.5 summarises the microfacies analysis of the Cármenes South Mound.

Samples	SMF	Characteristics	Interpretation
1 and 3 (basal)	7- Bafflestone	Algal bafflestone. <i>In-situ</i> growth of Donezelleaceans with baffled sediments of thrombolytic textures.	Shallow depth, restricted environment. Below wave base.
2, 4, 5 and 6 (mound)	21, 16- Laminate, 11	laminar fenestral cavities and thrombolytic and laminated peloidal micrite with low biodiversity.	Very shallow depth, restricted environment. Possibly supra- tidal with exhumation.

TABLE - 4.5 Summary of the main standard microfacies, characteristics and interpretations of the Cármenes South mound.

4.8 San Martín Mound

30T 279070.51 4758646.38

The San Martín Mound is found on a small farm track just to the east of the village of San Martín de la Tercia in the Bernesga Valley. The mound is exposed in a road cutting and is 14m wide and roughly the same height. The outcrop is a light, creamy grey, veined, micritic mound with rare shell fragments found. The mound is heavily fractured and contains abundant calcite filled fractures. The basal beds appear to be siltier than the mound material and contain some 'phylloid' algae. The mound is found as part of one of several limestone units which are observed cutting through the Bernesga Valley, these units are bounded by grassy intervals in which siltstones and fine sands can be found a few centimetres below surface levels. The Samples for this mound are separated into two facies, a basal- and a mound facies. The mound facies consists of two further sub-facies. Although the sample number for this mound is low when compared to other mounds, a big difference in facies types can be seen between the basal sample and the mound samples.

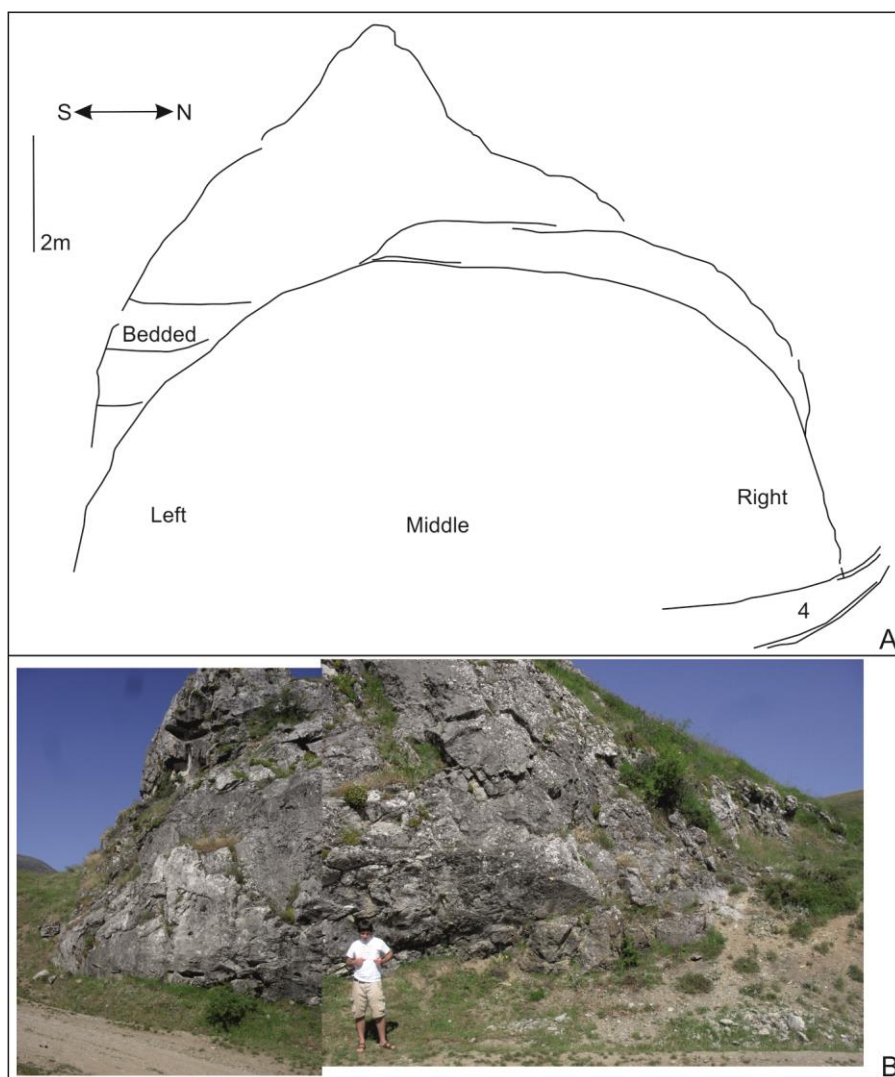


FIGURE - 4.42 A. An annotated field sketch of the San Martín Mound, sample points are highlighted. B. Field photo.

4.8.1 Basal Facies

The basal facies (**sample SMM 4**) consists of laminar ‘phylloid’ algal thalli and tube-like branching Donezella-like thalli within a microcrystalline calcite and clastic cement. *Archaeolithophyllum* occurs as isolated, laminar sheets, often in association with encrusting forms - both calcimicrobes and encrusting foraminifera. *Donezella* is found as both broken fragments and as branching, frame-building masses. The characteristic barrel like thalli with branching occurring perpendicular to the wall indicates that the specimens observed are *Donezella lunaensis*

Rącz. Several foraminifera can be observed though the ultrastructure of their walls is not preserved. Other bioclasts include rare ostracods and echinoderm plates. The ostracods are white in colour which may suggest a shallow burial depth for the San Martín Mound. The matrix in this facies has a packstone like texture and consists of micrite with a relatively high component of silty, clastic material. The clastic material often occurs as laminations of microgranular quartz crystals, where stylolites exist the clastic component is often concentrated along them. Stylolites are often bedding parallel occurring as irregular anastomosing seams. Cavity networks are absent.

SMF 8. *Wackestone with whole fossils.* This is characterised by whole ‘phylloid’ algae with *Donezella* and a packstone like matrix consisting of micrite and microcrystalline quartz (Fig. 4.43).

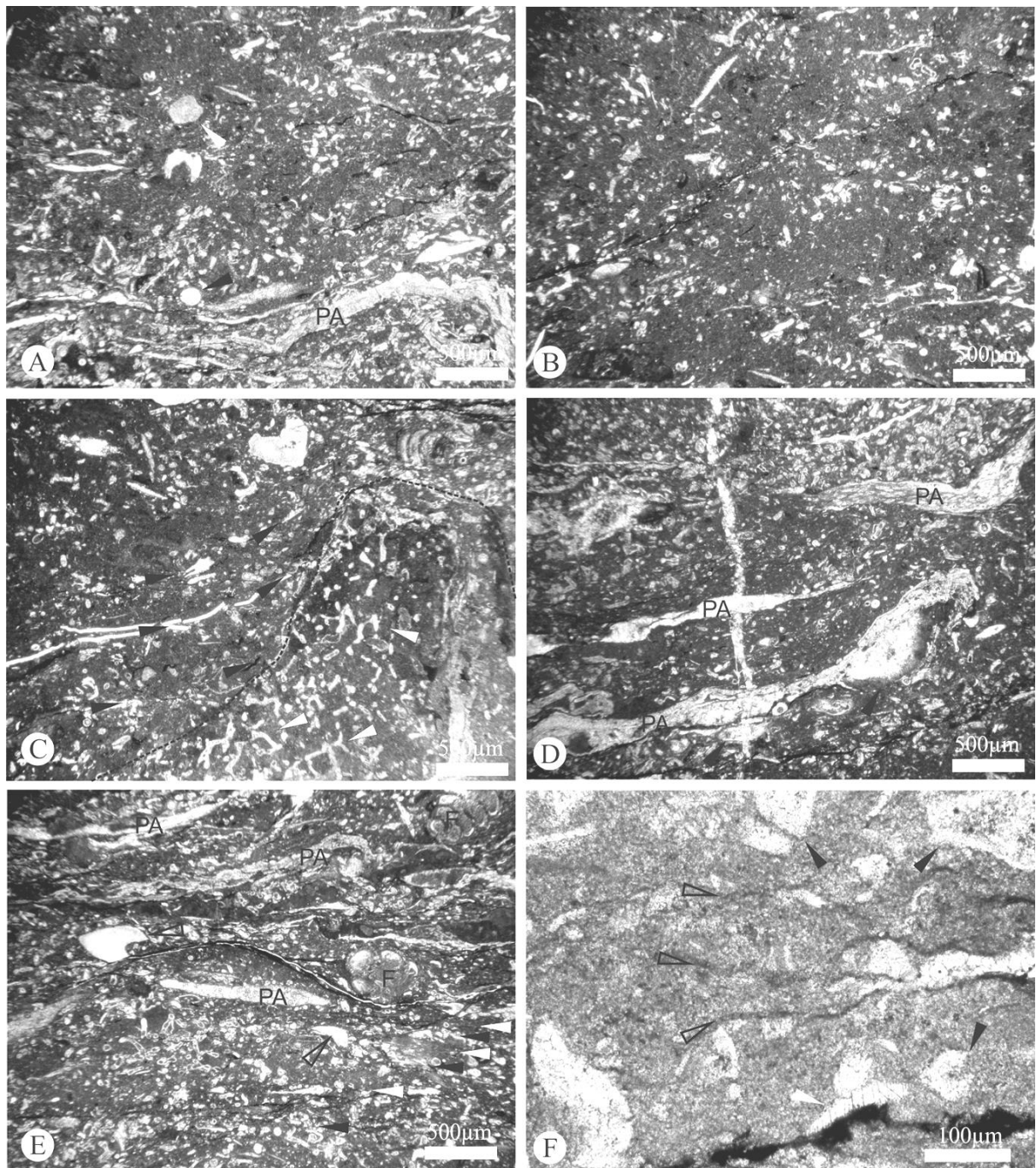


FIGURE - 4.43

A. (SMM4) 'Phylloid' algal thalli (PA) with *Donezella* thalli in a packstone like matrix. Ostracod and echinoderm plates are present. Bedding parallel stylolites can be seen, in some areas styloaccumulate consisting of clastic and most probably organic material can be found associated with the stylolites. Note the near homogenous nature of the matrix material.

B. (SMM 4) This photomicrograph was taken directly above that of A., and so represents a vertical shift in sediment from bioclast dominated, to matrix dominated sediment. Similar to A.

but with the absence of whole ‘phylloid’ algae. This photomicrograph shows the nature of the packstone like matrix with broken *Donezella* suspended within it. There is a low biodiversity.

C. (SMM 4) Here *Donezella lunaensis* Rácz can be seen as a framework within a rhodoid (outlined), the *Donezella* thalli can be seen to branch (white arrows) with a homogenous micritic sediment baffled between. Some encrustation has occurred on the rim of the cortoid. ‘Phylloid’ algae and some laminated bioclasts appear to show onlap (black arrows) on to the cortoid suggesting that the *Donezella* growth formed a topographic high and was truly, ‘shrub like’.

D. (SMM 4) ‘Phylloid’ algal thalli (PA) with *Donezella* thalli in a micritic matrix. Heavily recrystallised cavities can be seen in what would have been a cryptic environment beneath one of the ‘phylloid’ algae (black arrows). Stylolites parallel to the ‘phylloid’ algae can be seen (white arrows).

E. (SMM 4) Some poorly developed laminations can be observed in this photomicrograph, laminar alterations of matrix rich (white arrows) and *Donezella* fragment rich (black arrows) deposits can be observed. This laminated sequence may represent changes in either depositional depth or a change in energy levels or currents within the basin. Fragments of an echinoderm plate (open arrows) and two relatively large foraminifera (F) are present as well as some recrystallised ‘phylloid’ algae (PA).

F. (SMM 4) A close-up of the matrix material, the lighter clasts are broken *Donezella* thalli (black arrows) and a small fragment of an echinoderm plate (white arrow). A stylolite with styloaccumulate can be observed along the bottom of the image whilst several less well developed stylolites can be observed as dark lines (open arrows). Note the homogenous nature of the matrix.

4.8.2 Mound Facies

The mound facies is separated into two sub-facies. Sub-facies one (**sample SMM L**) has common fenestral cavities, whilst sub-facies two (**samples SMM M and R**) consists of pack/grainstones of varying types. Sub-facies one consists of whole and broken bioclasts and some cortoids within a micritic matrix, laminar cavities are common and constitute 30% of the rock. Bioclasts are generally coated in an envelope of micrite and are often abraded with some recrystallisation. Several cortoids are present and consist of rounded clasts of dark homogenous micrite, often with broken, tube like algal thalli (interpreted as broken *Donezella*) as a nucleus. The cavities are fenestral and birds-eye cavities filled with blocky, clear spar and some internal sedimentary fill. The sedimentary matrix consists of homogenous and peloidal micrite. Sub-facies two consists of bioclasts in a peloidal micrite matrix. Peloids are rounded and show no lamination, some peloids are made of dark micrite. Bioclasts consist mostly of *Donezella* fragments, which are found as both whole and broken thalli. Where whole, branching thalli exists as a framework it is in association with dark homogenous micrite. Other bioclasts include foraminifera and some

cortoids. The majority of bioclasts exhibit a micritic envelope and some show evidence of recrystallisation. Most of the specimens consist of a packstone with bioclasts within a peloidal micrite framework, however, this sedimentary framework is absent from a small area where a blocky spar cement is present instead. **SMF 21-Fen** and **SMF 10**. *Fenestral packstone and bioclastic packstone with worn skeletal grains*. These sub-facies are characterised by worn and abraded bioclasts within a pelmicritic sedimentary framework, which is occasionally replaced by sparry cement. Fenestral and birds-eye cavity networks are present in high abundance in some areas (Fig. 4.44).

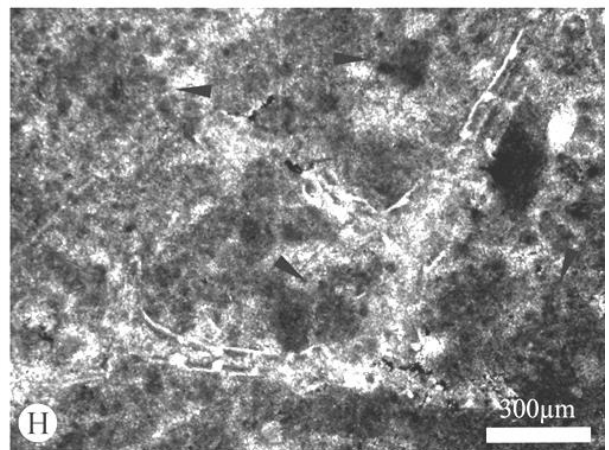
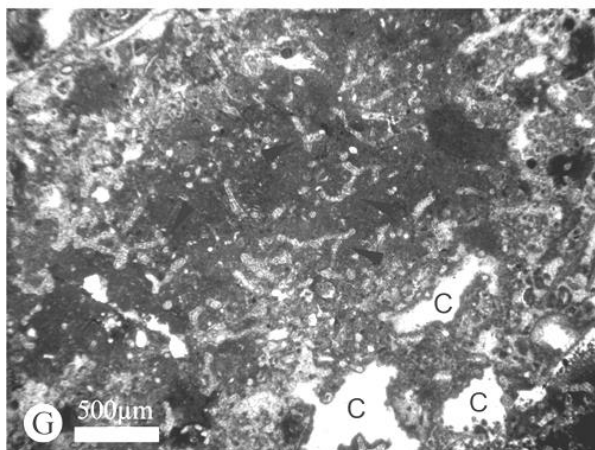
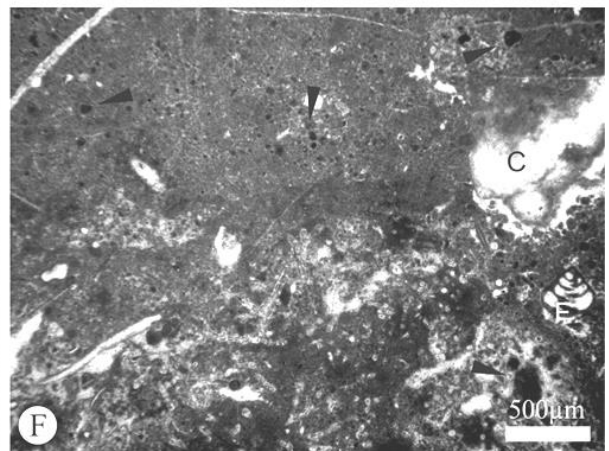
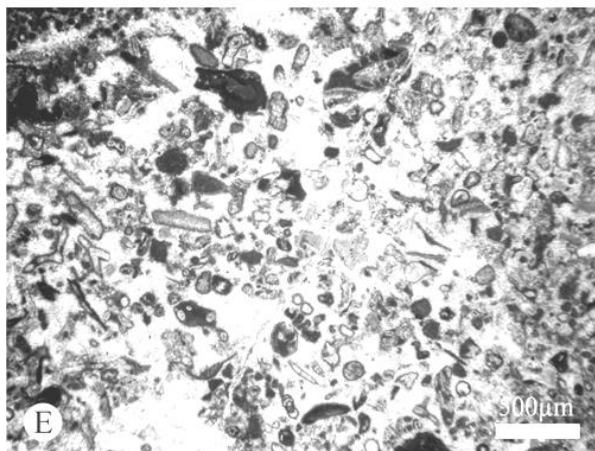
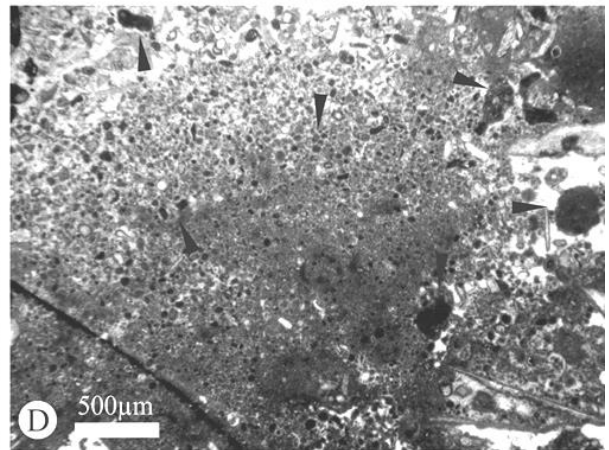
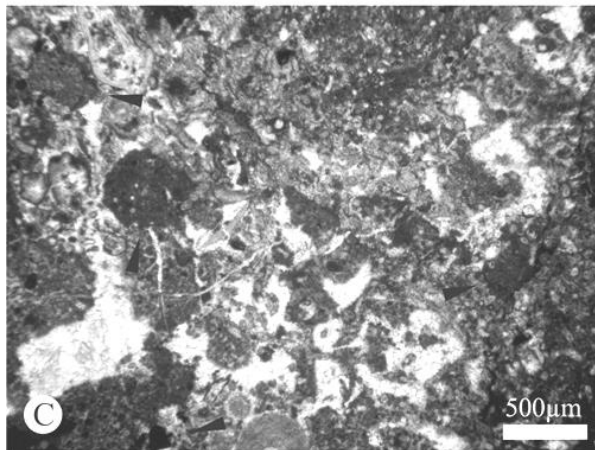
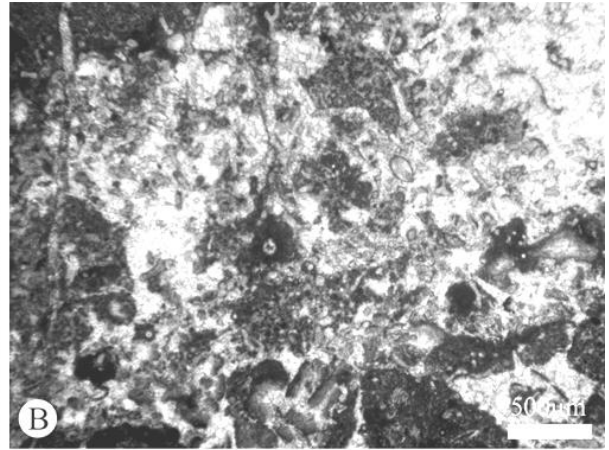
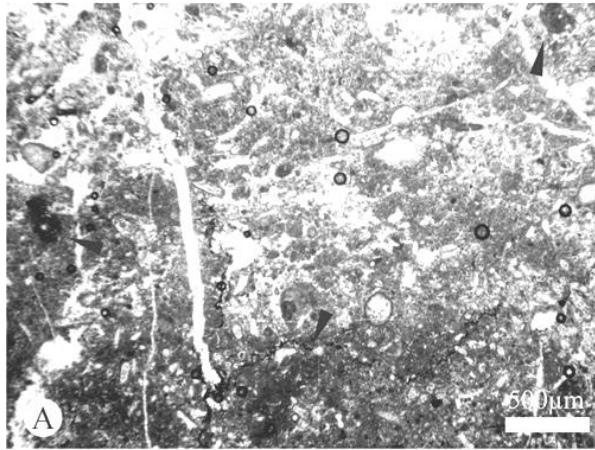


FIGURE-4.44

A. (SMM L) Fenestral cavity networks with a laminar geometry, the cavities tend to have a flat bottom (with some internal sedimentation) and an undulating roof. The cavities are filled with clear, blocky cement. Bioclasts generally consist of small, broken fragments of *Donezellacean* thalli. Some cortoids (arrows) are present and appear as rounded clasts of dark homogenous micrite, with a bioclast nucleus.

B. (SMM L) Cavity networks within a *Donezella* and pelmicritic grainstone texture, most bioclasts have a thin micritic envelope and appear to be broken. Cavities lack internal sediments but often have bioclasts, or blocks of sediment within them 'floating' in a blocky spar.

C. (SMM L) Bioclasts and cortoids (arrows) partially surrounded by fenestral cavities. Cortoids are formed of homogenous dark micrite, and tend to have tube like bioclasts as a nucleus.

D. (SMM M) A grainstone consisting of peloids and some bioclasts. Toward the centre of the image the peloids are supported by micrite, whereas toward the top, a blocky cement is supporting them. Some peloids and cortoids (white arrows) are formed of dark homogenous micrite similar to that which is observed baffled within *Donezella* thickets, it is possible that these dark peloids and the cortoids are reworked as broken chips of this micrite (see G.). This would imply deposition within wave base levels and the abrasion and reworking of the *Donezella* thickets.

E. (SMM M) A packstone texture consisting of oncoids, cortoids and coated and abraded bioclasts, supported by clear blocky spar.

F. (SMM M) Bioclastic packstone which has two distinct fabrics, the bottom of the image is dominated by branching *Donezella* thalli within a homogenous, to clotted micrite, whilst the top half is almost void of bioclasts and is instead dominated by peloids and small micritised grains. The lower half probably represents a *Donezellacean* thicket whilst the upper half is representative of the 'background' sedimentation. Dark peloids (arrows) may originate from the reworking and break-up of calcitic muds which are baffled by the *Donezella* growths. An irregular cavity (C) and a foraminifera (F) are present in this image

G. (SMM M) Branching *Donezella* thalli which have baffled a homogenous micrite. The characteristic barrel-like thalli and branching of the *Donezella* can be readily identified (arrows). Several cavities (C) can be seen which appear to be shaped directly by the *Donezella* thalli around them, the cavities are filled with a clear blocky cement.

H. (SMM M) A close-up of the area highlighted in F. *Donezella* thalli, with characteristic branching and barrel like segments of the tubular wall structure. In this specimen a bright outer wall and a darker inner wall can be observed. The micrite surrounding the *Donezella* thalli is homogenous to clotted with some possible thrombolytic textures apparent, these could be the micritised remains of calcareous tubes or calcimicrobial growths (arrows).

4.8.3 Interpretation

The San Martín Mound shows a heterolithic nature within the mound facies. The worn bioclasts with a pelmicritic sedimentary framework, which include several rhodoliths of *Donezella* are interpreted to have been deposited in shallow, warm waters, the low biodiversity suggesting a restricted environment. Peloids are likely to be reworked calcitic muds and algal thalli, the dark

colour of some peloids may indicate that they are micritised and reworks bioclasts. The basal facies is interpreted to have been deposited in a deeper, less restricted environment than the mound facies. Whole ‘phylloid’ algae and some larger foraminifera are present and there is evidence of some clastic input to the system, the microcrystalline quartz grains would suggest a very low energy level of deposition, and a very low clastic input into the basin. Onlapping of laminated sediments onto larger rhodoliths within the basal facies indicates that sedimentation with a deepening sea level was coeval with *Donezella* growth. As the mound facies is found above these deposits it is suggested that the San Martín Mound formed as a result of a regression from open marine conditions to a restricted environment. Facies change and the heterolithic nature within the mound facies is interpreted to represent cyclic sea-level change with sub-facies one shallowing, and sub-facies two deepening. Table 4.6 below summarises the microfacies analysis of the San Martín Mound.

Samples	SMF	Characteristics	Interpretation
4	8	Whole ‘phylloid’ algae with <i>Donezella</i> and a packstone like matrix	Open marine, below wave base
L	21-Fen	Common laminar fenestral cavities with cortoids.	Very shallow depth, restricted environment. Possibly super-tidal with exhumation. Low - moderate energy, lagoonal environment.
M and R	10	Bioclasts in a peloidal matrix	Shallow depth, restricted, protected environment, within wave base. Low - moderate energy, lagoonal environment.

TABLE - 4.6 Summary of the main standard microfacies, characteristics and interpretations of the San Martín mound.

4.9 Chapter Summary

The distinct microfacies observed between the mound, basal, flank and capping facies for the mounds observed indicates that each mound studied here is a primary mound and not a diagenetic mound of Hensen *et al.* (1995). The mounds of the San Emiliano Valley are compositionally different to those of the Bernesga Valley. San Emiliano Valley mounds are dominated by a community of *Donezella* with accessory biota including the encrusting *Rothpletzella* and *Claracrusta*. Sediments are mostly homogeneous, clotted and peloidal micrites. Laminar cavities are present along with constructed and stromatactoid cavities. Basal, flank and capping beds have a more diverse biological assemblage with shelly fauna and corals often present. Abraded and coated grains are common and peloidal micrite is the dominant sediment texture. Mounds are interpreted to have formed in shallow (occasionally extremely so), warm and restricted environment which was most probably hypersaline and possibly lagoonal. It is interpreted that San Emiliano Valley mounds formed during a sea level transgression, superimposed atop of a general regressive trend. Carbonate sedimentation is thought to have been relatively rapid, with mound accretion particularly fast. Mounds ceased to form when they were either smothered (by an influx of clastic rich sediments) or drowned. Basal, flank and capping beds are interpreted to have formed in a shallow, lagoonal environment, within wave base. Non-mound bearing units consisting of cyclical limestone and marl beds contain a higher biodiversity, and higher siliciclastic component than mound bearing limestones. The limestone and marl beds are typically associated with 'phylloid' algae, auloporida corals and bryozoans with accessory encrusting biota (*Rothpletzella*, *Claracrusta* and *Girvanella*). The Bernesga Valley mounds generally have less of a *Donezella*, *Rothpletzella* and *Claracrusta* dominated assemblage, while *Thartharella* is found exclusively within them. Whilst Donezellaceans are still found within the majority of the mounds it is less common and is more commonly associated with a wider diversity of biota. Bryozoans, corals, foraminifera, dasyclad algae, worm tubes and evidence for siliceous sponges are all conspicuously present. Bernesga Valley mounds clearly resemble the description of them given by Samankassou (2001). Peloidal micrite is much more common as are transported, abraded and

micritised grains. Stromatactoid and laminar cavities are common. These deposits are interpreted to have formed in a less restricted environment than the San Emiliano mounds and show far less evidence for formation during a transgressive sea level. The Bernesga mounds formed due to the accumulation of peloidal micrite which may have been stabilised by the formation of laminar stromatactoid cavity networks.

Mounds from the type locality of the San Emiliano Formation are the result of an organically driven accumulation of carbonate muds and are interpreted as microbial in nature. Sedimentation was a result of 'in house' production, stabilisation, baffling and binding of carbonate muds by *Donezella* and, perhaps more importantly, *Claracrusta* and *Rothpletzella* and other microscopic encrusters. Carbonate mud is most likely to have derived from the local abrasion and break down of algal thalli and precipitation of carbonate material from the water column.

5. Ultrafacies Analysis

An ultrafacies analysis of cut, polished and slightly etched samples has been undertaken to examine the textural features of the cements, matrix material and bioclasts within the studied carbonate rocks (see chapter 3. *Methods and Materials*). The samples chosen for this study reflect those chosen for microfacies analysis. The Candemuela Mound will be the primary focus, with a sample from each sub-group (as recognised from the microfacies analysis) being analysed. A specimen from each other local sampling site will also be analysed to compare and contrast results. An ultrafacies analysis on the mud mounds of the San Emiliano Formation has not been conducted before and will contribute to environmental and diagenetic reconstructions of the formation. Both high resolution images (SEM) and elemental maps (EDS) have been used to carry out this ultrafacies analysis. Element maps have been utilised to confirm grain types and to investigate the elemental composition for various structures. EDS images used in this chapter represent mixed element maps, for individual element maps and the associated spectrum for each EDS image used in this chapter see *Appendix 2. EDS Maps*. Features which are specifically investigated are the size, shape and etched condition of crystals and (depending upon preservation status) the ultra-skeletal structure of various biota (see chapter 6. *Palaeontology*). Using SEM derived images for the ultrafacies the probable original mineralogy of precursor soft sediments will be established, this is done by identifying relics of aragonite within a microspar matrix. Aragonite Dominated Precursors (ADP) and Calcite Dominated Precursors (CDP) can be distinguished by: ADP – aragonite relics, pitted crystal surfaces, common microspar fabrics and elevated strontium levels. CDP – absence of aragonite relics, smooth crystal surfaces and the dominance of very small (micrite) crystals (Lasemi & Sandberg, 1984; Munnecke *et al.*, 1997 and Flügel, 2004). It should be noted that Strontium is not within limit of detection of the EDS used, i.e. the instrument is not sensitive enough to definitively determine the presence of Strontium with statistical certainty (Rousseau, 2001).

An accessory investigation was also made on the size of framboidal pyrite found within parts of the samples where they are present. By measuring the diameter of the framboids it is possible to determine if the pyrite was formed in a sulfidic water column (syngenetic) or within sediments underlying an oxic water column (diagenetic) (Wilkin *et al.*, 1996).

Abbreviations used in text: PMS (Pitted Microspar), LPM (Less-Pitted Microspar), NPM (Non-Pitted Microspar), SS (Smooth Spar), PM (Pitted Micrite), NPM (Non-Pitted Micrite), PD (Pitted Dolomite), DOL (Dolomite), CC (Clastic Component), FP (Framboidal Pyrite), PY (Pyrite), IO (Iron Oxide) and SP (Spicule).

5.1 Candemuela Section

The samples from the Candemuela Section consist of one cut, polished and etched block from each sub-facies group recognised in the microfacies analysis. The ultrafacies data will be used to complement the microfacies analysis and give an insight into the diagenetic path the mud mounds have followed and shed light upon the soft sediment state of the depositional environment; making for more accurate environmental reconstructions. In total 10 samples from the Candemuela Section underwent ultrafacies Analysis, which breaks down as two from the 'Basal Facies', five from the 'Mound Facies' and three from the 'Capping Facies'. The ultrafacies analysis has shown that the majority of calcite crystals are pitted, with those that are smooth (i.e. without pitting) making up microcrystalline wall structures, small clumps or cavity filling spar crystals. Dolomite is present in most samples with a low abundance, dolomite is often observed as pitted, isolated 'floating' rhombs or in association with alumina-silicates. Framboidal pyrite is commonly associated with alumina-silicates and in some samples is quite common. Several examples of what are most likely to be iron oxides are present, but rare. Bioclasts show good morphological preservation but the skeletal ultra-structure is often not well preserved. Stylolites are observed in several samples.

5.1.1 Basal Limestone Facies

Sample 1 (Fig. 5.1) and Sample 4 (Fig. 5.2) (also representing samples 2 and 3) show the crystal textures which are observable throughout all samples analysed for the Candemuela Mound. The majority of the material consists of pitted micrite and microspar. These crystals are blocky when observed in the matrix fraction of the samples but often fibrous and elongated when the crystals form part of a bioclast, or as a partial fill of said bioclasts. The pitted material ranges from $<2\ \mu\text{m}$ to $30\ \mu\text{m}$ (crystals only reach $30\ \mu\text{m}$ when they are elongated along one axis preferentially, blocky crystals reach $20\ \mu\text{m}$ in diameter). Blocky crystals show no preferred orientation of growth and have distinct crystal boundaries. Elongated and fibrous crystals grow perpendicular to the substrate, which in these samples is generally as part of a wall structure or other biological structure. Pits are preferentially etched patches observable on the polished surfaces of the cut samples, these pits are often $1\text{--}3\ \mu\text{m}$ in diameter and often circular; although they are also observed as elongated grooves. Some possible evidence for precursor, botryoidal cements can be observed in sample 1. Other crystal textures which occur are non-pitted micrites and smooth spar crystals. Non-pitted micrites are distributed in an ordered and arranged fashion – often forming recognisable biological structures (foraminiferal and calcispheric walls). They are often in equigranular layers. Smooth spar (spar crystals that have a smooth surface after etching) are observed as cavity fill within fossils. Evidence for slight clastic input is observable in these samples. Framboidal pyrite occurs as isolated features. See Figures 5.1 and 5.2 for examples and details.

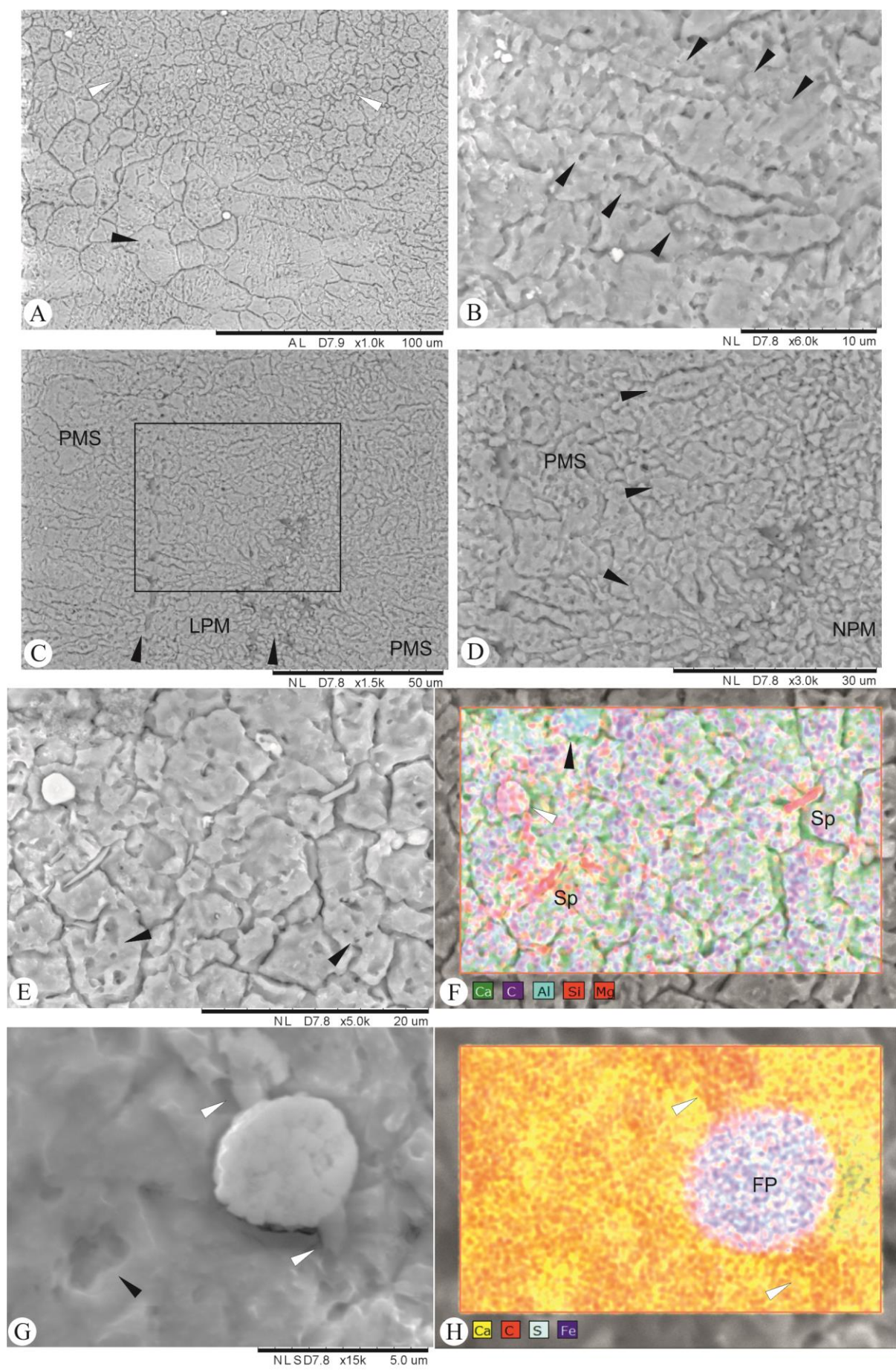


FIGURE - 5.1

A. An overview image of two of the major textures encountered within this sample (and every other sample). The white arrows indicate non-pitted micrite and microspar, the crystals range from 2 μm to 20 μm , their surfaces are smooth and granular in appearance. The non-pitted micrite and microspar forms a semi-circular structure which may represent a biological structure which has been exposed to slight aggrading neomorphism. The surrounding crystals are pitted microspars, notice that some crystals are preferentially pitted, whereas others have areas of pitting and smooth areas (black arrow).

B. Pitted microspars which are elongated from left to right of the image. The black arrows indicate lines upon which the majority of the 'pits' are aligned. These discontinuities within the crystals are reminiscent of 'dust lines' observed within botryoidal, aragonitic cements. The alignment of the pits along them might suggest that these 'dust lines' were once thin layers of high Mg-micrite, which are now preferentially etched.

C. An image of one of the few bioclasts identifiable in this sample. The black arrows both sit on the walls of an algal thalli. The walls consist of non-pitted micrite which grades into pitted micrites and microspar. Crystals within the walls are less pitted than those surrounding it. The obscured boundaries of the wall is due to a slight aggrading neomorphism of the surrounding microspars.

D. Zoomed in image of the area highlighted in C. The right hand edge of the image is dominated by non-pitted, tabular micrite ($<4 \mu\text{m}$) crystals. The black arrows indicate several pitted microspars which are elongated across the bioclast.

E. and F. Element map of pitted microspar with some accessory minerals. Notice the nature of the pitted surfaces (black arrows) they are often cylindrical holes and often show alignment with other pits nearby. F shows a shale component (black arrow), a quartz (sand) component (white arrow) and also what are possibly sponge spicules within the dominantly calcitic sample.

G. and H. A specimen of framboidal pyrite, in G again note the aligned pits with rounded, tube like morphologies. The white arrows indicate a cylindrical crystal which the framboid appears to have formed around. This structure has an elevated carbon content in contrast to the surrounding crystals which may indicate that it was an organic fragment.

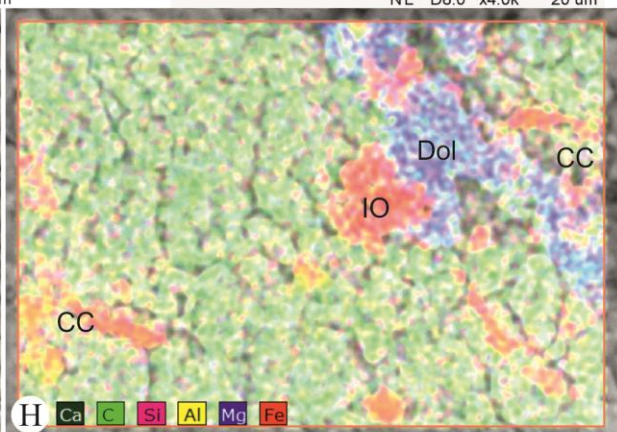
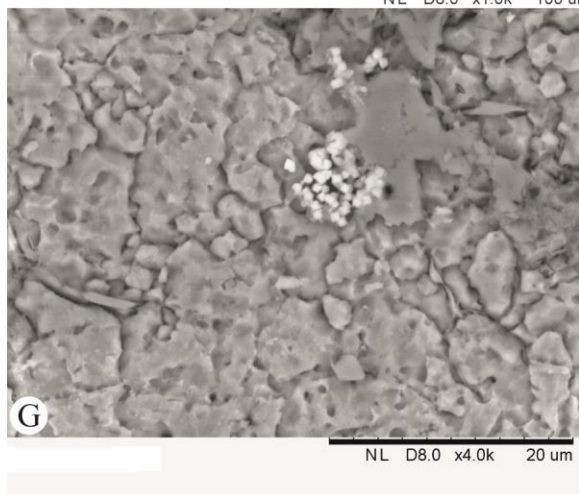
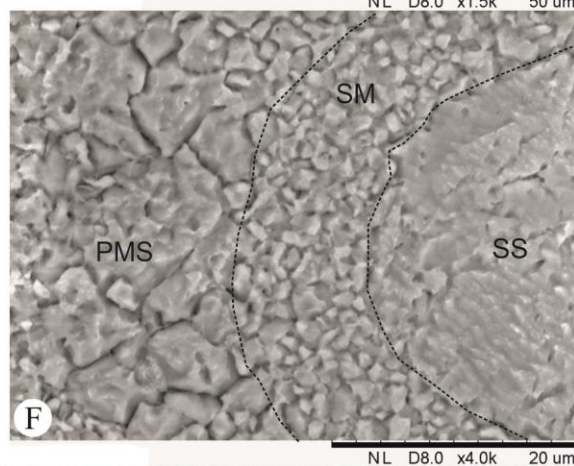
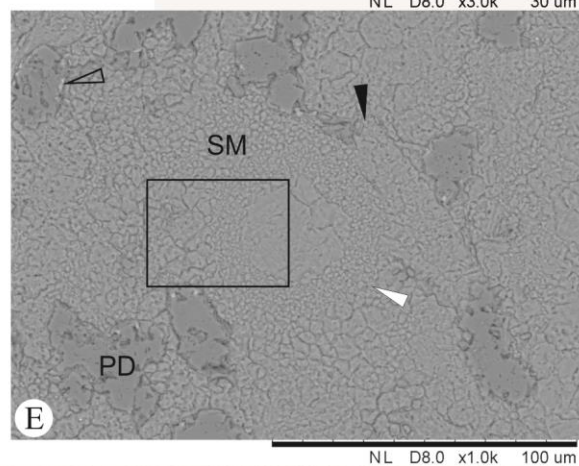
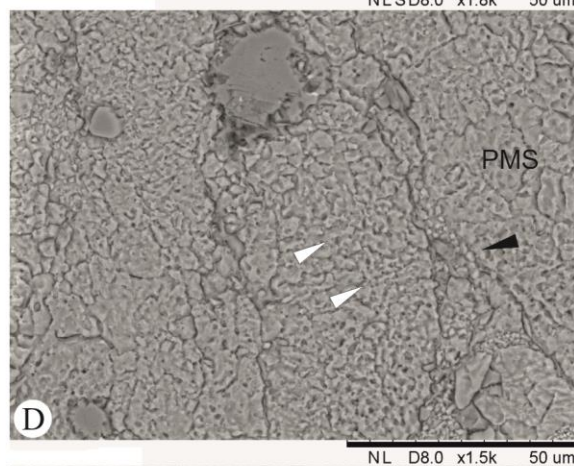
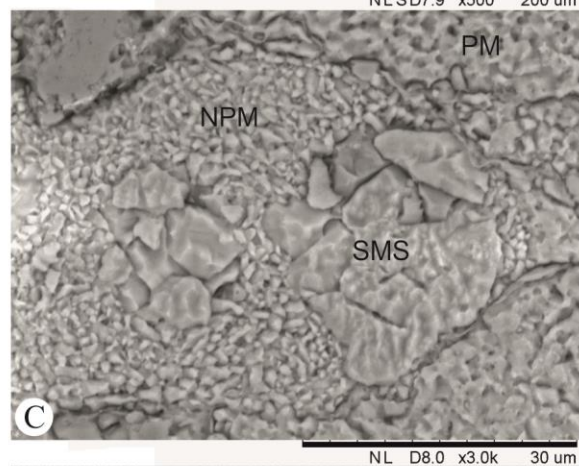
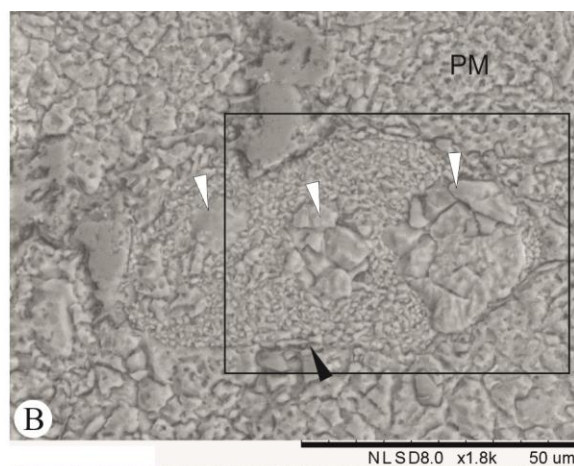
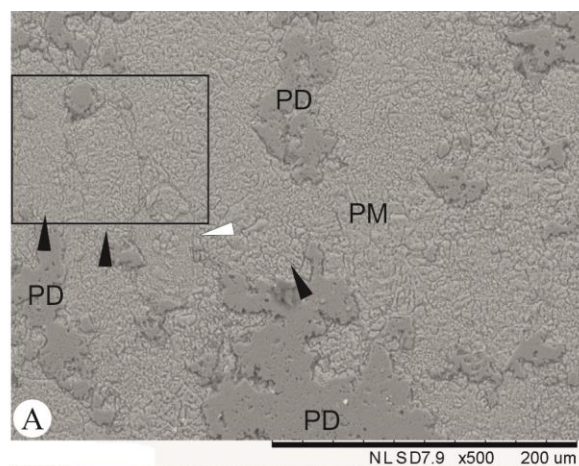


FIGURE - 5.2

A. An overview of the main constituents observed within this sample. The black arrows indicate algal thalli which can be seen throughout the sample in both longitudinal and cross section. Generally the algal thalli are recognised by a sharp boundary with surrounding material and little evidence of compression. The white arrow indicates a microfossil with a microcrystalline wall. Pitted dolomite is observable in this image, the dolomite is in association with a clastic component (see G and H) and occurs as both isolated rhomb's or as patches no greater than a few millimetres in size. The dolomite often has a pitted surface and rhomb's are generally deformed.

B. This image shows a close-up of the microfossil highlighted in A. A sharp and distinct boundary (as indicated by the black arrow) can be observed between the microgranular wall of the fossil and the surrounding pitted micrite (PM). Three cavities can be seen (white arrows) within the microcrystalline wall. This microfossil is interpreted to be of the family Ovummuridae (Munnecke *et al.*, 2000).

C. A close-up of the area highlighted in B. Several textures can be recognised in this image. The wall of the microfossil is made up of small ($<3\text{ }\mu\text{m}$) tabular crystals. The crystals are arranged in layers and have sharp boundaries. The surfaces are smooth. The cavities consist of smooth microspar/spar crystals (SMS). The surrounding micrite and microspar exhibits a well pitted surface.

D. Pitted microspar is often observed as fibrous/elongate crystals (white arrows), in this example the elongate crystals are confined to the algal thalli, whilst the surrounding matrix (PMS) shows a more granular texture. Note the encrusting form, with microcrystalline wall attached to the algae (black arrow)

E. In this image a pitted dolomite and pitted microspar surround a calcisphere (white arrow) which consists of a spherical wall of smooth micrite. Elongate structures consisting of elongate pitted microspars again indicate the presence of algal thalli (black arrow), here it can be seen that the dolomite forms around the bioclasts in association with a clastic component (open arrow).

F. Close-up of the highlighted area in E. The wall of the calcisphere can be seen to comprise of a near smooth spar crystal, some small defects on the crystal surface are evident but these do not resemble pits observed elsewhere (e.g. the pitted microspar to the left of this image), the shallow gouges here may be a result of twinning in the crystal or as a result of sample preparation.

G. and H. An image of pitted microspar, dolomite and the clastic component of this sample. The element map clearly shows the carbonate (calcite and dolomite) and clastic components with associated iron deposits. In this sample no sulphur was detected so the iron constituent is likely to be an iron oxide, possibilities include magnetite and hematite. The iron carbonate siderite is ruled out as no carbon is present.

5.1.2 Mound Facies

Sample 5 (Fig. 5.3) (also representing samples 7 and 10), **Sample 6 (Fig.5.4 and 5.5)** (also representing sample 11), **Sample 6a (Fig. 5.6 and 5.7)**, **Sample 12 (Fig. 5.8)** (also representing samples 9 and 18), **Sample 14 (Fig.5.9)** (also representing samples 13 and 16) and **Sample 17 (Fig 5.10)** (also representing sample 19). These samples make up the mound facies as characterised in the previous chapter. The textures observed in the basal samples can also be seen abundantly in these samples, however, some elongated pitted crystals can be observed that are not linked to an obvious biological structure. Several radial groups of elongated crystals that diverge away from the substrate are observed. Sparitic cavity fill is also observable in these samples as well as dolomite and associated clastic material. Smooth spar occurs as blocky crystals which often exhibit evidence of twinning, the spar is found as a cavity fill and is often in association with a rim of non-pitted micrite as a rim to the cavity. Some cavities are found with dolomite rhombs lining the roof and clastic material lining the base. Dolomite also occurs as isolated rhombs which often have pitted faces much like most of the calcite observed. Clastic material and dolomite can be observed together in layers, often between bioclasts and occasionally as stylolites.

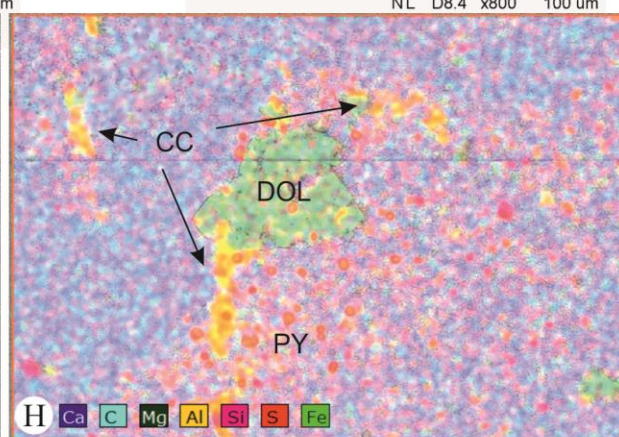
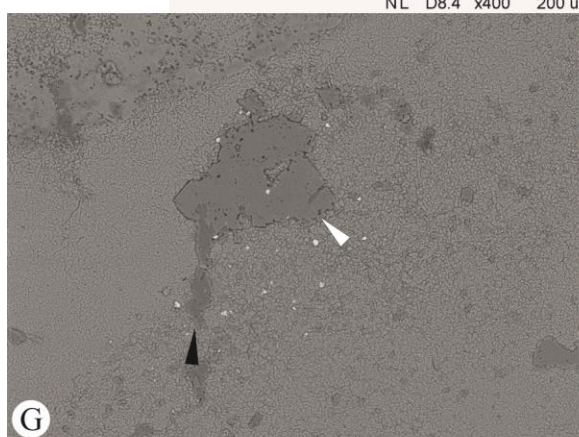
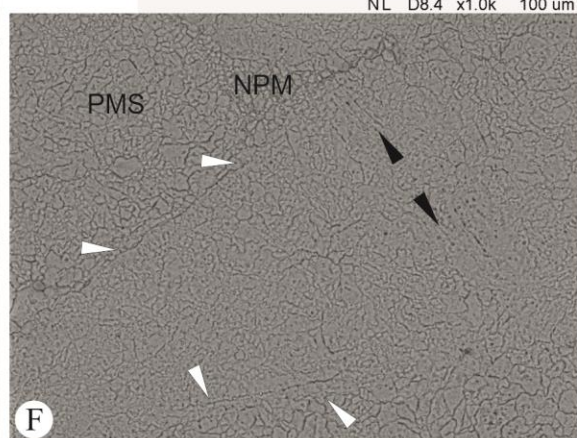
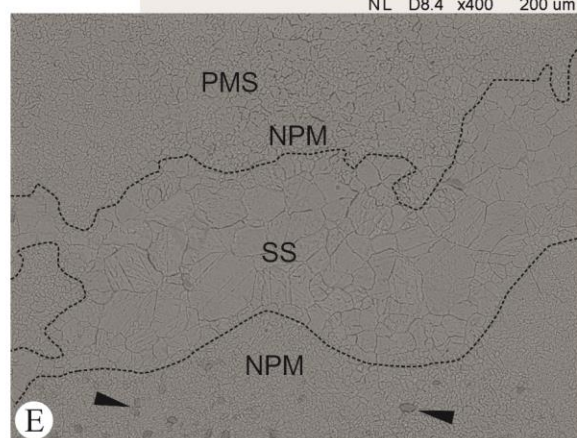
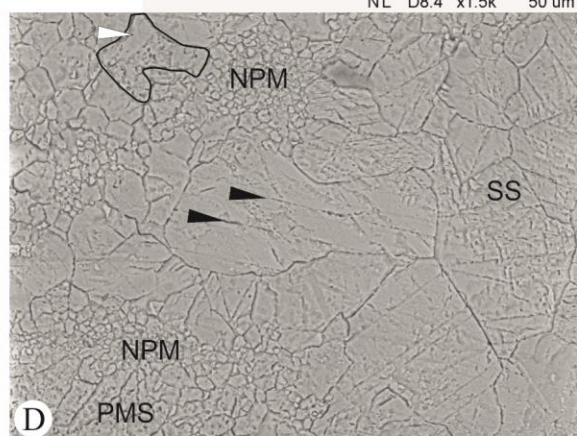
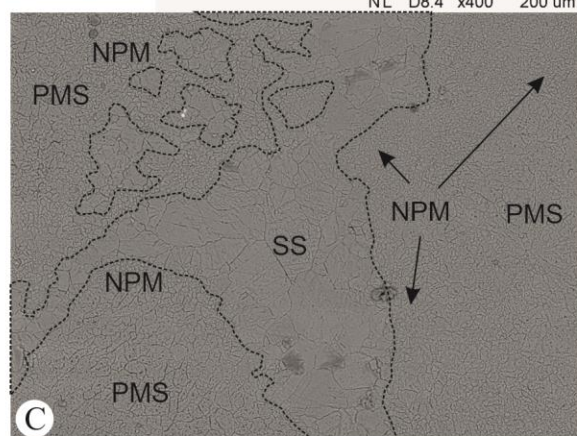
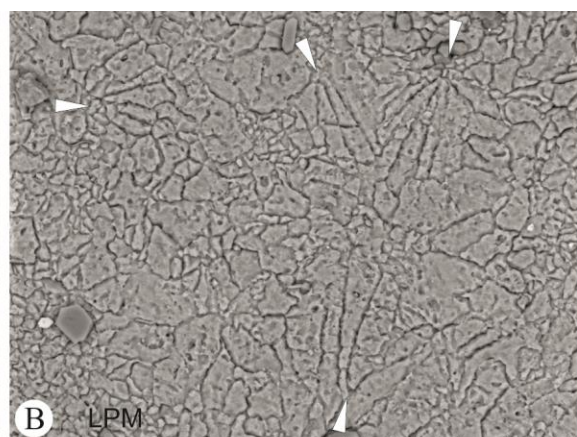
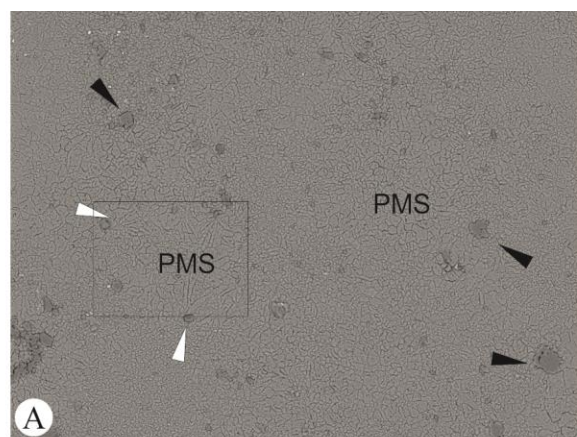


FIGURE - 5.3

A. Overview image of the microspar with a pitted surface texture. The black arrows indicate several individual or 'floating' dolomite rhomb's whilst the white arrows indicate small quartz grains, these are also observed to be individual or 'floating'.

B. A zoomed in image of the area highlighted in A. Here the pitted microspar can be clearly seen to form as radial crystals. Pitting seems to be aligned along these elongated radial crystals. The fans of crystals appear to be radiating from small patches of non-pitted micrite (arrows). This texture is interpreted to represent a peloidal fabric.

C. This image is of a fenestral cavity (outlined) with a blocky, drusy sparitic fill. The cavity filling spar can be seen coarsening toward the centre, the surfaces of the crystals show very few pits but do show evidence of twinning. The matrix surrounding the cavity consists of non-pitted micrite (NPM) which is located around the rim of the cavity and also as small clumps as indicated by the arrows. The non-pitted micrite then grades into pitted microspar. The proximity of the non-pitted micrite to the cavity and as small clumps may indicate aggrading neomorphism is the process behind its formation.

D. This image clearly shows the relationship between the smooth spar (SS), non-pitted micrite (NPM) and pitted microspar (PMS) seen in this sample. The smooth spar shows little evidence of pitting but does show evidence of twinning (black arrows). Although the majority of spar is without pits there are several examples at the edges of the cavity, in some cases single crystals exhibit pitting toward the rim of the cavity (highlighted crystal, white arrow points to the pitted half). The transition from spar to micrite to microspar can be seen in the bottom half of this image.

E. Non-pitted micrite can be seen distributed around the edge of the cavity. Toward the top, the transition into pitted microspar can also be seen. The arrows indicate small quartz grains, these grains are not observed above the cavity and may, along with the surrounding non-pitted micrite, represent internal cavity sedimentation.

F. An algal thalli, probably a *Donezella* 'barrel' - interpreted from morphology (white arrows indicate the wall structure). The small collection of non-pitted micrite (NPM) probably belongs to an encrusting organism, which attached its self to the algal thalli. Other than the small section of NPM this image shows various crystal arrangements of pitted microspar, the microspar that makes up the bioclast is elongated and has pits aligned perpendicular to the walls. The microspar which makes up the matrix is blocky with crystals not showing any preferred growth habits.

G. and H. Pitted dolomite rhombs, clastic fragments and pyrite can be clearly identified within the carbonate sample in both the SEM image (G.) and more obviously within the EDS (H.) The dolomite (DOL) appears lighter in colour than the clastic component (CC) and also has a smoother polished surface. Pyrite is formed as small isolated crystals <10 µm, and appears white in the SEM image.

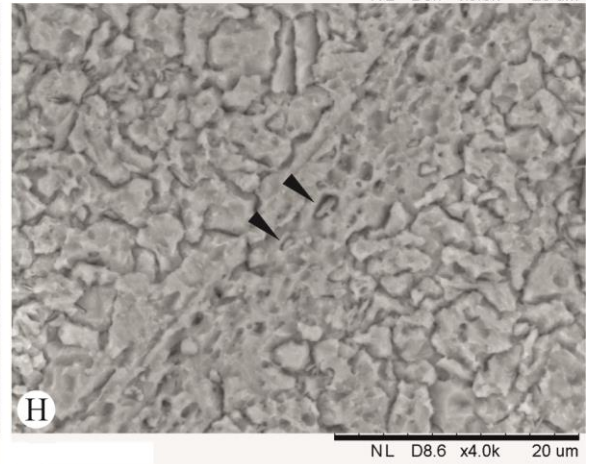
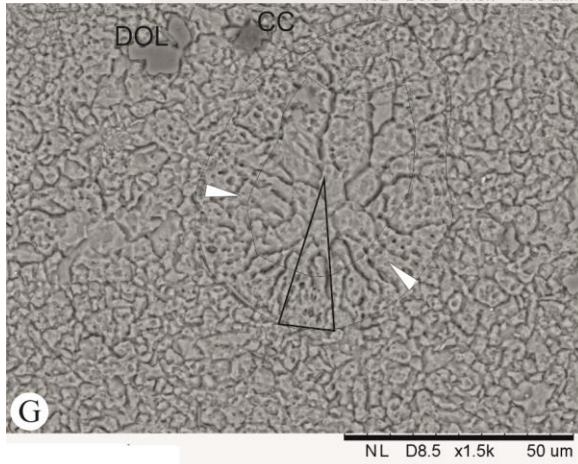
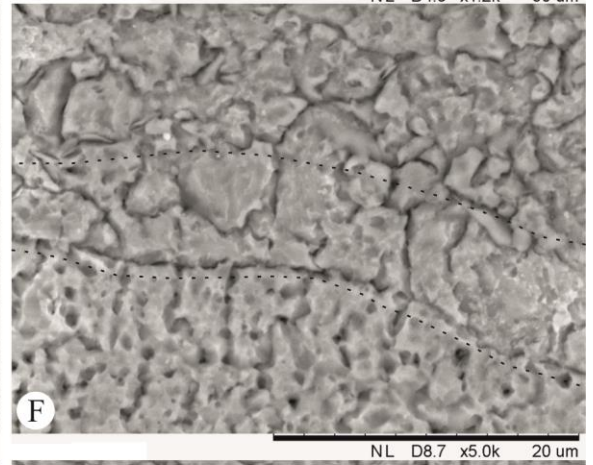
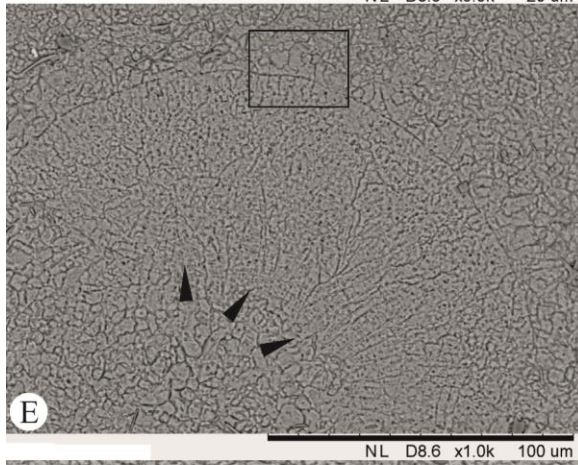
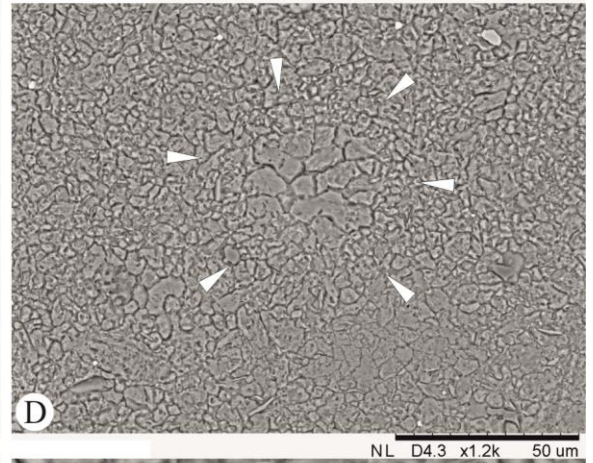
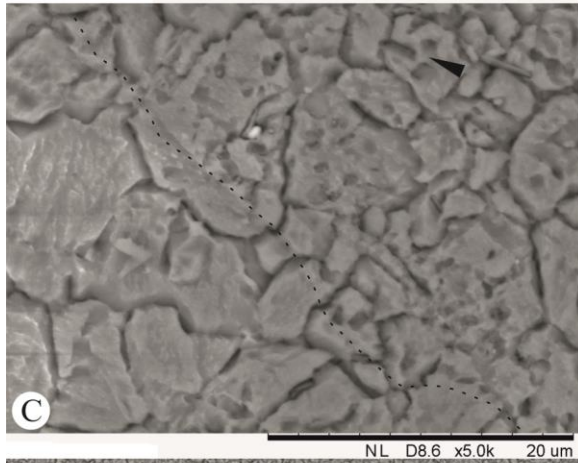
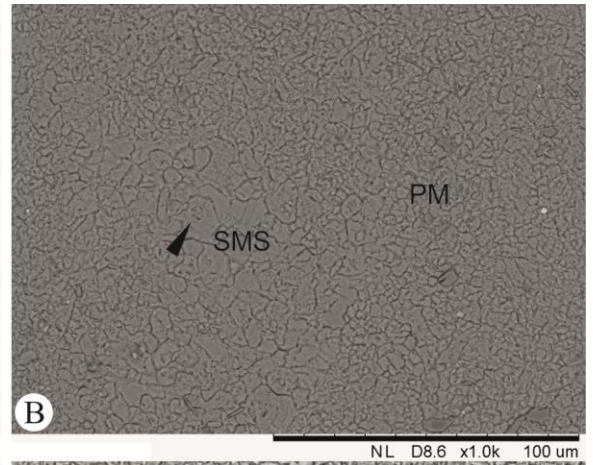
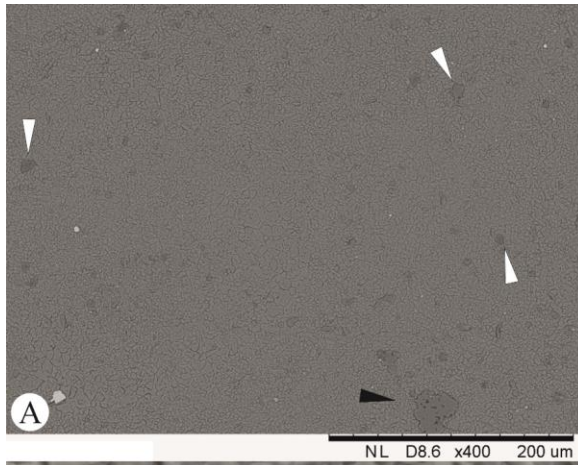


FIGURE - 5.4

A. This overview image shows the near homogenous nature of this sample, it consists almost entirely of pitted micrite and microspar with rare isolated quartz grains, dolomite rhombs and small pyrite crystals. Several stylolites run through the sample.

B. Textures observable in this image are smooth microspar (which is confined to a small, fenestral cavity) and pitted micrite which surrounds it. The arrow indicates a pit which appears to have a relic crystal within it.

C. A gradational relationship between non-pitted spar and pitted microspar boundaries is clearly shown in this image. The dashed line represents the boundary between the two textural features (non-pitted spar being below the line). However it can be clearly seen that this is a transitional boundary and several pits can be found within the spar component near to the boundary, suggesting that the same or similar processes are responsible for the precipitation of both sets of crystals. Several of the pitted surfaces are elongate and may represent the shape of pre-cursor aragonitic needles (arrow).

D. The arrows are arranged at the boundary of a calcisphere, the structure of the calcisphere is not well preserved. The wall has likely had slight aggrading neomorphism affecting it.

E. A specimen of *Tuberitina* displaying a pitted surface in comparison to other pitted textures observed, the pitting is also strongly aligned, radiating out from the central point along the flat side of the chamber (see arrows). The surrounding crystals are granular, pitted microspars.

F. A close-up of the area highlighted in F. Here the wall of the *Tuberitina* chamber can be observed, below the wall the highly pitted surface can be seen with many of the alignments of pitting tracing into the wall itself.

G. A calcisphere with a highly pitted wall, the central cavity is filled with non-pitted microspars which get progressively more pitted toward the wall, the large triangle highlights a good example of this. Again the pitted texture is dominantly aligned radially from the centre of the bioclast.

H. In this image an unidentified bioclast is observable running through the centre, non-pitted micrite is arranged directly next to this highly pitted bioclast, with pitted microspar making up the matrix around it. The arrows highlight pits which appear to have small clasts within them.

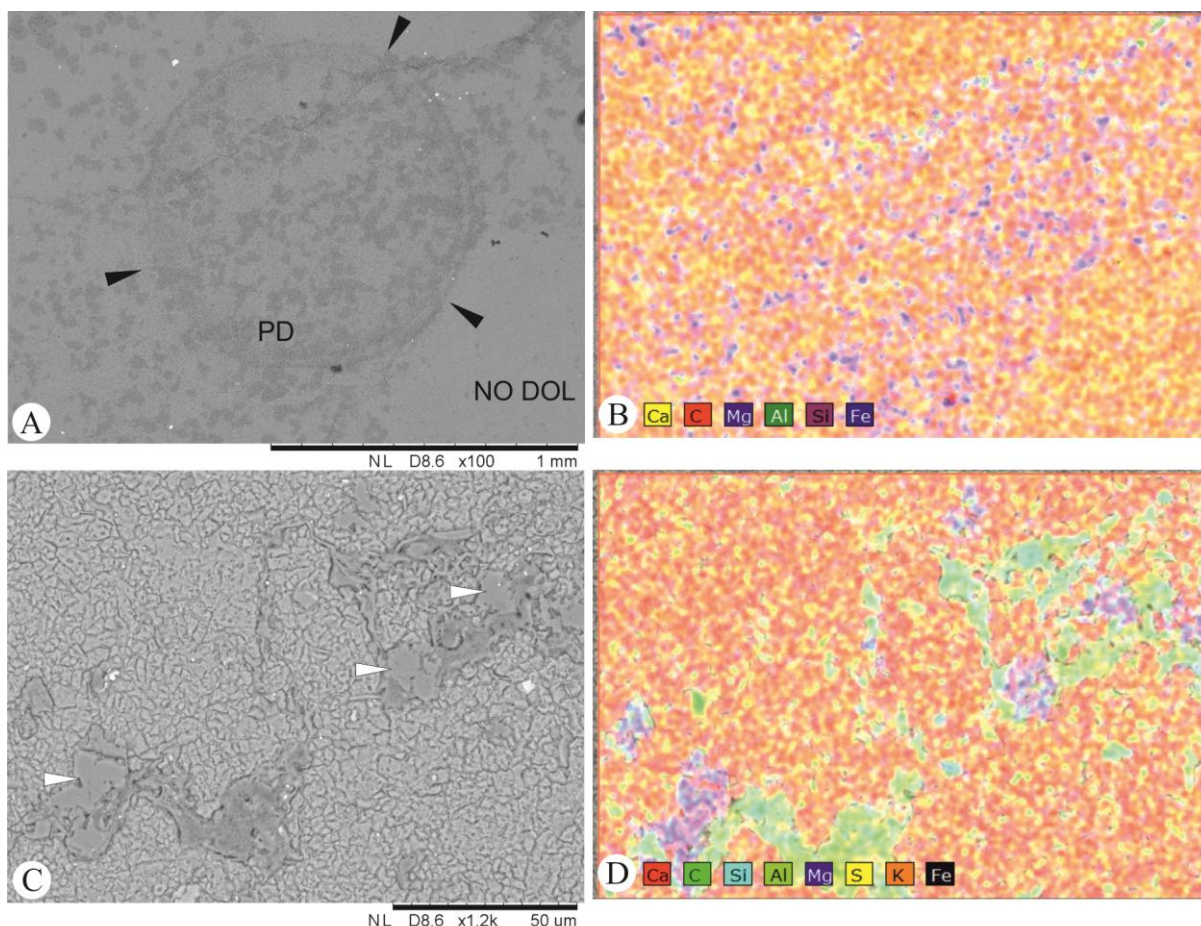


FIGURE - 5.5

A. and B. A large calcisphere (arrows) which has dolomite precipitated around, and within it. The dolomite has a pitted texture and is distributed in fine laminae, several of which are associated with clastic grains. The lower right corner of the image shows pitted microspar with no dolomite, and as seen in the previous Figure dolomite is not common within this sample. This indicates that dolomite precipitation was a selective process. Several pyrite crystals can be observed near the top of the image.

C. and D. An SEM image and element map of a part of one of several stylolites that were observed from this sample. The stylolite is composed of clastic material and dolomite rhomb's. In the image the clastics appear darker and have a 'gritty' texture whereas the dolomite rhomb's are darker than the calcite but lighter than the clastics (white arrows). Again, several pyrite crystals are present in association with the dolomite and clastics.

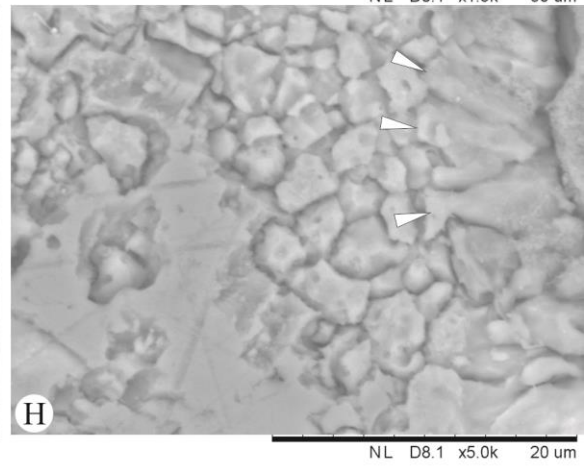
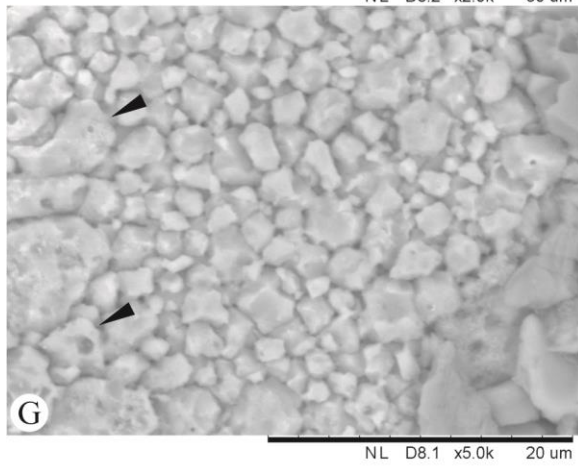
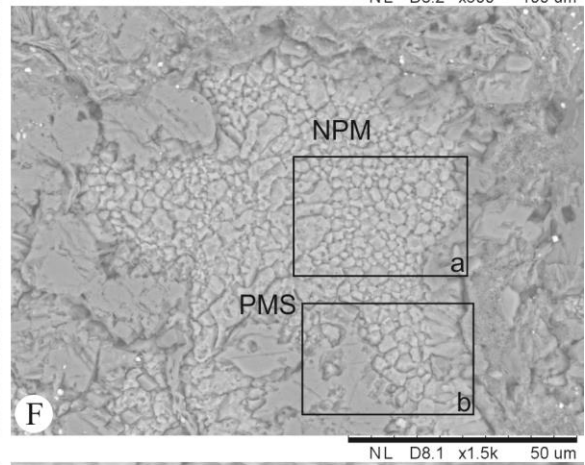
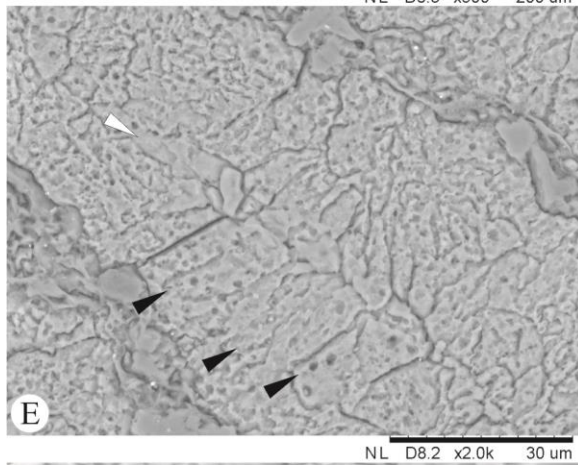
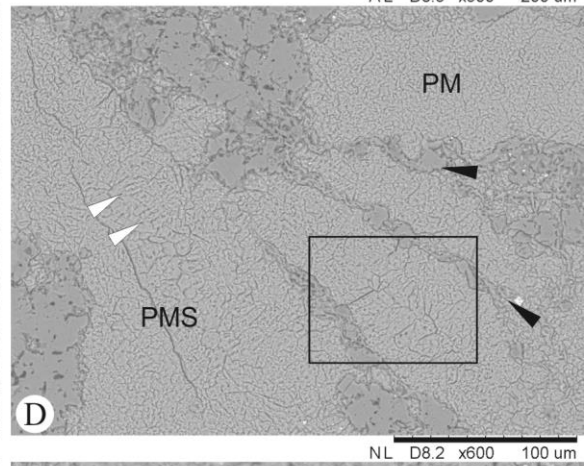
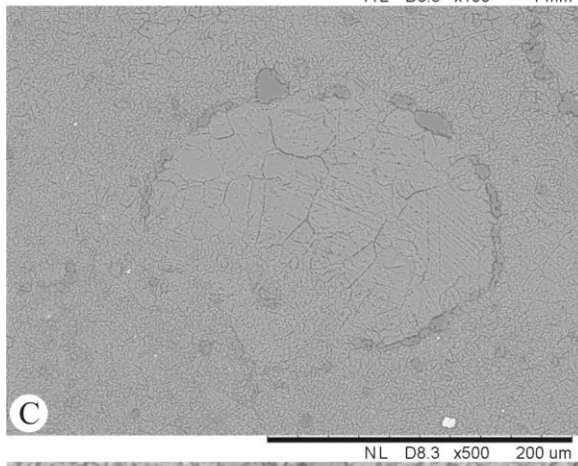
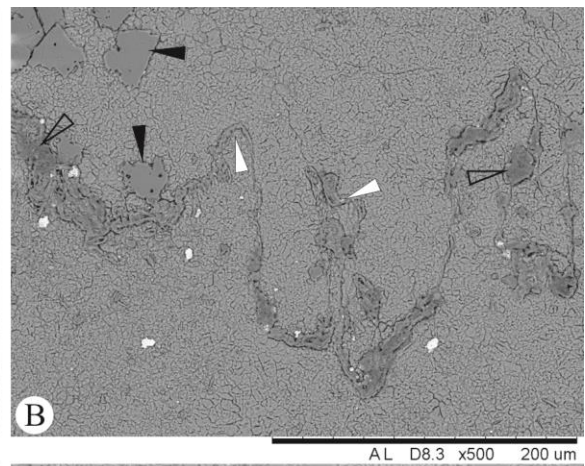
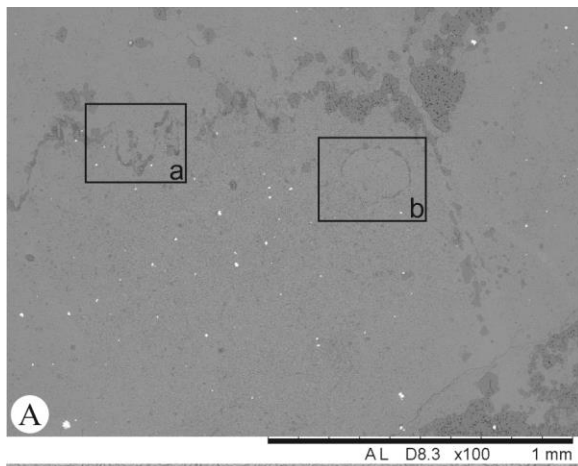


FIGURE - 5.6

A. An overview of the sample, a stylolite runs along the top of the image with dolomite, clastic grains and pyrite dotted throughout. Several bioclasts are also observable.

B. Highlighted area 'a' from A. A zoomed in image of part of the observed stylolite. Several crenulations can be seen. Clastic grains are often in the form of plates which are deformed along the path of the stylolite. Pitted dolomite can be observed in the upper left corner and pyrite is distributed along the length of the stylolite.

C. Highlighted area 'b' from A. A bioclast coated in clastic material can be clearly seen. The bioclast has a twinned sparitic fill and is sitting within a pitted microspar matrix.

D. Several bioclasts surrounded by clastic rich material are observable. The bioclast in the upper right area of the image is very angular and consists of pitted micrite. The other bioclasts are more ovoid in morphology and are mostly fibrous pitted microspars growing normal with respects to the bioclast walls (white arrows), these are most likely algal in origin. The distribution of clastic material appears to be directly linked to the bioclasts (black arrow) and may represent the baffling of sediments.

E. Highlighted area from D. The fibrous crystals with a pitted texture can be seen (black arrows) to end at a thin cavity (filled with non-pitted micrite/microspar) running through the centre (white arrow).

F. A microcrystalline walled microfossil within a clastic matrix. The microfossil consists of a non-pitted micrite wall which is granular and arranged in distinct layers. The central cavity of the microfossil is filled by pitted microspar.

G. Highlighted area 'a' from F. Layered, granular micrite, without pitting. This indicates that the crystals were biologically mediated. The arrows indicate the pitted microspar which fills the cavity between the microgranular walls.

H. Highlighted area 'b' from F. Indicated are acicular crystals growing normal to the wall, crystals are elongated parallel to the c-axis, the non-pitted surface texture of these crystals may suggest a low Mg-calcite origin, which like the non-pitted micrite would have been biologically mediated.

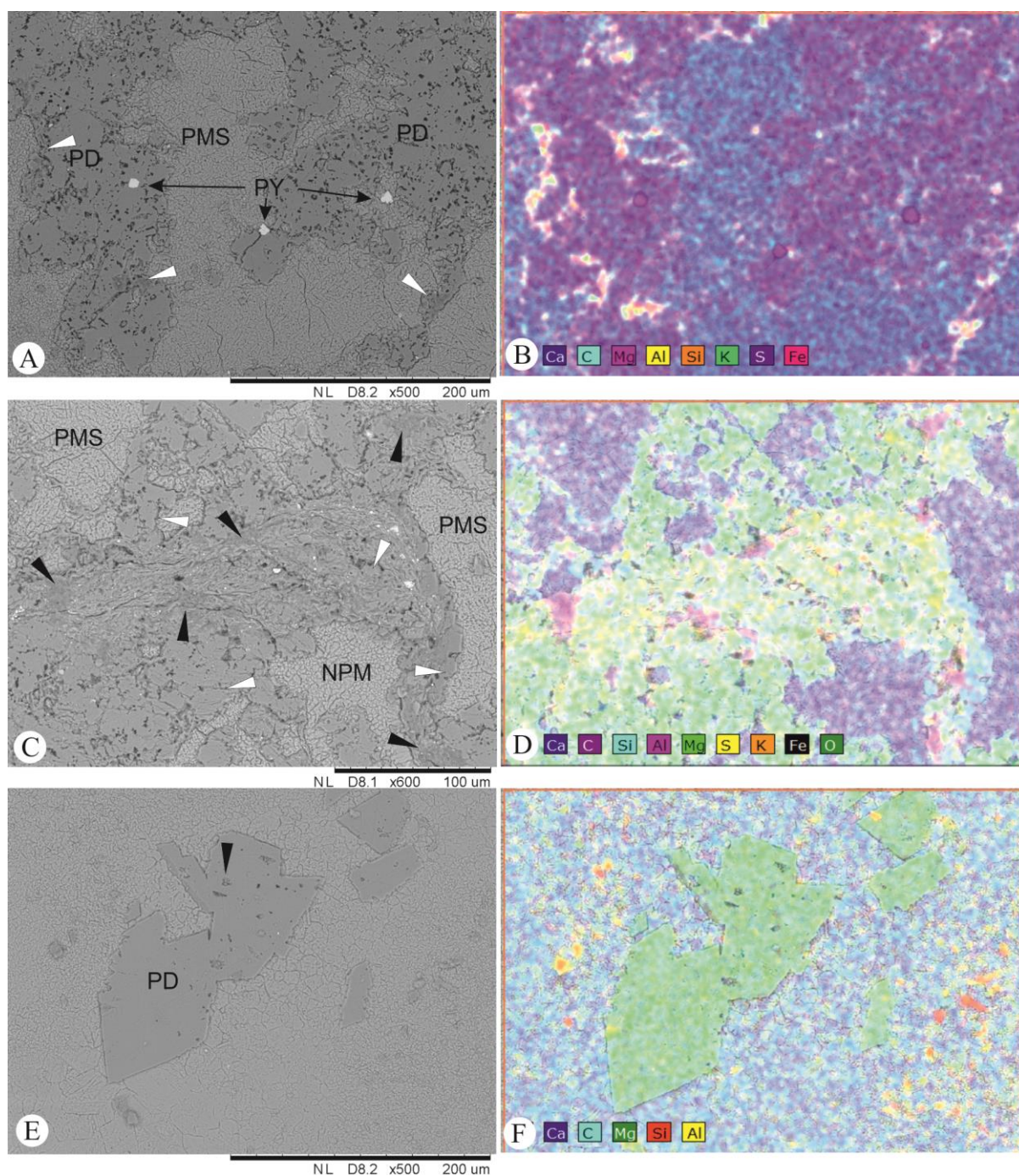


FIGURE - 5.7

A. and B. These images show the relationship between dolomite (PD) and calcite (PMS) in this sample. The calcite, which is pitted microspar, has very few grains of clastic material included within it, whereas the dolomite, which is pitted dolomite, frequently has patches (white arrows) of clastic material included. Pyrite is also confined to the dolomite fraction (PY).

C. and D. The dolomite (white arrows) fraction in these images is again in close association with the clastic fraction (black arrows). Pyrite is confined to the clastics. Calcite is represented by both pitted microspar (PMS) and non-pitted micrite, which again show very few inclusions.

E. and F. Rhombic dolomite (PD) with several pits (arrow), these rhomb's are isolated and appear to be 'floating' in the calcitic material.

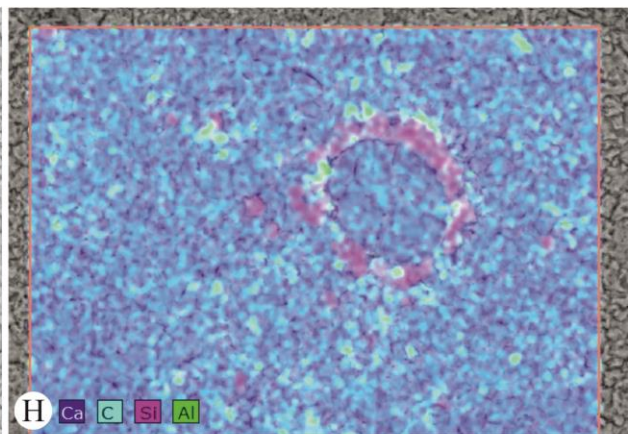
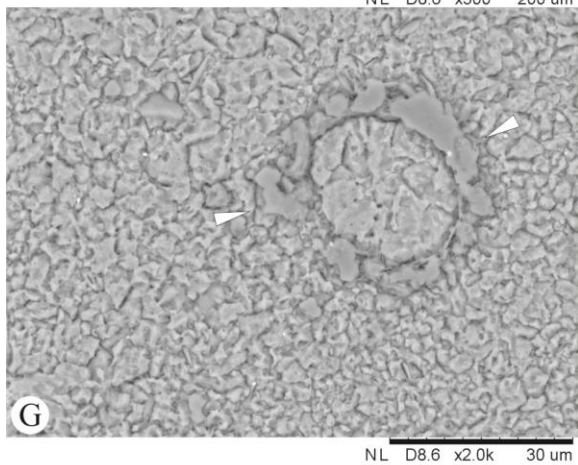
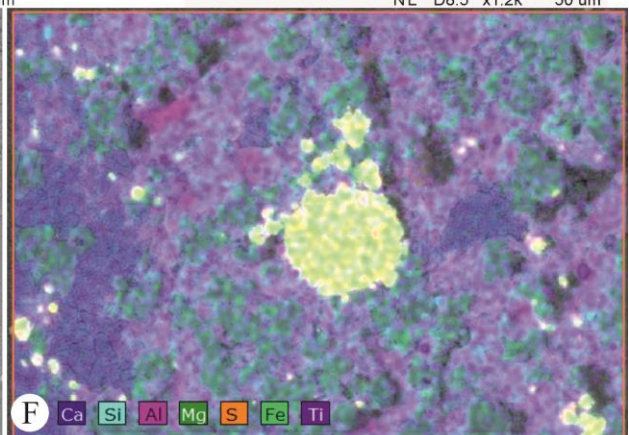
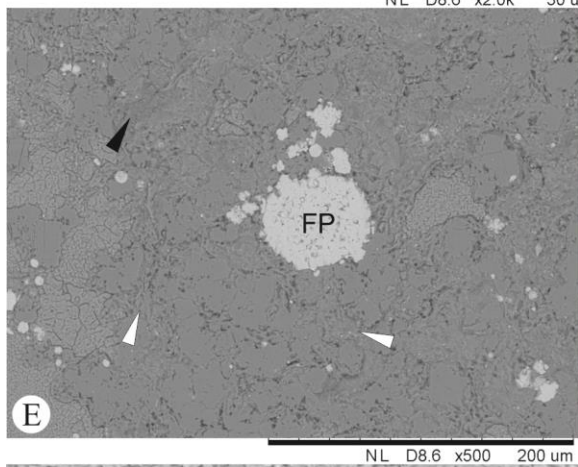
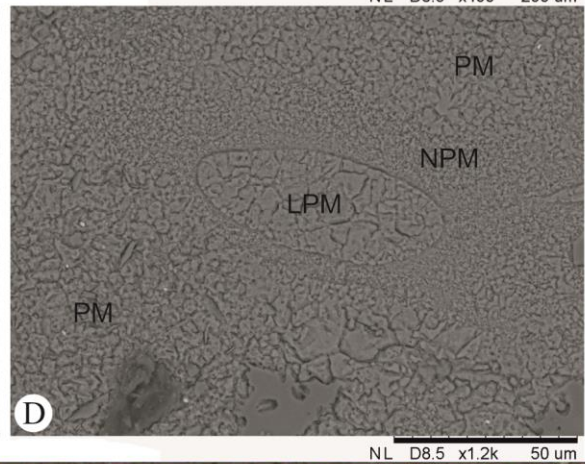
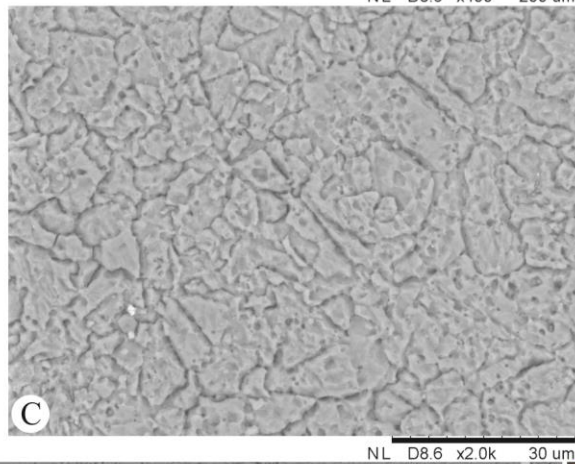
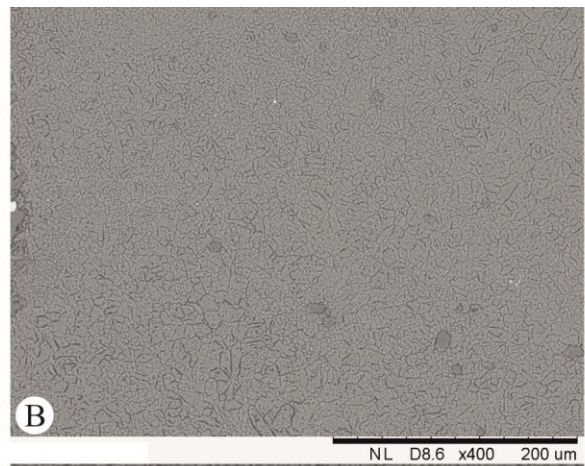
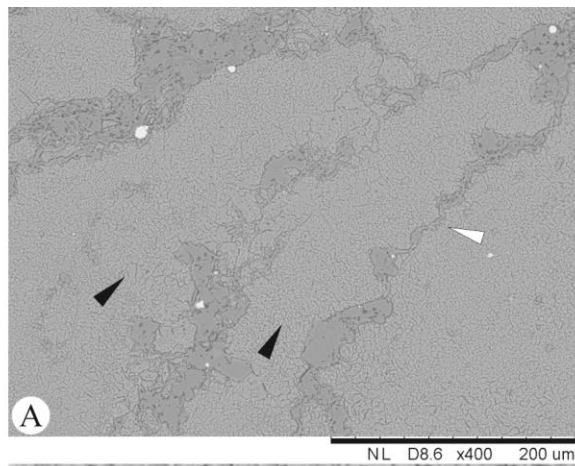


FIGURE - 5.8

A. Algal thalli (black arrows) consisting of pitted microspars, surrounded by clastic material and dolomite, the surfaces of the bioclasts are not smooth, with the clastic/dolomite fraction forming mini stylolites between them, this is evidence of some minor compaction of the sediments, pressure dissolution may have played a small role.

B. An overview showing the general constituent of this sample, pitted micrites and spars with accessory clastic grains and isolated dolomite rhomb's.

C. Blocky, pitted microspar crystals. Typical of most crystals observed within the Candemuela Mound. Some crystals are possibly elongated (arrow).

D. A microcrystalline walled microfossil within a pitted micrite (PM) matrix. The microfossil has a non-pitted micrite (NPM) wall. Although the microspar which fills the fossil cavity (LPM) is pitted, it is less pitted than the microspar surrounding the fossil.

E. and F. Dominantly dolomite (white arrow) and clastic grains (black arrow) with a high number of framboidal pyrite (FP) associated. The labelled framboid is 80 μm in diameter, whilst the smaller framboids range from 4 μm to 25 μm . The element map clearly shows that the framboids are associated with the dolomite and clastic fractions of the sample.

G. and H. The majority of crystals in this image show no or little pitting, the spherical object shows a larger crystal with possibly aligned pits, and is surrounded by clastic material.

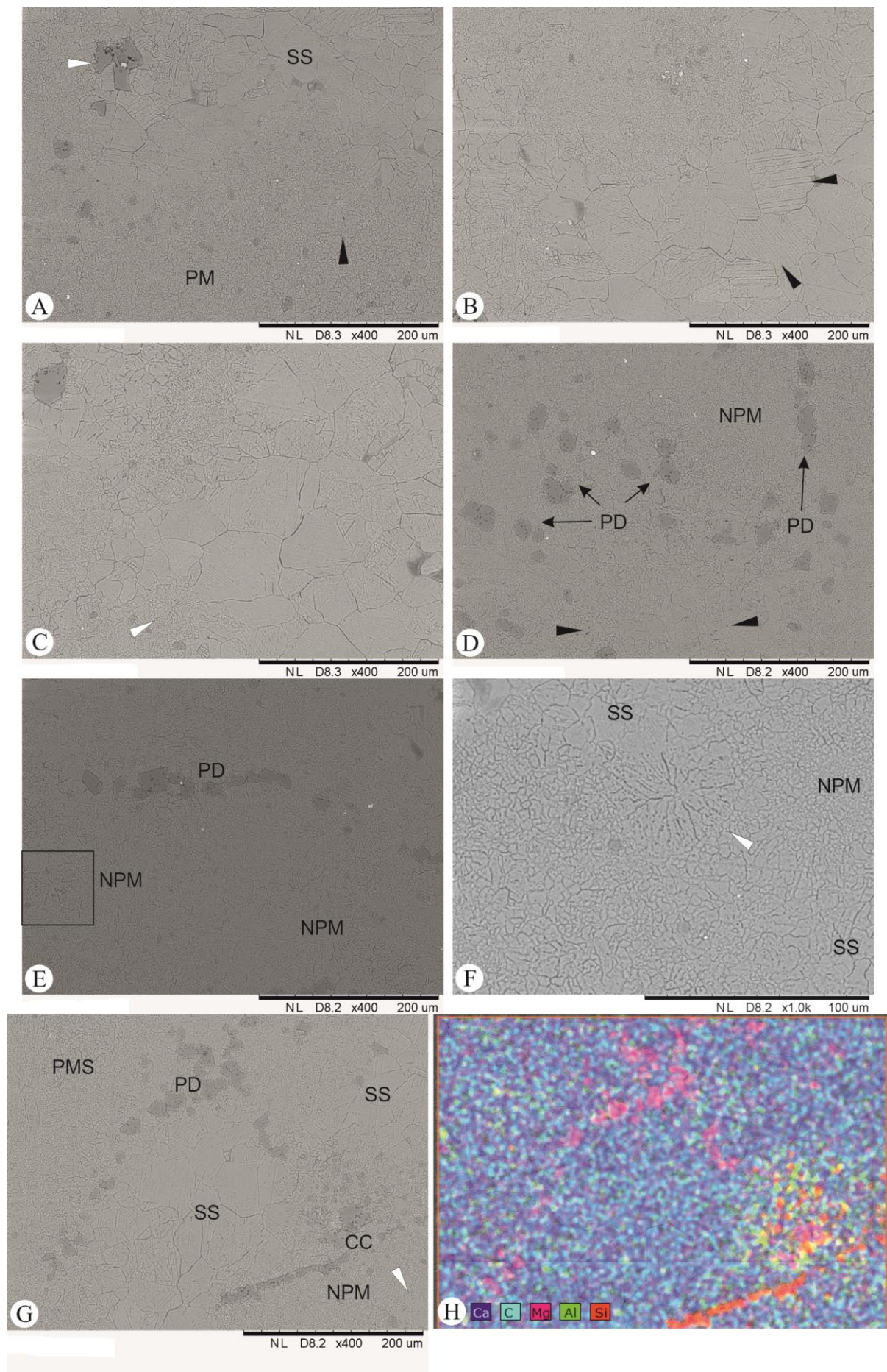


FIGURE - 5.9

A. Pitted micrite (PM) crystals and a fenestral cavity filled with a smooth spar (SS) fill. Pitted dolomite (white arrow) isolated toward the top of the cavity in association with (non-framboidal) pyrite.

B. Granular non-pitted micrite and microspar with smooth spar crystal as cavity fill. The spar shows well developed, regular twinning (black arrows).

C. Cavity fill can be seen as smooth blocky spar with twinning, surrounded by non-pitted micrites and some lightly pitted microspars. A calcisphere is indicated by the white arrow.

D. Non-pitted micrite (NPM) and slightly pitted microspars with 'floating' dolomite rhomb's. These rhomb's have a surface that is more pitted than other examples of dolomite observed. The white arrows indicate deep, and well pronounced pits that are present in the microspars and micrite. Although the overall amount of pitting is lower than that of other samples the depth and clarity of them is slightly elevated in this sample.

E. Non-pitted micrite (NPM) with fenestral, spar filled, cavities. Pitted dolomite (PD) occurs as a distinct band at the top of one of these cavities. Non-pitted micrite appears as intertwined clumps and lenses within this sample, these small clumps of micrite with pitted microspars are most likely peloids.

F. Highlighted area from E. An attached microorganism can be seen (white arrow) preserved as heavily pitted radial crystals. Evidence of a single layered, microcrystalline wall is observable. The organism appears to be attached to smooth spar which may indicate the dissolution of certain organic entities before or during diagenesis. The non-pitted micrite (NPM) can be clearly seen here in small clumps surrounded by pitted microspar and smooth spar.

G. and H. An image and element map of a cavity. The cavity fill is smooth spar (SS) with some evidence of twinning, the bottom of the cavity is filled with non-pitted micrite and clastic sediments (CC). The top of the cavity is coated in pitted dolomite (PD). The surrounding material is the common pitted microspar observed in most images.

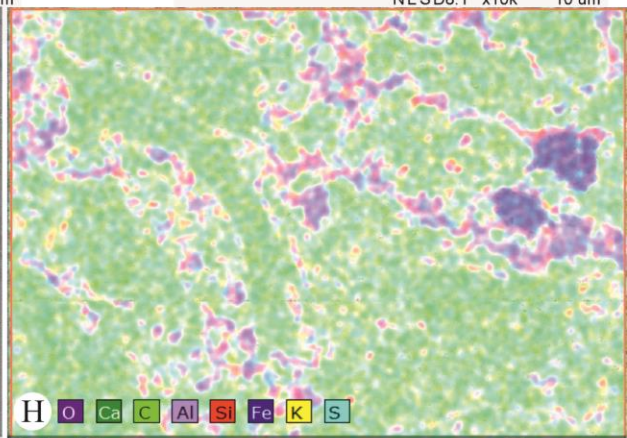
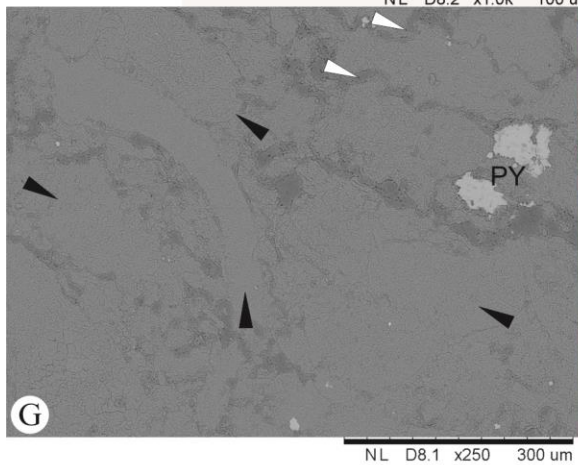
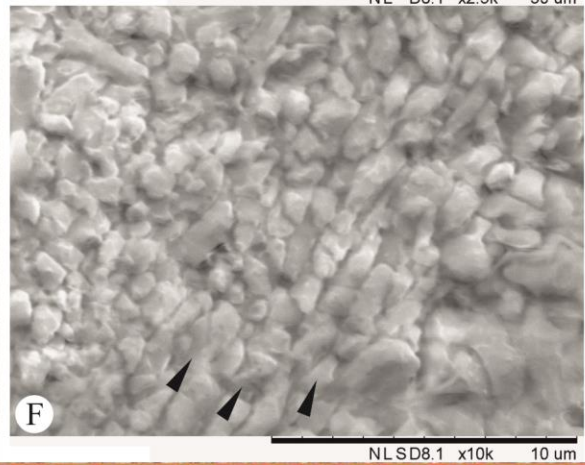
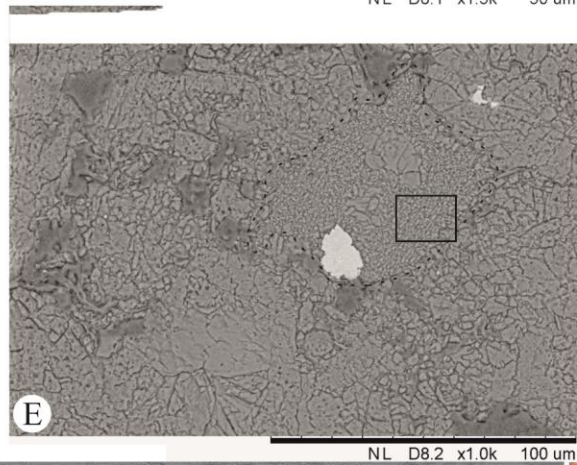
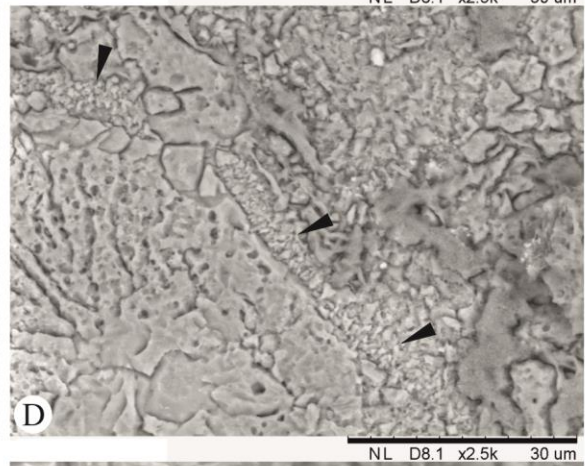
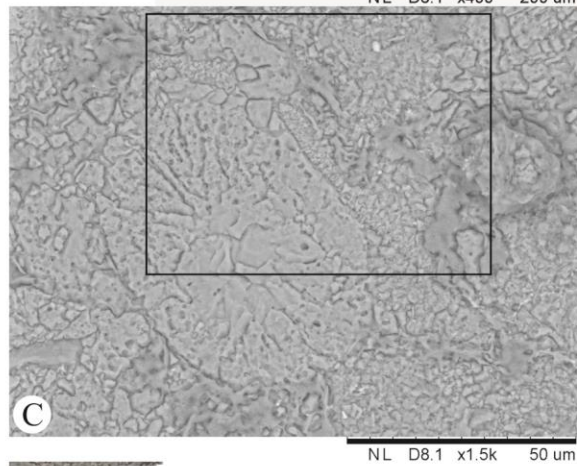
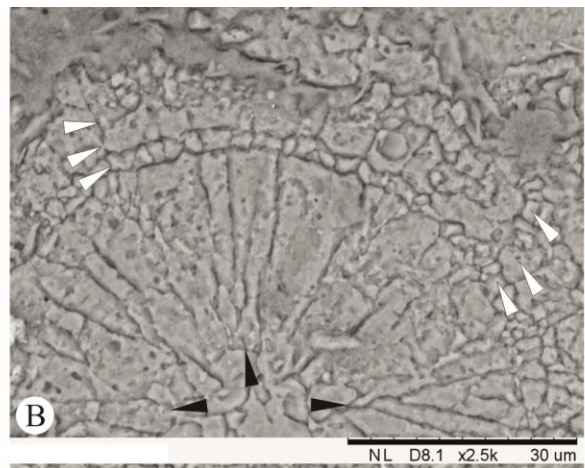
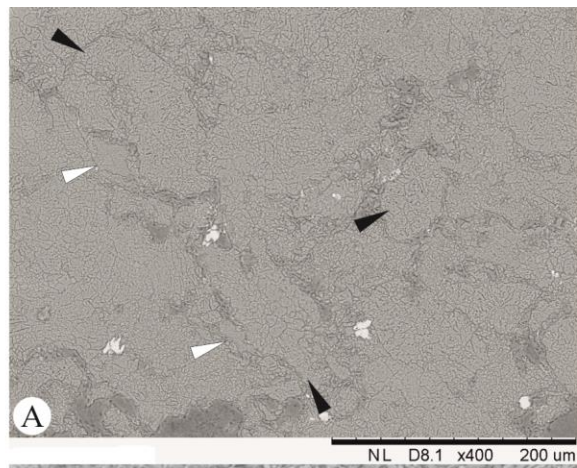


FIGURE - 5.10

A. Overview image showing well defined bioclasts (black arrows) with a clastic and dolomite fraction baffled between them. The bioclasts seen are longitudinal and cross sections through algal thalli. Also present here are several iron rich clasts, which are a ferric oxide (note the crystal morphology in comparison to the framboidal pyrite observed elsewhere (see 5.3 *Framboidal Pyrite*)).

B. A well preserved *Tuberitina* specimen, the chamber fill is radial, pitted crystals with less pitting toward the centre. The wall consists of one, to possibly three layers. The first, definite layer consists of equigranular, microcrystalline blocks, they are 1 - 3 μm in size (lowest arrows). The next layers (upper sets of arrows) are possibly part of the wall though it is not as obvious as to whether they are or not due to discontinuities in size and arrangement of the crystals, the crystals also exhibit a pitted texture, which the wall layer does not.

C. Several bioclasts with differing textural features are identified. The large spherical bioclast appears to be a cross section through Donezellacean thalli, and is pitted with a smooth central cavity fill. The other identifiable texture is that of the tubular bioclast attached to the algal thalli. This attached bioclast consists of microcrystalline crystals which are elongated from the algae wall.

D. Close-up of the highlighted area in C. Here both the pitted crystals and the microcrystalline texture of the attached bioclast can be seen clearly. Note how prominent the pits are in this sample and that the smooth spar toward the bottom left of the image also contains several, well defined pits. The microcrystalline texture consists of crystals with slight elongation from the walls, they have smooth surfaces and are $<2\ \mu\text{m}$.

E. A microcrystalline walled fossil within a pitted, blocky microspar, spar and dolomite/clastic matrix.

F. Close-up of the microcrystalline wall as highlighted in E. The crystals are well organised into layers and are non-pitted. They are roughly 2 μm in size with little deviation. The arrows indicate several of the layers within the wall.

G. and H. Several bioclasts are indicated by black arrows whereas the clastic/dolomitic/pyrite fraction is seen to fit around the bioclasts. This arrangement indicates that the clastic component in this sample has been baffled by the organisms.

5.1.3 Capping Facies

Sample 15 (Fig. 5.11), Sample 20 (Fig. 5.12) (also representing sample 21) and **Sample 22 (Fig. 5.13)**. Within these samples, which are representative of the Capping facies a much higher abundance of both dolomite and clastic material can be observed than in the Base and Mound facies. Bioclasts are preserved as the pitted micrites and spars and non-pitted micrites as observed in the other samples. Bioclasts are filled with either smooth spar and/or dolomite/clastic grains. The number of pyrite framboids is much higher in these samples than in any others from the Candemuela Mound.

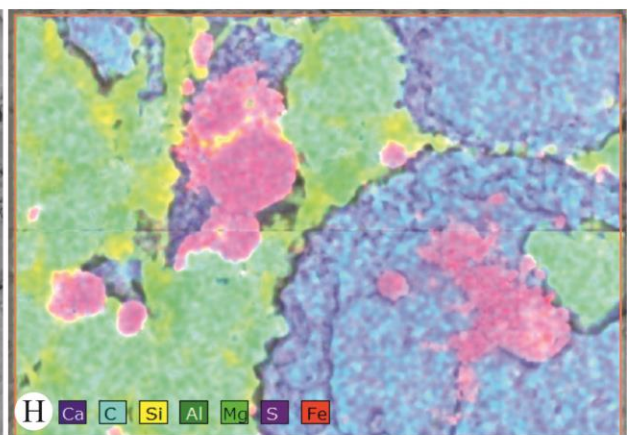
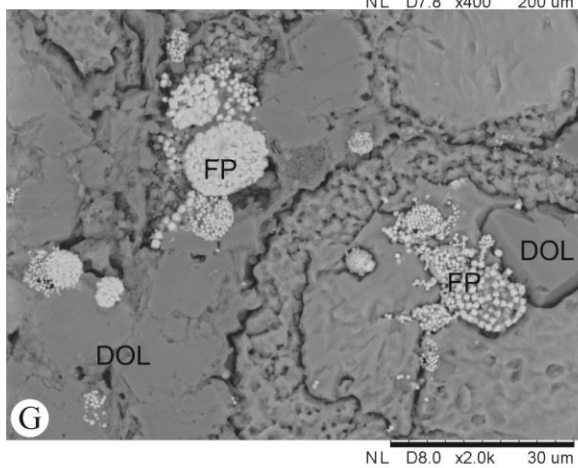
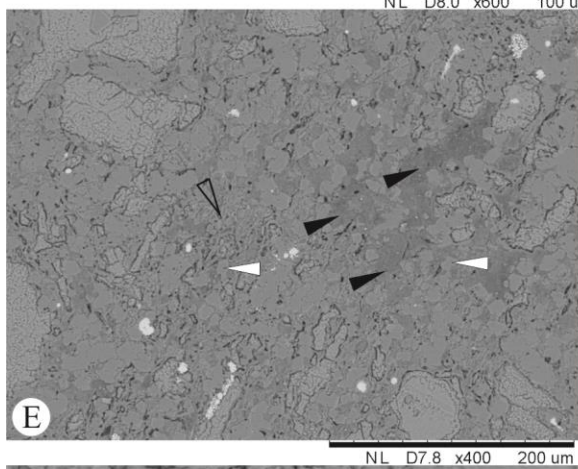
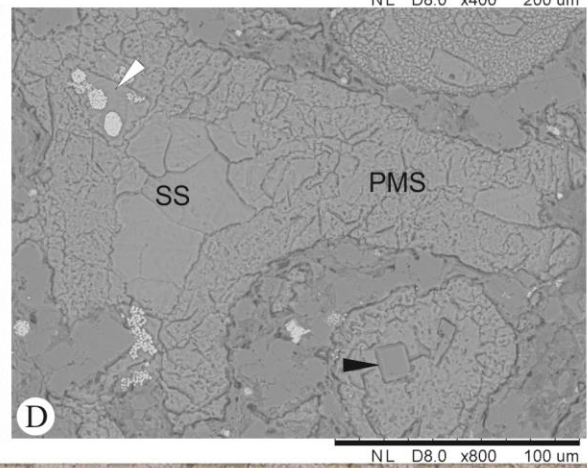
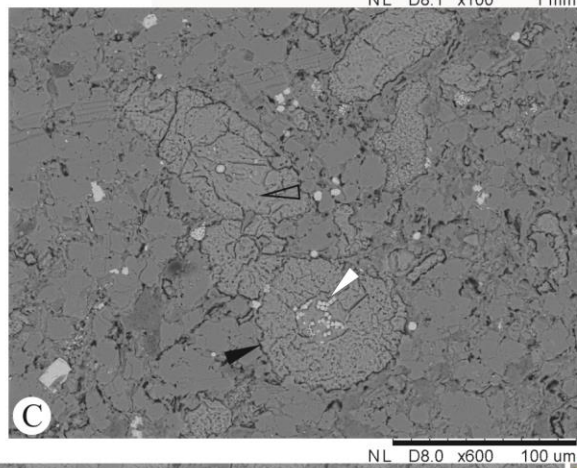
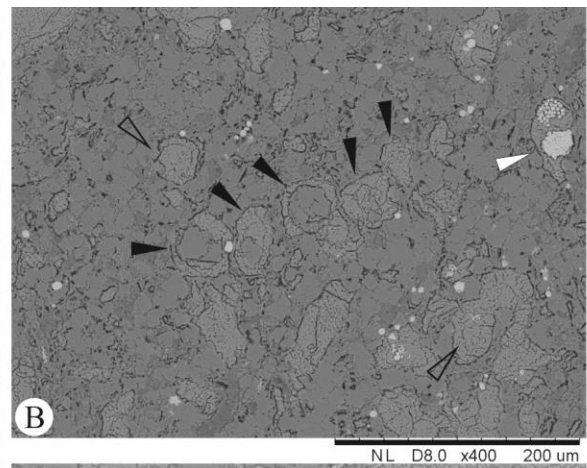
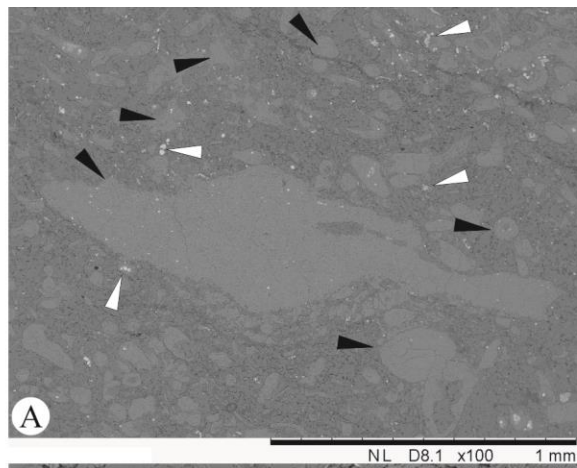


FIGURE- 5.11

A. Calcitic bioclasts (black arrows) can be seen within a matrix of clastic materials. The bioclasts appear to have maintained their original morphologies so compaction is deemed to be minimal. Framboidal pyrite is common throughout the sample (white arrows).

B. The darker material is clastic and dolomitic, this image shows several bioclasts (black arrow) arranged as a layer, these laminae can be observed through the sample. The bioclasts indicated by the black arrows all show a level of dolomite as cavity fill, the amount ranges from a few rhombs to the entire cavity fill. Bioclasts indicated by the open arrows have a pitted spar fill. The white arrow indicates a microcrystalline walled microfossil which has a pyrite fill.

C. An algal thalli preserved by heavily pitted fibrous microspar crystals (black arrow), the internal cavity is filled with less pitted spar (open arrow) and pyrite (white arrow).

D. A *Donezellacean* specimen clearly showing pitted microspar (PMS) walls with a smooth sparitic fill. Framboidal pyrite is also present (white arrow) within the fill material, as are dolomite rhombs (black arrow). The circular bioclast toward the upper right of the image shows an equigranular, non-pitted microgranular texture.

E. and F. The laminated nature of the sample can be seen particularly well in these images. The dominance of clastic and dolomitic material can be seen in the element map. Black arrows indicate the shale dominant component whereas the open arrow indicates the quartz. White arrows highlight some particularly rhombic dolomite crystals. The element maps indicate that the quartz fraction is often associated with Potassium.

G. and H. Calcitic bioclasts, dolomite, framboidal pyrite and aluminium/silicon rich clastic fractions can all be easily identified. The bioclasts have a pitted wall texture with a smooth calcite, dolomite and framboidal pyrite fill.

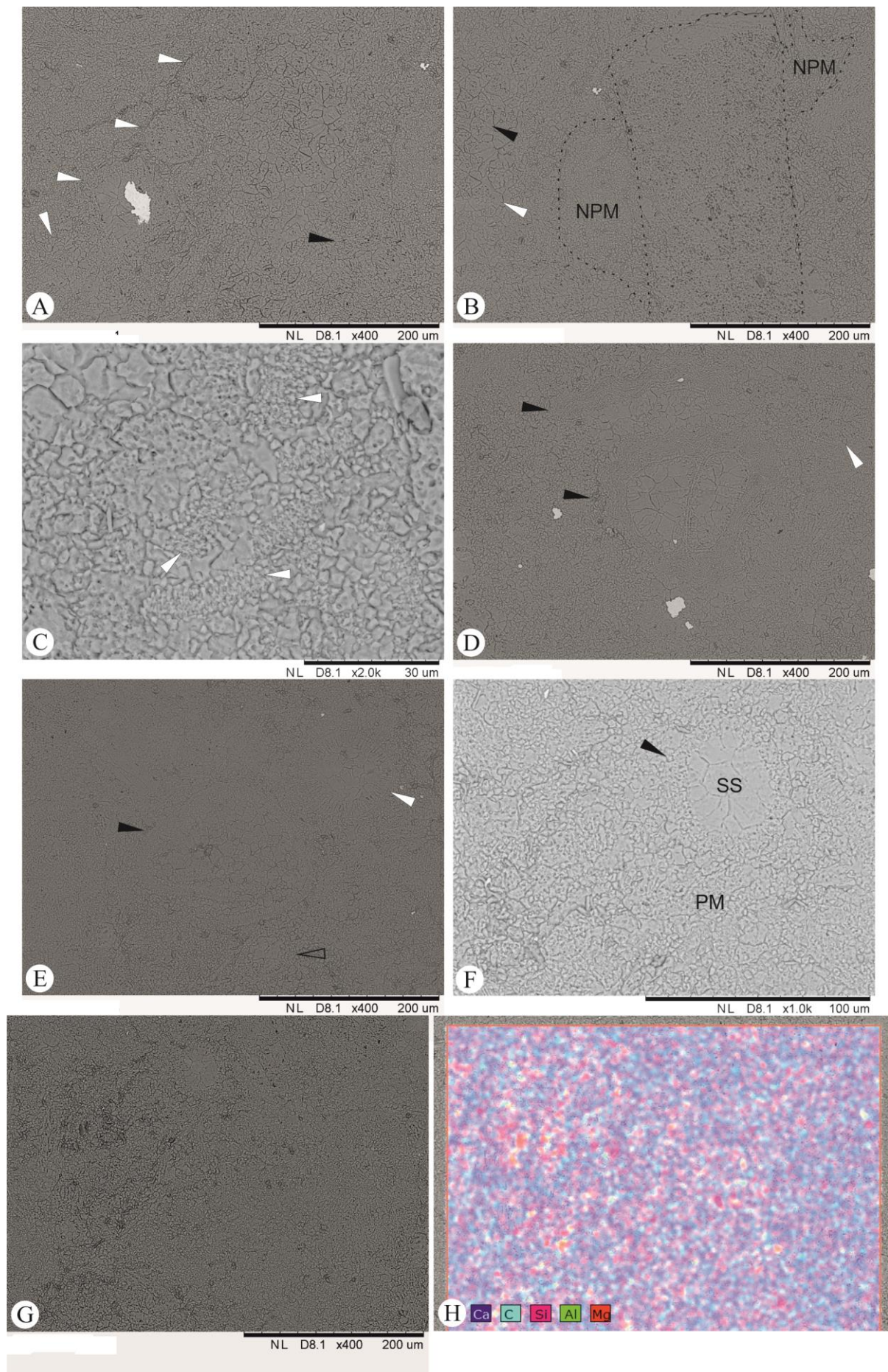


FIGURE - 5.12

A. Overview showing bioclasts (white arrows) and the major constituent – pitted microspar and micrite. The black arrow indicates very pitted crystals.

B. The central outlined bioclast is a *Donezellacean* thalli showing a heavily pitted texture. Attached to the algal thalli are two non-pitted micrite walled encrustating forms, the micrite is equigranular. The surrounding cements are mostly pitted microspar with some smooth spar (white arrow), some crystals have a half pitted, half smooth surface (black arrow).

C. Highlighted are several microcrystalline structures, the structures are found as small clumps or as tubular objects, the microgranular crystals are elongated with regard to the walls. These structures most resemble a calcimicrobial organism (due to size and morphology, and probably represent longitudinal and cross sections through *Girvanella* tubes.) The surrounding cements are both pitted and non-pitted micrites.

D. A bryozoan can be seen in this image (arrows). The wall structure consists of laminar, equigranular micrite ‘slabs’. See the chapter 6. *Palaeontology* for more detail.

E. Various bioclasts are present in this image: the white arrow indicates a *Tuberitina*, the open arrow a calcisphere and the black arrow an algal wall.

F. Highly pitted microspar and micrite (PM). A calcisphere (black arrow) with a regularly pitted wall and smooth spar fill.

G. and H. These images show the dominance of calcitic crystals in this sample, dolomite rhomb's and clastic grains are often isolated and found ‘floating’ in a calcite cement.

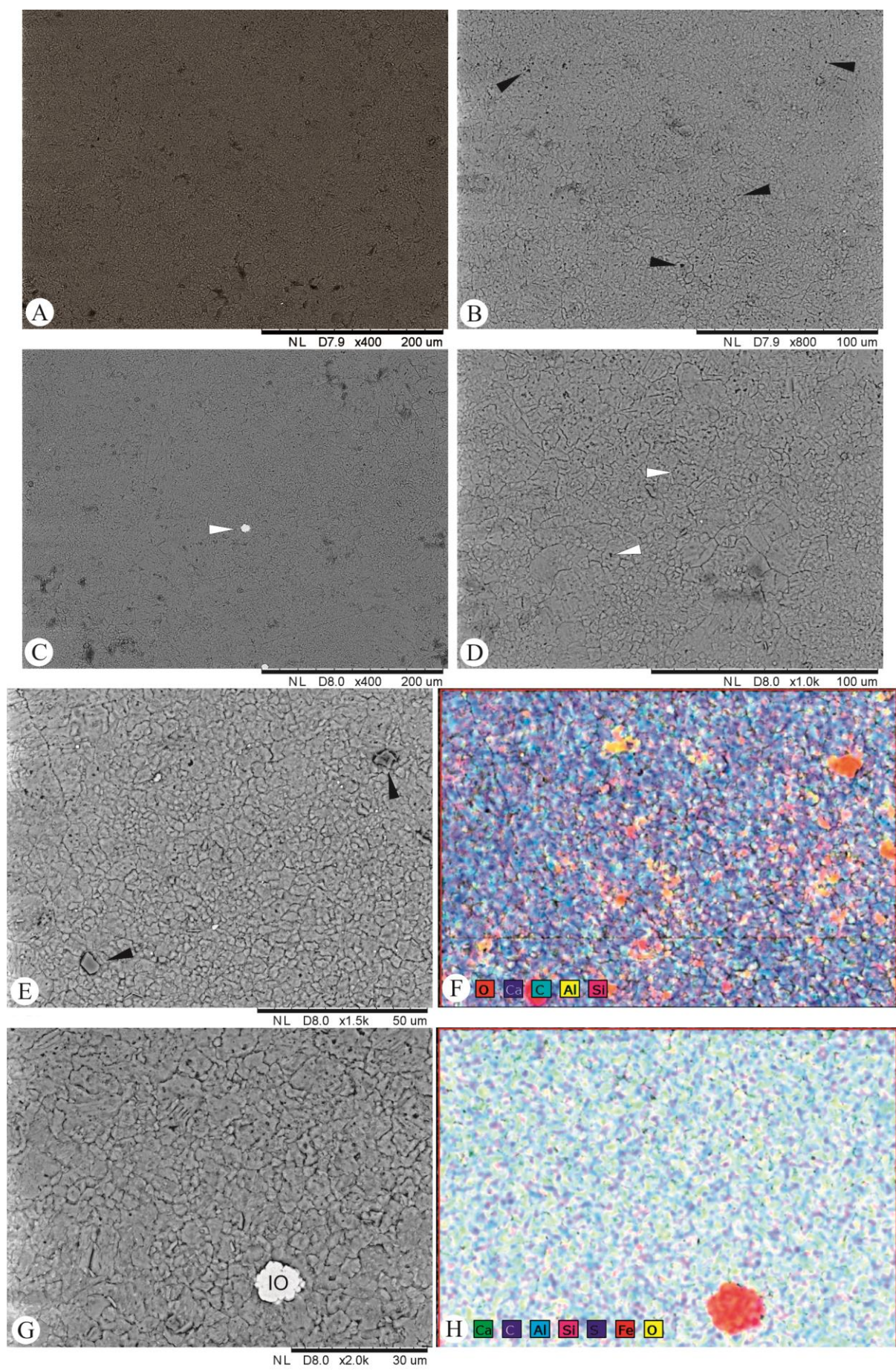


FIGURE - 5.13

A. This sample has a large amount of pitted microspars and some smooth spar. Toward the bottom of this image some large pits can be observed.

B. The pitted microspar is less pitted in terms of the abundance, but the pits are far more pronounced than in other samples, the arrows indicate several of these distinctive pits.

C. Another image showing the dominance of calcite. The arrow shows a rare patch of ferrous oxide.

D. Pitted microspar, the distinctively well-developed pits are again evident (arrows)

E. and F. It can be seen in these images that there is a clastic component to this sample but it is not distributed in patches or layers like elsewhere, here the grains are small ($<5\ \mu\text{m}$) and are isolated.

G. and H. Here an isolated patch of ferric oxide (IO) can be seen within a pitted microspar.

Interpretation

The major textures observed within the samples are dominantly micrite, microspar and spar crystals with associated dolomites and clastics, the latter two in much lower abundance. Micrite and spar crystals are mostly observed as smooth crystals whilst microspar has a pitted surface. The textures observed indicate several important factors about the diagenesis of the carbonate mud mounds and inter-mound carbonates and of the palaeoenvironment that they formed in. The pitted surfaces observed throughout the sample are created by the preferential etching of certain parts of the polished, cut blocks. This preferential etching is an indicator of a precursor structure, around which the calcite crystals observed have formed. These structures are observed both within the matrix material, and in algal thalli. This similarity suggests that both the algal thalli and the soft-sediment precursor to the calcite were both similar; indeed the soft sediment was potentially partially formed from the breakdown of the calcareous algae. The pitted structures are most probably the relics of a precursor aragonite (Lasemi and Sandberg, 1984) and possibly early high-Mg calcite crystals. The aragonite needles would form both chemically and also through bio-mediation. The breakdown of aragonitic skeletons along with chemical precipitation of aragonite and high-Mg calcite would form a mesh of needles, small crystals and bioclasts. Under normal diagenetic conditions low-Mg calcite will begin to precipitate preferentially over the unstable high-Mg calcite and aragonite (Folk, 1974; Tucker and Wright, 1990 & Munnecke and Samtleben,

1996). The low-Mg calcite crystals would presumably nucleate between needles subsequently overgrowing and engulfing the aragonite needles (Steinen, 1982). The precipitation of aragonite and high-Mg calcite at the time of sediment deposition (Bashkirian to Moscovian) can be attributed to global climate. During the Pennsylvanian the Earth was under icehouse conditions (e.g. Crowell, 1978; Oyarzun *et al.*, 1999; & Scotese *et al.*, 1999) and oceans were ‘aragonite seas’ where inorganic carbonate precipitates as aragonite or high-Mg calcite (Sandberg, 1983; Wilkinson and Given, 1986; Stanley and Hardie, 1998; Lowenstein *et al.*, 2001 & Mohammad, 2004). Cavities are generally filled with a smooth spar which suggests low-Mg calcite formed in the cavity networks at the same time the neomorphic overgrowth of aragonite occurred. Neomorphism takes place with the dissolution of aragonite and high-Mg calcite and precipitation of low-Mg calcite.

5.2 Other mounds

The textures observed within the analysis of the Candemuela Mound are observable for the other mounds found locally and within the San Emiliano Formation (the mounds analysed within the Microfacies chapter). The similarity in textures, including smooth spar and micrite crystals and microspars showing various levels of pitting, along with similar accessory inclusions (framboidal pyrite and clastics) suggests that the carbonate precipitation and diagenesis within the San Emiliano region is generally homogeneous, and that the mounds have similar nucleation and growth histories. One major difference observed is a dominance of homogenous smooth microspar with few bioclasts preserved within the isolated mounds observed within the Lois-Cigüera Formation (Sena de Luna, Cármenes South and San Martín mounds). This texture could represent prolonged neomorphism within these mounds or a less aragonite dominated precursor sediment.

The **Pinos hairpin Limestone** (Fig. 5.14) has a higher clastic component than any of the other samples, often the only substantial carbonate components are bioclasts. Where predominant carbonates occur it is either as a bioclast, where the walls are generally radial crystals of non-pitted micrite with smooth spar fills, or, it occurs as spars and microspars which have little pitting. Because of the polished nature of the samples no micro-topographic features of the clastic

component can be observed, however is it apparent that between the majority of carbonate crystals sits clastic fraction.

Ultrafacies analysis of the **Pinos East Mound** (Fig. 5.15) shows several of the textures observed within the Candemuela samples. Smooth spars and micrites with pitted microspars are common, NPM is often observed in small clusters around which PMS are arranged. Some SS occur within this mesh of crystals, it is noted that although they are generally smooth, several spar crystal can be observed to exhibit pits on their outer edges - suggesting a similar formation mechanism and timing as the PMS. The clustered texture probably represents the peloidal or clotted fabrics observed in thin sections. Dolomite is present as well formed rhomb's in places.

The main texture observed within the **San Martín Mound** consists of pitted microspars with a clastic component. The pits observed are generally well defined but do not occur within every crystal. Where microfossils are present the walls are well preserved NPM, often with a radial arrangement, within fossil cavities a non-pitted spar occurs as the fill, this texture also often exhibits a radial element. Pressure dissolution seams (stylolites) and fractures are present within the samples. Stylocumulate texture (see Fig. 5.16 A) is often observable within the direct vicinity of the stylolites, as are cubic pyrite crystals, which can be found distributed in bands oriented in a similar fashion to the stylolites. Fractures are found filled with a carbonaceous material with clastics along the rim (and some grains suspended) of the fracture. Generally fewer microfossils were observed from this location.

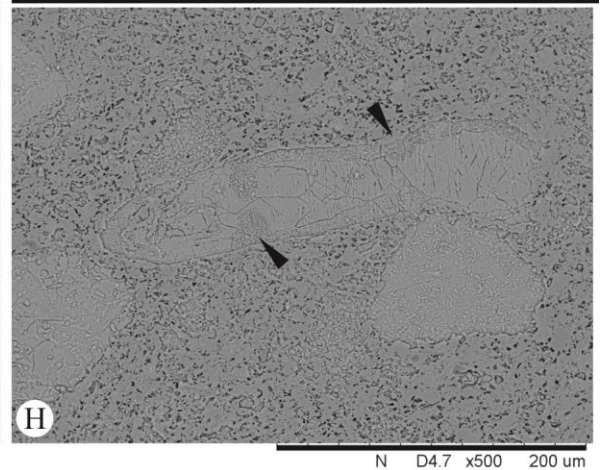
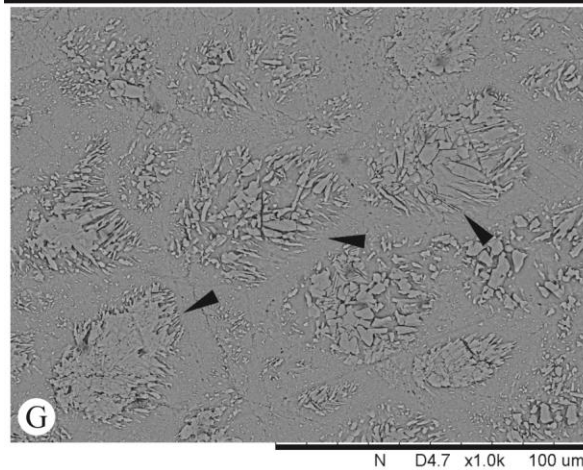
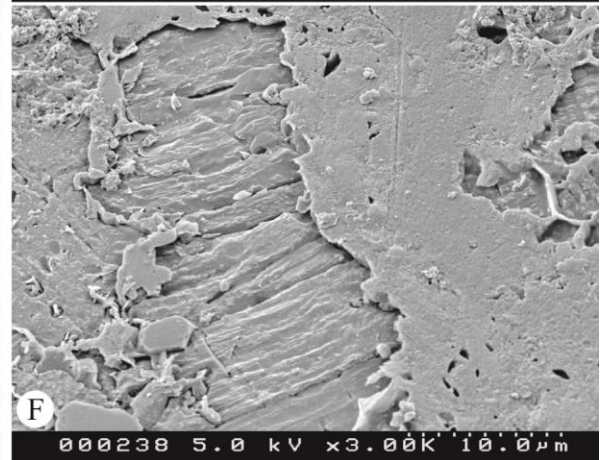
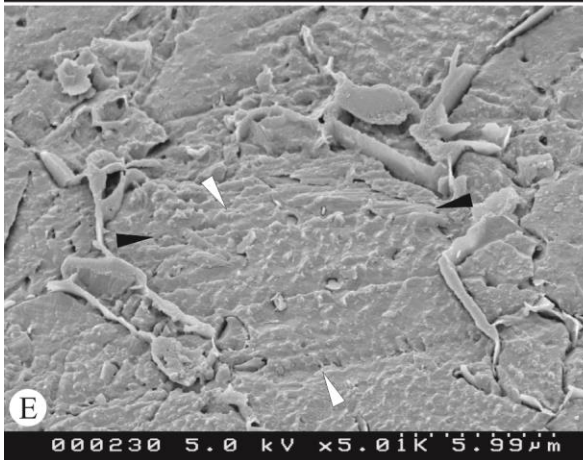
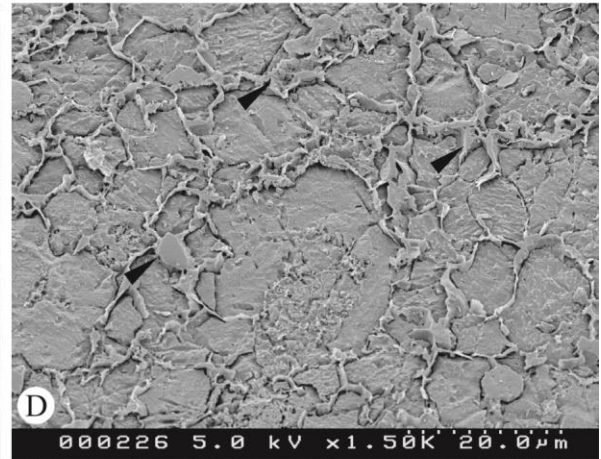
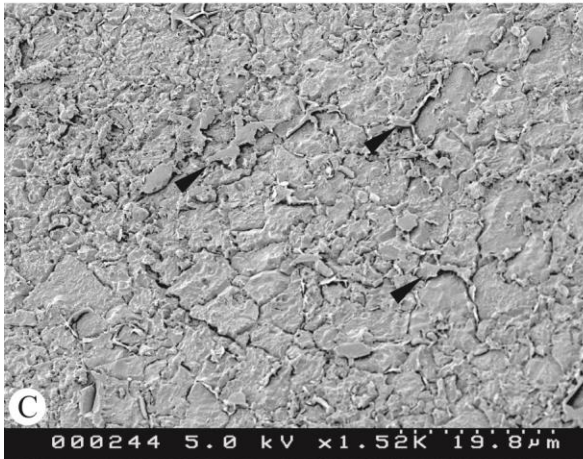
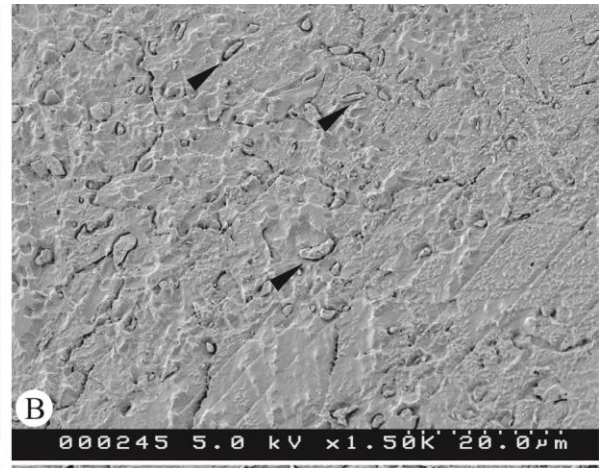
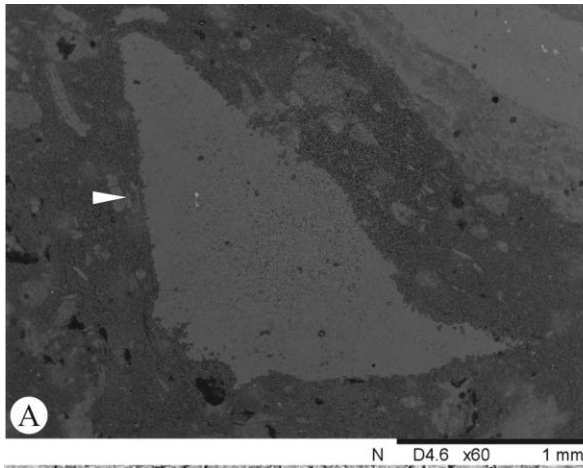


FIGURE - 5.14

A. In this image an overview of the Pinos Hairpin Limestone can be observed. The darker material consists of clastic fragments within a carbonate cement - due to the polishing of the samples, this component shows no textural features. The lighter material observed are calcium carbonate and are mostly bioclasts. The large 'bowl' shaped clast (white arrow) which dominates the image is a juvenile sponge (see G.).

B. Spar crystals exhibiting several smaller elongate micrite crystals (arrows) which are found sitting in etched pits.

C. and D. Microspar and spar crystals with clastics (see arrows for examples) between each crystal, this is likely due to the effects of pressure dissolution.

E. A microspar crystal surrounded by blade like clastics, cleavage is indicated by the arrows.

F. Fibrous microspar crystals surrounded by clastics. The clastics toward the right of the image are an example of the featureless surfaces found due to the polishing of the samples and the lack of reaction to etching. The fibrous crystals are roughly 10 μm in length and are around 1 μm wide. The crystals are quite needle like, and represent the wall structure of an organism which originally had aragonitic walls.

G. This image is a close-up of the ultrastructure of the sponge observable in A. Spicules are clearly visible in what would have been pore space. The spicules are well preserved and consist of calcareous needle like structures (the arrows point to a few examples) often measuring around 40 μm in length and several microns in width.

H. An example of a specimen of *Donezella*. The wall structure and internal cavity can be clearly seen, as can the internal divides (arrows) which form the barrel like shape of the thalli. In some cases the wall structure is exceptionally well preserved (see *Chapter 6. Palaeontology* below). The matrix seen here has a high siliciclastic component (un-etched material).

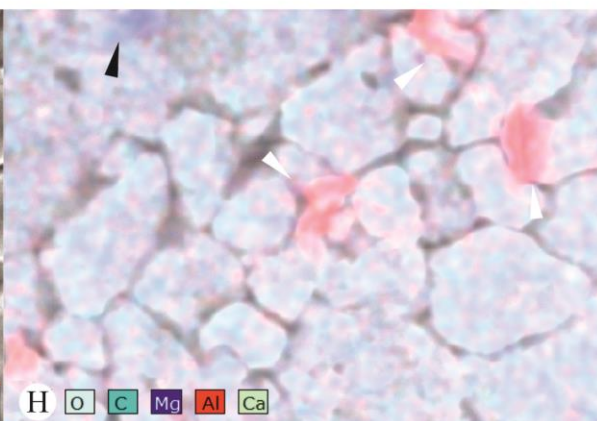
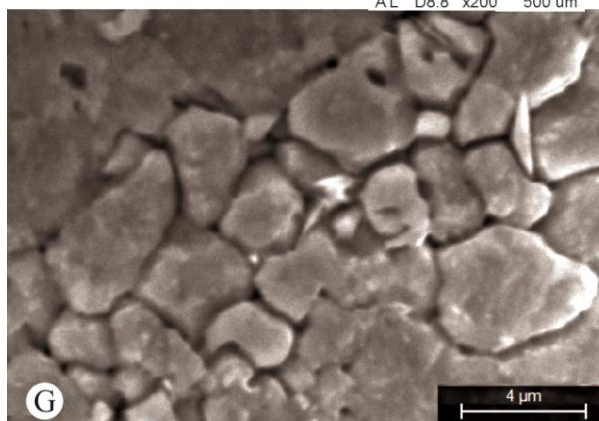
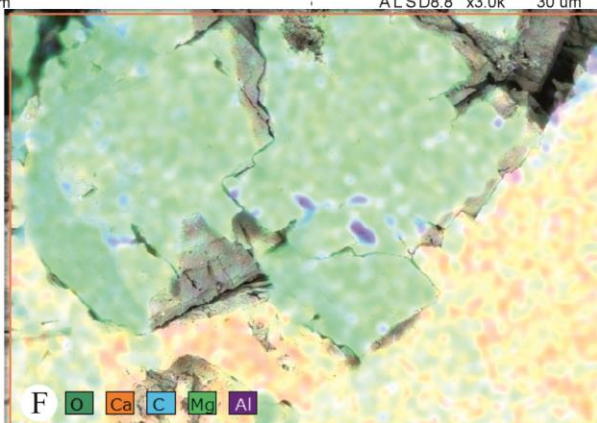
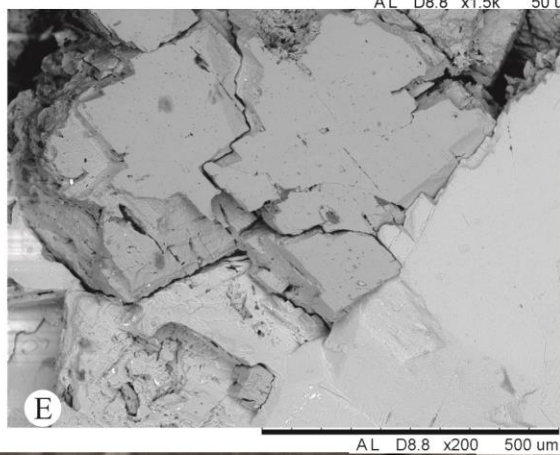
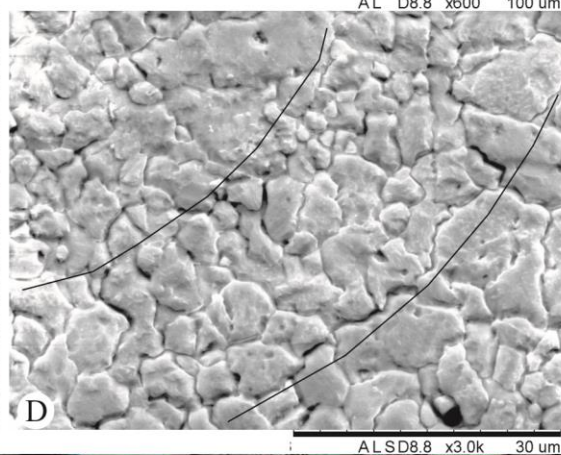
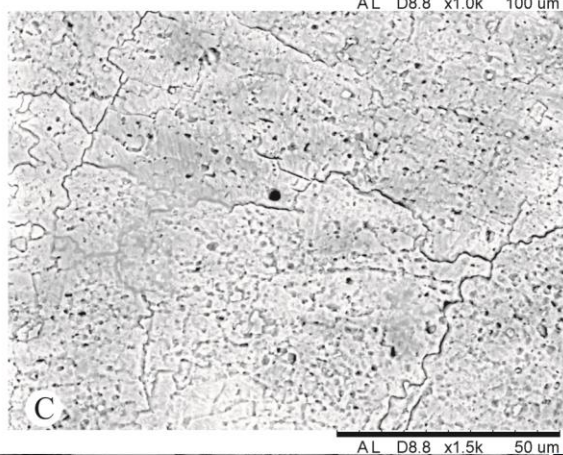
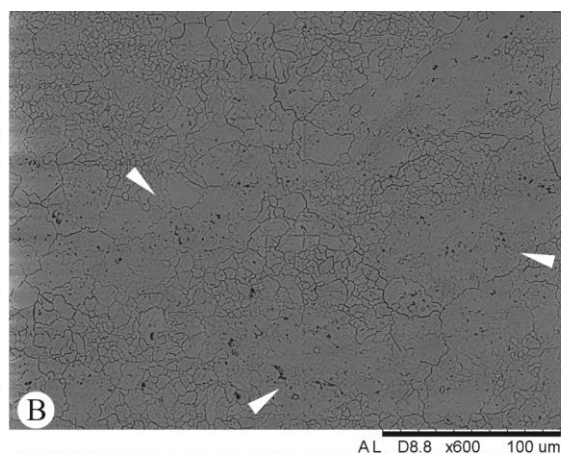
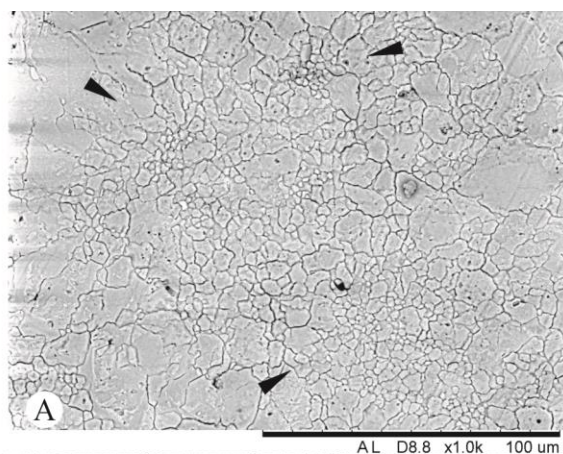


FIGURE - 5.15

A. This image shows a common texture observed within the mounds studied. Small clumps of micrite can be seen often surrounded by radial microspar crystals (arrows), spar crystals are occasionally found between these structures that somewhat resemble the head of a flower. These structures are thought to be what are responsible for clotted and peloidal textures observed under the microscope. The majority of crystals seen here show some pitting, The larger spar crystals generally have pitting restricted to the extremities of the crystal.

B. In this image some large pits can be observed within microspar and spar crystals. The pits are generally less than 3 μm in size but are often elongated along one axis. The pitted material is often confined to the microspars.

C. Heavily pitted spars, the pits are well developed, often rounded and no larger than 3 μm . In this sample several micro-fractures can be observed, they appear to have two perpendicular orientations.

D. Small spar crystals (15-30 μm) can be seen to form part of a wall structure surrounded by larger spar crystals (lines mark wall edges). The crystals show some evidence for pitted surfaces though the pits are not as well developed as in other samples. This is an example of extended neomorphism, where the original wall structure has been overgrown, the few, poorly developed pits may indicate more neomorphism has occurred within this sample than that observed for the Candemuela Mound. The relative lack of bioclasts found may also be an indication of prolonged neomorphism.

E. and F. This back scatter image and element map show the relationship between a well-developed dolomite rhomb (light green) and the surrounding calcium carbonate.

G. and H. This image and element map show several microspars with some clay flakes (white arrows) and a dolomite rhomb (black arrow).

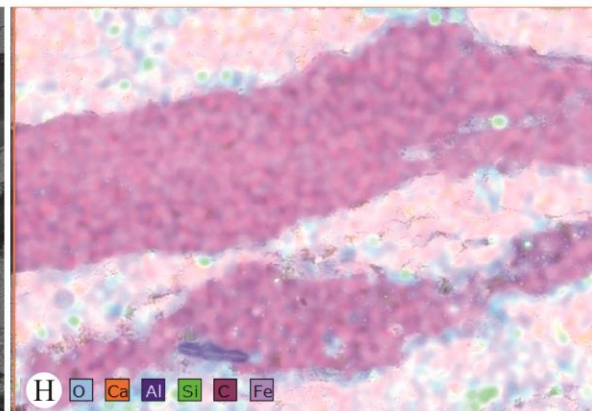
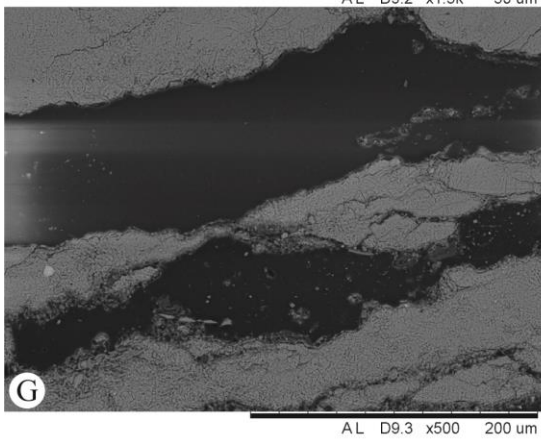
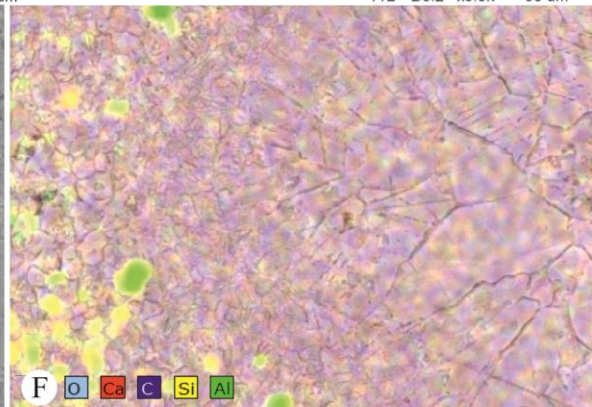
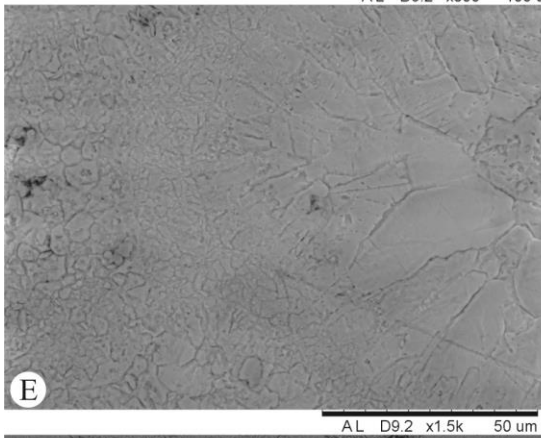
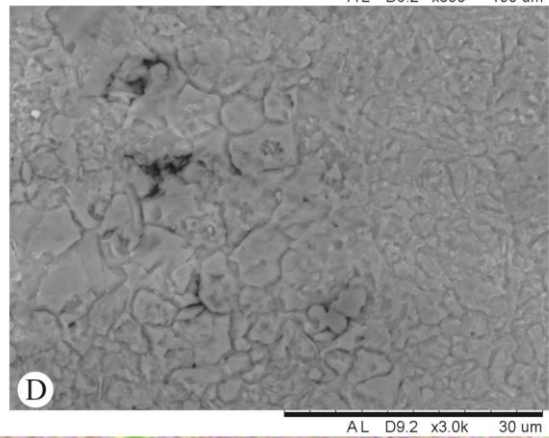
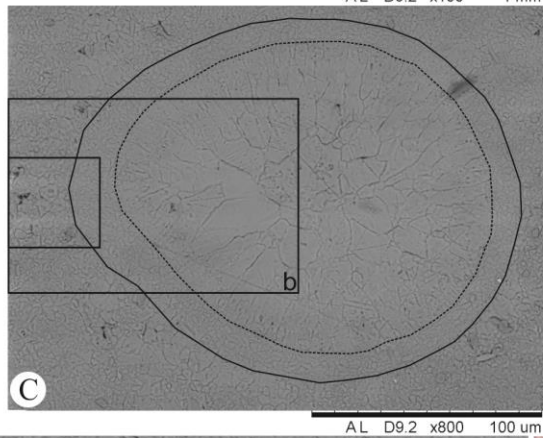
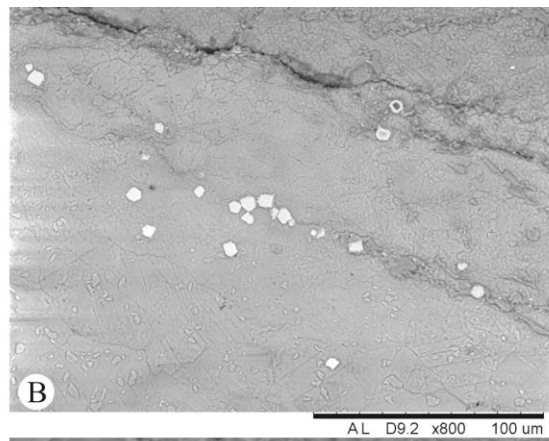
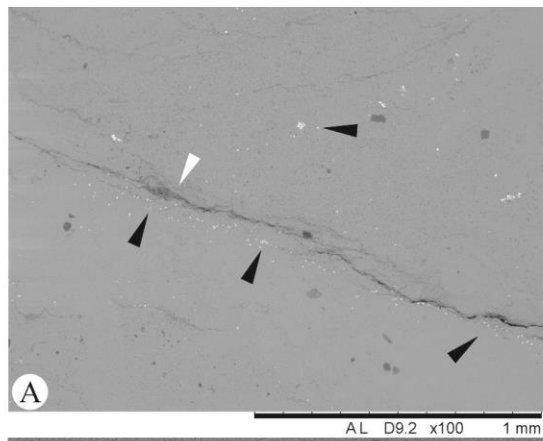


FIGURE - 5.16

A. A stylolite along which cubic pyrite appears to have formed (black arrows). Some stylolite can be observed along the length of the pressure dissolution seam (white arrow).

B. A closer image of the cubic pyrite as well as the crystal textures observed in this sample. Here, mostly pitted spars are observable.

C. A Tubertinidae within pitted microspars. In this image larger, smooth spars can be seen inside the wall formed cavity of the organism. The wall has well-defined edges, the outer surface is highlighted by the solid line, whilst the inner surface is highlighted by the dashed line.

D. A close-up of the square area (a) from C. Here the wall material can be clearly seen to be different from that of the surrounding material. The wall consists of smooth, equigranular micrite whereas the surrounding material is of pitted microspars. Several deep pits are observable toward the left of the image.

E. and F. A close-up of area b as highlighted in C. This element map shows that the bioclast wall structure and internal cavity contains no clastic fragments.

G. and H. In hand and under a microscope evidence for pyrobitumen within the Pinos East mound is present. A fracture which is filled with a carbonaceous material can be observed. The fractures also have a concentration of clastic material on their edges, which may be a result of migrating fluids.

5.3 Framboidal Pyrite

Framboidal pyrite are minute raspberry-shaped spherical aggregates, 2-50 μm in diameter, composed of assemblages of tiny crystallites of 0.5-2 μm (Folk, 2005). Average diameter measurements of framboidal pyrite can be used to indicate the euxinic and dysoxic and oxic state of the water column in which they precipitated (Wilkin *et al.* 1996). Framboids formed in sulphidic water columns tend to be smaller and less variable in size than those of framboids formed within sediments below an oxic water column. Pyrite was observed both in a framboidal (Fig. 5.17) and cubic form, the former being by far the most common. Framboids were observed as clusters within several samples from San Emiliano valley mounds. Framboids were rare, usually absent, from sediments of the Bernesga valley mounds and the Pinos Hairpin Limestone. Cubic pyrite was more commonly observed within samples where framboids were either extremely rare, or totally absent. The occurrence of abundant framboids is often observed within deep marine sediments, particularly mudstones (Wilkin *et al.*, 1996, 1997, Wignall and Newton, 1998, Wignall *et al.*, 2005, Bond and Wignall, 2010 & Liao *et al.*, 2010). Within shallow water sediments framboids have been observed as a result of the upwelling of anoxic waters during the Permo-Triassic mass extinction (Liao *et al.*, 2010). Pyrite has also been observed to form in anoxic sediments beneath the cover of microbial mats whilst the waters above remain oxygenated (Cavalazzi *et al.*, 2007).

Samples containing a higher clastic component were found to host the greatest number of pyrite framboids within the studied material. The majority of samples contained zero, to just a few framboids and were excluded from the framboids count. The use of “Box and Whisker” plots is suggested by Wignall and Newton (1998) to be a useful way to display changes in framboids size through sedimentary sections. Nevertheless, due to the small number of samples containing framboids (not representing full successions through sedimentary strata) the results here, are displayed using the scheme of Wignall *et al.* (2005). Framboids were found to have an average diameter of around 5 μm (Fig. 18) for the majority of samples (sample CAN 1 had an average of 3.54 μm). The range of size for framboids was from 2.66 to 17.29 μm . The small size of the

average pyrite framboid suggests that they were formed in an anoxic environment, however, the total number of framboids would be expected to be much higher if anoxia was pervasive throughout the environment (Wilkin *et al.*, 1997). It is interpreted that these framboids, found in isolated clusters, formed in anoxic conditions beneath microbial and algal accumulations within the sediment. These accumulations are envisaged to have been formed by laminar buildups of the genera *Claracrusta*, *Rothpletzella*, *Girvanella* and *Donezella* (see Chapter 6 Palaeontology). The water column above would have been fully oxygenated. The mounds of the Bernesga valley were observed to have few framboids, this suggests that a fully oxygenated environment was present (Bond and Wignall, 2010). This is likely to be the result of a lower number of encrusting, sheet-like, forms and the bioturbation of the sediments by worms (Samankassou, 2001).

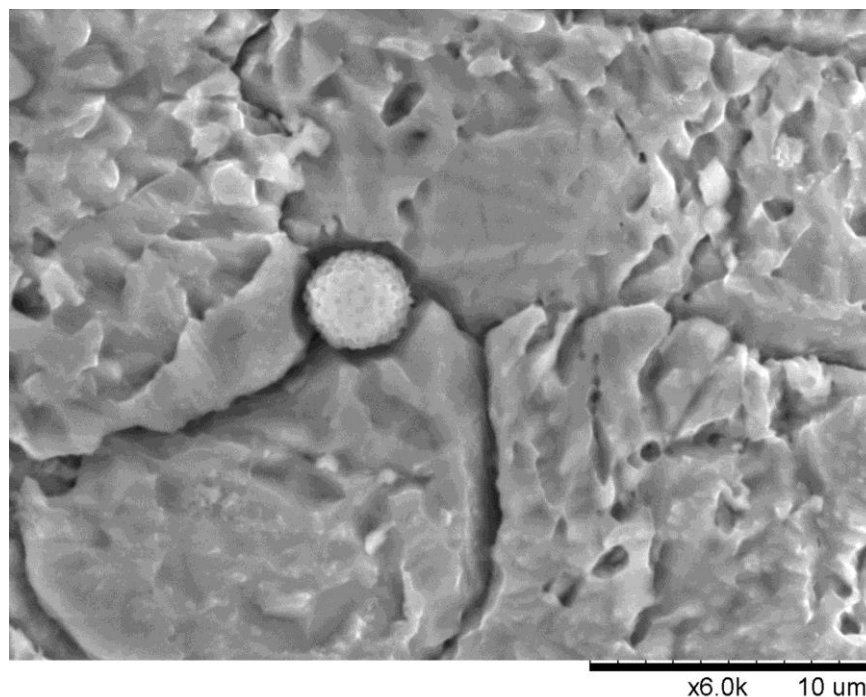


FIGURE - 5.17 An example of framboidal pyrite, here observed between several pitted microspar crystals. This framboid resembles those associated with nannobacterial origin, as discussed by Folk (2005).

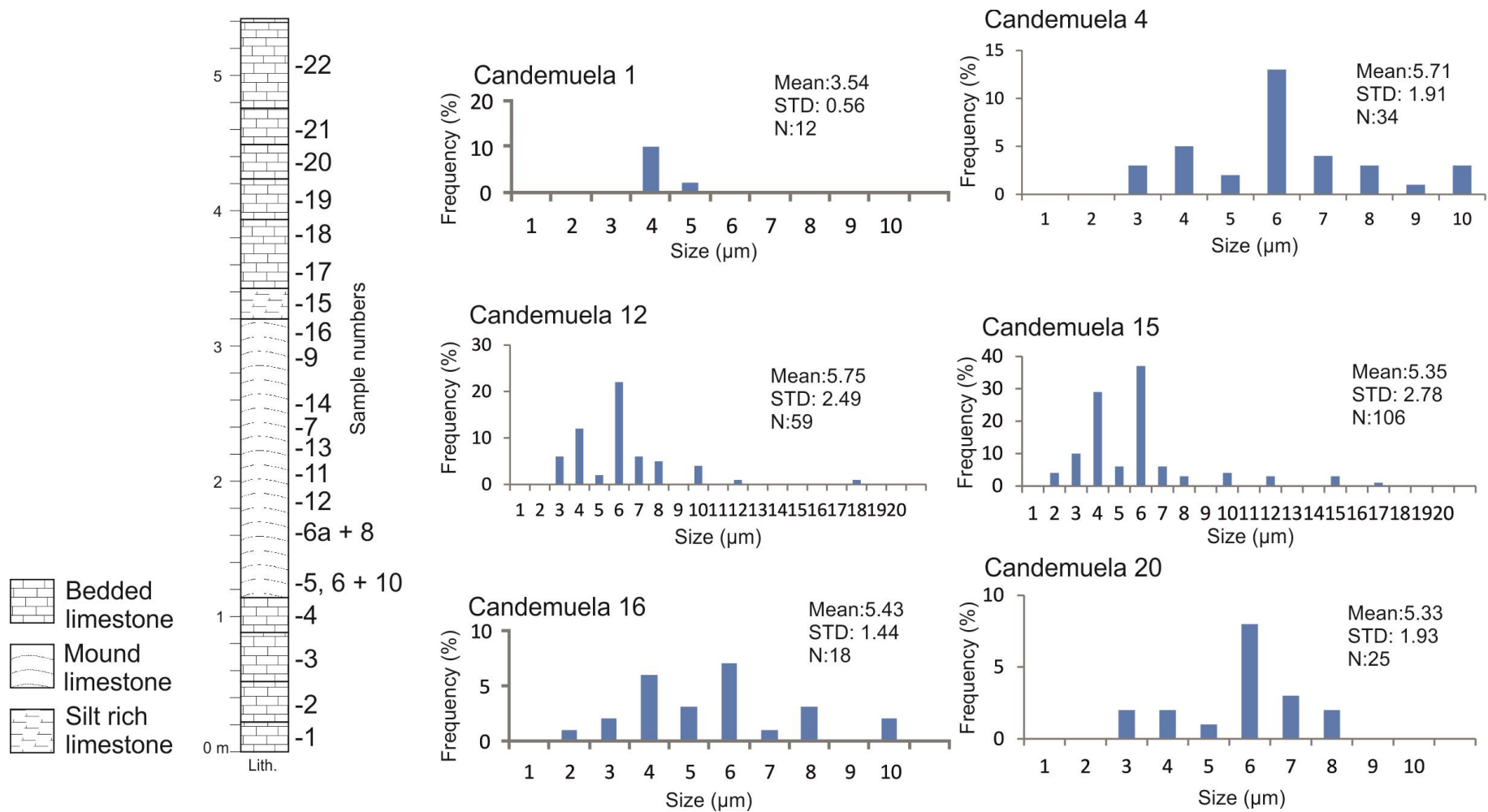


FIGURE - 5.18 A set of size frequency graphs for the samples with measured pyrite framboids. The litho-strat column is a schematic through the Candemuela mound, indicating where the samples are from in the succession. Mean = mean average, STD = standard deviation and N = total framboids observed from the sample.

5.4 Chapter Summary

The Candemuela Mound provided a case study for the area (due to its excellent exposure) and was the main focus of the ultrafacies analysis. The dominant textures observed within the ultrafacies analysis were generally constant throughout the sampled material. Micrite, microspar and spar crystals with subordinate dolomites and clastics were observed. Pits, which in many cases resembled a needle-like shape, were a commonly observable feature on microspar and spar surfaces. This pitting, along with the abundance of microspars and rare aragonitic relics indicates (though not conclusively) an Aragonite-Dominated Precursor for the carbonates of the San Emiliano and Lois-Cigüera Formations. Carbonate muds would have been formed from a mesh of aragonitic needles, derived either from the breakdown of aragonitic algal bodies or from chemical precipitation of carbonate. The presence of an aragonitic dominated carbonate population fits well with the predicted aragonite seas of the Pennsylvanian (Lowenstein *et al.*, 2001). The weight percentage of carbonate in Pennsylvanian ocean waters must have been far higher than those of today. Framboidal pyrite is commonly found within areas with relatively high clastic components. The framboids measured indicate that they formed in isolated anoxic sediments below a water column that was oxic. The isolated anoxic areas forming beneath microbial and algal accumulations.

6. Palaeontology

A major constituent of, and control upon, the formation of the San Emiliano and Lois-Cigüera Formation carbonates are various organisms. These organisms can be directly responsible for the precipitation of carbonate or may act as a baffler or binder of transported material (Tucker and Wright, 1990, Flügel, 2004). Ecological niches are filled by biota which are specifically suited to them, therefore different assemblages of biota can shed light on environmental and depositional conditions including photic levels, sea level, temperature, salinity, wave activity and more (e.g. Bosence and Allison, 1995; Fürsich, 1995; Brett and Baird, 1997 & Fischer and Wefer, 1999).

This chapter presents a description, review and interpretation of the biota observed from microscopy and SEM investigations. Biota which are found within both the mound facies and surrounding (basal/capping) facies are described here. The likely role which important biota has been interpreted to play in the formation of the studied carbonates is also considered. Comparisons with other occurrences of biota are considered for many important fossils which are thought to play a role in the formation of the carbonates within the study area. The chapter is separated into sections indicating the most important biota types (e.g. Algae, Cyanobacteria); within these sections important genera and species are covered along with broader classifications for less important or rare biota. The majority of fauna found within this study are not thought to play a direct role in mound formation, or are so rare that a systematic taxonomic review of each would not be prudent. Therefore only the systematics of those fauna which are new, or are abundant enough to provide new information, is supplied toward the end of this chapter.

Abbreviations used in text: CAN (Candemuela Mound), CSM (Cármenes South Mound), PEM (Pinos East Mound), PHL (Pinos Hairpin Limestone), PPM (Pinos Pylon Mound), SDL (Sena de Luna Mound), SMM (San Martín Mound), UNT (Unit 8 Limestone).

6.1 Algae

Algae are important contributors to modern carbonate reefs and platforms and it is inferred that they have played this important role since the Palaeozoic (Wray, 1977). The algae from the San Emiliano and Lois-Cigüera Formations are dominated by Donezelloids (within this study Donezelloids refers to: *Donezella*, *Beresella* and *Dvinella*) and ‘phylloid’ algae (e.g. *Archaeolithophyllum*). Also observed are several dasycladales and ancestral coralline red algae (‘true’ coralline red algae are found from the Jurassic age onwards (Basson and Edgell, 1971), ancestral coralline red algae share similar features and are believed to have been the evolutionary fore-runners of the algal family (Aguirre *et al.*, 2010)). Within the samples observed Donezelloids are mostly confined to the mound and intermound facies whereas ‘phylloid’ algae are found in association with marly carbonates in cyclic beds and some basal mound facies. Preservation ranges from broken and completely recrystallized to well-preserved specimens with wall and internal cell structures still present. The described algae are all thought to have been photosynthetic and so, light dependent (indicating a habitat within the photic zone), the abundance of algae indicates a warm water temperature (Mamet and Villa, 2004). Rácz (1964) provides an excellent review of the algae from the San Emiliano and Lois-Cigüera Formations whilst various authors have subsequently investigated algal bearing carbonates from the Cantabrian Mountains (e.g. Bowman, 1979; Hensen, *et al.*, 1995; Della Porta *et al.*, 2002; Choh and Kirkland, 2006 & Corrochano *et al.*, 2012). Mamet and Villa (2004) provide a useful review of the shallow water, Pennsylvanian red and green algae of the Cantabrian zone. The microflora described in this study are typical of the western Palaeo-Tethys Ocean (Fig. 1.3) carbonates of Carboniferous age. The most important algae that contribute to Carboniferous, western Palaeo-Tethyan carbonates are: [1] *Archaeolithophyllum*, *Kasimophyllum* and *Archaeolithoporella* (encrusting red algae), [2] Bereselloids (*Beresella*, *Dvinella*) (green algae), [3] *Donezella* (see below for a discussion on taxonomic status), [4] *Komia-Ungdarella* (red algae), [5] *Petschoria* (red algae), [6] ‘Phylloid’ algae (*Eugonophyllum*, *Ivanovia*, *Neoanchicodium*), [7] *Tubiphytes*, [8] *Uraloporella* (green algae) (Mamet and Villa, 2004, and references therein). Of the flora listed the latter two groups,

“[7] *Tubiphytes*” are extremely rare, and “[8] *Uraloporella*” are absent in the current study indicating that the carbonates observed were above the dysphotic zone (Madi *et al.*, 1996).

Note that within this study *Claracrusta* and *Wetheradella* are grouped under the heading of algae and are considered algae *incertae sedis*.

6.1.1 *Donezella*

Donezella was first described by Maslov (1929) and is one of the most prominent biotas found within the samples examined in this study. *Donezella* consists of branching, cylindrical tubes with a distinct wall structure; an outer clear calcite wall (possibly formed from a mucilage sheath) and a darker, thinner, perforate, inner micritic wall. At regular intervals the thicker inner wall can be observed to grow inwards, perpendicular to the thalli surface forming segmentations, at these intersections a constriction of the tubes can occur causing the tube to appear barrel like (Fig. 6.1). Several examples show evidence of further segmentation by thinner walls. Tubes range from 70 to 160 μm in diameter (Rich, 1967) and branch at an angle of 45 to 90° (Groves, 1983). *Donezella* was cosmopolitan within the northern hemisphere during the Carboniferous and is a common western Palaeo-Tethyan flora; it was rare from late Viséan to Serpukhovian times, very abundant during Bashkirian to Moscovian times before once again becoming rare during the late Carboniferous and early Permian (Mamet, 1991 & 1992). *Donezella* accumulations are often interpreted to have grown within a warm, shallow (low to moderate energy, below fair-weather wave base) environment but have been shown to thrive over a range of water depths up to 200 m (Della Porta *et al.*, 2002; Choh and Kirkland, 2006 & Corrochano *et al.*, 2012). Environmental conditions from quiet to quite agitated have been interpreted (Rácz, 1964 and Bowman, 1979). *Donezella* colonies have been found to form in a range of environments ranging from platform interiors to deep-slopes (Della Porta *et al.*, 2002). This cosmopolitan habit and ability of *Donezella* to occupy a variety of environments, quickly establishing itself and growing to maturity suggest that *Donezella* may be an example of the “opportunistic” species of Connell and Slatyer (1977). The affinity of *Donezella* is problematic (Riding, 1979) and its systematic position has been somewhat

controversial. *Donezella* has been assigned to various different taxonomic groups. Maslov (1929) originally assigned *Donezella* to the red algae (Johnson, 1963), however, in successive subsequent studies *Donezella* has been considered to be: green (Codiaceae) alga (Rácz, 1964), alga *incertae sedis* (Rich, 1967), Foraminifera (Riding, 1979), calcareous sponges (Termier *et al.*, 1977), microproblematica (Riding, 1979 & Chuvashov and Riding, 1984), green (Paleosiphonocladales) algae (Shuysky, 1985 & Ivanova, 1999), green algae of *incertae familiae* (Groves, 1986), green (Dasycladales) algae (Deloffre, 1988) and pseudo-algae (Vachard *et al.*, 1989). Recent work regarding *Donezella* refers to the genus as green (Chlorophycophyta) algae (Mamet and Villa, 2004), algae *incertae sedis* (Mamet and Zhu, 2005), algaospongia (Vachard and Cózar, 2010) or more commonly, microproblematica (Samankassou, 2001; Della Porta *et al.*, 2002; Choh and Kirkland 2006 & Corrochano *et al.*, 2012). The reason *Donezella* has caused so much controversy over its taxonomic position is because there is no categorical morphological evidence that it belongs to any particular taxa. The environmental range which it is found in and the general morphology tends to suggest that if it is indeed an algae then it would most likely be a member of the Rhodophyta as opposed to the Chlorophyta. *Donezella* has been interpreted to have behave as a baffler, binder and constructor (Eichmüller, 1985; Hensen *et al.*, 1995 and Choh and Kirkland, 2006) in respect to the ‘guild’ concept (constructor, baffler and binder) of Fagerstrom (1988, 1991) and is known to form oncoids (Chuvashov and Riding, 1984) and build bioherms and carbonate mud mounds (see Table 1. in Della Porta *et al.*, 2002 and Table 1. in Choh and Kirkland, 2006).

Within this study *Donezella* is observed as either whole, bush or shrub like colonies often up to several centimetres in diameter, as sheet like encrustations of entwined thalli which appear to encrust the subjacent surface or as broken thalli which have been reworked. Thalli are found to range from 50 to 275 µm in diameter with an average diameter of 140 µm. *Donezella* is generally observed within the mound and basal facies of the observed mounds. Where *Donezella* is found *in situ* (as either a shrub like growth or as an encrusting sheet) it is always the dominant biota with very few other biotas found in association. Evidence for bio-cementation between the thalli

exists in the form of a thin sheath like layer of clear calcite. The bush like growths of *Donezella* occasionally show a very ordered branching which appears to form a cubic pattern (Fig 6.1). Examples of some of the rare biota found with *Donezella* includes other algae - *Beresella*, *Dvinella*, *Komia* and *Ungdarella*, several Foraminifera including attached *Tetrataxis*, as well as both attached and free floating forms of *Tuberitina*. Possibly the most important biotas found commonly to be in association with *Donezella* were calcimicrobial encrusters, including *Rothpletzella*, *Girvanella* and (the algae) *Claracrusta*. These biota are often found forming encrustations between individual thalli or as sheet like bodies on top of *Donezella* growths. Sediments associated with *Donezella* range from homogenous to clotted and peloidal micrites baffled between entwined and branching *in situ* growths, and from clotted to peloidal micrites when in association with broken thalli. Cavities are often found in association with framework forming growths of *Donezella*, the cavities are irregular, fenestral and are filled with a clear spar cement, the geometry of the cavities appears directly related to the position of *Donezella* thalli. The cavities observed appear much like the ‘constructed cavities’ described by Choh and Kirkland (2006) and, similar to the cavities described there, these are also filled by dark micrite coatings, fine-grained internal sediments, peloidal micrite and calcite cement and are rarely the subject of selective dolomitisation. The isopachous fringes described by Samankassou (2001) are not observed in association with *Donezella* related constructed cavities and are confined to cavities associated with peloidal micrite. There are two commonly occurring species of *Donezella* recognisable in this study, and a rarer, third new morphotype described in this study. *Donezellasp.* 1 is larger than the other two species observed and has thicker walls with a more bulbous appearance. The two common species are the type species, *Donezella lutugini* Maslov and *Donezella lunaensis* Rácz. The characteristic differences are described below in section 6.6 *Systematic Palaeontology*. It should be noted that recrystallization often means identification is difficult if not impossible. The occurrence of *Donezella* in the studied samples indicates that it played a direct role in the formation of the carbonates of the San Emiliano Formation, it is observed to both baffle and bind (in association with several encrusting organisms, specifically *Claracrusta*, *Rothpletzella* and *Girvanella*) and at a millimetre scale may be considered to be a

constructor. In association with microscopic encrusters, *Donezella* was a successful baffler, binder and constructor so in regards to mound formation, *Donezella* must be considered as an integral component and directly linked to the nucleation, growth and success of carbonate mud mound formation within the San Emiliano Formation. *Donezella* is commonly found in all but the Sena de Luna Mound, where it is rare. Within the carbonates peloids often resemble reworked, abraded and micritised *Donezella* thalli, it is proposed that a component of the micrite of which the mounds are composed of originated from algal thalli.

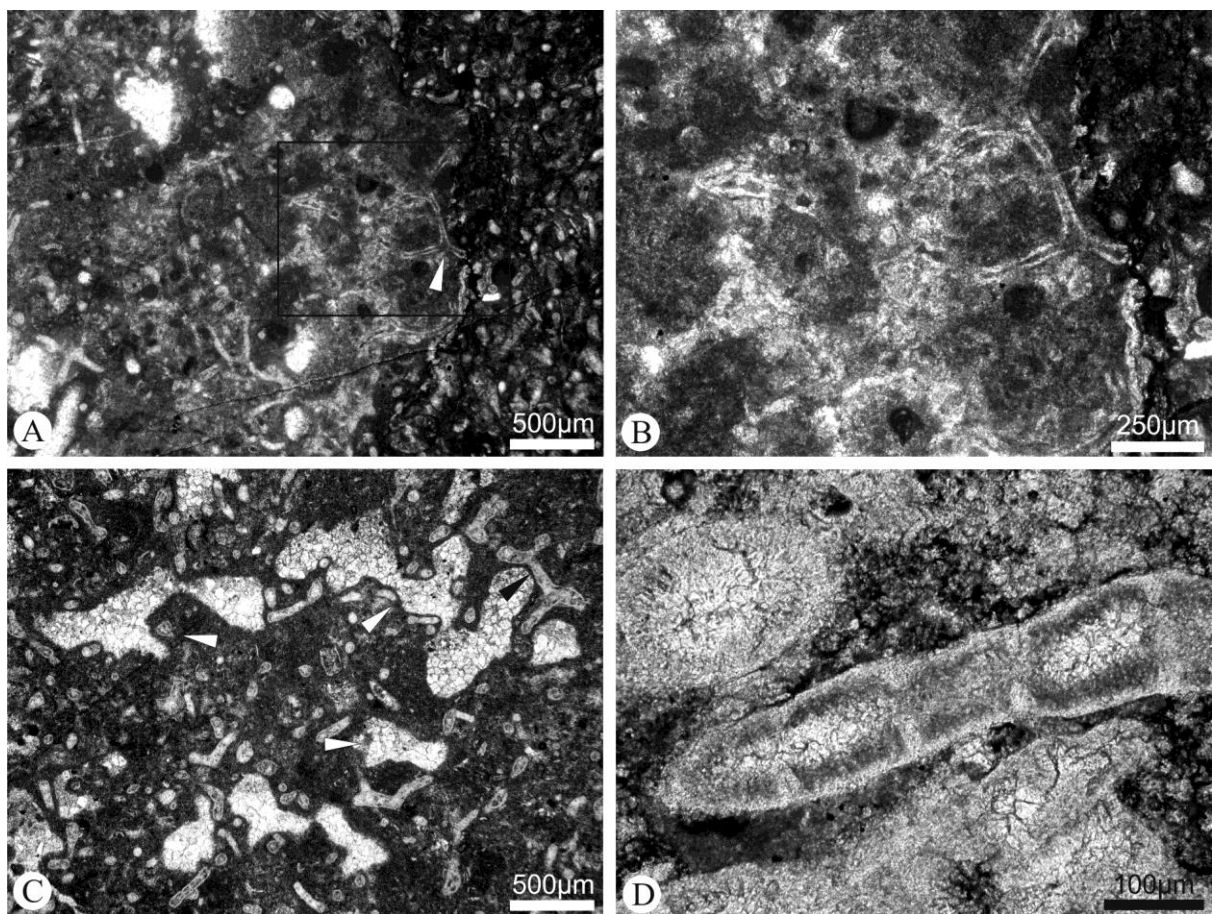


FIGURE - 6.1 When found in growth position *Donezella* often exhibits a cubic growth pattern. A, (CAN18) in this photomicrograph branching *Donezella* can be seen forming a baffling network in a cubic like pattern (arrow), the baffled sediment consists of homogenous to clotted micrite. B (CAN18) shows a zoomed in image of the area highlighted in A, the cubic branching of the *Donezella* is conspicuous. C, (CAN6a) this image is of an example of branching *Donezella* (black arrow) forming constructed cavities (white arrows). D, (CAN2) an example of a longitudinal (centre) and traverse section (top left) through a *Donezella* thalli, the wall and “barrel” like structures can be seen.

6.1.2.1 *Donezella* Ultrastructure

The skeletal ultrastructure of *Donezella* was analysed by means of SEM and EDX analytical system (see 3. *Methods and Materials* chapter). The wall structure of *Donezella* has been well preserved in several specimens found within the study with a distinctive ultrastructure observable. The wall consists of calcite and the ultrastructure was apparent in several specimens. The ultrastructure consists of fine laminae of alternating dark and light carbonate material which run parallel with the orientation of the wall. The laminae consist of <1 µm thick layers, partitioned by perpendicular rows of pits. The lighter carbonate layers, when compared against the darker laminae, have relatively higher C and Mg concentrations (Fig. 6.2). It may therefore be interpreted that these laminae are the result of varying C and Mg concentrations, which could possibly be linked to fluctuating water temperatures (Flajs, 1977). These laminations are cross-cut by lineaments of pits. The laminar features observed are reminiscent of the wall ultrastructure described for coralline algae in the work of Flajs (1977). A layer which would equate to the organic layer plus a primary and several secondary wall layers can be interpreted. The pitted lines which form perpendicular to the laminae show some similarities to the stacked ‘tubes’ of cells found within the solenoporacean algae. The overall morphology and wall ultrastructure suggest an algal affinity. Although the wall structure is reminiscent of the coralline alga *Donezella* was present far too early in geological history to be true coralline algae. *Donezella* is interpreted here to belong to algae *incertae sedis*, with it most likely being an ancestral red algae.

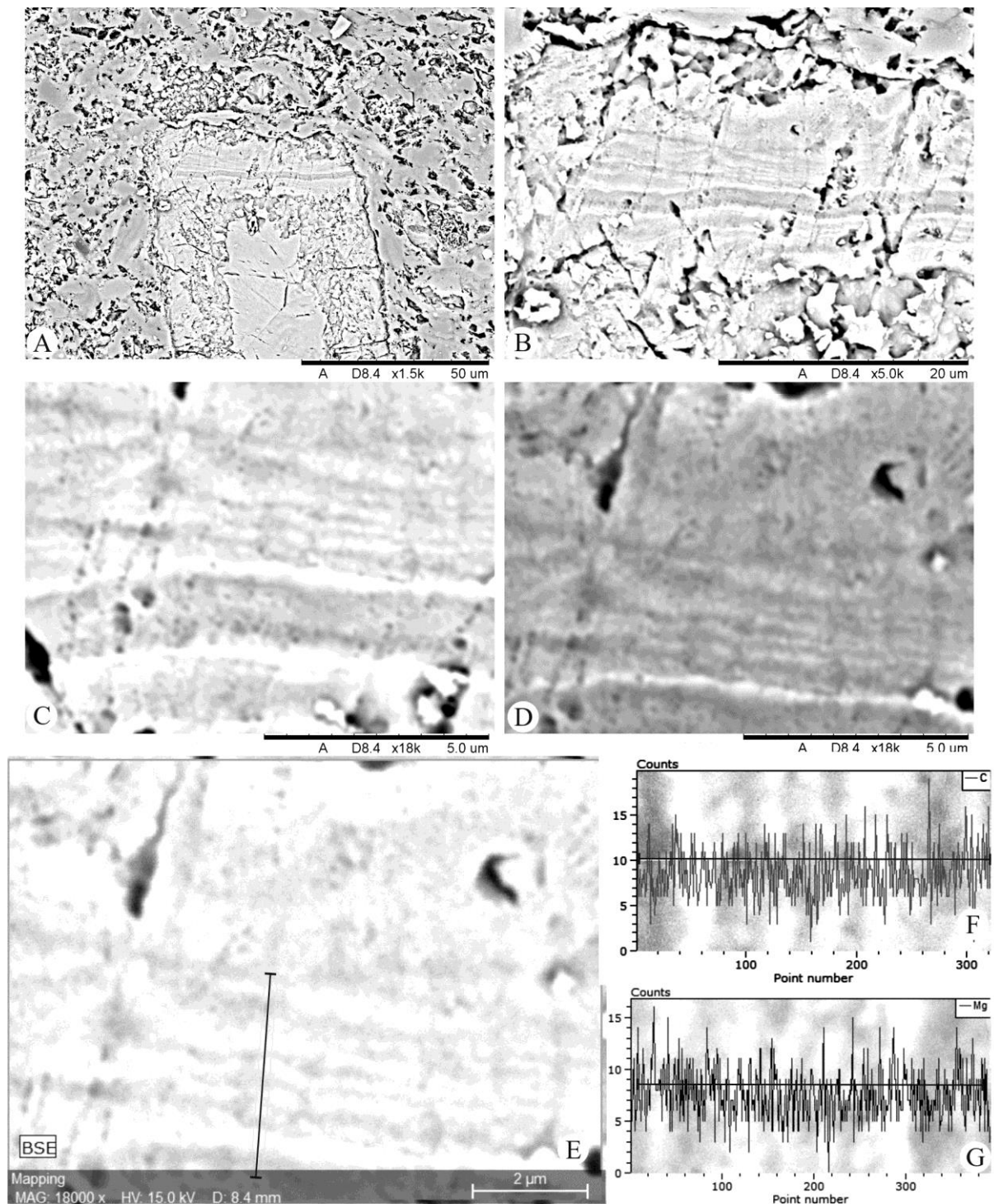


FIGURE - 6.2 A photo plate showing the enigmatic wall structure of *Donezella*. Specimen is from the Pinos Hairpin Limestones.

A. A segment of *Donezella* can be observed with the wall and central cavity both visible.

B. A close up of the partition seen in A., here laminae parallel to the wall surface can be seen, as can numerous pitted lineaments which run perpendicular to the laminations.

C. A further close up of the section seen in B., the laminae, which in the back scatter image consist of consecutive layers of lighter and darker material, can be seen to be partitioned by the

perpendicular rows of pits. The larger lamination is interpreted to be the primary wall structure with the thin laminations propagating from it.

D. Detail of the thin laminae and the pitted lineaments are shown. The thin laminae appear to be formed of “chains” of sausage shaped segments, partitioned by the pitted lines. The pits which form the lines appear to be relatively regular in size (0.1 μm) and are rounded.

E. F. and G. These three images are taken using EDX software. E. is a backscatter image of an area on which an element map was made. The black line on the image represents the line through which the linescans in F. and G. were taken. F. a linescan showing the concentration of C through the laminations, it appears that the C concentration is lower in the lighter (white) laminae when compared to the darker (grey) laminations. G. shows concentrations of Mg along the linescan, an increased concentration of Mg can potentially be seen within the lighter laminations.

6.1.2 *Beresella*

Beresella is found in association with *Donezella* forming bafflestones, it is also observed to form constructed cavities in places. Within the study beresellids are restricted to the Candemuela Mound, although recrystallised fragments which are probably *Beresella* are present within other mounds. Beresellids have an unbranching, cylindrical thallus which tapers toward the end. The thallus of beresellids found in this study were up to several millimetres in length and ranged from 200 to 325 μm wide, so on average, larger than *Donezella*. A distinction is easily made between the porous wall and an inner section. The inner portion is filled with clear, calcite cement. The wall consists of a thicker micrite wall which is punctuated by small pores and a thinner, outer, clear calcite wall. The pores form perpendicular to the long axis of the thallus and are often teardrop-shaped, the thicker part of the pore is located on the outer side of the wall (Fig. 6.3). The pores are arranged in a spiral configuration throughout the thallus. Mamet and Villa (2004) report a specimen that has a diameter of 500 μm with pores that range from 70 to 200 μm long. *Beresella* are known to have formed bafflestones throughout the Bashkirian and Moscovian and are considered typical Western Palaeo-Tethyan flora (Mamet, 1992). Unlike the similar *Donezella*, which has a controversial taxonomic position, beresellids are considered to be green algae. *Beresella* and *Donezella* are almost the same other than the primary pores of *Beresella* and the

branching of *Donezella*. The occurrence of *Beresella* is much rarer than that of *Donezella* but is often associated with the same biota and very occasionally it is found to be the dominant biota.

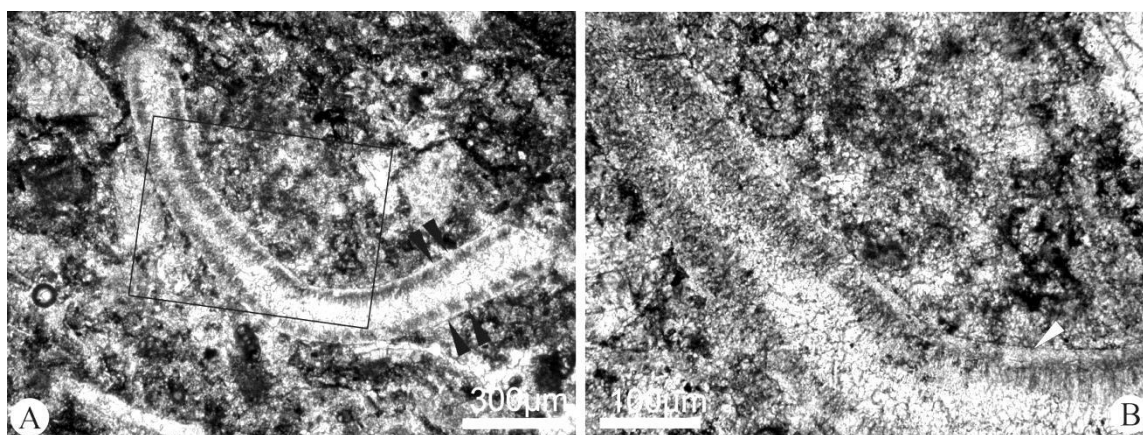


FIGURE - 6.3 Photomicrographs of a *Beresella* thalli. A. (CAN1) shows the entire thalli, including rounded ends. The outer and inner portions can be clearly see, the outer being much darker and perforated whilst the inner portion is clear. Note that the pores of the outer wall do not line up perpendicularly across the thalli, indicating a spiral arrangement (black arrows), the pores can also be seen to exhibit the characteristic teardrop-like shape. B, a close up of the area highlighted in A., here the darker outer wall and clear inner sections can be observed as well as the thin outer calcite wall (white arrow).

6.1.3 *Dvinella*

Dvinella and *Beresella* are almost identical. *Dvinella* consists of a cylindrical, unbranching thallus.

It has a central section which is filled with a clear, calcite cement and has a wall which consists of two elements, the first is an outer calcite wall with regular inward facing ‘teeth’, between these ‘teeth’ sits the second, dark micritic layer. The outer wall layer ranges from 5 to 15 µm whilst the second, inner wall is thicker at 25 to 35 µm, the ‘teeth’ of the outer layer are generally uniformly spaced at around 50 µm apart. The diameter of the cylindrical tubes encountered within this study were around 250 µm, a diameter up to 290 µm was recorded by Rich (1967). *Dvinella* are considered as Beresellids in regards to the western Palaeo-Tethyan flora as described by Mamet (1992) and have a similar stratigraphic range as *Beresella*. When first describing *Dvinella* Khvorova (1949) assigned them to the Dasycladacea, however, as reiterated by Rich (1967) she admitted that the specimens were poorly preserved. Rich (1967) refers to *Dvinella* as *Algae incertae sedis*, stating that until such time that a more thorough analysis is conducted, the taxonomic position of *Dvinella* (and *Beresella*) cannot be established. *Dvinella* is a rare

component of the sample material and occurs as individual thalli (Fig. 6.4), often in association with *Donezella* and related sediments (homogenous, clotted and peloidal micrite). In one case a specimen of *Dvinella* is observed with calcareous, encrusting forms which are reminiscent of the calcified bacteria *Renalcis* (see Fig. 4.4 in *Microfacies* chapter and Fig. 6.4 below).

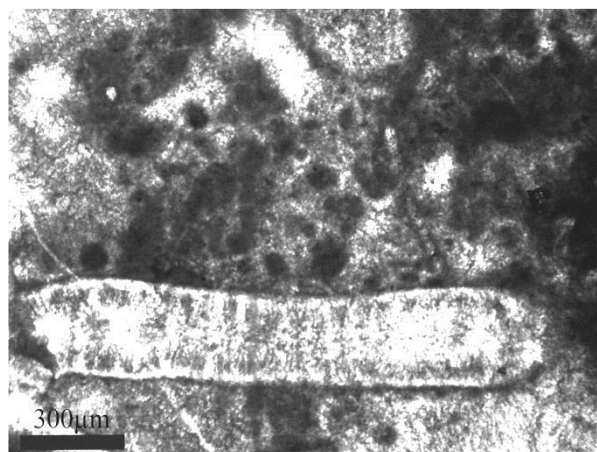


FIGURE - 6.4 A *Dvinella* thalli, the similarities to *Beresella* are clear. The characteristic partitions originating in the outer calcite wall can be seen to separate the second darker wall (CAN7). The thrombolitic peloids and tube-like forms attached to the *Dvinella* specimen are reminiscent of *Renalcis*.

6.1.4 *Komia* and *Ungdarella*

Komia and *Ungdarella* are late Palaeozoic ungdarellacean (problematic red) algae which often reach several millimetres in size (Flügel 2004). These taxa are often referred to as ‘ancestral red algae’ or ‘ancestral coralline algae’ due to their ramified thalli with rows of subquadratic or rectangular cells and hypo- and perithallus structures which are reminiscent of corallinacean algae. The skeletal elements of both are branching and often yellow or honey coloured which is indicative of original aragonitic mineralogy (Flügel 2004). *Komia* and *Ungdarella* are often difficult to distinguish from each other, hence they are grouped under the same heading here. The genera were cosmopolitan and have a stratigraphic range of the early Carboniferous to the Permian, they were abundant in Viséan to Moscovian times and are commonly used in the stratigraphic and environmental subdivision of carbonate ramps and platforms (Flügel, 2004). *Komia* and *Ungdarella* are considered important Palaeo-Tethyan flora (Mamet, 1992). *Komia* is thought to have grown within intermediate energy environments (Mamet and Villa, 2004).

Both types of ungdarellacean algae are observed within the mound facies, as well as outside of the mound facies (Fig. 6.5). Where they are found it is often in association with a relatively diverse biotic assemblage, associated biotas include *Archaeolithophyllum*, *Petschoria*, *Donezella*, various calcimicrobial encrusters as well as bryozoans and foraminifera. Both of these algae are commonly found as transported clasts, often in association with abraded and coated bioclasts which show evidence of transportation. *Komia* and *Ungdarella* are interpreted to have thrived in a more open environment than that of the *Donezella* dominated one, they are most likely to represent slightly deeper environment which is more open (hence the association with a more diverse biological assemblage and the occurrence of mobile/free floating foraminifera). *Komia* and *Ungdarella* are not in a high enough abundance to play a major role in the formation of the carbonates but do provide an indicator for when the depositional environment becomes more open and less restricted.

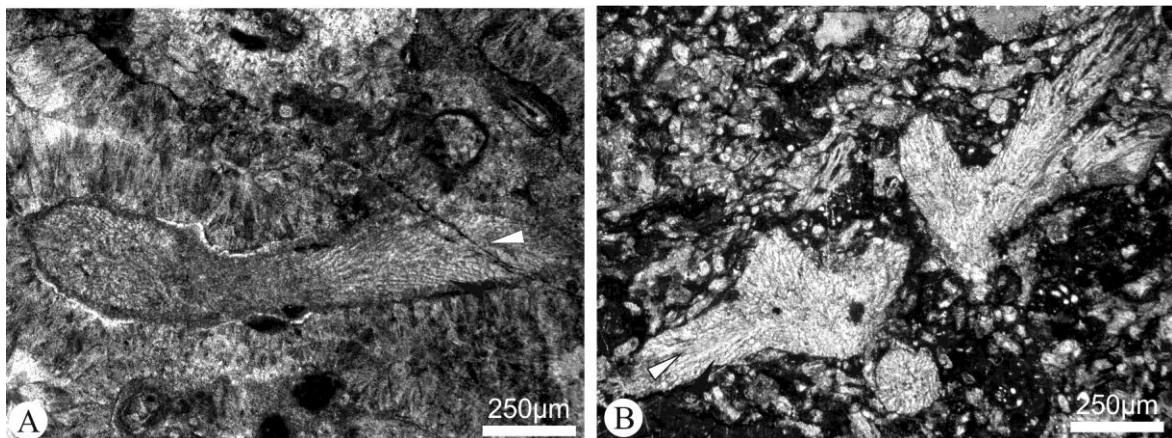


FIGURE - 6.5 Two photomicrographs of ungdarellacean algae. Sub-quadratic cells of the hypo- and perithallus can be observed in A (PEM11) and B (black and white arrows.) In B (PHL7) the characteristic branching behaviour can be seen. Preservation of bioclasts of this size was typical where ungdarellaceans were found.

6.1.5 *Claracrusta*

Specimens of *Claracrusta* are observed as laminar rows of irregular, often bean and ovoid to sub-quadratic shaped cells which have a honey or yellow coloured calcite wall. The wall cells are partitioned by inward growths of the wall creating segmentation similar to that observed in *Donezella* thalli. This creates the appearance of braid-like or chain-like laminations. The cells

have been referred to as tubular (Cózar, 2005, and elsewhere), but here, appear to be ovoid or sub-quadratic, agreeing with Mamet and Villa (2004). Individual cells have been observed to range from 10 to 110 μm but the average cell size is around 50 μm . Encrustations have the characteristic growth form of a concordant first lamination with subsequent encrusting laminations becoming more and more undulating, the space between laminations is generally filled with homogenous micrite or more rarely encrusting forms. *Claracrusta* appears to be non-selective in what it encrusts, although *Donezella* and *Archaeolithophyllum* appear to be the most commonly encrusted objects. Several examples of entire *Donezella* florets being encrusted have been observed and the preservation level is usually particularly high for these *Donezella* specimens. These florets are generally associated with homogenous micrite and constructed cavities which have been selectively dolomitised. *Claracrusta* in association with *Rothpletzella*, *Girvanella* and to a lesser extent *Wetheredella*, are considered to be important binders and stabilisers of *Donezella* growths and therefore the role they play within the formation of carbonate mounds within the San Emiliano Formation (particularly within the San Emiliano Valley) is very important.

This encruster forms laminations of filaments similar to those of *Rothpletzella* (see 6.2.2 *Rothpletzella* below), the major difference between the genera is that whilst *Rothpletzella* encrustations grow parallel to the substrate. *Claracrusta* encrustations become more and more undulose with each lamination. The taxonomic position of *Claracrusta* is uncertain with various authors assigning the genus as *incertae sedis* - (Mamet and Villa, 2004 & Cózar, 2005) Donezelloidea (Vachard *et al.*, 2001), Algospongia (Krainer *et al.*, 2009 & Rodríguez *et al.*, 2012), problematic algae (Said *et al.*, 2010) and cyanobacteria (Pille *et al.*, 2010). Vachard and Cózar (2010) assigned *Claracrusta* to the Algospongia, along with *Donezella*. *Claracrusta* differs from the cyanobacteria by the type of calcitic wall, which is often yellowish and hyaline, and the presence of a septation (Vachard and Cózar, 2010). The wall structure of *Wetheredella* could also hypothetically put them in this group (Vachard *et al.*, 2001). Within this study *Claracrusta* and *Wetheredella* are grouped with algae. *Rothpletzella* shares many similarities with *Claracrusta* and may also belong within the *incertae sedis* algae. Although appearing as a microscopic encruster in

several carbonate successions, the presence of *Claracrusta* is generally mentioned with no further detailed description or mention that it plays an important role in the formation of the host lithology. Mamet and Villa (2004) describe the stratigraphic range of the genus as possibly Serpukhovian to Early Permian. *Claracrusta* along with several other genera and species are apparently characteristic taxa from the northern border of the Palaeo-Tethys (Pille *et al.*, 2010).

Claracrusta was a relatively common component of the samples observed (Fig. 6.6); only missing from the Bernesga Valleys Sena de Luna and San Martín Mounds. *Claracrusta* is regularly observed in association with *Donezella* in mound facies, along with other microscopic encrusters (*Rothpletzella*, *Girvanella* and *Wetheradella*) and less extensively, with ‘phylloid’ algae (again in combination with other encrusters). The association of *Donezella* and *Claracrusta* in Bashkirian to Moscovian age strata of North Spain has been observed before (Mamet and Villa, 2004).

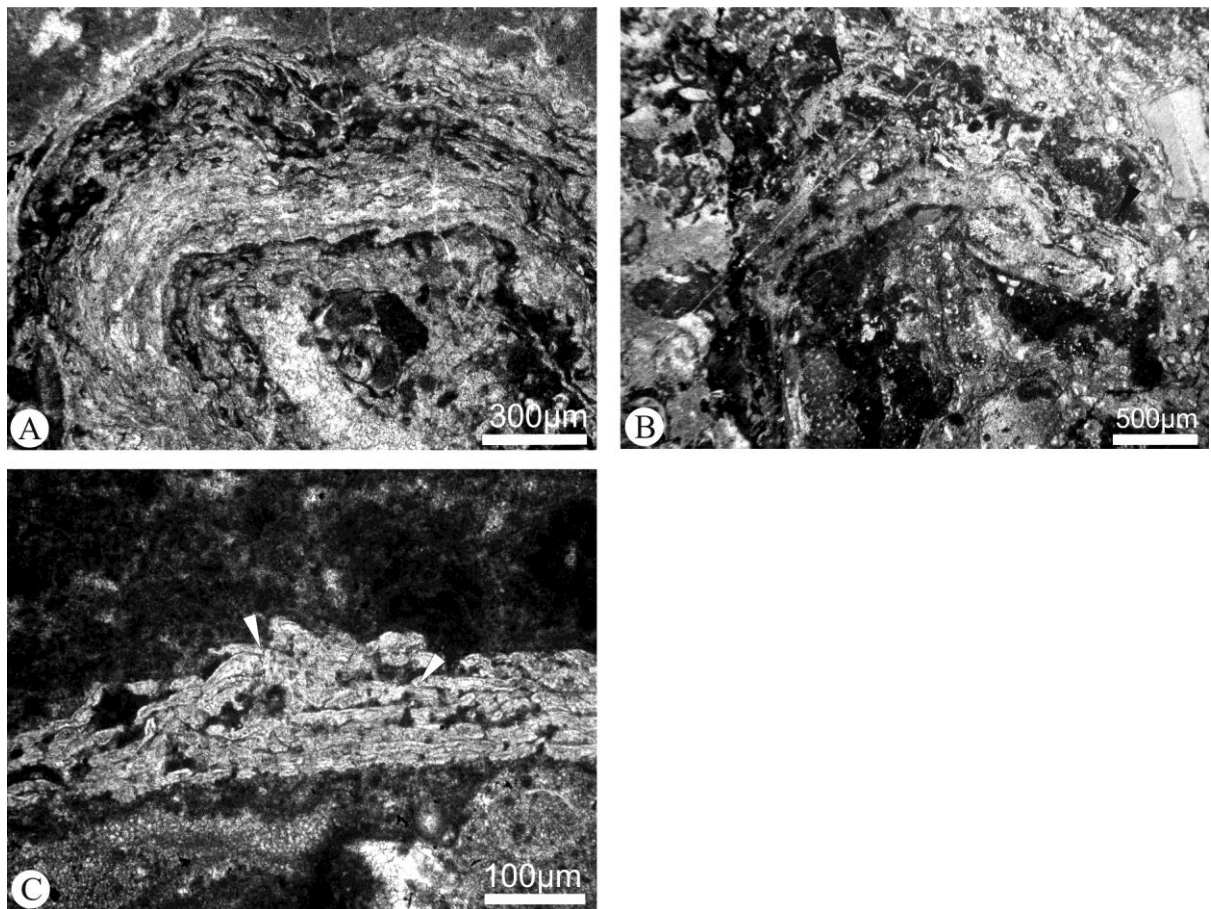


FIGURE - 6.6 *Claracrusta* encrusting various substrates. A. (PHL29), here a relatively thick laminar encrustation of *Claracrusta* can be seen. The layers of *Claracrusta* become successively

more divergent from the substrate, which in this example is a ‘phylloid’ algae thalli. B., (PHL56) here *Claracrusta* can be seen to encrust a variety of objects, apparently in a non-selective manner. C. (PPM14), the individual *Claracrusta* chambers can be seen to be ‘sausage’ or ‘bean’ like ovoid and sub-quadratic in shape. The manner in which successive rows become more divergent from the substrate is observable here (arrows).

6.1.6 *Wetheredella*

Wetheredella is generally referred to as a calcimicrobe, cyanobacteria, foraminifera (Feng *et al.*, 2010) or microproblematicum (Jarochowska and Munnecke, 2014) but is here regarded as algae *incertae sedis* due to the similarities its wall shares with the Moravamminida (Vachard *et al.*, 2001). Interestingly *Wetheredella*-like biostructures have been proposed to represent a possible form of lichen symbiosis (Taylor *et al.*, 1997). The genus is similar to *Claracrusta*, in that it is often mentioned within literature as having been observed but rarely described in any detail. The genus is characterised by microscopic, cystose growths forming thin laminar chains and rows. Individual tubular filaments are often hemispherical or ovoid in shape. The wall is thin and micro-sparitic and is a true exoskeletal element (Vachard *et al.*, 2001). A central cavity is filled by clear, blocky calcite (Fig. 6.7). *Wetheredella* appears to co-occur with *Rothpletzella* regularly (e.g. Flügel, 2004; Adachi *et al.*, 2007 and Feng *et al.*, 2010) the latter being seemingly more abundant in these relationships. Munnecke and Jarochowska (2013) have suggested that a symbiotic relationship may exist between *Wetheredella* and *Rothpletzella* and *Girvanella*. Indeed, within this study *Wetheredella* is found within close vicinity to *Rothpletzella*. The occurrence within this study is rare and where it does occur it is often only a thin row of cystoids within a larger encrustation.

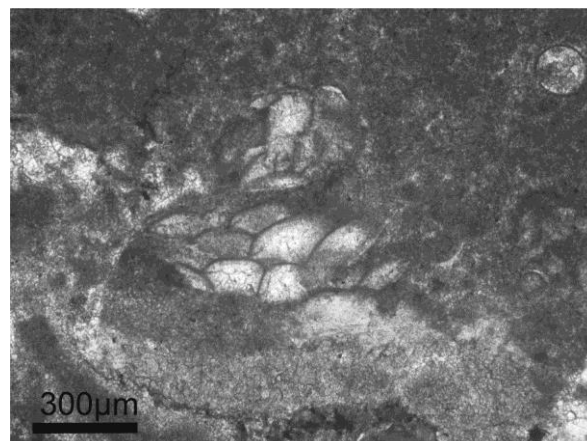


FIGURE - 6.7 (CAN21) A small encrustation of cystoid chambers. In this image *Wetheredella* is observed to occur without an abundance of other encrusting forms; a rare occurrence.

6.1.7 *Archaeolithophyllum*

Both the Pinos Hairpin Limestones and the basal facies of the Pinos Pylon Mound contain abundant specimens of the red (possibly ancestral coralline) algae *Archaeolithophyllum* (often referred to as a ‘phylloid’ algae due to its leaf-like shape). *Archaeolithophyllum* is a common component of algal banks, carbonate mud mounds and bedded carbonate deposits of Carboniferous age lithologies of mid-continent USA (e.g. Wray, 1964, Frost, 1975 - Kansas, Heckel and Cocke 1969 - Kansas and Oklahoma, Wiggins, 1986 - Texas) and of Europe (e.g. Krainer *et al.*, 2003 - Austria, Vachard and Aretz, 2004, Pille and Vachard 2011 - France, Rácz, 1964, Eichmüller, 1985, Samankassou, 2001 - Spain). *Archaeolithophyllum* has a stratigraphic range from the Viséan to Late Permian, it is cosmopolitan (Flügel, 2004) and falls under the encrusting red algae of Mamet’s (1992) Paleao-Thethyan flora. In the majority of reports from midcontinent USA *Archaeolithophyllum* is found as a major mound constructor and encruster, indeed the majority of carbonate mud mounds reported from the upper Carboniferous are termed ‘Phylloid’ mounds due to the dominance of ‘phylloid’ algae, such as *Archaeolithophyllum*. The role of *Archaeolithophyllum* in European examples is often not as a constructor but it is considered as an important encruster which may play a role in stabilising sediments (Mamet and Stemmerick, 2000). *Archaeolithophyllum* consists of undulating, irregularly shaped crusts of various thickness, which grow as isolated individual crusts or as multi-layered, stacked masses (Wray, 1964). The thalli can be separated into an easily recognisable, thick, central hypothallus and a thinner outer perithallus (Fig. 6.8). The hypothallus is made up of rows of polygonal cells whilst the perithallus consists of thin rows of rectangular cells which run parallel to the surfaces of the thallus (Rácz, 1964 and Wray, 1964). Concepticals are distributed irregularly over the surface of the thallus. The algae often exhibit a honey or yellowish colour hyaline structure, suggesting an aragonitic precursor (Flügel, 2004). The majority of ‘phylloid’ algal specimens observed within the study are recrystallised and identification is difficult, although in some cases monostromatic and differentiated characteristics of the thallus could be recognised - the differentiated forms are

possibly *Archaeolithophyllum* though it is conceded that they may also belong to several other genera, including *Eugonophyllum* and *Ivanovia*. Several well preserved specimens were found and are interpreted to be *Archaeolithophyllum johnsoni* Rácz and possibly *Archaeolithophyllum missouriense* Johnson. Observed thalli were up to several centimetres in length and occasionally over a millimetre in thickness. Several whole individual thalli were obtained in the field, well preserved in a marly material. The marly material was removed (see chapter 4. *Methods and Materials*) leaving well preserved thalli measuring around 12 to 8 cm in size and over a millimetre in thickness. The thalli were slightly undulose with the shape controlled by the subjacent surface. Arranged on the top of these thalli were uniformly spaced, stout tubes, which were originally thought to be conceptacles but were later identified to be aulopodid corals. *Archaeolithophyllum* thrived within quiet water environments (Frost, 1975). Although they have been reported to represent higher energy environments (Rácz, 1964 & Mamet and Villa 2004). *Archaeolithophyllum* is often attributed to the formation of cavities which were formed by a puckering effect caused by evaporation, so a very shallow environment is envisaged. Within the studied material *Archaeolithophyllum* act as an encruster and stabiliser in sediments often rich in detrital siliclastic materials at the base of mounds. ‘Phylloid’ algae plays no role within the formation of the mounds observed but does indicate changes in light levels and sedimentary input for the material it is found in. It is interpreted to have grown in a (sometimes extremely) shallow environment which had a steady sediment input, leading to the stacking of thalli and in some cases the bending upward of thalli as the algae attempts to stay above the deposited sediment. *Archaeolithophyllum* is an important sedimentary stabilizer, playing an important role in the formation of both the Pinos Hairpin Limestones and the basal facies of the Pinos Pylon Mound, it is thought that the algae were not suited to the slightly deeper environments of deposition of the mound facies. Littler and Littler (1980) investigated the morphological attributes of thallus forms of macroalgae and the relationship different forms may have with various survival strategies. Algae with thin sheet-like thalli were found to be very early colonisers which grow quickly and dominate pioneer communities (Johnson, 1963; Wray, 1964; Littler and Littler, 1980 & Mamet and Stemmerick, 2000).

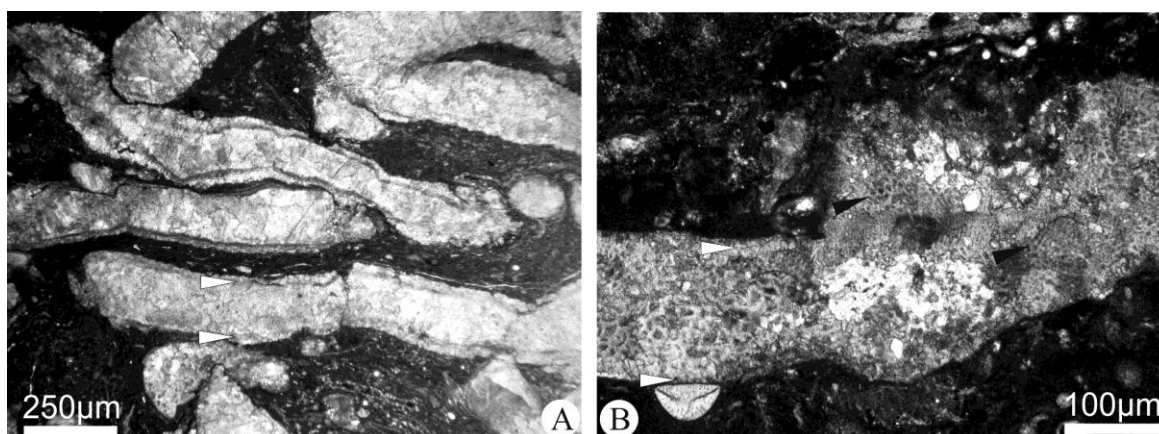


FIGURE - 6.8. In these images *Archaeolithophyllum* can be observed in both a recrystallised, A (PHL30), and well preserved state B (PHL42). A. the thick hypothallus and thin perithallus (white arrows) can be identified. B. Well preserved, sub-quadratic cells can be observed. Smaller cells form the perithallus (white arrows) whilst larger cells form the central hypothallus (black arrow).

6.1.8 *Petschoria*

Petschoria is another flora regarded as a typical Palaeo-Tethyan biota (Mamet, 1992 & Mamet and Villa, 2004). It is a red algae which has a wide dispersal and has been reported from the Urals (Russia), Yukon Territory (Canada), New Mexico (USA), the Tarim Basin (China) (Mamet and Zhu 2005) and Cantabria (Spain) (Rácz, 1964) though it is usually scarce (Mamet and Zhu, 2005). Mamet and Villa (2004) suggest that *Petschoria* and 'phylloid' algae are thought to have grown in low energy environments, within this study *Petschoria* is found in association with both *Archaeolithophyllum* and ungdarellacean algae, which are thought to represent low and intermediate energies respectively. *Petschoria* has a branched, rounded thallus which can be divided into a hypothallus and a perithallus of an even thickness. Most specimens are heavily recrystallized with the structure of the hypothallus being completely destroyed, the perithallus appears to be filamentous with individual filaments standing perpendicular to the surface of the hypothallus. *Petschoria* is not found within the mound facies in this study and is mostly confined to the basal facies. It is commonly associated with *Archaeolithophyllum*, encrusting bryozoans and aulopodid corals and where it is found, it appears to play the role of constructor.

6.1.9 *Fourstonella*

Fourstonella is a red algae which consists of overlapping, curvilinear rows. The alga can grow to up to 3 mm in length and around 600 µm in height. The thallus often appear as a crescent or hemispherical shape. Within the study the only specimen belonging to this genus, which belongs to the species *Fourstonella? Johnsoni* Flügel, was found. The lone specimen occurred within the capping material of the Candemuela Mound. The classification of the species is somewhat complicated and Mamet and Villa (2004, pg. 167) refer to the species as being in “...taxonomic chaos.” The confusion surrounding the species is attributed to different morphological geometries of various specimens being different, leading to the establishment of the genus *Eflugelia* (*Efluegelia*), however, these morphological differences were described to be the result of differing substrates. The status of genera *Cuneiphyucus* and *Foliophycus* adds to the confusion. The alga is cosmopolitan and common in Carboniferous and Permian carbonates of Eurasia. The genus tend to attach to phaeophyta or sponge megasclere (Mamet and Villa, 2004). The extreme rarity of the genus within the observed samples in conjunction with the rarity of sponge spicules is interpreted to suggest a scarce sponge population.

6.1.10 Solenoporacean Red Algae

An extinct group of encrusting algae which often grew with nodular or branching morphologies, ranging from several hundred microns to several centimetres in size. Solenoporacean algae are known from the Cambrian to early Neogene and have been regarded as possible ancestors to the coralline algae (Flügel, 2004). These algae form as radially or vertically divergent filaments, which show distinct growth zonation. Individual cells from the radial filaments often grow perpendicular to the subjacent cell, resulting in a “tube like” appearance. Within the present study rare specimens measuring just a few hundred microns are observed (Fig. 6.9). They play no role within the construction of the carbonate mud mounds, though Solenoporaceans have been known to do so; specifically small Frasnian and Famennian buildups (e.g. Shen *et al.*, 1997).

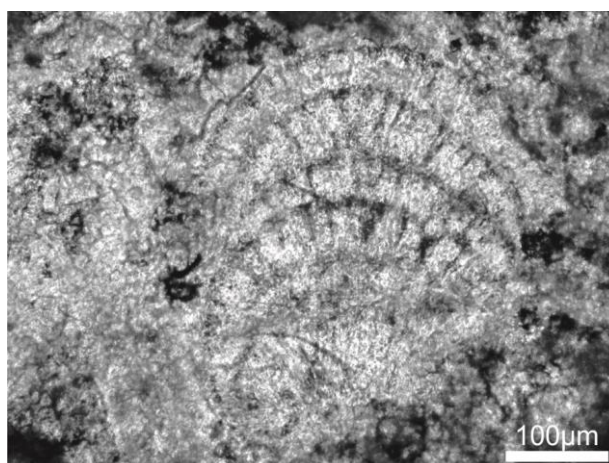


FIGURE - 6.9. An example of a Solenoporacean red algae showing radially divergent filaments and distinct growth zonation (CAN4).

6.1.11 Dasyclad algae

Dasyclad algae are known from the Cambrian and have maintained a relatively consistent morphology through to the present day (Zechman, 2003). The general morphology of a Dasycladale consists of microscopic, tube-like growths of varying styles (e.g. spherical, clavate and rod shaped) which forms a central stem. From this central stem one or several whorls of branching laterals form. Reproductive organs often form on or between the laterals or within the central stem (Flügel 2004). Diagnostic criteria for Dasycladales are based upon: morphology of the main stem, undulations and articulations of the main stem, arrangement of laterals, number of laterals and the shape of laterals (Berger and Keaver, 1992). Dasycladales are important rock builders and Flügel (2004) indicates that they are generally the most important calcareous algae used in microfacies analysis. Dasycladales are often classified based upon morphological reconstructions from thin sections with identification coming from morphological reconstructions established from variously orientated cuts through the algae. In this study Dasycladales are relatively poorly represented (Fig. 6.10), generally occurring outside of the mound facies and are seen as abraded and coated bioclasts, often in association with a variety of other abraded and coated bioclasts. The lack of Dasyclad algae is interpreted as evidence for a restricted environment

of deposition, their occurrence as abraded, coated and therefore transported grains indicates that they have been transported from elsewhere in the basin.

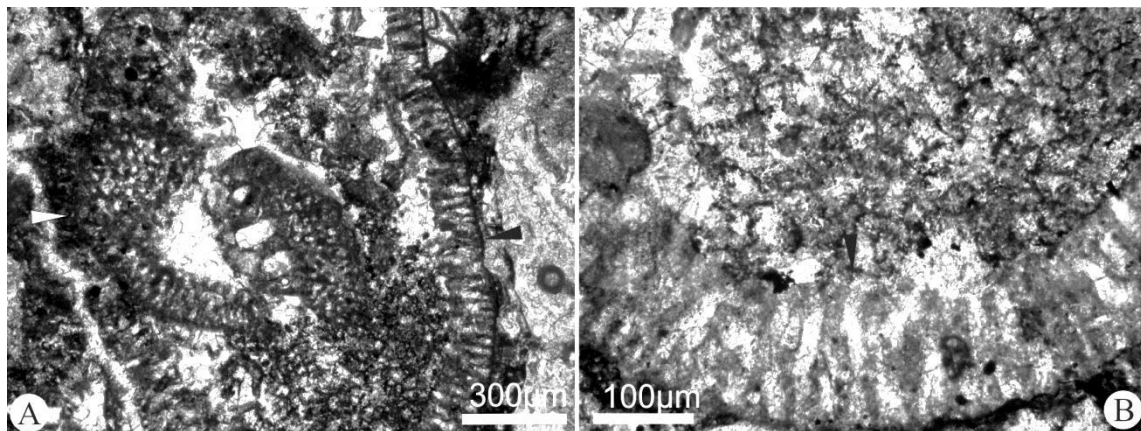


FIGURE - 6.10 Photomicrographs of Dasyclad algae (possibly *Epimastopora*?). A., various cuts through a Dasyclad, the white arrow indicates a tangential cut whereas the black arrow indicates a longitudinal cut through the wall. B., the pore structure of the wall can be seen (both CAN2).

6.2 Cyanobacteria, Calcimicrobes and Microproblematica

Cyanobacteria and calcimicrobes are a group of often problematic calcareous microfossils known from the Precambrian; for at least 2.7 billion years (Buick, 1992) and probably up to 3.4 to 3.5 billion years (Golubic and Seong-Joo, 1999). Cyanobacteria are phototrophic Procaryota (Stanier and Cohen-Bazire, 1977 & Rippka *et al.*, 1979) with an extremely varied morphological range. Cells are arranged in colonies with various growth forms, including sheet like, radial clusters, erect shrub like growths and clump like coccoid forms. Individual cells are generally arranged in thread like forms which may branch. The cells are protected by a mucilaginous sheath (glycocalyx). This sheath is composed of extracellular polymeric substances or exopolymers (Pratt, 2001). Sheaths have been observed upon modern cyanobacteria (e.g. Arp *et al.*, 1999), where, depending upon environmental conditions, carbonate is precipitated within, or as an encrustation upon, the mucilaginous sheath. The mineralogy of the carbonate is likely to reflect water chemistry (freshwater low Mg calcite whereas marine and restricted environments induce high Mg and aragonite (Folk, 1974)). Cyanobacteria only become calcified when the supersaturation of the water in respect to CaCO_3 minerals occurs, and it has been shown by Arp *et*

al. (2001) (although this was suggested by Merz-Preiß and Riding 1999) that Phanerozoic oceans which sustained calcified cyanobacteria must have had a considerably higher concentration of calcium than recent oceans as marine calcification is virtually unknown today, although calcification is widespread in freshwater lakes and streams in limestone areas (Riding, 1999). Calcification of cyanobacterial sheaths produces tube and sausage like “microfossils” generally ranging from tens to hundreds of microns in diameter and up to a centimetre in length. These calcified microfossils, referred to as calcimicrobes, often occur as tubes and irregular bodies which can be classified based upon morphological similarities. Individual tubes and other growth forms generally occur as colonies which exhibit laminations with thrombotic or dendrolitic qualities. The general classification of calcified cyanobacteria as described by Riding (1999) has been used in this study. Various morphologies have been observed with *Girvanella*, *Rothpletzella*, *Shamovella*, *Renalcis*, *Ortonella* and *Archaeolithoporella* having all been identified from thin section.

Cyanobacteria are a common component of the thin sections studied. The specimens are generally well preserved, although there are several examples which are most likely cyanobacterial in origin but have been micritised. The most common growth forms observed include laminar accumulates of bean and sausage shaped tubes, as well as encrusting, entwined and clustered tubes. Various cyanobacteria are found in association with the mound facies of several of the studied mounds, though it appears that they are preferentially found within the mounds of the San Emilliano Valley (indeed, the mound facies of the Candemuela Mound has specimens of each of the major groups focused on within this chapter present) and less so in their Bernesga Valley counterparts. Cyanobacteria are commonly associated with *Donezella* growths and are observed to form a baffling and binding action in association with *Donezella*. It is probable that the various cyanobacteria acted as encrusters upon the dendritic *Donezella* growths and stabilised them.

6.2.1 *Girvanella*

Girvanella (Nicholson and Etheridge, 1878) was first described from Silurian deposits of the Girvan area, Ayrshire. *Girvanella* are rarely-branching tubes which occur in varying habits, Høeg (1932) described three groups based upon aggregation and mode of preservation: [1] *typicalis* tightly packed masses of threads, [2] *lumbricalis* with sparsely scattered and loosely aggregated tubes and [3] *moniliformis*, isolated tubes within a calcareous matrix. *Girvanella* tubes range from 10 to 40 µm in diameter (Pratt 2001) and are often preserved with a micritic wall. Examples are known from the Neoproterozoic (Knoll *et al.*, 1993) to at least the Miocene (Pratt, 2001). *Girvanella* has been reported as the dominant framework builder of reefs particularly in Neoproterozoic (Turner *et al.*, 2000) and deep-water Cambrian reefs (Pratt, 1995, 2000). *Girvanella* was described as a Foraminifera by various authors on the basis that the tubes were similar to those of the recent foram *Hyperammina vagans* (Wood, 1957, and references therein). A large number of species have been established, though a general dictum to use just the generic name has become common practice (e.g. Riding, 1991 and Pratt, 2001).

Well preserved tubes of *Girvanella* are commonly found in association with *Donezella* and are found within non-*Donezella* dominated 'flank' deposits at just one location. The genus is also observed in association with other cyanobacteria. Large cyanobacterial growths including a *Girvanella* component are common within 'phylloid' algal dominated specimens. Along with other cyanobacteria it is found behaving as both an encruster and in many cases it is found as tangled clumps within homogenous micrite and a thin microspar envelope (which is a biocement) between *Donezella* thalli acting as a binder. When found in association with other cyanobacteria and encrusting algae, especially *Claracrusta* and often *Rothpletzella* it sometimes forms cyanoliths which can reach up to centimetres in diameter. These cyanoliths generally have algal thalli as a nucleus, but encrustation by *Girvanella* appears to be non-selective. *Girvanella* tubes have a typical micritic wall. Tubes with a diameter of 30 µm have been observed but the majority of specimens observed have a diameter of 10-15 µm (Fig. 6.11). Tubes appear as encrusting masses of aggregated tubes, as tightly entwined bundles and as loosely aggregates tubes, often within a

homogenous micrite. Within the sampled mounds *Girvanella* is more common within San Emiliano Valley examples when compared to Bernesga Valley counterparts. In association with other cyanobacteria and encrusting algal forms it is believed to play a critical role in the stabilisation of mound carbonates. The bias toward San Emiliano Valley mounds indicates preferential environmental conditions, interpreted here as quiet, warm and restricted. *Girvanella* is also commonly found associated with the ‘phylloid’ algae dominated silty carbonates of the Pinos Hairpin Limestones. Within this facies *Girvanella* (and other encrusting cyanobacteria) take advantage of the calcareous substrates provided by ‘phylloid’ algae and are very successful at colonising and in some cases binding homogenous micrite in place, it is generally on heavily encrusted and bound specimens of ‘phylloid’ algae where the best preservation is found.

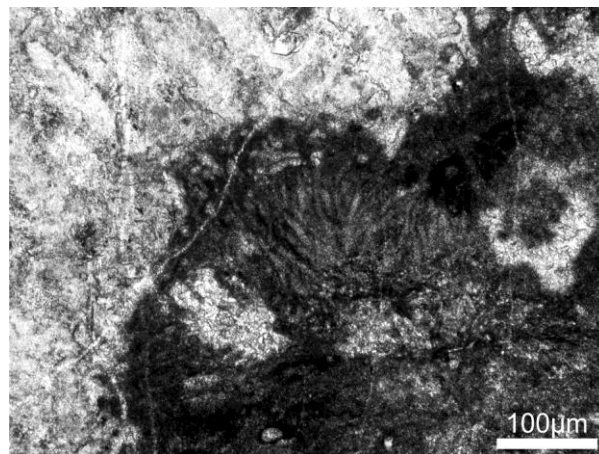


FIGURE - 6.11 An example of “*typicalis*” *Girvanella*. A mass of tightly packed threads can be seen.

6.2.2 *Rothpletzella*

This genus was first described by Wood (1948) as a cyanobacteria or green algae. However Riding (1991) considered *Rothpletzella* to be a microproblematicum as no extant analogues are known to indicate a cyanobacterial classification. Nether the less, *Rothpletzella* is still generally referred to as a calcimicrobe/cyanobacteria by many authors (e.g. Webb, 1996; Shen *et al.*, 1997; Wood, 2000 and Adachi *et al.*, 2006). *Rothpletzella* is characterised by laminar sheet-like growths of branching tubes which lie parallel to the substrate. In transverse sections *Rothpletzella* often resembles a

chain or bead like structure with individual filaments ovoid in shape, often resembling beans or sausages. Individual filaments have been reported to range from 13 to 37 μm (Adachi *et al.*, 2007) in diameter. Longitudinal cuts reveal dichotomous branching of filaments. Filaments branch often and can form fan like structures. Filaments have a thin micritic wall and are filled with clear sparry cement. *Rothpletzella* grows as thin crusts and oncoids (Feng *et al.*, 2010) and platy growths (Wood, 2000). Growths are laminar and undulate to mimic the subjacent micro-topography. *Rothpletzella* from Frasnian reefs of the Canning Basin (Australia) are thought to be representative of the deeper parts of reef growth (Wood, 2000). *Rothpletzella*, *Wetheredella* and *Girvanella* in combination have been known to grow together symbiotically (Wood, 1948) forming what is essentially a microbial organism where boundaries between the various components are impossible to see with the naked eye / optical microscope. This microbial organism was mistakenly interpreted as a single fossil and named *Sphaerocodium* (Wood, 1948 and Adachi *et al.*, 2007). *Rothpletzella* is known to co-occur with *Wetheredella* (see 6.1.6 *Wetheredella* above), and is seen to co-occur within this study. *Rothpletzella* is observed to be much more abundant than *Wetheredella*, a relationship also observed by Feng *et al.* (2010).

Rothpletzella is a commonly observed calcimicrobe in this study and is often found as well preserved laminations of juxtaposed ovoid filaments (Fig. 6.12). The genus is often found in association with other encrusting alga and calcimicrobes, especially *Claracrusta* and *Girvanella* and more rarely *Wetheradella*. These calcimicrobes often form variously layered growths. Several examples have a microsparitic wall and are filled with micrite with the filaments measuring up to 50 μm in height (width was not measured as it is unsure if the cutting angle is completely perpendicular to the filament). Several of the laminar growths of *Rothpletzella* reach up to a millimetre in height. The genus is usually found encrusting various bioclasts, in particular *Donezella* thickets and 'phylloid' algae. This genus is interpreted to play an important role in the binding and stabilisation of *Donezella* thickets within the San Emiliano Valley mounds, it is found commonly within these mounds but was completely absent within the Bernesga Valley mounds.

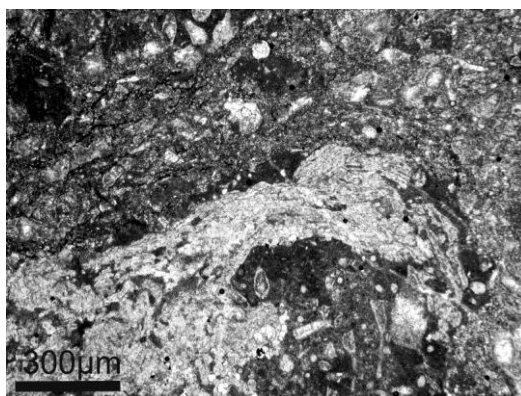


FIGURE - 6.12 A photomicrograph showing rows of *Rothpletzella* encrusting a *Donezella* colony (CAN6a). Note that unlike *Claracrusta*, successive rows of *Rothpletzella* are concordant with the previous row.

6.2.3 *Renalcis* and *Epiphyton*

Microfossils belonging to the ‘*Renalcis* group’ (see Flügel, 2004, pg 409) of calcified cyanobacteria consist of clusters of micrite walled, cystose to clotted forms. Individual forms grow erect and apparently branch. The genus is commonly found in reefs (Flügel, 2004) from the Cambrian, where it plays a major constituent in archaeocyath reefs. It is known from the Ediacaran of the Precambrian (Kontorovich *et al.*, 2008) and has been reported (without evidence) from the Triassic of southern China by Lehrmann (1999). It often occurs along with *Epiphyton* which is more tube or rod like than *Renalcis*. Several rare filamentous growth forms which resemble *Renalcis* and *Epiphyton* are found (see Fig. 6.4) and many clotted micrites and peloidal micrites also bear a resemblance to the filaments of these calcified cyanobacteria. The scarcity of intact specimens suggests that they did not play a major role in the construction, binding or baffling of the mounds. The peloids which resemble filaments may suggest that a proportion of micrite originated from the abrasion and micritisation of calcimicrobes.

6.2.4 *Shamovella* (= *Tubiphytes*)

Shamovella is also commonly called *Tubiphytes*. Both are valid names though due to reasons of priority, *Shamovella* is used here (Riding, 1993 and Senowbari-Daryan, 2013). It is one of the most problematic Late Palaeozoic organisms with an uncertain systematic affinity. *Shamovella* occurs with various growth morphologies, typically divided into two sub-groups; a cylindrical

form and a segmented aggregate (Flügel, 2004). A rare component of the carbonates in this study *Shamovella* is only observed within the Candemuela and possibly within the Cármenez Mounds. It is observed in association with other microscopic encrusters and appears as a segmented aggregate of hemispherical, helmet or ovoid shaped ‘envelopes’ of dark micrite. Each aggregate has a small microspar filled cavity. It has been suggested that the organism may be a group/combination of cyanobacteria, foraminifera and possibly sponges (Schmid, 1995 & Senowbari-Daryan, 2013). *Shamovella* does not play an important role in mound formation and its rare occurrence suggests that the environment of deposition may not have been well suited to its growth.

6.2.5 *Archaeolithoporella*

Archaeolithoporella is a relatively common constituent of many Permo-Carboniferous reefs, however, its taxonomic position is not clear (e.g. Flügel, 1981 & Wang *et al.* 1994). It consists of alternating laminations of thin, dark homogenous micrites and rows of slightly undulating, thin clear sparitic or microsparitic layers. The fossil has been considered an algae (e.g. Riding and Guo, 1991 and Wood *et al.*, 1996) and a microbial crust (Flügel, 1989) but is commonly referred to as a microproblematica. This problematic fossil forms encrustations on hard surfaces (marine hardgrounds, clasts and other fossils) and acts as baffler and binder. *Archaeolithoporella* is uncommon within the studied material. Where it does occur, it is associated with microfacies which are dominated by fellow microscopic encrusters. It should be noted that several authors have considered *Archaeolithoporella* to be abiotic in origin (see Kendall and Iannace, 2001, and references therein).

6.3 Foraminifera

Foraminifera are small, unicellular heterotrophs which construct chambered tests. The frequently changing composition of the fauna provides excellent information regarding evolution, habitat adaption and extinctions (Loeblich and Tappan, 1987 & Tappan and Loeblich, 1988). In microfacies analysis foraminifera are of high importance as they are excellent environmental

proxies and can be used to establish depositional environments in ancient samples (Flügel, 2004). From the San Emiliano Formation fusulinid foraminifera (along with brachiopods, spores and macroflora) have been used to indicate a stratigraphic age of early Bashkirian to end Moscovian (see chapter 1. *Introduction*). Foraminifera were present in almost all slides investigated, but rarely formed a large component. Observed forams were often 100 to 250 µm in size but occasionally larger specimens of up to 600 µm were observed. Several specimens of Fusulinid foraminifera were observed but the ultrastructure of their shell was obliterated, meaning classification further than Fusulinid was unlikely (Leppig *et al.*, 2005). Two forms of foraminifera were relatively commonly present; these were the Tetritaxidae, *Tetrataxis* and the Lasiodiscidae, *Lasiodiscus*. Whilst investigating the stratigraphic position of the San Emiliano Formation van Ginkel and Villa (1996) reported the occurrence of foraminifera including *Pseudostaffella* and *Millerella* from the lower limestone units of the La Majúa member and the appearance of abundant Archaediscidae from the upper most unit. The Archaediscidae which they report include “...*Archaediscus*, *Asteroarchaediscus* etc.” These forms were not observed within the current material, but as mentioned above abundant Lasiodiscidae have been observed.

6.3.1 *Tetrataxis*

Tetrataxis is a foraminifera which is conical, trochospirally coiled with a microgranular test wall, with additional radial fibrous calcite on the umbilical surface (Leoblich and Tappan, 1987). This genus is well known from Carboniferous sequences globally and was once considered to be free living or an encruster. The work of Cossey and Mundy (1990) suggested that *Tetrataxis* was, most probably, a loosely attached to adherent mobile form which grazed over its substrate in search of food. The occurrence of attached tetrataxids has been interpreted to represent a limpet-like behaviour in response to adverse environmental conditions.

Several, well preserved, specimens of *Tetrataxis* have been observed (e.g. Fig. 6.13) and in most cases there is evidence of them being attached to a substrate. This attachment suggests that the environment in which they were deposited was not favourable for them.

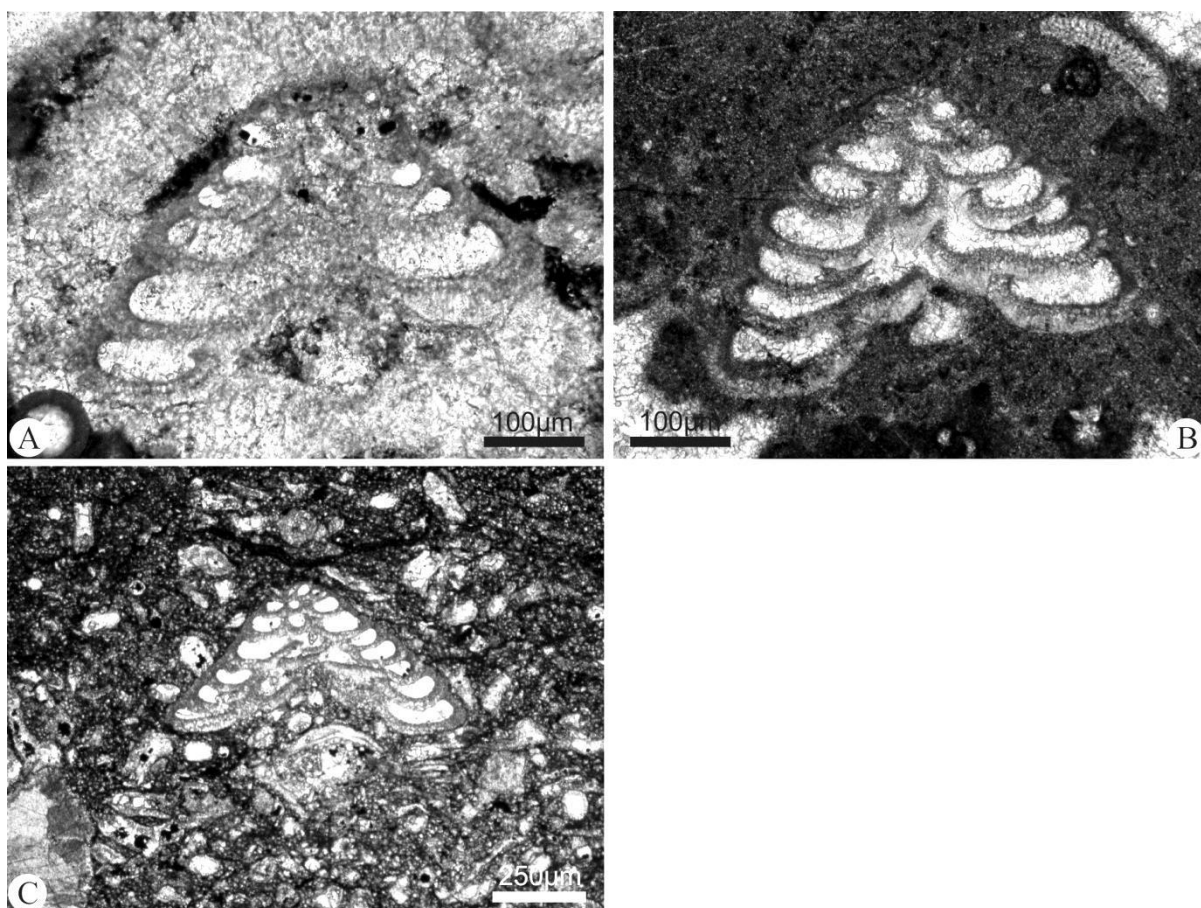


FIGURE - 6.13 Three cross sections through the foraminifera *Tetrataxis*. The characteristic coiled whorls can be clearly observed. A (CAN4) appears to be attached to an algal thalli whilst B (CSM2) and C (CAN15) do not appear to be attached, however at the base of C it appears that several grains have accumulated/become baffled.

6.3.2 *Lasiodiscus*

The Lasiodiscidae are a family of foraminifera which are known from the Carboniferous (Cózar and Mamet, 2001) through to the latest Permian (Groves and Altiner, 2005). Within the samples studied three distinct forms have been identified (from axial sections), the first is that of *Lasiodiscus sellieri* Dessauvage and Dağ, with the second two representing newly described morphotypes. The fossils consist of small tests with a planispiral coiling. Within the specimens observed a spherical proloculum proceeded by a second, undivided tubular chamber which forms a planispiral coil around the proloculum. The second chamber becomes very slightly conical as the tube becomes larger with consecutive spirals. *L. sellieri* shows 9 to 10 volutions of the second coiled chamber whilst *L. sp. 1* shows 7 and *L. sp. 2* has a range of 7 to 9, note that like *L. sellieri*

the last coil is not always aligned with the general plane of coiling. All forms show characteristic hyaline columns on the dorsal face whilst tubular appendages are present upon the ventral face. Other than the number of volutions of the coiled second chamber it is the morphology of these tubular appendages which make the identified specimens morphologically distinct. *L. sellieri* has small appendages (smaller than the total thickness of the second chamber) which converge toward the proloculum whilst *L. sp. 1* has longer appendages which become increasingly elongated (from the proloculum), these appendages are divergent from the proloculum, bending at around three quarters of their length to form talon like shapes. *L. sp. 2* has similarly long appendages to *L. sp. 1* but these lack the curvature of shape and are consistently divergent from the proloculum. Both new morphotypes (*Lasiodiscus sp. 1* and *Lasiodiscus sp. 2*) slightly resemble *Lasiodiscus medusa* Miklukho-Maklay except the secondary, coiled chamber is not as conical and the appendages are divergent from the proloculum and not convergent as in *L. medusa*. The Upper Permian species *L. rugosus* Miklukho-Maklay, is similar to, but differs from *L. sp. 2*, in that the second chamber continues to increase in height with consecutive volutions and it has shorter ventral appendages.

See section 6.6 *Systematic Palaeontology* for further description. Within the study the Lasiodiscidae do not form a major component and compared to some other taxa are relatively rare. It is interesting to note that other Carboniferous age Lasiodiscidae have been identified from a carbonate mud mound facies (Cózar and Mamet, 2001).

6.3.3 Fusulinids

The Lasiodiscidae and the Tetrataxidae are both examples of smaller fusulinid foraminifera found within the samples. There are several other smaller forams also present, but often the section through them is oblique and classification difficult. Larger fusulinids are also present in the samples studied (e.g. Fig. 6.14). However, the wall structure of these has been obliterated and classification further than fusulinid is difficult in many cases. Classification of fusulinids is based upon the general overall morphology of the tests, which consist of coiled and folded chambers. The consequence of not being able to successfully classify genera and species is that these forams

cannot be used for biostratigraphic purposes in the present study (however this has been successfully completed by other authors - see chapter 1. *Introduction*). Several of the specimens resemble the genera *Earlandia* and *Priscella*. Fusulinid foraminifera were adapted to warm, shallow, tropical and sub-tropical regions (Flügel, 2004). Although they are not particularly abundant they are found within every mound analysed in this study, adding further evidence to the interpretation of a shallow and warm environment. The relative scarcity of them may also indicate a restricted environment.

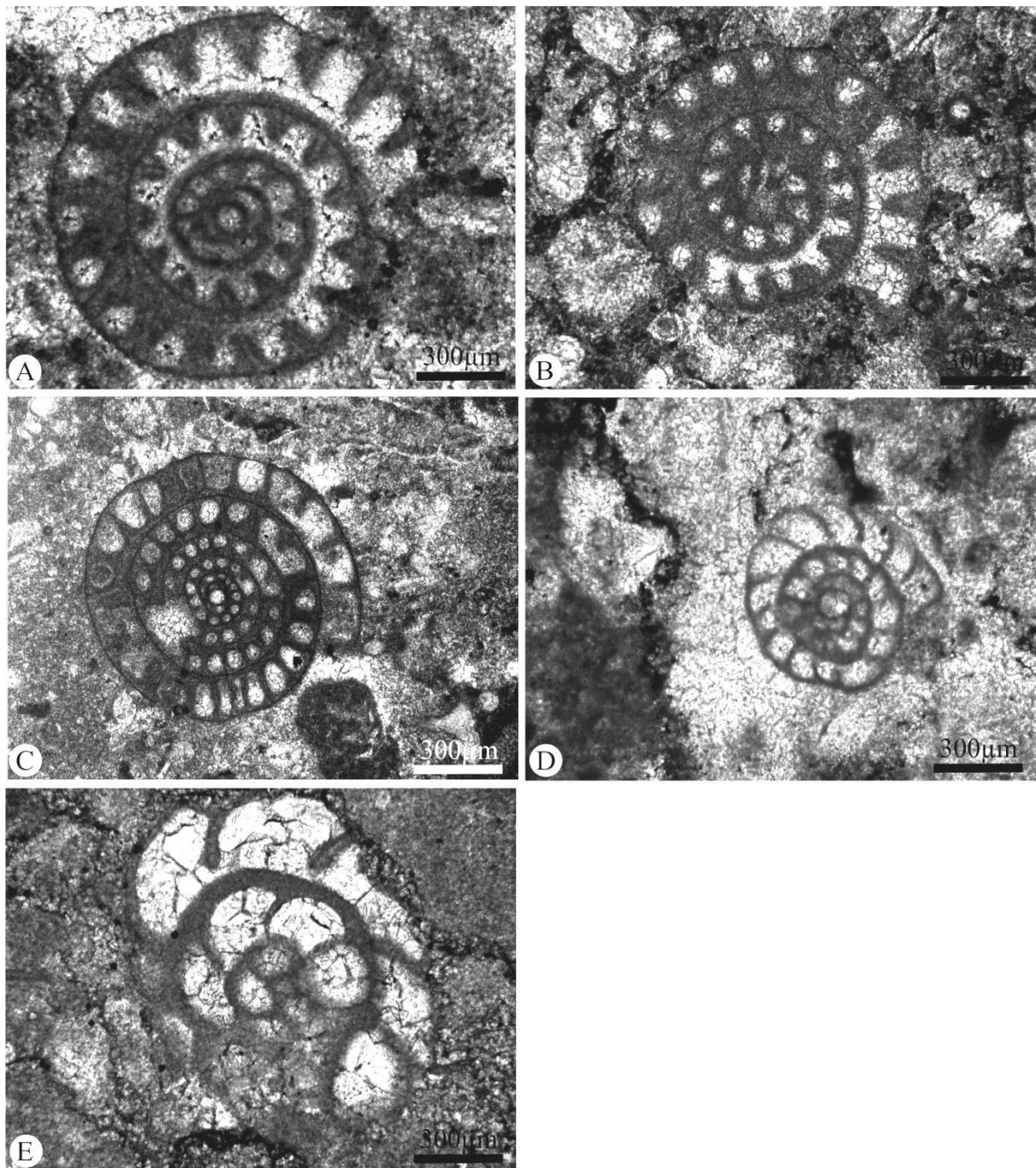


FIGURE - 6.14 Photomicrographs of several examples of fusulinid foraminifera observed within the study (specimens were not found in the appropriate cross sections for determination). Wall structure can be seen to be destroyed. A (SDL4), B (CAN17), C (CAN18), D (CAN1), E (CAN6).

6.3.4 Miliolinids

Miliolinid foraminifera have a porcelaneous calcareous wall which often appears very dark under transmitted light. There are several small clusters of numerous specimens within the Candemuela and Pinos East mounds which have been interpreted as miliolinid foraminifera (Fig. 6.15).

Although they are a rare component they may indicate an important factor. Flügel (2004) reports that miliolids are well suited to high carbonate concentrations in hypersaline marine water. In this study several tightly packed clusters of planispiral miliolinids have been observed. They appear to have a spherical initial chamber with several volutions of subsequent chambers present.

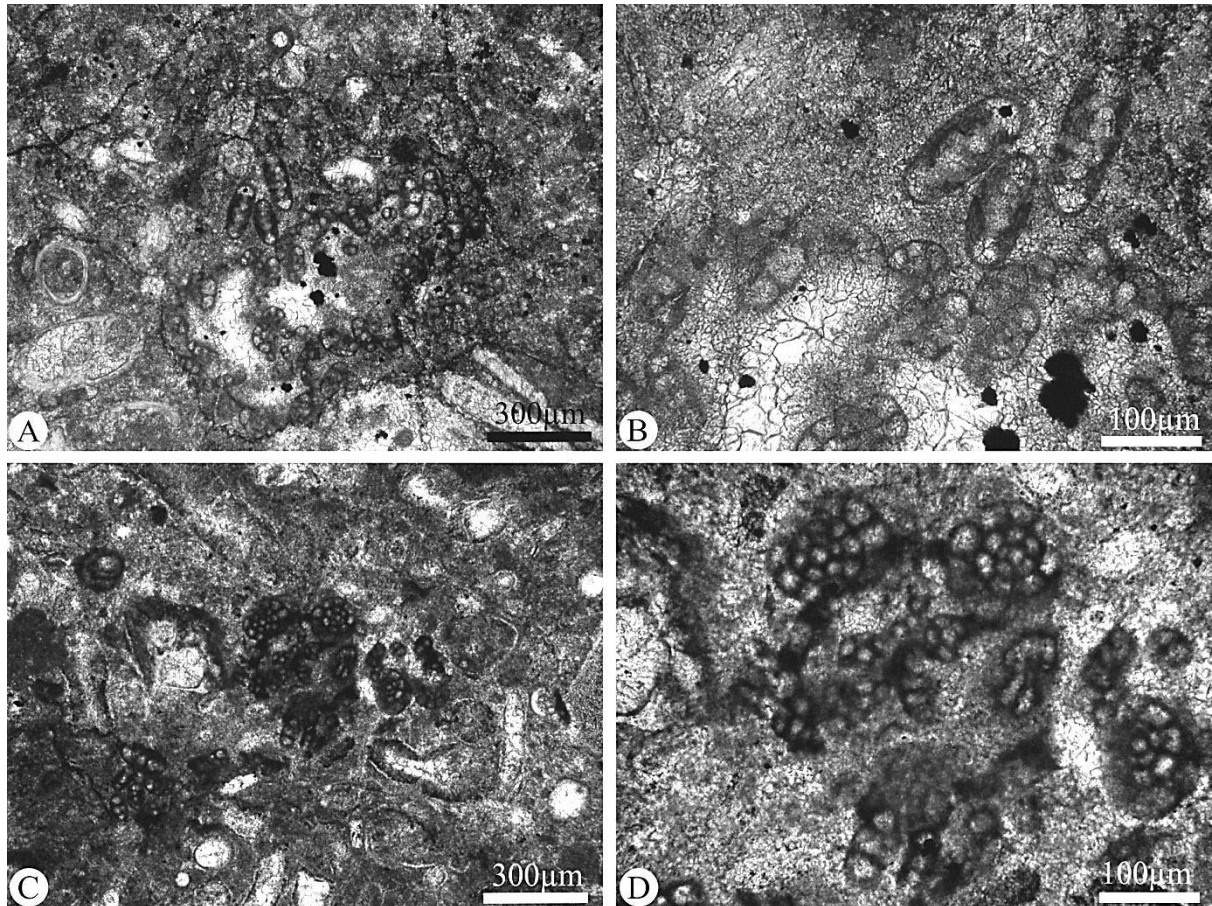


FIGURE - 6.15 Examples of Miliolinid forams observed within this study (CAN20). The characteristically dark porcelaneous wall is a distinctive feature. The forams are generally 100 µm in diameter. A. and B., in these microphotographs axial sections through the forams seem to be mostly present. B. is a zoomed in image of several of the forams seen in A. C. and D., Here mostly equatorial sections can be observed. D. is a zoomed in image of several of the forams seen in C.

6.4 Bryozoans

Bryozoans are widely distributed, known from a wide variety of water depths and latitudes both in modern examples and fossil examples (Bassler, 1953). Bryozoans are essentially colonies of individual animals (zooids) which form by budding from a primary individual. Bryozoans form a

wide variety of morphologies and sizes and were recognised within both the micro- and ultrafacies analyses (Fig. 6.16).

Bryozoans from the Carboniferous of the Cantabrian Mountains have been well documented by Ernst and Minwegen (2006) and Ernst and Winkler Prins (2008). Bryozoans are abundant in the carbonate material of the Cantabrian mountains and are generally well preserved. The majority of bryozoans are thought to be fenestrate (Ernst and Winkler Prins, 2008). Bryozoans observed within this study are generally reminiscent of the fistuliporids and are found in most locations (all except the Cármenez South and San Martín mounds). Bryozoans are best preserved when in association with the encrusting guild of organisms observed (e.g. *Rothpletzella*, *Claracrusta*). Within the Pinos Hairpin Limestones bryozoans are observed to act as encrusters and likely played a role in stabilising sediments. Broken and reworked fragments of bryozoans are often found within the facies associated with off-mound deposits. Bryozoans did not play a role in the formation of mounds but are occasionally found within them, though they are never considered to be an important component.

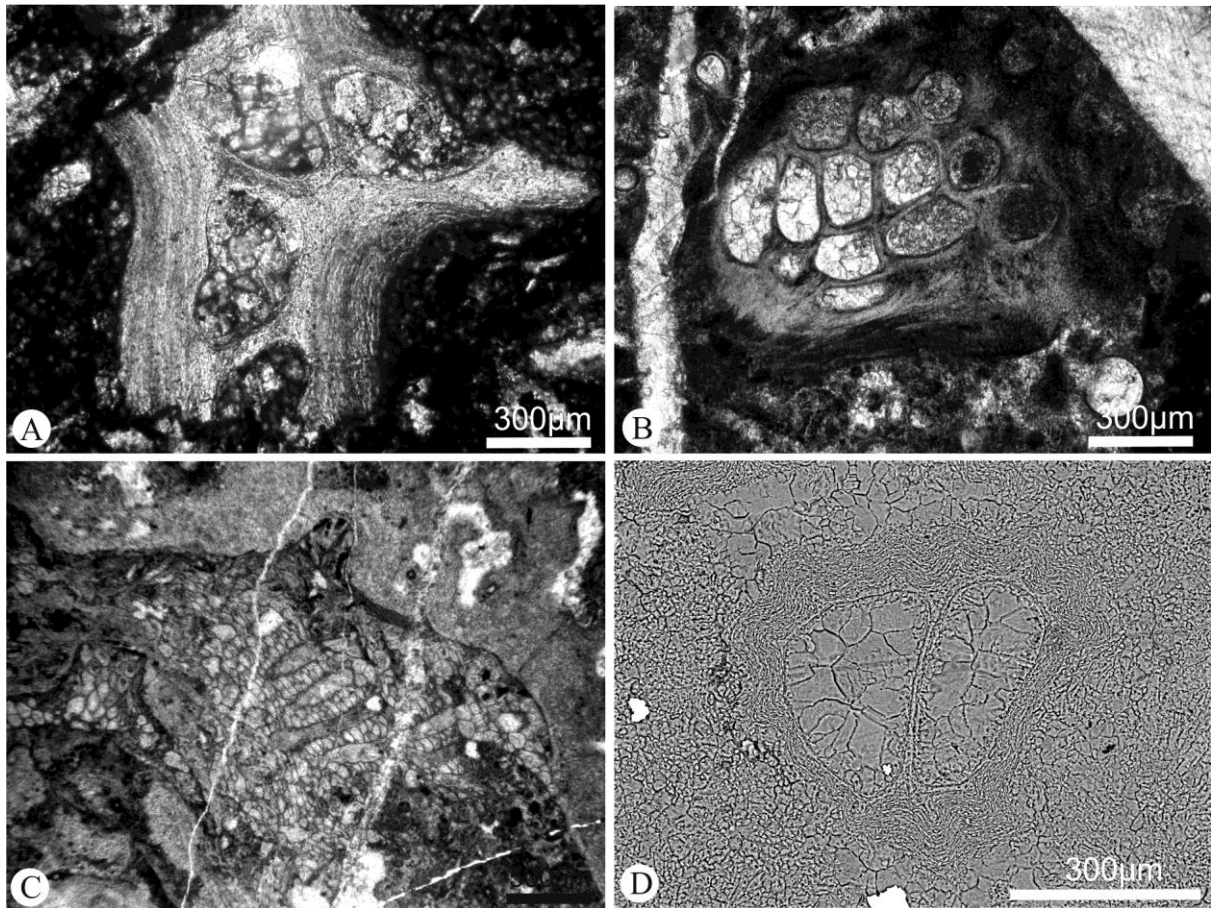


FIGURE - 6.16 Several examples of bryozoans. A., (CAN15) and B., (CAN20) show broken and transported fragments of bryozoans. The characteristic wall structure of the bryozoans can be seen in both images. The walls consist of laminar rows of 'slab-like'. C., (PEM21) An encrusting colony of bryozoans, upward growing zooecia can be seen. D., (CAN15) an SEM image of a small bryozoan frond, the laminar wall, characteristic of the bryozoa, can be seen.

6.5 Other Fossils

The following fossils are all present within the studied material but are not believed to play a major role within mound nucleation, formation or growth. Several of these fossils, including corals, gastropods and brachiopods, can be observed in hand specimens and represent the macro fossil content of the material (other than 'phylloid' algae). Although these fossils are not believed to have played an important role in the formation of carbonate mud mounds from the San Emiliano Formation they do provide evidence for environmental interpretations and are sometimes reasonably abundant within off mound sediments.

6.5.1 Corals

Corals are present in the form of both rugosa and auloporids. Solitary rugose corals are observable within both mound and off mound sediments. The largest specimens are found within the marly beds of the Pinos Hairpin Limestone, where they can often be seen in life position. The rugose corals can often be observed growing upright, but where clastic sediment input is increased the corals can be seen to grow more parallel to bedding. Within the mound facies rugose corals are rare and are always heavily encrusted. Thick walled, encrusting auloporidae corals which consist of tube-like ‘chimneys’ growing from a thin, laminar base are found within samples associated with ‘phylloid’ algae. The auloporids observed resemble *Multithecopora* sp. (Coronado and Rodríguez, 2014). Both the Pinos Hairpin and the Pinos Pylon Mound (specifically the basal but including the mound facies) have auloporidae communities. Whilst the auloporids found within marly beds can be observed to grow successfully within a community of other encrusters (including both microscopic encrusters - *Rothpletzella*, *Girvanella*, *Clavocrusta* and ‘phylloid’ algae) auloporids are generally absent from mound limestones. The small auloporids which are found within the Pinos Pylon Mound provide evidence that sedimentation may have been too rapid for the organisms to keep up with. Corals play no major role within the formation of mounds or the stabilisation of off-mound sediments.

6.5.2 Shelly Fauna

Rare gastropods, bivalves and brachiopods can be found as whole specimens and observed in thin section. These fossils are often found in association with transported clasts. Brachiopods have been used to help establish the stratigraphic age of the San Emiliano Formation. Winkler Prins (1968) and Martínez Chacón (1979) first described the brachiopods of the San Emiliano Formation before presenting a summary and further works together (Martínez Chacón and Winkler Prins, 1984, 2010). Gastropods are occasionally found in association with ‘phylloid’ algae.

6.5.3 Tuberitinidae

The Tuberitinidae are a group of enigmatic organisms which are commonly observed (though they contribute little to the overall composition) within the studied material. The biological affinity of the Tuberitinidae is uncertain, as a result the Tuberitinidae have been placed within several different taxonomic groups. They have generally been associated with foraminifers (e.g. Rich, 1970, 1980; Toomey, 1972; Toomey and Winland, 1973; Conil *et al.*, 1977; Wendt *et al.*, 2002; Nestell and Nestell, 2006; Enpu *et al.*, 2007; BouDagher-Fadel, 2008 and Błażejowski, 2009) or calcispheres (e.g. Jones and Somerville, 1996 referred to the tuberitine species *Mendipsia leesi* as a calcisphere). Vachard *et al.*, (2001, pg 396) placed the family within the *incertae sedis* (calcispherids) – noting that doubt surrounding the Family exists due to “...conspicuous generations...” within their morphological range and that certain genera are based upon “...diagenetic modifications of the wall...”. Other authors have also previously expressed doubt concerning the taxonomic position of the Tuberitinidae. Warthin (1930) remarks that the genus *Tuberitina* has no clear relationship to any Family of the Foraminifera, and probably belongs to another order. Gaillot *et al.* (2009) placed the Family within the Foraminifera but questioned this taxonomical assignment, by remarking that unlike the Foraminifera, the Tuberitinidae have a free and an attached stage and that there is an apparent lack of apertures. Vachard *et al.* (2010, and previous references therein) suggest that the group are probably not foraminifera. Conil *et al.* (1977) recognised distinct life stages which they called [1] spherical, [2] stretched, [3] diplospheric and [4] tuberitine. This observation suggested that the Tuberitinidae were not true foraminifera, as similar life stages are not observable within the forams. Vachard and Miconnet (1994) recognised that morphological differences between some genera and species may be due to taphonomic effects, e.g. different stages of recrystallisation of the wall structure.

Several morphologies related to different life stages within the *Tuberitina* are recognised (Fig. 6.17), including attached and free floating forms. Several authors have interpreted environments similar to those envisaged for the San Emiliano Formation (e.g. shallow and warm) for other Tuberitinidae bearing lithologies: Rich (1970) describes an environment that is low energy,

shallow and has little terrestrial input, and notes that the Tuberitinidae are often associated with the algal genera *Donezella*, *Dvinella* and *Komia*. Both Toomey and Winland (1973) and Vachard and Miconnet (1994) report specimens of the Tuberitinidae from a lagoonal, intertidal environment, whilst Nestell and Nestell (2006) found specimens from both proximal forereef and backreef lagoonal deposits. Browne and Pohl (1973) and Rich (1980) encountered examples of free floating Tuberitinidae only, the former study from deltaic silts and the latter from a wackestone and packestone with pelloidal grains. Interestingly, no attached forms were reported from these higher energy environments. This suggests that assemblages of Tuberitinidae could be used as a tentative proxy for energy conditions. A full cohort of life stages may suggest a low energy, shallow environment that may be a newly opened ecological niche. Assemblages containing just free floating stages of the life cycle may indicate a higher energy environment, possibly deeper water, and represent the dispersal of Tuberitinidae. A full range of morphologies was observed, possibly indicating a low energy, shallow, newly opened niche.

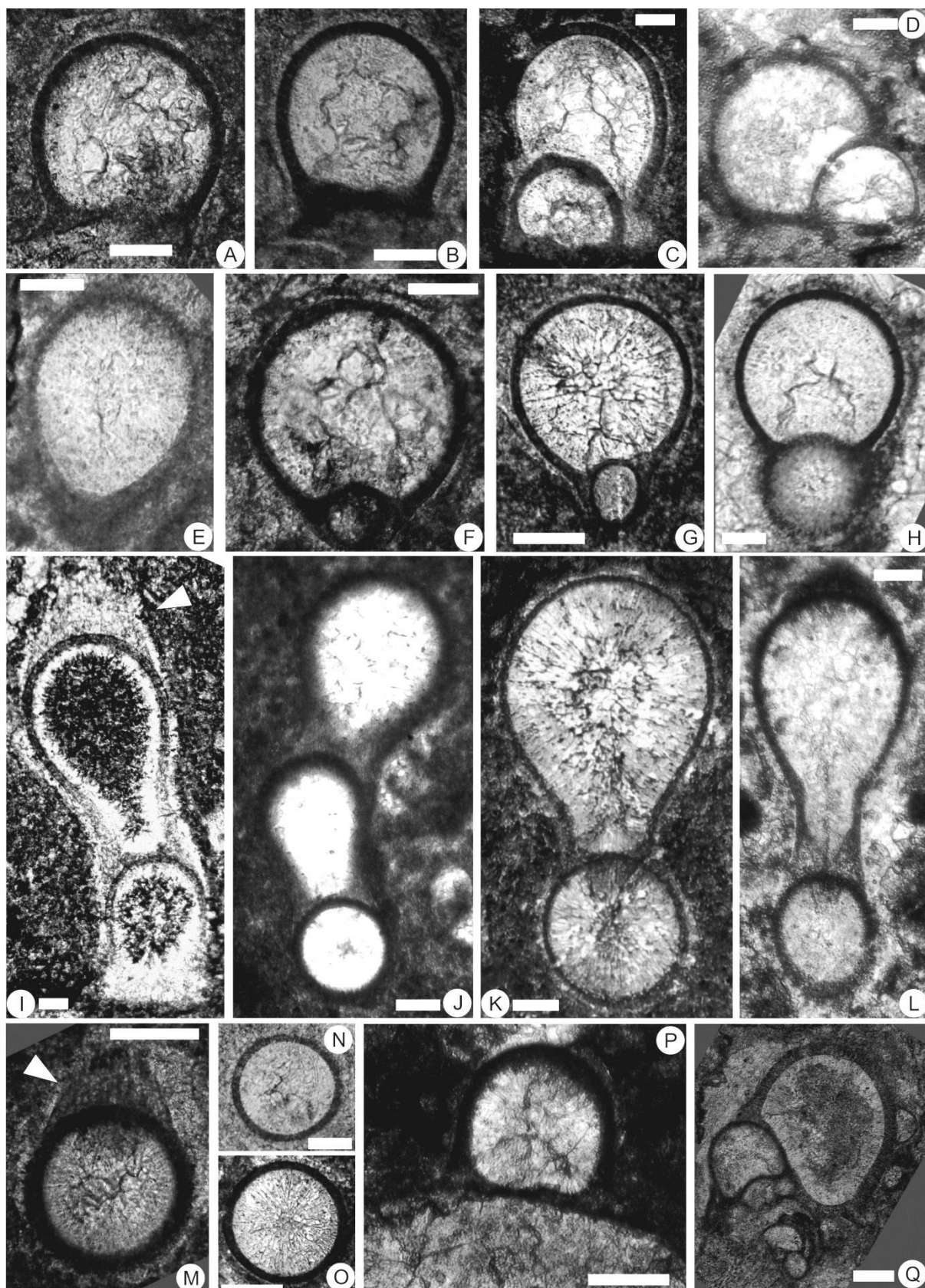


FIGURE - 6.17 Photomicrographs of examples of the morphological variation in chamber shape, size and preservation of Tubertinids, all scale bars = 50 μm . A, B and P, attached stage individuals, note how basal discs vary depending upon substrate, attached forms are often observed in association with algae (e.g. P). C and D, attached specimens showing growth of

second chambers. E, free floating individual, note the slightly elliptical shape. Tapered portion (bottom of photomicrograph) was once attached to chamber similar to those in A-D. F-H and J-L, diplosphaerine specimens showing increasing size, and also separation from new generation, spherical chamber. Note rectilinear growth pattern in J. I and M, I is a multi-chambered, rectilinear attached specimen whilst M is an individual free floating chamber, both show evidence of previous attachment (see arrows). M, N and O, spherical, free floating specimens. Q, an example of several specimens within close proximity of one another.

6.5.4 Others

Other fossils observed within this study and reported by other authors are thought to be of little importance to the formation of the San Emiliano Mounds and are often very rare. Sponges (e.g. Samankassou, 2001 and Garcíá-Bellido & Rigby, 2004), trilobites (Gandl, 1987) ostracods (Fernández Lopez and Sánchez de Posada, 1987) and echinoderms (Winkler Prins, 1968) were all observed from the studied specimens and have been described by the referenced authors. These organisms are rarely found within hand or thin specimen and play a very minor constituent role within the carbonates studied. These organisms did not play any major contributing role to the nucleation, formation or growth of mud mounds (or the carbonates in general).

6.6 Systematic Palaeontology

Taxonomic descriptions are provided for the Donezellacea and the Lasiodiscidae due to the new morphotypes discovered within the families. The new taxa described are a new morphotype of *Donezella*; *Donezellasp.* 1, as well as two new Lasiodiscidae morphotypes; *Lasiodiscus* sp. 1 and *L.* sp. 2. Other taxa are well known (i.e. *Archaeolithophyllum*) or the preservation or occurrence of the material is too poor to justify entry within sytematics. Several other new morphotypes /taxa may be present but more of the sample material would need to be investigated.

GENUS *Donezella* Maslov, 1929

Type species *Donezella lutugini* Maslov, 1929

The thallus consists of regularly branched tubes consisting of barrel shaped segments partitioned by a section of wall which grows perpendicular to the wall of the tubes. These partitioning walls are envisaged to allow communication between segments via a small hole at their centre, this apparent perforation is only visible in longitudinal cross-sections where the thallus has been sliced in half. The thallus is easily divided into two parts, a central cavity which is filled by a clear calcite cement and an outer wall structure which is often yellowish in colour and is surrounded by dark micrite. The inner part of the wall is often observed as a micritic layer between the calcite partitions, in several cases this layer appears to be formed by needle like structures which may represent further, finer, partitions across the tubes. Branching is often perpendicular to the wall of the tube, but not always. Where perpendicular branching occurs a distinctive quadratic growth form is observable.

In cross section the thallus is observed to be round with the two way division between wall and internal cavity still obvious. In cross section the wall appears almost as thick as the central cavity. This is seen as further evidence for the needle like segmentations between the main calcite segmentations.

The species *Donezella lutugini* Maslov and *Donezella lunaensis* Rácz are recognised along with *Donezella* sp. 1. These three morphologies are differentiated by the form and dimensions of the barrel like tube segments, differences in partitioning and differences in branching style (Fig. 6.18). *Donezella* shows a close affinity with the encrusting forms *Claracrusta*, *Rothpletzella*, *Girvanella* and to a lesser extent several other calcimicrobes.

Wall ultrastructure consists of alternating laminations of calcite with varying Mg concentrations.

Donezella lutigini Maslov, 1929

The thallus consists of round tubes which form arch-like shapes. The arching is formed by regular branching of the thallus which occurs at a variety of angles to the tube wall. Constrictions occur where partitions segment the tubes into barrel-like divisions. Partitions are small and are always observed to form a perforation between segmentations. A calcite 'shell' is often observed on the outside of the tubes.

Donezella lunaensis Rácz, 1964

The thallus is larger than that of *D. lutigini* but often less distinct. The thallus is tube-like and loosely arranged. A wall structure and a central cavity are clearly discernible. Segmentations divide the thallus into pronounced barrel-like sections as a constriction of the tubes is observed at the location of partitioning. Partitions are generally perpendicular to the wall of the thallus. The central cavity is filled with clear calcite. The wall consists of an outer, thin calcite shell and an inner, thick, darker coloured micritic rim which can be observed to consist of fine needle like structures.

Donezella sp. 1

Fig. 6.18 and 6.19

Holotype. Slide name: Candemuela Mound 8, deposited at the University of Keele, UK.

Type locality and horizon. Carbonate units within the La Majúa Member of the San Emiliano Formation (29T 744467.52 4763114.34). Bashkirian to Moscovian.

Association. Other Donezelloids, Ungdarellaceans.

Description. The thallus is tube-like and consists of isolated, branching growths. The wall is thick and leaves a narrow central cavity. Constrictions are pronounced at locations of internal segmentations along the thalli, resulting in bulbous, lump shaped segments along the tube. Where branching occurs a distinct thickening of the thallus can be observed. The wall consists of a thin, outer, and inner calcite shell with an inner, darker layer. Within the darker layer needle like perforations can sometimes be observed. *Donezella* sp. 1 has a larger thallus than both *D. lutigini* and *D. lunaensis* and the barrel-like segments of the thallus are much more pronounced.

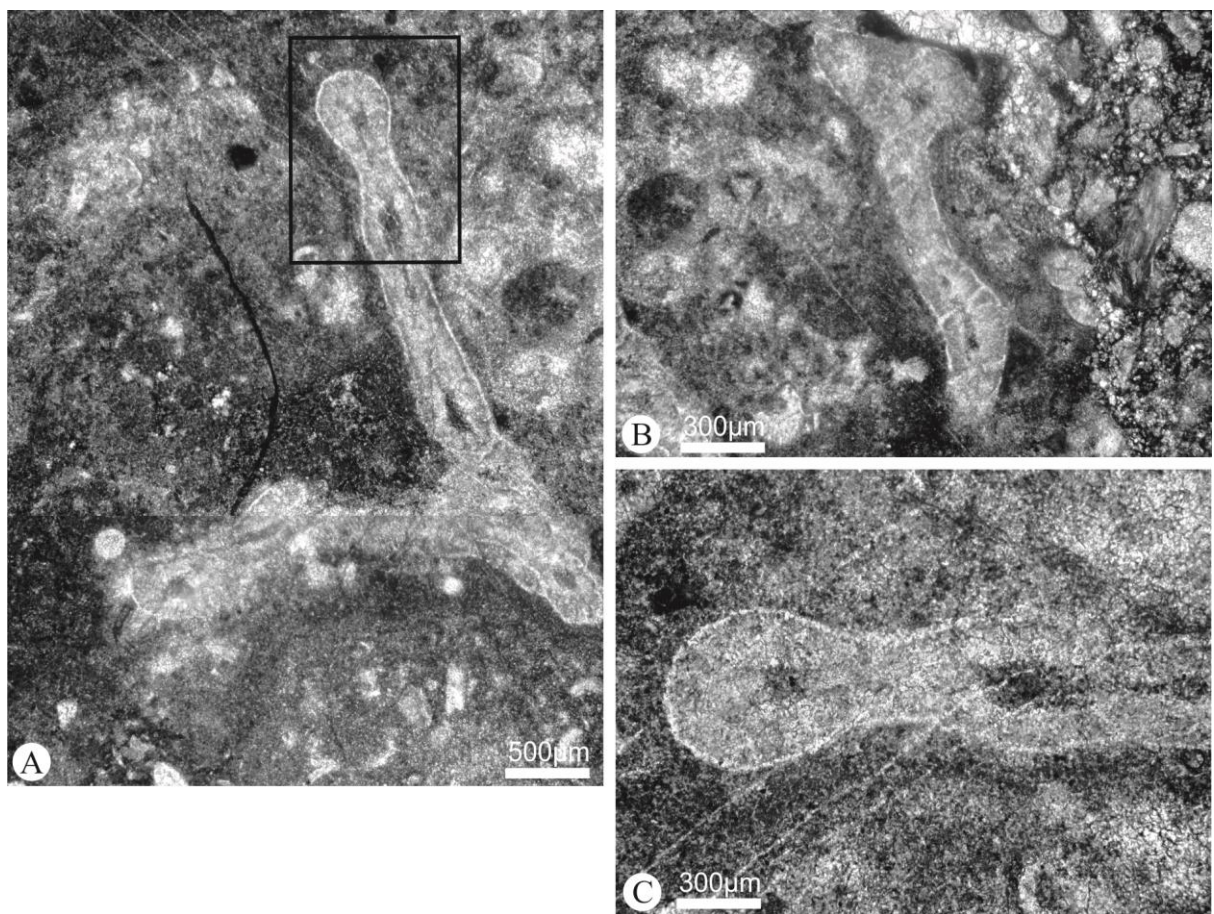
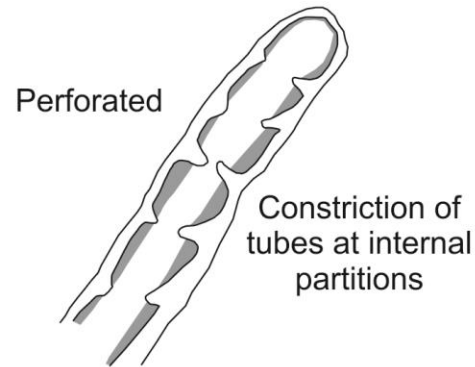


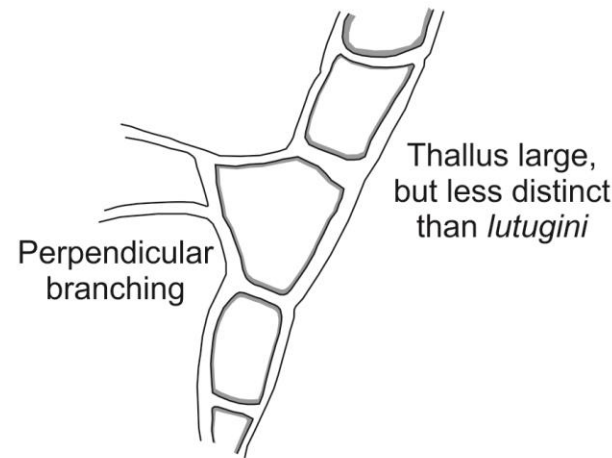
Figure 6.18. *Donezella* sp. 1. Pronounced constrictions along the thalli can be observed, note the thickness of the individual thalli. C. Area highlighted in A.

Donezella lutugini Maslov, 1929



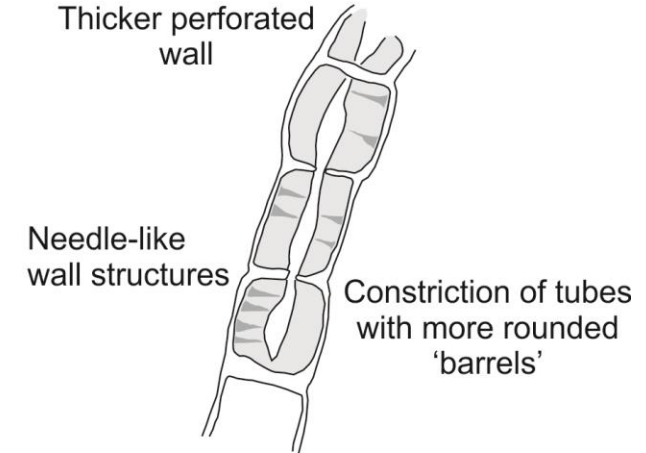
Tube length: 150-600µm
 Tube diameter: 25-100µm
 Diameter of inner part: 16-65µm
 Wall thickness: 8-20µm
 Partition thickness: 5-20µm
 Partition distance: 20-70µm

Donezella lunaensis Rácz, 1964



Tube length: 1000-2200µm
 Tube diameter: 50-275µm
 Diameter of inner part: 100-120µm
 Wall thickness: 33-50µm
 Perforated wall thickness: 23-35µm
 Thickness of calcite layer: 10-20µm
 Partition thickness: 12-20µm
 Partition distance: 100-225µm

Donezella sp. 1



Tube length: 1250-1850µm
 Tube diameter: 200-425µm
 Diameter of inner part: 25-75µm
 Wall thickness: 50-75µm
 Partition thickness: 25-35µm
 Partition distance: 150-475µm

FIGURE - 6.19 Schematic sketches of the three *Donezella* species observed within this study. Major measurements are supplied for each species.

PHYLUM Foraminifera

ORDER Fusulinida

FAMILY Lasiodiscidae Reitlinger, 1956

Genus *Lasiodiscus* Reichel, 1946

Type species *Lasiodiscus granifer* Reichel, 1946

The proloculum is spherical, with a second chamber, tubular, undivided with a planispiral coiling. The secondary chamber increases regularly in size with consequent volutions. The upper (dorsal) side of the coil is concave, whilst the lower (ventral) side is often flat to convex. The wall consists of a clear, hyaline, outer layer and a dark (slightly thicker) micritic inner layer. Along the dorsal side a hyaline cover, consisting of short hyaline pillars, can be found. This cover is thickest toward the proloculum resulting in a flat surface. Along the ventral side the micritic inner layer of the wall forms tubular appendages.

Lasiodiscidae are often found isolated and in samples with a very low diversity amongst foraminifera. Only Tetrataxidae are observed to commonly appear alongside them. The three *Lasiodiscus* described here are differentiated by several factors: the number of volutions of the second chamber, the coiling pattern of the second chamber, the length of ventral appendages and the form and growth direction of these appendages (Fig. 6.19 and 6.20).

Note that all descriptions are from thin sections and all specific characteristics are described from axial and transversal equatorial cuts through individuals from whole rock samples.

Lasiodiscus sellieri Dessauvagie and Dağ, 1963

A spherical proloculum with a diameter of around 20 µm. The second chamber is tubular, undivided, with a planispiral coiling. The second chamber develops 7-10 volutions increasing regularly in size. The total diameter is around 200 µm. The wall consists of a clear, hyaline, outer

layer and a dark (slightly thicker) micritic inner layer. After the first two volutions which are cylindrical the second chamber becomes flattened and slightly kidney shaped. The last volutions are often not in the general plane of coiling. The dorsal side is slightly concave and has a hyaline cover. The ventral side is flat to convex and has short, tubular, appendages which converge toward the proloculum. Fig. Fig. 6.20 A-D and 6.21.

Lasiodiscus sp. 1

Fig. Fig. 6.20 E and 6.21.

Holotype. Slide name: Pinos East 6b, deposited at the University of Keele, UK. Fig. 6.20 E.

Type locality and horizon. Carbonate units within the La Majúa Member of the San Emiliano Formation (30T 258465.30 4763828.33). Bashkirian to Moscovian.

Association. *Donezella*, *Tetrataxis*.

Description. A rounded, slightly flattened, proloculum with a diameter of around 20 µm. The second chamber is tubular, undivided, with a planispiral coiling. The second chamber develops 7 volutions increasing regularly in size. The total diameter is around 200 µm. The wall consists of a clear, hyaline, outer layer and a dark (slightly thicker) micritic inner layer. The secondary chamber shows a kidney-like shape along the entire length of the coil. The dorsal side is concave and has a hyaline cover consisting of hyaline tubes. The ventral side is flat and has appendages, formed from the inner, micritic layer of the wall. Appendages are roughly twice as long as the width of the volution to which they are rooted. The appendages are divergent from the proloculum. Appendages have a distinctive talon like morphology, which results in the tips of the appendages converging toward the proloculum. The morphological variation resembles *Lasiodiscus medusa* Miklukho-Maklay except the secondary, coiled chamber is not as conical and the appendages are divergent from the proloculum and not convergent as in *L. medusa*.

Lasiodiscus Sp. 2

Fig. 6.20 F-I and Fig. 21.

Holotype. Slide name: Pinos East 6a, deposited at the University of Keele, UK. Fig. 6.20 G.

Type locality and horizon. Carbonate units within the La Majúa Member of the San Emiliano Formation (30T 258465.30 4763828.33). Bashkirian to Moscovian.

Association. *Donezella*, *Tetrataxis*.

Description. A spherical proloculum with a diameter of around 20 µm. The second chamber is tubular, undivided, with a planispiral coiling. The second chamber develops 6 volutions with the size increasing to the third volution and then stays the same. The total diameter is around 200 µm. The wall consists of a clear, hyaline, outer layer and a dark (slightly thicker) micritic inner layer. The dorsal side is slightly concave and has a hyaline cover consisting of hyaline tubes. The ventral side is flat to slightly convex and has appendages, formed from the inner, micritic layer of the wall. Appendages are roughly three to four times as long as the width of the volution they are rooted to and are divergent from the proloculum. Appendages are straight. This morphological variation resembles *Lasiodiscus medusa* Miklukho-Maklay except the secondary, coiled chamber is not as conical and the appendages are divergent from the proloculum and not convergent as in *L. medusa*. The Upper Permian species *L. rugosus* Miklukho-Maklay, is similar to, but differs from *L. sp. 2*, in that the second chamber continues to increase in height with consecutive volutions and it has shorter ventral appendages.

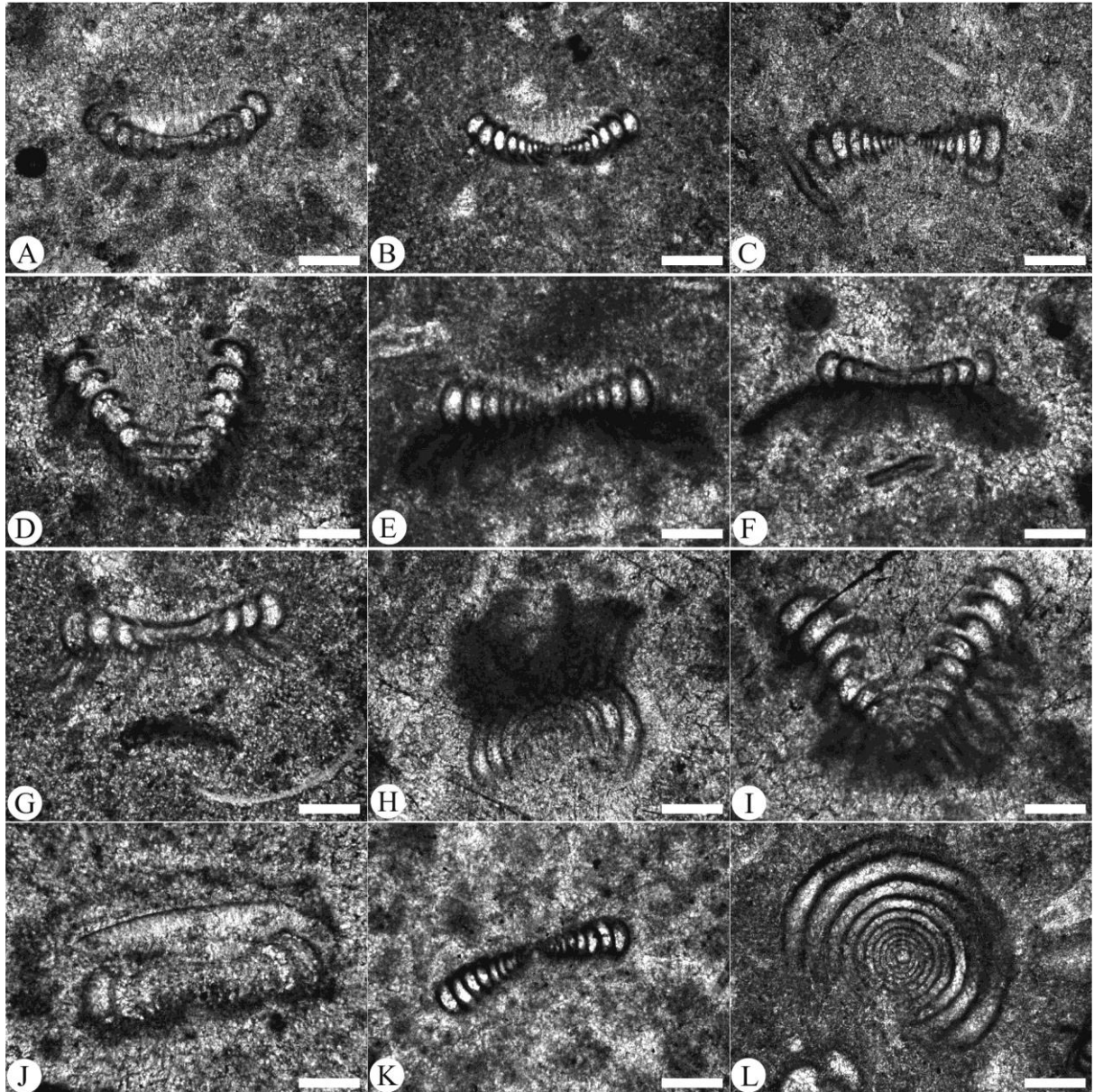
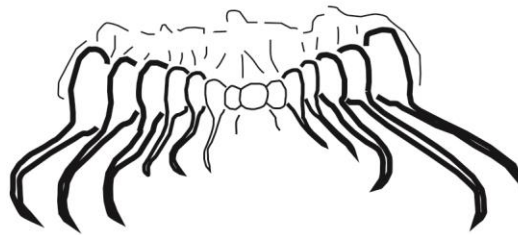


FIGURE - 6.20 Photomicrographs of Lasiodiscidae. A (UNT35), B (CAN14), C (CAN21) and D (PEM9) are specimens of *Lasiodiscus sellieri*. E (PEM6a) shows *Lasiodiscus* sp. 1, note the talon like tubular appendages. F (PEM6b), G (PPM3), H (PEM3), I (PEM3) shows several specimens of *Lasiodiscus* sp. 2, the long tubular appendages can be seen to be divergent from the proloculum. J (SDL10), K (CAN1) and L (CAN21) are images of *Lasiodiscus* sp. The scale bar for all images is 100 μ m. D and I are the result of an oblique cut through the specimens. Note the hyaline columns on the dorsal (concave) sides of the specimens.

Lasiodiscus sellieri Dessauvage and Dağ, 1963



Lasiodiscus Sp. 1



Lasiodiscus Sp. 2

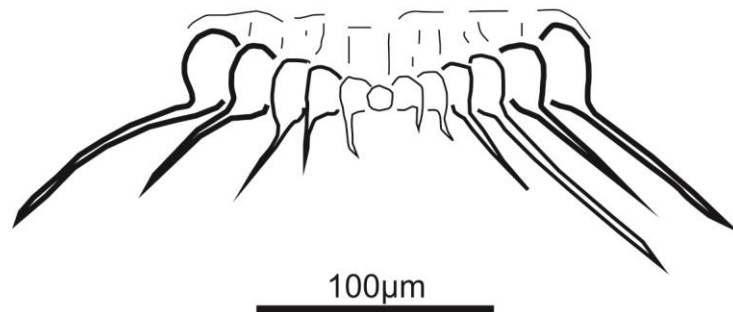


FIGURE - 6.21 Sketches based upon specimens observed within the study. Sketched lines correspond to the darker, microgranular wall of the *Lasiodiscus*. The proloculum and second, coiled chamber is similar in all three species whilst the form and size of appendages varies greatly.

6.7 Chapter summary

Donezellaceans were major components of nearly all of the mounds studied. Indeed, the Sena de Luna Mound was the only location with little evidence of Donezellaceans. Mounds from the San Emiliano Valley have a characteristic biological community consisting of *Donezella* and several encrusting forms. *Donezella* was often found with colonies of *Rothpletzella*, *Claracrusta*, *Girvanella* and occasionally *Wetheredella*. In some examples *Girvanella* could be observed between entwined *Donezella* thalli, often cemented by cement very similar to that of the carbonate shell found on *Donezella*. It is thought that this shell acted as a bio-cement between entwined *Donezella* thalli, and between *Donezella* and other clasts (including other bioclasts) juxtaposed against them. In other cases *Rothpletzella* and *Claracrusta* can be found to encrust, bind and stabilise *Donezella* thickets. Carbonate mud mounds from the San Emiliano Formation (at the type locality) are the result of a relationship between *Donezella* and various encrusting organisms, namely *Rothpletzella* and *Claracrusta*. These biota assumedly formed wave resistant, topographic mounds. The presence of bound and stabilised *Donezella*/encruster assemblages may have encouraged consecutive colonisation of the same area by subsequent *Donezella* and encrusters by acting as substrates. Other biota observed consist of low diversity assemblages and often consist of biota which may represent organisms living in a stressed environment (e.g. *Tetrataxis*, miliolinid foraminifera). There appears to be a reduced population or complete lack of grazers within environments where they would normally be expected. Bryozoans, corals and other biota often associated with carbonate deposits are generally restricted to mixed clastic and bedded carbonate lithologies and are rarely seen within mounds within the San Emiliano Valley. Dasyclad algae, foraminifera, bryozoans, corals and other shelly fauna are more common within Bernesga Valley mounds. *Thartharella* and calcisponges, which were reported as a main component of mounds from the Bernesga Valley (Samankassou, 2001) are absent from the San Emiliano Valley.

Several, distinct palaeoecological assemblages are recognisable from the studied material. Mound and off-mound carbonates (i.e. those carbonates found within the same unit as mounds) exhibit similar biological communities, however, distinct variations were observed between the

abundance of certain biota between the communities. Bedded limestones (in particular those of the Pinos Hairpin and the Pinos Pylon Mound) are associated with a palaeoecological assemblage distinct to those from mound bearing strata.

Mound bearing units are typically dominated by *Donezellacean* algae and the associated encrusting forms *Rothpletzella*, *Claracrusta*, *Girvanella* and several less common forms. Foraminifera are present, but in low numbers. Where found within mounds the preservation of the biota is generally very good. Off-mound carbonates tend to exhibit the same biological assemblage as the mounds they surround; in addition, they often show a higher biodiversity with corals and bryozoans being observed, with Foraminifera becoming more common. Preservation of off mound biota is typically lower than that of mound biota.

Bedded limestones were found to host the highest biodiversity with communities of *Archaeolithophyllum*, *Ungdarella* (and some *Komia*) and *Petschoria* being the dominant biota. *Donezella*, *Rothpletzella*, *Girvanella* are using the dominant biota as a substrate as are rare stromatoporoids and chaetetid sponges. Foraminifera and Tuberitinids, whilst not common, are present.

It can be seen from the sedimentology of the area that environmental conditions and therefore environmental niches evolved quickly during deposition (the rapid changes from clastic material to carbonate being an example). The presence of a restricted biota within an environmental niche that is newly opened suggests that the biota observed within this study most likely represents a colonial, pioneer assemblage.

Three new morphological variants of species are presented: *Donezella* sp. 1, *Lasiodiscus* sp. 1 and *Lasiodiscus* sp. 2.

7. Siliciclastic Units

The relationship between the sedimentology of the three constituent members of the San Emiliano Formation represents a coarsening upwards megasequence, with small scale cyclicity observable within each. As discussed in Chapter 1, the depositional setting of the San Emiliano Formation is generally agreed to be within a foreland basin system at the head of the Variscan orogeny (e.g. Bahamonde *et al.*, 2002). Bowman (1979, 1982, 1985) described the clastic sediments of the San Emiliano Formation in detail and concluded that the majority of clastic material was deposited at river dominated delta lobes in a regressive environment. Whilst the carbonate units of the La Majúa Member were the result of marine transgressions.

The major limestone units of the La Majúa Member of the San Emiliano Formation are separated by regressive deltaic and shallow marine clastics (see Chapter 1.2 *Geological setting and Sedimentology of the San Emiliano Formation*). The clastic intervals are much thicker than the carbonate units. The carbonate units are generally 3 - 5 m in thickness (though in places are much thicker, i.e. the Pinos Pylon Mound) whilst the clastic units range from around 20 - 45 m in thickness. The La Majúa Member is conformably sandwiched between the lower Pinos Member, which consists of shales, silts and some thin sandstones and the upper, Candemuela Member, which consists of deltaic sediments, seatearths and coal seams. A detailed microfacies analysis has revealed the depositional environment of the carbonates from the San Emiliano Formation, a study of the clastic material will allow a better environmental model to be constrained. Within foreland basin systems it is well documented, from both models and modern examples, that characteristic sedimentation takes place in 'facies belts' parallel to the advancing orogenic front (DeCelles and Giles, 1996 & Mutti *et al.*, 2003). By logging the sediments and comparing them to those of the modelled and modern examples it should be possible to constrain the position of the San Emiliano Formation in relation to the foreland basin (to a better degree than the 'foredeep', which refers to the type of basin and not a depozone, as given by Bahamonde *et al.*, 2002).

Foreland basins are formed as a result of flexural subsidence due to the load of an orogenic wedge upon a 'foreland plate'. Each foreland basin differs in terms of geological (structural style, sedimentation source and deposition) and geodynamic style but their overall evolution is essentially the same (Mutti *et al.*, 2003). Firstly, the foreland initiates and the foredeep remains under-filled in regards to sediment and experiences progressive subsidence. The second stage involves the migration of the foredeep due to the advancing orogenic wedge and the dominance of turbidite deposition. The final stage sees turbidite deposition halt, being replaced with fluvio-deltaic and alluvial sedimentation (Covey, 1986). The foreland consists of four discrete depozones which are referred to as: the wedge-top, foredeep, forebulge and back-bulge depozones (Fig. 7.1).

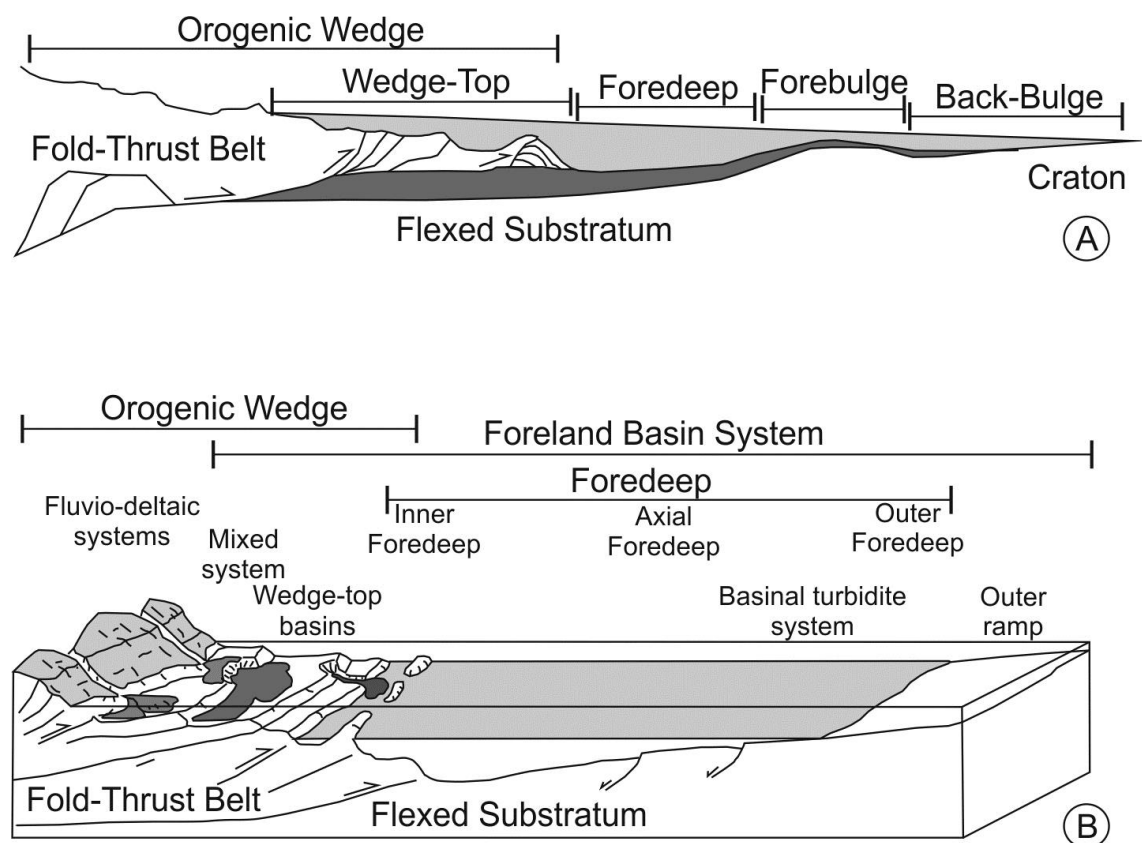


FIGURE - 7.1 Schematic diagrams of idealised foreland basins. A, Schematic cross-section showing the four discrete foreland depozones of the foreland basin system. Deposits are shown as light grey. After DeCelles and Giles, 1996. B, A schematic diagram showing the main depositional areas and associated sedimentology expected of an alpine type foreland basin. After Mutti *et al.*, 2003.

Three sedimentary logs were taken which encompassed clastic intervals associated with the three different types of carbonate unit commonly found within the La Majúa Member. These carbonates are: non-carbonate mound bearing micrites (see 7.1 Log - Unit 3 below), cyclical ‘phylloid’ dominated micrite and marl beds (see 7.2 Log - Unit 4 below), and carbonate mound bearing micrites (see 7.3 Log - Unit 8 below). The logs were taken from well exposed sections along roads, the locations of which can be seen on Figure 7.2. UTM’s of locations for each log are given at the beginning of each section.



FIGURE - 7.2 Location map indicating where the three logs presented here were taken. The colour of each arrow reflects the unit number that it is associated with (see legend).

The sediments encountered tended to range from silts to coarse sand with all grades in-between observed (Fig. 7.3). Weathered surfaces ranged from a tan brown to purples and greys, fresh surfaces were grey. The sediments were sub-rounded and well sorted, beds in which the sedimentary grade fined upwards were common. The units showed a general coarsening trends over several metres. Silts were often present toward the base of the sections into sands. Rare, thin micro-conglomerates were observed toward the base of unit 8. Some thin coal bands were observed and in places small lenses of coal were found. Sedimentary features observed included ripples, channels, some minor cross bedding and some laminar units. The sediments generally

reacted with HCl indicating that the cement was most likely calcareous in nature. Plant fossils were commonly observed within all of the clastic successions and within all of the individual lithologies, other fossils were rare, but gastropods, brachiopods and isolated corals (rugose and aulopodid) were found. The presence of corals may suggest the transportation of talus material from a local carbonate producing area. The studied sections often exhibited several fractured areas, as these sections are exposed due to road cuttings it is difficult to ascertain if these fractures were geologically (and/or) anthropogenically generated. Several areas of extensive weathering and vegetation cover are also present.

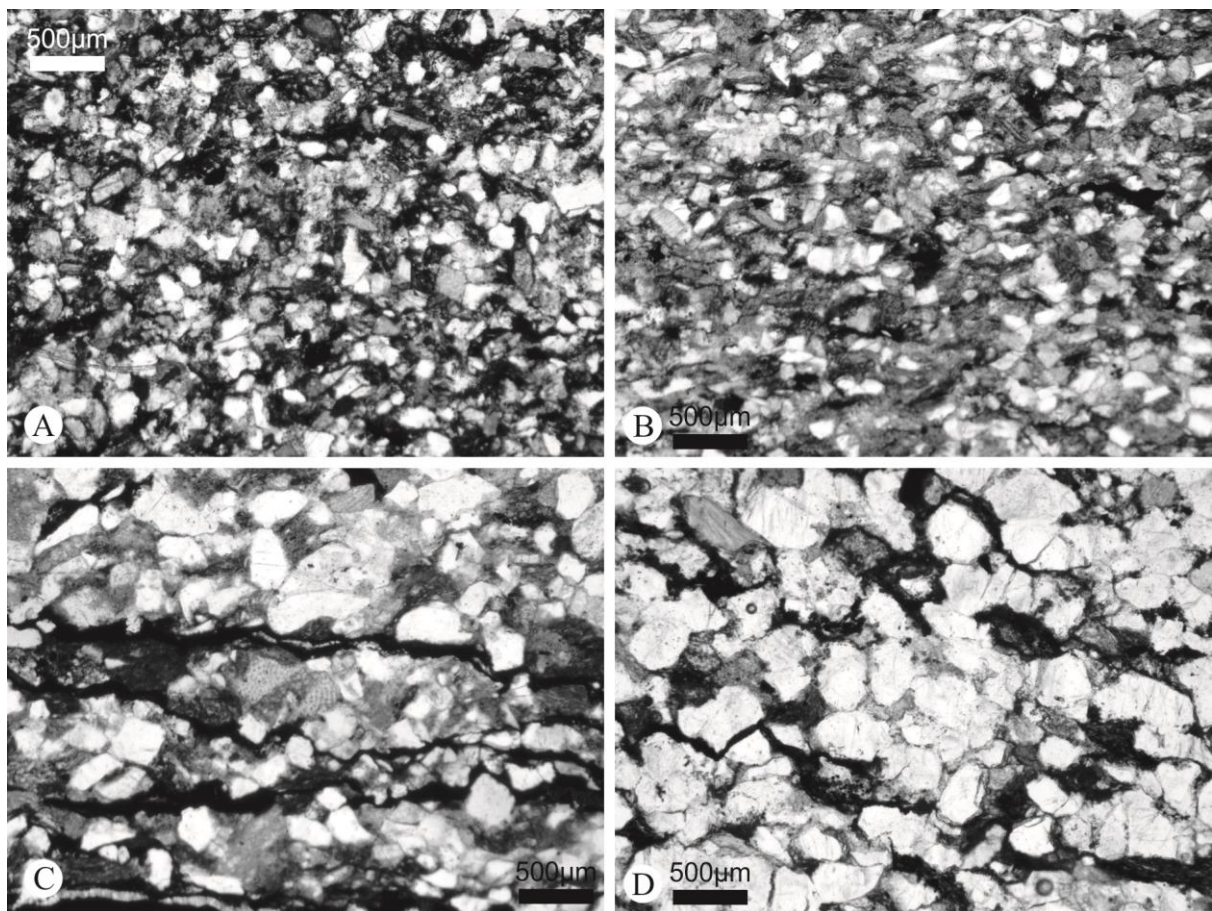


FIGURE 7.3 - Photomicrographs of silt (A and B), fine grained sand (C) and medium/coarse grained sandstone (D). In each example the white grains are quartz and the darker material is calcareous cement (grey colour) or organic content (black colour). The grains are sub-rounded and pore space is filled by cement and organic matter.

87.1 Log - Unit 3

(29T 744591.61 476521.26)

A log of Unit 3 comprises just over 46 m of mixed siltstone and sandstones with interbedded limestones and two prominent coal bands. The majority of clastic material occurs as cyclic units consisting of basal siltstones, grading up to coarse/very coarse sandstones, in places limestones are found at the base of these cycles and coals are found at the top. Cyclic units span up to 6 metres in thickness in parts of this succession (Fig. 7.4). A typical cycle consists of approximately 2 m of calcareous, fissile siltstones with rare nodular inclusions, these siltstones are highly fossiliferous with both plant remains and shelly fauna common. Above the siltstones are around 1 m of interbedded silt- and fine grained sandstones. This grades into 2.5 m of fine to coarse sandstones which are rippled and show cross bedding toward the top. Within this coarsening upward sequence many, small scale coarsening up sequences can be observed, often as individual graded beds. Shelly fauna including brachiopods and gastropods are observable within many of the sandstone beds. A thin coal is generally found at the top of a sequence. Several fining upward sequences were observed within this unit, these were generally much thinner than the coarsening upwards sequences (approximately 1 m). Sands are generally well rounded. The conspicuous carbonate unit at the top of this sequence consists of bedded micrite, which is a dark blue/grey in colour and exhibits a characteristic porcelaneous fracture. See Appendix 3. *Sedimentary Logs* for full log.

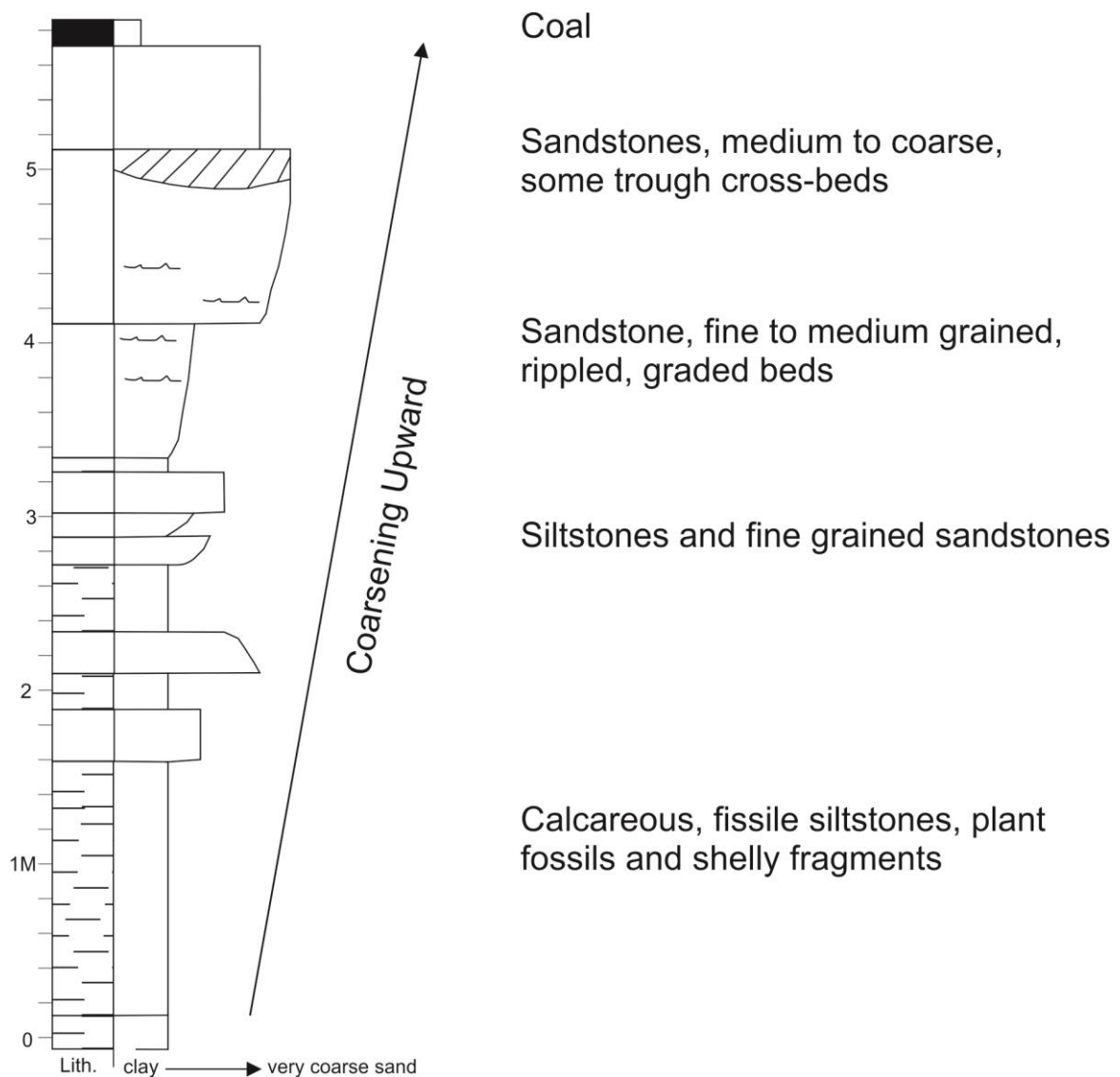


FIGURE - 7.4 Schematic sketch of a typical cyclic unit associated with the sediments of Unit 3. Dashed lithology = silts, blank lithology = sandstone, black lithology = coal seam.

7.2 Log - Unit 4

(30T 257817.79 4763455.88)

The log of Unit 4 is the shortest of the representative logs taken, measuring just over 20 m of loggable sediments and 28 m in total thickness. Cyclicity is observed on a much smaller scale within this log than elsewhere and beds are much thinner. The sediments are predominantly clastic, with carbonates representing just the final 3 m of the log. The clastic sediments consist of thin beds (centimetre scale) of siltstone to fine sandstone. Often,, repetitions of siltstone/fine sandstone laminae (millimetre scale) can be observed within beds, these may represent tidal

bundles. Coarsening upward cycles interpreted for the sediments generally span a metre of lithological thickness (Fig. 7.5). Some crossbedding, ripples and load structures are found throughout the section (particularly toward the top of a coarsening upward sequence. The majority of this log consists of sediments with a very consistent coarseness (mostly siltsto fine sands), indicating that the energy levels of the environment of deposition were relatively constant. The fine grained nature and related sedimentary structures (ripples and cross bedding) indicates a shallow depositional environment, possibly on top of a delta lobe. The associated carbonate unit consists of 3m of alternating ‘phylloid’ algal dominated limestones and marls. See Appendix 3. *Sedimentary Logs* for full log.

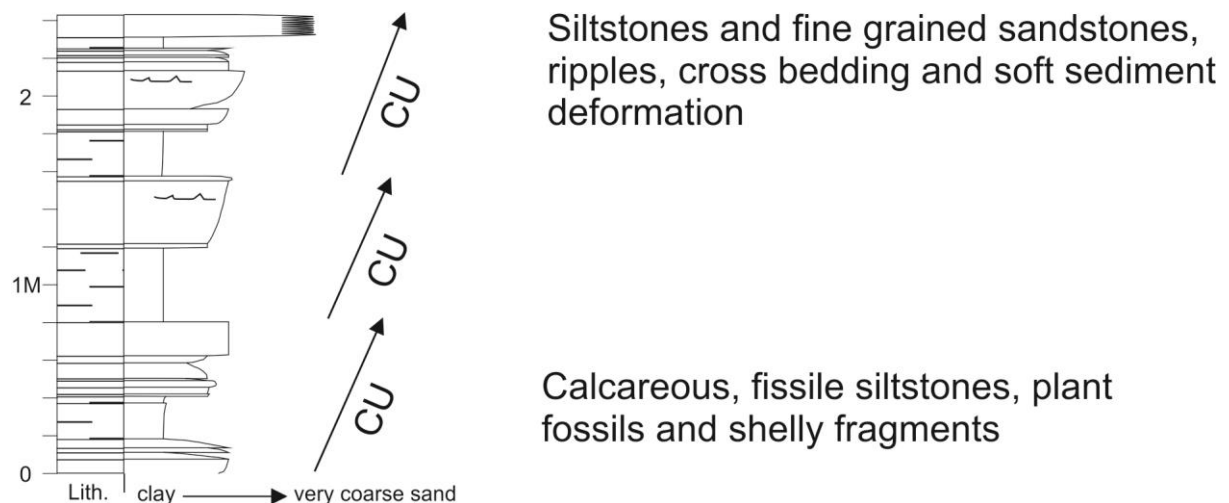


FIGURE - 7.5 Schematic sketch of a typical cyclic unit associated with the sediments of Unit 4. Dashed lithology = silts, blank lithology = sandstone.

7.3 Log - Unit 8

(29T 744475.93 4763092.62)

Measuring approximately 51 m in total thickness, this log is the longest of the representative logs taken. The section consists of cyclic units which generally consist of 1 to 3 m of coarsening upward sediments (Fig. 7.6). Siltstones, often with a calcareous cement form the base of the cycles

which grade up to medium, and quite often coarse grained sandstones. Ripples are a common feature observed in places as is the presence of plant material, which on occasions is preserved as stems and leaves of up to 9.5 cm in length. Several micritic limestone beds, averaging around 50 cm in thickness, are found throughout the sequence. The upper most carbonate unit associated with this log is an 8 m thick mound-bearing limestone. The majority of cycles interpreted for this log are regressive with rare transgressive events. Regressive events are represented by sedimentation of several metres thick, often consisting of very fine to fine sandstones with cross bedding and ripple marks grading upwards into coarse and very coarse sandstone beds. Several metres of beds from this section show similar grain sizes and small scale (individual beds) coarsening upwards trends. The coarsening upwards cycles may represent the sedimentary filling of the basin being more rapid than subsidence. Cycles where grain size is roughly the same for several metres probably represents times where the sediment filling of the basin is equal to the subsidence and may therefore represent prolonged tectonically active periods as flexure driven basin subsidence keeps pace with the overriding eustatic sea-level rise. See Appendix 3. *Sedimentary Logs* for full log.

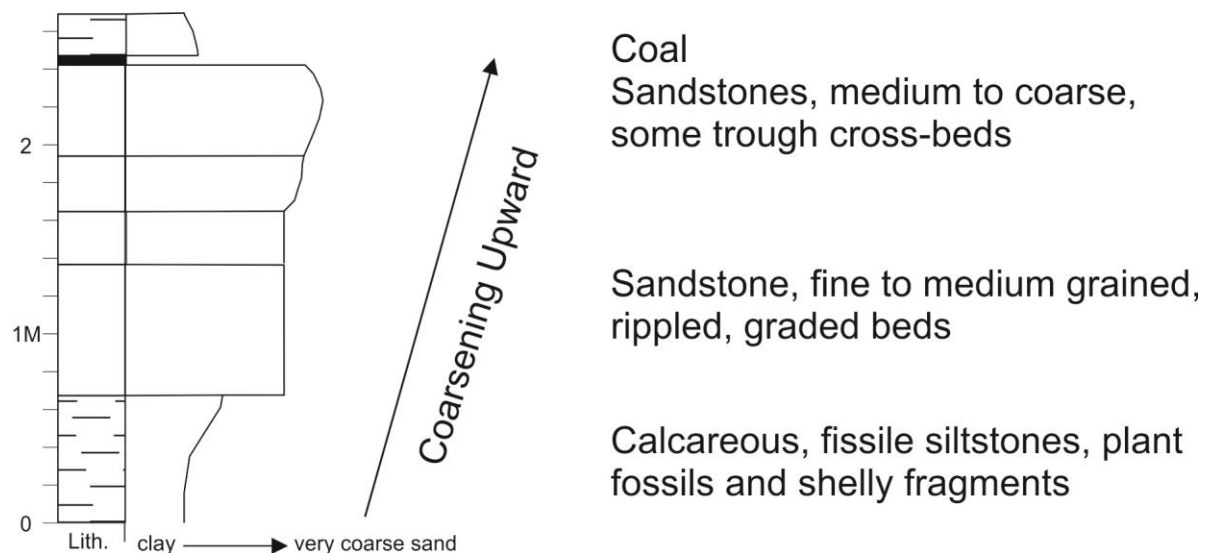


FIGURE - 7.6 Schematic sketch of a typical cyclic unit associated with the sediments of Unit 8. Dashed lithology = silts, blank lithology = sandstone, black lithology = coal seam.

7.4 Interpretation

As discussed by Bowman (1979, 1982 and 1985) the clastic units of the La Majúa Member of the San Emiliano Formation represent coarsening upward cycles. These cycles reflect periods of deltaic progradation into a shallow marine environment. The prevalence of plant fossils throughout the entire succession indicates a short transport distance and a low energy environment. The limestone units which are found within the La Majúa Member are interpreted to have been deposited during marine transgression. The type of sediments encountered seem to imply that sedimentation of the San Emiliano Formation took place in peripheral foredeep depozones. The sediments of the San Emiliano Formation are almost devoid of folds, faults or rotated cleavages - all of which are excellent evidence for deposition within a wedge top depozone (DeCelles & Giles, 1996). Early San Emiliano sediments consist of fissile siltstones and 'black shales' which are indicative of deep-marine sedimentation, whilst the La Majúa and Candemuela Members show increasing evidence for the shallowing of the basin (i.e. coals). The presence of deltaic deposits may be an indication that the wedge top depo-zone was subaerial and the foredeep was submarine, or that the foredeep was tilted, the delta occupying the transition zone (Miall, 1981 and Baltzer & Purser, 1990). The lack of unconformities might suggest that deposition took place within the axial part of the foredeep depozone. Regressive sedimentation is expected within a foreland basin, rapid subsidence as a result of the load provided by the advancing mountain front and a ready supply of sedimentary material derived from said mountain front would result in the observed coarsening upward cycles. The load related to tectonic movement would create subsidence (creating accommodation space) in the basin; this would be filled by locally (hinterland) derived sediments which would progressively fill the basin. Further loading would create more subsidence which, again, will be filled by locally derived sediments. Several fine sediment horizons often associated with thin coal bands and ripple structures are interpreted to represent shallow environments above a delta lobe - possibly as a result of the basin becoming filled. Transgressive events may be related to climatically driven sea-level change (glacio-eustasy), or may be the result of tectonic activity. Sudden transgressive events are most

likely a response of a deepening basin due to the advancing thrust front. Transgressions generally result in the deposition of a carbonate unit as the delta lobes were abandoned. Bowman (1985) provided sedimentation rates for the formation, stating that for the San Emiliano Formation sedimentation rates were at least 35 to 40cm per 1000 years (a relatively high rate of sedimentation/subsidence). The 8 main carbonate units within the La Majúa Member occur every 100 to 200 metres, taking the higher sedimentation rate of 40cm per 1000 years this would mean a temporal scale of 100 m of sediment per 250,000 years, or 200 m of sediment per 500,000 years for the deposition of each cyclic unit (1cm per 2.5 years). At the upper end of predicted sedimentation rates (i.e. 40 cm per 1000 years) this apparent cyclicity fits the timings of the first Milankovitch cycle - eccentricity (413,000 years per cycle). This would mean that the depositional environments in which the limestone units were deposited is the result of glacio-eustatic driven eustatic sea level rise and fall, superimposed upon tectonically (and sedimentologically) driven relative (basin wide) sea level rise and fall.

Compared to the sediments of the Bernesga Valley (i.e. the Lois-Cigüera Formation) the San Emiliano Formation appears to have been deposited coevally, but in different depositional environments. Bowman (1985) reports turbidity driven sequences consisting of both sandstones and carbonates. He produced a generalised palaeogeography which showed the San Emiliano Formation being deposited close to a rising hinterland whilst the Bernesga Valley sediments are deposited as a submarine fan, both bounded by the Cantabrian Block to the north. When considering more recent foreland basin reconstructions and models (i.e. those of DeCelles & Giles, 1996 and Mutti *et al.*, 2003, and similar) along with Bowman's (1985) work and the logs and microfacies evidence from this study the depositional environment can be further constrained.

7.5 Chapter Summary

San Emiliano Formation sediments are dominated by cyclothems controlled by an overall regressive trend punctuated by transgressions. Clastics comprise of calcareous siltstones and sandstones which have a high organic (plant debris) component. Clastics were deposited on the

top of a delta lobe whilst carbonates were deposited in a time of clastic input quiescence. Deposition took place in the transitional zone between an envisaged sub-aerial wedge top and the axial zone of the foredeep of a foreland basin. The Late Carboniferous sediments of the San Emiliano Valley were deposited in a shallower environment to those of the Bernesga Valley.

8. Geochemistry

Element and stable isotope analysis of carbonate rocks can provide important data on both the sedimentological (including environment of deposition and composition) and diagenetic histories of any particular sample. Analysis can take place as a whole rock, bulk analysis or can focus on individual components of the rock. Individual fossils or cements or specific parts of these (fossil walls or cement crystals) can be investigated. In an attempt to investigate the possible causes of nucleation and formation for the carbonate mud mounds analysed in this work pilot studies of both the elemental composition and oxygen and carbon stable isotopes were conducted (see 3. *Methods and Materials*). These pilots were designed to determine whether two, well documented, nucleation and growth mechanisms were operating within the San Emiliano Formation at the time of carbonate development. These mechanisms were hydrothermal venting (e.g. Belka 1998 and Mounji *et al.* 1998) and hydrocarbon seepage (e.g. Peckmann *et al.* 1999; Sager *et al.* 2003 and Naeth *et al.* 2007, see 2.5.1 *Hydrothermal Venting and Hydrocarbon Seepage* for details. The isotope ratios of $^{18}\text{O}/^{16}\text{O}$ and $^{13}\text{C}/^{12}\text{C}$ can be used to infer processes operating at the time of carbonate production and the subsequent lithification and diagenesis. Oxygen isotope ratios can be used to predict temperature of the fluid from which the carbonate mud precipitated whereas carbon isotope ratios can indicate the contribution of hydrocarbons to precipitation (Wu and Chafetz, 2002, Peckmann and Thiel, 2004 & Campbell, 2006 etc.). A chemostratigraphic log was made utilising a handheld XRF (see 3. *Methods and Materials*) in an attempt to document cyclical sedimentation (as seen in the field and sedimentary logs), to investigate if tectonic activity could be recognised within the San Emiliano Formations sediments and to see if this had any recognisable effect on the formation of the mud mounds. Orbitally forced stratigraphy has been successfully recognised since Hays *et al.* (1976) at a range of scales and in stratigraphy representing a wide range of climatically sensitive lithologies from all geological ages (Hinnov, 2000). Tectonic activity juxtaposed atop of a cyclic pattern has also been previously recognised in such studies (e.g. Müller *et al.*, 2001).

8.1 Stable Isotope Geochemistry

$^{18}\text{O}/^{16}\text{O}$ and $^{13}\text{C}/^{12}\text{C}$ isotope ratios were obtained for six whole rock samples. Four of the samples are from the eight carbonate unit of the La Majúa Member (one sample from the Candemuela mound and three from across Unit 8) of the San Emiliano Formation within the San Emiliano Valley, one came from a mound from the very base of the La Majúa Member (Pinos East Mound) and the remaining sample was from a mound in the Bernesga Valley (San Martin Mound). When plotted as a scatter graph the data can be clustered into two groups; the first group (Group 1) consists of the four samples from Unit 8 (i.e. the three from across Unit 8 and the Candemuela Mound) and a second group (Group 2) consisting of the other two mounds (Table 8.1 and Fig. 8.1). Group 1 has a slightly positive $\delta^{13}\text{C}$ value which averages +2.8‰ with a range of +2.4 to +3‰. The group has a negative $\delta^{18}\text{O}$ value which averages -6.7‰ and has a range of -4.8 to -7.7‰. Group 2 has a $\delta^{13}\text{C}$ averaging +4.1‰ with a range of +3.9 to +4.4‰. $\delta^{18}\text{O}$ values for the sample average -3.3‰ with a range of -2.9 to -3.7‰, and these values mean that Group 2 has a more positive $\delta^{13}\text{C}$ and $\delta^{18}\text{O}$ value than that for group 1. Carbonates which are related to hydrocarbon seepage have been found to be strongly depleted in $\delta^{13}\text{C}$ (e.g. Peckmann *et al.*, 2001, Campbell *et al.*, 2002 & Peckmann and Thiel, 2004). In modern carbonate precipitation found at methane seeps, Peckmann *et al.* (2001) found the deposits to have $\delta^{13}\text{C}$ values which ranged from -28.9 to -37.3‰. In ancient samples $\delta^{13}\text{C}$ values have been found to be as low as -69‰ (Campbell *et al.*, 2002). The data show that the carbonates from the studied material is slightly enriched in regards to $\delta^{13}\text{C}$, and that the carbonates have not inherited a low $\delta^{13}\text{C}$ value and are therefore, not related to hydrocarbon seeping. Mounji *et al.* (1998) observed $\delta^{18}\text{O}$ levels of between -11.2 and -8.5 for the Kess-Kess mounds of Morocco, which they interpreted to give a minimum temperature of 31°C for carbonate precipitation.

Sample	$\delta^{13}\text{C}$ PDB	$\delta^{18}\text{O}$ PDB	UTM	STD	$\delta^{13}\text{C}$ PDB	$\delta^{18}\text{O}$ PDB
CANDEMUELA-7	+3.0	-4.8	29T 744475.20 4763112.26	CC73857/MCS-21	-0.7	-9.2
U8-4	+2.4	-7.0	29T 739261.17 4761443.03	CC73863/MCS-21	-0.7	-9.2
U8-23	+2.9	-7.7	29T 741934.59 4762183.92	CC73868/MCS-21	-0.7	-9.2
U8-39	+2.8	-7.4	29T 743609.17 4762848.74			
PINOS-EAST-G	+4.4	-3.7	30T 258483.65 4763822.54			
SAN-M-M	+3.9	-2.9	30T 279065.53 4758616.59			

TABLE - 8.1 The readings from the stable isotope pilot study, including the six samples from the study area (dark grey) and three standards (light grey). PDB = Pee Dee Belemnite.

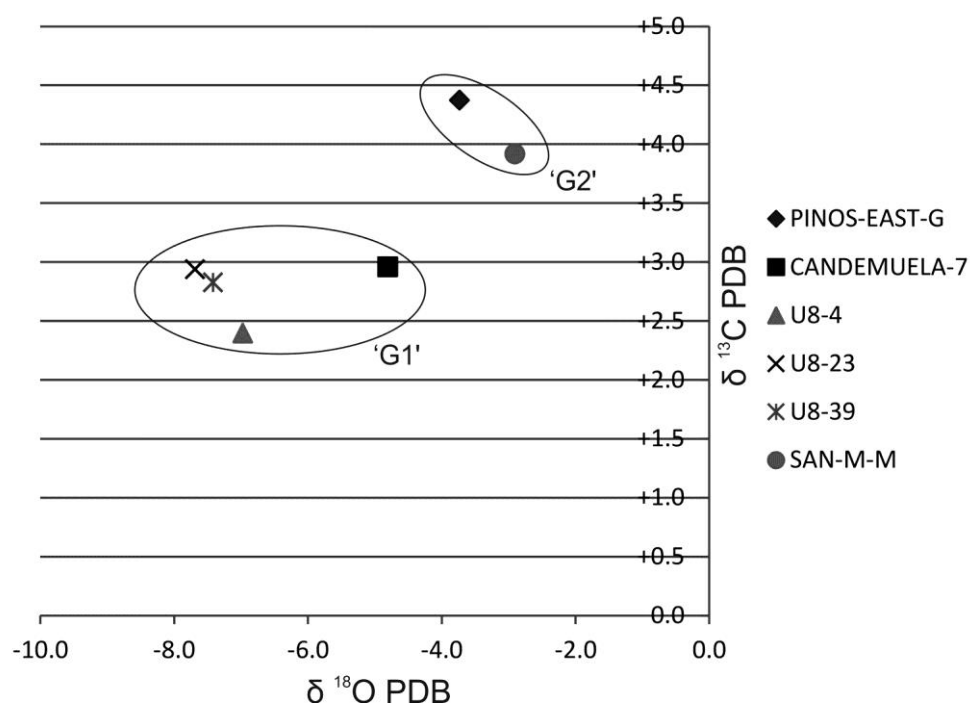


FIGURE - 8.1 A scatter graph showing the relationship between $\delta^{13}\text{C}$ and $\delta^{18}\text{O}$ ratios for the three samples analysed. The samples have been clustered into two groups, G1 - group 1 and G2 - group 2. PDB = Pee Dee Belemnite.

8.2 X-Ray Fluorescence Geochemistry

A pilot study was undertaken to investigate if hydrothermal venting may have been operational at the time of mound nucleation and formation. The pilot study was conducted on powdered tablets made from whole rock samples, the chosen samples were the same samples upon which the isotope pilot was conducted. To recognise hydrothermal venting the presence of elevated levels of certain elements are

looked for. Elements commonly associated with hydrothermal deposits include Cu, Ni, Zn, Co, Ca and Ba (Corliss *et al.*, 1978). From the pilot no elevated levels of these elements were observed.

A chemostratigraphic log (consisting of 600 locations separated approximately 10cm apart) was compiled along the Candemuela Mound road section, the log included the clastic sediments below the mound, and the mound itself. The handheld XRF used provided an analytical range of 31 elements: Mg, Al, Si, P, S, Cl, K, Ca, Ti, V, Cr, Mn, Fe, Co, Ni, Cu, Zn, As, Se, Bi, Rb, Sr, Zr, Nb, Mo, Pd, Ag, Cd, Sn, Sb and Ba. Of these, 10 elements were detected with an error of lower than 10%, these were: Al, Si, K, Ca, Ti, Mn, Fe, Rb, Sr and Zn. The major elements (those elements which have > 1000 ppm: Al, Si, K, Ca and Ti) are displayed as a weight % (they are converted to oxides). Trace elements (those elements with < 1000 ppm: Mn, Rb, Sr and Zr) are displayed in ppm (see *Appendix 4. XRF Data* for raw data). Line graphs of both the major and trace elements were produced (Figs. 8.2 and 8.3). The line graphs show that the elements recorded show a similar pattern, the exception being Ca, which shows the opposite (Fig. 8.4 emphasises this). Al, Si, K, Ti, Mn, Rb, Sr and Zr all show a relatively stable profile for the first 300 readings, at which point they show an increase in concentrations before peaking just before 500 and then dramatically reduce or are completely absent. The carbonate component of the stratigraphy is conspicuous. A carbonate rock is defined as containing at least 50% carbonate by weight (Flügel, 2004), and this component is highlighted on figures 8.2, 6.3, and 8.4. As observed in the sedimentary log for the Candemuela mound and its related exposure, carbonates are mostly restricted to the top of the log; the carbonate percentage of the lithologies suggests that several of the limestones logged as such are more likely to be highly carbonate rich clastics or marls. Where deposition of carbonates occur, the clastic components are greatly reduced or absent. As the Ca values increase when the values for the other elements decrease (and *vice versa*) it is logical to assume that all measured elements bar Ca have a detrital (clastic) origin. To establish relationships between the individual elements cross-plots were produced. In order to interpret any signals (orbital, autocyclic or tectonic) recorded within the chemostratigraphic log several of the elements were investigated in more detail and are presented in a correlation panel (Fig. 8.6).

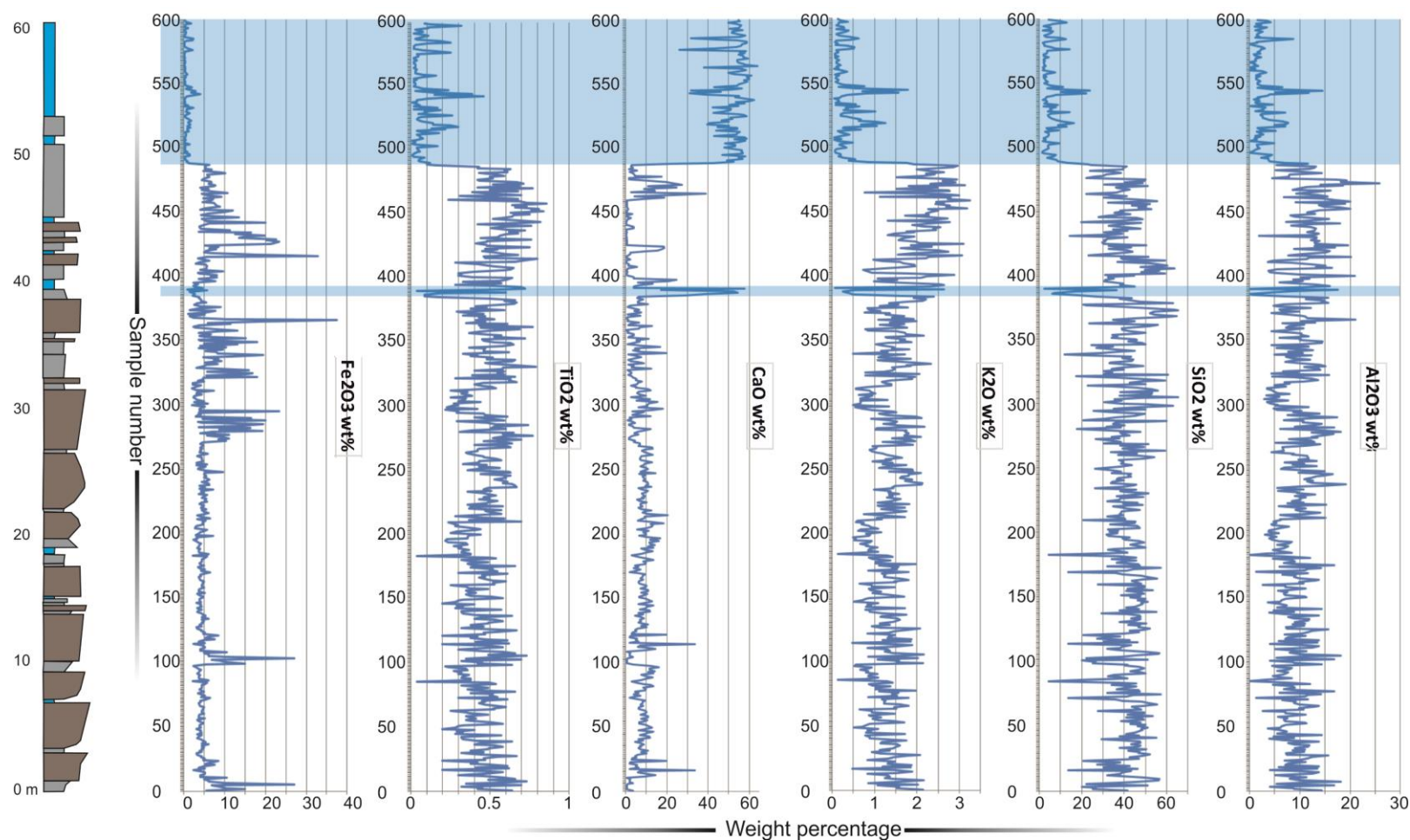


FIGURE - 8.2 A correlation panel of chemostratigraphic logs corresponding to the weight % for the oxides of Al, Si, K, Ca, Ti and Fe. The light blue boxes represent carbonate lithologies due to the weight % of CaO being above 50%. The other oxides (which are all interpreted as having a detrital origin) show a negative correlation with CaO). The line plots for Al, K and Ti oxides show an increase in weight % before a dramatic drop (i.e. the start of carbonate material). Schematic log included for reference, lithologies; grey = siltstone, brown = sandstone, blue = limestone.

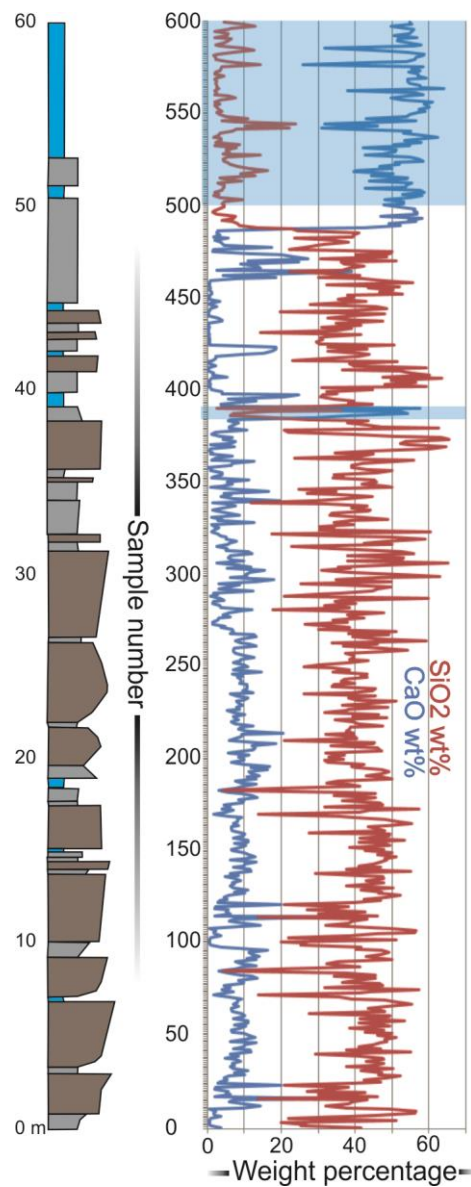


FIGURE - 8.3 A comparison between CaO (blue line) and SiO₂ (red line), this figure emphasises the negative correlation between the two. The blue boxes indicate where carbonate sedimentation occurs, CaO can be seen to be above 50% weight, indicating the sample is a carbonate. Schematic log included for reference, lithologies; grey = siltstone, brown = sandstone, blue = limestone.

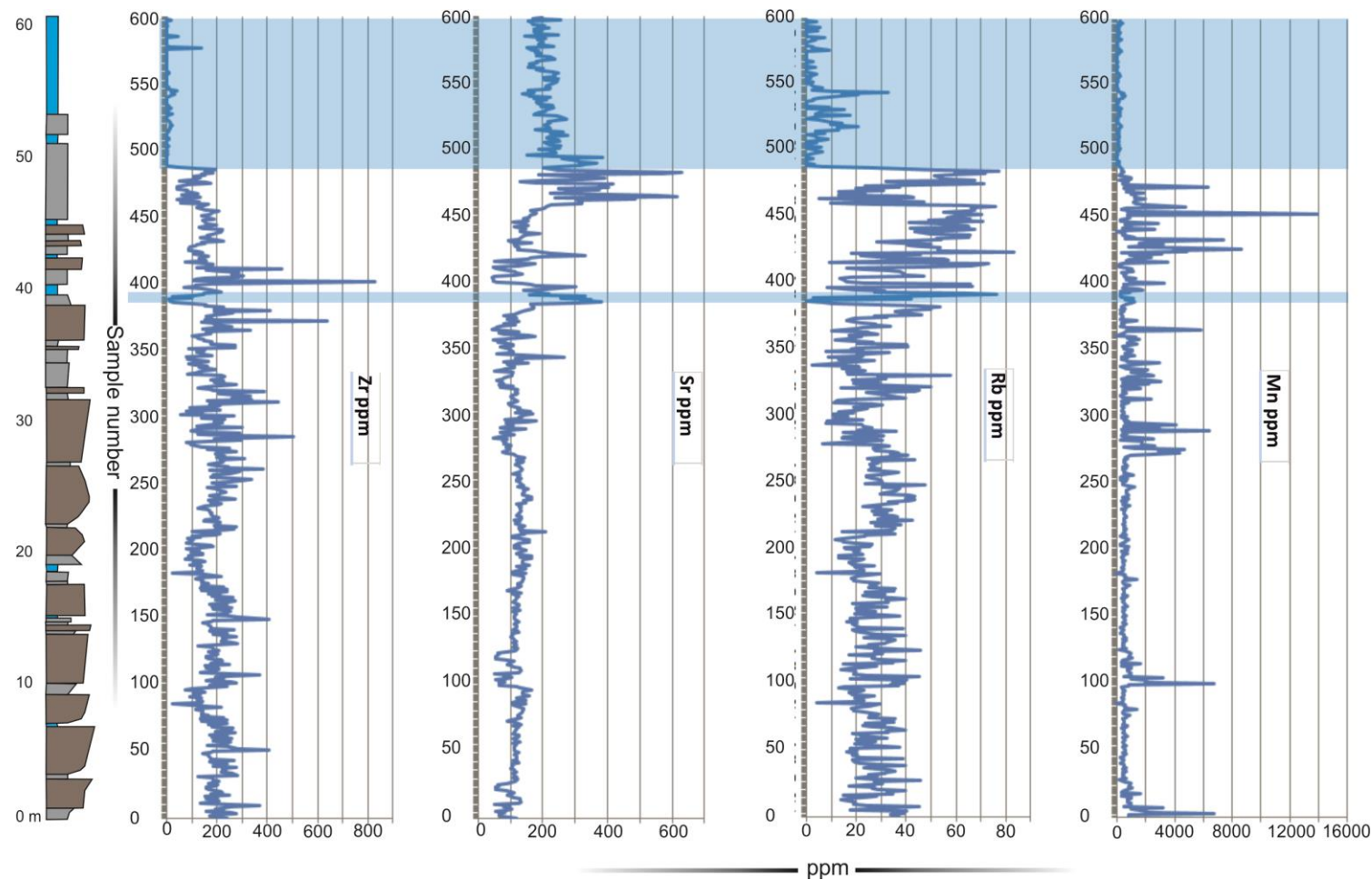


FIGURE - 8.4 A correlation panel of trace element line plots (all readings are in ppm). As with Fig. 8.2 a distinction between clastic and carbonate deposition is easy to define, and is highlighted by the blue boxes. The general trend of these line graphs (particularly of Zr and Rb) are similar to those seen in Fig 8.2. for the major elements (except Ca). Schematic log included for reference, lithologies; grey = siltstone, brown = sandstone, blue = limestone

The provenance of an element can be checked by cross-plotting with Al or Ti and Zr. These elements are commonly detrital, are scarce in sea water, and are not affected by burial or diagenetic processes. Elements which show linear relationships with these elements are quite likely to be of detrital origin. Ti has also been successfully related to grain size of sediments and can be used as a proxy for depositional environment. Ti is generally associated with heavy minerals (e.g. rutile), these minerals are most likely to be found within higher energy environments (i.e. coastal, shallow). Higher Ti values may therefore indicate a higher energy depositional environment (Morton and Hallsworth, 1999) and could indicate a tentative depositional factor (e.g. switching delta lobes). Ti values could also be of use to indicate relative sea level (if it is assumed that the higher the energy environment, the shallower it is). In Fig. 8.2, a clear increase in Al_2O_3 , K_2O and TiO_2 can be observed (from around sample 320), followed by a sharp drop (at roughly sample 490) before carbonate production takes control. The increase of these elements is interpreted to represent a regressive event which is abruptly ended as either a transgression occurs, or detrital input into the basin ceases, as indicated by a rapid decrease in Ti values. A linear relationship between Si, Ti and Zr are strong indications for detrital input, these elements can be seen to negatively correlate to Ca (Fig. 8.5). Sharp changes in detrital input, juxtaposed atop of the larger scale cyclicity, are interpreted to represent tectonic loading as a result of thrusting, these events occur at sample number 200, 390 and 490 (they are highlighted in Fig.8.6). Thick carbonate units may have resulted from a sharp transgressive event in association with a sea-level low stand. Within several of the cross plots, some points appear relatively 'scattered' from the trend lines (e.g. SiO_2 vs Al_2O_3 , SiO_2 vs K_2O and SiO_2 vs TiO_2). These divergent values are possibly the result of readings taken from sandstones which are rich in organic matter (i.e. plant fragments and coal bearing layers). For example TiO_2 vs. Fe_2O_3 shows a trend line with an R^2 value of 0.042, however, it is clear that this trend has been greatly skewed by data points which are most likely to be related to organic rich components. Moving averages with a period of 10 for the elements Al, Si, K, Ca, Ti, Rb and Zr as well as the ratios of Rb/K and Zr/Ti (both $\times 10^2$) have shown cyclicity is apparent within the logged sediments (Fig. 8.6). Al, K and Ti show apparent cyclicity with a periodicity of 45 samples, sample space is at 10 cm so this is roughly every 4.5 m. Si, Zr and the ratios between Rb/K and Zr/Ti all show cyclicity with a

periodicity of roughly 90 samples, or 9 m. This cyclicity is possibly the result of glacio-eustatic sea-level change. The cyclicity observed is disrupted (as mentioned above) at around 200 (20 m) 390 (39 m) and 490 (49 m) these breaks in the cyclicity are attributed to the juxtaposition of tectonic (in this case thrust faulting) activity over the cycles observed. The onset of carbonate production coincides with the zenith of the tectonic activity. The ratios of Zr/Ti and of Rb/K can be used as proxy signatures, for provenance and salinity respectively (Scheffler *et al.*, 2003). Zr/Ti ratios indicate that the provenance for the sediments is stable with variation matching cyclicity observed elsewhere (forced orbital cyclicity linked with climatic variation being responsible for the cyclicity observed). The ratio drops considerably where carbonate deposition is dominant, suggesting that the provenance of sediments may have changed or ceased at this point. The Rb/K ratio (Campbell and Williams, 1965) indicates that salinity is also linked to the observed cyclicity and remains relatively stable throughout the bulk of the log, only shifting dramatically at around sample 490, where carbonate production begins. This decrease in ratio indicates a decrease in salinity, however, it must be noted that the readings for Rb and K past the point of sample 490 within the log is often zero (as clastic deposition is greatly reduced allowing carbonate deposition to occur), this negatively skews the moving average, greatly reducing its reliability. Nevertheless, the sharp drop in ratio indicates that the environment is becoming more restricted.

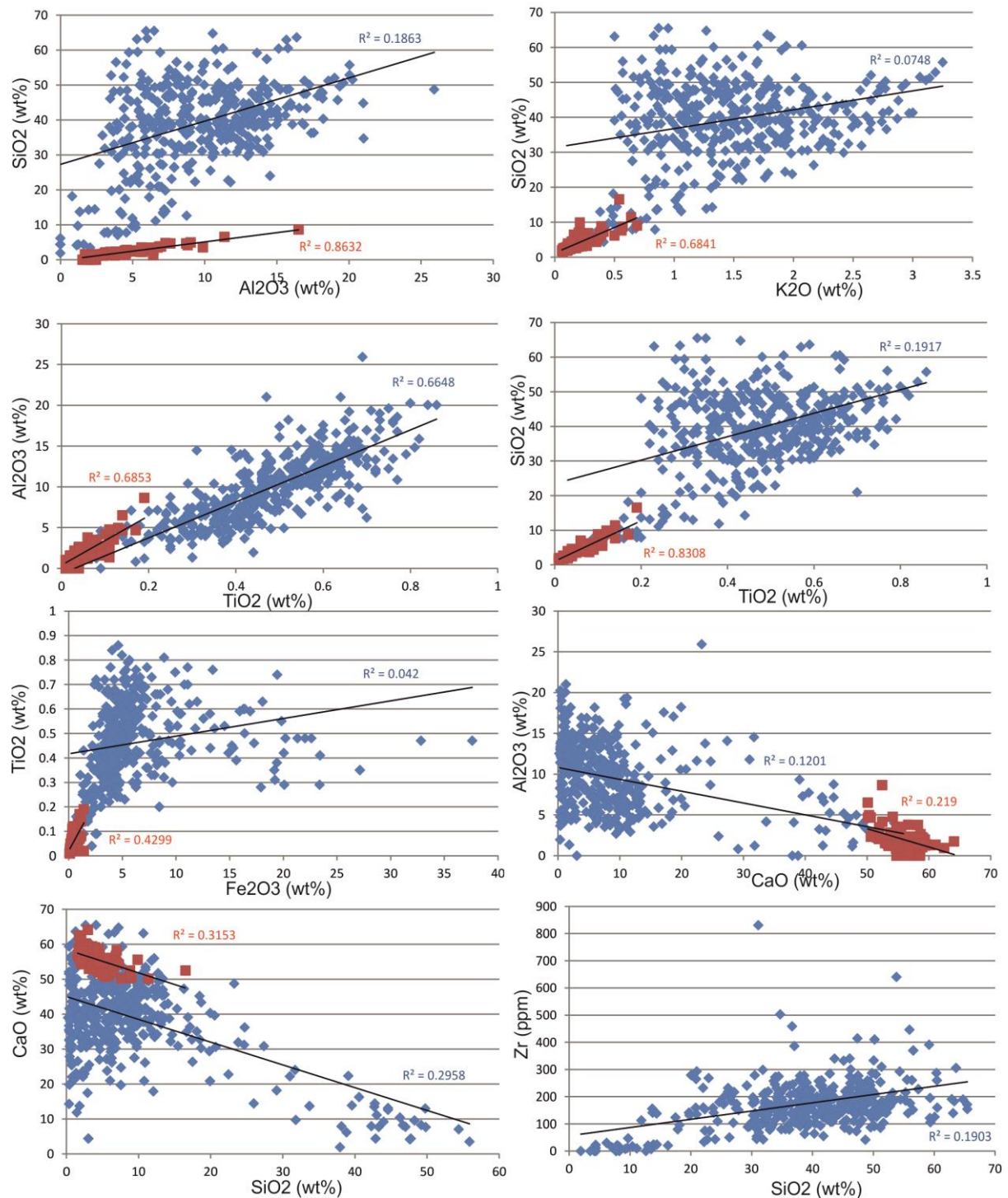


FIGURE - 8.5 Cross-plots between several of the elements recorded (mostly major elements). Blue diamonds represent readings from the clastic component, whilst red squares represent the carbonate component. These cross plots show that the elements associated with a detrital clastic component (i.e. Si, K, Ti, Al and Zr) have positive correlations. A negative correlation can be seen between both Al and Si with Ca. These plots suggest that the clastic components are detrital in origin, possibly with the same if not similar provenance. These cross plots, in agreement with the line graphs (see Fig 8.2 and 8.3) indicate that carbonate deposition took place when clastic deposition was at a minimum.

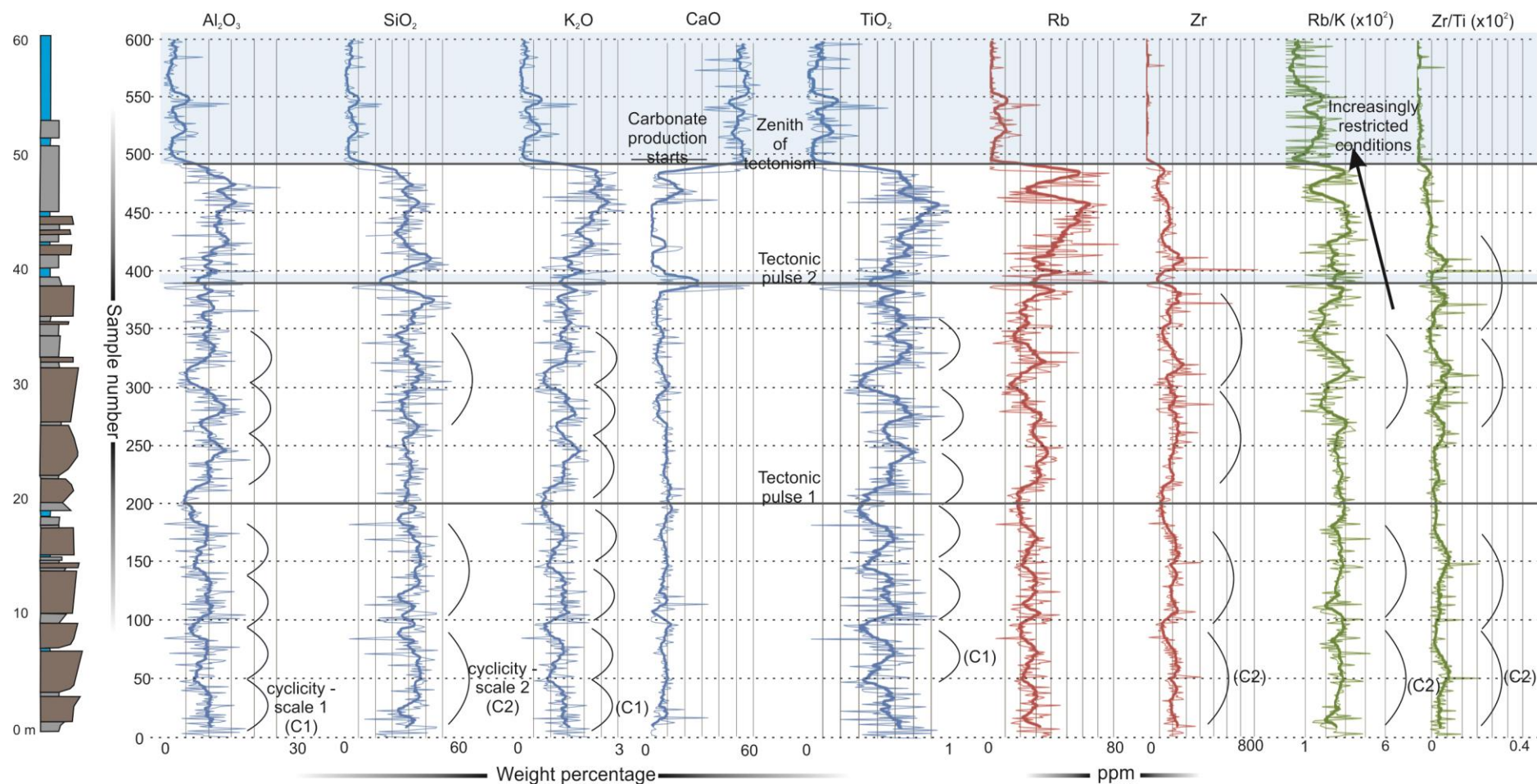


FIGURE 8.6. Moving averages of elements (and ratios) that can be interpreted to show cyclicity or evidence of other events. Shown are Al, Si, K, Ca and Ti (major elements) in blue, Rb and Zr (trace elements) in red and ratios between Rb/K and Zr/Ti in green. Cyclicity is observable in many of the elements and pronounced cycles are highlighted by black crescents, two obvious periodicities can be observed, cyclicity - scale 1 and 2. The cycles are roughly 45 and 90 readings long (each reading is spaced 10cm apart) respectively. The observed cyclicity is disrupted at several points, these events are interpreted as thrust fault related movement within the foreland basin setting, with the main stage of carbonate production coinciding with the maximum tectonism. The Rb/K ratio indicates that as the sedimentation switches from clastic to carbonate dominated the environment possibly becomes more restricted.

Time-frequency analysis in the form of Continuous Wavelet Transform (Morelet) analysis is used to transform one dimensional elemental compositional data into a two dimensional time-frequency representation. This reveals the persistency of periodicities along the Candemuela section (Fig. 8.7). The time-frequency analysis complements the evidence for cyclicity as observed in Figure 8.6. Evidence for two cycles is clearly visible whilst evidence for two more could possibly be interpreted. Amplitude modulation, which is typical of repetitive cycles are observed within each wavelet transform conducted. When considering cyclostratigraphy, as observed here, it is necessary to take into account the Astronomical (or orbital forcing) timescale (House, 1995 and Hinnov and Ogg, 2007). Orbitally forced cyclicity at the geological timescale is the result of: the Earth-Sun distance (precession, 19 and 23 ka at present), Earth's tilt in regards to the Earth's orbit around the Sun (obliquity, 41 and 54 ka at present) and changes in the Earth's orbit around the Sun (eccentricity, around 123 and 413 ka at present) these cycles are generally referred to as Milankovich band cycles, they are named after Milutin Milankovich (1920 and 1941) who first calculated the effects of orbital forcing to explain ice ages. Both precession and obliquity are dependent upon interactions between the Earth and Moon (House, 1995), evidence suggests that the lunar month has changed through time, as a result, so would the periodicity of precession and obliquity. Berger *et al.* (1989a and 1989b) provided a calculation to correct this through geological time, the range of precession and obliquity, in years, is estimated to be 17,272 - 20,468 and 32,954 - 40,403 respectively for the Upper Carboniferous. Berger *et al.* (1989a) also produced a figure indicating the shift in precession and obliquity through time (Fig 8.8). Eccentricity is not affected by changes in the Earth - Moon system.

A broad modulation is observed in each image which is interpreted to represent the large scale cyclicity responsible for the clastic/carbonate cyclothems of the La Majúa Member (i.e. eccentricity cycles), this is represented by a dashed line on images in Fig. 8.7. and shows the clastic to carbonate changes (i.e. the 8 carbonate units) within the La Majúa Member of the San Emiliano Formation. These repetitive transgressive sequences are most likely to represent eccentricity cycles (based upon the given sedimentation rates of the San Emiliano Fm. (see *Chapter 7*) - which have previously been observed in Carboniferous sediments (Davydov *et al.*, 2010). A bifurcation pattern was observed in each image at

similar times (x axis) and periods (y axis). The spacing of this bifurcation (Fig. 8.7, marked on the images) was measured for each image and it was found to have a period of 9.7 m (mean) on average (mode = 8 m, range = 6 to 13 m). This pattern is likely to be the same pattern observed from the gliding averages observed in Figure 8.6 (cyclicality scale 2). A cycle with a period of 9.7 m stratigraphically represents around 24,250 years of deposition (see chapter 7. *Clastic Intervals* for discussion on sedimentation rates). This cycle does not fit with the expected periodicities associated with Milankovich style cyclicality (Berger *et al.*, 1989a & 1989b). Two other bifurcation patterns may be present, however, they are not as clear as the pattern described above. These possible patterns are found above and below the marked pattern. The lower pattern may represent obliquity whilst the higher pattern would represent a cycle with a low period - possibly an autocyclic response caused by tectonics or sedimentation.

An eccentricity cycle appears to be apparent, whilst shorter periodicities, whilst evident, are not attributable to Milankovitch cyclicality based upon the data presented here. This problem has been observed in other Carboniferous sedimentary successions which are believed to be transgressive cycles (Schwarzacher, 1993). There are several factors which may have resulted in the measured section resulting in intervals which do not fit the expected Milankovitch periodicities, these include non-deposition of sediments and the erosion of deposited sediment. Schwarzacher (1993) concluded that positive proof of Milankovitch cyclicality in the Pennsylvanian of North America does not exist, but conceded that the cycles were "...of the order of orbital cycles and that no satisfactory alternative explanation has yet been given." A similar conclusion must be drawn here.

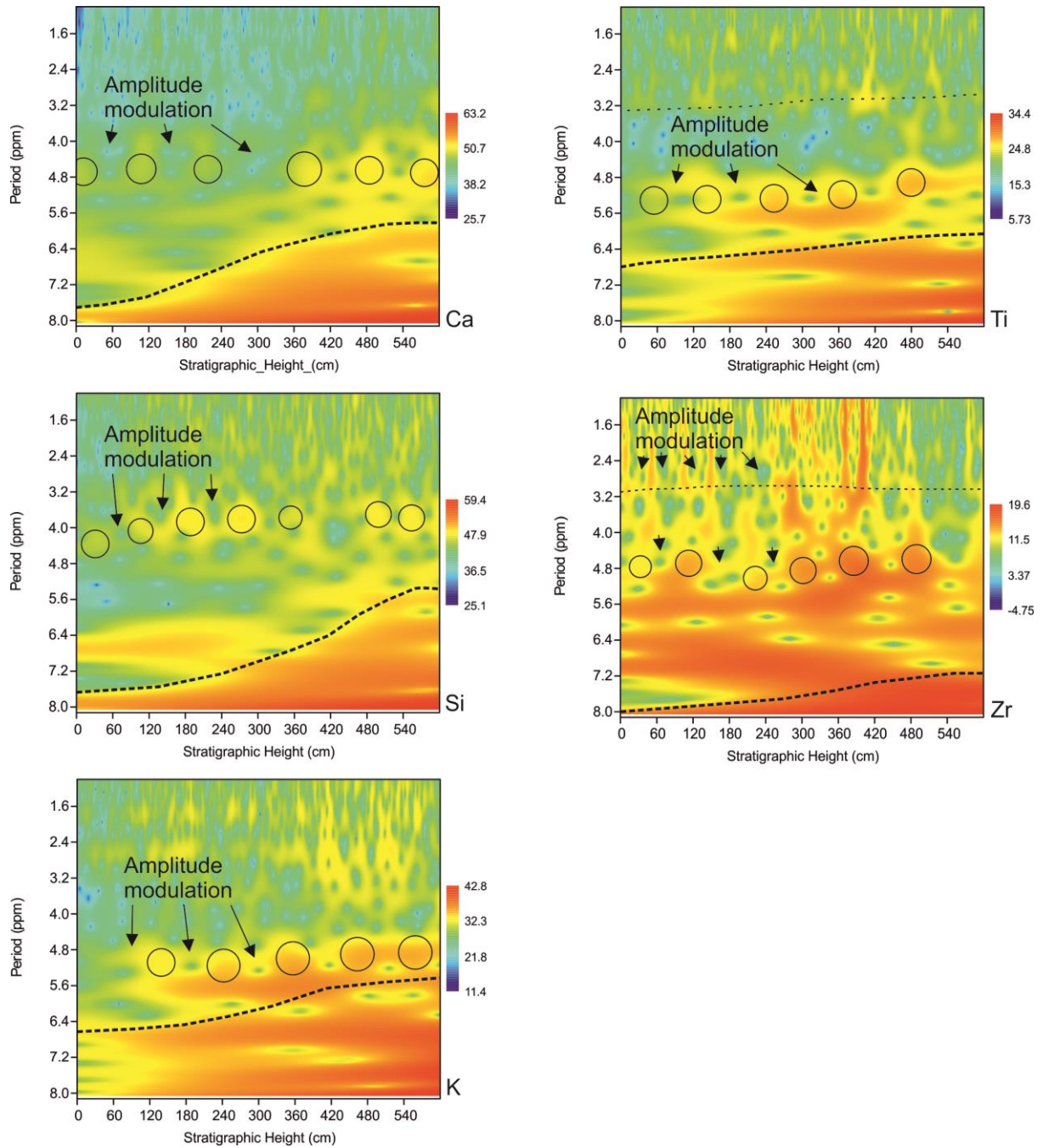


FIGURE- 8.7 Time-Frequency images resulting from Continuous Wavelet (Morlet) Transformation analysis. Letters indicate the element to which each image relates. Hot colours indicate at which stratigraphic level (x axis) and period (y axis) elements are characterised by high spectral power. Thick dashed lines indicate the period related to eccentricity. Circles and arrows indicate a bifurcation pattern which is indicative of the amplitude modulation of a cycle with a 24250 period. The thin dashed line in Zr and Ti may represent a cycle with a small period, possible evidence is found in the other images. Below the rows of circles a second bifurcation pattern may exist but is not as clear as the pattern indicated.

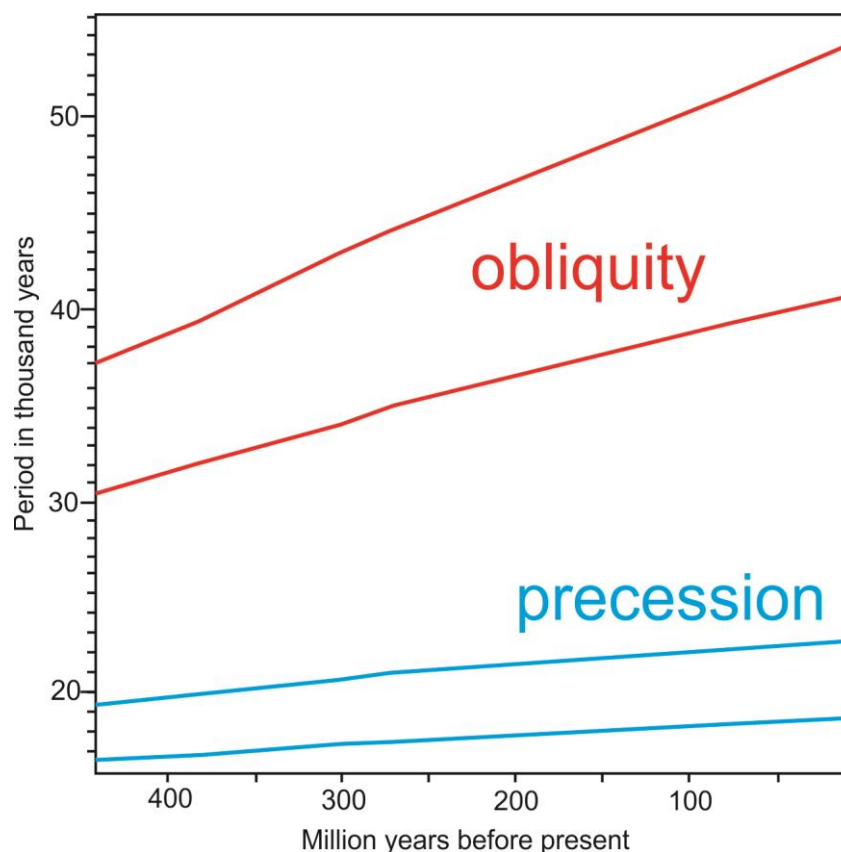


FIGURE - 8.8 Correction for the periodicity of obliquity and precession cycles through time due to Earth - Moon interaction. After Berger *et al.*, 1989a.

The recognition of cyclicity within the clastic component of the chemostratigraphic log, juxtaposed with the sharp carbonate production boundary indicates that an event occurred which disrupted the ‘normal’ cyclicity within the sedimentary basin (i.e. glacio-eustatic sea-level change). Given the foreland basins setting, it is likely that this event involved tectonics, specifically thrusting (agreeing with the interpretation presented in the previous chapter). Flexural subsidence related to this thrusting would cause a transgression within the basin. The regressive event interpreted for the increased deposition of Al_2O_3 , K_2O and TiO_2 directly before carbonate deposition becomes dominant may represent a period of time where the advancing mountain front was providing increased amount of eroded material into the basin (leading to a regression) before the rate of uplift outstripped the rate of erosion and clastic sedimentation became mainly terrestrial. The geochemical data and interpretation provided here fit well with the interpretation reached from the analysis of the clastic sedimentology in the previous chapter.

8.3 Chapter Summary

Hydrocarbon seepage and hydrothermal venting as the initiation mechanism for the carbonate mud mounds from the San Emiliano Formation can be dismissed. Samples from the Bernesga Valley show higher $\delta^{13}\text{C}$ and $\delta^{18}\text{O}$ values than their San Emiliano counterparts, neither set of isotope data indicate an extreme environment (i.e. seep sites etc.) for deposition of the studied mud mounds. Elemental compositions for the Candemuela section indicate that the sequence has an overall regressive trend with a transgressive event beginning at the time of major carbonate production. At this transgression the mound bearing carbonate unit occurs. Milankovitch scale cyclicity is probably recognised in the sequence, eccentricity and a shorter orbital cycle are recognised. A cycle with a very short period, most likely the result of autocyclic feedback is apparent. A possible cause of the autocyclic mechanisms in the depositional environment would be delta lobe collapse. It is suggested that the large carbonate units of the La Majúa Member represent tectonic thrusting events (juxtaposed upon Milankovich scale orbital driven climatic cyclicity), causing initial regression, before relative sea-level rise occurs due to subsidence related to basin flexure.

9. Discussion

In this chapter several strands of evidence are integrated and discussed in order to better understand the nucleation, formation, growth and demise of the studied mud mounds. The composition of the carbonate mud mounds from the San Emiliano Formation, their depositional environment and nucleation and growth mechanisms are all discussed. The mounds from this study are compared and contrasted with other mounds worldwide.

9.1 Mound description

The carbonate mud mounds from the San Emiliano Formation are a skeletal-microbial pack-wackestone often associated with fenestral cavities. The mounds vary in size ranging from 2 to 50 m in thickness and are steep sided, lens to mound shaped. Mounds appear as either isolated build-ups or as superimposed complexes of two or more mounds. The basal facies consists of well-preserved thickets of *Donezella* and *Beresella* with cyanoliths and cortoids. Cyanoliths and cortoids suggest a shallow subtidal back-reef environment (Flügel, 2004). The mound facies is dominated by packstones. Donezellacean algae are the most common fossil and are commonly associated with the encrusting forms *Rothpletzella*, *Claracrusta*, *Girvanella* and, less commonly, several other encrusting forms. A peloidal, clotted and homogenous micrite matrix is the dominant sediment, clotted peloids have been inferred to represent microbial activity (Samankassou *et al.*, 2013). Cavities are fenestral and are filled with peloidal micrite and marine cement or are stromatactoid in nature. The morphology of the cavities can often be seen to be directly controlled by Donezellacean thalli. Mound fossils are less common than those of the carbonates external to the mounds and represent a more restricted biological assemblage. The *mound facies* was deposited in a low energy, shallow environment. Microfacies evidence indicates an increase in sea level throughout the formation of the mounds from the San Emiliano Valley (Fig. 9.1). The capping facies shows an increased clastic input and the appearance of relatively

large, reworked and abraded bioclasts, often reef derived (assumedly from the ‘Caliza Masiva’, see Fig. 9.6 for Palaeogeographical reconstructions). Diversity increases and several foraminifera not encountered within the basal or mound facies are found, indicating a more open environment.

The presence of whole, well-preserved fossils and the presence of cavity networks, which show evidence for connectivity (i.e., well-developed stromatactoid cavities), indicate rapid lithification after deposition.

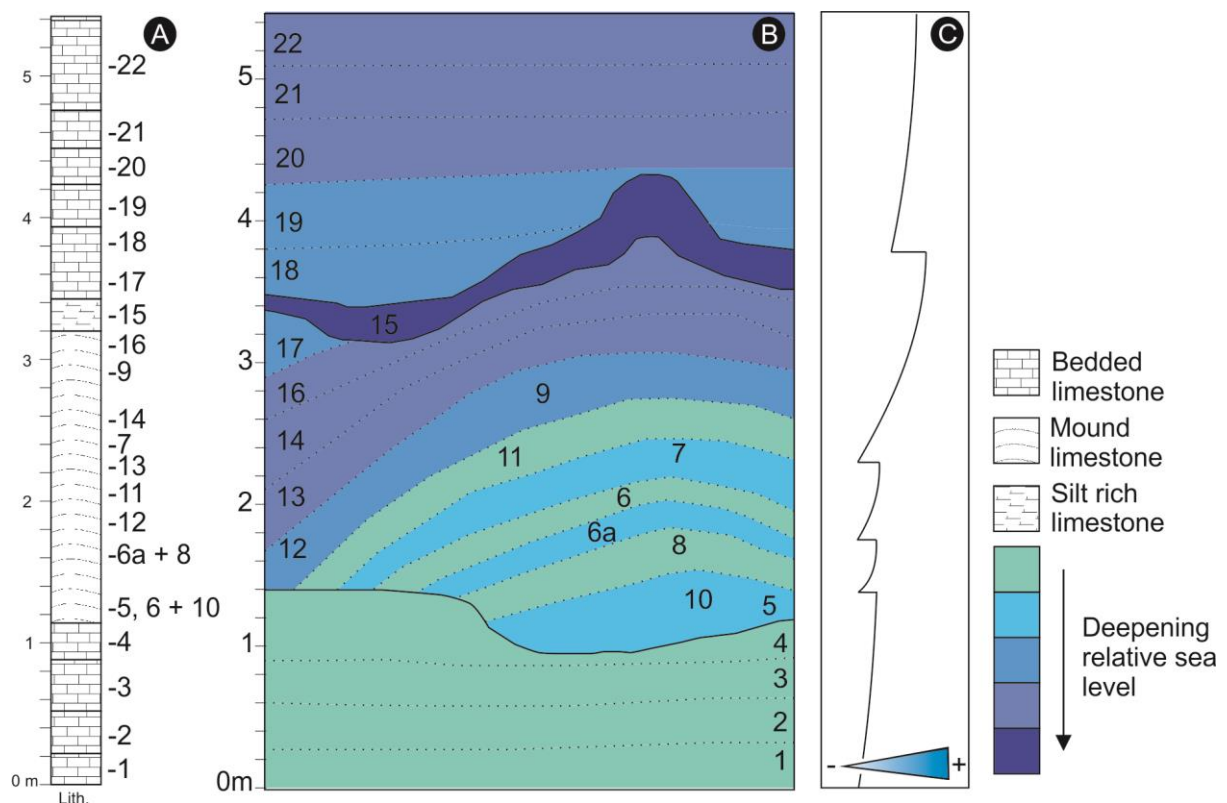


FIGURE - 9.1 A diagram showing the general sea-level rise interpreted for the depositional environment of the San Emiliano mounds, using the Candemuela mound as an example. A, a schematic log showing the major lithology and the level at which each sample originated. B, a cartoon of the Candemuela mound with bedding drawn as dotted lines, numbers correspond to the position from which samples were obtained. Colours correspond to different Standard Microfacies which have been attributed to different sea levels, the hotter the colour the deeper the sea level at time of deposition of the represented unit. Note that “bedding” drawn for the mound is based upon changes in Standard Microfacies and are not beds observable in the field. C, a sea-level curve based upon depth of deposition, a general transgression can be observed, punctuated by several rapid shallowing events.

Mounds from the Bernesga Valley are fundamentally different from those formed at the San Emiliano type locality. Investigation from the Bernesga Valley in this work and Samankassou's (2001) study show that Donezelloids are again the dominant fossils. Unlike the San Emiliano Valley mounds, they are associated with agglutinated worm tubes (*Thartharella*), calcisponges and a greater number of metazoans (e.g. corals and bryozoans). The disparity between mounds from the separate locations is shown in Fig. 9.2. These mounds formed in a low-energy environment below wave base and deeper than their San Emiliano Valley counterparts. Bryozoans, corals, dasyclad algae and foraminifera are more common within the Bernesga Valley. The Bernesga Valley mounds also formed on non-biogenic carbonate banks (ooid and oncoids bars) whereas the San Emiliano Valley mounds form above biogenic *Donezella* thickets. The mounds from the Bernesga Valley are interpreted to have a strong association with platform-derived carbonates of the 'Caliza Masiva' (see 9.6 *Depositional Environment* below).

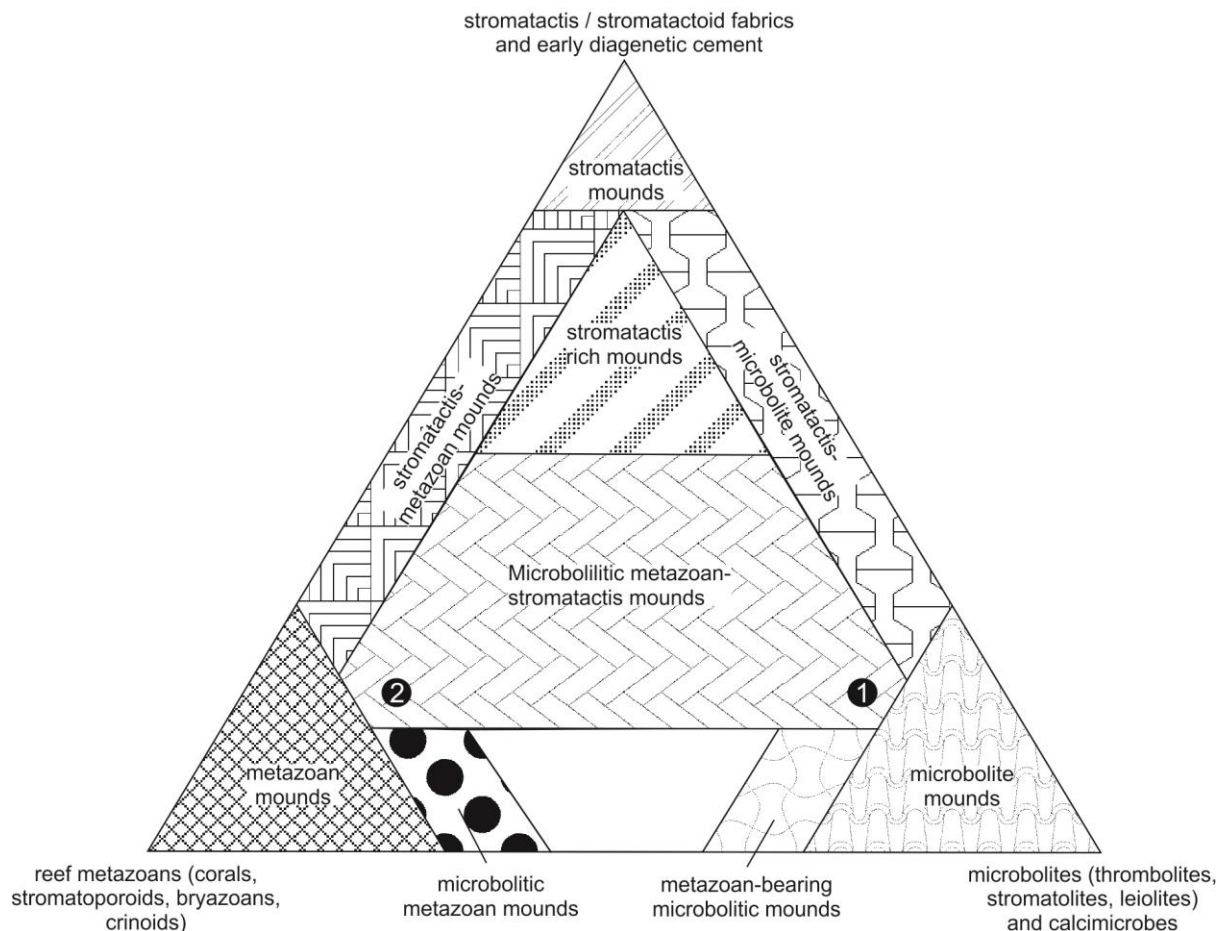


FIGURE - 9.2 Palaeozoic mound types. Mounds have a minimum content of 25% carbonate mud. 1, this marker corresponds to the mounds found at the type locality of the San Emiliano Formation. The mounds contain abundant metazoans (Donezellaceans), microbes (calcimicrobes and microscopic encrusters) and cavity networks (both stromatactoid and fenestral). 2, the Bernesga Valley Mounds have less of a microbial association and commonly contain larger metazoans such as corals and bryozoans. It is interesting to note that Lower Devonian mounds from the La Vid Formation of the Cantabrian Mountains plot in a similar position. After Schmid *et al.*, 2001.

Non-mound bearing ‘phylloid’ algae bearing carbonates are dominated by whole fossil wackestones and bioclastic packstones which form cyclic beds of micrite to marl cycles. These carbonates are interpreted to represent a more open marine setting than the mound bearing carbonates and may represent the transitional slope between the shallow depositional environment of the San Emiliano mounds and the deeper one of the Bernesga Valley.

9.2 Palaeoecology: interpretation

The palaeoecological assemblage found with the studied carbonates is dominated by a low diversity of biota. The algal assemblage is typical of those found within the euphotic zone of western Palaeo-Tethyan ocean carbonates (Mamet and Villa, 2004 and Madi *et al.* 1996) and shows similarities to assemblages observed by others studying carbonates of comparable ages (e.g. Della Porta *et al.*, 2002; Choh and Kirkland, 2006 & Corrochano *et al.*, 2012). The low diversity of biota indicates a restricted environment. Littler and Littler's (1980) investigation of morphological attributes of thallus forms of macro-algae, and its relationship with various survival strategies, indicate the dominant biota found represent very early colonisers which grow quickly and dominate pioneer communities. Similarly, the widespread nature of *Donezella*, both spatially and environmentally, suggest that the species fit the role of "opportunistic" in the mechanisms of ecological community succession (Connell and Slatyer, 1977). Opportunistic species are those which arrive first and occupy empty space (i.e. newly opened environmental niches), have a broad dispersal range and rapidly grow to maturity. It is thought that opportunistic species struggle to establish themselves in the presence of mature specimens of other species, although some may be able to change local conditions to better suit their proliferation once established (Connell and Slatyer, 1977). Within the La Majúa Formation, the carbonate units are characterised by 'phylloid' algal packstone (Pinos Hairpin), or skeletal-microbial boundstone (San Emiliano Valley mounds and inter mound carbonates). Both of these are dominated by non-complex algal forms which show little evidence of reworking. The ecological group observed represents that of a pioneer community, found within an environment of relatively shallow water, with low energy levels. Low diversity assemblages characterised by dominant algal communities have been attributed to the exclusion of other biota from the living space via both chemical defence (poisons produced by the algae) and through the occupation of all available living space (Toomey, 1976 & 1991; Forsythe *et al.*, 2002; Samankassou and West, 2003 & Enpu *et al.*, 2007).

Other microbial mounds have been found to dominate environments where reef ecosystems might be expected. A good example for this colonisation of microbial biota occurred on a global scale for 4-8 m.y. after the end Permian mass extinction (Pruss and Bottjer, 2004). During this period of biotic recovery there was an absence of metazoans from reef ecosystems, resulting in the colonisation of the now open niches (Baud *et al.*, 1996 and 2002; Lehrmann, 1999; Lehmann *et al.*, 2003; Schubert and Bottjer, 1992; Wignall and Twitchett, 2002 & Pruss and Bottjer, 2004) by so called “disaster forms” (Schubert and Bottjer, 1992).

9.2.1 The Role of *Donezella* and its Associated Biota

As discussed in chapter 6. *Palaeontology*, *Donezella* acted as the framework builder within the mounds and also as a baffler and binder. Accumulations of carbonate mud by *Donezella* was proposed by Bowman (1979) as the mechanism responsible for the mounds of the San Emiliano Formation. Riding (1979), however, doubted the ability of sparsely distributed *Donezella* patches to accumulate such a large amount of carbonate mud. Here, *Donezella* is seen to be relatively common and often forms dense thickets, which would supposedly be able to baffle substantial amounts of sediment. In agreement with Riding (1979), it is not envisaged that *Donezella* thickets alone are responsible for mound formation. A dynamic relationship between *Donezella* and various laminar encrusting forms has been observed and it is this interaction between the different members of the community which is envisaged to be responsible for the accumulation of mud mounds within the San Emiliano Formation. The association with *Rothpletzella*, *Claracrusta*, *Girvanella* and other microscopic encrusting forms is a relationship that has been identified before (Mamet and Villa, 2004) but never attributed to the formation of carbonate buildups. The encrusting forms are interpreted to have played an important role binding and stabilising the *Donezella* growths. The stabilised growths providing a further substrate for subsequent colonisation by *Donezella*. The encrusters observed here play the role taken by calcareous sponges and worm tubes for those mounds of the Bernesga Valley (Sammankassou, 2001). The occurrence of the encrusters *Rothpletzella* and *Claracrusta* indicate changing environmental conditions,

laminae of these encrusters are not observed to occur between individual *Donezella* thalli (as *Girvanella* is observed to do). The encrusting of *Rothpletzella* and *Claracrusta* occurs as laminar sheets of branching fillements; both tightly, and loosely packed growths, with sediment and spary cement between the individual laminae. Encrusting communities are found on top of *Donezella* growths and not within them, and *vice versa* (other than rare *Girvanella* between *Donezella* thalli). This indicates that the encrusters and the (micro) framework forming *Donezella* did not grow coevally. *Donezella* has been observed from various environments and appears to be prolific where found (see chapter 6. *Palaeontology*). The accumulation of *Rothpletzella* and *Claracrusta* (plus associated enrusters) on successive surfaces of the *Donezella* built framework indicate periods where the algae *incertae sedis* either ceases to grow, or struggles to compete with the filamentous encrusting forms. This relationship clearly indicates interruptions to *Donezella* growth which corespond to changing environmental conditions. A similar relationship has been observed between *Graticula*-like red algae, *Rothpletzella* and laminar stromatoporoids in Lower Devonian age bindstones by Adachi *et al.* (2007). They interpreted that the *Rothpletzella* encrustations represented deteriorating environmental conditions whilst the growth of the framework builder indicated improved habitat conditions. In the light of *Donezella* having a tolerance for a variety of environmental conditions, the interpretation of Adachi *et al.* (2007) is adopted for the relationship between framework and encrusters observed in the San Emiliano Mounds. Laminar growths of encrusting *Rothpletzella* and *Claracrusta* represent periods of deteriorating environmental conditions whilst framework growth represents a return to less restricted environmental conditions. The repetitive nature of this relationship indicates fluctuating environmental conditions which may be related to sea-level change imposed on an already shallow environment. This relationship also indicates direct competition for habitat between the framework forming *Donezella* and the encrusting *Rothpletzella* and *Claracrusta* (Fig. 9.3).

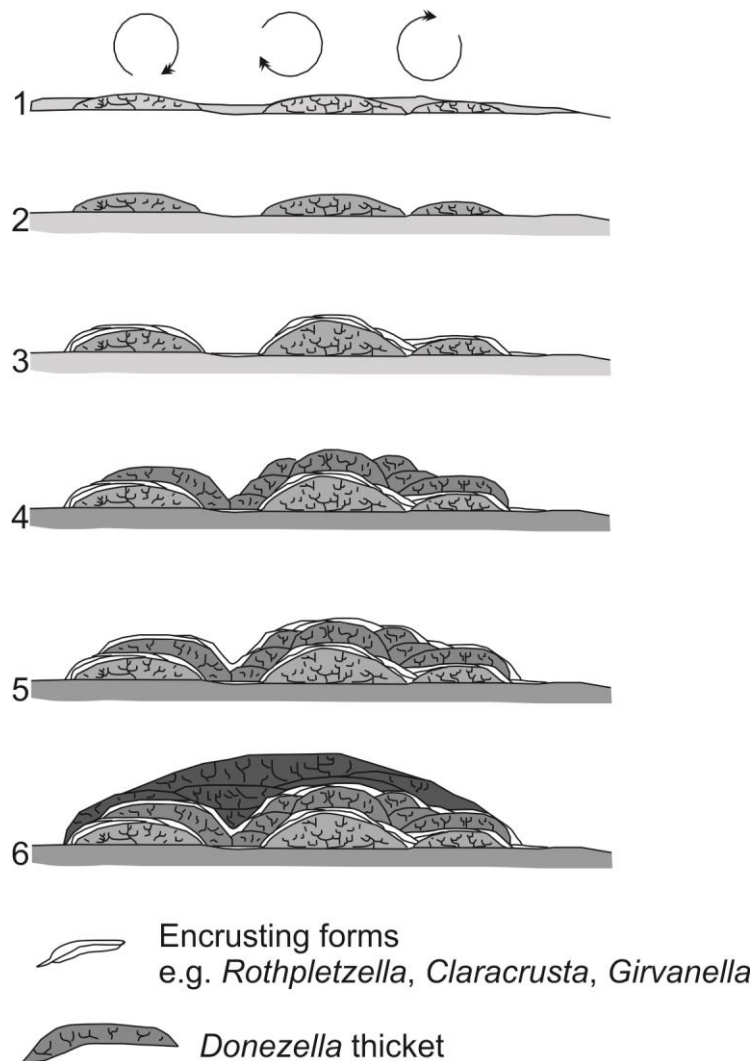


FIGURE - 9.3 A schematic representation of mound formation. 1] *Donezella* grows and is broken and abraded by local wave action and currents. 2] *Donezella* grows on top of the accumulated, broken *Donezella*. 3] Environmental conditions deteriorate and laminar encrusters colonise the substrate provided by the *Donezella* thickets. 4, 5 and 6] Environmental conditions continue to fluctuate resulting in the repetition of *Donezella* growth, and stabilisation by encrusting forms.

9.3 Origin of Micrite

The ‘micrite problem’ (as discussed in chapter 2. *Literature review*) considers the origin of carbonate muds and the resulting micrites in Phanerozoic age lithologies. The polygenetic nature of carbonate muds mean that identifying a source for ancient rocks is often very difficult. Several formation mechanisms have been suggested including faecal pellets (Perry *et al.*, 2011), the *in situ* calcification of cyanobacteria (Każmierczak *et al.*, 1996) and commonly the disaggregation of bioclasts (Tucker and Wright, 1990; Flügel, 2004). Micrite and microspar are observed as

homogenous, clotted and peloidal textures within the sampled material. Optical Light Microscopy revealed that peloids are rounded but are not always spherical, or the same size. This disparity amongst peloids tends to suggest that faecal pellets be ruled out. The inclusion of calcimicrobial sheaths and algal thalli within many peloids probably indicates that carbonate mud originated from the disaggregation of bioclasts, namely *Donezella*, *Girvanella* and other encrusting forms. *Donezella* can be observed in various stages of preservation, often, poorly preserved specimens are associated with a micritic coating, this may suggest micritization prior to breakdown of the algae. *Girvanella* is often observed between *Donezella* thalli and can be found within peloids. Pratt (2001) suggested that *Girvanella* was a good candidate responsible for carbonate mud formation. It is therefore likely that other filamentous encrusters (e.g. *Claracrusta*) are also potential candidates for disaggregation. The micrite which forms the carbonates of the San Emiliano Fm. is interpreted to be autochthonous micrite which formed as a result of surplus organic matter formed by microbial degradation of *Donezella* (see Neuweiler *et al.*, 1999 and 2000, plus, chapter 2. *Literature Review*) and other, less common biota. Several environmental triggers have been proposed which are thought to give rise to this accumulation of autochthonous micrite, one of them being a reduced sediment supply (Kirkby, 1997). The environmental trigger fits well with the depositional environmental proposed for the mud mounds of the San Emiliano Formation (see 9.6 below)

9.3.1 Does the Carbonate have an Aragonitic Origin?

Identifying an aragonite-dominated precursor in carbonates is possible by identifying several characteristic features: aragonite relics, pitted crystal surfaces, common microspar fabrics and elevated strontium levels. Of these characteristics, the first three were identified within the ultrafacies study conducted. Further evidence observed within the microfacies analysis includes hyaline structures observed for both foraminifera and alga. Hyaline crystals often exhibit a honey-like colour and are generally thought to have been formed with aragonite (Flügel, 2004). The occurrence of limestone-marl alternations may also provide a link to an environment with

preferred aragonitic deposition (Westphal and Munnecke, 2003 & Munnecke and Westphal, 2004). Strontium is near the detection limit of the analytical equipment implemented within this study, so data regarding its presence (or absence) is not quantitatively reliable. Nevertheless, even in the absence of the relevant geochemical data the recognition of aragonite precursors is possible, and has been carried out by several authors (e.g. Mazzullo and Cys, 1979 & Grotzinger and Reed, 1983). The presence of these features strongly suggests an aragonite-dominated precursor, though evidence supported by geochemical data would clarify this further. When compared to similar investigations, the microspars observed here strongly resemble those of other authors who have suggested an aragonitic precursor. If an aragonitic precursor were present it is assumed to have formed a mesh-like calcareous mud consisting of needle-like crystals. As discussed in chapter 2. *Literature review*, these aragonitic precursor muds would have undergone aggrading neomorphism. Aragonite and fibrous-high Mg calcites would be replaced by low Mg microspar crystals. These crystals would nucleate between aragonite/high Mg calcite crystals, engulfing them and replacing them. Evidence for aggrading neomorphism is apparent within the studied material with specimens highly resembling stages of the reconstructed diagenetic path suggested by Munnecke *et al.* (1997). When a comparison is made between carbonatates from the San Emiliano mounds and those from both the Pliocene of the Bahamas and the upper Silurian of Gotland, similarities are evident (Fig. 9.4). The likely presence of an aragonite precursor introduces potential difficulties in trying to interpret isotope data. Whereas isotopic fractionation has been well documented and verified for calcite (Epstein *et al.*, 1953) the isotopic fractionation of aragonite is not as well defined and the use of ^{18}O and ^{13}C data to interpret palaeotemperatures is hampered by the lack of accurate fractionation data (Grossman & Ku, 1986).

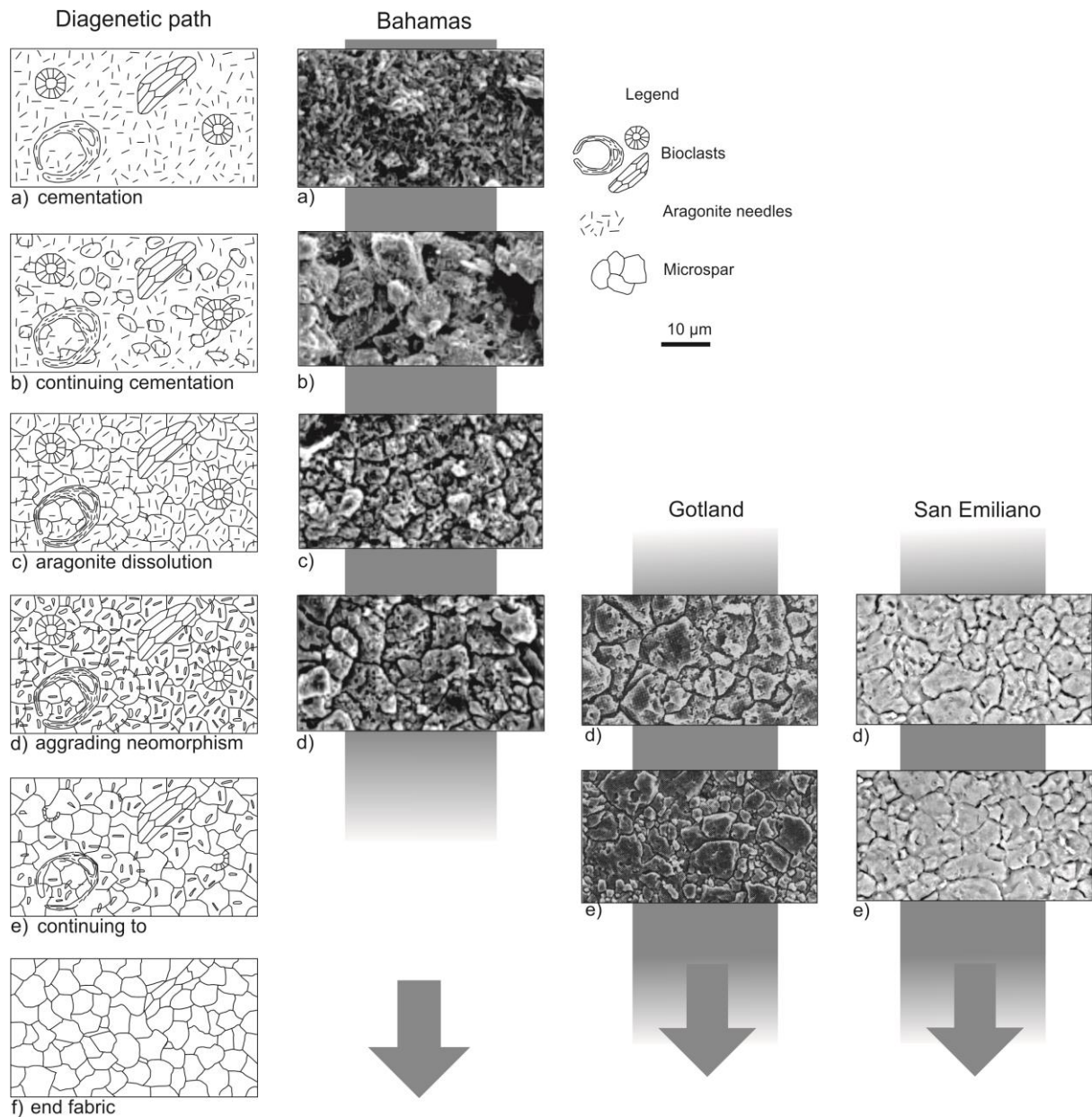


FIGURE - 9.4 Evidence for aggrading neomorphism from the San Emiliano Mounds presented next to that of Munnecke *et al.* (1997). The carbonates show textures from stages d and e which represent a pitted texture as a result of the dissolution of aragonite needles and microspar as a result of continued aggrading neomorphism. If neomorphism had continued the final stage would be represented by equigranular microspar with a smooth surface. After Munnecke *et al.* (1997).

9.4 Water Depth

A sea-level curve based upon the sedimentary log, geochemical profile and microfacies analysis (of carbonates) has been drawn for the cyclothem of Unit 8 of the La Majúa Member of the San Emiliano Formation (Fig. 9.5). Where clastic sediments are dominant the sedimentary profile and

the Ti values are used to predict clastic input (Friedrich *et al.*, 2011) and the relative water level. Rutile (the most common form of TiO_2) is a heavy mineral often associated with shallower deposition. When the sediments become dominantly carbonates then both Ti values and sediment profile become less useful (no clastic input means no rutile incorporation) and the microfacies analysis is implemented. The resulting sea-level curve shows an overall regressive sequence with carbonate deposition being related to transgressive events. The general regressive trend is likely related to the glaciation of the Pennsylvanian, the zenith of glaciation is thought to have been during the Moscovian. The waxing and waning of the glaciers whilst building to the Moscovian ice sheet maximum would have resulted in high-frequency sea-level change on an overall regressive sequence. The transgression associated with increased carbonate deposition is most likely related to tectonic pulsing in an active thrusting environment. Due to the rapid and disruptive manner in which the transgressions have been observed to occur in (Fig. 8.6, *Chapter 8*) they are interpreted as tectonically, rather than eustatically driven. The transgression is a result of flexural subsidence of the basin. The overall regressive sequence related to clastic deposition is probably a consequence of the infilling of the basin, the rate of regression appears to increase just before the deposition of the major carbonate unit. This increased regression fits well with the interpretation of tectonic thrusting, as thrusting (uplift) begins, an increased amount of sediment is supplied to the basin as more material is pushed above local sea-level and is eroded. This increase in sediment supply stops when the rate of uplift outstrips the rate of erosion, flexural subsidence of the basin takes place as a response to the advancing mountain load and transgression occurs. At this point it is envisaged the clastic sediments are deposited sub-aerially and do not make it to the (still relatively) shallow basin.

The sea-level is generally shallow, with ripples, crossbedding and some channelisation observed within the clastic component and evidence of shallow deposition within the microfacies analysis of the carbonate component. This evidence suggests that the carbonate units of the San Emiliano Formation formed in times of tectonic thrusting juxtaposed onto orbital force (most probably

Milankovitch scale) cyclicity, with mounds forming during tectonic activity in association with lowstands (i.e. climatically/sedimentary infill driven shallowing of relative sea level with sudden transgression due to tectonics). Carbonate units formed of ‘phylloid’ dominated sequences may be the result of tectonic activity juxtaposed upon a highstand; ‘phylloid’ dominated communities establishing themselves in relatively (compared to mound bearing units) deep water which still have some distal clastic sediment deposition.

Similar Pennsylvanian cyclothems are common from the Midcontinent of North America (e.g. Heckel, 1977, 1980, 1986 & 1990a) and the north of England (e.g. Johnson, 1959; Shiells, 1963; Johnson, 1984; Tucker, 2003; Tucker *et al.*, 2003 & Tucker *et al.*, 2009). Typical sequences of North American cyclothems consists of a thin transgressive limestone, thin offshore dark phosphatic shale and a thick regressive limestone and were deposited in a shelf to foreland basin setting that was distant from tectonic processes (Heckel, 1990b). Heckel (1990b) concluded that the cyclothems of Midcontinental North America were controlled by global glacio-eustatic sea-level rise and ultimately to Milankovitch orbital forcing. He also suggested that tectonic forces had no discernible control over the cyclothems formation; this conclusion was drawn from the vast lateral persistence of the cyclothems across local tectonic features. Glacio-eustatic sea-level rise and fall in the Pennsylvanian is thought to have been of an order of around 100 m (e.g. Joachimski *et al.*, 2006), this global control must mean that glacio-eustasy had an underlying control over all Pennsylvanian aged shallow marine sediments. In contrast to the solely eustatic controlled cyclothems of North America the San Emiliano Fm. clearly show tectonic overprint, they must also have been closer to a detrital source than the North American counterparts as evidenced by the clastic sediments found for the majority of the formation. Local sea level at the time of deposition of the San Emiliano Fm. would have been controlled by the complex interplay of glacio-eustatic, tectonic and sedimentary controlled relative sea-level rise. The carbonate dominant cyclothems of North America are likely missing here due to the siliciclastic input into the basin, which would have stopped carbonate production.

Yoredale cyclothems of northern England are typically mixed clastic and carbonate successions. Individual cycles range from 5 - 50 m in thickness and generally consist of a lower carbonate component overlain by a clastic section, that is topped by thin coal seams in places. The clastic sections show coarsening upwards (shallowing upwards) units (Tucker *et al.*, 2009). The Yoredale cyclothems cover a relatively large area (some 10,000km²) and were deposited on an epicontinental platform (Holliday *et al.*, 1975 & Tucker, 2009). The cyclicity which is apparent within these cyclothems is attributed to orbital (short eccentricity Milankovitch) forcing. The cyclothems of the San Emiliano Fm. and the Yoredale cyclothems of northern England share several characteristics. Both have clastic (mostly deltaic) and carbonate components, with some thin coals. The clastic sections of both show coarsening upward units. The carbonate units of the Yoredale sequences are found at the base of each cycle and represent the deepest relative sea-level, for the San Emiliano Fm. cyclothems the carbonates appear at the top of each sequence and show no evidence of being deeper than the clastic component. The San Emiliano Fm. cyclothems record a greater degree of sedimentary filling of the basin and tectonically forced sea-level change than the Yoredale cyclothems.

The discussed above, Milankovitch style orbital forcing was the major control on Pennsylvanian aged sediments exhibiting repetitive patterns. The Cyclothems from North America and those of northern England are both examples of this. The San Emiliano Fm. cyclothems also exhibit evidence of orbital forcing, however, they also show a great deal of tectonically (and most likely sedimentologically) forced relative sea-level change. Due to the proximity of the basin to a tectonic and sediment source, this is perhaps unsurprising, and it is speculated that the relatively small size of the basin into which the San Emiliano Fm. was deposited has (when compared to those of the North American and northern England counterparts) intensified the relative sea-level change associated with tectonic flexure and sedimentary infilling and loading.

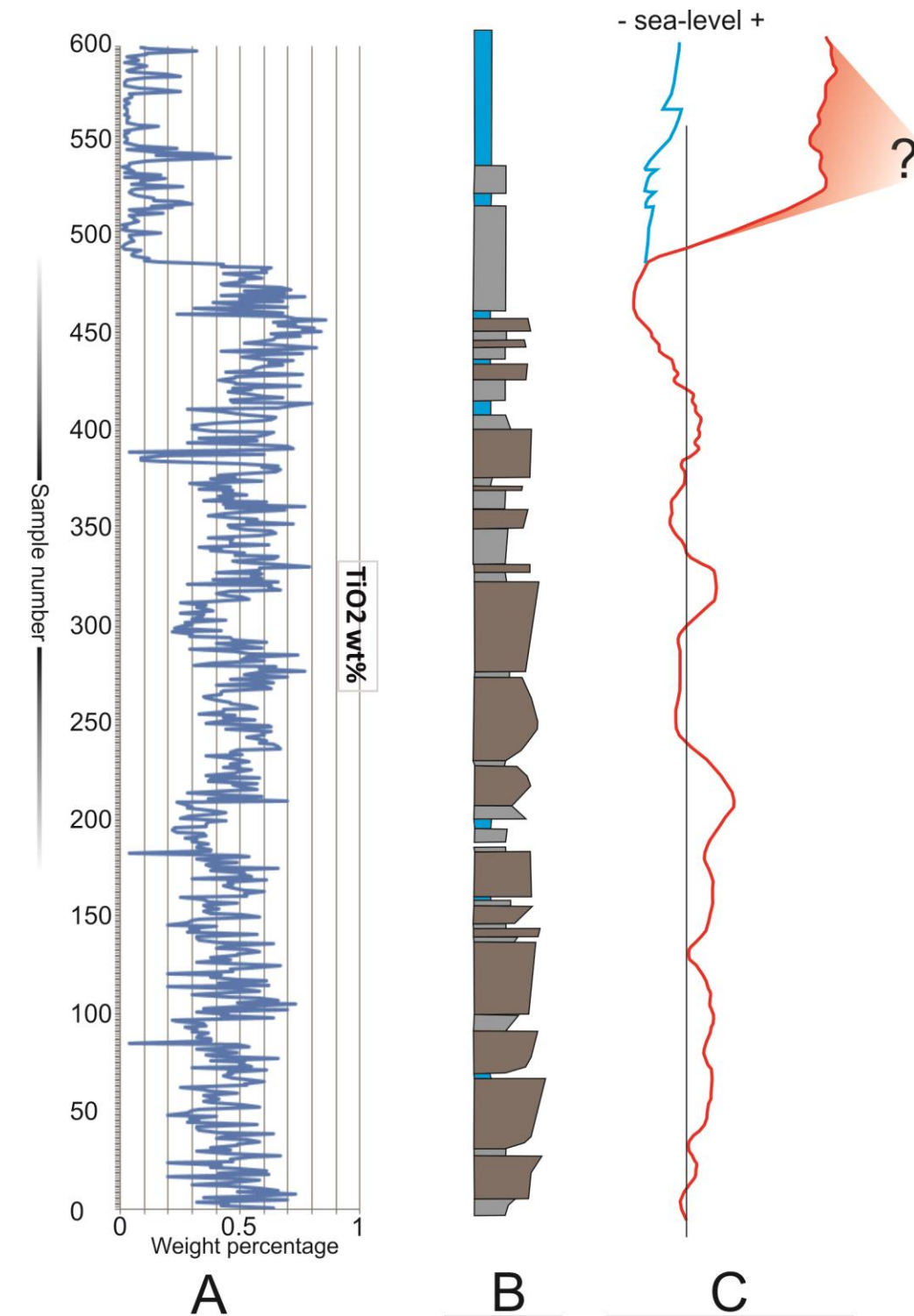


FIGURE - 9.5 Sea-level curve based upon geochemical and sedimentary logs and microfacies interpretations. A, shows Ti values (wt%) from Unit 8 of the La Majúa Member, Ti was used as it was shown to be a detrital element (see chapter 8. *Geochemistry*), higher Ti values represent shallower depositional environments. B, a sketch of the sedimentary log of the section. C, sea-level curve (red line) based on Ti values and the sedimentary log, toward the top of the curve the Ti values are less useful as detrital input into the basin has stopped, instead microfacies data is used (blue line) (see Fig. 9.1).

9.5 Salinity

Organisms can be excellent proxies for many palaeoenvironmental conditions, including salinity. Normal salinities are often associated with a high biodiversity whereas both brackish and hypersaline environments would be expected to house restricted assemblages of biota (Murray, 1991). Sodium (Na) has also been used as a proxy for hypersalinity (Veizer *et al.*, 1977). Although a reliable Na value was not obtained from XRF analysis in this study. It is suggested that the palaeoenvironment of the depositional area had fluctuating salinity levels, though it was generally slightly saline. Salinity levels are thought to have been mostly higher than normal, as indicated by the low biodiversity observed; a dominance of a few algae genera and the rarity of benthic foraminifera with several appearances of miliolinid foraminifera (Murray, 1991). The basin is thought to have been restricted and there is evidence for the sub-aerial/extremely shallow deposition of the sediments (coals), this restricted nature in association with evaporation of the shallow body of water may have driven this increased salinity.

9.6 Depositional Environment

The deposition of sediments took place within a foreland basin at the front of the advancing Variscan orogenic wedge. Palaeogeographical reconstructions indicate that the basin was west of the Palaeo-Tethys Ocean and that communication with the Palaeo-Tethys was partially restricted (i.e. the basin was a narrow sea-way connected to the Palaeo-Tethys).. DeCelles and Giles (1996) and Mutti *et al.* (2003) reported examples of basin characterisation where foreland basins are separated into several facies belts parallel to the orogenic front. These belts reflect changes in basin depth, sediment provenance and input rate. Sediments show different characteristics depending upon the facies belt they are deposited in. For example, sediments tend to be coarser and more angular on the wedge-top than in the foredeep. Carbonates are generally considered to be deposited on the forebulge. However, the studied carbonates are interpreted to have been deposited within the shallow foredeep of a tilted piggy back basin. The rationale for this is based

mainly upon the disparity between the San Emiliano and Bernesga Valley mounds. Palaeogeographic reconstructions (Fig. 9.6) have been made which help explain the relationship between the shallower, restricted, laterally continuous San Emiliano sediments and their coeval, deeper, less restricted, more gravity induced related sediments of the Bernesga Valley. The logs of clastic sequences and the microfacies analysis of the carbonate material indicate a relatively shallow depositional environment for the mound bearing La Majúa Member of the San Emiliano Formation, whereas others have indicated that the Carboniferous age Bernesga Valley sediments show evidence for a deeper deposition (e.g. Bowman, 1985). The deltaic sediments of the San Emiliano Fm. at the type locality also indicate a tilted foreland. In modern foredeep depozones sub-aerial forelands which become submarine along tectonic strike have large deltas accumulating within the transition zone (Miall, 1981; Baltzer and Purser, 1990 & DeCelles and Giles, 1996).

In a foreland basin setting it is widely accepted that climatic change, eustatic, tectonic and localised autocyclic mechanisms all play a role in controlling basin characteristics and sediment deposition (Blair and Bilodeau, 1988; DeCelles and Giles, 1996 & Mutti *et al.*, 2003). Clastic sediments are often thought to represent periods of tectonic activity where non-deposition may represent times of quiescence. Blair and Bilodeau (1988) argued that fine grained material was an indicator of tectonic activity, mainly based upon the disparity between erosion rates and tectonic uplift with uplift rates being 8 times higher than denudation rates (up to 117 times higher in arid environments). They argue that it is unlikely that a clastic wedge (especially of coarse clastics) could form during an active tectonic episode. Applying this thinking to the foreland basin development it is suggested that carbonate deposition (specifically the 8 major units from the La Majúa Member) represents tectonic activity (thrusting). The uplift of the hinterland and related flexural subsidence in the foreland exceeds erosion and deposition rates; this leads to a period where sedimentation is 'confined' to the hinterland / foreland boundary (possibly resulting in continental fan type deposits) before marine sediment routes, deltas and fans are once again established. This period represents a time of non-deposition of detrital material within the basin,

allowing the colonisation of the basin by pioneer communities of carbonate producing biota. The transitional event recorded within the mound bearing Unit (Unit 8) supports this idea, with transgression representing basin subsidence. The regressive nature of the sea-level curve throughout the clastic component of the sedimentary sequence represents a restricted basin being filled with sediments and/or climatically driven regression.

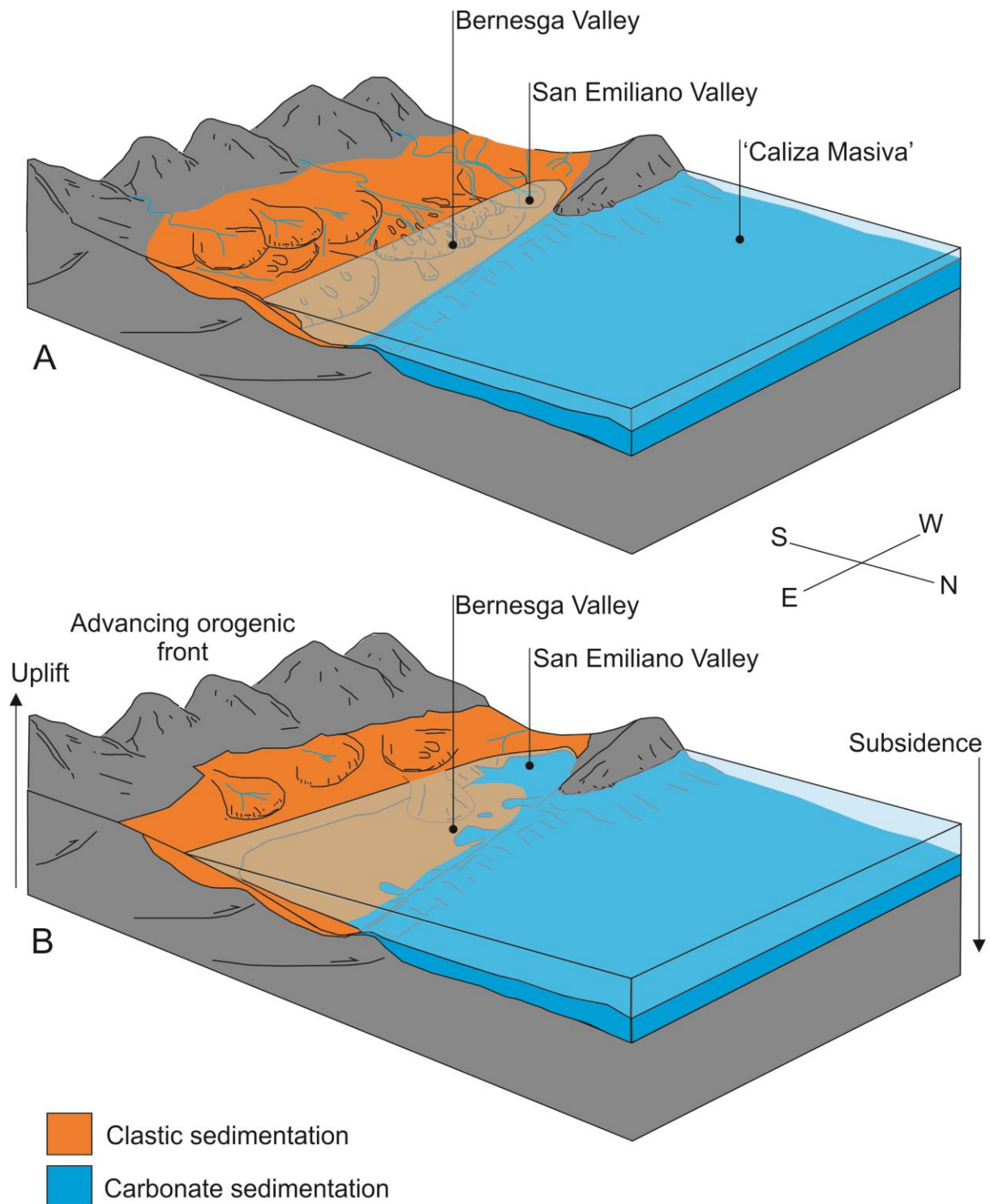


FIGURE - 9.6 A cartoon reconstruction of the depositional environments for the clastic and carbonate deposits of the La Majúa Member of the San Emiliano Formation. A, the clastic deposition is dominated by delta lobe deposits into a narrow, tilted, piggyback foreland basin, to the west is continental Pangea. Sedimentation within the foredeep depozone of the foreland basin transitions from subaerial to submarine in the vicinity of San Emiliano, characterised by deltaic

sediments. Toward the north is a carbonate platform, the 'Caliza Masiva', which bound the basin into which the San Emiliano Fm. is deposited. East of the San Emiliano Valley deposits the water depth increases due to the tilted nature of the basin, turbidites and other gravity driven slumps can be found here. B, this cartoon represents the palaeoenvironment after a tectonic event. The basin subsides resulting in relative sea-level rise. Denudation and transport of sediment into the basin is greatly reduced as uplift rates out-pace erosion rates, leading to a relatively clastic free basin. Carbonate production is established within the basin and platform derived olistoliths slump into the deeper part of the basin as a result of mass wasting of the 'Caliza Masiva'. The tilted nature of the thrust and piggyback basin restricts the basin from the larger foreland, especially to the west.

9.7 Initiation, Growth and Demise

The carbonate mud mounds from the type locality of the San Emiliano Formation initiated as the result of several interacting factors. The combination of a newly opened niche within a restricted, warm and shallow basin encouraged the growth of pioneer or opportunist organisms. The absence of detrital clastic input allowed for carbonate producers to fully establish themselves, resulting in an 'in house' production of carbonate mud. Growth of the mounds resulted from the interaction of the genus *Donezella* and several encrusting forms including the genera *Rothpletzella* and *Claracrusta*. Fluctuating environmental conditions allowed the encrusting forms to bind and stabilise the framework building and carbonate mud baffling *Donezella* growths. *Donezella* grew during 'normal' environmental conditions within the basin whilst the encrusters, which were direct competitors for the environmental niche, flourished during deteriorating conditions. The resulting stabilised (and likely wave resistant) encrusted *Donezella* thickets provided a substrate for further *Donezella* growth when environmental conditions became more tolerable. The mounds ceased to form when detrital sediment deposition returned to the basin. Microfacies analysis indicated that the environment became more open with encrusting forms becoming less common whilst (relatively) large and mobile metazoans become more common. The *Donezella*/encruster relationship ceased and mounds could no longer form. The major factors responsible for mound formation can be attributed to: a] biological community present, b] a restricted basin and c] a lack of clastic input.

Mounds from the Bernesga Valley have a higher affinity with ‘larger’ metazoans (corals and bryozoans) than the San Emiliano Mounds and are associated with worm tubes and sponges. These mounds are interpreted to have formed in a deeper environment with sponges and agglutinated worm tubes playing the role that encrusting forms play in the San Emiliano Mounds. Several of the mounds in the Bernesga Valley are most likely olistoliths which originated from the ‘Caliza Masiva’ to the north. The mounds are well preserved in part due to the rapid lithification of the carbonates.

9.8 Comparison with other Mounds

Various mound types, ranging from Waulsortian-type mounds, biodetrital and microbial mounds, stromatactoid mounds, Tepee Buttes and several others, have been reported both temporally and spatially (e.g. Monty, 1995; Pratt, 1995; Kauffman *et al.*, 1996; Neuweiler *et al.* 2001 & Krause *et al.*, 2004). The different mound types are generally distinguished by their varying biological, sedimentological and setting types. There is also a distinction between Palaeozoic and Mesozoic buildups (Schmid *et al.* 2001). Throughout the Pennsylvanian Series, carbonate units associated with a dominance of *Donezella* growths are relatively common. Several examples also exist from the Permian, although these are far less abundant. These carbonates have been reported to form a wide variety of geometries and features including mud mounds, bioherms, biostromes (see Table 9.1 below) and as carbonate ramps and platforms (Della Porta *et al.*, 2002 & Choh and Kirkland, 2006 and references within). Other mounds (including bioherms and biostromes) containing *Donezella* are summarised in Table 9.1 and are loosely grouped into geographical location. Several common biological associations are apparent. An association with *Petschoria*, *Archaeolithophyllum*, *Komia* and *Ungdarella* is plain to see within the majority of these mounds. Several of the mounds, including those from the Bernesga Valley, are associated with worm tubes and siliceous sponges. No other mounds (other than those in this study), bioherms or biostromes have a reported biological association between *Donezella*, *Claracrusta*, *Rothpletzella*, *Girvanella* and other microscopic encrusting forms. The mud mounds of the San Emiliano Valley have a

composition which is unique when compared to other mounds with a *Donezella* component. Nevertheless, it is likely that mounds of Bashkirian to Moscovian age share a similar growth and nucleation mechanism (see 9.2.1 *The Role of Donezella and its Associated Biota*). Whereas the encrusting forms helped stabilise the *Donezella* growths within the San Emiliano Formation, it is suggested that a similar relationship occurs between *Donezella* and siliceous sponges, worm tubes and *Petschoria*, *Archaeolithophyllum*, *Komia* and *Ungdarella* for other mounded structures. The depth at which the San Emiliano mounds formed may be the cause for this unique biological assemblage with most other *Donezella* mounds forming at a deeper sea level.

Mound description	Age	Location	Reference
Low-energy buildups	Lower Permian	Central Texas (USA)	Wiggins, 1986
<i>Donezella</i> mounds with siliceous sponges, <i>Archaeolithophyllum</i> and worm tubes	Lower Permian	Ouachita Mountains (Oklahoma, USA)	Choh and Kirkland, 2000
<i>Donezella</i> -Siliceous sponge dominated carbonate buildup with worm tubes	Lower Pennsylvanian	Ouachita Mountains (Oklahoma, USA)	Choh and Kirkland, 2006
<i>Donezella</i> low bank to mound controlled by water depth and energy	Moscovian	Hueco Mountains (W Texas and SE New Mexico)	Lambert, 1986 & Lambert and Stanton, 1988
Skeletal microbial <i>Donezella</i> - <i>Tubiphytes</i> (= <i>Shamovella</i>) biostromes	Bashkirian	California (USA)	Watkins, 1999
<i>Donezella</i> baffled mounds associated with <i>Petschoria</i> , <i>Komia</i> and <i>Archaeolithophyllum</i>	Bashkirian - Moscovian	Cantabrian Mountains (Spain)	Rácz, 1964
<i>Donezella</i> mounds with <i>Komia</i> , <i>Ungdarella</i> , encrusting foraminifers, 'phylloid algae' and dasyclads	Bashkirian - Moscovian	Cantabrian Mountains (Spain)	Bowman, 1979
Mounds sparse of <i>Donezella</i> (5-10%).	Bashkirian - Moscovian	Cantabrian Mountains (Spain)	Riding, 1979

<i>Donezella</i> mounds with <i>Petschoria</i> , <i>Komia</i> , <i>Ungdarella</i> , encrusting foraminifers, <i>Archaeolithophyllum</i> and bryozoans	Bashkirian - Moscovian	Cantabrian Mountains (Spain)	Eichmüller, 1985
Skeletal-microbial boundstone. <i>Donezella</i> , agglutinated worm tubes and calcisponges	Bashkirian - Moscovian	Cantabrian Mountains (Spain)	Samankassou, 2001
Skeletal microbial <i>Donezella</i> - <i>Tubiphytes</i> (=Shamovella) mounds	Bashkirian - Moscovian	Cantabrian Mountains (Spain)	Samankassou, 2001
Clotted microbial peloids with <i>Donezella</i> and ‘phyloid algae’	Pennsylvanian	Cantabrian Mountains (Spain)	Samankassou <i>et al.</i> , 2013
<i>Donezella</i> pack- wackestones mounds with <i>Rothpletzella</i> and <i>Claracrusta</i>	Bashkirian - Moscovian	Cantabrian Mountains (Spain)	This study
<i>Donezella</i> mounds with <i>Beresella</i> , <i>Komia/Ungdarella</i> , bryozoans, crinoids, encrusting foraminifers and ostracods	Late Surpukhovian to early Bashkirian	Ellesmere Island (Canadian Arctic Archipelago)	Davies and Nassichuk, 1989
Skeletal <i>Donezella</i> - <i>Tubiphytes</i> (=Shamovella) mounds	Carboniferous	Kazakhstan	Cook <i>et al.</i> , 2007
<i>Donezella</i> and <i>Ungdarella</i> buildups	Bashkirian	Western Urals (Russia)	Proust <i>et al.</i> , 1996

TABLE - 9.1 Summary of documented occurrences of *Donezella* related buildups, the mound type, age, location and original reference is given. Mounds, bioherms and biostromes are all included in this table. It should be noted that Riding (1979) concluded that *Donezella* was not responsible for the formation of the studied mounds. Mounds are grouped into geographical locations.

9.9 The Distribution of Carbonate Mud Mounds through Space and Time

Carbonate mud mounds are present in every Phanerozoic System Period (Figs. 9.7 to 9.13) in a wide variety of environments (see *Appendix 5.Distribution Database* for full references). Mounds appear to peak in abundance during the lower Carboniferous (Mississippian) with high numbers

also found in the Devonian and upper Carboniferous (Pennsylvanian). The global distribution of mounds is highly dominated by their locations in the present Northern hemisphere, especially Northern America and Western Europe. This is probably less due to the actual distribution of mud mounds and more likely a cultural bias (i.e., North American and European Geologists describe mud-mounds frequently, perhaps due to the economic importance that mud mounds have gained as petroleum and mineral exploration targets - Peterson, 1966a 1966b, 1966c; Hovland, 1990; Krause *et al.*, 2004 & De Vos *et al.*, 2005).

Distribution throughout time suggests that the preferred environment for mud mound initiation and growth is within the tropics (i.e., 23°, see lower Carboniferous, Fig. 9.10). Mounds also appear farther pole-ward. Where groups of mounds are observed at higher latitudes, very few mound locations are reported from more equatorial latitudes (see distribution for Lower and Middle Devonian, Fig. 9.9). Isolated mounds are more common within the tropics, higher latitude mounds appear to cluster together (see Lower and Middle Devonian, Fig. 9.9; Jurassic, Fig. 9.12 and Cenozoic, Fig. 9.13).

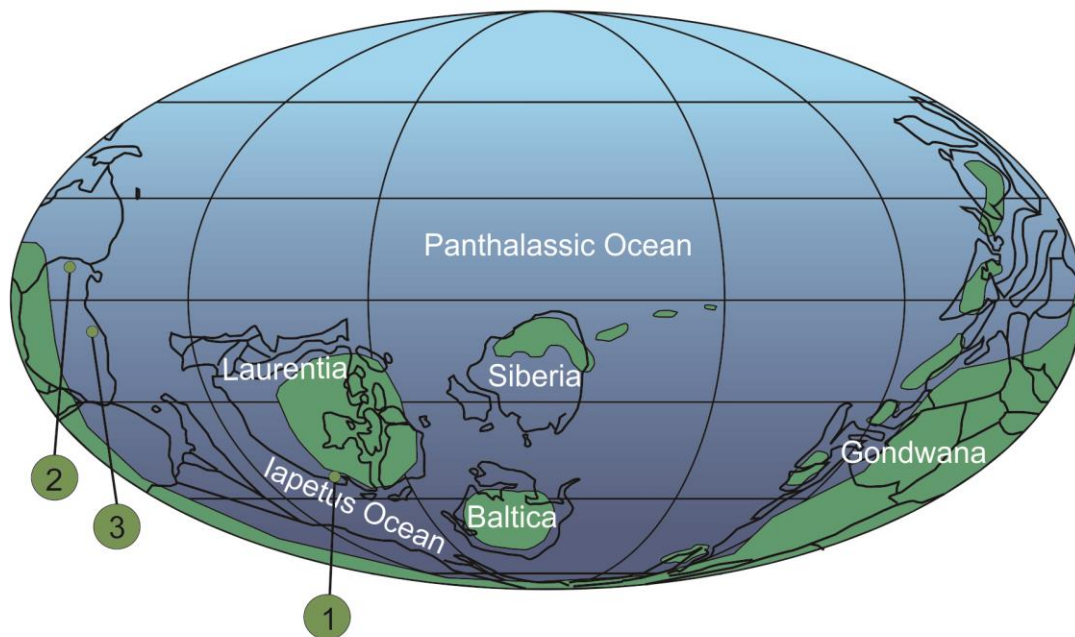
The first recorded mud mounds occur in the Cambrian and numbers steadily increase throughout the lower Palaeozoic until a peak is reached in the lower Carboniferous (Mississippian). Numbers then fall for the upper Carboniferous and continue to decrease for the Permian. The distribution of mounds for this time appears to be dominantly within or bordering the tropics, the biggest exception for this being the Lower and Middle Devonian (Fig. 9.9). Numbers of recorded mounds are the highest within the Palaeozoic where, for example, Krause *et al.* (2004) suggest that well over 2000 mud mounds from the Mississippian of Ireland exist.

The greatest of known extinctions on Earth marks the Permian-Triassic boundary, this extinction brought about the loss of 95% of the known fossil species, with the loss of marine species being the most extreme. It is not surprising then that the abundance in carbonate mud mound numbers sharply decreases between the Permian and Triassic (Fig. 9.11). The Jurassic and Cretaceous

periods see a revival in mound numbers, where the majority of known mounds formed outside or on the borders of the tropics.

The majority of Cenozoic mounds have only been discovered recently due to the contemporary association of mud-mounds with hydrocarbons and the advancement of multibeam bathymetry and side-scanning sonar imagery and the continued use of 2D seismics on shelf areas. Increased recognition of the scientific and possible economic potential of mud-mounds and cool-water corals has led to the European Union funded ACES, ECOMOUND and GEOMOUND research programmes, which have led to the rise in reports on modern mounds (van Weering *et al.*, 2003 & Foubert *et al.*, 2008).

Lower Cambrian Palaeogeography (535Ma)



Middle and Upper Cambrian Palaeogeography (495Ma)

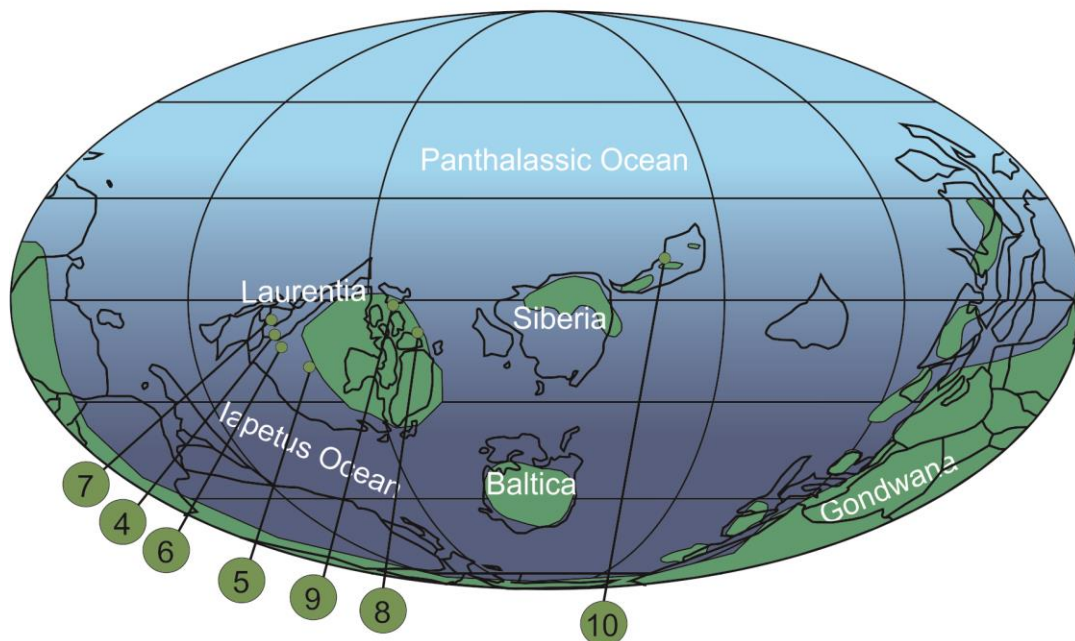
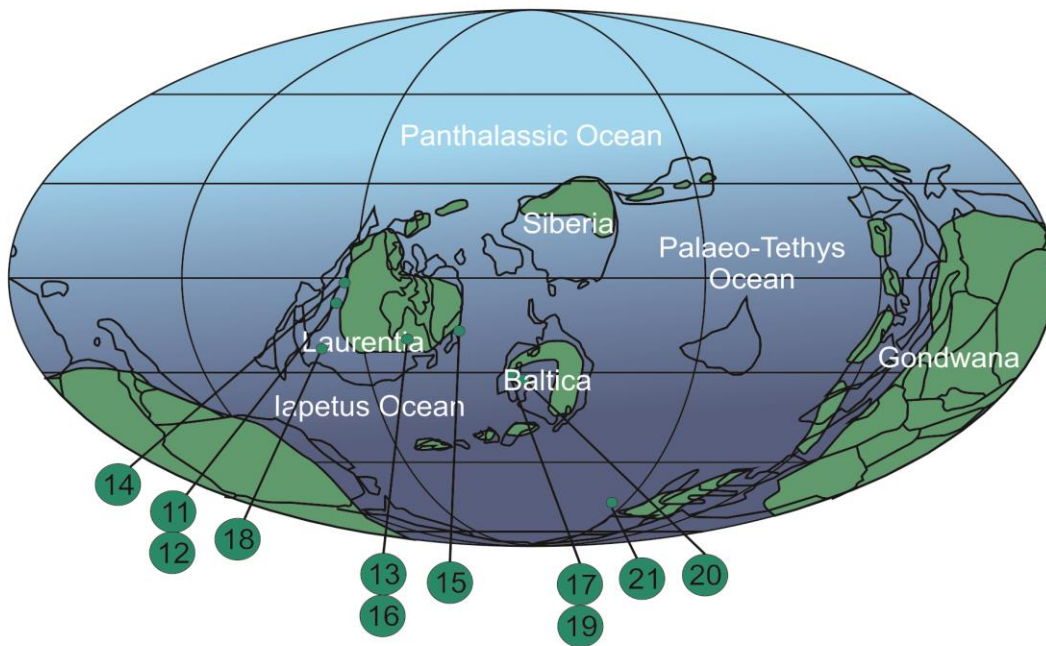


FIGURE - 9.7 Palaeogeographic distribution of known mound locations for the Cambrian, numbers refer to references - see Appendix 5 (After Eldridge *et al.*, 1998).

Middle and Upper Ordovician Palaeogeography (450Ma)



Silurian Palaeogeography (425Ma)

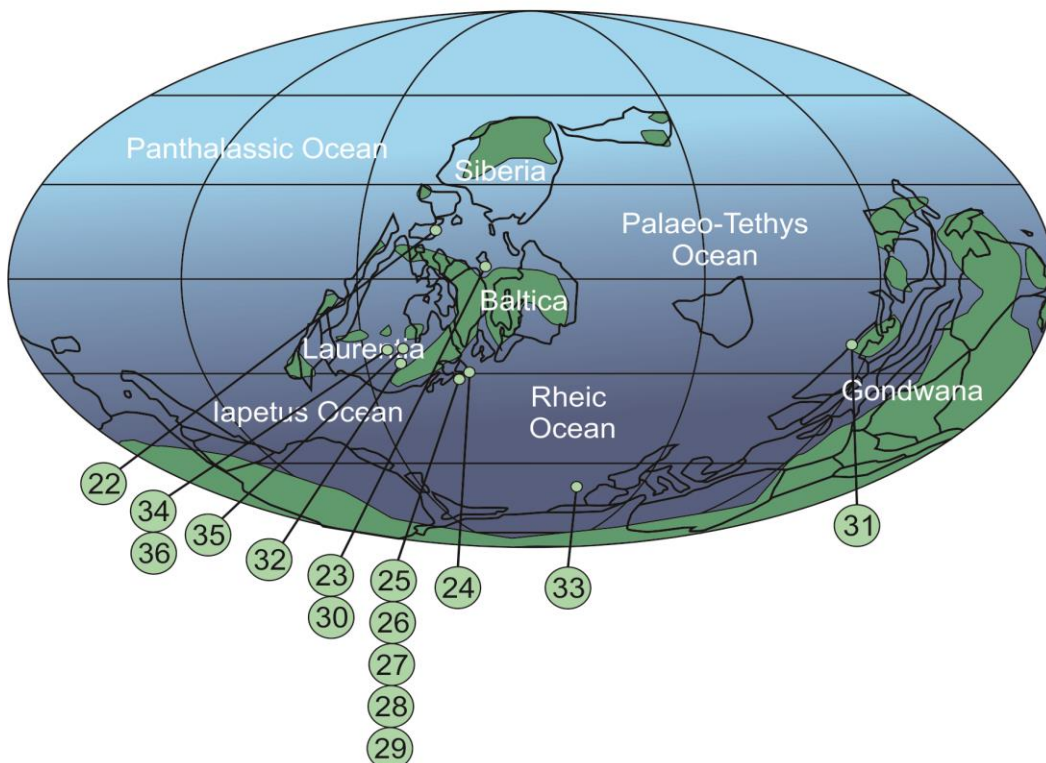
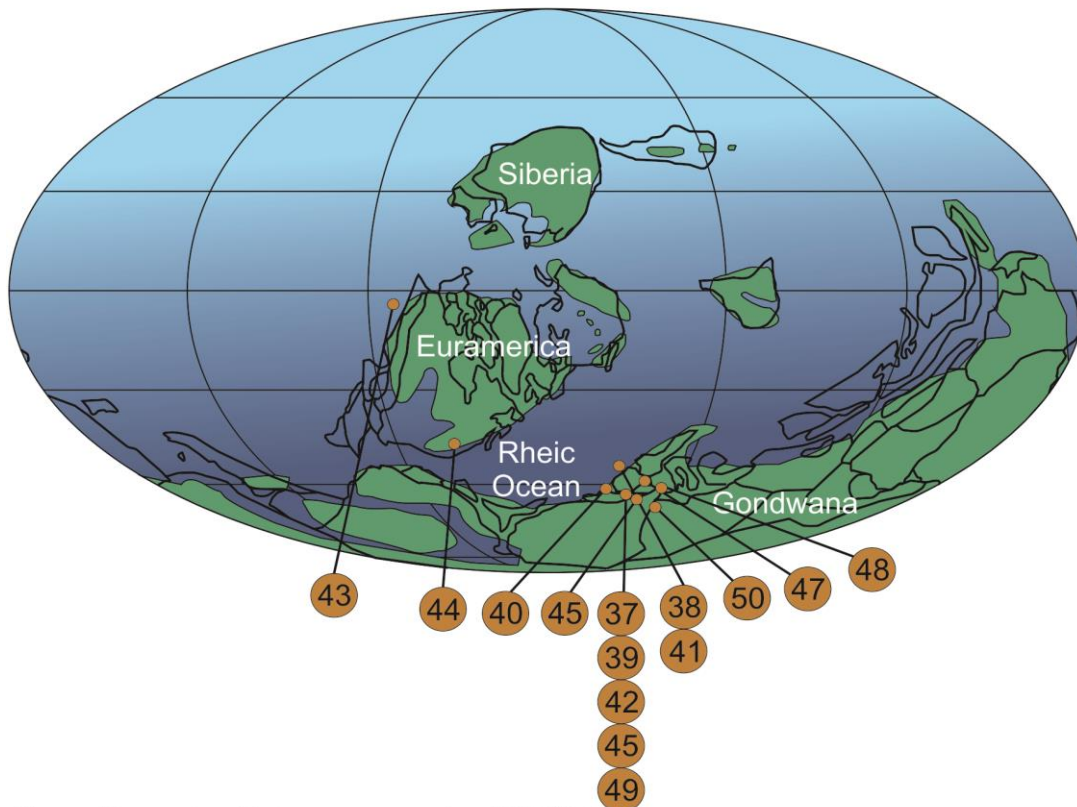


FIGURE 9.8 Palaeogeographic distribution of known mound locations for the Ordovician and Silurian, numbers refer to references - see Appendix 5 (After Eldridge *et al.*, 1998).

Lower and Middle Devonian Palaeogeography (410Ma)



Upper Devonian Palaeogeography (370Ma)

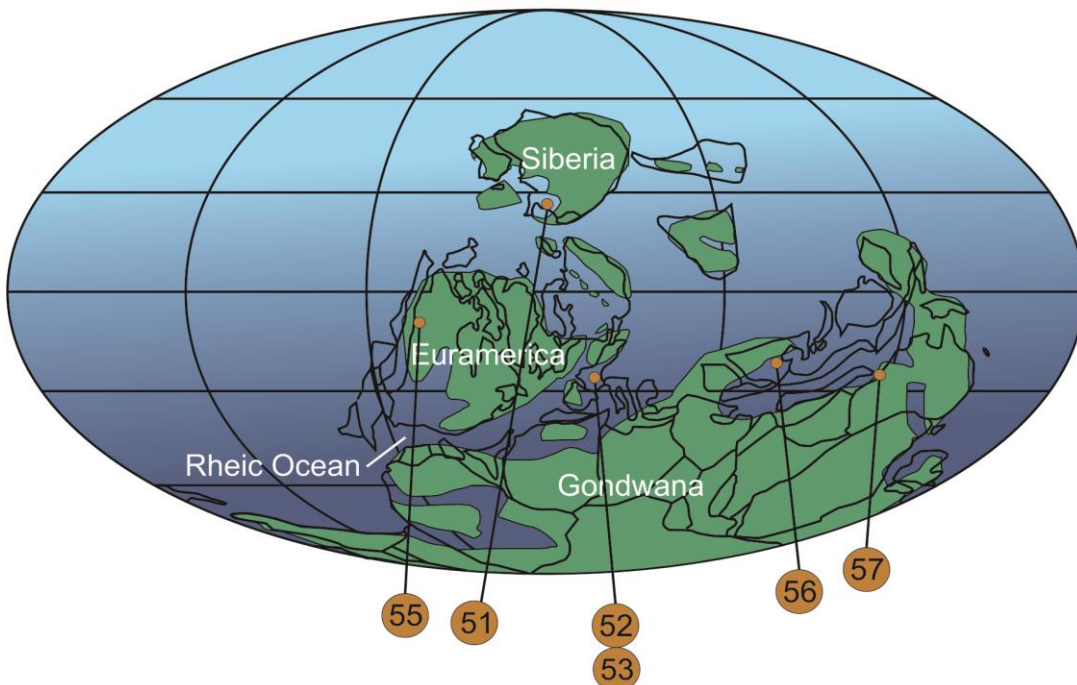
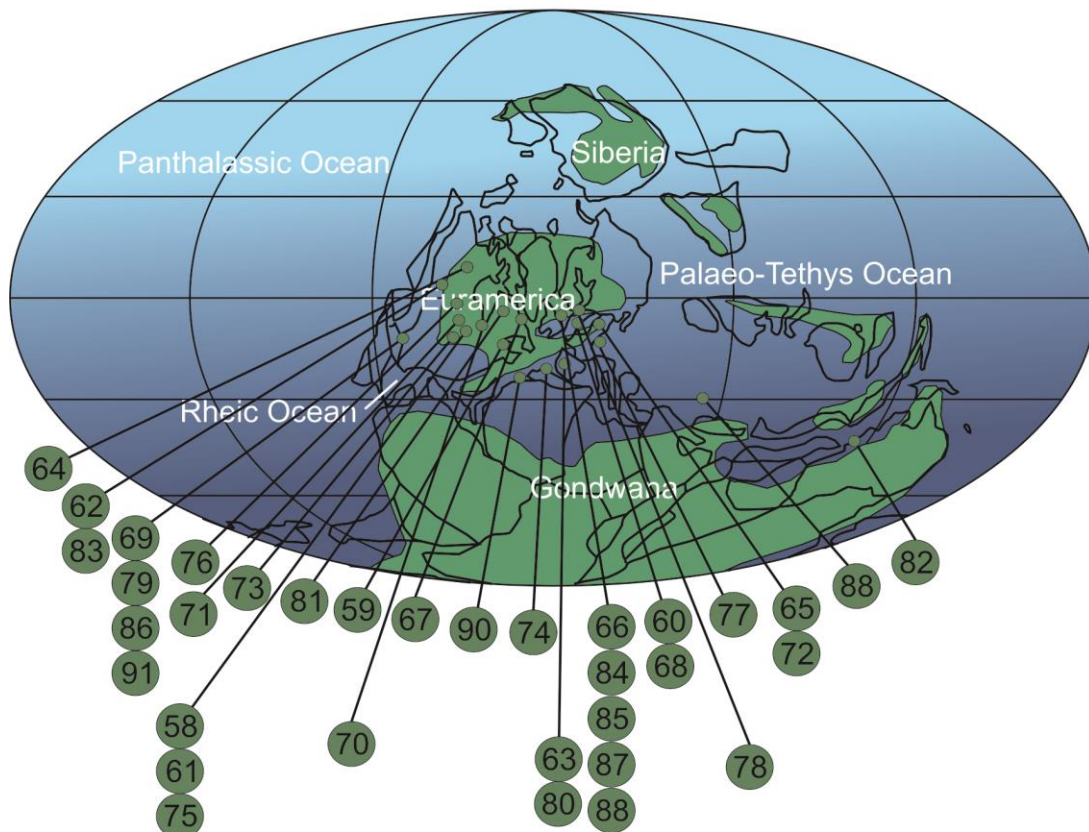


FIGURE 9.9 Palaeogeographic distribution of known mound locations for the Devonian, numbers refer to references - see Appendix 5 (After Eldridge *et al.*, 1998).

Lower Carboniferous (Mississippian) Palaeogeography (340Ma)



Upper Carboniferous (Pennsylvanian) Palaeogeography (300Ma)

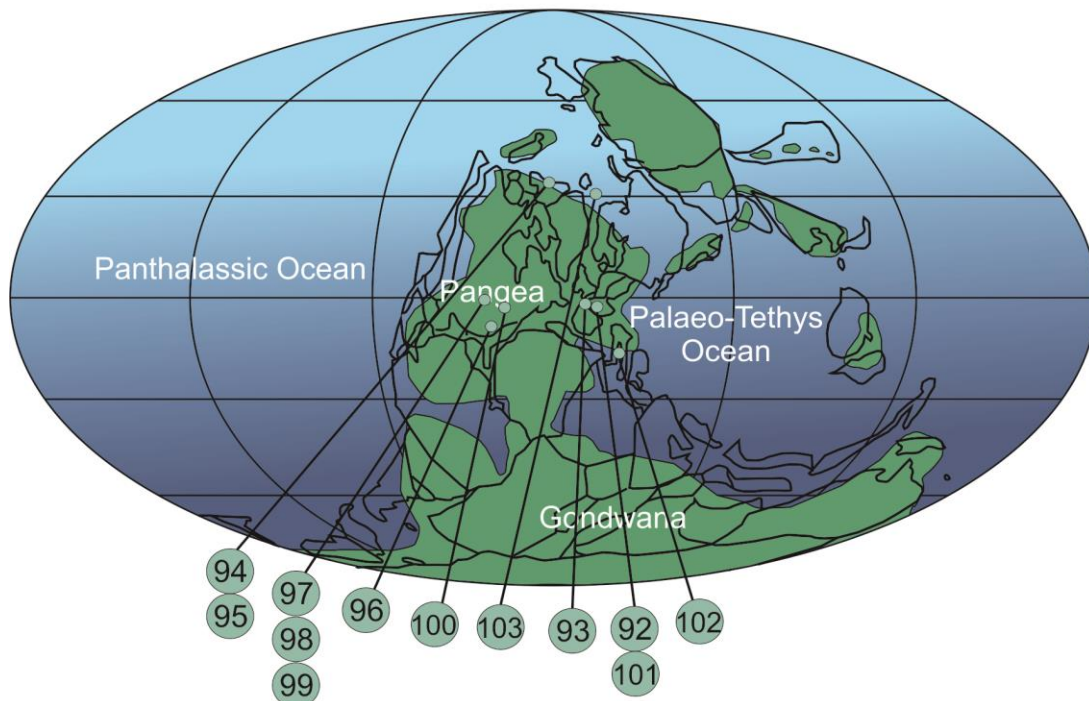
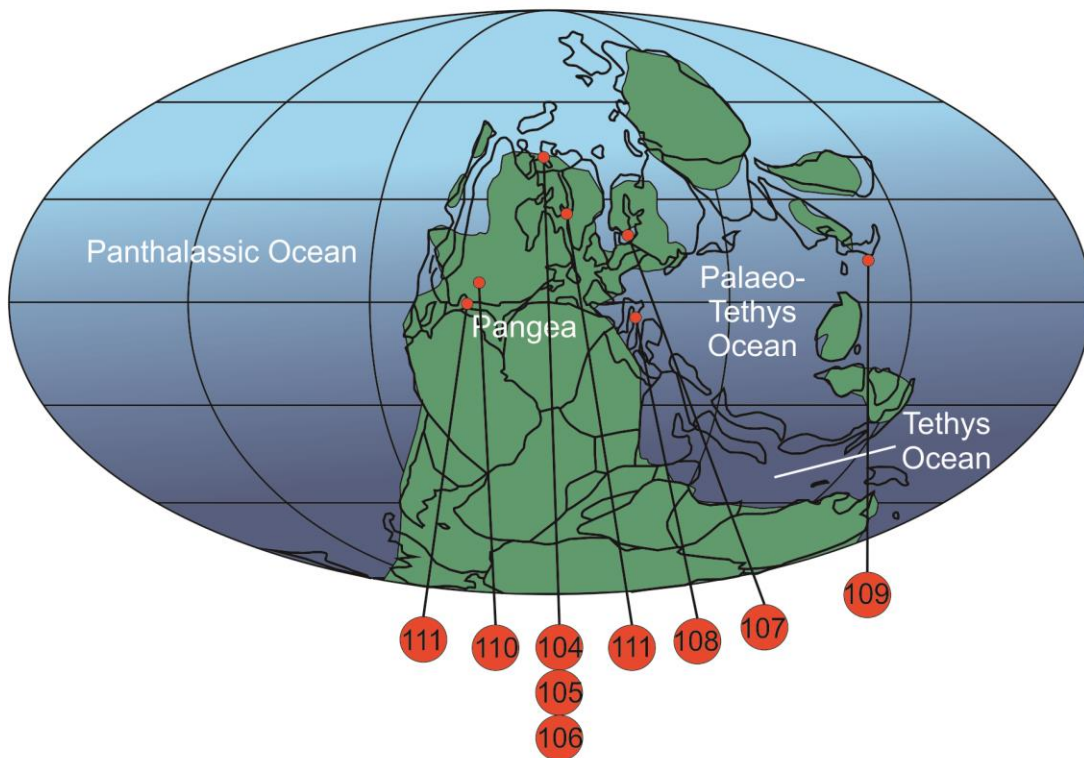


FIGURE 9.10 Palaeogeographic distribution of known mound locations for the Carboniferous, numbers refer to references - see Appendix 5 (After Eldridge *et al.*, 1998).

Permian Palaeogeography (275Ma)



Triassic Palaeogeography (230Ma)

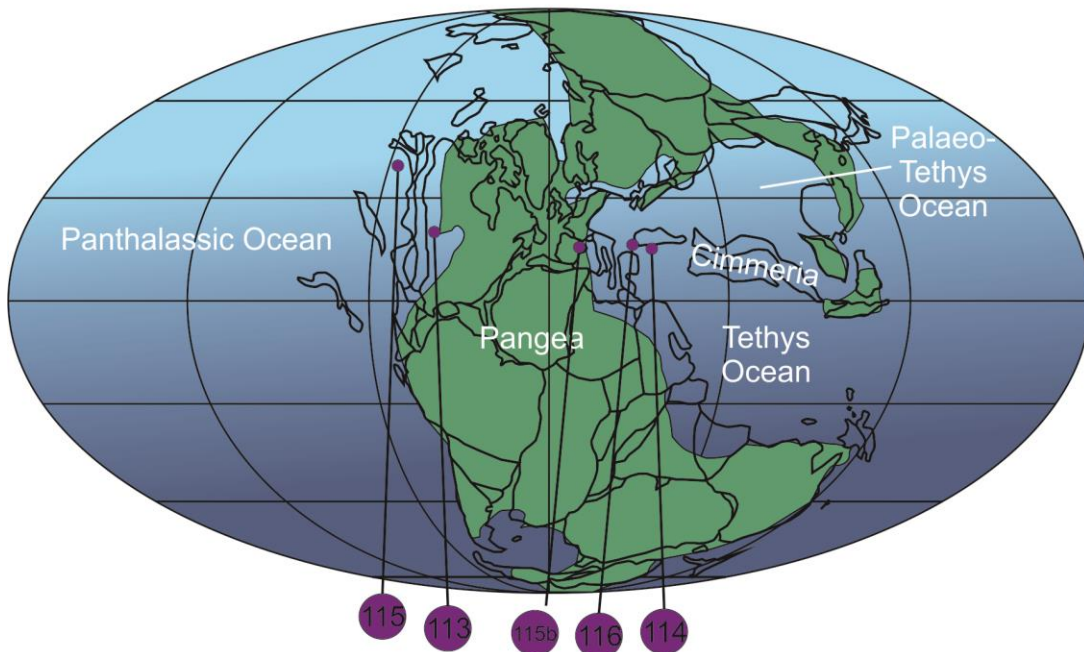
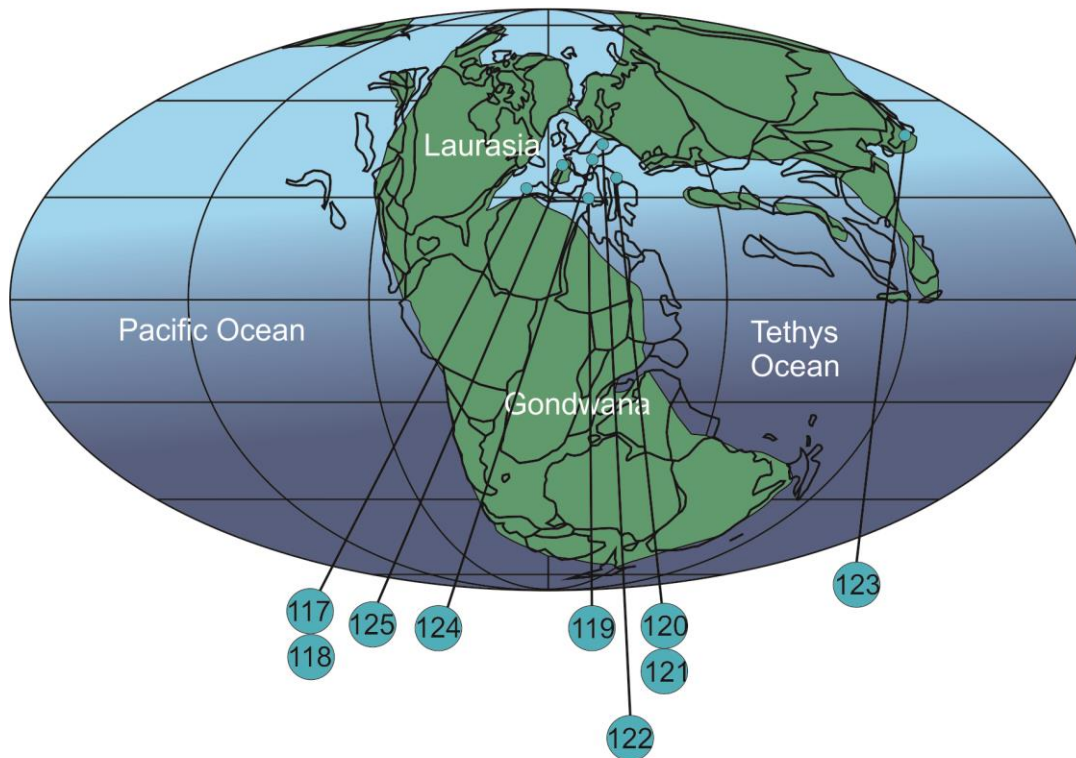


FIGURE 9.11 Palaeogeographic distribution of known mound locations for the Permian and Triassic, numbers refer to references - see Appendix 5 (After Eldridge *et al.*, 1998).

Jurassic Palaeogeography (165Ma)



Cretaceous Palaeogeography (100Ma)

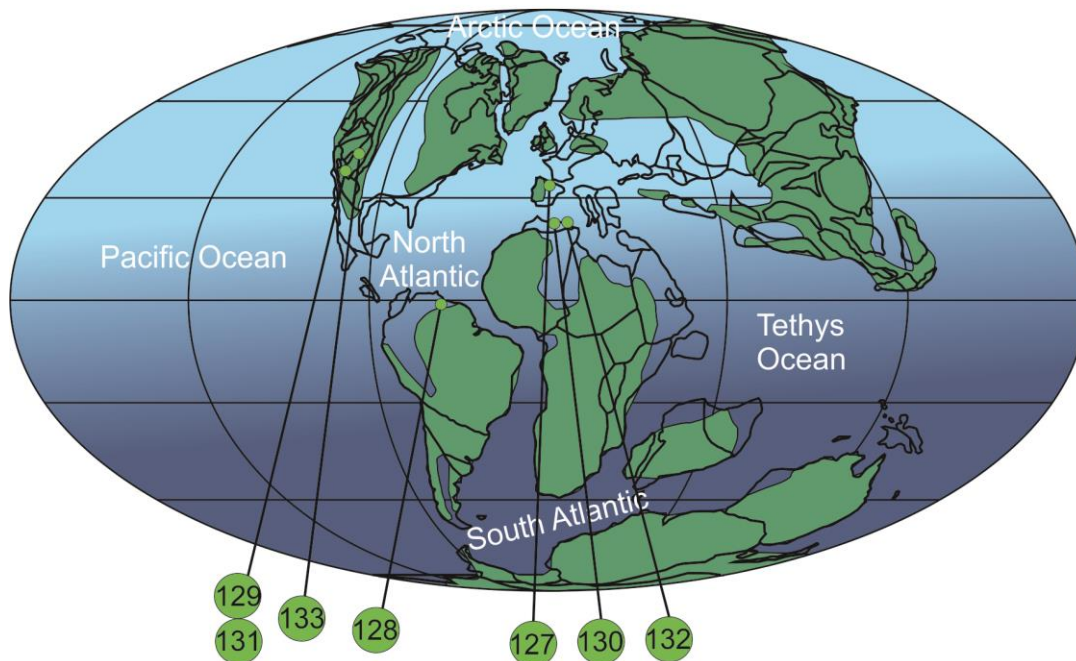


FIGURE 9.12 Palaeogeographic distribution of known mound locations for the Jurassic and Cretaceous, numbers refer to references - see Appendix 5 (After Eldridge *et al.*, 1998).

Cenozoic Palaeogeography (45-0Ma)

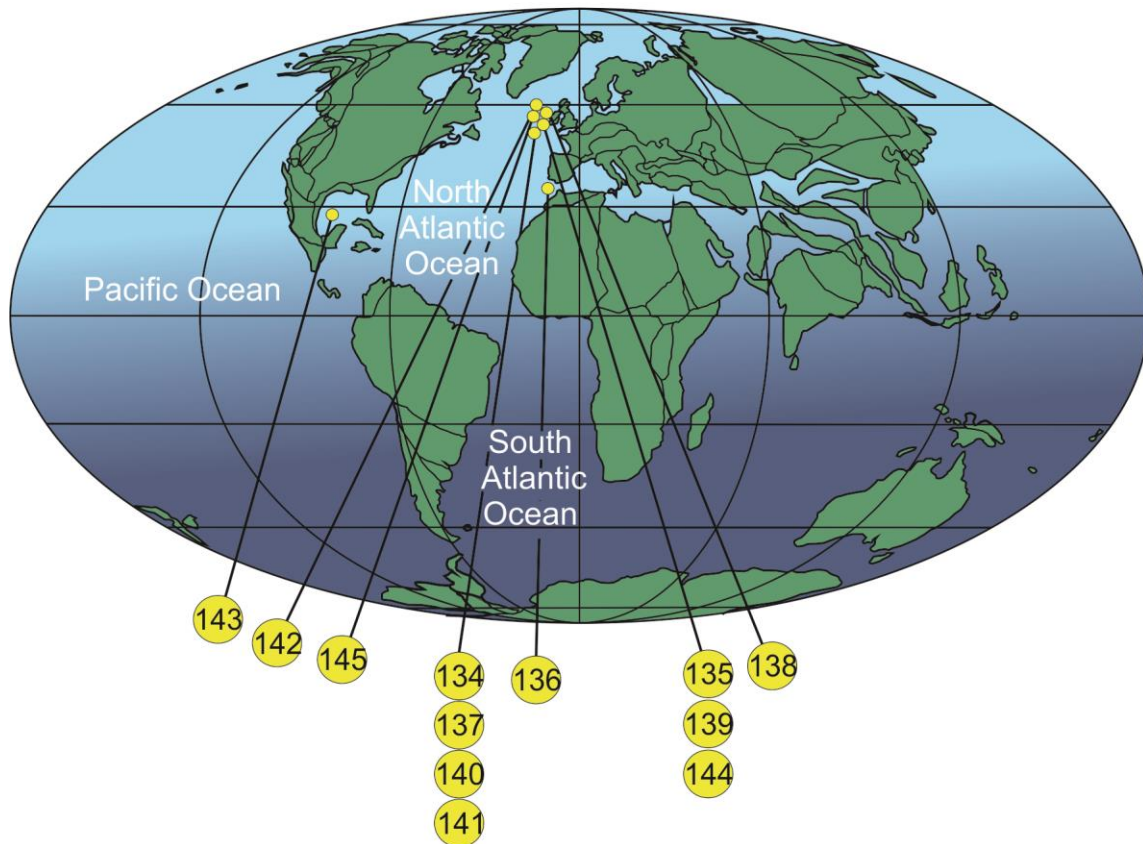


FIGURE - 9.13 Palaeogeographic distribution of known mound locations for the Cenozoic, numbers refer to references - see Appendix 5 (After Eldridge *et al.*, 1998).

By comparing and contrasting the palaeogeographic reconstructions it would appear that mounds can form in a variety of environments but ‘prefer’ low latitudes (i.e., equatorial seas). The dominance of mounds at lower latitudes during the Mississippian age is an example of this bias. So why are mounds not always found at the equator? Why are they often found occupying higher latitudes? An explanation for this may be that mud mounds and ‘ecological’ reefs share the same preferred environments and are competitors. Where reefs are generally found (see Flügel and Flügel-Kahler, 1992), mounds are not and *vice versa* (James and Bourque, 1992). This suggests that reefs are a more successful guild of biota than mounds and it seems likely that mounds thrive in areas where reefs cannot. So for the Mississippian, the abundance of mounds in equatorial

waters could be explained by the combination of a cool climate and the extinction of major reef builders at the end of the Devonian, which would ultimately allow mound biota to infiltrate and occupy niches usually dominated by reefs. The presence of mounds could then be fortified by their ‘in house’ nature of existence; with no input from outside sources mounds continue to grow. Organic matter degradation and sulphur reduction on mounds would further increase growth and pH is regulated by microbes to a pH level which suits their proliferation better, further decreasing other species abilities to encroach. Mound communities related to seeping of methane and other fluid dispersion sites are found at all latitudes throughout geological history which would suggest that whilst mounds can occupy this niche, reefs cannot.

9.10 Chapter Summary

The carbonate mud mounds of the San Emiliano Formation (at the type locality) are skeletal-microbial pack- wackestone often associated with fenestral cavities. The mounds are dominated by two common biological assemblages; Donezellaceans (most commonly *Donezella* but also including *Beresella* and *Dvinella*) and laminar encrusters (including *Claracrusta*, *Rothpletzella*, *Wetheredella* and *Girvanella*). Fluctuating environmental conditions lead to a succession of repetitive conditions favouring one set of organisms. This led to the repetition of encrusters growing on, and stabilising, Donezellacean thickets. The encrusters were then, in turn used as a substrate for further Donezellacean growth. The mounds nucleated and grew on the flank of a tilted foreland basin within a shallow, warm and restricted environment. Mounds from the Bernesga valley area are compositionally different from those of the San Emiliano Valley. The Bernesga valley mounds contain far less of the typical encrusting biota of the San Emiliano valley and are instead associated with sponges and worms. The calcite which the carbonate units of the San Emiliano Formation are now composed of originated as the polymorph aragonite, which has since undergone neomorphism. The San Emiliano Fm. was deposited into the foredeep of a tilted foreland basin at the front of the advancing Variscan front. The distribution of carbonate mud mounds throughout the Phanerozoic suggests that mounds and reefs may compete for the same

ecological niche. Reef biota is interpreted to be a more successful guild of biota than that of mounds. Mounds become more dominant when reef biota is restricted.

10. Conclusion

The overall aims of this research were to provide a detailed microfacies, palaeontological and geochemical analysis of the carbonate mud mounds of the San Emiliano Formation and associated deposits. The rationale for this being that the carbonate lithologies of the San Emiliano Formation were relatively poorly understood when compared with the clastic lithologies of the formation. Inherent in achieving the aims of this research were four main objectives. This chapter provides a summary of the research which completes the main objectives as well as identifying the significant outcomes of the study.

The first objective was “*To characterise the sedimentary nature of the La Majúa Member of the San Emiliano Formation with emphasis on the carbonate units*”. The San Emiliano Formation consists of shallow marine sediments of both clastic and carbonate lithologies. Deposition took place on the flanks of a tilted foreland basin at the front of an active thrust belt (the Variscan Orogeny). Clastic deposition took place on top of a delta lobe whereas carbonates were deposited in a time of clastic input quiescence. The zone within the foreland basin in which deposition took place is interpreted to be the transitional zone between a sub-aerial wedge top and the axial part of the foredeep depo-zones. Clastic sediments consist of eight coarsening sequences consisting of siltstones and sandstones with occasional limestone beds and thin coals, these were deposited by delta lobes prograding into a shallow marine environment. The carbonate units of the La Majúa Mb. were deposited on top of the delta lobes responsible for the clastic successions during a time of clastic input quiescence, and are represented by four main facies. Three distinctive microfacies are recognised between mound, basal and capping material whereas a fourth facies is recognised which is dominated by cyclical micrite and marl. Carbonate mud mounds from the carbonate units of the member are interpreted as skeletal-microbial pack-wackestones with various cavity networks. Specific microfacies types recognised within the mound included: 1] fenestral packstones with peloids and *Donezella*, 2] whole fossil bioclastic floatstones (*Donezella*

dominated) and 3] bioclastic packstones with non-laminated homogenous micrite and whole *Donezella* thalli. The mounds vary in size ranging from 2 to 50 m in thickness and are steep sided, lens to mound shaped. Mounds are composed of homogenous, peloidal and clotted micrites. Peloids are of various shapes and sizes, many grains observed had a micritic envelope. Five distinct sub-facies were recognised for the cyclical micrite-marl beds, these were: 1] bioclastic packstone (high diversity), 2] microbial and algal baffle/boundstone, 3a] *Donezella* boundstone, 3b] *Donezella* bafflestone, 4] *Petschoria* and ‘phylloid’ algae bafflestone and 5] Whole fossil wackestone (with dominant ‘phylloid’ algae). The coevally deposited sediments of the Bernesga Valley, which have been mistakenly referred to as the San Emiliano Formation and should be referred to as the Lois-Cigüera Formation, were deposited in a deeper environment.

The second objective was to “*Constrain the palaeontological community associated with the carbonate mud mounds present*”. The dominant palaeontological communities were low diversity assemblages reflecting a pioneer or opportunist community living in a newly opened (relatively restricted) niche. The dominant mound communities were: a *Donezella* community, with rare foraminifera (*Tetrataxis* and *Lasiodiscus*) and a laminar encrusting community comprising mostly of the genera *Rothpletzella*, *Claracrusta* and *Girvanella*. These two communities competed for habitat and had a dynamic relationship controlled by fluctuating environmental conditions. Off mound sediments (basal and capping facies) were commonly associated with higher biodiversity, including biota such as bryozoans, corals and foraminifera. A unique palaeontological assemblage related with cyclical micrite and marl beds was also identified. This assemblage was dominated by ‘phylloid’ algae, auloporid corals and encrusting forms. Microbial activity was present as inferred from clotted peloids. Three new morphotypes are identified and presented.

The third objective was to “*Identify external and internal controls on sedimentary deposition of the carbonate mud mounds present*”. Sedimentary deposition of the mounds was characterised by autochthonous micrite, in the “in-house” manner, typical of many microbial mounds. Clotted

peloids of different sizes and shapes and algal thalli in various states of preservation suggest that the carbonate deposition is the result of degradation of algal thalli. The sediments were most probably originally aragonitic and would have been a mesh of aragonitic needles. Aggrading neomorphism being responsible for the calcite found today. Carbonate precipitation occurred due to a hiatus in siliciclastic deposition. Siliciclastic deposition into the basin was controlled by climatic and tectonic activity as well as autocyclic mechanisms. Carbonate deposition took place in times of clastic quiescence as a result of an advance of the Variscan Orogenic front. Clastic input into the foreland basin was briefly increased as tectonics raised the hinterland, increasing potential for erosive product. Tectonic uplift of the hinterland continued, eventually outstripping the rate of erosion leading to a drastic reduction in clastic deposition into the foreland basin.

The fourth objective was to “*Identify processes (physical, biological or chemical) responsible for mound nucleation and growth*”. Geochemical analysis ruled out hydrothermal or hydrocarbon seepage as a nucleation or growth mechanism for the carbonate mud mounds. The process identified as being responsible for the nucleation and growth of the mounds is a dynamic relationship between the *Donezella* dominated community and the laminar encrusting form dominated community. As indicated by microfacies analysis the environmental conditions of deposition fluctuated. Where conditions were near normal, *Donezella* flourished, acting as a microscopic framework builder as well as a baffler. Environmental degradation led to the encruster guild becoming dominant. Laminar encrusters grew in a non-selective manner covering the majority of grain types. Commonly the encrusters could be found atop of *Donezella* thickets, stabilising and protecting the (supposedly) delicate *Donezella* thalli. When environmental conditions returned to suit *Donezella* the laminar encrusters provide a suitable substrate for new growth. Mounds ceased to form due to drowning by a deepening sea-level or by an increase in clastic sediment resulting in a clastic-rich bed draped over the mound.

10.1 Future Work

Several potential avenues of research have presented themselves as a result of this work. The main possibilities are:

1. A complete review of *Donezella* and of *Tuberitina*, two genera which have proved taxonomically controversial. A review of both genera would be welcomed. Using methods which are becoming increasingly accessible and affordable (e.g. SEM analysis) the taxonomic confusion surrounding both genera might be reduced. Palaeoecological studies of the genera would greatly contribute to the understanding of their ecological distribution and their use as “environmental proxies”.
2. The spatial and temporal relationship between carbonate mud mounds and a comparison of different mound types, nucleation and growth mechanisms compared with global trends and events. This would build on from the spatial and temporal comparison presented here.
3. The application of the hypothesis that limestone - marl alternations favour deposition in settings that favoured aragonite deposition (Westphal and Munnecke, 2003 & Munnecke and Westphal, 2004). Using the sequences observed at the Pinos Hairpin and beneath the Pinos Pylon Mound may provide further evidence for an aragonitic precursor sediment for mound carbonates.
4. Throughout the study the Standard Microfacies Types and the environmental distribution in Facies Zones is based upon those of the rimmed carbonate platform model. Microfacies types frequently described in studies dealing with Palaeozoic and Mesozoic foreland basins could be incorporated into a depositional model to better constrain SMF types (Flügel, 2004).

References

- Adachi, N., Ezaki, Y. and Pickett, J. W. 2007. Interrelations between framework-building and encrusting skeletal organisms and microbes: more-refined growth history of Lower Devonian bindstones. *Sedimentology*. Vol. 54. Pg. 89-105
- Aguirre, J., Perfectti, F. and Braga, J. C. 2010. Intergrating phylogeny, molecular clocks, and the fossil record in the evolution of coralline algae (Corallinales and Sporolithales, Rhodophyta). *Paleobiology*. Vol. 36. Pg. 519-533
- Allègre, C. J. 2008. *Isotope Geology*. Cambridge
- Álvaro, J.J., Van Vliet-Lanoë, B., Vennin, E. and Blanc-Valleron, M. -M. 2003. Lower Cambrian paleosols from the Cantabrian Mountains (northern Spain): a comparison with Neogene-Quaternary estuarine analogues. *Sedimentary Geology*. Vol. 163. Pg. 67-84
- Antoshkina, A. I. 2006. Palaeoenvironmental implications of Palaeomicrocodium in Upper Devonian microbial mounds of the Chernshev Swell, Timan-northern Ural Region. *Facies*. Vol. 52. Pg. 611-625
- Aramburu, C., Truyols, J., Arbizu, M. 1992. El Paleozoico Inferior en la Zone Cantábrica. In: Gutiérrez Marco, J. C., Saavedra, J. and Rábano, I. (Eds.) *Paleozoico Inferior de Ibero-America*. University of Extremadura, Badajoz, 397-421
- Arp, G., Thiel, V., Reimer, A., Michaelis, W. and Reitner, J. 1999. Biofilm exopolymers control microbialite formation at thermal springs discharging into the alkaline Pyramid Lake, Nevada, USA. *Sedimentary Geology*. Vol. 126. Pg. 159-176
- Aubrecht, R., Szulc, J., Michalík, J., Schögl, J. and Wagreich, M. 2002. Middle Jurassic Stromatactis Mud-mound in the Pieniny Klippen Belt (Western Carpathians). *Facies*. Vol. 47. Pg. 113-126
- Schlögl, J., Krobicki, M., Wierzbowski, H., Matyja, B. A. and Wierzbowski, A. 2009. Middle Jurassic stromatactis mud-mounds in the Pieniny Klippen Belt (Carpathians) - A possible clue to the origin of stromatactis. *Sedimentary Geology*. Vol. 213. Pg. 97-112
- Bahamonde, J. R., Colmenaro, J. R., Fernández, L. P., Moreno, C., Barba, P., Heredia, M. and González, F. 2002. Carboniferous. In: Gibbons, W. and Moreno, M. T. (Eds). *The Geology of Spain*. Geological Society, London. Pg. 93-116
- Baltzer, F and Purser, B. H. 1990. Modern alluvial fan deltaic sedimentation in a foreland tectonic setting: the lower Mesopotamian Plain and the Arabian Gulf. *Sedimentological Geology*. Vol. 67. Pg. 175-197
- Barham, M., Murray, J., Joachimski, M. M. and Williams, D. M. 2012. The onset of the Permo-Carboniferous glaciation: reconciling global stratigraphic evidence with biogenic apatite $\delta^{18}\text{O}$ records in the late Viséan. *Journal of the Geological Society*. Vol. 169. Pg. 119-122
- Bathurst, R. G. C. 1970. Problems of lithification in carbonate muds. *Geologists Association Proceedings*. Vol. 81. Pg. 429-440
- 1975. *Carbonate sediments and their diagenesis*. Developments in Sedimentology (2nd Ed.). Elsevier
- 1980. Stromatactis - Origin related to submarine-cemented crusts in Paleozoic mud mounds. *Geology*. Vol. 8. Pg. 131-134

- 1982. Genesis of stromatactis cavities between submarine crusts in Palaeozoic carbonate mud buildups. *Journal of the Geological Society of London*. Vol. 139. Pg. 165-181

Barnaby, R. J. and Read, F. 1990. Carbonate ramp to rimmed shelf evolution: Lower to Middle Cambrian continental margin, Virginian Appalachians. *Geological Society of America Bulletin*. Vol. 102. Pg. 391-404

Barrois, C. 1882. Recherches sur les terrains anciens des Asturies et de la Galice. *Mémoires de la Socite Géologique de Nord*. Vol. 2. Pg. 1-630

Bassler, R. S. 1953. Bryozoa. In: Moore R. C. (ed.). *Treatise on Invertebrate Paleontology*. Part G. Geological Society of America and University of Kansas Press

Basson, P. W. and Edgell, H. S. 1971. Calcareous algae from the Jurassic and Cretaceous of Lebanon. *Micropaleontology*. Vol. 17. Pg. 411-433

Baud, A., Cirilli, S. and Marcoux, J., 1996. Biotic response to mass extinction: the lowermost Triassic microbialites. In: Reitner, F., Neuweiler, F., Monty, C. (Eds.) *Biosedimentology of Microbial Build-Ups—IGCP Project No. 380*. Facies, vol. 36. pg. 238– 242

- Richoz, S., Cirilli, S. and Marcoux, J., 2002. Basal Triassic carbonate of the Tethys: a microbialite world. *16th International Sedimentological Congress*. Rand Afrikaans University, Johannesburg, South Africa, pg. 24-25

Beauchamp, B. and Savard, M. 1992. Cretaceous Chemosynthetic Carbonate Mounds in the Canadian Arctic. *Palaios*. Vol. 7. Pg. 434-450

Beckhoff, B., Kanngießer, B., Langhoff, N., Wedell, R. and Wolff, H. 2006. *Handbook of Practical X-Ray Fluorescence Analysis*. Springer-Verlag Berlin Heidelberg

Belka, Z. 1998. Early Devonian Kess-Kess Carbonate Mud Mounds of the Eastern Anti-Atlas (Morocco), and their relation to submarine hydrothermal venting. *Journal of Sedimentary Research*. Vol. 68. Pg. 368-377

Berger, A., Loutre, M. F. and Dehant, V. 1989a. Influence of the changing lunar orbit on the astronomical frequencies of Pre-Quaternary insolation patterns. *Paleoceanography*. Vol. 4. Pg. 555-564

-, - and -. 1989b. Pre-Quaternary Milankovitch frequencies. *Nature*. Vol. 323. Pg. 87-110

Berger, S. & Kaeffer, M. J. 1992. *Dasycladales: An Illustrated Monograph of a Fascinating Algal Order*. Thieme, Stuttgart

Berkýová, S. and Munnecke, A. 2010. “Calcspheres” as a source of lime mud and peloids - evidence from the early Middle Devonian of the Prague Basin, the Czech Republic. *Bulletin of Geosciences*. Vol. 85. Pg. 585-602

Beyer, A. 2001. High-resolution bathymetry of the European continental slope. *Contributions to 16 Hydrographentag 2001* . German Hydrographic Society

- 2006. Seafloor analysis based on multibeam bathymetry and backscatter data = Meeresbodenanalyse auf der Basis von Bathymetrie und akustischer Rückstreuung. *Berichte zur Polar- und Meeresforschung (Reports on Polar and Marine Research)*. Bremerhaven, Alfred Wegener Institute for Polar and Marine Research

- Chakraborty, B. and Werner Schenke, H. 2007. Seafloor classification of the mound and channel provinces of the Porcupine Seabight: an application of the multibeam angular backscatter data. *International Journal of Earth Sciences*. Vol. 96. Pg. 11-20

Birgel, D., Peckmann, J., Klautzsch, S., Thiel, V. and Reitner, J. 2006. Anerobic and aerobic oxidation of methane at Late Cretaceous seeps in the Western Interior Seaway, USA. *Geomicrobiology Journal*. Vol. 23. Pg. 565-577

Blair, T. C. and Bilodeau, W. L. 1988. Development of tectonic cyclothems in rift, pull-apart, and foreland basins: Sedimentary response to episodic tectonism. *Geology*. Vol. 16. Pg. 517-520

Blakey, R. 2011. *Palaeogeography of Europe*. Colorado Plateau Geosystems. <http://cpgeosystems.com/europaleogeography.html> (Accessed 26/05/15)

Błażejowski, B. 2009. Foraminifers from the Treskelodden Formation (Carboniferous-Permian) of south Spitsbergen. *Polish Polar Research*. Vol. 30. Pg. 193-230

Blendinger, W., Bowlin, B., Zijp, F. P., Darke, G. and Ekroll, M. 1997. Carbonate buildups flank deposits: an example from the Permian (Barents Sea, northern Norway) challenges classical facies models. *Sedimentary Geology*. Vol. 112. Pg. 89-103

Bond, D. and Wignall, P. B. 2010. Pyrite framboids study of marine Permian-Triassic boundary sections: a complex anoxic event and its relationship to contemporary mass extinction. *Geological Society of America Bulletin*. Vol. 122. Pg. 1265-1279

Bosellini, A. 1989. Dynamics of Tethyan carbonate platforms. *SEPM Special Publication*. Vol. 44. Pg. 3-13

Bosence, D. W. J. 1995. Anatomy of a Recent biotrital mud-mound, Florida Bay, USA. In: Monty, C. L. V. Bosence, D. W. J. Bridges, P. H. and Pratt, B. R. (Eds.) *Carbonate Mud-Mounds Their Origin and Evolution*. International Association of Sedimentologists. Blackwell Science. Vol. 23. Pg. 775-493

- and Allison, D. W. J. 1995. (Eds.) *Marine paleoenvironmental analysis from fossils*. Geological Society of London, Special Publication. Vol. 83.

- and Bridges, P. H. 1995. Origin and evolution of carbonate mud-mounds. In: Monty, C. L. V. Bosence, D. W. J. Bridges, P. H. and Pratt, B. R. (Eds.) *Carbonate Mud-Mounds Their Origin and Evolution*. International Association of Sedimentologists. Blackwell Science. Vol. 23. Pg. 3-9

Boudagher-Fadel, M. 2008. Evolution and Geological Significance of Larger Benthic Foraminifera. *Developments in Paleontology and Stratigraphy*. Vol. 21

Bourque, P-A. and Gignac, H. 1983. Sponge-constructed stromatactis mud mounds, Silurian of Gaspé, Quebec. *Journal of Sedimentary Research*. Vol. 53. Pg. 521-532

- and Amyot, G. 1988. Stromatoporoid-coral reefs of the Upper West Point Reef Complex, Late Silurian, Gaspé peninsula, Quebec. In: Geldsetzer, H. H. J., James, N. P. and Tebbutt, G. E. (Eds.), *Reefs, Canada and Adjacent Area*. Canadian Society of Petroleum Geologists. Memoir 13. Pg. 251-257

- Raymond, L. 1994. Diagenetic alteration of early marine cements of Upper Silurian stromatactis. *Sedimentology*. Vol. 41. Pg. 255-269

- Amyot, G., Desrochers, A., Gignac, H., Gosselin, C., Lachambre, G. and Laliberte, J. Y. 1986. Silurian and Lower Devonian reef and carbonate complexes of the Gaspé Basin, Quebec - A summary. *Bulletin of Canadian Petroleum Geology*. Vol. 34. Pg. 452-489

Bowman, M. B. J. 1979. The depositional environments of a limestone unit from the San Emiliano Formation (Namurian/Westphalian), Cantabrian Mts., NW Spain. *Sedimentary Geology*. Vol. 24. Pg. 25-43

- 1982. The Stratigraphy of the San Emiliano Formation and its relationship to other Namurian/Westphalian A sequences in the Cantabrian Mts., N W Spain. *Trabajos de Geologia*. Vol. 12. Pg. 23-35
 - 1985. The sedimentology and paleogeographic setting of late Namurian-Westfalian. A basin-fill succession in the San Emiliano and Cármenes areas of NW león, Cantabrian Mountains, NW Spain. In: Lemos de Sousa, H. J. and Wagner, R. H. (Eds.) *Papers on the Carboniferous of the Iberian Peninsula (Sedimentology, Stratigraphy, Paleontology, Tectonics and Geochemistry)*. Annales da Faculdade de Ciências, Universidade do Porto, Special Supplement to Vol. 64 (1983). Pg. 117-168
- Brett, C. E. and Baird, G. C. 1997. (Eds.) *Paleontological events: stratigraphical, ecological, and evolutionary implications*. Columbia University Press
- Brouwer, A. and van Ginkle, A. C. 1964. La succession Carbonifère dans la partie méridionales des montagnes Cantabriques (Espagne Nord-Ouest). *Comptes Rendus, 5éme Congrès sur la Carbonifère, Paris*. Vol. 1. Pg. 307-319
- Brown M. A. and Dodd, J. R. 1990. Carbonate Mud Mounds in Middle Mississippian strata of Southern Indiana and Northern Kentucky: End members of a Middle Mississippian Mud Mound spectrum? *Palaaios*. Vol. 5. Pg. 236-243
- Brown, R. G. and Pohl, E. R. 1973. Stratigraphy and genera of calcareous foraminifera of the Fraileys facies (Mississippian) of central Kentucky. *Bulletins of American Paleontology*. Vol. 64. Pg. 173-240
- Brunton, F. R. and Dixon, O. A. 1994. Siliceous Sponge-Microbe Associations and Their Recurrence through the Phanerozoic as Reef Mound Constructors. *Palaaios*. Vol. 9. Pg. 370-387
- Buick, R. 1992. The antiquity of oxygenic photosynthesis: Evidence from stromatolites in sulphate-deficient achaeon lakes. *Science*. Vol. 255. Pg. 74-77
- Cachán Santos, L. J. 1978. Palinoflora del Westfaliense A superior y B inferior de la Cuenca hullera de Teverga (Oviedo, España). *Palinología*. Vol. 1. Pg. 103-113
- Calner, M. Lehnert, O. and Joachimski, M. 2010. Carbonate mud mounds, conglomerates, and sea-level history in the Katian (Upper Ordovician) of central Sweden. *Facies*. Vol. 56. Pg. 157-172
- Camoin, G. and Maurin, A-F. 1988. Rôles des micro-organismes (bactéries, cyanobactéries) dans la genèse des “Mud Mounds”. Exemples du Turonien des Jebels Biréno et Mrhila (Tunisie) *Comptes rendus de l'Académie des sciences. Série 2, Mécanique, Physique, Chimie, Sciences de l'univers, Sciences de la Terre*. Vol. 307. No. 4. Pg. 401-407
- Campell, K. A., Farmer, J. D. and Des Marais, D. 2002. Ancient hydrocarbon seeps from the Mesozoic convergent margin of California: carbonate geochemistry, fluids and palaeoenvironments. *Geofluids*. Vol. 2 Pg. 63-94
- 2006. Hydrocarbon seep and hydrothermal vent paleoenvironments and paleontology: Past developments and future research directions. *Palaeogeography, Palaeoclimatology, Palaeoecology*. Vol. 232. Pg. 362-407
- Campbell, F.A. and Williams, G.D. 1965. Chemical composition of shales of Mannville Group (Lower Cretaceous) of central Alberta, Canada. *American Association of Petroleum Geologists Bulletin*. Vol. 49. Pg. 81-87

Carballeira, J., Corrales, I., Valladares, I., Naval, A., Ruiz, F., Lorenzo, S., Martínez Chacón, M. L., Mendez, C., Sanchez De Posada, L. C. and Truyols, J. 1985 Aportaciones al conocimiento de la estratigrafía de la Formación San Emiliano (Carbonífero, Cordillera Cantábrica) en su area-tipo. *Compte Rendu 10ème Congrès sur le Carbonifere, Madrid, 1983*. Vol. 1. Pg. 345-362.

Cavalazzi, R., Barbieri, R. and Ori, G. G. 2007. Chemosynthetic microbialites in the Devonian carbonate mounds of Hamar Laghdad (Anti-Atlas, Morocco). *Sedimentary Geology*. Vol. 200. Pg. 73-88

Chafiki, D., Canerot, J., Souhel, A., Hariri, K. E. and Eddine, K. T. 2004. The Sinemurian carbonate mud-mounds from central High Atlas (Morocco): stratigraphy, geometry, sedimentology and geodynamic patterns. *Journal of African Earth Sciences*. Vol. 39. Pg. 337-346

Chidsey, T. C. Jr., Brinton, L., Eby, D. E. and Hartmann, K. 1996. Carbonate-Mound Reservoirs in the Paradox Formation: an Outcrop Analogue along the San Juan River, Southeastern Utah. *Geology and Resources of the Paradox Basin*. Pg. 139-150

Choh, S-J. and Kirkland, B. L. 2000. Microfacies, biota, and depositional environment of an early Pennsylvanian (Morrowan) *Donezella*-siliceous sponge dominated bioherm, Frontal Ouachita Thrust Belt, Oklahoma, USA (abstract). *SEPM-IAS Research Conference on Permo-Carboniferous Platforms and Reefs. El Paso, Texas, 15-16 May 2000*. Pg. 37

- 2006. Sedimentological role of microproblematica *Donezella* in a Lower Pennsylvanian *Donezella*-siliceous sponge-dominated carbonate buildup, frontal Ouachita thrust belt, Oklahoma, U.S.A. *Journal of Sedimentary Research*. Vol. 76. Pg. 152-161.

Chuvashov, B. and Riding, R. 1984. Principle floras of Palaeozoic marine calcareous algae. *Palaeontology*. Vol. 27. Pg. 487-500

Cook, H. E., Zhemchuzhnikov, V. G., Zempolich, W. G., Lehmann, P. J., Alexeiev, D. V. Ya. Zhaimina, V. and Ye. Zorin, A. 2007. Devonian and Carboniferous Carbonate Platform Facies in the Bolshoi Karatau, Southern Kazakhstan: Outcrop Analogs for Coeval Carbonate Oil and Gas Fields in the North Caspian Basin. In: Yilmaz, P. O. and Isaken, G. H. (Eds.) *Oil and Gas of the Greater Caspian Area*. American Association of Petroleum Geology Studies in Geology. No. 5. Pg. 159-163

Conil, R., Grossens, E. and Lys, M. 1977. Étude micropaléontologique de la tranchée d'Yves-Gomezée (Tn 3c V 1-V 2, Belgique). *Bulletin de la Société belge de géologie*. Vol. 82. Pg. 201-239 (imprinted 1973)

Connell, J. H. and Slatyer, R. O. 1977. Mechanisms of Succession in Natural Communities and Their Role in Community Stability and Organization. *The American Naturalist*. Vol. 111. Pg. 1119-1144

Corliss, J. B., Lyle, M. and Dymond, J. 1978. The chemistry of hydrothermal mounds near the Galapagos rift. *Earth and Planetary Science Letters*. Vol. 40. Pg. 12-24

Coronado, I. and Rodríguez, S. 2014. Carboniferous auloporids from the Iberian Peninsula: palaeocology, diversity, and spatio-temporal distribution. *Journal of Iberian Geology*. Vol. 40. Pg. 61-85

Corrochano, D., Barba, P. and Comenero, J. R. 2012. Transgressive-regressive sequence stratigraphy of Pennsylvanian *Donezella* bioherms in a foreland basin (Lena Group, Cantabrian Zone, NW Spain). *Facies*. Vol. 58. Pg. 457-476

Cossey, P. J. and Mundy, D. J. C. 1990. *Tetrataxis*: a loosely attached limpet-like foraminifera from the Upper Palaeozoic. *Lethia*. Vol. 23. Pg. 311-322

Covey, M. 1986. The evolution of foreland basins to steady state: evidence from the western Taiwan foreland basin. In: Allen, P. A. and Homewood, P. (Eds.). *Foreland Basins*. International Association of Sedimentologists, Special Publication. Vol. 8. Pg. 77-90

Cózar, P. 2005. Early Serpukhovian (late Mississippian) microflora from the Guadiato Area (southwestern Spain). *Geological Journal*. Vol. 40. Pg. 405-424

- and Mamet, B. L. 2001. *Planohowchinia* (Lasiodiscidae, Foraminiferida), a New Late Viséan Genus, southwestern Spain. *Journal of Foraminiferal Research*. Vol. 31. Pg. 228-232

Crow, C. J., Brande, S., Turner, M. E., Stock, C. W. and Benson, D. J. 2001. Random sampling of carbonate mounds: an example from the Upper Ordovician of Alabama. *Sedimentary Geology*. Vol. 145. Pg. 173-187

Crowell, J. C. 1978. Gondwanan Glaciation, Cyclothems, Continental Positioning, and Climate Change. *American Journal of Science*. Vol. 278. Pg. 1345-1372

Crowley, T.J., and Baum, S.K. 1991. Estimating Carboniferous sea-level fluctuations from Gondwanan ice extent. *Geology*. Vol. 19. Pg. 975-977

- 1992. Modeling late Paleozoic glaciation. *Geology*. Vol. 20. Pg. 507-510

Davies, G. R. and Nassichuk, W. W. 1989. Upper Carboniferous tubular algal boundstone reefs in the Otto Fiord Formation, Canadian Arctic Archipelago. In: Geldsetzer, H. H. J., James, N. P. and Tebbutt, G. E. (Eds.). *Reefs, Canada and Adjacent Area*. - Canadian Society of Petroleum Geology. Vol. 13. Pg. 649-657

Davydov, V. I., Crowley, J. L., Schmitz, M. D. and Poletaev, V. I. 2010. High-Precision U-Pb Zircon Age Calibration of the Global Carboniferous Time Scale and Milankovitch Band Cyclicity in the Donets Basin, Eastern Ukraine. *Geochemistry, Geophysics, Geosystems*. Vol. 11. Pg. 1-22

de Hass, H., Mienis, F., Frank, N., Richter, T. O., Stienacher, R., de Stigter, H., van der Land, C. and van Weering, T. C. E. 2009. Morphology and sedimentology of (clustered) cold-water coral mounds at the south Rockall Trough margins, NE Atlantic Ocean. *Facies*. Vol. 55. Pg. 1-26

de Vleeschouwer, D., Rakociński, M., Racki, G., Pond, D. P. G., Sobieñ, K. and Claeys, P. 2013. The astronomical rhythm of Late-Devonian climate change (Kowala section, Holy Cross Mountains, Poland). *Earth and Planetary Science Letters*. Vol. 365. Pg. 25-37

de Vos, W., Bastida, M. J., Demetriades, A., Duris, M., Lexa, J., Lis, J., Marsina, K. and O'Connor, P. J. 2005. Metallogenic mineral provinces and world class ore deposits in Europe. In: Salimen, R., Plant, J. and Reeder, S. (Eds.), *Geochemical Atlas of Europe*. Part 1, Background Information, Methodology and Maps. Epso, Finland, Geological Survey of Finland. [Online Version] <http://www.gtk.fi/publ/foregsatlas/article.php?id=8> (accessed 08/03/10)

DeCelles, P. G. and Giles, K. A. 1996. Foreland basin systems. *Basin Research*. Vol. 8. Pg. 105-123

Dehantschutter, J. A. E. and Lees, J. 1996. Waulsortian build-ups of Waulsort, Belgium. *Geological Journal*. Vol. 31. Pg. 123-142

Della Porta, G., Kenter, J. A. M. and Bahamonde, J. R. 2002. Microfacies and paleoenvironment of *Donezella* accumulations across and Upper Carboniferous high-rising carbonate platform (Asturias, NW Spain). *Facies*. Vol. 46. Pg. 149-168

- Deloffre, R. 1988. Nouvelle taxonomic des algues dasycladales. *Bulletin des Centres de Recherches Exploration-Production Elf-Aquitaine*. Vol. 12. Pg. 165-217
- Dessauvage, T. F. J. and Dağ, Z. 1963. Occurences of Lasiodiscidae in Anatolia. *Mineral Research and Exploration Institute of Turkey*. Vol. 60. Pg. 75-82
- Devuyst, F-X. and Lees, A. 2001. The initiation of Waulsortian buildups in Western Ireland. *Sedimentology*. Vol. 48. Pg. 1121-1148
- DiFilippo, E. L., Hammond, D. E. and Corsetti, F. A. 2003. Geochemical constraints for coexisting CO₂ gas hydrate and calcite: implications for sheet like cracks, stromatactis, zebra and tepee-like structures. *Sedimentary Geology*. Vol. 160. Pg. 1-6
- Dingle, P. S., Bader, B., Hensen, C., Minten, B. and Schäfer, P. 1993. Sedimentology and Paleoecology of Upper Carboniferous Shallow-Water Carbonate Complexes of the Carmenes Syncline (Cantabrian Mts., N-Spain). *Zeitschrift der Deutschen Geologischen Gesellschaft*. Vol. 144. Pg. 370-395
- Dodd, J. R. and Nelson, C. S. 1998. Diagenetic comparisons between non-tropical Cenozoic limestones of New Zealand and tropical Mississippian limestones from Indiana, USA: Is the non-tropical model better than the tropical model? *Sedimentary Geology*. Vol. 121. Pg. 1-21
- Doherty, P. D., Soreghan, G. S. and Castagna, J. P. 2002. Outcrop-Based Reservoir Characterization: A Composite Phylloid-Algal Mound, Western Orogrande Basin (New Mexico). *The American Association of Petroleum Geologists*. Vol. 85. Pg. 779-795
- Dronov, A. V. 1993. Middle Paleozoic Waulsortian-type Mud Mounds in Southern Fergana (Southern Tein-Shan, Commonwealth of Independent States): The Shallow-water Atoll Model. *Facies*. Vol. 28. Pg. 169-180
- Dunham, R. J. 1962. Classification of carbonate rocks according to depositional texture. In Ham, W. E. (Ed.). *Classification of Carbonate Rocks. Memoirs of the American Association of Petroleum Geology*. Vol. 1. Pg. 108-121
- Dupont, E. 1881. Sur l'origine des calcaires dévoniens de la Belgique. *Bulletin de l'Académie royale des Sciences, des Lettres et des Beaux-Arts de Belgique*. Vol. 2. Pg. 264-280
- Egorov, A. V., Crane, K., Vogt, P. R. and Rozhkov, A. N. 1999. Gas hydrates that outcrop on the sea floor: stability models. *Geo-marine Letters*. Vol. 19. Pg. 68-75
- Eichmüller, K. 1985. Die Valdeteja Formation: Aufbau und Geschichte einer oberkarbonischen Karbonatplattform (Kantabrisches Gebirge, Nordspanien). *Facies*. Vol. 13. Pg. 45-154.
- Eldridge, J., Walsh, D. and Scotese, C. R. 1998. Plate Tracker v2.0. PALEOMAP Software. University of Texas
- Elrick, M. and Snider, A. C. 2002. Deep-water stratigraphic cyclicity and carbonate mud mound development in the Middle Cambrian Marjum Formation, House Range, Utah, USA. *Sedimentology*. Vol. 49. Pg. 1021-1047
- Embry, A. F. and Klovan, J. S. 1971. A Late Devonian reef tract on northeastern Banks Island. *Bulletin of Canadian Petroleum Geology*. Vol. 4. Pg. 730-781

- Enpu, G., Samankassou, E., Changqing, G., Yongli, Z. and Baoliang, S. 2007. Paleoeecology of Pennsylvanian phylloid algal build-ups in south Guizhou, China. *Facies*. Vol. 53. Pg. 615-623
- Ernst, A. and Minwegen, E. 2006. Late Carboniferous Bryozoa from La Hermida, Spain. *Acta Palaeontologica Polonica*. Vol. 51. Pg. 569-588
- and Winkler Prins, C. 2008. Pennsylvanian bryozoans from the Cantabrian Mountains (northwestern Spain). *Scripta Geologica (Leiden)*. Vol. 137. Pg. 1-123
- Schäfer, P. and Reijmer, J. J. G. 2005. Stenolaemate Bryozoa from the Upper Carboniferous of the Cantabrian Basin, Northern Spain. *Senckenbergiana Lethaea*. Vol. 85. Pg. 301-317
- Fagerstrom, J. A. 1988. A structural model for reef building communities. *Palaios*. Vol. 3. Pg. 217-220.
- 1991. Reef-building guilds and a checklist for determining guild membership. *Coral Reefs*. Vol. 10. Pg. 47-52
- Feng, Q., Gong, Y-M. and Riding, R. 2010. Mid-Late Devonian Calcified Marine Algae and Cyanobacteria, South China. *Journal of Paleontology*. Vol. 84. Pg. 569-587
- Fernández Lopez, M. G. and Sánchez de Posada, L. C. 1987. Hollinomorpha y Kirkbyocopina (Ostracoda) del Bashkiriense del N. de León (Cordillera Cantábrica, NW. de España). *Revisita Española de Micropaleontología*. Vol. 19. Pg. 465-485
- Fernández, L. P. 1993. La Formacion San Emiliano (Carbonifero de la zona Cantabrica, no de España): estratigrafía y extension lateral. Algunas implicaciones paleogeograficas. *Trabajos de Geologia*. Vol. 19. Pg. 97-122
- Nose, M., Fernandez-Martinez, E., Mendez-Bedia, L., Schroder, St. and Soto, F. 2006. Reefal and mud mound facies development in the Lower Devonian La Vid Group at the Colle outcrops (Leon province, Cantabrian Zone, NW Spain). *Facies*. Vol. 52. Pg. 307-327
- Fernández-Matínez, E., Tourneur, F. and López-Alcántara. 2003. A new Middle Devoinian heterocoral from Spain. *Acta Palaeontologica Polonica*. Vol. 48. Pg. 531-546
- Fischer, A. G., Honjo, S. and Garrison, R. E. 1967. *Electron Micrographs of Limestone and their Nannofossils*. Princeton University Press
- Fischer, G. and Wefer, G. 1999. *Use of proxies in paleoceanography*. Springer
- Flajs, G. 1977. Die Ultrastrukturen Des Kaslkalgenskeletts. *Palaeontographica Abteilung B*. Vol. 160. Pg. 69-128
- and Hüssner, P. D. H. 1993. A microbial model for the Lower Devonian stromatactis mud mounds of the Montagne Noire (France). *Facies*. Vol. 29. Pg. 179-193
- Vigener, M., Keupp, H., Meischner, D., Neuweiler, F., Paul, J., Reitner, J., Warnke, K., Weller, H., Dingle, P., Hensen, C., Schäfer, P., Gautret, P., Leinfelder, R. R., Hüssner, H. and Kaufmann, B. 1995. Mud mounds: A polygenetic spectrum of fine-grained carbonate buildups. *Facies*. Vol. 32. Pg. 1-69
- Floquet, M., Neuweiler, F. and Léonide, P. 2012. The Impact of Depositional Events and Burial Rate on Carbonate-Silica Diagenesis In A Middle Jurassic Stromatactis Carbonate Mud Mound, Sainte-Baume Massif, Se France. *Journal of Sedimentary Research*. Vol. 82. Pg. 521-539
- Flügel, E. 1972. Mikrofazielle Untersuchungen in der alpinen Trias: Methoden und Probleme. *Mitteilungen der Gesellschaft der Geologie- und Bergbaustudenten in Österreich*. Vol. 21. Pg. 6-64
- 1967. Elektronenmikroskopische Untersuchungen an mikritischen Kallen. *Geologische Rundschau*. Vol. 56. Pg. 341-358

- 1981. Lower Permian Tubephytes/Archaeolithoporella buildups in the southern Alps (Austria and Italy). *The Society of Economic Paleontologists and Mineralogists (SEPM) Special Publication*. Vol. 30. Pg. 143-160
- 1989. 'Algen/Zement'-Riffe. *Archivfur Lagerstättenforschung. Geologie*. Vol. 10. Pg. 125-131
- 2004. *Microfacies of carbonate rocks: Analysis, interpretation and application*. Springer.
- and Flügel-Kahler, E. 1992. Phanerozoic Reef Evolution: Basic Questions and Data Base. *Facies*. Vol. 26. Pg. 167-278

Folk, R. L. 1959. Practical petrographic classification of limestones. *American Association of Petroleum Geology Bulletin*. Vol. 43 No. 1. Pg. 1-38

- 1965. Some aspects of recrystallization in ancient limestones. In: Pray, L. C. and Murray, R. C. (Eds.). *Dolomitization and Limestone Diagenesis*. Special Publication - Society of Economic Paleontologists and Mineralogists. Vol. 13. Pg. 14-48

- 1974. The natural history of crystalline calcium carbonate: effect of magnesium content and salinity. *Journal of sedimentary Petrology*. Vol. 44 No. 1. Pg. 141-153

- 1993. SEM imaging of bacteria and nannobacteria in carbonate sediments and rocks. *Journal of Sedimentary Petrology*. Vol. 63 No. 5. Pg. 990-999

- 2005. Nannobacteria and the formation of Framboidal pyrite: Textural evidence. *Journal of Earth System Science*. Vol. 114. Pg. 369-374

Forsythe, G. T. W., Wood, R. and Dickson, J. A. D. 2002. Mass spawning in ancient reef communities: evidence from Late Paleozoic phylloidalgae. *Palaios*. Vol. 17. Pg. 615-621

Fortey, R. 2000. Olenid trilobites: The oldest known Chemoautotrophic symbionts? *Proceedings of the National Academy of Sciences*. Vol. 97. Pg. 6574-6578

Foubert, A., Depreiter, D., Beck, T., Maignien, L., Pannemans, B., Frank, N., Blamart, D. and Henriot, J-P. 2008. Carbonate mounds in a mud volcano province off north-west Morocco: Key to processes and controls. *Marine Geology*. Vol. 248. Pg. 74-96

Friedrich, O., Voigh, S., Kuhnt, T. and Kock, M. C. 2011. Repeated bottom-water oxygenation during OAE 2: timing and duration of short-lived benthic foraminiferal repopulation events (Wunstorf, northern Germany). *Journal of Micropalaeontology*. Vol. 30. Pg. 119-128

Frost, J. G. 1975. Winterset algal-bank complex, Pennsylvanian, eastern Kansas. *American Association of Petroleum Geologists, Bulletin*. Vol. 59 Pg. 265-291

Fürsich, F. T. 1995. Approaches to paleoenvironmental reconstructions. *Geobios, Memoire Special*. Vol. 18. Pg. 183-195

Gailliot, J., Vachard, D., Galfetti, T. and Martini, R. 2009. New latest Permian foraminifers from Laren (Guangxi Province, South China): Palaeobiogeographic implications. *Geobios*. Vol. 42. Pg. 141-168

García-Alcalde, J. L., Carls, P., Pardo Alonso, M. V., Sanz-López, J., Soto, F., Truyols-Massoni, M. and Valenzuela-Ríos, J. I. 2002. Devonian. In: Gibbons, W. and Moreno, M. T. (Eds). *The Geology of Spain*. Geological Society, London. Pg. 67-91

Garcia-Bellido, D. C. and Rigby, J. K. 2004. Devonian and Carboniferous sponges from Spain. *Journal of Paleontology*. Vol. 78. Vol. 431-455

García-Fuente, S. 1952. Geología del Concejo de Tavera (Asturias). *Boletín Instituto Geológico y Minero España*. Vol. 64. Pg. 345-456

García-López, S. and Bastida, F. (Eds.) 2002. *Palaeozoic conodonts from Northern Spain*. Instituto Geológico y Minero de España, serie Cuadernos del Museo Geominero.

Gandl, J. 1987. Die Karbon-Trilobiten des Kantabrischen Gebirges (NW Spanien), 4: Trilobiten aus dem höheren Namur und tieferen Westfal. *Abhandlungen der Senckenbergischen Naturforschenden Gesellschaft*. Vol. 543. Pg. 1-79

Garland, J., Neilson, J. Laubach, S. E. and Whidden, K. J. (Eds.) 2012. *Advances in carbonate exploration and reservoir analysis*. Geological Society of London, Special Publications. Vol. 370. Pg. 1-15

Golubic, S. and Seong-Joo, L. 1999. Early Cyanobacterial fossil record: preservation, palaeoenvironments and identification. *European Journal of Phycology*. Vol. 34. Pg. 339-348

Gómez de Llarena, J. and Rodríguez Arango, C. 1948. Datos para el estudio geológico de la Babia Baja (León). *Boletín Instituto Geológico y Minero España*. Vol. 61. Pg. 79-206

Grammer, G. M. and Ritter, A. L. 2009. Phylloid Algal Mounds in the Paradox Basin, Southwestern USA: An Alternative to the *in situ* Constructional Growth Model? In: P. K. Swart, G. P. Eberli, J. A. McKenzie, I. Jarvis and T. Stevens (Eds.) *Perspectives in Carbonate Geology: A Tribute to the Career of Robert Nathan Ginsburg*. John Wiley & Sons

Grossman, E. L. and Ku, T-L. 1986. Oxygen and carbon isotope fractionation in biogenic aragonite: temperature effects. *Chemical Geology (Isotope Geoscience Section)*. Vol. 59. Pg. 59-74

Grotzinger, J. P. and Reed, J. F. 1983. Evidence for primary aragonite precipitation, lower Proterozoic (1.9 Ga) Rocknest dolomite, Wopmay orogeny, northwest Canada. *Geology*. Vol. 11. Pg. 710-713

Groves, J. R. 1983. Calcareous foraminifers and algae from the type Morrowan (Lower Pennsylvanian) region of northeastern Oklahoma and northwestern Arkansas. *Oklahoma Geological Survey, Bulletin*. Vol. 133. Pg. 1-65
- 1986. Calcareous algae and associated microfossils from mid-Carboniferous rocks in east-central Idaho. *Journal of Paleontology*. Vol. 60. Pg. 476-496
- and Altiner, D. 2005. Survival and recovery of calcareous foraminifera pursuant to the end-Permian mass extinction. *Comptes Rendus Palevol*. Vol. 4. Pg. 487-55

Gutiérrez-Alonso, G., Fernández-Suárez, J., Gutiérrez-Marco, J. C., Corfu, F., Murphy, J. B. and Suárez, M. 2007. U-Pb depositional age for the upper Barrios Formation (American Quartzite facies) in the Cantabrian zone of Iberia: Implications for stratigraphic correlation and paleogeography. In: Linnemann, U., Nance, R. D., Kraft, P. and Zulauf, G. (Eds.) *The evolution of the Rheic Ocean: From Avalonian-Cadomian active margin to Alleghenian-Variscan collision*. Geological Society of America Special Paper. Vol. 423. Pg. 287-296

Gutiérrez-Marco, J. C., Robardet, M., Rábano, I., Sarmiento, G. N., San José Lancha, M. A., Herranz Araújo, P. and Pieren Pidal, A. P. 2002. Ordovician. In: Gibbons, W. and Moreno, M. T. (Eds.) *The Geology of Spain*. Geological Society, London. Pg. 31-49

Gutteridge, P. 1995. Late Dinantian (Brigantian) carbonate mud-mounds of the Derbyshire carbonate platform. In: Monty, C. L. V. Bosence, D. W. J. Bridges, P. H. and Pratt, B. R. (Eds.) *Carbonate Mud-Mounds Their Origin and Evolution*. International Association of Sedimentologists. Blackwell Science. Vol. 23. Pg. 289-307

Hammer, Ø., Harper, D. A. T. and Ryan, P. D. 2001. *PAST: Paleontological Statistical Software Package for Education and Data Analysis*. Palaeontological Association.
- 2005. PAST - Palaeontological Statistics, ver. 1.34. User Manual. Online resource: <http://www.uq.edu.au/dinosaurs/documents/past.pdf> - Accessed 07/04/14

Harper, D. A. T., Jin, J., Mac, C. and Rasmussen, Ø. 2014. Late Ordovician carbonate mounds from North Greenland: a peri-Laurentian dimension to the Boda Event? *Journal of the Geological Society of Sweden*. Accessed online (31/01/2014). DOI:10.1080/11035897.2013.865669

Harris, M. P., Kendall, C. G. St. C. and Lerche, I. 1985. Carbonate cementation – a brief review. In: Schneidermann, N. and Harris, P (Eds.) *Carbonate Cements*. Society of Economic Paleontologists and Mineralogists. Special Publications 36. Pg. 79-96

Hays, J. D., Imbrie, J. and Shackleton, N. J. 1976. Variations in the Earth's orbit: pacemaker of the ice ages. *Science*. Vol. 194. Pg. 1121-1132

Heckle, P. H. 1977. Origin of phosphatic black shale facies in Pennsylvanian cyclothems of Midcontinent North America. *American Association of Petroleum Geologists Bulletin*. Vol. 61. Pg. 1045-1068

- 1980. Paleogeography of eustatic model for deposition of Midcontinent Upper Pennsylvanian cyclothems. In: Fouch, T. D. and Magathan, E. R. (Eds) *Paleozoic paleogeography of westcentral United States, Society of Economic Paleontologists & Mineralogists, Rocky Mountain Section, Paleogeography Symposium I*. Pg. 197-215

- 1986. Sea-level curve for Pennsylvanian eustatic marine transgressive-regressive depositional cycles along Midcontinent outcrop belt, North America. *Geology*. Vol. 14. Pg. 330-334

- 1990. Updated Middle-Upper Pennsylvanian eustatic sea-level curve for Midcontinent North America and preliminary biostratigraphic characterization. XI International Carboniferous Congress, 1987, *Compte Rendu, Academia Sinica*, Beijing, China.

- 1990b. Evidence for global (glacial-eustatic) control over upper Carboniferous (Pennsylvanian) cyclothems in midcontinent North America. In: Hardman, R. F. P. and Brooks, J. (Eds) *Tectonic Events Responsible for Britain's Oil and Gas Reserves*, Geological Society Special Publication. Vol. 55. Pg. 35-47

- and Cocke, J. M. 1969. Phylloid Algal-Mound Complexes in Outcropping Upper Pennsylvanian Rocks of Mid-Continent. *American Association of Petroleum Geologists Bulletin*. Vol. 53. Pg. 1058-1074

Henson, C., Dingle, P. and Schäfer, P. 1995. Primary and diagenetic mud mound genesis in the San Emiliano Formation of the Cármenes syncline (Westphalian B/C, Cantabrian Mts., Spain). In: Reitner, J. and Neuweiler, F. (Eds.) *Mud Mounds: A Polygenetic Spectrum of Fine-grained Carbonate Buildups*. Facies. Vol. 32. Pg. 1-70

Herrmann, R. and Hubmann, B. 1994. Devonian Udoteacean Green Algae from the Cantabrian Mountains (Santa Lucía Formation), NW Spain. *Revista Española de Paleontología*. Vol. 9. Pg. 195-202

Hillis, L. W. 1999. Phylogeny of Halimeda (Bryopsidales): linking paleontological, morphological and molecular data. *Acta Palaeontologica Romaniae*. Vol. 2. Pg. 183-189

Hinnov, L. A. 2000. New Perspectives on Orbitally Forced Stratigraphy. *Annual Review OF Earth and Planetary Sciences*. Vol. 28. Pg. 419-475

- Ogg, J. G. 2007. Cyclostratigraphy and the Astronomical Time Scale. *Stratigraphy*. Vol. 4. Pg. 239-251

- Hladil, J. 2005. The formation of stromatactis-type fenestral structures during the sedimentation of experimental slurries - a possible clue to a 120-year-old puzzle about stromatactis. *Bulletin of Geosciences*. Vol. 80. Pg. 193-211
- Růžička, M. and Koptíková, L. 2006. Stromatactis cavities in sediments and the role of coarse-grained accessories. *Bulletin of Geosciences*. Vol. 81. Pg. 123-146
- Hoefs, J. 1997. *Stable Isotope Geochemistry Fourth Completely Revised, Updated, and Enlarged Edition*. Springer.
- Høeg, G. J. 1932. Ordovician algae from the Trondheim area. *Spitzbergexpeditionen Norske Vidensk. Akad i Oslo Math-Nat. Kl.* Vol.63
- Honjo, S. 1969. Study of the fine grained carbonate matrix: sedimentation and diagenesis of 'micrite'. *Paleontological Society of Japan Special Paper*. Vol. 14. Pg. 67-82
- House, M. R. Orbital forcing timescales: an introduction. In: House, M. R. and Gale, A. S. (Eds.), *Orbital Forcing Timescales and Cyclostratigraphy*. Geological Society Special Publication. No. 85. Pg. 1-18
- Hovland, M. 1990. Do carbonate reefs form due to fluid seepage? *Terra Review*. Vol. 2. Pg. 8-18
- 2007. Discovery of prolific natural methane seeps at Gullfaks, northern North Sea. *Geo-Marine Letters*. Vol. 27. Pg. 197-201
- and Thomsen, E. 1989. Hydrocarbon-Based Communities in the North Sea? *Sarsia*. Vol. 74. Pg. 29-42
- Insalaco, E., Skelton, P. and Palmer, T. J. 2000. Carbonate platform systems: components and interactions – an introduction. In: Insalaco, E., Skelton, P. and Palmer, T. J. (Eds.), *Carbonate platform systems: components and interactions*. Geological Society, London, Special Publications. No. 178. Pg. 1-8
- Ivanova, R. M. 1999. Some calcareous algae from the Carboniferous of the Urals. *Paleontological Journal*. Vol. 33. Pg. 681-685.
- James, N. P. 1980. Reef Environments. In: Scholle, P. A., Bebout, D. G. and Moore, C. H. (Eds.), *Carbonate Depositional Environments*. Memoire of the American Association of Petroleum Geologists. Vol. 33. Pg. 346-444
- 1983. Reefs. In: Walker, R. G. (Ed.), *Facies Models*. Geoscience Canada reprint series. Vol. 1. Pg. 121-132
- and Bourque, P-A. 1992. Reefs and mounds. In: Walker, R. G. and James, N. P. (Eds.), *Facies Models, Response to Sea Level Change*. Geological Association of Canada, Geotext. Vol 1. Pg 323-347
- and Gravestock, D. I. 1990. Lower Cambrian shelf and shelf margin buildups, Flinders Ranges, South Australia. *Sedimentology*. Vol. 37. Pg. 455-480
- and Wood, R. A. 2010 Reefs and Reef Mounds. In: Dalrymple, R. and James, N. P. (Eds.) *Facies Models: Response to Sea Level Change*. St Johns Newfoundland. Geological Association of Canada
- Jeffery, D. L. and Stanton, R. J. Jr. 1996. Growth history of Lower Mississippian Waulsortian mounds: Distribution, stratal patterns, and geometries, New Mexico. *Facies*. Vol. 35. Pg. 29-58
- Jenkins, R. and De Vries, J. L. 1969. *Practical X-Ray Spectrometry*. Springer-Verlag New York

- Joachimski, M. M., von Bitter, P. H. and Buggisch, W. 2006. Constraints on Pennsylvanian glacioeustatic sea-level change using oxygen isotopes of conodont apatite. *Geology*. Vol. 34. Pg. 277-280
- Johnson, G. A. L. 1959. The Carboniferous stratigraphy of the Roman Wall district in western Northumberland. *Proceedings of the Yorkshire Geological Society*. Vol. 32. Pg. 83-130
- 1984. Subsidence and sedimentation in the Northumberland Trough. *Proceedings Yorkshire Geological Society*. Vol. 45. Pg. 71-83
- Johnson, J. H. 1963. Pennsylvanian and Permian algae. *Colorado School of Mines, Quarterly*. Vol. 58. Pg. 1-211
- Jones, G. LL. and Somerville, I. D. 1996. Irish Dinantian biostratigraphy: practical applications. *From: Strogon, P., Somerville, I. D. And Jones, G. LL. (eds). 1996. Recent Advances in Lower Carboniferous Geology*, Geological Society Special Publication. Vol. 107. Pg. 371-385
- Julivert, M., 1978. Hercynian orogeny and Carboniferous paleogeography in north-western Spain: a model of deformation-sedimentation relationship. *Deutsche Geologische Gesellschaft*. Vol. 129. Pg. 565-592
- Kaufmann, B. 1998a. Facies, stratigraphy and diagenesis of Middle Devonian reef- and mud-mounds in the Mader (eastern Anti-Atlas, Morocco). *Acta Geologica Polnica*. Vol. 48. Pg. 43-106
- 1998b. Middle Devonian reef and mud mounds on a carbonate ramp: Mader Basin (eastern Anti-Atlas, Morocco). *Geological Society, London, Special Publications*. Vol. 149. Pg. 417-435
- Arthur, M. A., Howe, B. and Scholle, P. A. 1996. Widespread venting of methane-rich fluids in late Cretaceous (Campanian) submarine springs (Teepee Buttes) Western Interior seaway, USA. *Geology*. Vol. 24. No 9. Pg. 799-802
- Kaul, N., Foucher, J.-P. and Heesemann. 2006. Estimated mud expulsion rates from temperature measurements on Håkon Mosby Mud Volcano, SW Barents Sea. *Marine Geology*. Vol. 229. Pg. 1-14
- Kaźmierczak, J., Coleman, M. L., Gruszczyński, M. and Kempe, S. 1996. Cyanobacterial key to the genesis of micritic and peloidal limestones in ancient seas. *Palaeontologica Polonica*. Vol. 41. Pg. 319-338
- Keller, M., Bahlburg, H. and Reuther, C-D. 2008. The transition from passive to active margin sedimentation in the Cantabrian Mountains, Northern Spain: Devonian or Carboniferous? *Tectonophysics*. Vol. 461. Pg. 414-427
- Kendall, A. C. and Iannace, A. 2001. 'Sediment'-cement relationships in a Pleistocene speleothem from Italy: a possible analogue for 'replacement' cements and *Archaeolithoporella* in ancient reefs. *Sedimentology*. Vol. 48. Pg. 681-698
- Kenyon, N. H., Akhmetzhanov, A. M., Wheeler, A. J., van Weering, T. C. E., de Haas, H. and Ivanov, M. K. 2003. *Marine Geology*. Vol. 195. Pg. 5-30
- Kharaka, Y. F., Law, L. M. Carothers, W. W. and Goerlitz, D. F. 1986. Role of organic species dissolved in formation waters from sedimentary basins in mineral diagenesis. . In: Gautier, D. L. (Ed.) *Roles of organic matter in sedimentary diagenesis*. Society of Economic Paleontologists and Mineralogists. Special Publication 38. Pg. 111-122
- Khvorova, I. V. 1949. A New genus of Dasycladacea from the Middle Carboniferous of the Moscow tectonic valley. *Doklady Akademii Nauk SSSR*. Vol. 65. Pg. 749-752

King Jr., D. T. 1986. Waulsortian -type buildups and resedimented (Carbonate-turbidite) facies, Early Mississippian Burlington Shelf, Central Missouri. *Journal of Sedimentary Petrology*. Vol. 56. Pg. 471-479

Kirikoulakis, K., Bett, B. J., White, M. and Wolff, G. A. 2004. Organic biogeochemistry of the Darwin Mounds, a deep-water coral ecosystem, of the NE Atlantic. *Deep Sea Research Part I: Oceanographic Research Papers*. Vol. 51. Pg. 1937-1954

- Fisher, E., Wolff, G. A., Freiwald, A., Grehan, A. and Robers, M. J. 2005. Lipids and nitrogen isotopes of two deep-water corals from the North-East Atlantic: initial results and implications for their nutrition. In: Freiwald, A. and Roberts, J. M (Eds.) *Cold-water Corals and Ecosystems*. Springer-Verlag, Berlin, Heidelberg. 715-729

- Freiwald, A., Fisher, E. and Wolff, G. A. 2007. Organic matter quality and supply to deep-water coral/mound systems of the NW European Continental Margin. *International Journal of Earth Sciences*. Vol. 66. Pg. 159-170

Kirkby, K. C. 1997. Comparison of North American mound suites: implication for the Early Carboniferous ocean. *CSPG-SEPM Joint Convention: Sedimentary Events and Hydrocarbon Systems, Calgary*. Abstract with Program. Pg. 154

Knoll, H. H., Fairchild, I. J. and Swett, K. 1993. Calcified microbes in Neoproterozoic carbonates: Implications for our understanding of the Proterozoic/Cambrian transition. *Palaaios*. Vol. 8. Pg. 512-525

Koch, R. Moussavian, E., Ogorelec, B., Skaberne, R. and Bucur, I. I. 2002. Development of a Lithocodium (syn. Bacinella irregularis) reef mound - A patch reef within Middle Aptian lagoonal limestone sequence near Nova Gorica (Sabotin Mountain, W-Slovenia). *Geologija*. Vol. 45. Pg. 71-90

Kopaska-Merkel, D. C. and Haywick, D. W. 2001a. Carbonate mounds: sedimentation, organismal response, and diagenesis. *Sedimentary Geology*. Vol. 145. Pg. 157-159

-- 2001b. A lone biotrital mound in the Chesterian (Carboniferous) of Alabama? *Sedimentary Geology*. Vol. 145. Pg. 253-268

Kontorovich, A. E., Varlamov, A. I., Grazhdankin, D. V., Karlova, G. A., Klets, A. G., Kontorovich, V. A., Saraev, S. V., Terleev, A. A., Belyaev, S. Y., Varaksina, I. V., Efimov, A. S., Kochnev, B. B., Nagovitsin, K. E., Postnikov, A. A. and Filippov, Y. F. 2008. A section of Vendian in the east of West Siberian Plate (based on data from the borehole Vostok 3). *Russian Geology and Geophysics*. Vol. 49. Pg. 932-939

Krainer, K., Vachard, D. and Lucas, S. G. 2009. Facies, Microfossils (Smaller Foraminifers, Calcareous Algae) and Biostratigraphy of the Hueco Group, Doña Ana Mountains, Southern New Mexico, USA. *Rivista Italiana di Paleontologia e Stratigrafia*. Vol. 115. Pg. 3-26

- Flügel, E., Vachard, D. and Joachimski, M. M. 2003. A Close Look at Late Carboniferous Algal Mounds: Schulterkofel, Carnic Alps, Austria. *Facies*. Vol. 49. Pg. 325-350

Krause, F. F., Scotese, C. R., Nieto, C., Sayegh, S. G., Hopkins, J. C. and Meyer, R. O. 2004. Paleozoic stromatolites and zebra carbonate mud-mounds: Global abundance and palaeogeographic distribution. *Geology*. Vol. 32. Pg. 181-184

Krinsley, D. H., Pye, K., Boggs, S. Jr. and Tovey, N. K. 1998. *Backscattered Scanning Electron Microscopy and Image Analysis of Sediments and Sedimentary Rocks*. Cambridge University Press.

Kullmann, J. and Rodríguez, S. 1986. Hornförmige Einzelkorallen (Rugosa) aus frühoberkarbonischen Flachwasser-Sedimenten im Kantabrischen Gebirge (Nordspanien). *Neues Jahrbuch für Geologie und Paläontologie Mh.* Pg. 293-306

Kutterolf, S., Liebetrau, V., Mörz, T., Freundt, A., Hammerich, T. and Garbe-Schönberg, D. 2008. Lifetime and cyclicity of fluid venting at forearc mound structures determined by tephrostratigraphy and radiometric dating of authigenic carbonates. *Geology*. Vol. 36. Pg. 707-710

Lambert, L. L. 1986. Growth habitat of the microproblematical genus *Donezella* in the middle Magdalena, Hueco Mountains, West Texas. *Geological Society of America Abstracts with Programs*. Vol. 18. Pg. 250-251

- and R. J. Stanton, Jr. 1988 Carbonate facies and stratigraphic framework of the middle Magdalena (Middle Pennsylvanian), Hueco Mountains, West Texas. *American Association of Petroleum Geologists Bulletin*. Vol. 72. Pg. 101

Lasemi, Z. and Sandberg, P. A. 1984. Transformation of aragonite-dominated lime muds to microcrystalline limestones. *Geology*. Vol. 12. Pg. 420-423

Lecompte, M. 1937. Contribution à la connaissance des récifs du Dévonien de l'Ardenne. Sur la présence de structures conservées dans des efflorescences cristallines du type 'stromatactis'. *Bulletin du Musée Royal d'Histoire Naturelle de Belgique*. Vol. 13. Pg. 1-14

Lees, A. 1988. The Waulsortian buildups of the Dinant area. In: Herbolch, A. (Ed.) *IAS 9th European Regional Meeting Excursion Guidebook Lueven-Belgium*. Belgian Geological Survey. Pg. 177-185

- 1997. Biostratigraphy, sedimentology and palaeobathymetry of Waulsortian buildups and peri-Waulsortian rocks during the late Tournaisian regression, Dinant area, Belgium. *Geological Journal*. Vol. 32. Pg. 1-36

- and Miller, J. 1985. Facies variation in Waulsortian buildups. Part 2. Mid-Dinantian buildups from Europe and North America. *Geological Journal*. Vol. 20. Pg. 159-180

- and Miller, J. 1995. Waulsortian banks. In: Monty, C. L. V., Bosence, D. W. J., Bridges, P. H. and Pratt, B. R. (Eds.) *Carbonate Mud-Mounds Their Origin and Evolution*. International Association of Sedimentologists. Blackwell Science. Vol. 23. Pg. 191-271

Lehrmann, D. J. 1999. Early Triassic calcimicrobial mounds and biostromes of the Nanpanjiang basin, south China. *Geology*. Vol. 27. Pg. 359-362

- Payne, J.L., Felix, S.V., Dille, P.M., Youyi Yu, H.W. and Wei, J., 2003. Permian –Triassic boundary sections from shallow marine carbonate platforms of the Nanpanjiang Basin, South China: implications for oceanic conditions associated with the end-Permian extinction and its aftermath. *Palaio*. Vol. 18. Pg. 138-152

Leppig, U., Forke, H. C., Montenari, M. and Fohrer, B. 2005. A three- and two-dimensional documentation of structural elements in schwagerinids (superfamily Fusulinoidea) exemplified by silicified material from the Upper Carboniferous of the Carnic Alps (Austria/Italy): a comparison with verbeekinoideans and alveolinids. *Facies*. Vol. 51. Pg. 541–553

Li, L., Tan, X., Zeng, W., Zhou, T., Yang, Y., Hong, H., Lou, B. and Bian, L. 2013. Development and reservoir significance of mud mounds in Sinian Dengying Formation, Sichuan Basin. *Petroleum Exploration and Development*. Vol. 40. Pg. 714-721

Liao, W., Wang, Y., Kershaw, S., Weng, Z. and Yang, H. 2010. Shallow-marine dysoxia across the Permian-Triassic boundary: Evidence from pyrite framboids in the microbialite in South China. *Sedimentary Geology*. Vol. 232. Pg. 77-83

- Liñán, E., Gozalo, R., Palacios, T., Gámez Vintaned, J. A., Ugidos, J. M and Mayoral, E. 2002. Cambrian. In: Gibbons, W. and Moreno, M. T. (Eds). *The Geology of Spain*. Geological Society, London. Pg. 17-29
- Littler, M. M. and Littler, D. S. 1980. The evolution of thallus form and survival strategies in benthic marine macroalgae: field and laboratory tests of a functional form model. *The American Naturalist*. Vol. 116. Pg. 25-44
- Loeblich, A. R. and Tappan, H. 1987. *Foraminiferal Genera and Their Classification*. Van Nostrand Reinhold, New York
- Longman, M. 1981. A Process Approach to Recognising Facies of Reef Complexes. In: Toomey, D. F. (Ed.), *European Fossil Reef Models. Special Publication of the Society of Economic Paleontology*. Vol. 30. Pg. 9-40
- Lotze, F. 1945. Zur Gliederung der Varisziden der Iberischen Meseta. *Geotektonic Forschungen*. Vol. 6. Pg. 78-92
- Lowenstam, H.A., Epstein, S.A. 1957. On the origin of sedimentary aragonite needles of the Great Bahama Bank. *Journal of Geology*. Vol. 65. Pg. 364-375
- Lowenstein, T. K., Timofeeff, M. N., Brennan, S. T., Hardie, L. A. and Demicco, R. V. 2001. Oscillations in Phanerozoic Seawater Chemistry: Evidence from Fluid Inclusions. *Science*. Vol. 294. Pg. 1086-1088
- MacDonald, I. R., Sager, W. W. and Peccini, M. B. 2003. Gas hydrate and chemosynthetic biota in mounded bathymetry at mid-slope hydrocarbon seeps: Northern Gulf of Mexico. *Marine Geology*. Vol. 198. Pg. 133-158
- Madi, A., Bourque, P. A. and Mamet, B. 1996. Depth-related ecological zonation of a Carboniferous carbonate ramp: Upper Viséan of Béchar Basin, western Algeria. *Facies*. Vol. 35. Pg. 59-80.
- Mamet, B. 1991. Carboniferous calcareous algae. In: Riding, R (Ed.) *Calcareous algae and Stromatolites*. New York, Springer-Verlag. Pg. 370-451
- 1992. Paléogeographie des algues calcaires marines carbonifères. *Revue Canadienne des Sciences de la Terre*. Vol. 29. Pg. 174-194.
- and Stemmerik, L. 2000. Carboniferous algal microflora, Kap Jungersen and Foldedal formations, Holm land and Amdrup land, eastern North Greenland. *Geology of Greenland Survey Bulletin*. Vol. 187. Pg. 79-101
- and Villa, E. 2004. Calcareous marine algae from the Carboniferous (Moscovian-Gzhelian) of the Cantabrian Zone (NW Spain). *Revista Española de Paleontología*. Vol. 19. Pg. 151-190.
- and Zhu, Z. 2005. Carboniferous and Permian algal microflora, Tarmin Basin (China). *Geologica Belgica*. Vol. 8. Pg. 3-13.
- Marcos, A. and Pulgar, J. A. 1982. An Approach to the tectonostratigraphic evolution of the Cantabrian Foreland thrust and fold belt, Hercynian Cordillera of NW Spain. *Jbuch. Geol. Paläont. Abh.* Vol. 163. Pg. 256-260
- Martínez Chacón, M. L. 1977. New carboniferous stenoscismatacean brachiopods from Oviedo and León, Spain. *Palaeontology*. Vol. 20. Pg. 209-223
- 1979. Braquiópodos carboníferos de la Cordillera Cantábrica (Orthida, Strophomenida y Rhynchonellida). *Memoria del instituto Geológico y Minero de España*. Vol. 96.
- 1986. Nota sobre la edad de los materiales carboníferos de la region de Villamanín (Nde León; España). *Breviora Geologica Asturica*. Vol. 27. Pg. 17-20

- and Winkler Prins, C. F. 1979. The brachiopod fauna of the San Emiliano Formation (Cantabrian Mountains, NW Spain) and its connection with other areas. *Compte Rendu du 9ème Congrès sur le Carbonifère, Washington, Champaign-Urbana*, 1979. Vol. 5. Pg. 233-244.
- - 2010. Adaption to hard substrates on Pennsylvanian Productides (Brachiopoda) from the Cantabrian Mountains (north-west Spain). *Special Papers in Palaeontology*. Vol. 84. Pg. 225-241
- Maslov, V. P. 1929. Microscopic algae from Carboniferous limestones of the Donetz Basin. *Akademiya Nauk SSSR, Vsesoyuznii geologo-razvedochnii*. Vol. 40. Pg. 1519-1542
- Matte, P. 2001. The Variscan collage and orogeny (480-290 Ma) and the definition of the Armorica microplate: a review. *Terra Nova*. Vol. 13. Pg. 122-128
- Maurin, A. F. and Noël, D. 1977. A possible bacterial origin for Famennian micrite. In: Flügel, E. (Ed.) *Fossil Algae: recent results and developments*. New York, Springer-Verlag. Pg. 136-142
- Mazzullo, S. J. and Cys, J. M. 1979. Marine aragonite sea-floor growths and cements in Permian phylloid algal mounds, Sacramento Mountains, New Mexico. *Journal of Sedimentary Research*. Vol. 49. Pg. 917-936
- Teal, C. S., Bischoff, W. D., Dimmick-Wells, K. and Wilhite, B. W. 2003. Sedimentary architecture and genesis of Holocene shallow-water mud-mounds, northern Belize. *Sedimentology*. Vol. 50. Pg. 743-770
- McGovney, J. E. 1988. Thornton reef, Silurian, North-eastern Illinois. In: Geldsetzer, H. H. J., James, N. P. and Tebbutt, G. E. (Eds.), *Reefs, Canada and Adjacent Area*. *Canadian Society of Petroleum Geologists*. Memoir 13. Pg. 330-338
- Meijer, J. J. de. 1971. Carbonate petrography of algal limestones (Lois Cigüera Formation, Upper Carboniferous, León, Spain). *Leidse Geologische Mededelingen*. Vol. 47. Pg. 1-97
- Merz-Preiß, M. and Riding, R. 1999. Cyanobacterial tufa calcification in two freshwater streams: ambient environment, chemical thresholds and biological processes. *Sedimentary Geology*. Vol. 126. Pg. 103-124
- Miall, A. D. 1981. Alluvial sedimentary basins: tectonic setting and basin architecture. In: Miall, A. D. (Ed.) *Alluvial Basins*. Geological Association of Canada Special Paper. Vol. 23. Pg. 1-33
- Milankovitch, M. 1920. *Théorie Mathématique des Phénomènes Thermiques Produits par la Radiation Solaire*. Académie Yougoslave des Science et des Arts de Zagreb, Gauthiers-Villiers, Paris
- 1941. *Kanon der Erdbestrahlung und seine Anwendung auf das Eiszeitenproblem*. Academic Royale Serbe. Edition Speciale. Vol. 133
- Mohammad, A. 2004. A re-evaluation of aragonite versus calcite seas. *Carbonates and Evaporites*. Vol. 19. Pg. 133-141
- Monreal, L. N. 1879. Datos geológicos acerca de la Provincia de León, recogidos durante la campaña de 1878 a 1879. *Boletín de la Comisión del Mapa Geológico de España*. Vol. 7. Pg. 311-320
- Moore, L. R., Neves, R., Wagner, R. H. and Wagner-Gentis, C. H. T. 1971. The stratigraphy of Namurian and Westphalian rocks in the Villmanín area of northern León, NW Spain. *Trabajos de Geología*. Vol. 3. Pg. 307-363

- Monty, C. L. V. 1995. The rise and nature of carbonate mud-mounds: an introductory actualistic approach. In: Monty, C. L. V. Bosence, D. W. J. Bridges, P. H. and Pratt, B. R. (Eds.) *Carbonate Mud-Mounds Their Origin and Evolution*. International Association of Sedimentologists. Blackwell Science. Vol. 23. Pg. 11-48
- van Laer, P., Maurin, A. F. and Bernet-Rollande, M. C. 1988. The Upper Devonian mud mounds. Herbosch, A. (Ed.) *IAS 9th European Regional Meeting Excursion Guidbook Lueven-Belgium*. Belgian Geological Survey. Pg. 157-176
 - Bosence, D. W. J. Bridges, P. H. and Pratt, B. R. 1995. (Eds.) *Carbonate Mud-Mounds Their Origin and Evolution*. International Association of Sedimentologists. Blackwell Science.
- Morton, A. C., and C. R. Hallsworth. 1999. Processes controlling the composition of heavy mineral assemblages in sandstones. *Sedimentary Geology*. Vol. 124. Pg. 3-29
- Mounji, D., Bourque, P-A. and Savard, M. M. 1998. Hydrothermal origin of Devonian conical mounds (kess-kess) of Hamar Lakhdad Ridge, Anti-Atlas, Morocco. *Geology*. Vol. 26. Pg. 1123-1126
- Müller, J., Oberhänsli, H., Melles, M., Schwab, M., Rachold, V. and Hubberten, H.-W. 2001. Late Pliocene sedimentation in Lake Baikal: implications for climatic and tectonic change in SE Siberia. *Palaeoecology, Palaeoclimatology, Palaeoecology*. Vol. 174. Pg. 305-326
- Munnecke, A. and Samtleben, C. 1996. The Formation of Limestones and the Development of Limestone-Marl Alternations in the Silurian of Gotland, Sweden. *Facies*. Vol. 34. Pg. 159-176
- and Jarochowska, E. 2013. The Paleozoic micropaleontological *Wetheredella* is a wastebasket taxon. *Proceedings of the 3rd IGCP 591 Annual Meeting*. Pg. 234-235
 - Westphal, H., Reijmer, J. J. G. and Samtleben, C. 1997. Microspar development during early marine burial diagenesis: a comparison of Pliocene carbonates from the Bahamas with Silurian limestones from Gotland (Sweden). *Sedimentology*. Vol. 44. Pg. 977-990
 - Servais, T. and Vachard, D. 2000. A new Family of calcareous microfossils from the Silurian of Gotland, Sweden. *Palaeontology*. Vol 43. Pg. 1153-1172
 - and Westphal, H. 2004. Shallow-water aragonite recorded in bundles of limestone-marl alternations - the Upper Jurassic of SW Germany. *Sedimentary Geology*. Vol. 164. Pg. 191-202
- Murillo-Muñetón, G and Dorobek, S. L. 2003. Controls on the evolution of carbonate mud mounds in the Lower Cretaceous Cupido Formation, Northeastern Mexico. *Journal of Sedimentary Research*. Vol. 73. Pg. 869-886
- Murray, J. W. 1991. *Ecology and Palaeoecology of Benthic Foraminifera*. Routledge
- Mutti, E., R. Tinterri, G. Benevelli, D. DiBiase, and G. Cavanna, 2003. Deltaic, mixed and turbidite sedimentation of ancient foreland basins. In: E. Mutti, G.S. Steffens, C. Pirmez, M. Orlando, and D. Roberts (Eds.). *Turbidites; models and problems: Marine and Petroleum Geology*, Vol. 20. Pg.733-755
- Naeth, J., di Primio, R., Horsfield, B., Schaefer, R. G. and Krooss, B. M. 2007. On the relationship between hydrocarbon migration pathways and carbonate mound occurrence in the Porcupine Basin. *International Journal of Earth Science*. Vol. 98. Pg. 199-200
- Nestell G. P. and Nestell M. K. 2006. Middle Permian (Late Guadalupian) foraminifers from Dark Canyon, Guadalupe Mountains, New Mexico. *Micropaleontology*. Vol. 52. Pg.1-50
- Neumann, A.C., Land, L.S. (1975): Lime mud deposition and calcareous algae in the Bight of Abaco, Bahamas: a budget. *Journal of Sedimentary Petrology*. Vol. 45. Pg. 763-786

- Neuweiler, F., Gautret, P., Thiel, V., Langes, R., Michaelis, W. and Reitner, J. 1999. Petrology of Lower Cretaceous carbonate mud mounds (Albian, N. Spain): insights into organomineralic deposits of the geological record. *Sedimentology*. Vol. 46. Pg. 837-857
- Rutsch, M., Geipel, G., Remer, A. and Heise, K. H. 2000. Soluble humic substances from in situ precipitation microcrystalline calcium carbonate, internal sediment, and spar cement in a Cretaceous carbonate mud mound. *Geology*. Vol. 28. Pg. 851-854
- Bourque, P-A. and Boulvain, F. 2001. Why is stromatolites so rare in Mesozoic carbonate mud mounds? *Terra Nova*. Vol. 13. Pg. 338-346
- d'Orzio, V., Immenhauser, A., Geipel, G., Heise, K-H., Cocozza, C. and Miano, T. M. 2003. Fulvic acid-like organic compounds control nucleation of marine calcite under suboxic conditions. *Geology*. Vol. 31. No. 8. Pg. 681-684
- Nicholson, H. A. and Etheridge, R. 1878. *A monograph of the Silurian fossils of the Girvan District in Ayrshire with special reference to those contained in the 'Gray collection'*. Vol. 1. Edinburgh, Blackwood.
- Oyarzun, R., Dobleas, M., Ruiz, J. L., Cebria, J.-M. and Youbi, N. 1999. Tectonically-induced icehouse-greenhouse climate oscillations during the transition from the Variscan to the Alpine cycle (Carboniferous to Triassic). *Bulletin de la Société Géologique de France*. Vol. 170. Pg. 3-11
- Pas, D., Da Silva, A.-C., Dhital, M. R. and Boulvain, F. 2011. Sedimentology of a Mid-Late Ordovician carbonate mud-mound complex from the Katmandu nappe in Central Nepal. *Journal of Asian Earth Sciences*. Vol. 42. Pg. 452-467
- Pedley, M. and Carannante, G. 2006. Cool-water carbonate ramps: a review. In: Pedley, H. M. and Carannante, G. (Eds.) *Cool-water Carbonates: Depositional Systems and Palaeoenvironmental Controls*. Geological Society, London, Special Publications. No. 255. Pg. 1-9
- Peckmann, J., Walliser, O. H., Riegel, W. and Reimer, J. 1999. Signatures of Hydrocarbon Venting in a Middle Devonian Carbonate Mound (Hollard Mound) at the Hamar Laghdad (AntiAtlas, Morocco). *Facies*. Vol. 40. Pg. 281-296
- Reimer, A., Luth, U., Luth, C., Hansen, B. T., Heinicke, C., Hoefs, J. and Reitner, J. 2001. Methane-derived carbonates and authigenic pyrite from the northwestern Black Sea. *Marine Geology*. Vol. 177. Pg. 129-150
- and Thiel, V. 2004. Carbon cycling at ancient methane-seeps. *Chemical Geology*. Vol. 205. Pg. 443-467
- Perejón, A., Moreno-Eiris, E., Bechstädt T., Menéndez, S. and Rodríguez-Martínez, M. 2012. New Bilbilian (early Cambrian) archaeocyath-rich thrombolitic microbialite from the Láncara Formation (Cantabrian Mts., northern Spain). *Journal of Iberian Geology*. Vol. 38. Pg. 313-330
- Pérez-Estaún, A., Bastida, F., Alonso, J. L., Marquínez, J., Aller, J., Alvarez-Marrón, J., Marcos, A. and Pulgar, J. A. 1988. A thin-skinned tectonic model for an arcuate fold and thrust belt: the Cantabrian zone (Variscan Ibero-Armorican arc). *Tectonics*. Vol. 7. Pg. 517-537
- Perry, C. T., Salter, M. A., Harborne, A. R., Crowley, S. F., Jelks, H. L. and Wilson, R. W. 2011. Fish as major carbonate mud producers and missing components of the tropical carbonate factory. *Proceedings of the National Academy of Sciences of the United States of America*. Vol. 108. Pg. 3865-3869
- Peterson, J. A. 1966a. Genesis and Diagenesis of Paradox Basin Carbonate Mound Reservoirs. *Symposium on Recently Developed Geologic Principles and Sedimentation of the Permian-Pennsylvanian of the Rocky Mountains; 20th Annual Conference*. Pg. 67-86
- 1966b. Genesis of Paradox Basin Carbonate Mound Reservoirs in Relation to Regional Permian-Pennsylvanian Sedimentation. *Symposium on Recently Developed Geologic Principles*

and Sedimentation of the Permo-Pennsylvanian of the Rocky Mountains; 20th Annual Conference. Pg. 86a-86l

- 1966c. Stratigraphic Vs. Structural Controls on Carbonate-Mound Hydrocarbon Accumulation, Aneth Area, Paradox Basin. *Bulletin of the American Association of Petroleum Geologists*. Vol. 50. Pg. 2068-2081

Pickard, N. A. H. 1992. Depositional controls on Lower Carboniferous microbial buildups, eastern Midland Valley of Scotland. *Sedimentology*. Vol. 39. Pg. 1081-1100

- 1996. Evidence for microbial influence on the development of Lower Carboniferous buildups. *Geological Society, London, Special Publications*. Vol. 107. Pg. 65-82

Pille, L. and Vachard, D. 2011. Diploporaceae (calcareous green algae dasycladales) from the late Viséan (Mississippian) of Montagne Noire (southern France). *Revue de Micropaléontologie*. Vol. 54. Pg. 1-30

- Vachard, D., Somerville, I. D., Argyriadis, I. and Aretz, M. 2010. Revision of the late Viséan-Serpukhovian (Mississippian) calcareous algae, foraminifers and microproblematica from Balia-Maden (NW Turkey). *Geobios*. Vol. 43. Pg. 531-546

Pomar, L. and Hallock, P. 2008. Carbonate factories: A conundrum in sedimentary geology. *Earth-Science Reviews*. Vol. 87. Pg. 134-169

Prasolov, E. M., Tokarev, I. V., Ginsburg, G. D., Soloviev, V. A. and Eltsova, G. M. 1999. Helium and other noble gases in gas-hydrate sediments of the Håkon Mosby Mud Volcano. *Geo-Marine letters*. Vol. 19. Pg. 84-88

Priewalder, H. 1997. SEM-Revision of a Chitinozoan Assemblage from the Uppermost San Pedro Formation (Pridoli), Cantabrian Mountains (Spain). *Jahrbuch der Geologischen Bundesanstalt*. Vol. 140. Pg. 73-93

Pratt, B. R. 1995. The origin, biota and evolution of deep-water mud-mounds. In: Monty, C. L. V., Bosence, D. W. J., Bridges, P. H. and Pratt, B. R. (Eds.), *Carbonate Mud-Mounds Their Origin and Evolution*. International Association of Sedimentologists. Blackwell Science. Pg. 49-123

- 2000. Microbial contribution to reefal mud-mounds in ancient deep-water settings: Evidence from the Cambrian. In: Riding, R. and Awramik, S. M. (eds.), *Microbial Sediments*. Berlin, Springer-Verlag. Pg. 282-288

- 2001. Calcification of cyanobacterial filaments: *Girvanella* and the origin of lower Paleozoic lime mud. *Geology*. Vol. 29 Pg. 763-766

Prokoph, A., A.D. Fowler & R.T. Patterson. 2000. Evidence for periodicity and nonlinearity in a high-resolution fossil record of long-term evolution. *Geology*. Vol 28. Pg.867-870

Proust, J.-N., Vennin, E., Vachard, D., Boisseau, T., Chuvashov, B., Ivanova, R., Masse, P. and Maslo, A. 1996. Sedimentological and biostratigraphical analysis of the Bashkirian stratotype (Southern Urals, Russia). *Bulletin Centre Recherche Exploration-Production Elf-Aquitaine*. Vol 20. Pg. 341-365

Pruss, S. B. and Bottjer, D. J. 2004. Late Early Triassic microbial reefs of the western United States: a description and model for their deposition in the aftermath of the end-Permian mass extinction. *Palaeoecology, Palaeoclimatology, Palaeoecology*. Vol. 211. Pg. 127-137

Rác, L. 1964. Carboniferous Calcareous Algae and their Associations in the San Emiliano and Lois-Ciguera Formations (Prov. León, NW Spain). *Leidse Geologische Mededelingen*. 31. Pg. 1-112

Radig, F. 1962. Ordovizium /Silurian und die Frage Prävariszischer Faltungen in Nordspanien. *Geologische Rundschau*. Vol. 52. Pg. 346-357

Reed, S. J. B. 2005. *Electron microprobe analysis and scanning electron microscopy in geology*. Cambridge University Press.

Rees, M. N., Pratt, B. R. and Rowell, A. J. 1989. Early Cambrian reefs, reef complexes, and associated lithofacies of the Shackleton Limestone, Transantarctic Mountains. *Sedimentology*. Vol. 36. Pg. 341-361

Rich, M. 1967. *Donezella* and *Dvinella*, widespread algae in Lower and Middle Pennsylvanian rocks in East-Central Nevada and West-Central Utah. *Journal of Paleontology*. Vol. 41. Pg. 973-980

- 1970. The genus *Tuberitina* (Foraminiferida) in Lower and Middle Pennsylvanian rocks from the Eastern Great Basin. *Journal of Paleontology*. Vol. 44. Pg. 1060-1066

- 1980. *Carboniferous Calcareous Foraminifera from Northeastern Alabama, South-Central Tennessee, and Northwestern Georgia*. Cushman Foundation for Foraminiferal Research Special Publication. Vol. 18

Richardson, J. B., Rodríguez González, R. M. and Sutherland, S. J. E. 2000. Palynology and recognition of the Silurian/Devonian boundary in some British terrestrial sediments by correlation with Cantabrian and other European marine sequences - a progress report. *Courier Forschungstitut Senckenberg*. Vol. 220. Pg. 1-7

--- 2001 Palynological zonation of mid-Palaeozoic sequences from the Cantabrian Mountains, NW Spain: implications for inter-regional and inter-facies correlation of the Ludford/Pridoli and Silurian/Devonian boundaries, and plant dispersal patterns. *Bulletin of the Natural History Museum, Geology Series*. Vol. 57. Pg. 115-162

Riding, R. 1979. *Donezella* bioherms in the Carboniferous of the southern Cantabrian Mountains, Spain. *Bulletin Centre Recherche Exploration-Production Elf-Aquitaine*. Vol. 3. Pg. 787-794

-1991. Calcified Cyanobacteria. In: R. Riding (ed.) *Calcareous Algae and Stromatolites*. Springer-Verlag Berlin. Pg. 55-87

- 1993. *Shamovella obscura*: the correct name of *Tubiphytes obscurus* (Fossil). *Taxon*. Vol. 42. Pg. 71-73

- 2000. Microbial Carbonates: the geological record of calcified bacterial-algal mats and biofilms. *Sedimentology*. Vol. 47. Pg. 179-214

- 2002. Structure and composition of organic reefs and carbonate mud mounds: concepts and categories. *Earth Science Reviews*. No. 58. Pg 163-231

- and Gou, L. 1991. Permian marine calcareous algae. In: Riding, R. (ed.) *Calcareous algae and stromatolites*. Springer-Verlag, Berlin. Pg. 452-480

Ries, J. B. 2010. Review: geological and experimental evidence for secular variation in seawater Mg/Ca (calcite-aragonite seas) and its effects on marine biological calcification. *Biogeosciences*. Vol. 7. Pg. 2795-2849

Rippka, R., Derulles, J., Waterbury, J. B., Herdman, M. and Stanier, Y. 1979. Generic Assignments, Strain Histories and Properties of Pure Cultures of Cyanobacteria. *Journal of General Microbiology*. Vol. 111. Pg. 1-61

Robardet, M. and Gutiérrez-Marco, J. C. 2002. Silurian. In: Gibbons, W. and Moreno, M. T. (Eds). *The Geology of Spain*. Geological Society, London. Pg. 51-66

Roberts, J. M. and Freiwald, A. 2005. Integrated European Research into Cold-Water Coral Reefs. *The Journal of Marine Education*. Vol. 21. Pg. 41-45

- Henry, L.-A., Long, D. and J. P. Hartley. 2008. Cold-water coral reef frameworks, megafaunal communities and evidence for coral carbonate mounds on the Hatton Bank, north east Atlantic. *Facies*. Vol. 54. Pg. 297-316

Rodríguez, S., Somerville, I. D., Said, I. and Cózar, P. 2012. Late Viséan coral fringing reef at Tiouinine (Morocco): implications for the role of rugose corals as building organisms in the Mississippian. *Geological Journal*. Vol. 47. Pg. 462-472

Rodríguez Fernández, L.R. 1993. Tectonosedimentary evolution of a Carboniferous foreland basin related with arcuated fold-thrust belt. The example of NW Iberian Variscan belt. *Compte Rendu 12. International Congress of the Carboniferous-Permian stratigraphy and Geology, Buenos Aires*. Vol. 1. Pg. 435-445

Rodríguez González, R. M. 1983. *Palinología de las formaciones del Silúrico superior-Devónico inferior de la Cordillera Cantábrica, Noroeste de España*. Institución Fray Bernardino da Sahagún-Servicio de Publicaciones de la Universidad de León

Rodríguez- Martínez, M. Cózar, P. Mas, R and Rodríguez, S. 2003. Upper Viséan Saccaminopsis-Sponge Microbial Mud Mounds, Sierra de la Estrella, southwestern Spain. In: Ahr, W.M., Harris, P.M., Morgan, W.A., Somerville, I.D. (Eds.), *Permo-Carboniferous carbonate platforms and reefs*. Society of Economic Paleontologists and Mineralogists, Special Publication 78, and American Association of Petroleum Geologists, Memoir 83. Pg.. 189-200

Rollet, N., Logan, G. A., Kennard, J. M., O'Brien, P. E., Jones, A. T. and Sexton, M. 2006. Characterisation and correlation of active hydrocarbon seepage using geophysical data sets: An example from the tropical, carbonate Yampi Shelf, Northwest Australia. *Marine and Petroleum Geology*. Vol. 23. Pg. 145-164

Rousseau, R. M. 2001. Detection Limit and Estimate of Uncertainty of Analytical XRF Results. *The Rigaku Journal*. Vol. 18. Pg. 33-47

Russo, F., Neri, C., Mastandrea, A. and Baracca, A. 1997. The Mud Mound Nature of the Cassian Platform Margins of the Dolomites. A Case History:the Cipit Boulders from Punta Grohmann (Sasso Piatto Massif, Northern Italy). *Facies*. Vol. 36. Pg. 25-36

Sager, W. W., MacDonald, I. R. and Hou, R. 2003. Geophysical signatures of mud mounds at hydrocarbon seeps on the Louisiana continental slope, northern Gulf of Mexico. *Marine Geology*. Vol. 198. Pg. 97-132

Said, I., Rodríguez, S., Berkli, M., Cózar, P. and Gómez-Herguedas, A. 2010. Environmental parameters of a coral assemblage from the Akerchi Formation (Carboniferous), Adarouch Area, central Morocco. *Cuadernos de geología ibérica (Journal of Iberian Geology)*. Vol. 36. Pg. 7-19

Samankassou, E. 2001. Internal structure and depositional environment of Late Carboniferous mounds from the San Emiliano Formation, Cármenes Syncline, Cantabrian Mountains, North Spain. *Sedimentary Geology*. Vol 145. Pg. 235-252

- and West, R. R. 2002. Construction versus accumulation in phylloid algal mounds: an example of a small constructed mound in the Pennsylvanian of Kansas, USA. *Palaeogeography, Palaeoclimatology, Palaeoecology*. Vol. 185. Pg. 379-389

- - 2003. Constructional and accumulative modes of fabrics in selected Pennsylvanian algal-dominated buildups in eastern Kansas, Midcontinent, USA. In: Ahr, W. M., Harris, P. M., Morgan, W. A. and Somerville, I. D. (Eds) *Permo-Carboniferous platforms and reefs*. SEPM/AAPG Special Publication. Vol. 78. Pg. 219-237

- Tresch, J. and Strasser, A. 2005. Origin of peloids in early Cretaceous deposits, Dorset, South England. *Facies*. Vol. 51. Pg. 264-274

- Von Allmen, K. and Bahamonde, J. R. 2013. Growth Dynamics of Pennsylvanian Carbonate Mounds From A Mixed Terrigenous-Carbonate Ramp In The Pueblo De Lillo Area, Cantabrian Mountains, Northern Spain. *Journal of Sedimentary Research*. Vol. 83. Pg. 1099-1112

Sandberg, P. A. 1983. An oscillating trend in Phanerozoic non-skeletal carbonate mineralogy. *Nature*. Vol. 305. Pg. 19-22

Scheffler, K., Hoernes, S. and Schwark, L. 2003. Global changes during Carboniferous-Permian glaciation of Gondwana: Linking polar and equatorial climate evolution by geochemical proxies. *Geology*. Vol. 31. Pg. 605-608

Schlager, W. 2000. Sedimentation rates and growth potential of tropical, cool-water and mud-mound carbonate systems. *Geological Society, London Special Publications*. Vol. 178. Pg. 217-227

- 2003. Benthic carbonate factories of the Phanerozoic. *International Journal of Earth Science*. Vol. 92. Pg. 445-464

Schmid, D. U. 1995. "Tubiphytes" *morronesis* - eine fakultativ inkrustierende Foraminifere mi endosymbiotischen Algen. *Profil*. Vol. 8. Pg. 305-317

- Leinfelder, R. R. and Nose, M. 2001. Growth dynamics and ecology of Upper Jurassic mounds, with comparisons to Mid-Palaeozoic mounds. *Sedimentary Geology*. Vol. 145. Pg. 343-376

Schubert, J.K. and Bottjer, D.J., 1992. Early Triassic stromatolites as post-mass extinction disaster forms. *Geology*. Vol. 20. Pg. 883-886

Schwarzacher, S. 1993. Cyclostratigraphy and the Milankovitch Theory. *Developments in Sedimentology*. Vol. 52

Scotese, C. R. Gondwanan palaeogeography and palaeoclimatography. *Journal of African Earth Sciences*. Vol. 28. Pg. 99-114

- 2003. PALEOMAP Project. www.scotese.com (accessed 21/01/13)

Senowbari-Daryan, B. 2013. Tubiphytes Maslov, 1956 and description of similar organisms from Triassic reefs of Tethys. *Facies*. Vol. 59. Pg. 75-112

Shapiro, R. and Fricke, H. 2002. Tepee Buttes: Fossilized methane-seep ecosystems. In: Leonard, E. M., Hubbard, M. S., Kelley, S. A., Evanoff, E., Siddoway, C. S., Oviatt, C. G., Heizler, M. and Timmons, M. (Eds.) *High Plains to Rio Grande Rift: Late Cenozoic Evolution of Central Colorado*. GSA Field Guides. Pg. 59-93

Shen, J. W. and Hairuo, Q 2010.. Mississippian (Early Carboniferous) stromatolite mounds in a fore-reef slope setting, Laibin, Guangxi, South China. *International Journal of Earth Science*. Vol. 99. Pg. 443-458

- Yu, C. M. and Bao, H. M. 1997. A Late-Devonian (Famennian) Renalcis-Epiphyton reef at Zhajiang, Guilin, South China. *Facies*. Vol. 37. Pg. 195-210

Shiells, K. A. G. 1963. Yoredale Cyclothems of Northumberland. *Nature*. Vol. 197. Pg. 1098-1099

Shuysky, V. P. 1985. On the position of the Paleoberesellids and other segmented algae from the Siphonophyceae. *New data on the Geology, biostratigraphy and paleontology of the Urals*. *Akad. Nauk. SSSR, Ural, Nauchn. Centr, Inst. Geol. Geochem. Akad.* Pg. 86-95

- Sivhed, U., Erlstrom, M, Bojesen-Koefoed, L. A. and Löfgren, A. 2004. Upper Ordovician carbonate mounds on Gotland, central Baltic Sea: Distribution, composition and reservoir characteristics. *Journal of Petroleum Geology*. Vol. 27. Pg. 115-140
- Soja, M. and Riding, R. 1993. Silurian Microbial Associations from the Alexander Terrane, Alaska. *Journal of Paleontology*. Vol. 67. Pg. 728-738
- Stanier, R. Y. and Cohen-Bazire, G. 1977. Phototrophic Prokaryotes: The Cyanobacteria. In: Starr, M. P., Ingraham, J. L. and Balows, A. (Eds.) *Annual Review of Microbiology*. Pg. 225-274
- Stanley, S. M. and Hardie, L. A. 1998. Secular oscillations in the carbonate mineralogy of reef-building and sediment-producing organisms driven by tectonically forced shifts in seawater chemistry. *Palaeogeography, Palaeoclimatology, Palaeoecology*. Vol. 144. Pg. 3-19
- Steinen, R. P. 1982. SEM observations on the replacement of Bahaman aragonitic mud by calcite. *Geology*. Vol. 10. Pg. 471-475
- Stenzel, S. R. and James, N. P. 1995. Shallow-water stromatolite mud-mounds on a Middle Ordovician foreland basin platform, western Newfoundland. In: Monty, C. L. V. Bosence, D. W. J. Bridges, P. H. and Pratt, B. R. (Eds.) *Carbonate Mud-Mounds Their Origin and Evolution*. International Association of Sedimentologists. Blackwell Science. Vol. 23. Pg. 423-437
- Stephenson, M. H., Angiolini, L., Cózar, P., Jadoul, F., Leng, M. J., Millward, D. and Chenery, S. 2010. Northern England Serpukhovian (early Namurian) farfield responses to southern hemisphere glaciation. *Journal of the Geological Society*. Vol. 167. Pg. 1171-1184
- Stockman, K. W., Ginsburg, R. N. and Shinn, E. A. 1967. The production of lime mud by algae in south Florida. *Journal of Sedimentary Petrology*. Vol. 37. Pg. 633-648
- Stockmans, F. and Williér, Y. 1965. Documents paléobotaniques pour l'étude du Houiller dans le Nord-Ouest de l'Espagne. *Mémoires de l'Institut Royal des Sciences Naturelles de Belgique*. Vol. 79. Pg. 1-106
- Suárez, A., Heredia, N., López, F., Toyos, J.M., Rodríguez, L.R. and Gutiérrez, G. 1991. Mapa Geológico de España, Hoja 102 (Los Barrios de Luna, 1:50,000). *Instituto Geológico y Minero de España, Madrid*.
- Swennen, R. 1988. *IAS 9th European Regional Meeting Abstracts Lueven-Belgium*. Belgian Geological Survey. Pg. 245
- Taberner, M. C. and Bosence, D. W. J. 1995. An Eocene biodetrital mud-mound from the southern Pyrenean foreland basin, Spain: an ancient analogue for Florida bay mounds? In: Monty, C. L. V. Bosence, D. W. J. Bridges, P. H. and Pratt, B. R. (Eds.) *Carbonate Mud-Mounds Their Origin and Evolution*. International Association of Sedimentologists. Blackwell Science. Vol. 23. Pg. 423-437
- Tabor, N. J. and Montañez, I. P. 2004. Morphology and distribution of fossil soils in the Permian-Pennsylvanian Wichita and Bowie Groups, north-central Texas, USA: implications for western equatorial Pangean palaeoclimate during icehouse-greenhouse transition. *Sedimentology*. Vol. 51. Pg. 851-884
- and Poulsen, C. J. 2008. Palaeoclimate across the Late Pennsylvanian-Early Permian tropical palaeolatitudes: A review of climate indicators, their distribution, and relation to palaeophysiographic climate factors. *Palaeogeography, Palaeoclimatology, Palaeoecology*. Vol. 268. Pg. 293-310

- Tappan, H. and Loeblich, A. R. Jr. 1988. Foraminiferal evolution, diversification, and extinction. *Journal of Paleontology*. Vol. 62. Pg. 695-714
- Taylor, T. N., Hass, H. and Kerp, H. 1997. A cyanolichen from the Lower Devonian Rhynie chert. *American Journal of Botany*. Vol. 84. Pg. 992-1004
- Termier, H., Termier, G. and Vachard, D. 1977. On Moravamminida and Aoujgaliida (Porifera, Ischyrospongia): Upper Paleozoic "Pseudo Algae". In: Flügel, E. (Ed.) *Fossil Algae - Recent Results and Developments*. Berlin, Springer-Verlag. Pg. 215-219
- Textoris, D. and Carozzi, A. 1964. Petrography and evolution of Niagran (Silurian) reefs, Indiana. *Bulletin of the American Association of Petroleum Geologists*. Vol. 48. Pg. 397-426
- Toomey, D. F. 1972. The biota of the Pennsylvanian (Virgilian) Leavensworth Limestone, midcontinent region. Part 3: Distribution of calcareous foraminifera. *Journal of Paleontology*. Vol. 46. Pg. 276-298
- 1976. Paleosynecology of a Permian plant dominated marine community. *Neues Jahrb Geol Paläontol Abhandlung*. Vol. 152. Pg. 1-18
- and Winland, H. D. 1973. Rock and Biotic Facies Associated with Middle Pennsylvanian (Desmoinesian) algal buildup, Nena Lucia Field, Nolan County, Texas. *The American Association of Petroleum Geologists Bulletin*. Vol. 57. Pg. 1053-1074
- Tosolini, A.-M. P., Wallace, M. W. and Gallagher, S. J. 2012. Shallow water mud-mounds of the Early Devonian Buchan Group, East Gippsland, Australia. *Sedimentary Geology*. Vol. 281. Pg. 208-221
- Truyols, J., Philippot, A. and Julivert, M. 1974. Les Formations siluriennes de la Zone Cantabrique et leurs faunes. *Bulletin de la Société Géologique de France*. Vol. 16. Pg. 23-35
- Tucker, M. E. 2003. Mixed clastic-carbonate cycles and sequences: Quaternary of Egypt and Carboniferous of England. *Geologica Croatica*. Vol. 56. Pg. 19-37
- and Wight, V. P. 1990. Carbonate Sedimentology. *Blackwell Science*.
- Gallagher, J., Lemon, K., Leng, M., 2003. The Yoredale cycles of Northumbria: high frequency clastic-carbonate sequences of the Mid-Carboniferous icehouse world. *Open University Geological Society Journal*. Vol. 24. Pg. 5-10
- Gallagher, J. and Leng, M. J. Are beds in shelf carbonates millennial-scale cycles? An example from the mid-Carboniferous of northern England. *Sedimentary Geology*. Vol. 214. Pg. 19-34
- Turner, E. C., James, N. P. and Narbonne, G. M. 2000. Taphonomic control on microstructure in early Neoproterozoic reefal stromatolites and thrombolites. *Palaios*. Vol. 15. Pg. 87-111
- Vachard, D. and Miconnet, P. 1994. Foraminifera and Moravamminids from the Givetian and Frasnian of the Ligerian Realm (Amorican Massif, France). [Foraminifères et Moravamminides du Givetien et du Frasnien du Domaine Ligerien (Massif Amoricain, France)]. *Palaeontographica Abteilung A*, **231**, 1-92.
- and Aretz, M. 2004. Biostratigraphical precisions on the Early Serpukhovian (Late Mississippian), by means of a carbonate algal microflora (cyanobacteria, algae and pseudo-algae) from La Serre (Montagne Noire, France). *Geobios*. Vol. 37. Pg. 643-666
- and Cózar, P. 2010. An attempt of classification of the Palaeozoic *incertae sedis* Algospongia. *Revista Española de Micropaleontología*. Vol. 42. Pg. 129-241
- Perret, M. F. and Delvolvé, J. J. 1989. Algues, pseudo-algues et foraminifères des niveaux bachkiriens dans les secteurs d'Escarra et Aragon Subordan (Pyrénées aragonaises, Espagne). *Geobios*. Vol. 22. Pg. 697-723.

- Hauser, M., Martini, R., Zaninetti, L., Matter, A. and Peters, T. 2001. New Algae and Problematica of Algal Affinity from the Permian of the Aseelah Unit of the Batain Plain (East Oman). *Geobios*. Vol. 34. Pg. 375-404
- Pille, L. and Gaillot, J. 2010. Palaeozoic Foraminifera: Systematics, palaeoecology and responses to global changes. *Revue de Micropaléontologie*. Vol. 53. Pg. 209-254
- Vai, G. B. 2003. Development of the palaeogeography of Pangaea from Late Carboniferous to Early Permian. *Palaeogeography, Palaeoclimatology, Palaeoecology*. Vol. 196. Pg. 125-155
- Valley, J. W. and Cole, D. R. (Eds.) 2001. Reviews in Mineralogy & Geochemistry. *Mineral Society of America*. Vol 43
- Van De Graff, W. J. E. 1971. The Piedrasluengas limestone, a possible model of limestone facies distribution in the Carboniferous of the Cantabrian Mountains. *Trabajos de Geología*. Vol. 3. Pg. 151-159
- Van Gaever, S., Vanreusel, A., Hughes, J. A., Bett, B. J. and Kiriakoulakis, K. 2004. The macro- and micro-scale patchiness of meiobenthos associated with the Darwin Mounds (north-east Atlantic). *Journal of the Marine Biological Association of the UK*. Vol. 84. Pg. 547-556
- van Ginkel, A. C. 1965. Carboniferous fusulinids from the Cantabrian Mountains (Spain). *Leise Geologische Mededelingen*. Vol. 34. Pg. 1-225
- and Villa, E. 1996. Palaeontological data of the San Emiliano Formation (Cantabrian Mountains, Spain) and their significance in the Carboniferous chronostratigraphy. *Geobios*. 29. 149-170
- van Weering, T. C. E., de Haas, H., de Stiger, H. G., Lykke-Andersen, H. and Kouvaev, I. 2003. Structure and development of giant carbonate mounds at the SW and SE Rockall Trough margins, NE Atlantic Ocean. *Marine Geology*. Vol. 198. Pg. 67-81
- Veevers, J. J. and Powell, C. M. 1987. Late Paleozoic glacial episodes in Gondwanaland reflected in transgressive-regressive depositional sequences in Euramerica. *Geological Society of America Bulletin*. Vol. 98. Pg. 475-487
- Veizer, J., Lemieux, J., Lones, B., Gibling, M. R. and Savelle, J. 1977. Sodium: Paleosalinity indicator in ancient carbonate rocks. *Geology*. Vol. 5. Pg. 177-179
- Villa, E., Horvath, V., Martínéz Chacón, M. L. and Sanchez De Posada, L. C. 1988. Datos paleontológicos y edad de la sección de Villamanín (Carbonífero, C. Cantábrica, NW de España). *Congreso Geológico de España*, 1988. Vol. 1. Pg. 337-341
- Walter, L. M. 1986. Relative efficiency of carbonate dissolution and precipitation during diagenesis: A progress report on the role of solution chemistry. In: Gautier, D. L. (Ed.) *Roles of organic matter in sedimentary diagenesis*. Society of Economic Paleontologists and Mineralogists. Special Publication 38. Pg. 1-11
- Wagner, R. H. 1959. Flora fossil y estratigrafía del Carbonífero de España NW y Portugal N. *Estudios Geológicos*. Vol. 15. Pg. 393-420
- 1965. Palaeobotanical Dating of Upper Carboniferous Folding Phases in NW Spain. *Memorias del Instituto Geológico y Minero de España*. Vol. 66. Pg. 1-169
- and Bowman, M. B. J. 1983. The position of Bashkirian/Moscovian boundary in West European chronostratigraphy. *Newsletter on Stratigraphy*. Vol. 12. Pg. 132-161
- and Fernández-García, I. 1971. The Lower Carboniferous and Namurian rocks north of La Robla (León). *Trabajos de Geología*. Vol. 4. Pg. 507-531

- and Winkler Prins, C. F. 1985. The Cantabrian and Barruelian stratotypes: A summary of basin Development and biostratigraphic in Fm. In: Lemos de Sousa, H. J. and Wagner, R. H. (Eds.) *Papers on the Carboniferous of the Iberian Peninsula (Sedimentology, Stratigraphy, Paleontology, Tectonics and Geochemistry)*. Annales da Faculdade de Ciências, Universidade do Porto, Special Supplement to Vol. 64 (1983). Pg. 359-410
- Wang, S., Fan, J. and Rigby, J. K. 1994. Archaeolithoporella and tubiphytes: Affinities and paleoecology in Permian reefs of South China. *Science in China. Series B, Chemistry, Life Sciences & Earth Sciences*. Vol. 36. Pg. 723-743
- Wanless, H.R. and Sheppard, F.P. 1936. Sea level and climatic changes related to late Paleozoic cycles. *Geological Society of America Bulletin*. Vol. 47. Pg. 1177-1206
- Warthin, A. S. Jr. 1930. Micropaleontology of the Wetumka, Wewoka and Holdenville Formations. *Oklahoma Geological Survey Bulletin*. Vol. 53.
- Watkins, R. 1999. Upper Paleozoic biostromes in island-arc carbonates of the eastern Klamath terrane, California. *Paleontological Research*. Vol. 3. Pg. 151-161
- Watson, J. S. 1996. Fast, simple method of powdered pellet preparation for X-ray Fluorescence analysis. *X-Ray Spectrometry*. Vol. 25. Pg. 173-174
- Webb, G. E. 1996. Was Phanerozoic reef history controlled by the distribution of non-enzymatically secreted reef carbonates (microbial carbonate and biologically induced cement)? *Sedimentology*. Vol. 43. Pg. 947-971
- Weller, H. 1995. The Devonian mud mounds of Rubeland in the Harz Mountains/Germany. *Facies*. Vol. 32. Pg. 43-49
- Wendt, J., Belka, Z. and Moussine-Pouchkine, A. 1993. New Architecture of deep water carbonate buildups: Evolution of mud mounds into mud ridges (Middle Devonian, Algerian Sahara). *Geology*. Vol. 21. Pg. 723-726
- Kaufmann, B., Belka, Z., Farsan, N. and Bavandpur, A. K. 2002. Devonian/Lower Carboniferous stratigraphy, facies patterns and palaeogeography of Iran. Part I. Southeastern Iran. *Acta Geologica Polonica*. Vol. 52. Pg. 129-168
- West, R. R. 1988. Temporal changes in Carboniferous Reef Mound Communities. *Palaios*. Vol. 3. Pg. 152-169
- Westphal, H. and Munnecke, A. 2003. Limestone-marl alternations: A warm water phenomenon? *Geology*. Vol. 31. Pg. 263-266
- Wienberg, C., Beuck, L., Heidkamp, S., Hebbeln, D., Freiwald, A., Pfannkuche, O. and Monteys, X. 2008. Franken Mound: facies and biocoenoses on a newly-discovered "carbonate mound" on the western Rockall Bank, NE Atlantic. *Facies*. Vol. 54. Pg. 1-24
- Wiggins, W. D. 1986. Geochemical signature in carbonate matrix and their relation to deposition and diagenesis, Pennsylvanian Marble Falls Limestone, Central Texas. *Journal of Sedimentary Petrology*. Vol. 56. Pg. 771-783
- Wignall, P.B. and Newton, R. 1998. Pyrite framboid diameter as a measure of oxygen deficiency in ancient mudrocks. *American Journal of Science*. Vol. 298. Pg. 537-552
- and Twitchett, R.J., 2002. Permian-Triassic sedimentology of Jameson Land, East Greenland; incised submarine channels in an anoxic basin. *Journal of the Geological Society of London*. Vol. 159. Pg. 691-703

- Newton, R. and Brookfield, M. E. 2005. Pyrite framboids evidence for oxygen-poor deposition during the Permian-Triassic crisis in Kashmir. *Palaeogeography, Palaeoclimatology, Paleoecology*. Vol. 216. Pg. 183-188
- Wilkin, R. T., Barnes, H. L. and Brantley, S. L. 1996. The size distribution of framboidal pyrite in modern sediments: An indicator of redox conditions. *Geochemica et Cosmochimica Acta*. Vol. 60. Pg. 3897-3912
- Arthur, M. A. and Dean, W. E. 1997. History of water-column anoxia in the Black Sea indicated by pyrite framboids size distributions. *Earth Planetary Science Letters*. Vol. 148. Pg. 517-525
- Wilkinson, B. H. and Given, K. R. 1986. Secular variation in abiotic marine carbonates: constraints on Phanerozoic carbon dioxide contents and oceanic Mg/Ca ratios. *Journal of Geology*. Vol. 94. Pg. 321-333
- Wilson, J. L. 1975. *Carbonate Facies in Geologic History*. Springer-Verlag Berlin.
- Winkler Prins, C. F. 1968. Carboniferous Productidina and Chonetidina of the Cantabrian Mountains (NW Spain): systematics, stratigraphy and palaeoecology. *Leidse Geologische Mededelingen*. Vol. 43. Pg. 41-126
- Wood, A. 1948. "Sphaerocodium", a misinterpreted fossil from the Wenlock Limestone. *Proceedings of the Geologists Association*. Vol. 59. Pg. 9-22
- 1957. The type-species of the genus *Girvanella* (calcareous algae). *Palaeontology*. Vol. 1. Pg. 22-28
- Wood, J. 1986. Thermal mass transfer in systems containing quartz and calcite. . In: Gautier, D. L. (Ed.) *Roles of organic matter in sedimentary diagenesis*. Society of Economic Paleontologists and Mineralogists. Special Publication 38. Pg. 169-180
- Wood, R. 2000. Novel paleoecology of a postextinction reef: Famennian (Late Devonian) of the Canning basin, northwestern Australia. *Geology*. Vol. 28. Pg. 987-990
- 2001. Are reefs and mud mounds really so different? *Sedimentary Geology*. Vol. 145. Pg. 161-171
- Dickson, A. D. and Kirkland, B. L. 1996. New observations on the ecology of the Permian Capitan Reef, Texas and New Mexico. *Palaeontology*. Vol. 39. Pg. 733-762
- Wotte, T. 2009. Re-interpretation of a Lower-Middle Cambrian West Gondwanan ramp depositional system: a case study from the Cantabrian Zone (NW Spain). *Facies*. Vol. 55. Pg. 473-487
- Wray, J. L. 1964. *Archeolithophyllum*, an Abundant Calcareous Alga in Limestones of the Lansing Group (Pennsylvanian), Southeastern Kansas. *Kansas Geological Survey, Bulletin*. Vol. 170. Pg. 1-13
- 1977. *Calcareous algae*. Elsevier, Amsterdam.
- Wright, V. P. and Burgess, P. M. 2005. The carbonate factory continuum, facies mosaics and microfacies: an appraisal of some of the key concepts underpinning carbonate Sedimentology. *Facies*. Vol. 51. Pg. 17-23
- Wu, Y. and Chafetz, H. S. 2002. ¹³C-Enriched carbonate in Mississippian mud mounds: Alamogordo Member, Lake Valley Formation, Sacramento Mountains, New Mexico, U.S.A.. *Journal of Sedimentary Research*. Vol. 72. Pg. 138-145

Zechman, F. W. 2003. Phylogeny of the Dasycladales (Chlorophyta, Ulvophyceae) Based on Analyses of Rubisco Large Subunit (rbcL) Gene Sequences. *Journal of Phycology*. Vol. 39. Pg. 819-827

Ziegler, P. A. 1989. *Evolution of Laurussia - A Study in Late Palaeozoic Plate Tectonics*. Royal Geological and Mining Society of the Netherlands

- 1990. *Geological Atlas of Western and Central Europe*. Shell International Petroleum.

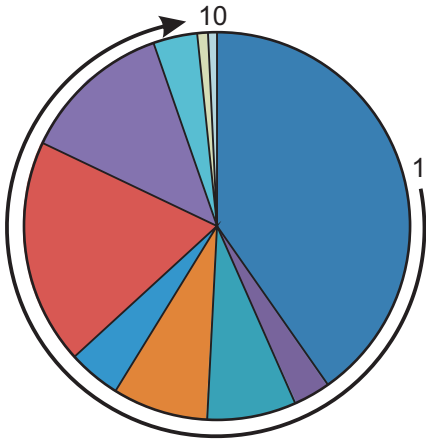
Zonneveld, J-P. 2001. Middle Triassic biostromes from the Liard Formation, British Columbia, Canada: oldest examples from the Mesozoic of NW Pangea. *Sedimentary Geology*. Vol. 145. Pg. 317-341

Acknowledgements

I would like to express my gratitude to my supervisors, Michael Montenari and Graham Williams. The technical staff: Rich Burgess, David Emley, Andy Lawrence, Ian Wilshaw, Peter Greatbatch and David Wilde (Pete n' Dave) have all been a great help. Thanks to Melanie Leng of NIGL for help with isotope analysis. To my numerous postgrad comrades, especially Jamie Hansen, Helen Doherty and Rosie Allen Smithells and my friends from near and far (Julie Boyce!), thanks for helping keep me relatively sane. The folks of the San Emiliano area are thanked for their exceptional attitude toward us, especially "Dutch" Pete. Stuart Egan, Ian Stimpson, Jamie Pringle, Nigel Cassidy and Graham Williams (deserves a second mention!) have all been a wondrous help throughout. Finally a special thanks to my family, especially Jen and Seb, for all of your continued help and love.

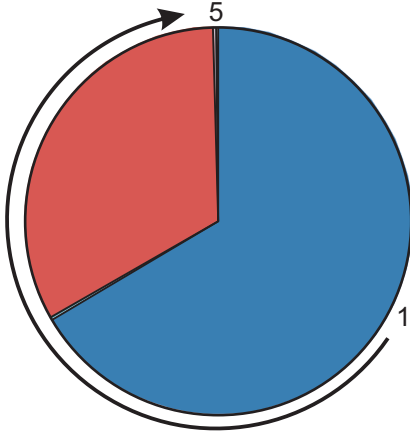
Appendix 1. Point Count

Candemuela Mound 1



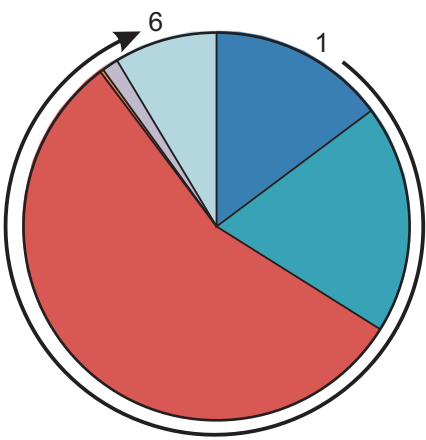
- 1) Homogenous Micrite 40%
- 2) Internal Micrite 3%
- 3) Sparite - Fenestral 7%
- 4) Sparite - Fossil fill 8%
- 5) Calcite Fracture 4%
- 6) Algae - Donezella/Beresellanids 19%
- 7) Algae - Komia etc. 13%
- 8) Algae - other 4%
- 9) Cyanobacterial mat 1%
- 10) Other 1%

Candemuela Mound 6



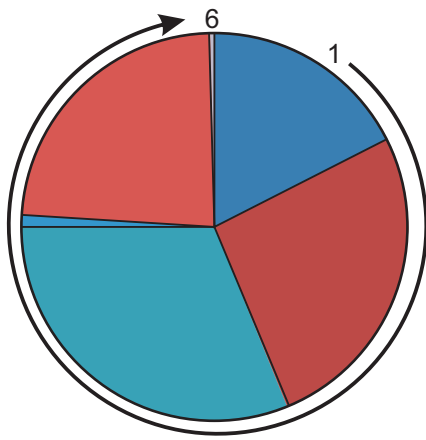
- 1) Homogenous Micrite 65%
- 2) Sparite - Fenestral 1%
- 3) Algae - Donezella/Beresellanids 32%
- 4) Tuberitinidae 1%
- 5) Other 1%

Candemuela Mound 2



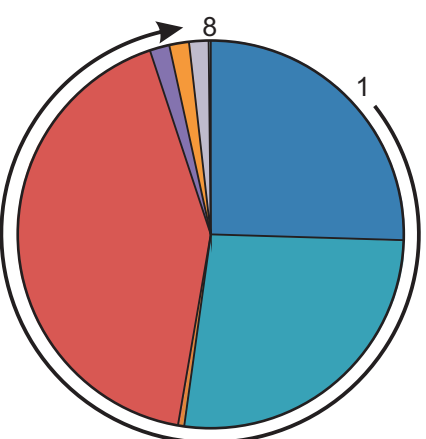
- 1) Homogenous Micrite 15%
- 2) Sparite - Fenestral 19%
- 3) Algae - Donezella/Beresellanids 56%
- 4) Foraminifera 1%
- 5) Tuberitinidae 1%
- 6) Other 8%

Candemuela Mound 7



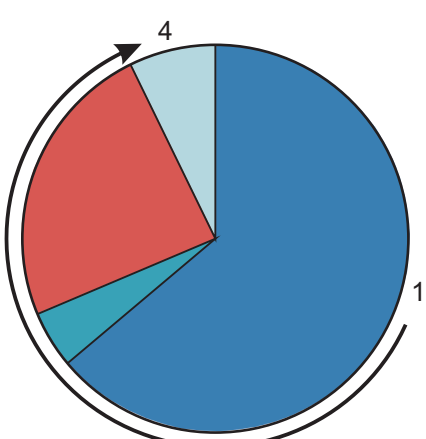
- 1) Homogenous Micrite 17%
- 2) Clotted Micrite 26%
- 3) Sparite - Fenestra 31%
- 4) Calcite Fracture 1%
- 5) Algae - Donezella/Beresellanids 24%
- 6) Tuberitinidae 1%

Candemuela Mound 3



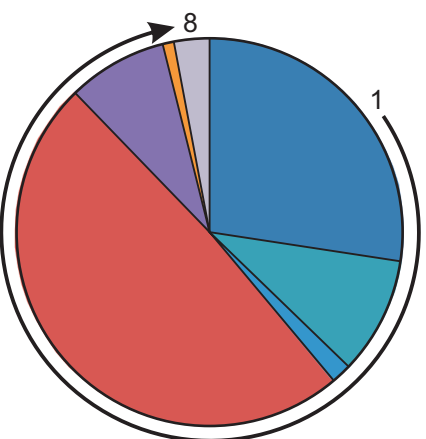
- 1) Homogenous Micrite 15%
- 2) Sparite - Fenestral 27%
- 3) Sparite - Fossil fill 1%
- 4) Algae - Donezella/Beresellanids 42%
- 5) Algae - Komia etc. 1%
- 6) Foraminifera 2%
- 7) Tuberitinidae 1%
- 8) Other 1%

Candemuela Mound 8



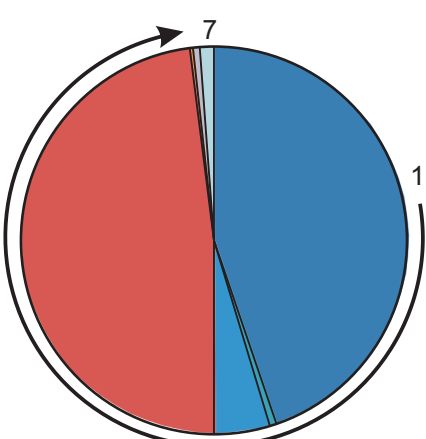
- 1) Homogenous Micrite 64%
- 2) Sparite - Fenestral 5%
- 3) Algae - Donezella/Beresellanids 24%
- 4) Other 7%

Candemuela Mound 4



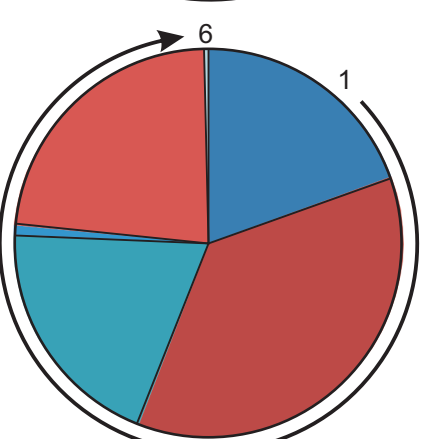
- 1) Homogenous Micrite 27%
- 2) Sparite - Fenestral 10%
- 3) Calcite Fracture 2%
- 4) Algae - Donezella/Beresellanids 49%
- 5) Algae - Komia etc. 8%
- 6) Foraminifera 1%
- 7) Tuberitinidae 3%

Candemuela Mound 9



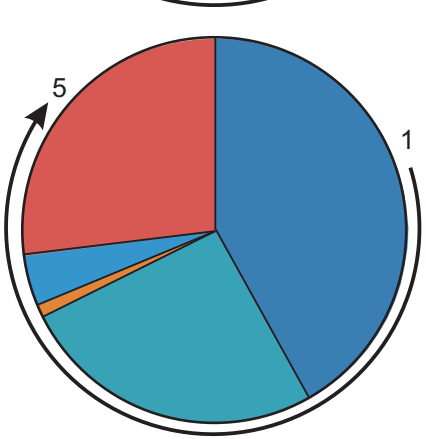
- 1) Homogenous Micrite 44%
- 2) Sparite - Fenestral 1%
- 3) Calcite Fracture 4%
- 4) Algae - Donezella/Beresellanids 48%
- 5) Foraminifera 1%
- 6) Tuberitinidae 1%
- 7) Other 1%

Candemuela Mound 5



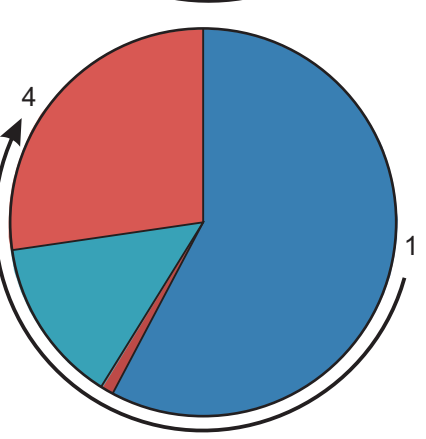
- 1) Homogenous Micrite 19%
- 2) Clotted Micrite 36%
- 3) Sparite - Fenestral 20%
- 4) Calcite Fracture 1%
- 5) Algae - Donezella/Beresellanids 23%
- 6) Other 1%

Candemuela Mound 10



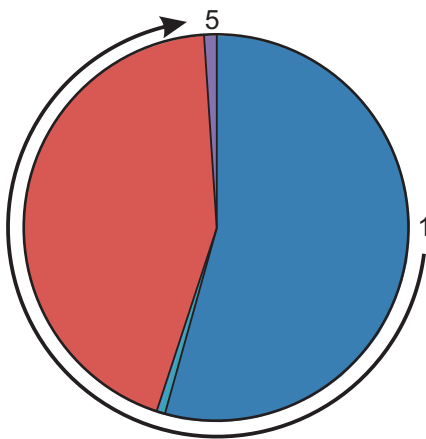
- 1) Homogenous Micrite 42%
- 2) Sparite - Fenestral 26%
- 3) Sparite - Fossil fill 1%
- 4) Calcite Fracture 4%
- 5) Algae - Donezella/Beresellanids 27%

Candemuela Mound 6A

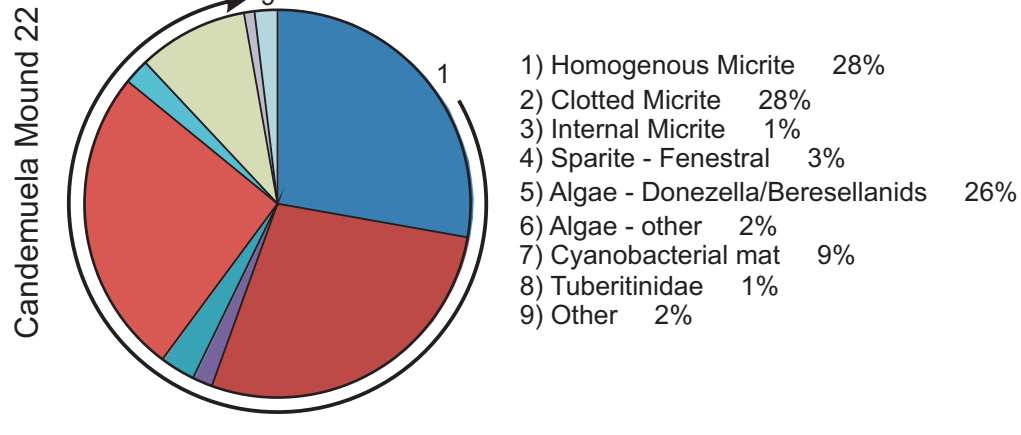
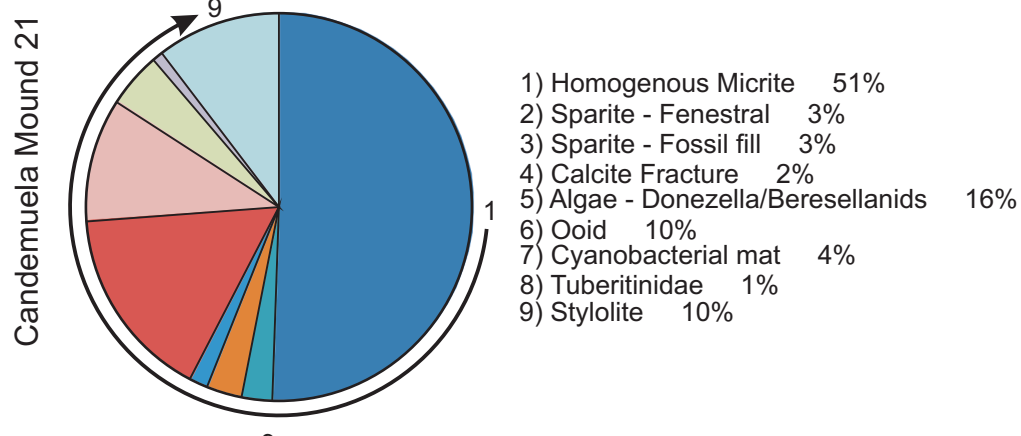
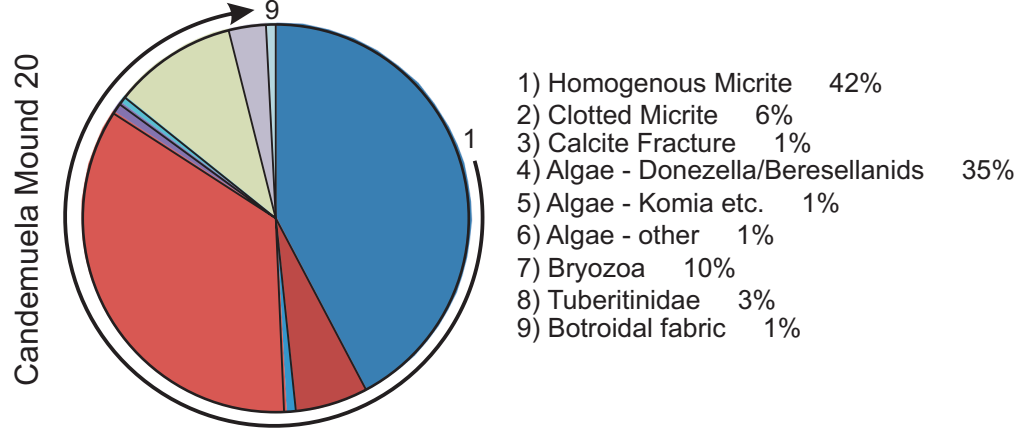
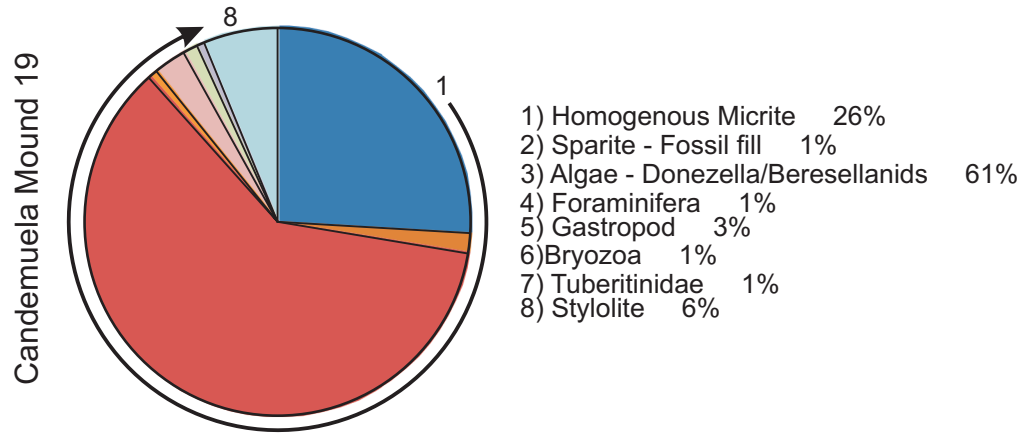
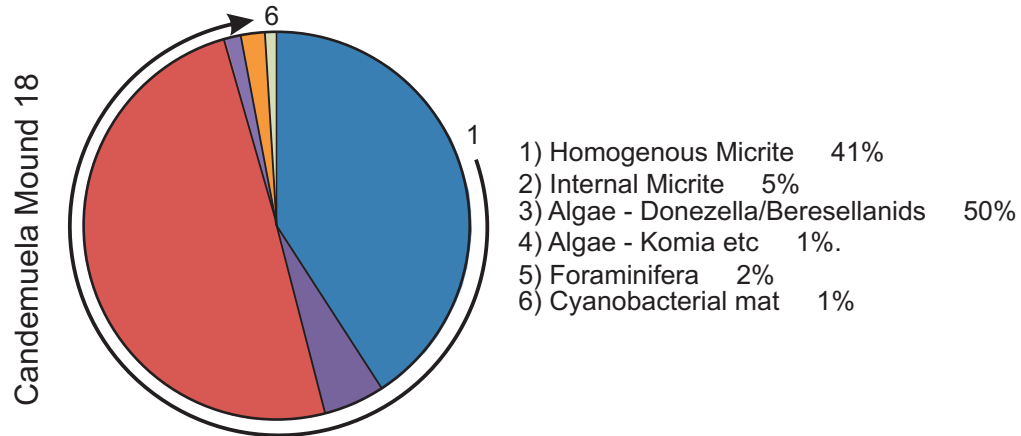
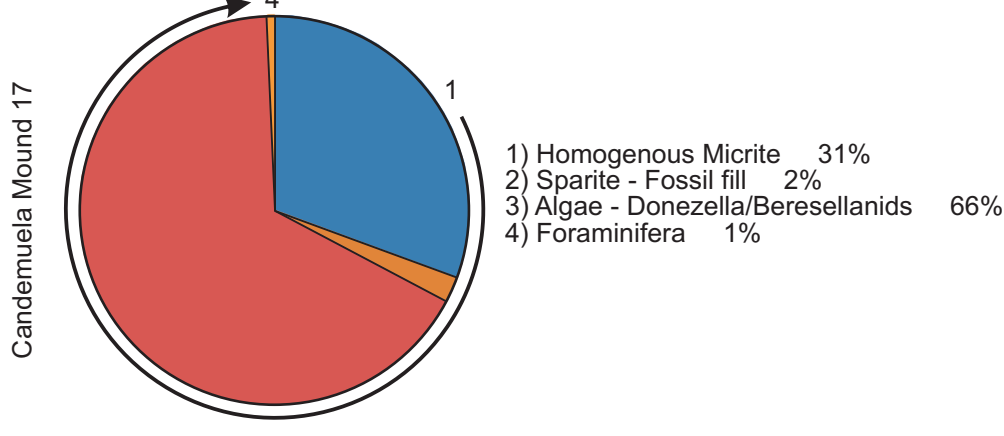
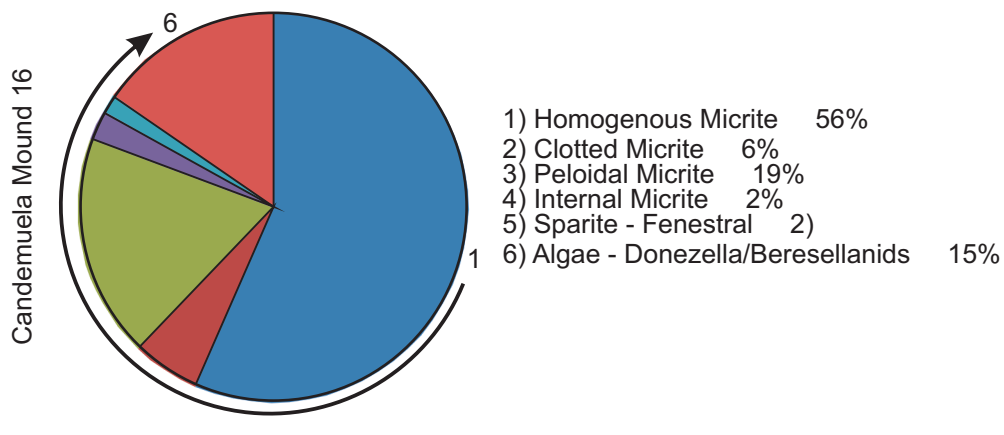
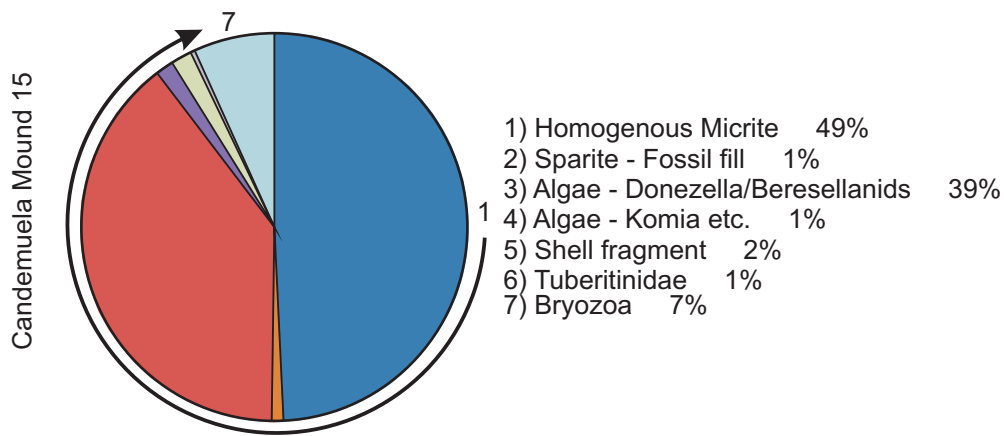
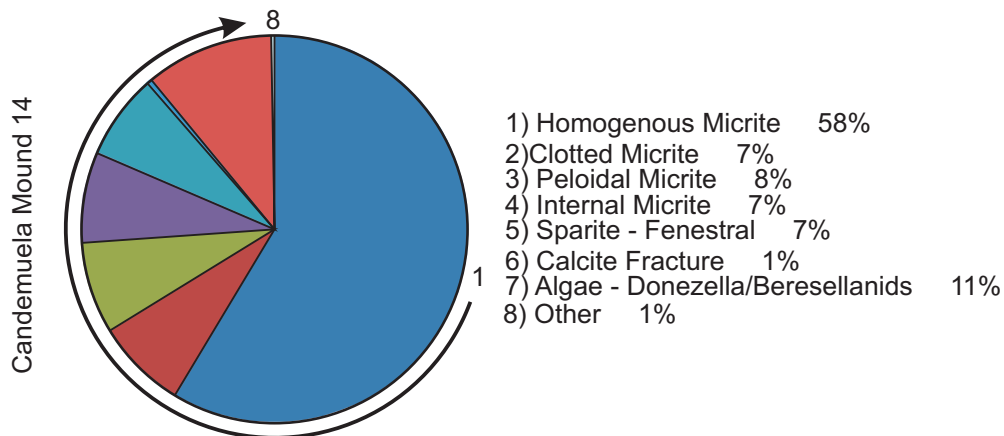
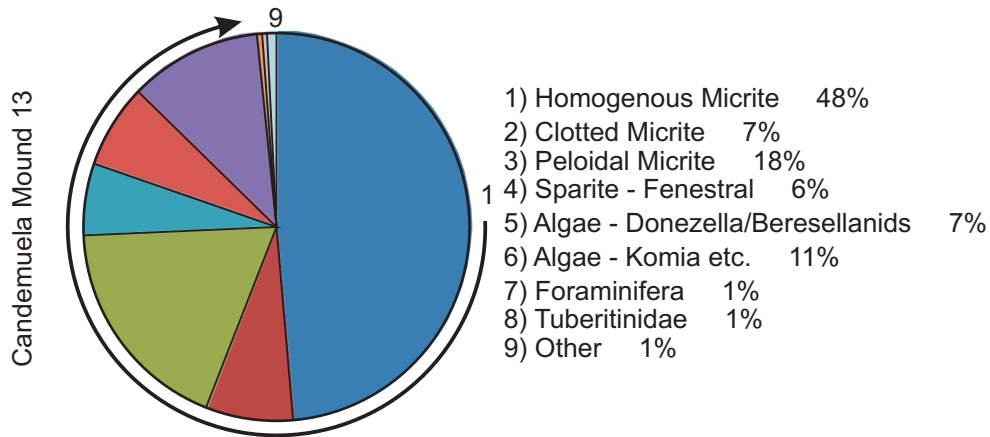
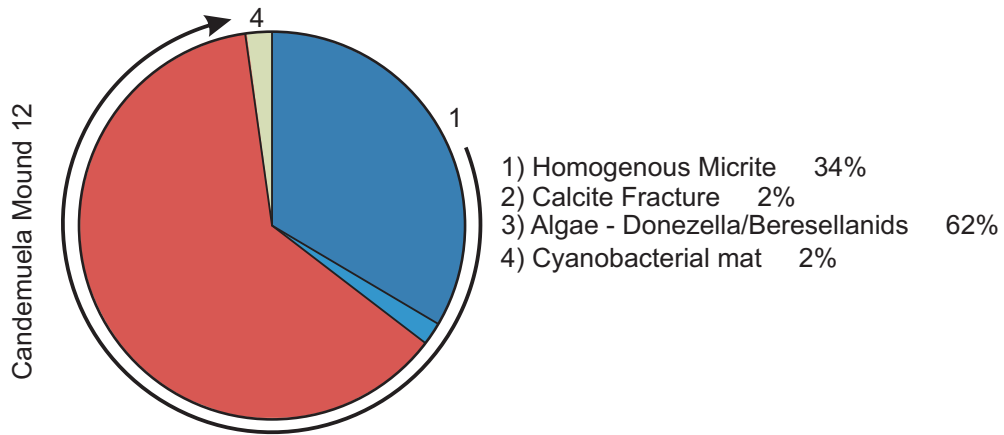


- 1) Homogenous Micrite 58%
- 2) Clotted Micrite 1%
- 3) Sparite - Fenestral 14%
- 4) Algae - Donezella/Beresellanids 27%

Candemuela Mound 11



- 1) Homogenous Micrite 54%
- 2) Sparite - Fenestral 1%
- 3) Calcite Fracture 1%
- 4) Algae - Donezella/Beresellanids 43%
- 5) Algae - Komia etc. 1%



Appendix 2. EDS Maps

Fig. 5.1 F

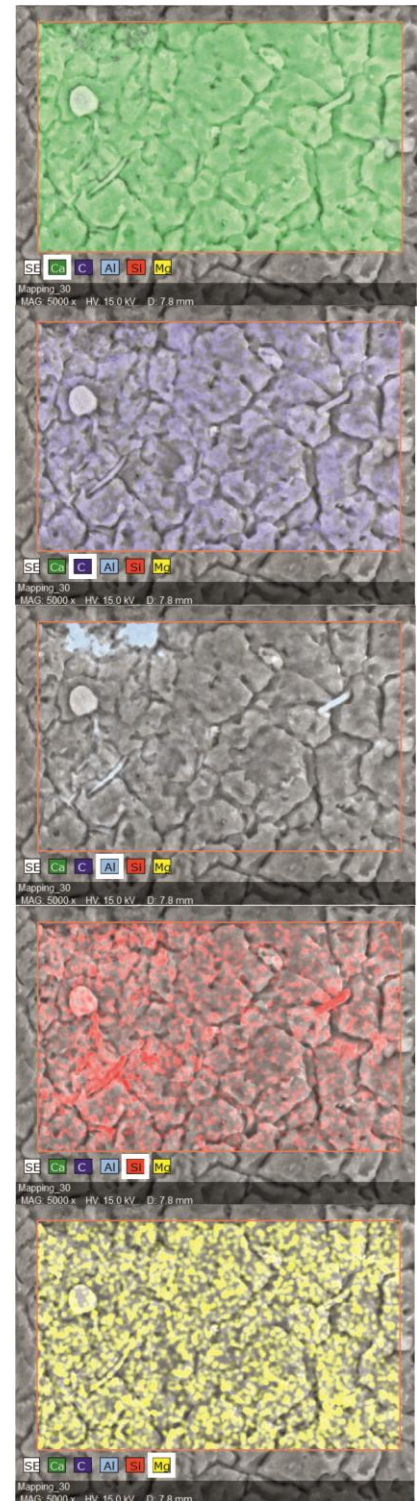
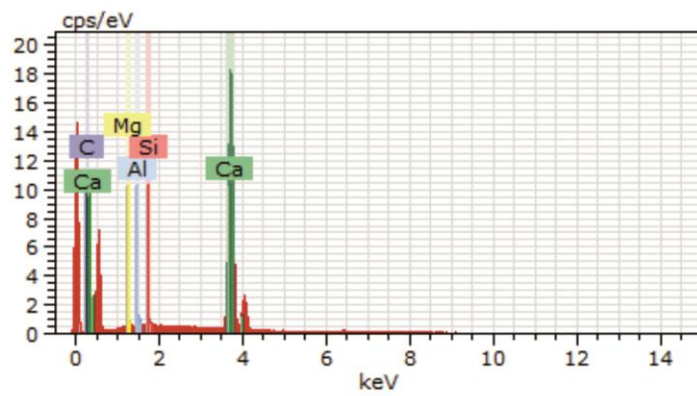
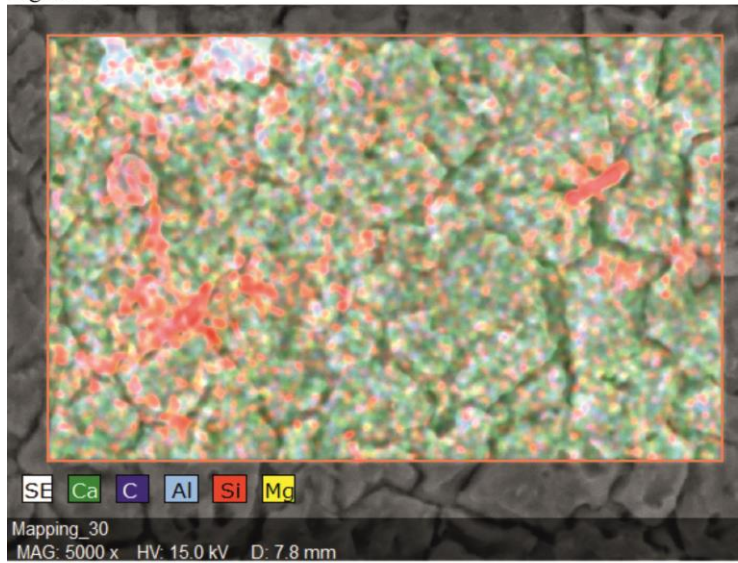


Fig. 5.1 H

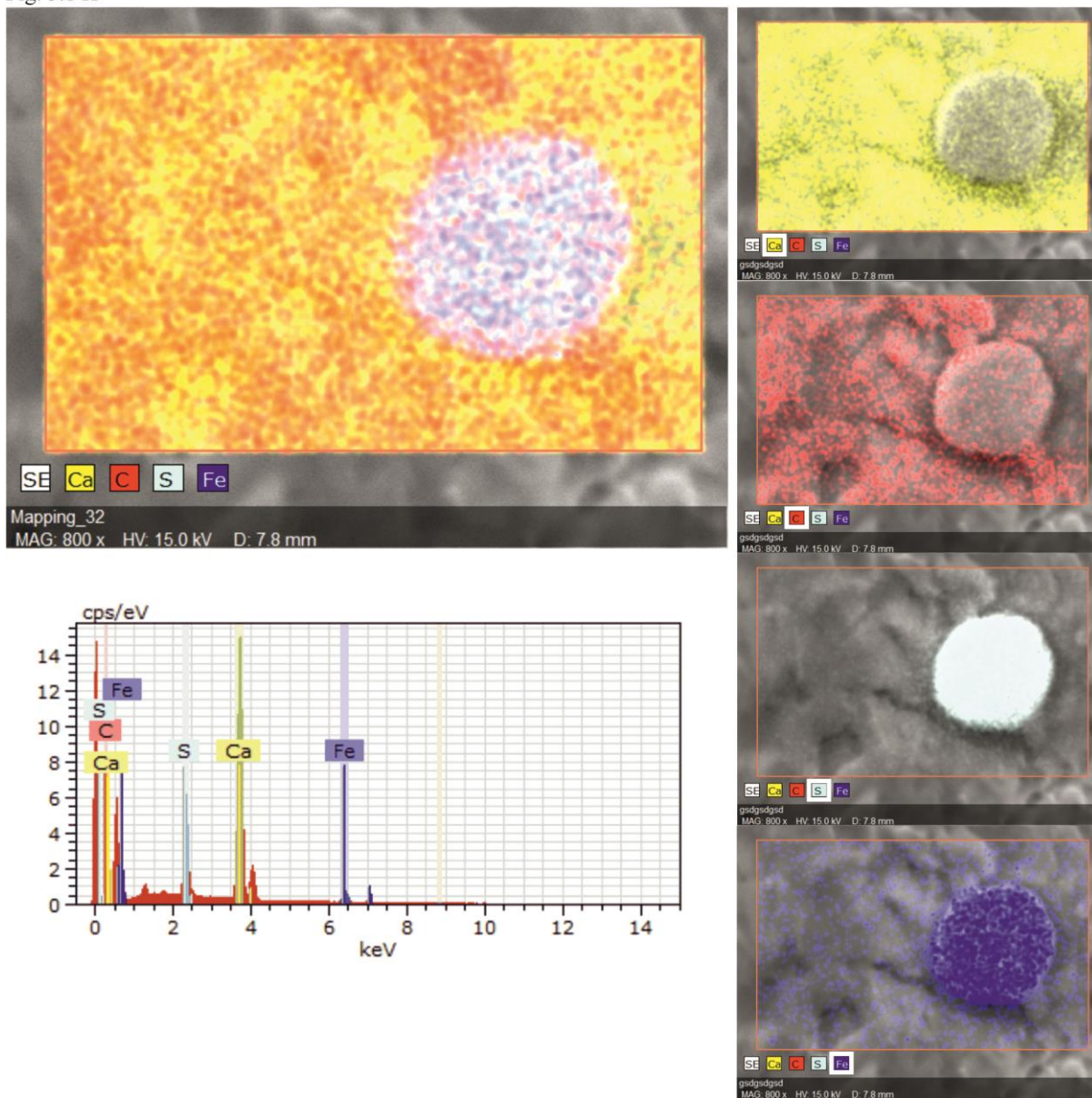


Fig. 5.2 H

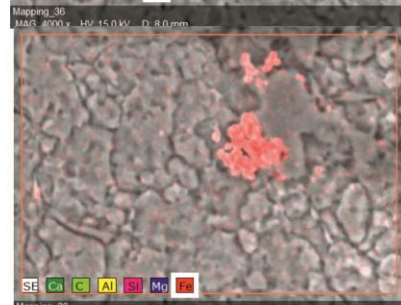
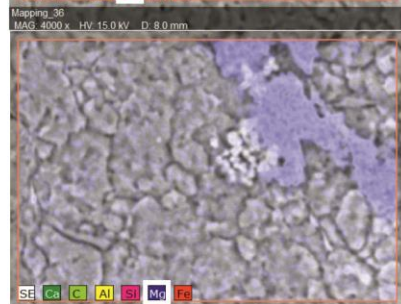
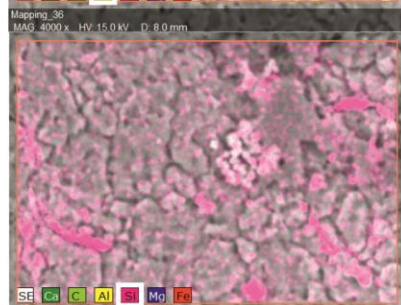
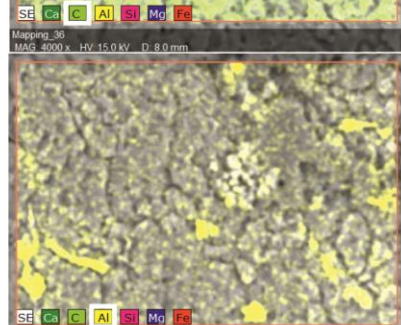
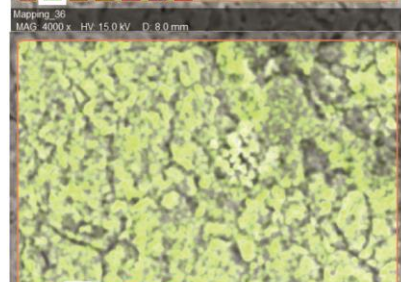
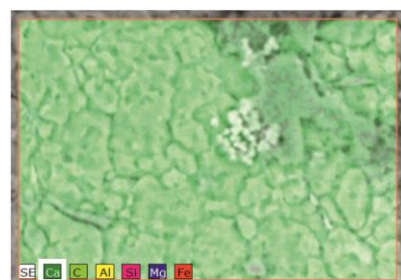
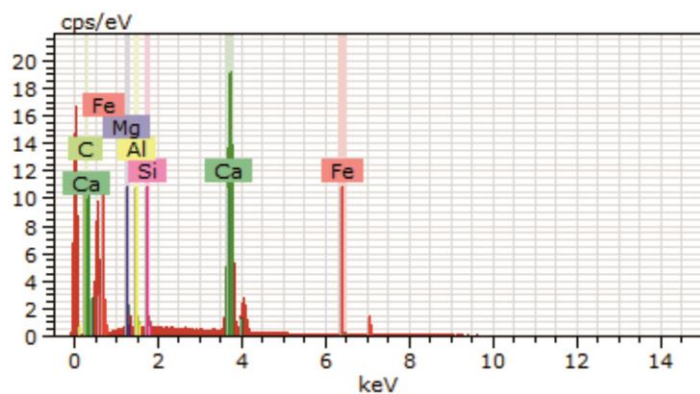
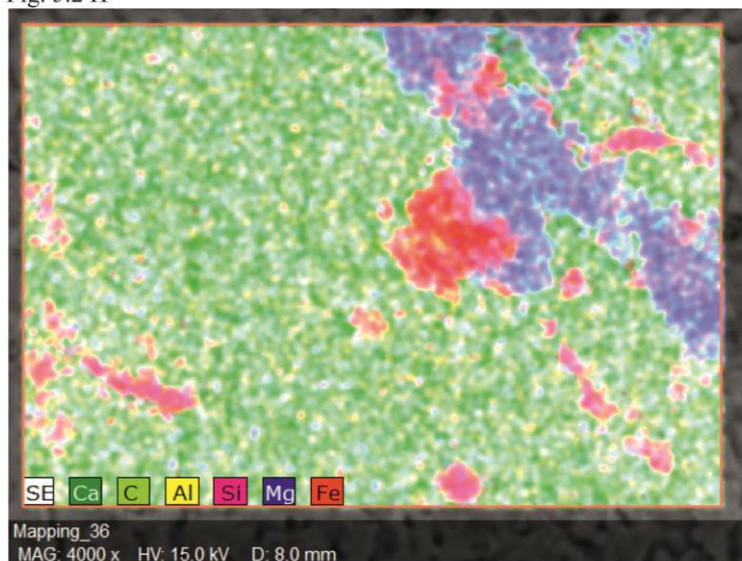


Fig. 5.3 H

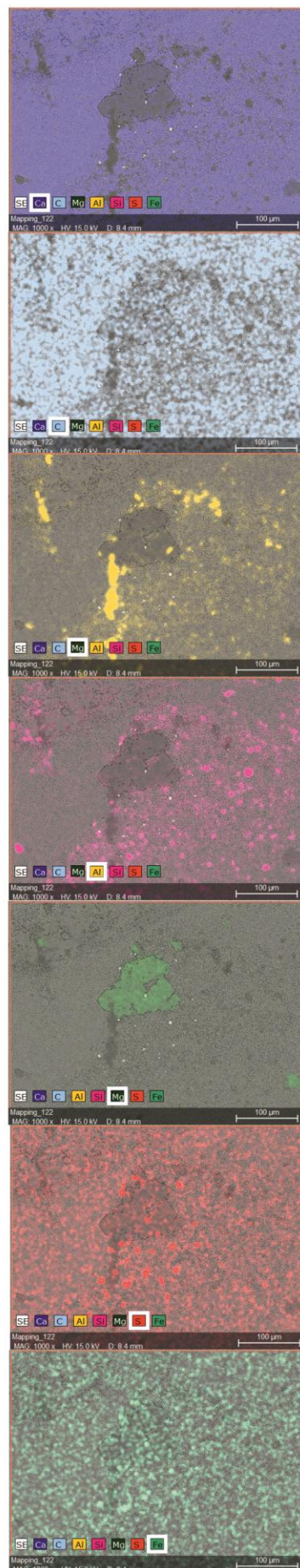
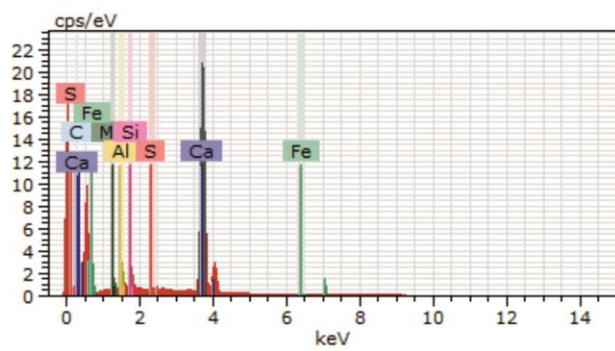
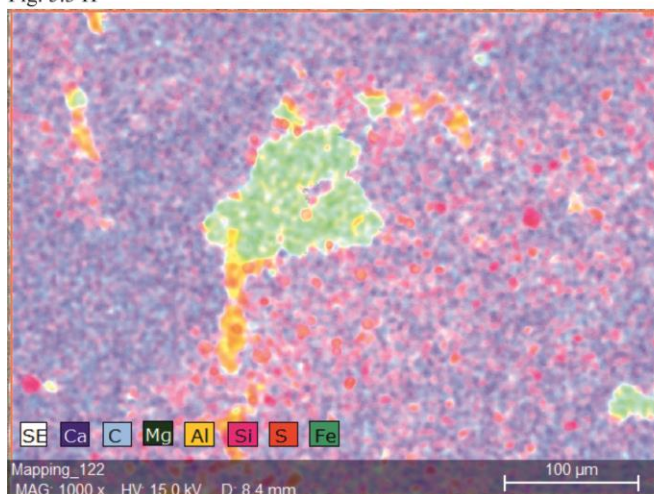


Fig. 5.5 B

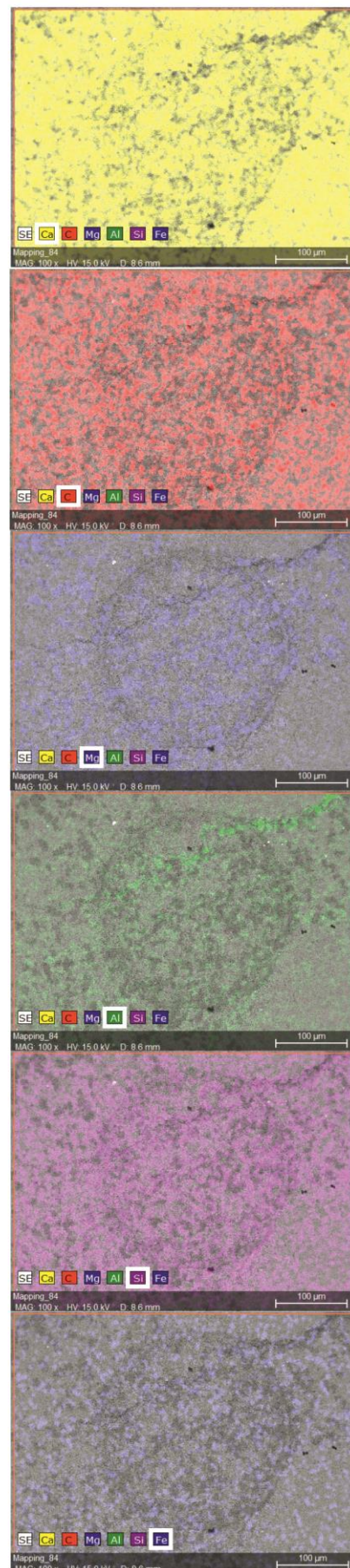
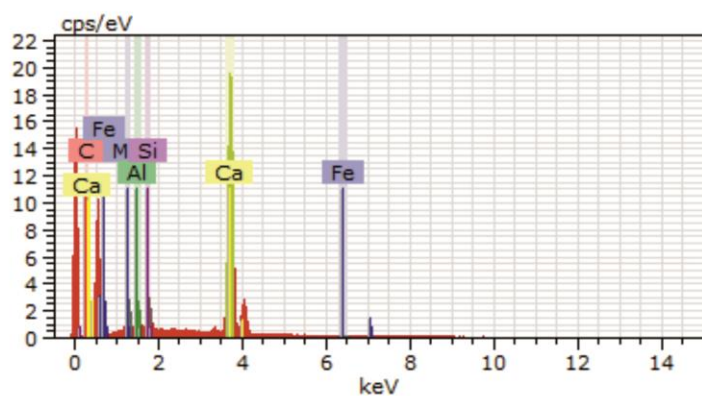
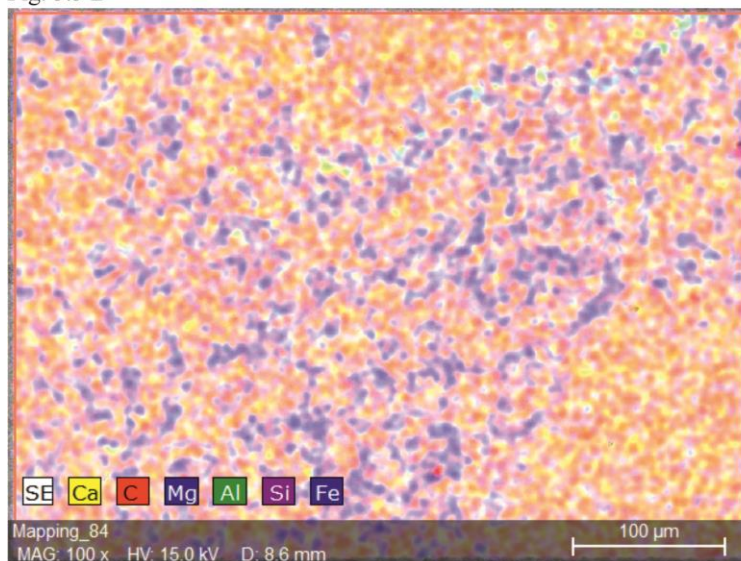
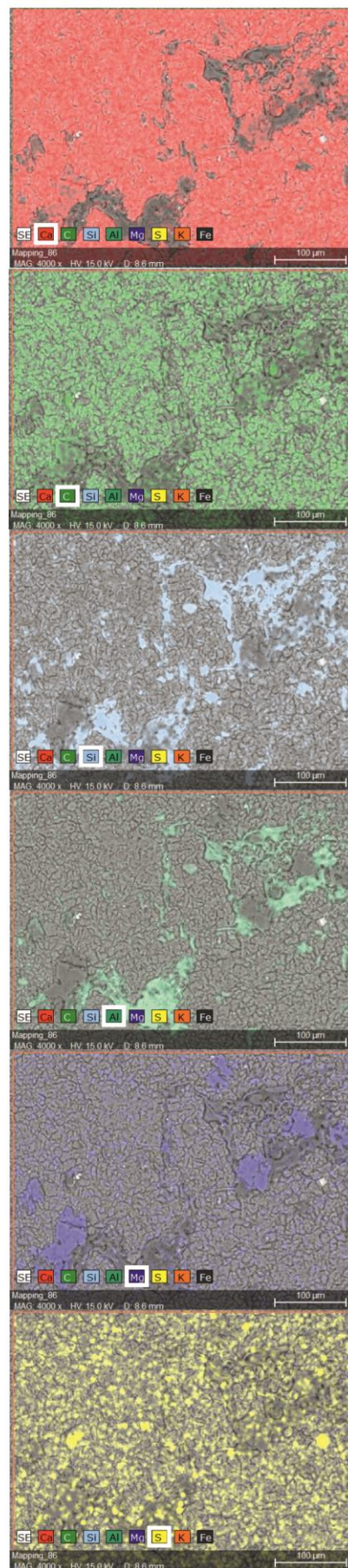
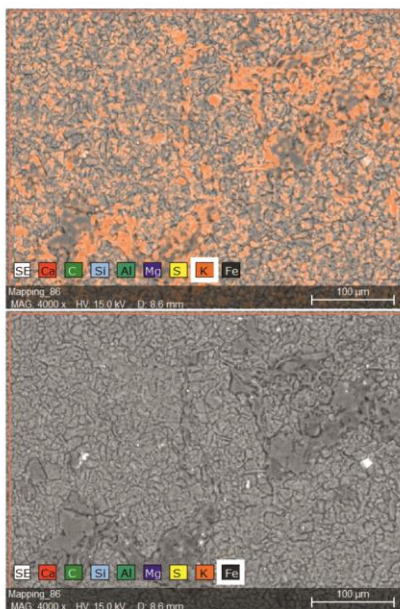
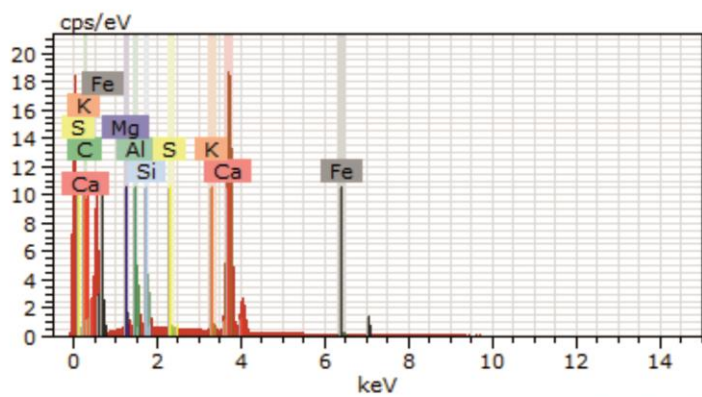
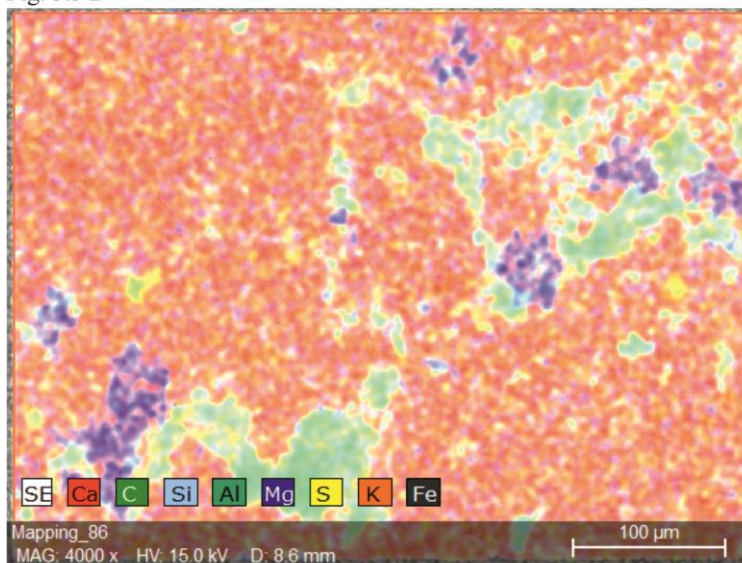


Fig. 5.5 D



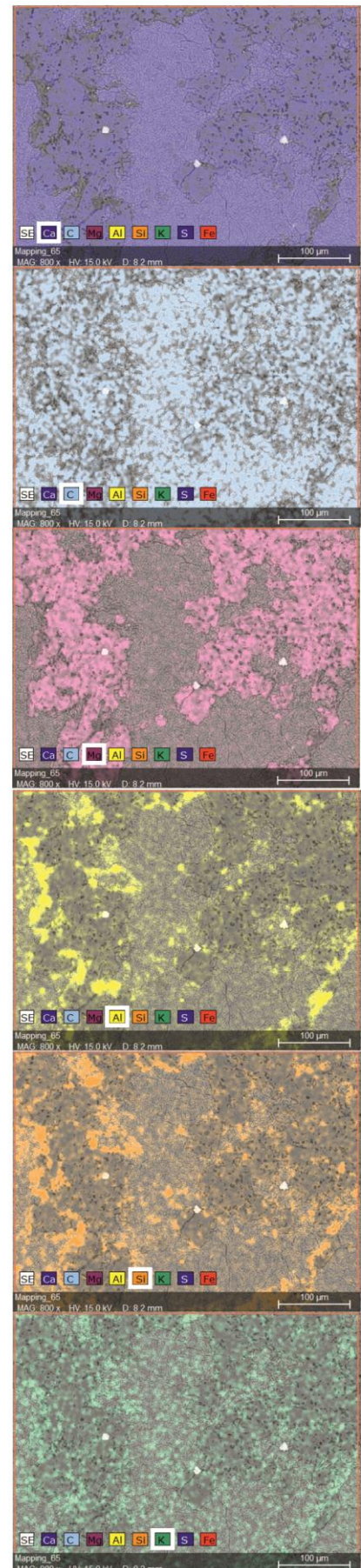
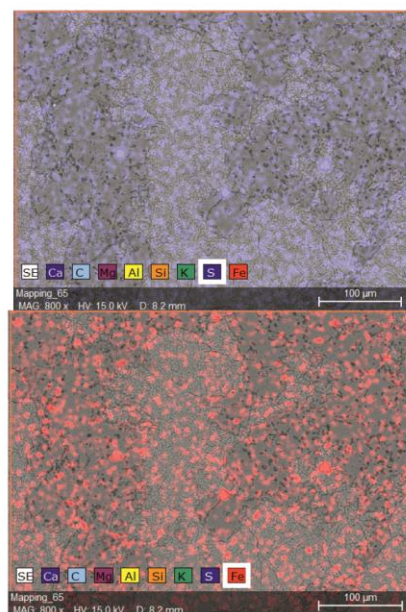
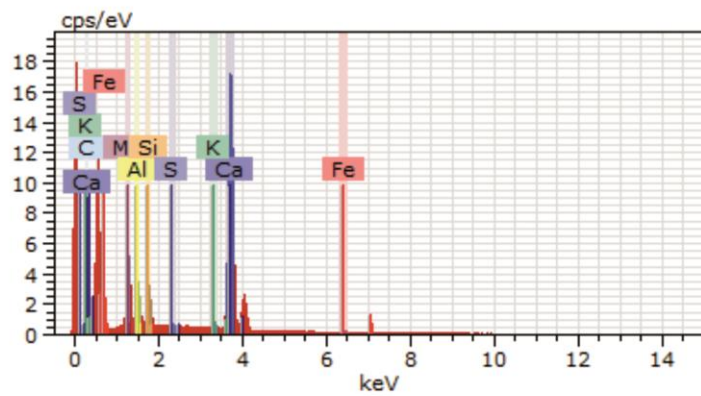


Fig. 5.7 D

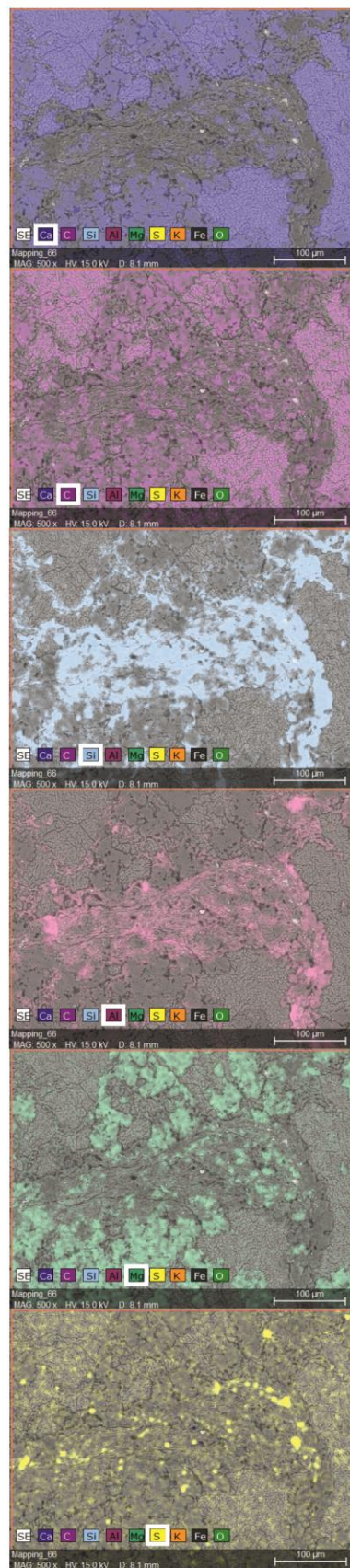
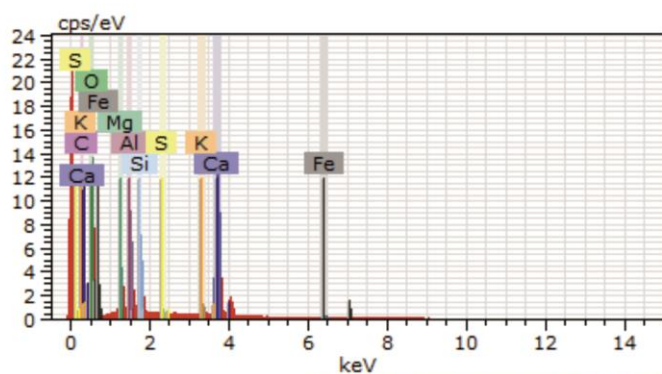
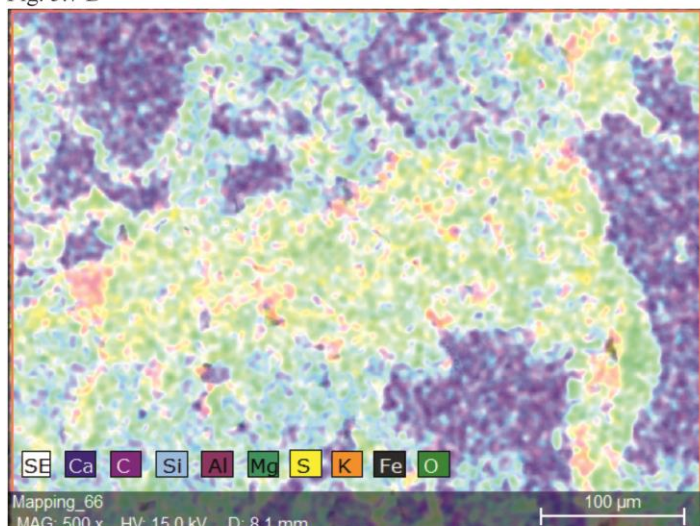


Fig. 5.7 F

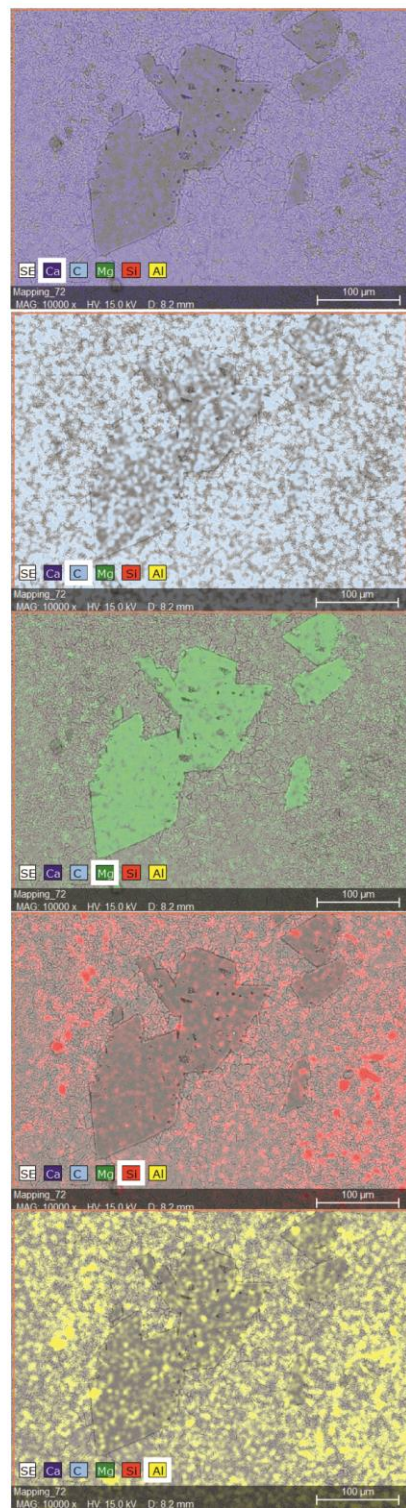
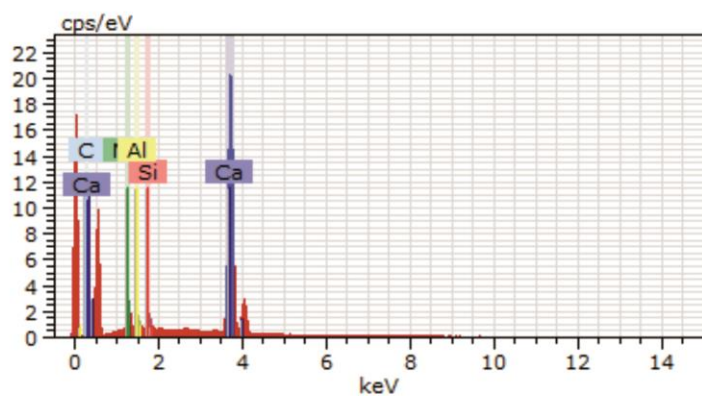
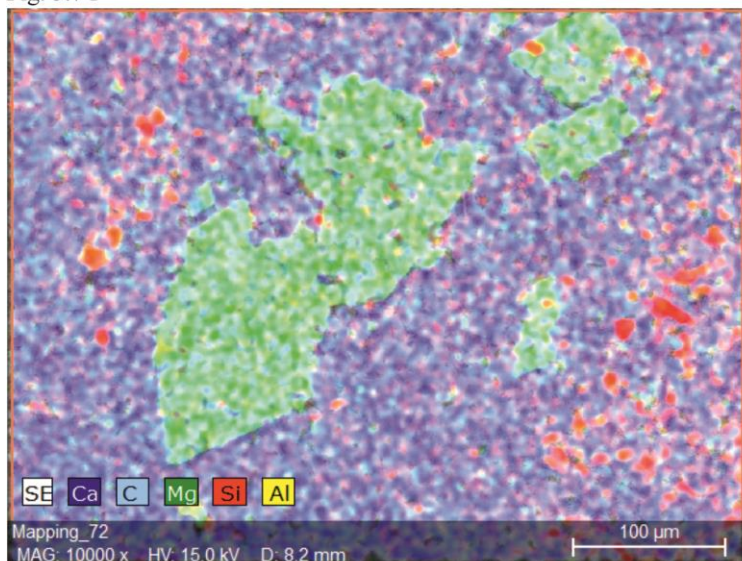


Fig. 5.8 F

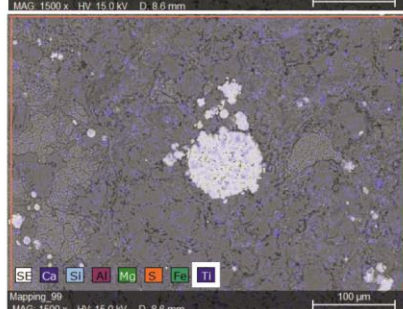
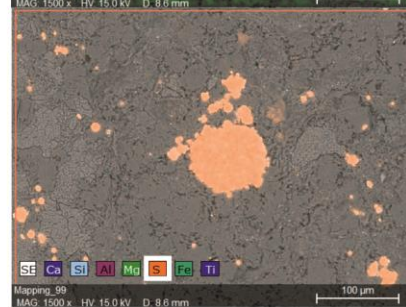
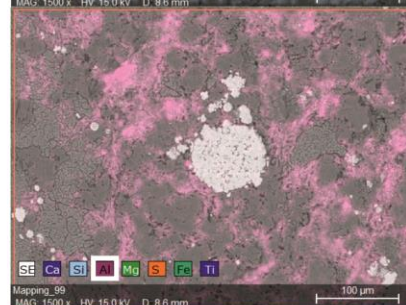
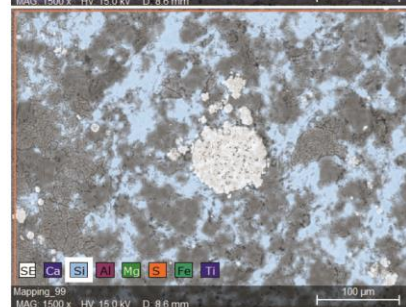
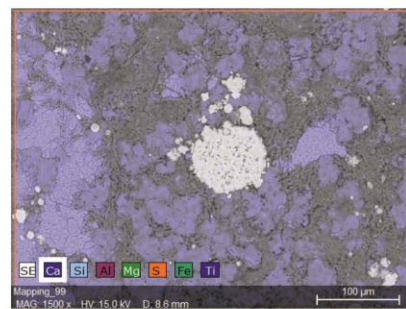
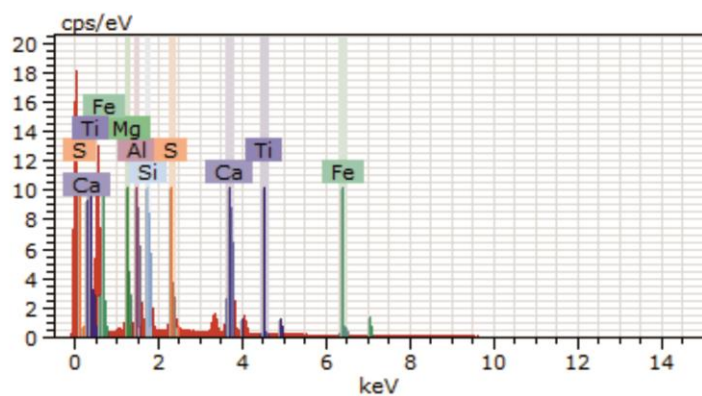
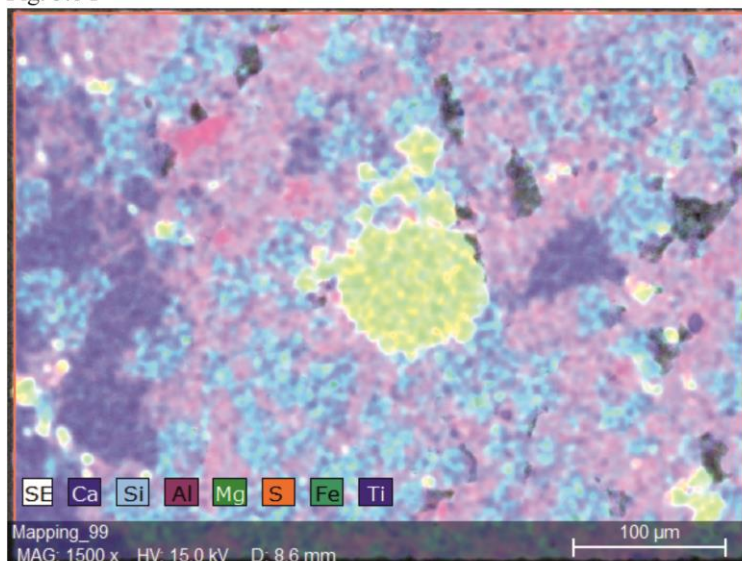


Fig. 5.8 H

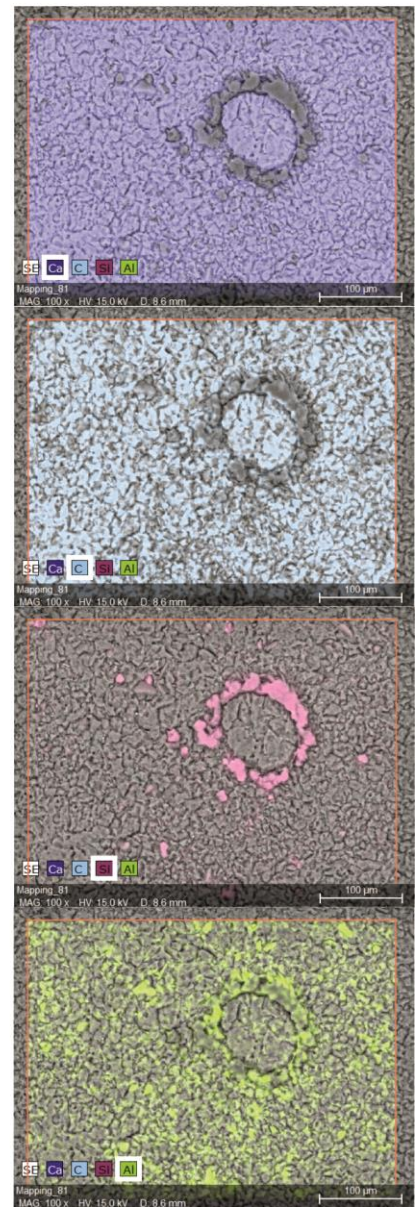
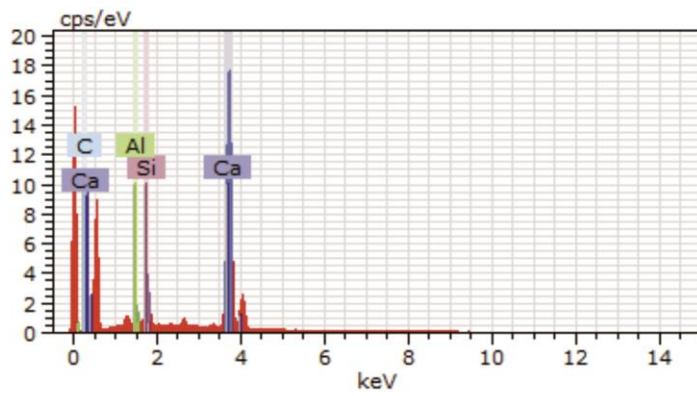
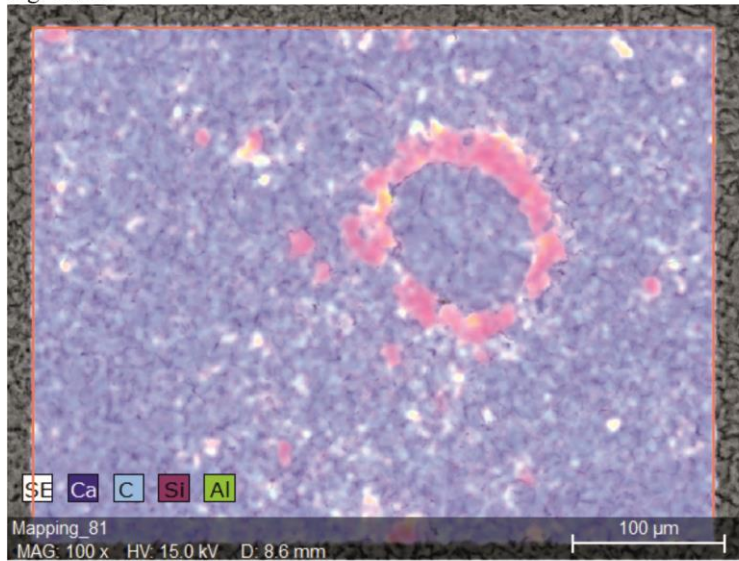
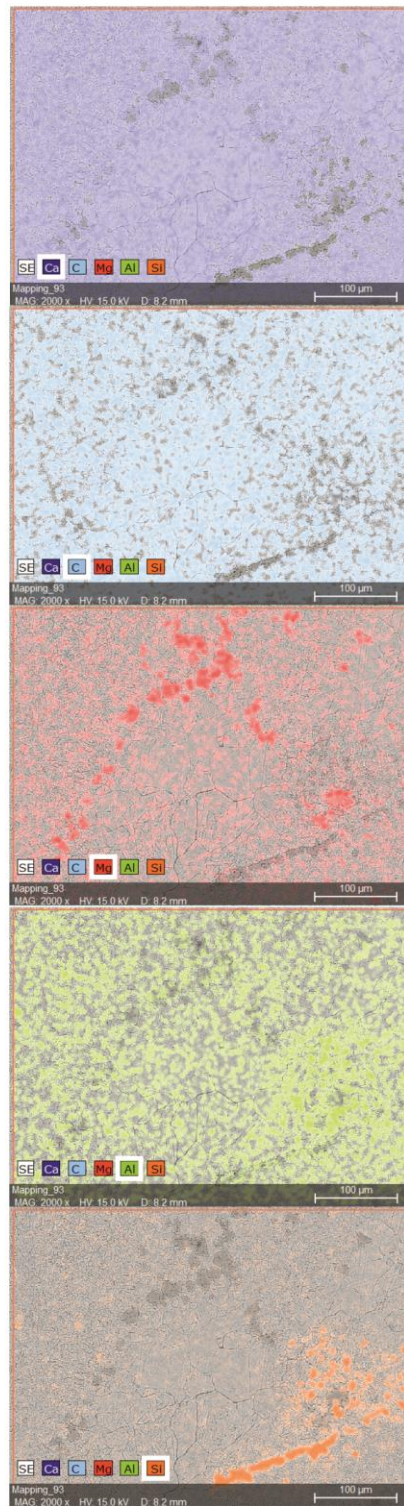
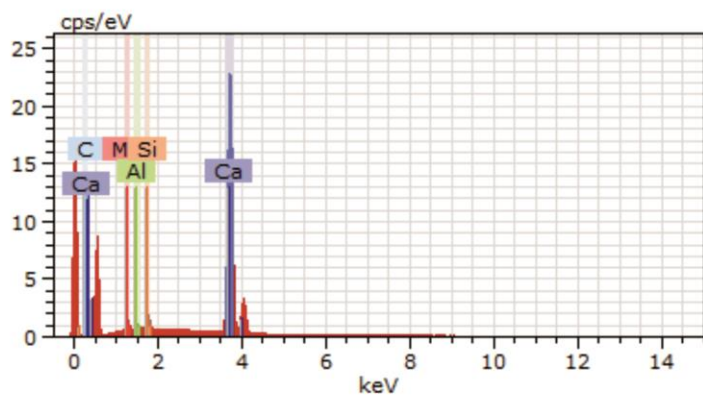
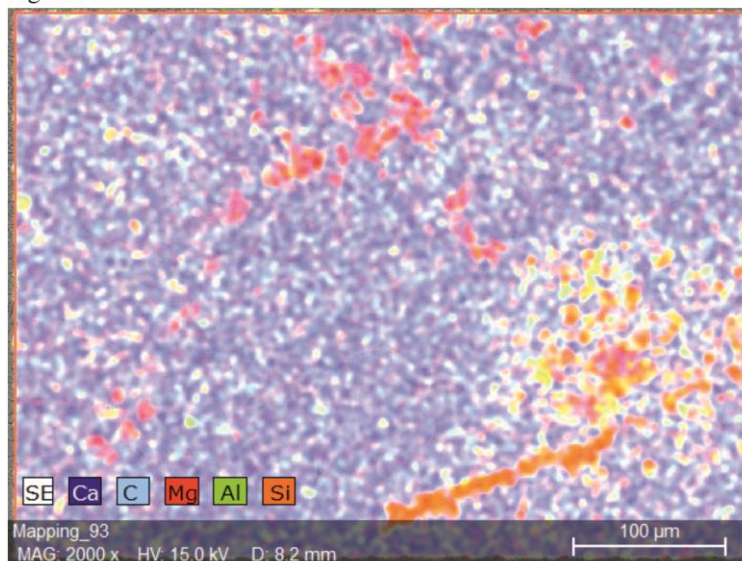


Fig. 5.9 H



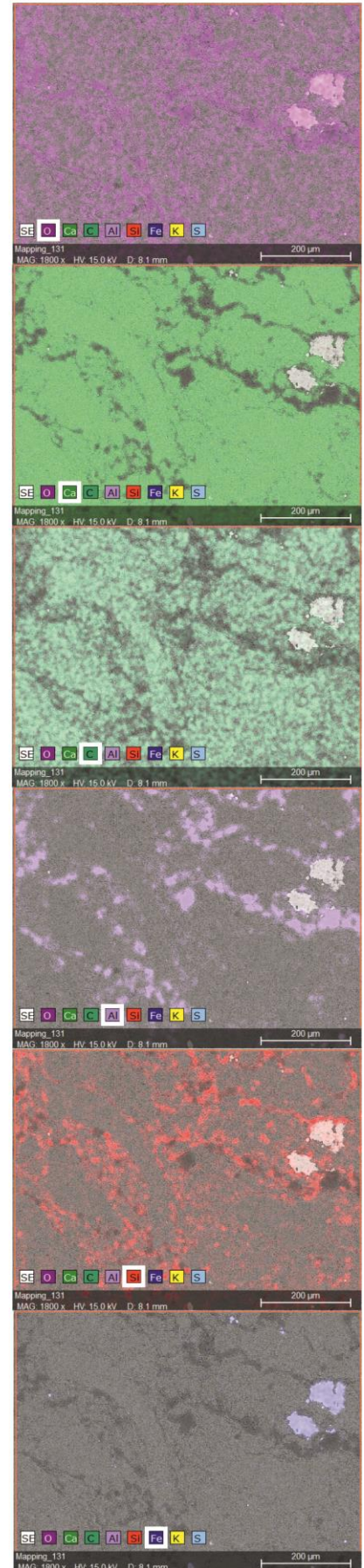
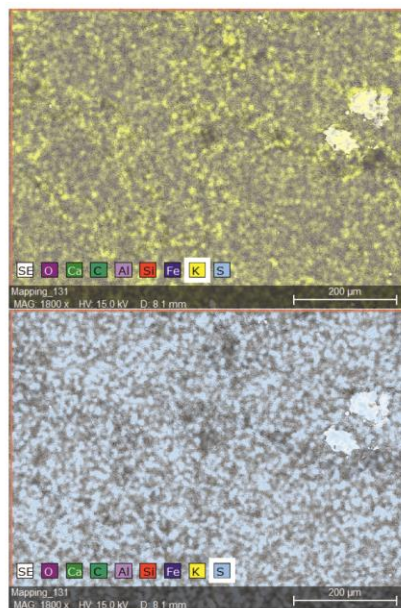
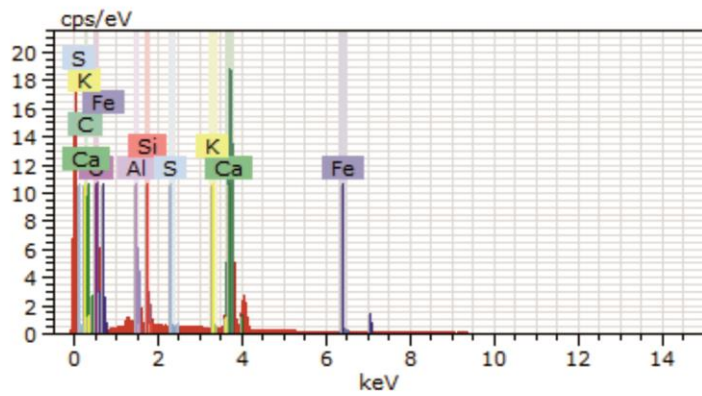


Fig. 5.11 F

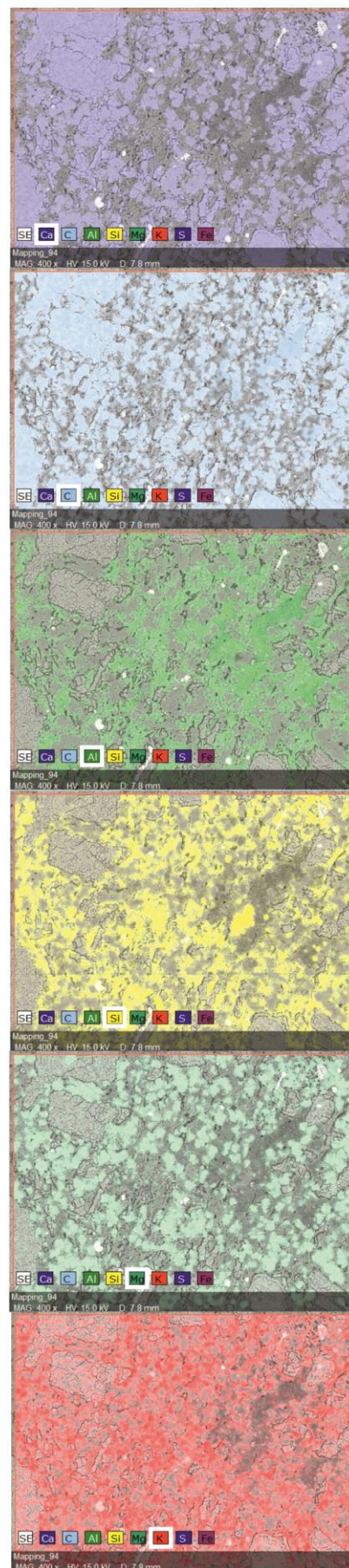
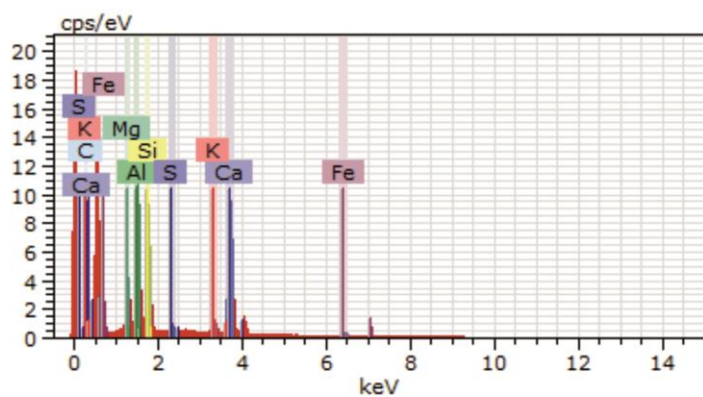
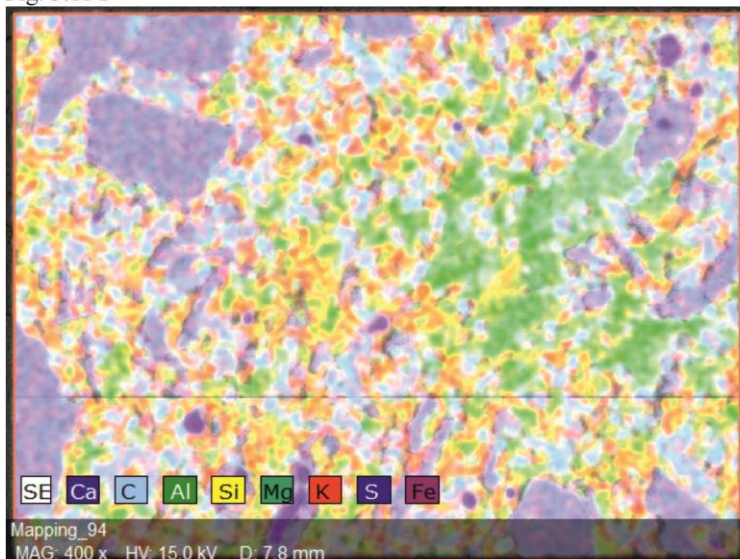


Fig. 5.11 H

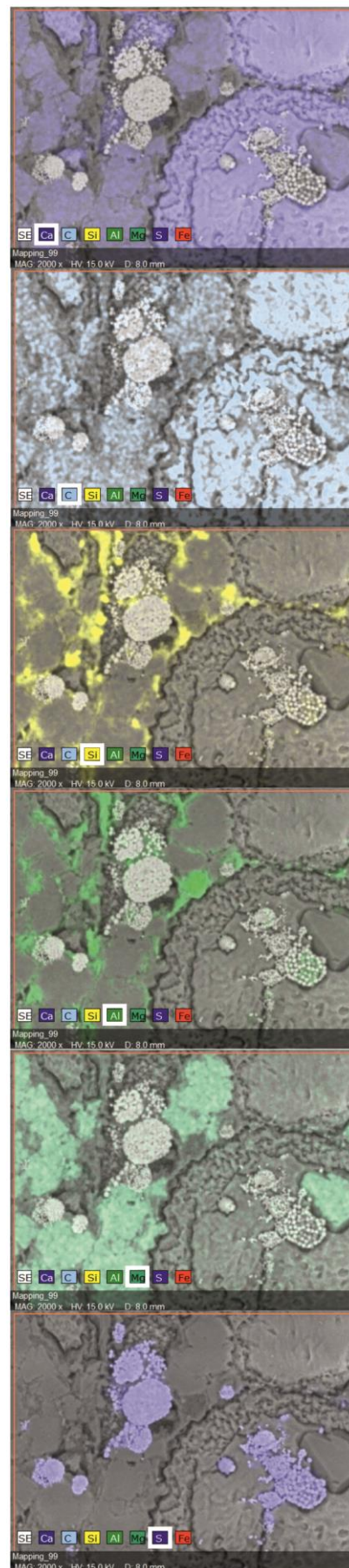
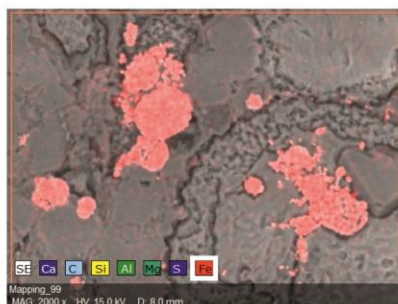
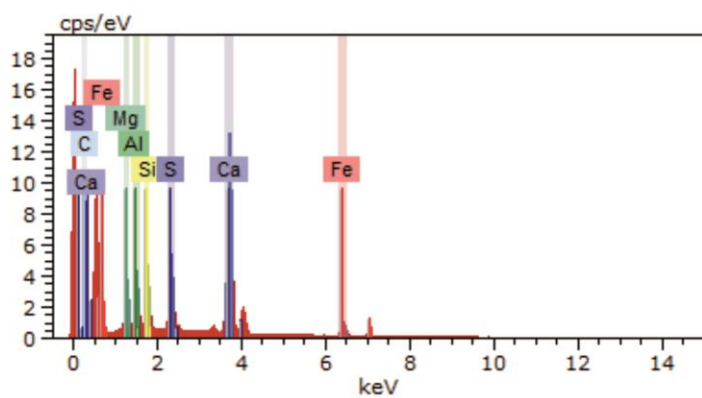
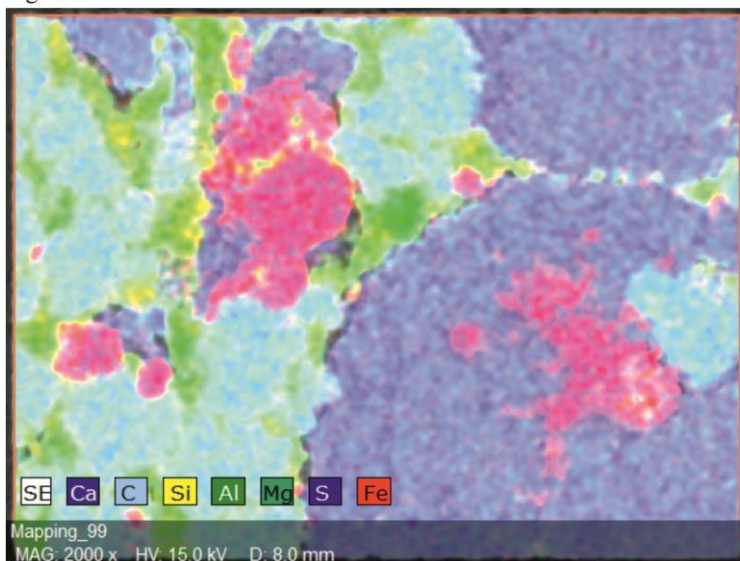


Fig. 5.12 H

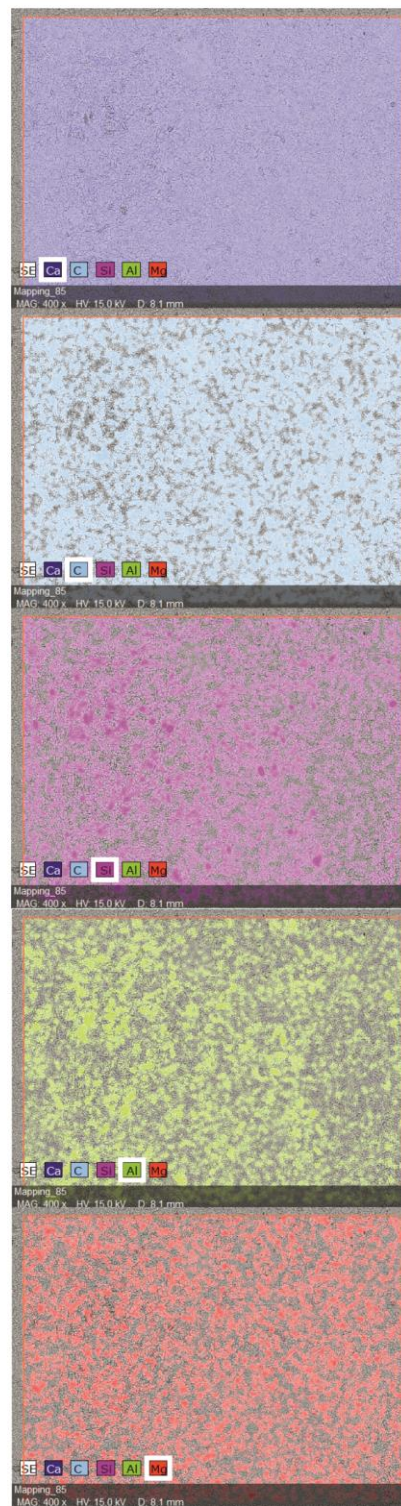
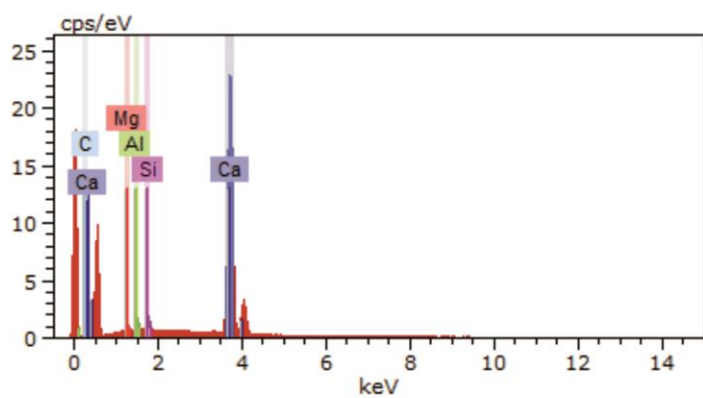
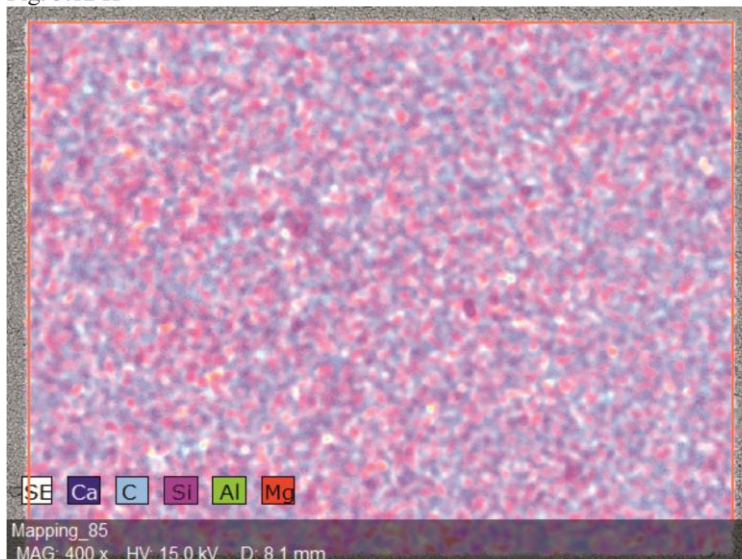


Fig. 5.13 F

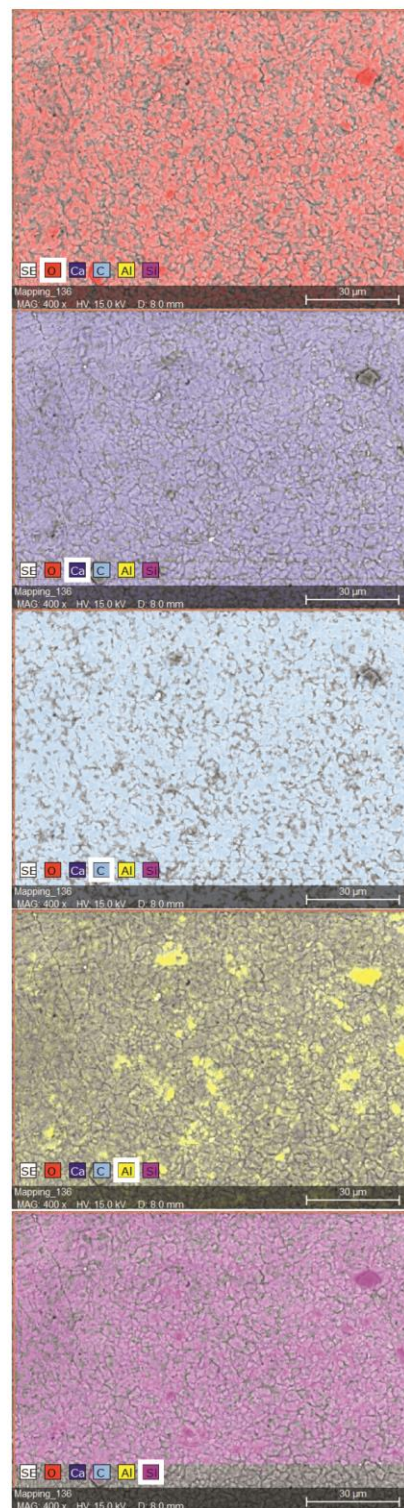
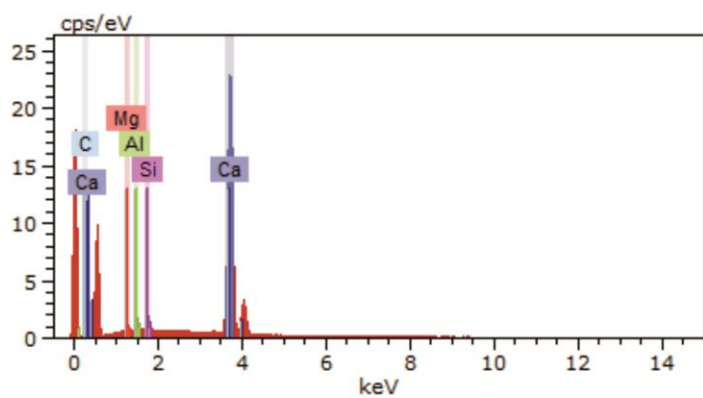
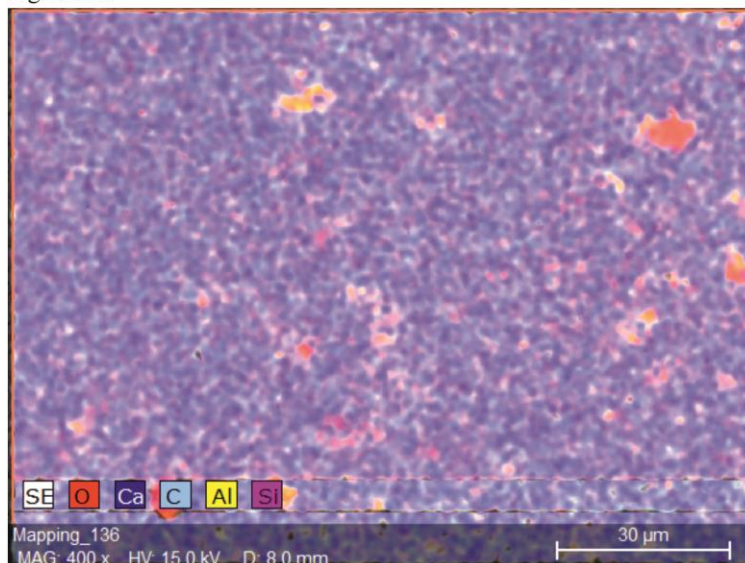


Fig. 5.13 H

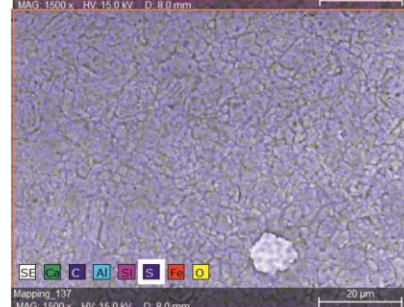
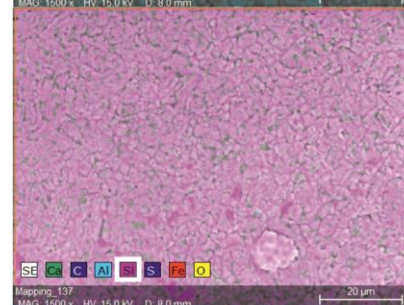
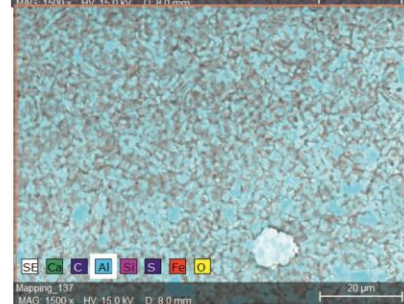
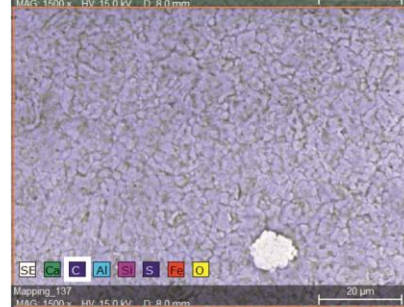
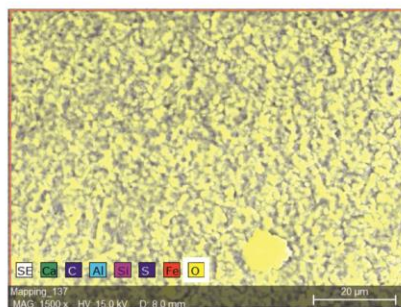
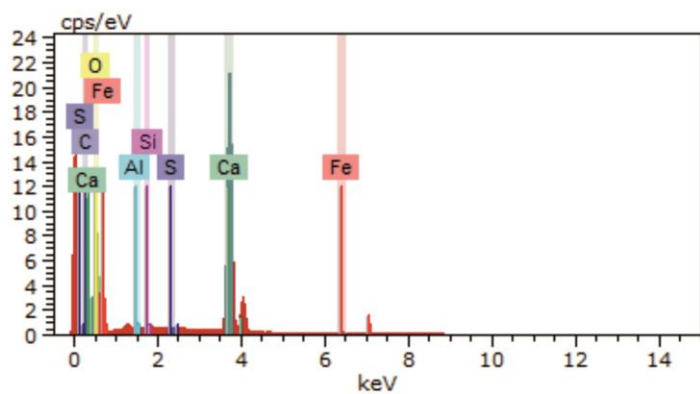
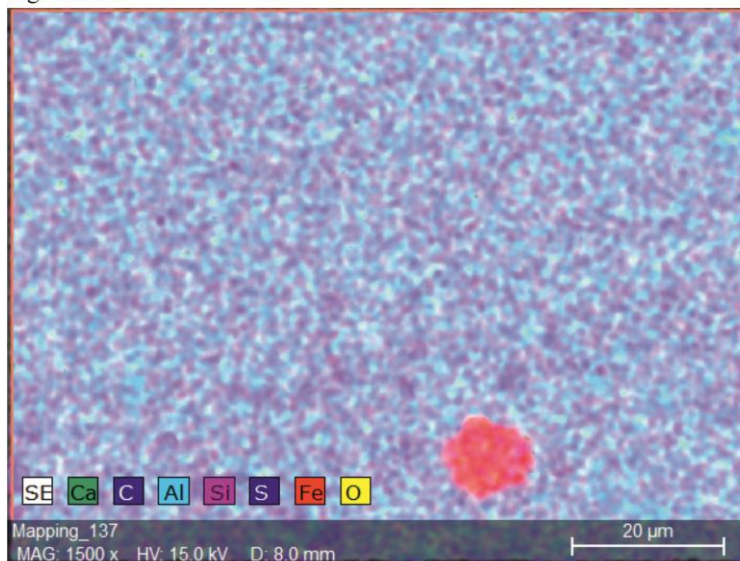


Fig. 5.15 F

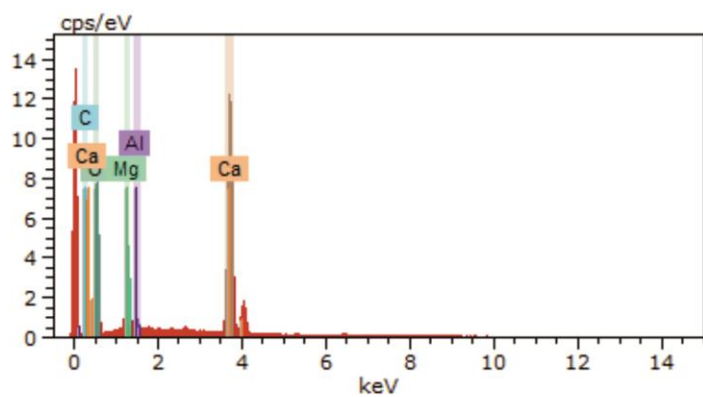
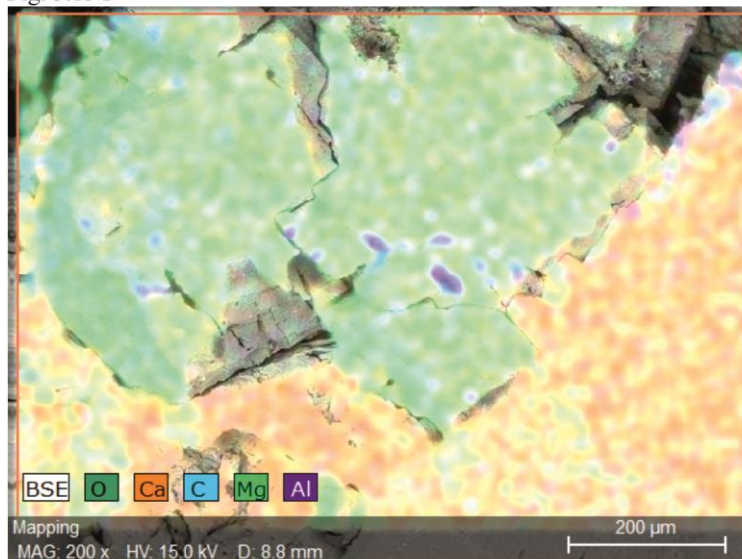


Fig. 5.15 H

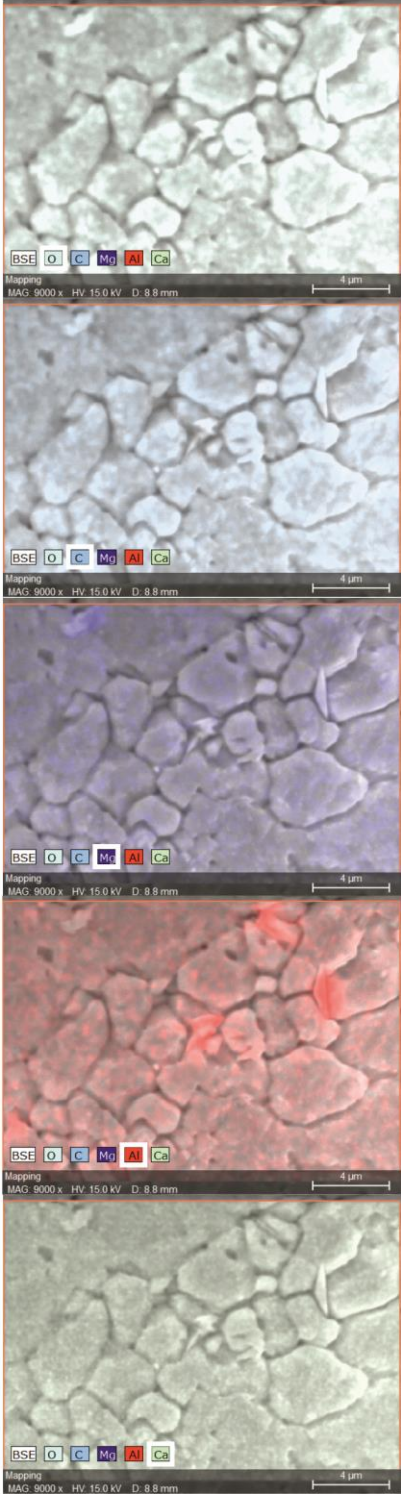
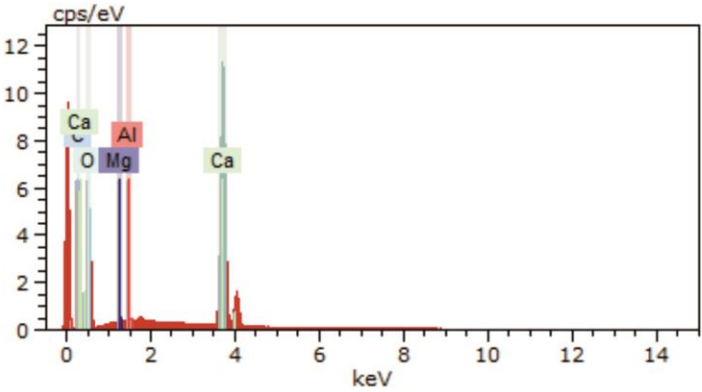
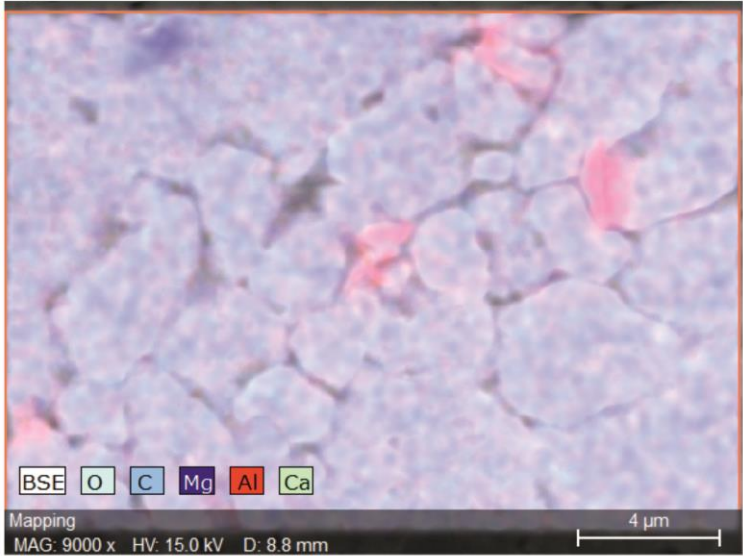


Fig. 5.16 F

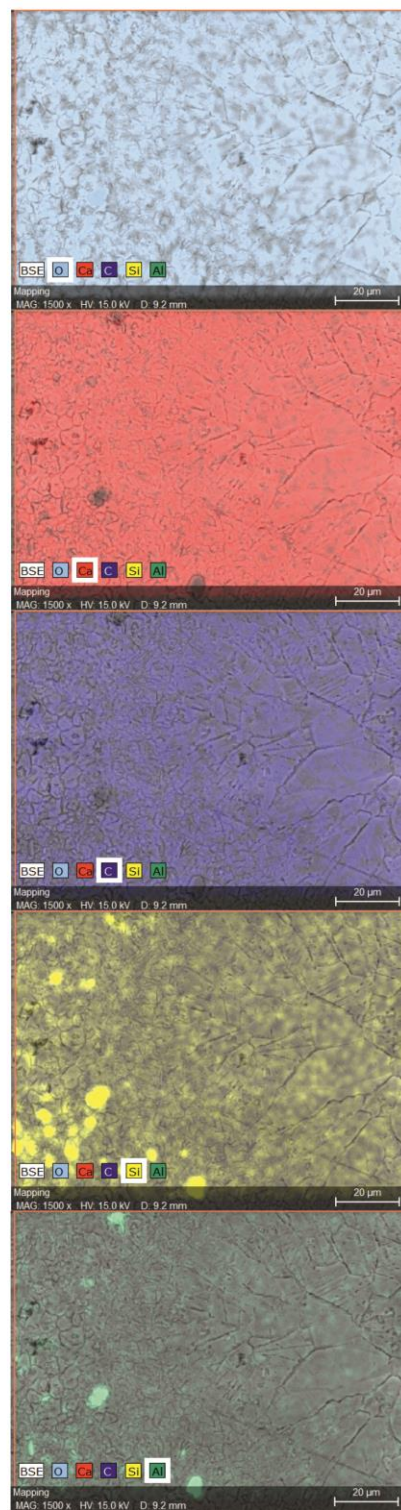
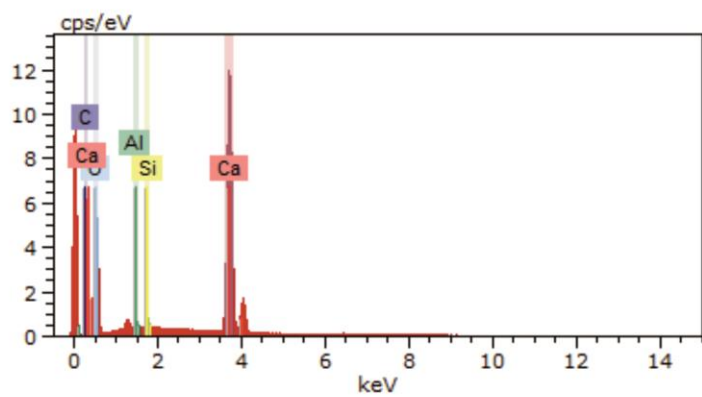
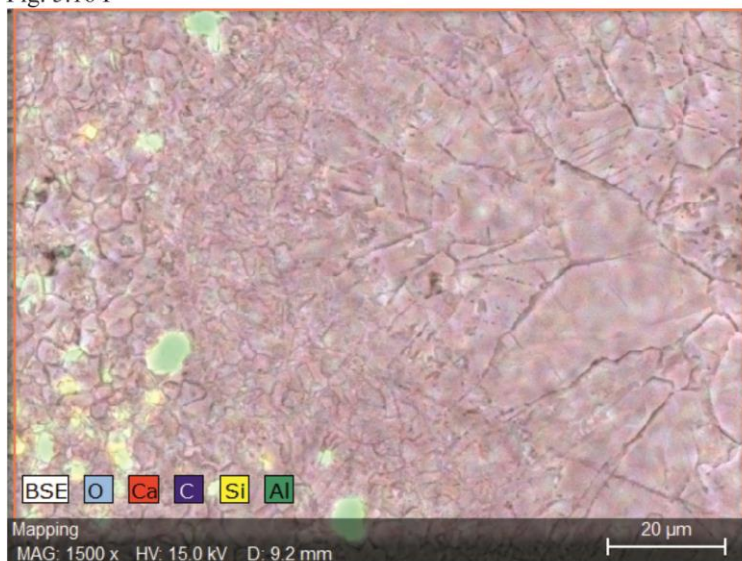
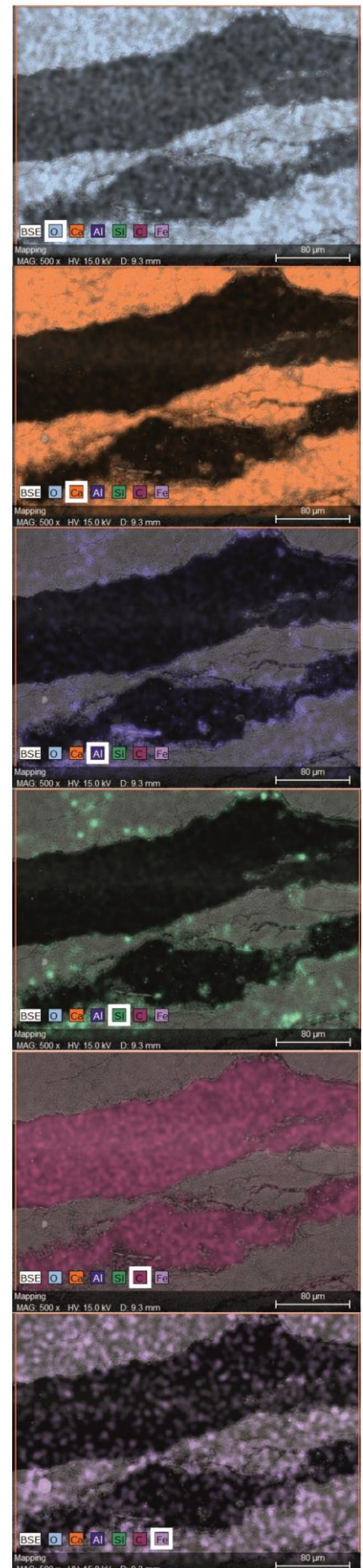
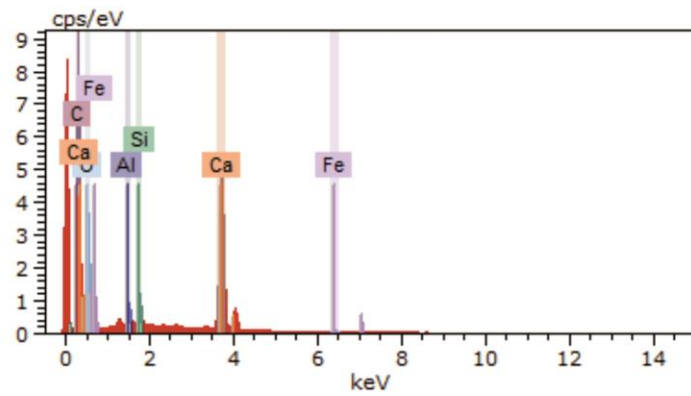
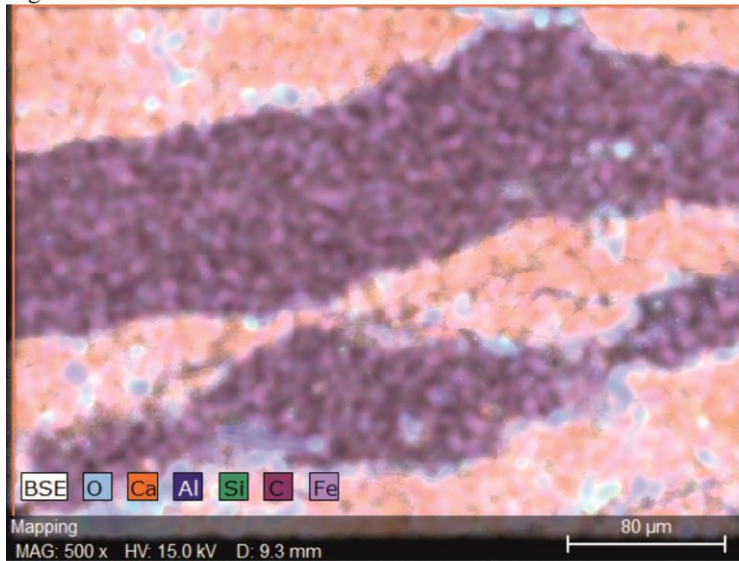


Fig. 5.16 H



Appendix 3. Sedimentary Logs

La Majúa Member, Candemuela Formation
Log of 'Unit 3'. (Originally logged 8/6/10)

-Sheet 1 of 2
-Some poor exposure for first 10metres
-less small scale cyclicity observed within
beds than other logs.

- cross bedding

load casts

nodular

ripples

algae

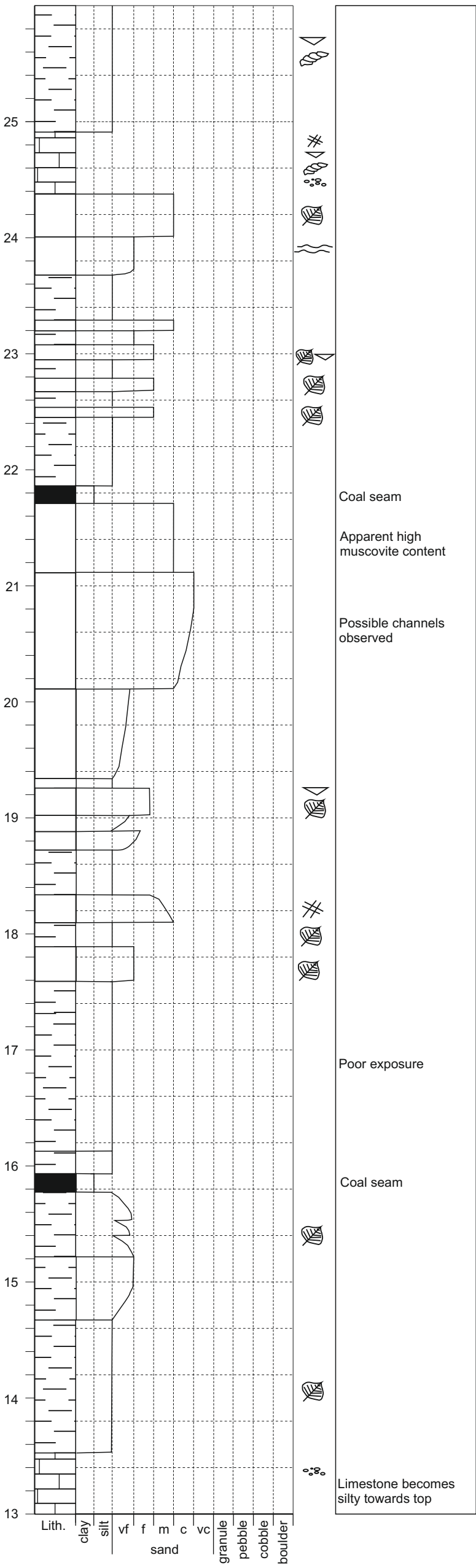
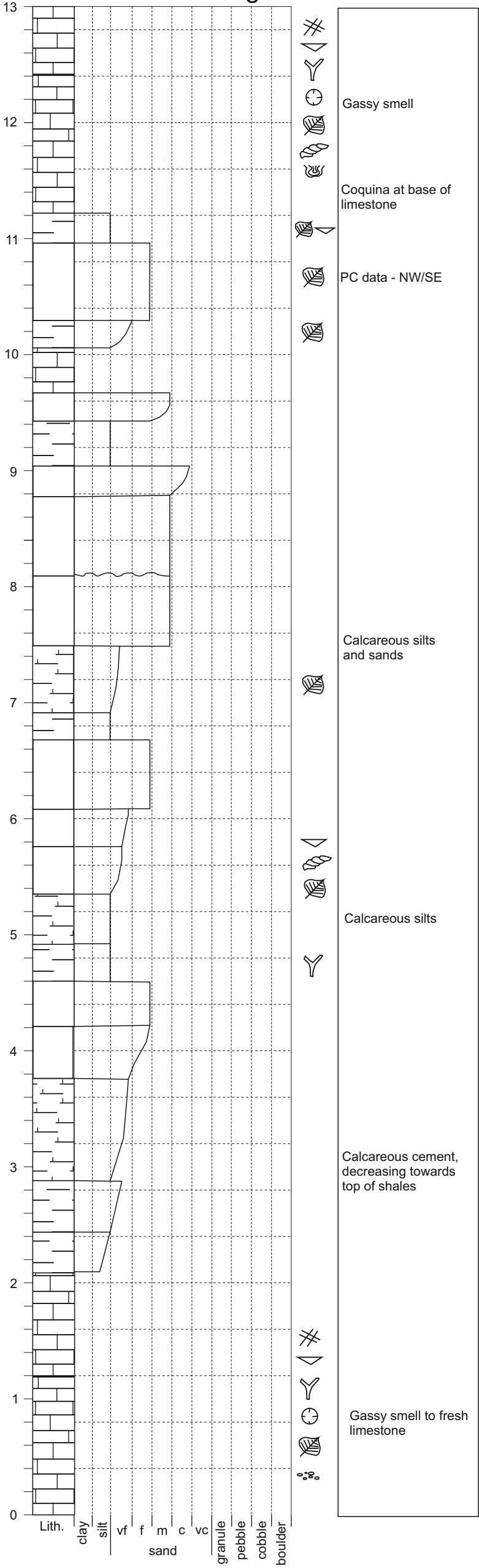
brachiopods

bryozoans

corals

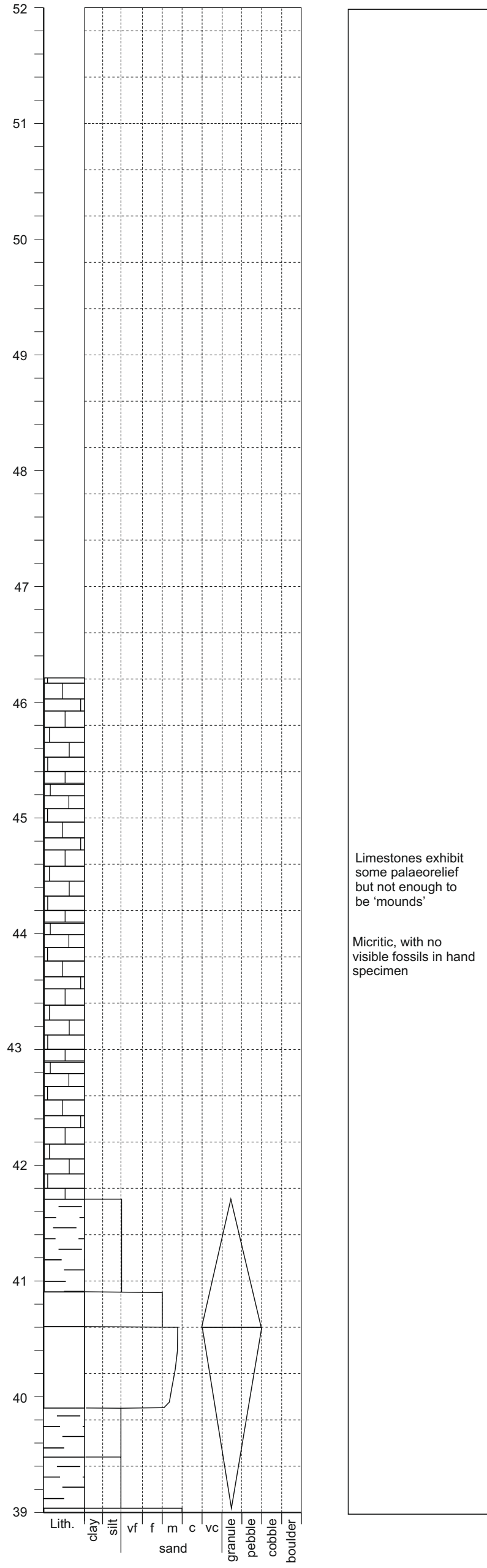
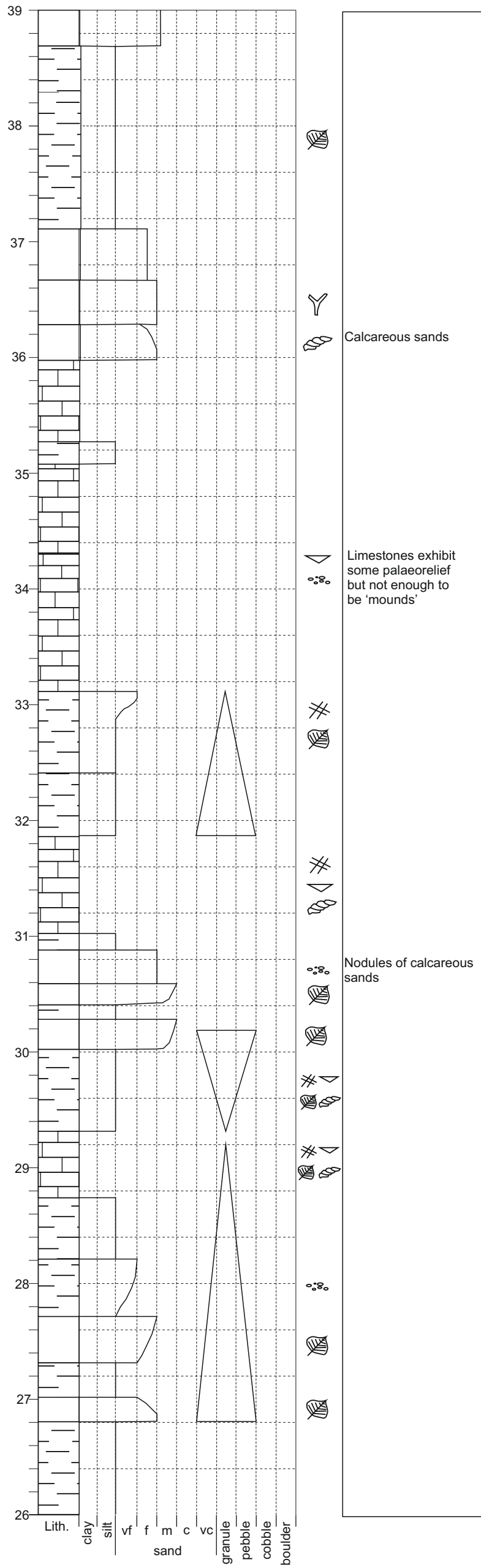
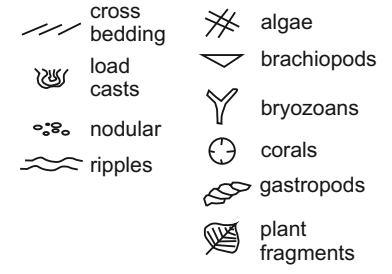
gastropod

plant fragments



La Majúa Member, San Emiliano Formation
Log of 'Unit 3'. (Originally logged 8-9/6/10)

-Sheet 2 of 2



La Majúa Member, San Emiliano Formation
Log of 'Unit 4'. (Originally logged 10/6/10)

-Sheet 1 of 1

- cross bedding

load casts

nodular

ripples

algae

brachiopods

bryozoans

corals

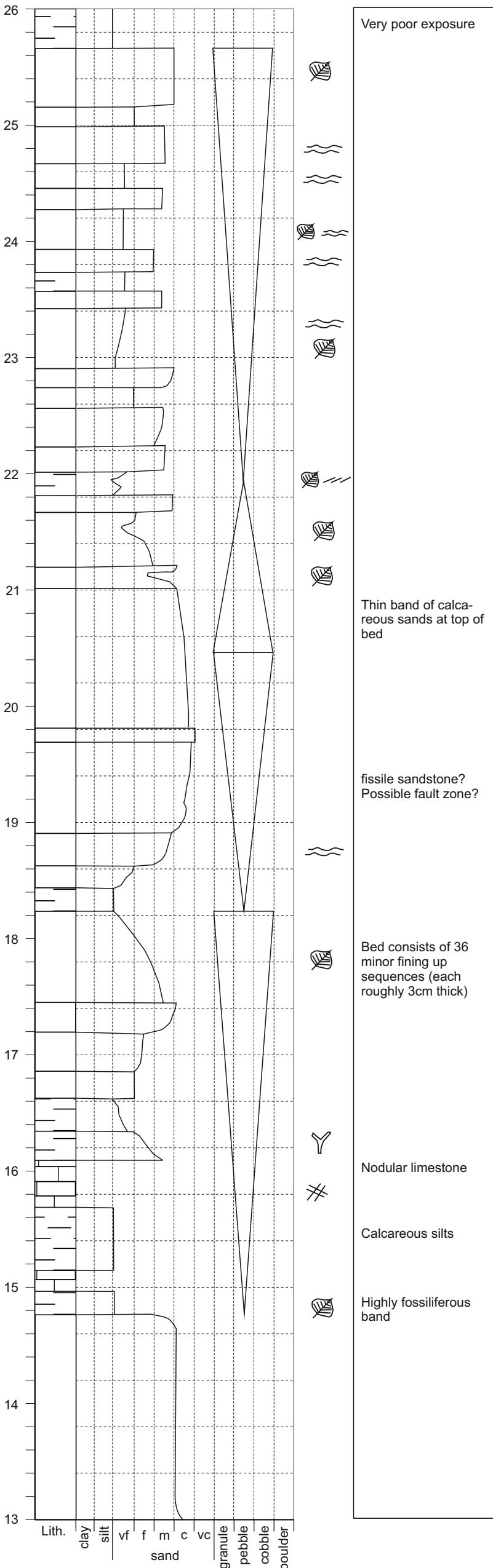
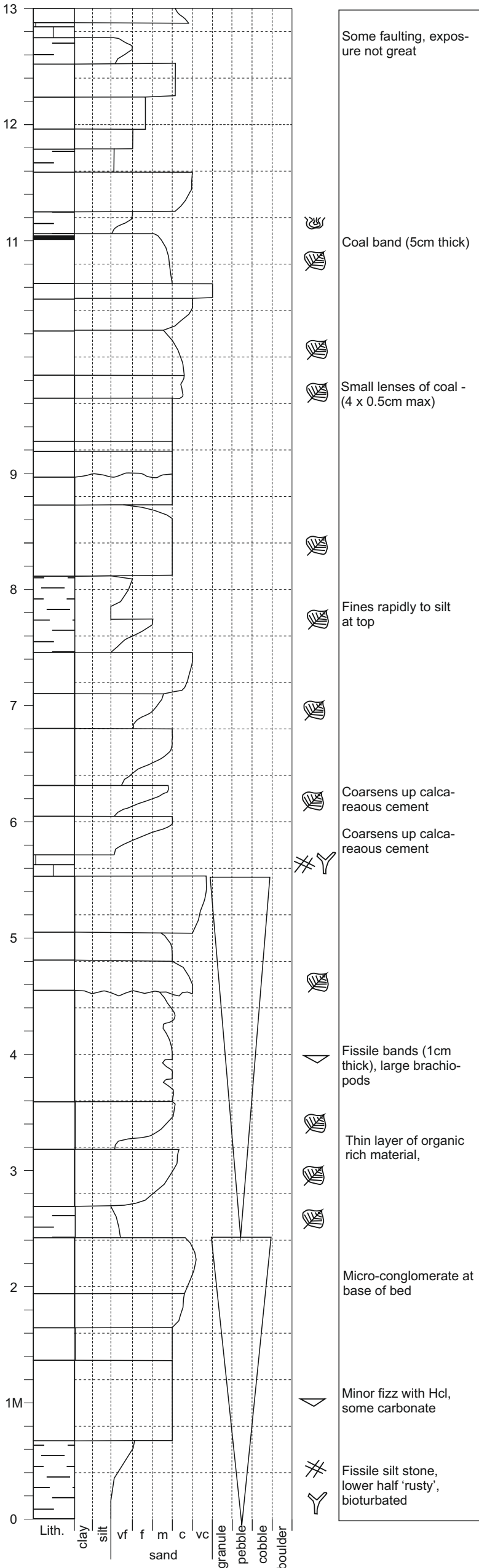
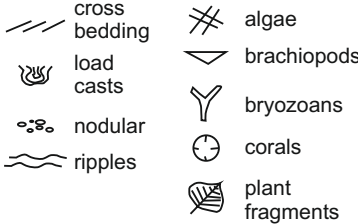
gastropods

plant fragments
- Stratigraphic log for Unit 4 (left column) showing depths from 0 to 13 meters. The log includes lithological descriptions (Lith., clay, silt, vf, f, m, c, vc, granule, pebble, cobble, boulder) and various sedimentary structures (cross bedding, load casts, nodular, ripples, algae, brachiopods, bryozoans, corals, gastropods, plant fragments). A limestone lense is noted within silts between 6 and 7 meters.
- Stratigraphic log for Unit 4 (right column) showing depths from 13 to 26 meters. The log includes lithological descriptions (Lith., clay, silt, vf, f, m, c, vc, granule, pebble, cobble, boulder) and various sedimentary structures (cross bedding, load casts, nodular, ripples, algae, brachiopods, bryozoans, corals, gastropods, plant fragments). A note identifies the section as bedded limestone, specifically the Pinos Hairpin Limestone, characterized by cyclic beds of phylloid dominated carbonates and marls.

La Majúa Member, San Emiliano Formation
Log of 'Unit 8'. (Originally logged 6/6/10)

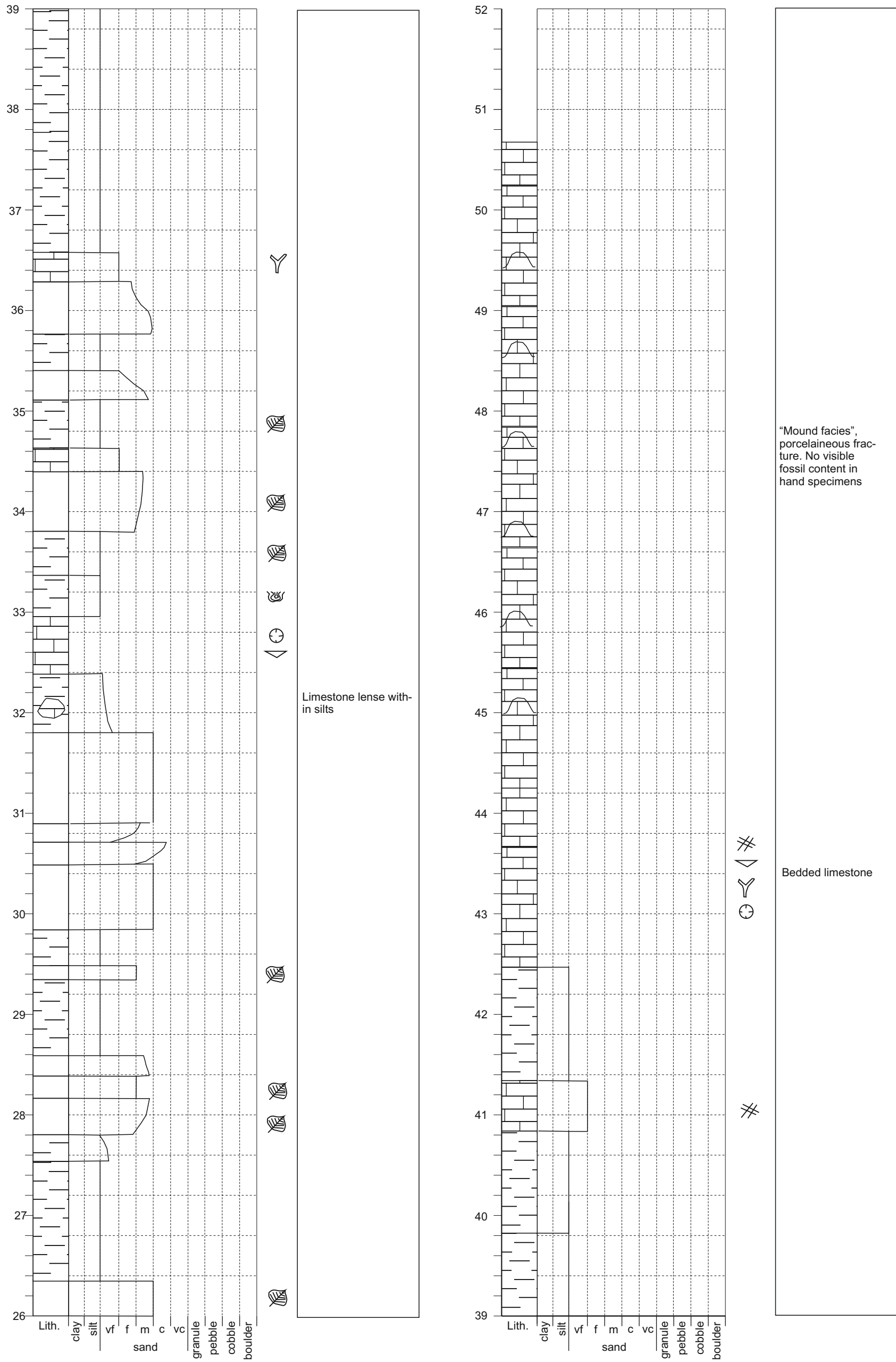
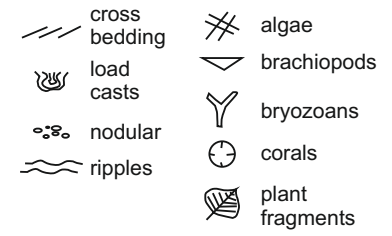
-Sheet 1 of 2

-Some areas of poor exposure



La Majúa Member, Candemuela Formation
Log of 'Unit 8'. (Originally logged 6/6/10)

-Sheet 2 of 2



Appendix 4. XRF Data

Major Elements, Clastic

Reading No	Fe2O3 wt%	TiO2 wt%	CaO wt%	K2O wt%	Al2O3 wt%	SiO2 wt%
1	5.54	0.64	3.73	2.14	14.37	41.59
2	14.91	0.42	0.73	1.53	8.92	25.4
3	10.42	0.45	0.61	1.59	8.76	26.66
4	8.88	0.32	0.5	1.08	4.08	20.06
5	6.83	0.7	0.64	2.02	16.92	51.18
6	27.14	0.35	0.8	0.85	5.45	22.05
7	10.13	0.53	3.57	1.59	11.28	38.8
8	6.13	0.73	2.05	2.16	18.18	46.12
9	6.05	0.49	1.77	1.44	9.99	56.36
10	4.89	0.66	2.38	1.24	8.05	56.55
11	10.46	0.58	0.5	1.37	11.33	49.25
12	3.93	0.45	9.58	1.32	8.56	37.77
13	3.97	0.3	14.45	0.83	5.15	32.18
14	5.22	0.47	10.01	1.52	12.54	38.24
15	5.2	0.58	6.05	1.9	13.76	39.34
16	4.51	0.5	7.37	1.48	11.41	43.36
17	2.41	0.2	33.7	0.47	4.15	13.68
18	5.15	0.62	2.07	1.85	13.59	46.22
19	3.63	0.41	6.23	1.19	5.82	30.18
20	4.92	0.61	4.95	1.87	13.8	42.76
21	7.59	0.49	5.57	1.32	7.09	27.13
22	5.31	0.38	1.96	1.34	7.68	33.22
23	6.62	0.42	2.4	1.48	11.19	38.26
24	8.45	0.2	19.92	0.84	7	20.82
25	4.76	0.47	2.97	1.33	10.12	40.04
26	5.16	0.46	3.31	1.46	11.6	47.15
27	4.12	0.55	5.4	1.79	12.56	42.46
28	4.38	0.67	4.62	2.08	15.67	48.64
29	3.34	0.44	5.82	1.15	7.39	52.25
30	3.11	0.32	10.21	0.93	7.33	46.59
31	4.45	0.46	7.41	1.37	10.94	47.42
32	3.82	0.38	10.94	1.12	8.57	41.8
33	4.49	0.49	7.11	1.43	11	50.42
34	4.31	0.49	6.08	1.5	8.99	37.86
35	5.02	0.58	7.47	1.61	11.62	45.41
36	4.44	0.53	6.9	1.54	11.87	47.87
37	6.12	0.4	8.98	1.15	8.91	43.19
38	4.31	0.44	7.52	1.18	7.67	47.72
39	5.28	0.64	4.68	1.75	13.78	47.49
40	4.52	0.41	8.57	1.17	6.77	41.23
41	4.35	0.33	6.17	0.89	3.98	29.2
42	3.25	0.32	11.8	0.89	8.89	55.31
43	3.55	0.32	11.52	0.78	4.83	37.77

Reading No	Fe2O3 wt%	TiO2 wt%	CaO wt%	K2O wt%	Al2O3 wt%	SiO2 wt%
44	4.47	0.57	6.92	1.72	14.36	47.14
45	3.26	0.28	9.81	0.81	5.55	40.98
46	4.43	0.33	10.24	0.92	6.75	44.96
47	4.08	0.29	13.34	0.84	7.37	46.97
48	4.21	0.4	6.25	1.1	5.97	48.7
49	3.01	0.2	9.85	0.51	3.7	48.08
50	4.15	0.28	12.84	0.71	6.09	51.19
51	3.9	0.3	11.29	0.81	6.38	46.22
52	3.76	0.33	10	0.88	7.25	50.21
53	4.53	0.58	6.68	1.7	11.38	42.86
54	4.69	0.51	6.5	1.44	11.05	47.78
55	3.75	0.38	8.98	1.09	7.07	38.48
56	3.28	0.35	10.41	0.95	6.91	49.5
57	5.04	0.41	7.39	1.16	7.62	47.91
58	3.65	0.37	10.99	0.9	5.65	41.06
59	3.71	0.35	10.98	0.87	7.97	53.44
60	3.78	0.49	7.16	1.49	11.14	41.47
61	4.87	0.37	9.55	0.93	7.08	49.29
62	4.37	0.35	10.12	0.93	7.14	49.46
63	4.46	0.25	9.43	0.65	2.7	27.51
64	4.66	0.53	6.86	1.52	10.82	48.07
65	4.78	0.52	6.37	1.47	9.87	46.16
66	4.93	0.6	6.58	1.81	13.07	43.52
67	4.09	0.52	8.41	1.6	13.86	49.02
68	3.77	0.47	7.17	1.22	9.91	55.55
69	3.56	0.43	8.19	1.22	8.82	51.46
70	4.17	0.47	8.3	1.26	9.13	48
71	4.03	0.45	9.4	1.18	6.48	39.1
72	5.41	0.61	5.64	1.81	11.57	35.67
73	6.39	0.3	1.83	0.86	1.34	13.73
74	4.16	0.55	5.01	1.53	11.06	41.26
75	5.11	0.5	7.14	1.41	11.7	44.32
76	4.04	0.52	4.01	1.57	14.3	57.39
77	3.41	0.38	6.1	1.11	5.9	31.91
78	4.96	0.66	4.66	1.97	16.87	47.47
79	4.14	0.39	9.59	1.02	8.42	46.77
80	3.79	0.36	9.78	1.03	6.84	36.65
81	4.47	0.49	8.52	1.38	9.01	40.47
82	4.43	0.39	13.63	0.96	8.55	45.59
83	4.42	0.32	12.06	0.87	4.64	34.24
84	5.13	0.54	8.93	1.44	12.08	45.72
85	5.77	0.49	5.66	1.29	7.26	37.74
86	2.15	0.04	3.04	0.13	0	4.36

Reading No	Fe2O3 wt%	TiO2 wt%	CaO wt%	K2O wt%	Al2O3 wt%	SiO2 wt%
87	6.02	0.38	7.56	0.79	3.54	19.7
88	3.81	0.38	9.86	1.1	8.39	41.45
89	3.67	0.32	13.16	0.85	6.39	37.89
90	3.58	0.33	9.42	0.89	4.62	32.27
91	3.94	0.37	7.7	1.08	6.66	35.36
92	3.24	0.3	13.34	0.8	7.45	50.17
93	3.68	0.32	10.76	0.85	7.75	47.17
94	3.84	0.27	14.09	0.67	5.47	42.97
95	4.24	0.36	12.01	0.88	7.81	47.16
96	3.68	0.35	11.39	0.94	8.42	49.4
97	3.07	0.24	16.28	0.53	5.86	47.21
98	2.26	0.22	11.76	0.56	4.46	40.37
99	5.54	0.64	3.73	2.14	14.37	41.59
100	14.91	0.42	0.73	1.53	8.92	25.4
101	10.42	0.45	0.61	1.59	8.76	26.66
102	8.88	0.32	0.5	1.08	4.08	20.06
103	6.83	0.7	0.64	2.02	16.92	51.18
104	27.14	0.35	0.8	0.85	5.45	22.05
105	10.13	0.53	3.57	1.59	11.28	38.8
106	6.13	0.73	2.05	2.16	18.18	46.12
107	6.05	0.49	1.77	1.44	9.99	56.36
108	4.89	0.66	2.38	1.24	8.05	56.55
109	10.46	0.58	0.5	1.37	11.33	49.25
110	3.93	0.45	9.58	1.32	8.56	37.77
111	3.97	0.3	14.45	0.83	5.15	32.18
112	5.22	0.47	10.01	1.52	12.54	38.24
113	5.2	0.58	6.05	1.9	13.76	39.34
114	4.51	0.5	7.37	1.48	11.41	43.36
115	2.41	0.2	33.7	0.47	4.15	13.68
116	5.15	0.62	2.07	1.85	13.59	46.22
117	3.63	0.41	6.23	1.19	5.82	30.18
118	4.92	0.61	4.95	1.87	13.8	42.76
119	7.59	0.49	5.57	1.32	7.09	27.13
120	5.31	0.38	1.96	1.34	7.68	33.22
121	6.62	0.42	2.4	1.48	11.19	38.26
122	8.45	0.2	19.92	0.84	7	20.82
123	4.76	0.47	2.97	1.33	10.12	40.04
124	5.16	0.46	3.31	1.46	11.6	47.15
125	4.12	0.55	5.4	1.79	12.56	42.46
126	4.38	0.67	4.62	2.08	15.67	48.64
127	3.34	0.44	5.82	1.15	7.39	52.25
128	3.11	0.32	10.21	0.93	7.33	46.59
129	4.45	0.46	7.41	1.37	10.94	47.42

Reading No	Fe2O3 wt%	TiO2 wt%	CaO wt%	K2O wt%	Al2O3 wt%	SiO2 wt%
130	3.82	0.38	10.94	1.12	8.57	41.8
131	4.49	0.49	7.11	1.43	11	50.42
132	4.31	0.49	6.08	1.5	8.99	37.86
133	5.02	0.58	7.47	1.61	11.62	45.41
134	4.44	0.53	6.9	1.54	11.87	47.87
135	6.12	0.4	8.98	1.15	8.91	43.19
136	4.31	0.44	7.52	1.18	7.67	47.72
137	5.28	0.64	4.68	1.75	13.78	47.49
138	4.52	0.41	8.57	1.17	6.77	41.23
139	4.35	0.33	6.17	0.89	3.98	29.2
140	3.25	0.32	11.8	0.89	8.89	55.31
141	3.55	0.32	11.52	0.78	4.83	37.77
142	4.47	0.57	6.92	1.72	14.36	47.14
143	3.26	0.28	9.81	0.81	5.55	40.98
144	4.43	0.33	10.24	0.92	6.75	44.96
145	4.08	0.29	13.34	0.84	7.37	46.97
146	4.21	0.4	6.25	1.1	5.97	48.7
147	3.01	0.2	9.85	0.51	3.7	48.08
148	4.15	0.28	12.84	0.71	6.09	51.19
149	3.9	0.3	11.29	0.81	6.38	46.22
150	3.76	0.33	10	0.88	7.25	50.21
151	4.53	0.58	6.68	1.7	11.38	42.86
152	4.69	0.51	6.5	1.44	11.05	47.78
153	3.75	0.38	8.98	1.09	7.07	38.48
154	3.28	0.35	10.41	0.95	6.91	49.5
155	5.04	0.41	7.39	1.16	7.62	47.91
156	3.65	0.37	10.99	0.9	5.65	41.06
157	3.71	0.35	10.98	0.87	7.97	53.44
158	3.78	0.49	7.16	1.49	11.14	41.47
159	4.87	0.37	9.55	0.93	7.08	49.29
160	4.37	0.35	10.12	0.93	7.14	49.46
161	4.46	0.25	9.43	0.65	2.7	27.51
162	4.66	0.53	6.86	1.52	10.82	48.07
163	4.78	0.52	6.37	1.47	9.87	46.16
164	4.93	0.6	6.58	1.81	13.07	43.52
165	4.09	0.52	8.41	1.6	13.86	49.02
166	3.77	0.47	7.17	1.22	9.91	55.55
167	3.56	0.43	8.19	1.22	8.82	51.46
168	4.17	0.47	8.3	1.26	9.13	48
169	4.03	0.45	9.4	1.18	6.48	39.1
170	5.41	0.61	5.64	1.81	11.57	35.67
171	6.39	0.3	1.83	0.86	1.34	13.73
172	4.16	0.55	5.01	1.53	11.06	41.26

Reading No	Fe2O3 wt%	TiO2 wt%	CaO wt%	K2O wt%	Al2O3 wt%	SiO2 wt%
173	5.11	0.5	7.14	1.41	11.7	44.32
174	4.04	0.52	4.01	1.57	14.3	57.39
175	3.41	0.38	6.1	1.11	5.9	31.91
176	4.96	0.66	4.66	1.97	16.87	47.47
177	4.14	0.39	9.59	1.02	8.42	46.77
178	3.79	0.36	9.78	1.03	6.84	36.65
179	4.47	0.49	8.52	1.38	9.01	40.47
180	4.43	0.39	13.63	0.96	8.55	45.59
181	4.42	0.32	12.06	0.87	4.64	34.24
182	5.13	0.54	8.93	1.44	12.08	45.72
183	5.77	0.49	5.66	1.29	7.26	37.74
184	2.15	0.04	3.04	0.13	0	4.36
185	6.02	0.38	7.56	0.79	3.54	19.7
186	3.81	0.38	9.86	1.1	8.39	41.45
187	3.67	0.32	13.16	0.85	6.39	37.89
188	3.58	0.33	9.42	0.89	4.62	32.27
189	3.94	0.37	7.7	1.08	6.66	35.36
190	3.24	0.3	13.34	0.8	7.45	50.17
191	3.68	0.32	10.76	0.85	7.75	47.17
192	3.84	0.27	14.09	0.67	5.47	42.97
193	4.24	0.36	12.01	0.88	7.81	47.16
194	3.68	0.35	11.39	0.94	8.42	49.4
195	3.07	0.24	16.28	0.53	5.86	47.21
196	2.26	0.22	11.76	0.56	4.46	40.37
197	3.34	0.23	16.85	0.5	3.91	39.1
198	3.03	0.36	9.91	0.87	5.43	42.47
199	7.23	0.36	6.62	0.9	4.52	32.79
200	2.92	0.37	9.83	0.81	3.07	31.81
201	3.57	0.44	9.82	1.16	5.87	36.89
202	3.95	0.25	8.43	0.61	3.72	32.97
203	4.7	0.29	11.31	0.69	3.93	37.18
204	5.67	0.41	5.63	1.09	4.93	32.23
205	2.73	0.44	10.16	0.92	6.08	47.22
206	2.87	0.37	12.5	0.87	7.82	46.79
207	3.16	0.28	13.04	0.7	4.62	46.09
208	4.8	0.3	12.23	0.75	4.38	33.42
209	4.6	0.27	18.47	0.57	5.33	45.14
210	4.53	0.24	13.31	0.6	4.88	45.29
211	5.34	0.7	6.05	1.17	6.23	20.96
212	3.25	0.37	7.68	1.05	6.11	40.58
213	6.43	0.59	9.32	1.73	15.11	40.02
214	4.41	0.46	9.32	1.32	8.91	32.18
215	3.28	0.28	20.55	0.75	6.08	39.59

Reading No	Fe2O3 wt%	TiO2 wt%	CaO wt%	K2O wt%	Al2O3 wt%	SiO2 wt%
216	4.4	0.47	10.69	1.41	11.06	37.72
217	6.09	0.57	8.34	1.76	14.15	38.45
218	4.92	0.51	9.45	1.5	10.19	38.88
219	4.42	0.47	12.48	1.16	9.11	47.55
220	5.56	0.57	7.69	1.72	11.21	41.08
221	4.13	0.37	6.37	1.12	9.68	39.53
222	4.49	0.38	8.36	1.08	5.86	34.75
223	4.85	0.58	7.25	1.82	15.23	48.66
224	3.87	0.36	7.19	1.07	7.51	39.51
225	4.33	0.48	10.28	1.39	10.79	46.51
226	5.7	0.49	6.92	1.53	8.41	31.91
227	5.13	0.55	5.44	1.62	10.2	37.82
228	5.42	0.43	8.84	1.29	10.08	38.31
229	4.41	0.5	8	1.43	11.14	48.93
230	4.89	0.46	9.59	1.35	8.97	36.54
231	5.73	0.54	8.38	1.59	13.07	44.71
232	3.67	0.51	7.84	1.33	9.49	51.35
233	5.02	0.46	9.94	1.38	9.73	40.47
234	4.2	0.36	10.96	0.99	5.69	38.34
235	7.14	0.51	7.86	1.45	10.75	45.7
236	3.9	0.46	6.3	1.41	5.5	26.13
237	5.1	0.49	12.41	1.48	9.98	39.21
238	3.87	0.67	9.52	2.11	14.54	44.64
239	6.16	0.66	10.73	2.13	19.22	45.67
240	6.12	0.64	10.76	1.96	12.45	33.87
241	4.4	0.58	10.63	1.73	11.52	34.3
242	5.55	0.61	8.68	1.9	12.6	40.01
243	6.16	0.56	9.44	1.61	10.87	36.34
244	5.53	0.53	8.95	1.63	12.42	37.08
245	4.91	0.6	8.24	1.8	13.31	43.46
246	5.54	0.59	9.59	1.8	14.9	41.8
247	4.97	0.63	6.71	2.1	16.56	43.43
248	5.21	0.44	14.65	1.34	9.74	34.09
249	9.57	0.63	7.16	1.91	14.97	38.64
250	5.16	0.62	8.76	1.9	11.14	34.11
251	3.53	0.36	10.9	1.11	6.21	26.12
252	3.69	0.43	9.75	1.31	7.04	30.58
253	5.34	0.56	7.13	1.76	13.4	38.44
254	3.08	0.43	8.92	1.19	8.63	43.63
255	5.74	0.48	9.15	1.43	10.95	38.45
256	3.09	0.33	12.68	0.96	7.03	39.62
257	4.56	0.43	9.75	1.4	13.39	39.61
258	4.66	0.43	7.65	1.27	9.68	37.5

Reading No	Fe2O3 wt%	TiO2 wt%	CaO wt%	K2O wt%	Al2O3 wt%	SiO2 wt%
259	4.31	0.57	7	1.66	11.83	49.46
260	4.46	0.54	7.07	1.49	11.61	54.34
261	3.31	0.46	7.48	1.3	11.44	47.14
262	3.84	0.46	13.13	1.2	8.46	37.01
263	5.79	0.4	11.2	1.08	8.93	46.1
264	3.87	0.36	9.15	0.93	4.3	33.84
265	4.28	0.35	7.76	0.88	6.91	59.32
266	3.93	0.42	9.62	1.04	6.73	45.23
267	4.61	0.42	13.3	1.06	6.64	39.36
268	4.06	0.43	12.78	0.96	6.54	49.3
269	4.5	0.63	6.34	1.91	11.35	38.31
270	4.51	0.6	7.05	1.63	14.08	51.35
271	3.97	0.4	6.83	1.2	5.26	30.21
272	4.62	0.64	3.76	1.96	13.01	38.58
273	10.32	0.58	4.68	1.85	12.22	34.6
274	8.43	0.46	1.57	1.41	7.89	26.52
275	11.1	0.7	1.44	2.09	13.51	37.95
276	9.41	0.52	2.73	1.7	12.32	34.09
277	5.77	0.58	3.09	1.74	14.57	42.59
278	11.09	0.77	6.08	1.8	16.77	39.06
279	4.08	0.58	4.11	1.73	12.41	38.09
280	7.03	0.65	5.92	1.76	18.18	47.73
281	19.22	0.31	9.2	1.03	14.47	32.63
282	8.7	0.39	12.05	1.05	6.15	17.86
283	16.29	0.6	3.79	2.18	16.9	38.61
284	3.72	0.51	3.48	1.51	9.04	31.84
285	14.52	0.53	1.57	1.21	12.77	40.18
286	19.44	0.74	1.74	1.47	14.34	34.7
287	4.43	0.54	4.5	1.54	10.55	36.25
288	3.49	0.48	3.37	1.33	10.76	60.07
289	20.09	0.29	0.94	0.92	6.77	20.98
290	4.61	0.59	2.78	2.12	10.69	30.55
291	16.4	0.5	1.77	1.97	17.38	36.21
292	2.93	0.4	12.33	1.29	9.86	44.9
293	3.51	0.61	3.18	1.11	7.51	46.29
294	4.18	0.47	5.87	1.51	14.02	49.77
295	3.65	0.46	8.86	1.44	8.73	35.71
296	23.37	0.29	3.16	0.93	10.4	25.47
297	3.87	0.3	13.27	0.72	5.48	49.94
298	3.78	0.22	18.07	0.55	4.77	35.04
299	4.52	0.42	6.17	1.35	11.85	46.51
300	5.22	0.23	10.67	0.5	5.3	63.1
301	1.97	0.26	10.44	0.66	5.7	51.52

Reading No	Fe2O3 wt%	TiO2 wt%	CaO wt%	K2O wt%	Al2O3 wt%	SiO2 wt%
302	5.95	0.3	11.59	0.68	4.09	38.37
303	2.55	0.27	15.48	0.66	3.55	30.84
304	5.03	0.44	5.39	1.32	7.7	38.79
305	3.35	0.3	11.71	0.67	2.92	35.57
306	2.67	0.34	8.16	0.83	4.61	48.46
307	2.36	0.35	2.67	0.95	5.94	65.41
308	2.6	0.25	9.91	0.63	3.4	37.95
309	4.41	0.39	6.87	1.02	7.98	52.75
310	3.13	0.35	5.69	0.92	5.61	53.18
311	3.28	0.32	6.1	0.89	4.99	38.15
312	7.38	0.36	12.18	0.57	4.57	55.95
313	2.91	0.25	10.98	0.57	3.51	52.74
314	2.04	0.37	5.03	0.86	3.45	46.11
315	2.88	0.54	5.3	1.39	7.24	33.65
316	4.26	0.51	2.53	1.39	4.93	22.92
317	2.21	0.45	5.52	1.26	8.07	50.06
318	2.11	0.4	6.04	1.18	6.95	42.52
319	4.94	0.46	7.89	1.38	10.75	48.96
320	3.45	0.67	5.03	1.9	13.62	59.16
321	4.72	0.62	5.15	1.8	12.34	49.49
322	4.77	0.63	3.71	1.96	8.72	36.27
323	17.91	0.28	2.94	0.79	4.48	17.47
324	5.42	0.66	1.14	2.07	15.78	60.51
325	15.62	0.39	2.12	0.78	4.34	30.49
326	16.91	0.59	2.98	1.23	9.8	34.37
327	5.62	0.55	1.96	1.43	6.69	30.38
328	15.94	0.59	1.04	1.49	14.07	39.78
329	8.16	0.4	12.57	1.42	13.6	34.23
330	3.17	0.58	2.76	1.85	10.9	39.12
331	4.77	0.58	3.87	1.76	15.18	49.03
332	5.51	0.79	1.25	2.34	13.98	42.07
333	8.27	0.66	8.79	1.88	10.3	33.22
334	5.04	0.5	5.66	1.24	7.13	33.86
335	9.29	0.47	2.48	1.08	8.96	43.62
336	7.29	0.64	1.43	1.85	12.08	44.15
337	8.55	0.66	4.3	1.09	8.49	39.17
338	4.79	0.48	7.65	1.22	7.23	43.39
339	11.8	0.52	4.97	1.73	12.43	32.1
340	19.4	0.38	1.43	0.49	4.99	11.87
341	8.25	0.42	19.82	1.31	10.55	29.36
342	8.01	0.33	7	1.16	7.67	38.09
343	5.3	0.62	3.65	1.83	12.69	44.83
344	9.67	0.46	6.48	1.42	11.13	35.5

Reading No	Fe2O3 wt%	TiO2 wt%	CaO wt%	K2O wt%	Al2O3 wt%	SiO2 wt%
345	3.72	0.46	4.59	1.47	5.35	26.98
346	10.41	0.47	16.65	1.21	11.83	34.88
347	4.08	0.37	7.57	1.04	4.39	24.68
348	13.17	0.58	0.93	1.33	9.97	50
349	4.9	0.65	3.93	1.87	14.38	48.53
350	18.07	0.63	6.86	1.61	14.59	42.06
351	4.04	0.53	5.3	1.72	10.1	45.89
352	3.69	0.46	11.2	1.29	10.14	45.29
353	15.2	0.45	1.23	1.26	5.96	34.01
354	5.08	0.72	1.71	2.16	11.73	36.75
355	3.76	0.53	3.93	1.74	10.26	34.44
356	6.7	0.57	3.84	1.72	10.27	46.31
357	3.69	0.49	0.8	1.52	8.78	50.16
358	8.23	0.37	1.22	0.86	4.39	43.31
359	13.2	0.44	0.35	0.79	8.26	39.15
360	7.56	0.5	6.52	1.77	10.83	39.01
361	2.83	0.69	6.87	1.57	7.32	42.21
362	2.37	0.44	12.72	1.13	7.99	51.68
363	3.9	0.77	1.25	1.7	10.86	56.04
364	11.44	0.43	2.29	1.36	6.62	23.66
365	5.9	0.61	6.69	2	13.08	41.86
366	19.16	0.35	0.78	1.09	10.38	45.12
367	37.6	0.47	1.31	1.92	21.02	34.68
368	10.32	0.41	0.69	1.42	11.49	45.31
369	2.28	0.53	1.01	1.7	11.27	60.45
370	1.39	0.43	7.23	1.27	10.56	64.74
371	5.1	0.47	0.86	1.36	7.54	54.46
372	1.09	0.33	6.24	0.77	4.39	52.22
373	5.47	0.46	7.69	1.14	9.83	53.8
374	7.72	0.33	4.12	0.87	6.49	65.45
375	1.38	0.29	6.66	0.83	6.02	63.31
376	3.5	0.59	3.54	1.79	12.28	50.72
377	8.99	0.38	1.05	1.12	5.77	39.27
378	4.08	0.48	2.31	1.57	4.85	22.02
379	2.58	0.41	10.79	1.35	6.85	20.87
380	3.19	0.57	5.86	1.81	15.66	62.9
381	5.57	0.65	5.87	2.13	14.37	47.38
382	4.12	0.67	7.16	2.21	15.02	43.01
383	4.24	0.59	8.47	1.93	11.21	37.97
384	3.71	0.66	5.56	2.41	15.68	43.69
385	3.79	0.49	6.29	1.6	6.92	27.42
386	2.09	0.17	29.15	0.49	0.81	18.16
387	2.63	0.09	38.83	0.4	0	6.15

Reading No	Fe2O3 wt%	TiO2 wt%	CaO wt%	K2O wt%	Al2O3 wt%	SiO2 wt%
388	2.5	0.09	54.4	0.25	3.97	7.05
390	5.71	0.6	17.12	2.64	17.56	36.33
392	4.64	0.59	4	2.32	8.83	32.33
393	2.56	0.72	3.77	2.65	15.94	44.84
394	2.4	0.7	6.66	2.54	13.36	38.22
395	3.44	0.5	13.2	1.68	10.88	39.57
396	2.36	0.28	5.76	0.99	6.02	34.07
397	7.82	0.57	20.71	1.54	10.58	30.56
398	6.38	0.33	24.65	1.07	8.66	31.2
399	3.57	0.56	3.87	2.09	11.98	35.25
400	8.14	0.61	3.92	2.23	10.36	32.43
401	6.67	0.64	1.28	2.88	20.99	44.76
402	8.17	0.39	0.75	1.78	9.82	31.1
403	3.86	0.3	0.42	0.93	5.35	59.39
404	3.39	0.32	0.87	0.84	4.14	48.19
405	9.67	0.3	0.67	0.73	3.85	56.51
406	4.04	0.4	0.5	1.25	5.57	49.76
407	5.43	0.59	1.28	1.78	16.38	63.59
408	5.45	0.63	5.5	1.96	13.29	47.58
409	5.73	0.65	1.33	1.94	15.13	60.37
410	5.35	0.53	1.65	1.69	11.92	55.31
411	2.8	0.49	0.37	1.6	8.29	52.07
412	3.74	0.42	0.38	1.21	3.66	36.66
413	6.28	0.28	0.37	0.98	4.75	59.3
414	5.39	0.66	2.19	2.21	11.4	39.65
415	3.36	0.72	0.55	2.29	11.98	38.61
416	5.67	0.8	0.38	3.06	20.25	51.49
417	32.83	0.47	1.35	1.55	7.7	23.11
418	17.27	0.46	2.17	1.93	10.59	31.93
419	6.81	0.68	2.33	2.75	15.07	41.23
420	5.01	0.6	9.83	2.5	16	43.96
421	5.59	0.54	15.33	2.06	15.07	41.5
422	7.88	0.45	17.4	1.62	8.94	32.69
423	6.27	0.55	18.68	2.36	17.05	43.31
424	8.47	0.47	18.5	1.85	12.88	32.69
425	5.16	0.75	0.59	3.11	19.61	50.56
426	21.32	0.48	0.59	2.07	13.1	30.48
427	22.02	0.48	0.58	1.98	12.98	29.65
428	23.43	0.41	0.58	1.57	13.96	31.39
429	20.19	0.48	0.47	1.64	12.23	30.75
430	22.61	0.48	0.4	1.7	13.24	32.48
431	13.43	0.76	0.45	1.95	13.44	41.54
432	15.34	0.44	0.37	1.32	1.95	14.26

Reading No	Fe2O3 wt%	TiO2 wt%	CaO wt%	K2O wt%	Al2O3 wt%	SiO2 wt%
433	19.83	0.55	0.43	1.47	13.01	35.31
434	12.56	0.56	0.41	1.95	13.76	39.18
435	16.41	0.6	0.54	1.76	11.47	30.86
436	3.64	0.68	0.42	2.45	12.97	41.58
437	11.25	0.62	0.44	2.38	13.13	34.87
438	4.23	0.72	3.86	2.56	13.3	47.68
439	3.74	0.6	4.06	2.16	12.18	40.73
440	3.91	0.51	2.86	1.89	8.24	32.73
441	4.91	0.61	0.23	2.29	12.52	38.93
442	6.27	0.76	0.43	2.77	18.08	48.2
443	20.04	0.42	0.43	1.31	7.27	19.79
444	5.49	0.72	0.56	2.34	12.15	38.12
445	4.96	0.82	0.8	2.73	15.86	48.8
446	4.3	0.68	2.49	2.28	13.85	45.79
447	13.6	0.52	0.46	1.72	9.12	27.84
448	5.46	0.57	0.45	2.29	8.21	32.73
449	4.26	0.64	3.34	2.21	13.09	43.1
450	6.06	0.65	0.38	2.34	11.43	35.49
451	9.93	0.75	0.5	2.5	12.22	39.76
452	11.97	0.63	0.52	2.27	14.02	38.06
453	4.05	0.84	1.22	3.19	20.04	52.86
454	5.33	0.76	1.1	2.7	17.82	46.84
455	8.9	0.81	0.62	2.77	14.82	50.3
456	8.07	0.66	0.74	2.44	13.8	43.57
457	7.73	0.73	0.59	2.65	19	52.02
458	7.28	0.64	0.46	2.46	9.15	32.45
459	4.62	0.86	0.69	3.25	20.04	55.7
460	6.65	0.73	0.77	2.72	17.04	47.44
461	7.15	0.69	8.13	2.8	14.62	41.81
462	4.8	0.24	18.67	1.12	6.82	30.24
463	9.25	0.68	4.24	3	15.59	41.32
464	5.63	0.51	23.82	2.57	13.74	31.89
465	4.46	0.31	39.08	0.76	9.33	22.31
466	10.78	0.7	2.52	2.78	12.59	36.55
467	6.92	0.5	14.27	2.74	16.08	38.71
468	4.32	0.39	13.6	1.51	8.59	42.55
469	6.02	0.68	8.99	2.49	9.91	37.15
470	4.07	0.5	24.71	1.8	11.55	36.2
471	7.29	0.77	11.01	3.14	18.57	51.17
472	7.65	0.42	27.39	2.31	14.07	30.82
473	6.07	0.69	23.27	2.91	25.91	48.7
474	6.77	0.52	19.93	2.61	18.22	40.31
475	6.56	0.71	11.18	2.94	19.36	49.57

Reading No	Fe2O3 wt%	TiO2 wt%	CaO wt%	K2O wt%	Al2O3 wt%	SiO2 wt%
476	4.41	0.67	1.49	2.61	17.26	50.08
477	4.89	0.43	1.59	1.52	4.56	22.3
478	6.24	0.42	17.48	2.17	7.88	26.35
479	6.01	0.52	4.65	2.42	7.93	29.9
480	5.65	0.5	4.28	2.21	8.06	31.7
481	10.13	0.59	3.57	2.65	14.33	38.39
482	9.27	0.54	2.05	2.25	10.18	33.8
483	4.79	0.43	5.66	1.99	5.27	23.75
484	6.89	0.61	1.68	2.63	12.06	39.53
485	5.12	0.59	3.42	2.87	12.84	39.58
486	5.37	0.63	2.5	2.97	13.25	41.15
487	5.11	0.42	2.86	1.93	5.37	24.41
488	6.3	0.43	22.47	1.76	11.63	22.72
489	1.31	0.16	42.69	0.85	7.1	13.47
491	0.87	0.12	49.19	0.55	3.83	8.25
495	1.41	0.09	47.02	0.21	4.57	7.74
501	0.33	0.05	47.77	0.28	1.61	4.4
504	1.36	0.17	48.27	0.49	4.98	9.56
510	0.53	0.08	42.86	0.41	1.24	4.38
514	1.21	0.18	43.97	0.68	5.23	9.21
517	1.57	0.22	44.6	1.06	7.15	13.1
519	1.67	0.3	39.58	1.27	7.29	13.86
520	1.3	0.25	40.58	1.01	7.72	16.24
522	1.79	0.14	46.65	0.68	3.87	8.21
528	1.34	0.26	42.75	1.03	7.19	14.42
529	0.39	0.05	47.62	0.28	1.13	4.13
532	2.31	0.19	42.28	0.65	3.24	7.93
542	2.97	0.2	38.15	0.84	4.07	7.87
543	3.94	0.46	30.99	1.57	11.79	22.19
544	1.77	0.15	46.24	0.72	5.17	10.39
545	2.87	0.39	31.72	1.79	14.53	24.01
548	1.95	0.24	43.02	0.77	6.6	11.12
559	0.7	0.16	49.81	0.36	3.31	7.64
563	0.33	0.03	37.93	0.1	0	1.9
577	2.2	0.25	25.99	0.52	2.38	14.4
578	0.94	0.15	43.31	0.53	3.05	7.71
585	2.18	0.25	44.59	0.64	8.75	12.61
586	2.27	0.19	31.81	0.45	1.21	9.71
587	0.22	0.04	55.9	0.17	2.05	3.47
598	1.8	0.32	49.76	0.38	4.29	12.98

Major Elements, Carbonate

Reading No	Fe2O3 wt%	TiO2 wt%	CaO wt%	K2O wt%	Al2O3 wt%	SiO2 wt%
389	1.41	0.19	52.45	0.54	8.65	16.51
391	0.87	0.04	57.81	0.07	0	2.46
490	0.59	0.1	52.46	0.39	4.15	8.81
492	0.36	0.06	56.66	0.28	3.77	6.87
493	0.31	0.05	54.71	0.16	2.27	3.85
494	0.34	0.06	58.24	0.2	3.76	6.98
496	1.4	0.02	56.95	0.08	1.36	2.44
497	0.1	0.01	56.86	0.07	0	1.53
498	0.93	0.02	56.01	0.07	0.79	1.8
499	0.21	0.04	56.33	0.11	1.17	3
500	0.35	0.06	51.91	0.35	2.04	4.39
502	0.36	0.04	53.21	0.17	1.66	3.98
503	0.22	0.04	53.31	0.19	1.47	4.43
505	0.19	0.03	55.16	0.15	1.87	3.4
506	0.11	0.01	58.27	0.06	0	1.81
507	0.4	0.03	52.92	0.23	1.53	3.14
508	0.1	0.01	58.94	0.06	1.04	1.97
509	0.29	0.04	57.75	0.21	2.23	3.92
511	0.42	0.06	53.71	0.28	2.81	4.6
512	0.42	0.06	54.15	0.2	2.04	4.54
513	0.2	0.04	55.55	0.14	1.47	2.74
515	0.81	0.08	54.13	0.25	2.21	4.45
516	0.88	0.04	54.23	0.27	1.64	3.27
518	0.87	0.13	50.33	0.69	4.96	9.03
521	1.04	0.14	50.11	0.64	6.51	11.37
523	1.16	0.08	51.97	0.5	3.45	6.22
524	0.79	0.06	51	0.34	2.59	5.37
525	0.28	0.04	58.65	0.2	2.63	4.47
526	0.26	0.05	57.46	0.2	2.14	4.15
527	0.58	0.07	54.92	0.27	2.51	5.5
530	0.59	0.1	50.93	0.38	2.74	5.86
531	0.68	0.09	51.22	0.33	2.64	5.01
533	0.17	0.02	54.77	0.09	0	2.05
534	1.03	0.17	50.59	0.57	4.67	8.72
535	0.15	0.02	57.94	0.08	1.29	2.36
536	0.27	0.06	53.47	0.18	1.2	3.75
537	0.21	0.04	59.33	0.15	1.98	3.57
538	0.12	0.01	62.49	0.06	0.94	1.76
539	0.28	0.04	58.21	0.19	2.08	3.11
540	0.31	0.04	53.09	0.23	1.62	3.51
541	0.7	0.11	55.05	0.38	3.49	6.74
546	1.15	0.14	50.14	0.56	4.66	7.63
547	0.4	0.03	56.53	0.15	1.59	3.84

Reading No	Fe2O3 wt%	TiO2 wt%	CaO wt%	K2O wt%	Al2O3 wt%	SiO2 wt%
549	0.59	0.08	54.06	0.28	2.3	5.07
550	0.31	0.04	54.99	0.16	1.67	3.41
551	0.2	0.02	57.07	0.08	1.57	2.54
552	0.23	0.03	59.05	0.14	2.17	3.97
553	0.35	0.03	57.42	0.15	1.95	3.2
554	0.13	0.02	60.2	0.08	1.27	2.67
555	0.18	0.02	59.57	0.11	1.37	1.98
556	0.4	0.04	58.83	0.17	2.25	3.45
557	0.23	0.02	61.09	0.07	1.34	2.06
558	0.79	0.08	52.87	0.21	2.09	3.66
560	0.37	0.08	54.72	0.22	2.44	5.69
561	0.22	0.03	58.58	0.06	0	1.87
562	0.32	0.03	56.37	0.15	1.14	2.55
564	0.37	0.04	64.08	0.2	1.73	2.98
565	0.14	0.02	57.73	0.13	0.9	2.46
566	0.15	0.03	57.65	0.11	1.19	2.52
567	0.22	0.03	55	0.1	0	2.15
568	0.21	0.03	54.33	0.18	1.37	2.61
569	0.2	0.02	54.28	0.11	1.23	2.07
570	0.13	0.02	59.38	0.07	1.23	2.38
571	0.21	0.04	57.12	0.16	2.33	4.6
572	0.11	0.02	57.25	0.07	1.14	2.02
573	0.14	0.02	54.68	0.07	0.9	2.19
574	0.18	0.05	57.66	0.15	2.21	3.5
575	0.2	0.05	55.52	0.12	1.67	3.72
576	0.22	0.04	58.52	0.11	2.22	3.9
579	0.58	0.08	53.94	0.36	2.54	5.39
580	0.19	0.02	56.31	0.09	1.09	2.31
581	0.17	0.02	56.63	0.13	0	2.33
582	0.19	0.02	58.68	0.07	1.56	1.7
583	0.16	0.03	58.96	0.1	1.45	2.92
584	0.53	0.11	54.15	0.41	4.76	7.28
588	0.15	0.03	58.04	0.11	1.47	2.34
589	0.28	0.07	54.48	0.15	1.68	4.52
590	0.48	0.11	51.6	0.3	2.22	5.69
591	0.46	0.09	51.93	0.39	2.64	6.45
592	0.15	0.02	56.9	0.1	1.13	1.87
593	0.37	0.08	50.61	0.29	2.32	5.45
594	1.02	0.07	54.78	0.28	3.49	5.62
595	0.2	0.03	55.35	0.11	1.02	2.11
596	0.35	0.11	56.03	0.16	2.27	5.52
597	0.42	0.11	53.79	0.16	1.35	6.44
599	0.4	0.12	55.52	0.21	3.53	9.88

Reading No	Fe2O3 wt%	TiO2 wt%	CaO wt%	K2O wt%	Al2O3 wt%	SiO2 wt%
600	0.34	0.09	54.97	0.14	1.57	4.39

Trace elements, clastic

Reading No	Zr	Sr	Rb	Mn
1	240.77	118.96	37.23	842.88
2	172.43	63.57	33.64	832.67
3	184.52	72.02	39.15	6738.28
4	279.12	66.84	34.62	1946.02
5	253.39	84.09	40.09	2028.91
6	159.76	55	17.76	1024.35
7	225.49	91.25	33.99	3222.94
8	196.19	104.58	45.18	509.92
9	260.26	80.28	24.27	999.33
10	369.79	95.75	19.07	892.7
11	245.62	51.93	19.85	997.03
12	135.41	125.4	19.4	784.4
13	175.25	133.25	14.14	747.66
14	209.54	129.76	17.12	980.08
15	158.28	130.76	23.07	962.15
16	203.7	108.29	28.43	314.54
17	155.24	103.33	15.07	647.51
18	249.18	91.9	34.58	1645.33
19	175.74	101.67	32.5	337.88
20	223.18	111.64	39.78	389.43
21	216.7	88.36	28.84	862.98
22	168.7	53.57	26.54	1093.44
23	158.49	56.07	27.38	850.82
24	158.95	53.11	17.27	900.64
25	194.47	65.43	30.8	931.19
26	203.71	61.01	29.88	1026
27	168.29	91.2	27.39	604.84
28	207.76	114.53	46.04	181.04
29	183.76	117.41	26.32	650.02
30	186.94	121.17	19.96	389.03
31	178.68	109.11	28.71	467.85
32	124.03	119.49	25.06	458.76
33	281.25	110.88	31.48	513.98
34	261	106.82	32.49	409.92
35	219.75	118.88	35.79	663.54
36	237.11	110.33	33.29	431.48
37	221.18	111.37	23.41	627.33
38	224.74	100.19	26.51	502.15
39	277.37	103.3	39.68	486.31

Reading No	Zr	Sr	Rb	Mn
40	184.82	108.08	28.36	521.99
41	240.45	103.45	21.31	280.99
42	185.21	126.62	19.48	448.69
43	171.05	121.18	18.4	465.18
44	269.02	108.29	38.85	374.63
45	175.47	120.65	21.81	279.38
46	177.55	119.69	20.42	516.13
47	168.97	120.84	18.34	526.01
48	169.14	112.21	20.33	660.93
49	143.55	117.1	16.41	417.73
50	176.92	125.37	20.4	552.55
51	186.88	115.82	17.78	558.94
52	409.93	113.33	17.45	507.45
53	284.41	111.14	37.6	441.54
54	246.16	111.85	30.71	630.05
55	161.62	117.23	19.43	467.24
56	242.08	120.87	24.02	462.41
57	241.55	106.58	27.92	431.01
58	257.16	131.33	20.24	599.74
59	185.5	120.07	20.08	506.37
60	260.02	106.9	32.6	445.71
61	179	122.39	21.66	725.57
62	242.62	124.72	21.97	619.02
63	173.08	124.6	18.72	576.17
64	223.94	107.32	32.9	455.82
65	274.3	111.82	32.2	494.01
66	192.84	115.92	39.78	476.96
67	258.42	119.63	34.14	371.95
68	262.43	120.13	25.76	646.75
69	181.36	124.62	22.68	719.3
70	212.46	108.6	31.36	414.61
71	165.84	132.7	23.87	498.92
72	239.98	115.19	35.17	506.45
73	141.12	91.04	30.42	490.37
74	240.73	102	35.68	406.14
75	135.06	118.84	25.26	637.49
76	227.15	134.51	28.4	695.73
77	140.88	123.69	25.29	876.41
78	166.65	123.34	29.24	510.38
79	140.9	135	22.63	445.43
80	142.27	137.76	19.04	492.65
81	142.46	138.47	19.54	1383.91
82	114.11	138.93	17.9	595.16
83	131.2	139.35	20.64	633.78

Reading No	Zr	Sr	Rb	Mn
84	215.76	130.75	25.32	500.24
85	146.76	107.61	29.86	550.02
86	22.02	147.39	4.03	0
87	140.98	105.87	20.38	379.61
88	145.96	117.69	23.16	408.13
89	123.5	147.42	21.66	491.71
90	120.22	136.44	19.32	358.23
91	137.44	118.89	27.37	389.95
92	91.56	158.97	18.59	476.47
93	133.75	140.15	18.06	507.25
94	107.54	137.92	17.17	429.44
95	151.38	138.04	21.86	621.97
96	134.56	140.56	22.96	438.94
97	73.31	165.69	13.05	436.61
98	101.78	130.53	15.15	369.44
99	240.77	118.96	37.23	842.88
100	172.43	63.57	33.64	832.67
101	184.52	72.02	39.15	6738.28
102	279.12	66.84	34.62	1946.02
103	253.39	84.09	40.09	2028.91
104	159.76	55	17.76	1024.35
105	225.49	91.25	33.99	3222.94
106	196.19	104.58	45.18	509.92
107	260.26	80.28	24.27	999.33
108	369.79	95.75	19.07	892.7
109	245.62	51.93	19.85	997.03
110	135.41	125.4	19.4	784.4
111	175.25	133.25	14.14	747.66
112	209.54	129.76	17.12	980.08
113	158.28	130.76	23.07	962.15
114	203.7	108.29	28.43	314.54
115	155.24	103.33	15.07	647.51
116	249.18	91.9	34.58	1645.33
117	175.74	101.67	32.5	337.88
118	223.18	111.64	39.78	389.43
119	216.7	88.36	28.84	862.98
120	168.7	53.57	26.54	1093.44
121	158.49	56.07	27.38	850.82
122	158.95	53.11	17.27	900.64
123	194.47	65.43	30.8	931.19
124	203.71	61.01	29.88	1026
125	168.29	91.2	27.39	604.84
126	207.76	114.53	46.04	181.04
127	183.76	117.41	26.32	650.02

Reading No	Zr	Sr	Rb	Mn
128	186.94	121.17	19.96	389.03
129	178.68	109.11	28.71	467.85
130	124.03	119.49	25.06	458.76
131	281.25	110.88	31.48	513.98
132	261	106.82	32.49	409.92
133	219.75	118.88	35.79	663.54
134	237.11	110.33	33.29	431.48
135	221.18	111.37	23.41	627.33
136	224.74	100.19	26.51	502.15
137	277.37	103.3	39.68	486.31
138	184.82	108.08	28.36	521.99
139	240.45	103.45	21.31	280.99
140	185.21	126.62	19.48	448.69
141	171.05	121.18	18.4	465.18
142	269.02	108.29	38.85	374.63
143	175.47	120.65	21.81	279.38
144	177.55	119.69	20.42	516.13
145	168.97	120.84	18.34	526.01
146	169.14	112.21	20.33	660.93
147	143.55	117.1	16.41	417.73
148	176.92	125.37	20.4	552.55
149	186.88	115.82	17.78	558.94
150	409.93	113.33	17.45	507.45
151	284.41	111.14	37.6	441.54
152	246.16	111.85	30.71	630.05
153	161.62	117.23	19.43	467.24
154	242.08	120.87	24.02	462.41
155	241.55	106.58	27.92	431.01
156	257.16	131.33	20.24	599.74
157	185.5	120.07	20.08	506.37
158	260.02	106.9	32.6	445.71
159	179	122.39	21.66	725.57
160	242.62	124.72	21.97	619.02
161	173.08	124.6	18.72	576.17
162	223.94	107.32	32.9	455.82
163	274.3	111.82	32.2	494.01
164	192.84	115.92	39.78	476.96
165	258.42	119.63	34.14	371.95
166	262.43	120.13	25.76	646.75
167	181.36	124.62	22.68	719.3
168	212.46	108.6	31.36	414.61
169	165.84	132.7	23.87	498.92
170	239.98	115.19	35.17	506.45
171	141.12	91.04	30.42	490.37

Reading No	Zr	Sr	Rb	Mn
172	240.73	102	35.68	406.14
173	135.06	118.84	25.26	637.49
174	227.15	134.51	28.4	695.73
175	140.88	123.69	25.29	876.41
176	166.65	123.34	29.24	510.38
177	140.9	135	22.63	445.43
178	142.27	137.76	19.04	492.65
179	142.46	138.47	19.54	1383.91
180	114.11	138.93	17.9	595.16
181	131.2	139.35	20.64	633.78
182	215.76	130.75	25.32	500.24
183	146.76	107.61	29.86	550.02
184	22.02	147.39	4.03	0
185	140.98	105.87	20.38	379.61
186	145.96	117.69	23.16	408.13
187	123.5	147.42	21.66	491.71
188	120.22	136.44	19.32	358.23
189	137.44	118.89	27.37	389.95
190	91.56	158.97	18.59	476.47
191	133.75	140.15	18.06	507.25
192	107.54	137.92	17.17	429.44
193	151.38	138.04	21.86	621.97
194	134.56	140.56	22.96	438.94
195	73.31	165.69	13.05	436.61
196	101.78	130.53	15.15	369.44
197	89.58	167.18	13.16	526.4
198	145.81	130.21	22.9	432.88
199	143.65	119.76	19.53	772.83
200	99.56	137.23	18.79	367.79
201	129.03	146.79	21.24	774.15
202	77.86	133.17	15.77	585.27
203	143.32	113.62	15.51	783.31
204	185.6	130.73	25.56	790.6
205	176.71	112.15	26.39	262.84
206	109.86	126.5	19.07	263.03
207	76.91	157.3	14.75	604.05
208	95.25	142.22	15.03	632.74
209	107.01	159	11.49	822.26
210	84.97	132.7	15.13	660.28
211	134.68	105.31	23.49	430.44
212	102.9	105	23.62	293.49
213	195.37	142.55	35.8	698.26
214	213.56	134.22	33.26	449.46
215	101.37	209.63	14.34	608.06

Reading No	Zr	Sr	Rb	Mn
216	206.97	130.83	33.88	481.29
217	266.89	135.96	35.89	665.84
218	194.93	127.6	34.06	525.63
219	276.37	145.66	27.68	503.14
220	190.45	127.86	38.15	563.67
221	206.83	116.12	29.18	427.55
222	213.11	121.87	25.76	544.72
223	146.86	128.7	42.77	464.79
224	152.52	113.17	28.82	461.06
225	205.03	134.06	31.36	513
226	208.56	131.95	36.62	627.34
227	186.51	117.76	34.73	630.27
228	177.39	122.58	27.14	546.24
229	182.67	124.74	32.28	540.04
230	173.73	128.22	26.22	522.44
231	172.95	132.09	34.43	602.03
232	161.89	131.24	28.31	371.76
233	125.57	134.6	29.7	633.26
234	155.44	125.17	22.52	586.05
235	204.83	133.51	31.67	889.29
236	218.39	117.82	36.67	418.45
237	178.21	146.73	33.06	629.94
238	184.71	142.16	41.2	308.71
239	165.29	164.36	43.66	763.68
240	272.05	152.21	39.69	836.08
241	187.96	165.18	43.71	440.06
242	172.23	150.7	41.28	727.09
243	206.95	138.21	29.69	821.99
244	213.28	137.17	31.4	647.38
245	237.31	145.08	34.93	647.55
246	219.9	140.39	35.92	625.55
247	193.09	153.64	37.42	868.02
248	160.59	140.5	30.46	941.37
249	277.86	123.4	36.35	1213.95
250	197.48	139.77	47.53	714.97
251	231.76	130.41	23.66	417.33
252	180.37	130.89	30.69	385.87
253	261.75	120.9	30.3	666.61
254	339.75	117.78	28.65	283.74
255	255.93	133.51	26.06	757.35
256	178.3	123.25	24.02	227.34
257	187.15	131.53	23.9	431.93
258	183.25	107.68	30.78	1191.04
259	254.37	117.36	37.1	480.41

Reading No	Zr	Sr	Rb	Mn
260	292.19	130.43	31.13	618.46
261	171.37	131.87	25.12	484.98
262	385.87	136.65	29.77	448.64
263	231.78	133.34	25.73	672.96
264	245.31	125.04	27.18	431.84
265	195.19	114.28	25.41	753.45
266	168.58	120.06	28.69	687.88
267	222.02	135.36	29.15	498.81
268	226.05	139.69	26.3	587.53
269	211.38	118.68	43.71	513.12
270	309.64	143.85	24.4	725.13
271	197.26	122.92	35.67	560.66
272	231.47	115.6	40.64	734.85
273	195.2	111.11	33.76	1018.53
274	197.19	86.01	37.24	4333
275	276.64	74.31	34.85	3196.83
276	230.98	90.6	27.63	2885.99
277	161.28	96.74	26.81	4670.2
278	251.62	88.12	29.7	1255.25
279	137.4	101.03	33.32	519.7
280	99.39	100.52	29.86	2676.01
281	95.73	78.28	6.62	1694.34
282	79.55	87.64	13.8	1760.86
283	179.3	76.89	30.57	1698.43
284	298.54	91.49	28.22	281.44
285	191.17	48.41	14.58	2542.99
286	502.74	63.42	14.98	1654.69
287	240.89	86.87	31.16	397.72
288	125.58	110.43	27.21	361.51
289	292.82	70.12	14.88	765.88
290	129.99	93.77	36.06	434.94
291	96.15	103.12	20.64	6389.4
292	144.22	149.53	25.16	343.15
293	299.88	67.28	26.5	2934.82
294	122.36	91.56	23.3	536.98
295	164.67	109.47	22.34	509.87
296	199.91	86.11	7.86	4102.78
297	221.05	151.35	14.1	558.25
298	189.8	181.5	8.48	790.87
299	231.89	83.89	22.7	515.98
300	138.92	135.21	11.06	639.48
301	144.78	125.86	16.54	296.91
302	269.78	145.7	10.59	776.24
303	53.67	170.05	10.54	329.88

Reading No	Zr	Sr	Rb	Mn
304	141.63	115.41	19.18	496.36
305	80.42	162.43	12.82	479.17
306	213.45	128.19	19.46	300.2
307	170.72	124.17	24.46	423.24
308	91.24	129.66	18.87	433.55
309	199.27	101.76	27.09	506.8
310	214.05	98.26	30.37	365.64
311	170.41	94.06	26.52	352.12
312	445.77	111.25	11.01	839.08
313	164.43	124.26	12.59	357.11
314	340.53	114.98	19.88	508.88
315	257.28	104.01	39.79	2397.28
316	268.21	99.53	36.62	618.82
317	333.1	105.5	33.72	309.13
318	208.25	118.32	31.1	229.55
319	205.69	123.51	24.19	704.66
320	390.91	116.56	43.42	385.57
321	187.23	123.46	45.61	566.94
322	173.63	102.93	43.15	459.27
323	123.41	67.25	13.74	1690.89
324	159.61	109.31	50.13	939.66
325	278.61	64.92	21.98	367.47
326	211.78	80.92	18.99	2245.75
327	190.13	77.71	29.26	386.28
328	225.09	59.14	23.9	3063.96
329	177.92	77.01	18.51	2335.1
330	213.89	79.54	32	328.8
331	231.34	91.4	28.89	669.79
332	219.05	106.03	58.03	709.31
333	85.96	104.07	16.49	2567.1
334	114.56	109.85	19.42	1762.51
335	128.29	49.94	16.32	997.53
336	149.54	71.63	23.64	1822.33
337	193.46	85.07	14.25	2169.31
338	131.67	111.23	21.19	687.25
339	163.1	112.28	20.76	500.69
340	112.55	90.92	2.48	279.75
341	88.42	155.94	9.44	1724.12
342	122.36	80.2	14.55	2993.78
343	165.24	123.18	27.57	725.41
344	81.61	137.6	13.18	694.19
345	103.73	116.11	21.79	300.21
346	79.79	266.5	8.8	783.32
347	179.1	130.59	22.94	359.97

Reading No	Zr	Sr	Rb	Mn
348	149.35	58.57	20.47	1272.46
349	150.1	108.33	33.47	579.07
350	121.84	108.37	8	736.1
351	152.7	97.35	22.75	1082.76
352	88.08	100.47	17.91	1047.17
353	271.45	67.95	21.06	460.87
354	245.13	106.69	40.89	584.85
355	274.54	109.06	40.47	380.32
356	174.95	89.45	20.54	1434.88
357	179.16	62.49	27.03	784.23
358	150.11	81.95	18.42	1049.66
359	146.92	48.4	11.72	908.01
360	126.03	140.77	16.99	1553.36
361	127.25	175.06	22.12	784.58
362	103.48	153.57	17.27	1332.66
363	175.69	78.2	28.72	0
364	158.57	65.4	25.44	433.06
365	187.17	125.54	24.39	544.16
366	331.94	43.8	10.43	690.19
367	142.22	53.51	20.18	5858.8
368	187.95	57.25	22.89	3765.18
369	260.1	72.96	33.98	721
370	189.61	113.76	27.86	281.98
371	189.64	80.47	27.79	480.84
372	140.87	126.82	21.61	336.99
373	639.79	111.76	16.41	625.15
374	154.38	90.59	17.82	1410.37
375	182.75	118.89	19.36	283.77
376	157.46	110.52	32.49	304.09
377	188.5	78.05	27.54	399.69
378	232.38	111.44	46.53	459.06
379	264.66	129.88	42.61	277.82
380	190.93	140.31	35.54	299.02
381	414.41	154.04	39.66	493.53
382	189.59	169.77	49.91	230.86
383	226.28	173.35	46.65	615.65
384	154.21	168.55	53.84	297.9
385	157.37	160.92	44.54	334.12
386	96.02	309.78	10.22	626.81
387	30.02	382	6.63	967.78
388	13.73	317.32	0	1226.73
390	102.54	256.74	41.98	558.34
392	112.21	160.39	54.8	374.78
393	146.23	219.21	76.36	231.47

Reading No	Zr	Sr	Rb	Mn
394	150.8	183.31	63.89	268.32
395	217.04	192.41	27.55	952.78
396	173.52	140.88	31.74	282.59
397	139.03	211.7	19.65	1837.09
398	67.78	302.71	8.53	1518.05
399	120.37	176.92	66.68	389.5
400	117.43	163.88	49.82	704.56
401	176.4	133.93	65.69	486.11
402	830.07	58.69	22.51	3271.22
403	105.26	48.19	16.15	875.5
404	114.48	48.73	15.06	1027.58
405	151.97	43.86	13.46	655.2
406	286.23	50.47	17.88	1332.48
407	305.26	114.68	47.44	623.62
408	260.08	135.67	38.72	513.6
409	287.04	119.93	39.21	678.22
410	215.6	116.38	37.4	325.69
411	156.4	73.73	31.89	1182.35
412	458.5	55.28	22.6	722.58
413	120.95	48.6	16.43	1069.75
414	173.32	126.96	47.77	690.44
415	184.87	150.86	66.27	196.4
416	144.64	177.44	73.37	170.66
417	74.34	48.96	9.18	505.3
418	158.34	102.24	30.11	3522.32
419	137.32	153.91	57.02	659.53
420	128.75	160.73	55.05	816.89
421	168.08	195.4	33.09	1460.62
422	133.26	332.8	21.67	2375.71
423	108.03	223.03	45.97	890.07
424	145.71	196.16	17.9	3144.51
425	125.96	177.4	83.21	330.92
426	89.12	123.3	53.59	4832.53
427	89.98	125.98	52.59	3983.13
428	93.68	125.58	53.88	8606.6
429	113.86	113.9	45.6	5058.16
430	119.54	111.25	40.93	862.74
431	151.32	166.95	49.91	3232.49
432	140.37	101.51	36.95	1537.45
433	228.39	92.15	28.2	2078.04
434	170.11	124.92	54.13	3847.09
435	134.44	128.99	52.45	7381.62
436	172.38	139.99	65.2	624.49
437	162.64	149.95	64.37	1225.89

Reading No	Zr	Sr	Rb	Mn
438	187.26	192.25	65.8	421.99
439	200.49	145.98	49.36	567.42
440	219.16	129.7	43.43	450.53
441	220.34	132.87	58.97	0
442	146	146.51	67.79	766.64
443	131.59	110.97	41.69	2611.44
444	157.9	154.08	65.17	403.6
445	198.63	146.47	64.96	1029.56
446	156.31	145.28	52.15	573.76
447	150.82	106.51	41.2	2883.68
448	144.27	154.47	70.8	1038.99
449	188.01	141.27	49.29	292.22
450	165.81	160.27	65.54	278.01
451	164.38	158.93	56.42	674.55
452	140.86	161.21	60.77	930.25
453	170.95	177.94	70.49	711.01
454	186.24	179.39	63.38	13930.51
455	208.57	163.65	55.29	8342.47
456	154.32	190.87	64.62	755.06
457	139.51	204.83	67.58	819.04
458	119.49	209.03	66.2	376.33
459	138.56	217.32	75.95	677.78
460	166.84	225.78	63.02	4745.15
461	55.3	319.04	26.4	1875.76
462	131.25	319.76	9.64	1339.02
463	92.84	307.94	47.18	1142.29
464	42.34	487.26	24.46	1253.03
465	74.67	239.34	4.92	1407.41
466	136.03	617.56	42.96	1947.88
467	62.69	553.67	40.12	1233.43
468	123.9	222.39	13.15	1349.48
469	102.92	316.79	23.73	1029.82
470	79.29	270.56	12.82	1909.34
471	85.29	375.18	30.84	669.47
472	44.16	248.01	26.27	1143.41
473	41.1	402.85	20.16	918.89
474	63.91	375.66	37.33	493.23
475	87.18	417.28	23.54	6327.42
476	174.46	175.76	71.24	473.22
477	153.56	129.68	45.85	453.58
478	49.95	207.04	32.19	650.72
479	102.84	323.31	67.62	866.28
480	135.88	394.09	55.67	166.59
481	108.94	270.29	54.3	978.8

Reading No	Zr	Sr	Rb	Mn
482	152.73	189.17	51.63	961.22
483	141.24	572.2	60.23	167.86
484	183.54	629.34	71.59	280.97
485	155.05	415.93	59.52	358.26
486	193.92	243.6	77.18	539.21
487	108.93	202.35	51.72	335.1
488	42.62	256.33	25.48	420.26
489	7.31	318.68	6.43	330.36
491	0	366.98	3.39	198.25
501	0	187.2	3.8	0
504	11.33	254.32	6.2	227.04
510	11.23	214.23	8.65	99.49
517	12.69	223.59	12.82	137.95
522	15.97	215.8	14.58	132.97
528	23.98	181.49	17.74	290.95
529	0	191.21	3.85	169.02
532	20.98	233.58	15.31	175.73
542	20.11	159.21	14.66	378.1
543	33.56	137	20.67	570.68
544	17.12	174.59	14.3	334.17
545	42.83	154.31	32.78	475.62
559	11.55	230.8	4.37	162.19
563	0	155.4	0	0
577	137.83	151.66	9.11	364.03
578	0	233.27	2.29	242.65
585	0	184.92	2.5	191.8
586	46.89	143.1	7.46	361.33
587	0	249.27	0	0
598	20.54	255.91	4.43	415.09
545	42.83	154.31	32.78	475.62
559	11.55	230.8	4.37	162.19
563	0	155.4	0	0
577	137.83	151.66	9.11	364.03
578	0	233.27	2.29	242.65
585	0	184.92	2.5	191.8
586	46.89	143.1	7.46	361.33
587	0	249.27	0	0
598	20.54	255.91	4.43	415.09

Appendix 5. Distribution database

Mound Number	Age	Locality	Formation	Setting	Reference
1	Lower Cambrian	Virginia Appalachians	Patterson Member	Continental margin (passive margin)	Barnaby, R. J. and Read, F. 1990. Carbonate ramp to rimmed shelf evolution: Lower to Middle Cambrian continental margin, Virginian Appalachians. <i>Geological Society of America Bulletin</i> . Vol. 102. Pg. 391-404
2	Lower Cambrian	Northern Flinders Ranges	Hawkers Group	Continental Margin Trough	James, N. P. and Gravestock, D. I. 1990. Lower Cambrian shelf and shelf margin buildups, Flinders Ranges, South Australia. <i>Sedimentology</i> . Vol. 37. Pg. 455-480
3	Lower Cambrian	Transantarctic Mountains	Shackleton Limestone	Carbonate platform	Rees, M. N. Pratt, B. R. and Rowell, A. J. 1989. Early Cambrian reefs, reef complexes, and associated lithofacies of the Shackleton Limestone, Transantarctic Mountains. <i>Sedimentology</i> . Vol. 36. Pg. 341-361
4	Middle Cambrian	Rocky Mnts, Canada	Burgess, Cathedral Formations	Passive Margin	Collom, C. J., Johnson, P.A. and Powell, W. G. 2009. Reinterpretation of 'Middle' Cambrian stratigraphy of the rifted western Laurentian margin: Burgess Shale Formation and contiguous units (Sauk II megasequence), Rocky Mountains, Canada. <i>Palaeogeography, Palaeoclimatology, Palaeoecology</i> . Vol. 277. Pg. 63-85
5	Middle Cambrian	House Range, Utah	Marjum Formation	Passive Margin	Elrick, M. and Snider, A. C. 2002. Deep-water stratigraphic cyclicity and carbonate mud mound development in the Middle Cambrian Marjum Formation, House Range, Utah, USA. <i>Sedimentology</i> . Vol. 49. Pg. 1021-1047

6	Middle Cambrian	Monarch, Canada	Burgess Shales	Passive Margin	Johnston, P. A. Johnston, K. J. Collom, C. J. Powell, W. G. and Pollock, R. J. 2009. Palaeontology and depositional environments of ancient brine seeps in the Middle Cambrian Burgess Shale at The Monarch, British Columbia, Canada. <i>Palaeogeography, paleoclimatology, Palaeoecology</i> . Vol. 277. Pg. 86-105
7	Middle Cambrian	Mackenzie Mnts, Canada	Rockslide Formation	?	Pratt, B. R. 1995. The origin, biota and evolution of deep-water mud-mounds. In: Monty, C. L. V., Bosence, D. W. J., Bridges, P. H. and Pratt, B. R. (Eds.), <i>Carbonate Mud-Mounds Their Origin and Evolution</i> . International Association of Sedimentologists. Blackwell Science. Pg. 49-123
8	Middle Cambrian	Virginia	?	Passive Margin - Outer Ramp	Read, J. F. 1989. Controls on Evolution of Cambrian-Ordovician Passive Margin, U. S. Appalachians. In: Crevello, P. D., Wilson, J. L., Sarg, J. F. and Read, J. F. (Eds.) <i>Controls on Carbonate Platform and Basin Development. Society of Economic Paleontologists and Mineralogists</i> . Special Publications. No. 44. Pg. 147-165
9	Upper Cambrian	Newfoundland	Shallow Bay Formation	?	Pratt, B. R. 1995. The origin, biota and evolution of deep-water mud-mounds. In: Monty, C. L. V., Bosence, D. W. J., Bridges, P. H. and Pratt, B. R. (Eds.), <i>Carbonate Mud-Mounds Their Origin and Evolution</i> . International Association of Sedimentologists. Blackwell Science. Pg. 49-123

10	Upper Cambrian	Maly Karatau, Kazakhstan	?	Rift-bounded Platform	Pratt, B. R. 1995. The origin, biota and evolution of deep-water mud-mounds. In: Monty, C. L. V., Bosence, D. W. J., Bridges, P. H. and Pratt, B. R. (Eds.), <i>Carbonate Mud-Mounds Their Origin and Evolution</i> . International Association of Sedimentologists. Blackwell Science. Pg. 49-123
11	Middle Ordovician	Nevada, USA	Antelope Valley Limestone	Outer Ramp	DiFilippo, E. L. Hammond, D. E. and Corsetti, F. A. 2003. Geochemical constraints for coexisting CO ₂ gas hydrate and calcite: implications for sheet cracks, stromatactis, zebra and tepee-like structures. <i>Sedimentary Geology</i> . Vol. 106. Pg. 1-6
12	Middle Ordovician	Nevada, USA	Antelope Valley Limestone	Outer Ramp	Krause, F. F. 2001. Genesis and geometry of the Meiklejohn Peak lime mud-mound, Bare Mountain Quadrangle, Nevada, USA: Ordovician limestone with submarine frost heave structures--a possible response to gas clathrate hydrate evolution. <i>Sedimentary Geology</i> . Vol. 145. Pg. 189-213
13	Middle Ordovician	Virginia and Tennessee	Effna/Murat and Holston Formations	Appalachian Foreland Basin	Pratt, B. R. 1995. The origin, biota and evolution of deep-water mud-mounds. In: Monty, C. L. V., Bosence, D. W. J., Bridges, P. H. and Pratt, B. R. (Eds.), <i>Carbonate Mud-Mounds Their Origin and Evolution</i> . International Association of Sedimentologists. Blackwell Science. Pg. 49-123

14	Middle Ordovician	Basin Ranges, USA	Lower Antelope Valley and Shingle Limestones	Outer-Shelf Belt	Ross, R. J. Jr., James, N. P., Hintze, L. F. and Poole, F. G. 1989. Architecture and Evolution of a Whiterockian (Early Middle Ordovician) Carbonate Platform, Basin Ranges of Western U.S.A. In: Crevello, P. D., Wilson, J. L., Sarg, J. F. and Read, J. F. (Eds.) <i>Controls on Carbonate Platform and Basin Development</i> . Society of Economic Paleontologists and Mineralogists. Special Publications. No. 44. Pg. 167-185
15	Middle Ordovician	Newfoundland (western)	Table Point Formation	Taconian Foreland Basin	Stenzel, S. R. and James, N. P. 1995. Shallow-water stromatactis mud-mounds on a Middle Ordovician foreland basin platform, western Newfoundland. In: Monty, C. L. V., Bosence, D. W. J., Bridges, P. H. and Pratt, B. R. (Eds.), <i>Carbonate Mud-Mounds Their Origin and Evolution</i> . International Association of Sedimentologists. Blackwell Science. Pg. 127-149
16	Middle Ordovician	Virginia, USA	Effna/Murat and Holston Formations	Appalachian Foreland Basin	Tobin, K. J. and Bergstrom, S. M. 2002. Implications of Ordovician (460Myr) marine cement for constraining seawater temperature and atmospheric pCO ₂ . <i>Paleogeography, Palaeoclimatology, Palaeoecology</i> . Vol. 181. Pg. 399-417
17	Upper Ordovician	Sweden	Upper Sandbian to Lower Katian Kullberg and Upper Katian to Hirnantian Boda Limestones	Carbonate Platform (Regressive Sea Level)	Calner, M. Lehnert, O. and Joachimski, M. 2010. Carbonate mud mounds, conglomerates, and sea-level history in the Katian (Upper Ordovician) of central Sweden. <i>Facies</i> . Vol. 56. Pg. 157-172

18	Upper Ordovician	Alabama, USA	Chickamauga Group	Appalachian Foreland Basin	Crow, C. J. Brande, S. Turner, M. E. Stock, C. W. and Benson, D. J. 2001. Random sampling of carbonate mounds: an example from the Upper Ordovician of Alabama. <i>Sedimentary Geology</i> . Vol. 145. Pg. 173-187
19	Upper Ordovician	Sweden	Boda Limestone	Carbonate Platform (Regressive Sea Level)	Schmid, D. U. Leinfelder, R. R. and Nose, M. 2001. Growth dynamics and ecology of Upper Jurassic mounds, with comparisons to Mid-Palaeozoic mounds. <i>Sedimentary Geology</i> . Vol. 145. Pg. 343-376
20	Upper Ordovician	Gotland (Sweden)	Klasen Limestoone	Marginal Zone	Sivhed, U. Erlstrom, M. Bojesen-Koefoed, J. A. and Lofgren, A. 2004. Upper Ordovician Carbonate Mounds on Gotland, Central Baltic Sea: Distribution, Composition and Reservoir Characteristics. <i>Journal of Petroleum Geology</i> . Vol. 27. Pg. 115-140
21	Upper Ordovician	Spain (East Iberian Chain)	Ashgill Cystoid Limestone Formation	Gondwanan Margin	Vennin, E. Alvaro, J and Villas, E. 1998. High-Latitude pelmatozoan-bryozoan mud-mounds from late Ordovician northern Gondwana platform. <i>Geological Journal</i> . Vol. 33. Pg. 121-140
22	Lower Silurian	Ellesmere Island, Canadian Arctic	Cape Philips and Allen Bay Formations	Platform Margin and Backstepped Platform	de Freitas, T. A. and Dixon, O. A. 1995. Silurian microbial buildups of the Canadian Arctic. In: Monty, C. L. V., Bosence, D. W. J., Bridges, P. H. and Pratt, B. R. (Eds.), <i>Carbonate Mud-Mounds Their Origin and Evolution</i> . International Association of Sedimentologists. Blackwell Science. Pg. 151-169

23	Lower Silurian	Anticosti Island, Canada	Jupiter Formation	?	Schmid, D. U. Leinfelder, R. R. and Nose, M. 2001. Growth dynamics and ecology of Upper Jurassic mounds, with comparisons to Mid-Palaeozoic mounds. <i>Sedimentary Geology</i> . Vol. 145. Pg. 343-376
24	Lower Silurian	Northern Greenland	Franklinian Reef Belt	?	Sonderholm, M. and Harland, T. L. 1988. Franklinian reef belt, North Greenland. Reefs, Canada and Adjacent Area. In: Geldsetzer, H. H. J., James, N. P. and Tebbutt, G. E. (Eds.), <i>Reefs, Canada and Adjacent Area</i> . Canadian Society of Petroleum Geologists. Memoir 13. Pg. 356-366
25	Upper Silurian	Gaspe, Canada	West Point Formation	Platform Margin?	Bourque, P-A. 2001. Sea-level, synsedimentary tectonics, and reefs: implications for Hydrocarbon exploration in the Silurian-lowermost Devonian Gaspe Belt, Quebec Appalachians. <i>Bulletin of Canadian Petroleum Geology</i> . Vol. 49. Pg. 217-237
26	Upper Silurian	Gaspe Peninsula, Canada	West Point Formation	Platform Margin?	Bourque, P-A. and Amyot, G. 1988. Stromatoporoid-coral reefs of the Upper West Point Reef Complex, Late Silurian, Gaspe peninsula, Quebec. In: Geldsetzer, H. H. J., James, N. P. and Tebbutt, G. E. (Eds.), <i>Reefs, Canada and Adjacent Area</i> . Canadian Society of Petroleum Geologists. Memoir 13. Pg. 251-257
27	Upper Silurian	Gaspe Peninsula, Canada	West Point Formation	Platform Margin?	Bourque, P-A. and Gignac, H. 1983. Sponge-constructed stromatactis mud mounds, Silurian Gaspe, Quebec. <i>Journal of Sedimentary Petrology</i> . Vol. 53. Pg. 521-532

28	Upper Silurian	Gaspe Peninsula, Canada	West Point Formation	Platform Margin?	Bourque, P-A. and Raymond, L. 1994. Diagenetic alteration of early marine cements of Upper Silurian stromatactis. <i>Sedimentology</i> . Vol. 41. Pg. 255-269
29	Upper Silurian	Gaspe Peninsula, Canada	Sayabec/La Vielle Formationsa. West Point Formation	Platform Margin?	Bourque, P-A., Amyot, G., Desrochers, A., Gignac, H., Gosselin, C., Lachambre, G. and Laliberte. J. Y. 1986. Silurian and Lower Devonian reef and carbonate complexes of the Gaspe Basin, Quebec - A summary. <i>Bulletin of Canadian Petroleum Geology</i> . Vol. 34. Pg. 452-489
30	Upper Silurian	Ellesmere Island, Canadian Arctic	Cape Philips and Allen Bay Formations	Platform Margin and Backstepped Platform	de Fretas, T. A., Dixon, O. A. and Mayr, U. 1993. Silurian pinnacle reefs of the Canadian Arctic. <i>Palaaios</i> . Vol. 8. Pg. 172-182
31	Upper Silurian	Southern Tien-Shan, Commonwealth of Independent States	Aktur Nappe	Shallow Water Atoll	Dronov, A. V. 1993. Middle Paleozoic Waulsortian-type Mud Mounds in Southern Fergana (Southern Tein-Shan, Commonwealth of Independent States): The Shallow-water Atoll Model. <i>Facies</i> . Vol. 28. Pg. 169-180
32	Upper Silurian	Indiana, USA	Louisville Formation	Shallow Reef Platform?	Lehman, P. J. and Simo, A. 1988. Depositional facies and diagenesis of the Pipe Creek Jr. reef, Silurian, Great Lakes Region, Indiana. In: Geldsetzer, H. H. J., James, N. P. and Tebbutt, G. E. (Eds.), Reefs, Canada and Adjacent Area. <i>Canadian Society of Petroleum Geologists. Memoir 13</i> . Pg. 319-329
33	Upper Silurian	Anti-Atlas, Morocco	Iriqui, Lmhaifid and Mersane Formations	High Energy, Current Swept Shelf in Cool Waters	Lubeseder, S. 2008. Palaeozoic low-oxygen, high-latitude carbonates: Silurian and Lower Devoinian nautiloid and scyphocrinoid limestones of the Anti-Atlas (Morocco). <i>Palaeogeography, Palaeoclimatology, Palaeoecology</i> .

					Vol. 264. Pg. 195-209
34	Upper Silurian	N E Illinois, USA	Kankakee	?	McGovney, J. E. 1988. Thornton reef, Silurian, Northeastern Illinois. In: Geldsetzer, H. H. J., James, N. P. and Tebbutt, G. E. (Eds.), <i>Reefs, Canada and Adjacent Area</i> . Canadian Society of Petroleum Geologists. Memoir 13. Pg. 330-338
35	Upper Silurian	Michigan Basin, USA	?	Deep Platform	Pratt, B. R. 1995. The origin, biota and evolution of deep-water mud-mounds. In: Monty, C. L. V., Bosence, D. W. J., Bridges, P. H. and Pratt, B. R. (Eds.), <i>Carbonate Mud-Mounds Their Origin and Evolution</i> . International Association of Sedimentologists. Blackwell Science. Pg. 49-123
36	Upper Silurian	Indiana, USA	Mississinewa Shale, Liston Creek Limestone and Huntington Dolomite	Shallow Reef Platform?	Textoris, D. and Carozzi, A. 1964. Petrography and evolution of Niagran (Silurian) reefs, Indiana. <i>Bulletin of the American Association of Petroleum Geologists</i> . Vol. 48. Pg. 397-426
37	Lower Devonian	Hamar Lakhad Ridge, Anti- Atlas, Morocco	Emsian Shales	Margin - Submarine Volcanism	Belka, Z. 1998. Early Devonian Kess-Kess Carbonate Mud Mounds of the Eastern Anti-Atlas (Morocco), and their Relation to Submarine Hydrothermal Venting. <i>Journal of Sedimentary Research</i> . Vol. 68. Pg. 368-377

38	Lower Devonian	Montange Noire, France	Minervois Nappe, Mont Peyroux Nappe and Pardailhan Nappe	Divergent Margin	Bourrouilh, R., Bourque, P-A., Dansereau, P., Bourrouilh-Le Jan, F. and Weyant, P. 1998. Synsedimentary tectonics, mud-mounds and sea-level changes on a Palaeozoic carbonate platform margin: a Devonian Montagne Noire example (France). <i>Sedimentary Geology</i> . Vol. 118. Pg. 95-118
39	Lower Devonian	Hamar Lakhad Ridge, Anti-Atlas, Morocco	Emsian Shales	Margin - Submarine Volcanism	Cavalazzi, B. 2006. KESS KESS carbonate mounds, Hamar Laghdad, Anti-Atlas, SE Morocco - A FIELD GUIDE
40	Lower Devonian	Cantabrian Zone, N W Spain	Valporquero Shale Formation	Passive Continental Margin	Fernandez, L. P., Nose, M., Fernandez-Martinez, E., Mendez-Bedia, L., Schroder, St. and Soto, F. 2006. Reefal and mud mound facies development in the Lower Devonian La Vid Group at the Colle outcrops (Leon province, Cantabrian Zone, NW Spain). <i>Facies</i> . Vol. 52. Pg. 307-327
41	Lower Devonian	Montange Noire, France	Minervois Nappe, Mont Peyroux Nappe and Pardailhan Nappe	Divergent Margin	Flajs, G and Hussner, H. 1993. A Microbial Model for the Lower Devonian Stromatactis Mud Mounds of the Montagne Moire (France). <i>Facies</i> . Vol. 29. Pg. 179-194
42	Lower Devonian	Hamar Lakhad Ridge, Anti-Atlas, Morocco	Emsian Shales	Margin - Submarine Volcanism	Mounji, D. , Bourque, P-A. and Savard, M. M. 1998. Hydrothermal origin of Devonian conical mounds (kess-kess) of Hamar Lakhdad Ridge, Anti-Atlas, Morocco. <i>Geology</i> . Vol. 26. Pg. 1123-1126
43	Middle Devoinian	Saskatchewan, Canada	Winnipegosis Formation	Intracratonic Basin	Fu, Q., Qing, H. and Bergman, M. 2004. Dolomitized calcrete in the Middle Devonian Winnipegosis carbonate mounds, subsurface of south-central Saskatchewan, Canada.

					<i>Sedimentary Geology</i> . Vol. 168. Pg. 49-69
44	Middle Devonian	New York, USA	Tully Limestone	Acadian Basin	Heckel, P. 1972. Possible inorganic origin for stromatactis in Calcilutite mounds in the Tully Limestone, Devonian of New York. <i>Journal of Sedimentary Petrology</i> . Vol. 42. Pg. 7-18
45	Middle Devonian	Mader (east Anti-Atlas, Morocco)	Mudstone/Shales?	Continental Margin	Kauffman, B. 1998. Facies, stratigraphy and diagenesis of Middle Devonian reef- and mud-mounds in the Mader (eastern Anti-Atlas, Morocco). <i>Acta Geologica Polonica</i> . Vol. 48. Pg. 43-106
46	Middle Devonian	Hamar Lakhad Ridge, Anti-Atlas, Morocco	Eifelian and Givetian Stages	Divergent Margin	Peckmann, J., Walliser, O. H., Riegel, W. and Reitner, J. 1999. Signatures of Hydrocarbon Venting in a Middle Devonian Carbonate Mound (Hollard Mound) at the Hamar Laghdad (Anti-Atlas, Morocco). <i>Facies</i> . Vol. 40. Pg. 281-296
47	Middle Devonian	Eifel Hills, Germany	Hillesheim Syncline	Tidal Flats/Deltacic/Shallow Marine?	Schmid, D. U. Leinfelder, R. R. and Nose, M. 2001. Growth dynamics and ecology of Upper Jurassic mounds, with comparisons to Mid-Palaeozoic mounds. <i>Sedimentary Geology</i> . Vol. 145. Pg. 343-376
48	Middle Devonian	Harz Mountains, Germany	Elbingerode	Foreland Basin?	Weller, H. 1995. The Devonian mud mounds of Rubeland in the Harz Mountains/Germany. <i>Facies</i> . Vol 32. Pg. 43-49
49	Middle Devonian	Morocco	?	Continental Margin	Wendt, J. 1993. Steep-sided carbonate mud mounds in the Middle Devonian of the eastern Anti-Atlas, Morocco. <i>Geological Magazine</i> . Vol. 130. Pg. 69-83

50	Middle Devonian	Algerian Sahara	Ahnet Basin	Shallow-pelagic Carbonate Shelf	Wendt, J., Belka, Z., Kauffman, B., Kostrewa, R. and Hayer, J. 1997. The wrld's most spectacular carbonate mud mounds (Middle Devonian, Algerian Sahara). <i>Journal of Sedimentary Research</i> . Vol. 67. Pg. 424-436
51	Upper Devonian	Chernyshev Swell, Timan N Ural Region	Chernyshev Swell	Pre-Urals Foredeep	Antoshkina, A. I. 2006. Palaeoenvironmental implications of Palaeomicrocodium in Upper Devonian microbial mounds of the Chernshev Swell, Timan-northern Ural Region. <i>Facies</i> . Vol. 52. Pg. 611-625
52	Upper Devonian	Dinant Area, Southern Belgium	Frasnes Group	Frasnian Basin - Pre Variscan Orogeny	Boulvain, F. 2001. Facies architecture and diagenesis of Belgian Late Frasnian carbonate mounds. <i>Sedimentary Geology</i> . Vol. 145. Pg. 269-294
53	Upper Devonian	Dinant Area, Southern Belgium	Frasnes Group	Frasnian Basin - Pre Variscan Orogeny	Boulvain, F., De Ridder, C., Mamet, B., Preat, A and Gillan, D. 2001. Iron Microbial Communities in Belgian Fransian Carbonate Mounds. <i>Facies</i> . Vol. 44. Pg. 47-60
54	Upper Devonian	Rock Mountains, Alberta, Canada	Nisku Formation	?	Pratt, B. R. 1995. The origin, biota and evolution of deep-water mud-mounds. In: Monty, C. L. V., Bosence, D. W. J., Bridges, P. H. and Pratt, B. R. (Eds.), <i>Carbonate Mud-Mounds Their Origin and Evolution</i> . International Association of Sedimentologists. Blackwell Science. Pg. 49-123
55	Upper Devonian	Dinant Area, Southern Belgium	Frasnes Group	Postorogenic Sedimentary Basin?	Rutten, M. G. 1956. Devonian reefs from Belgium: relation between geosynclinal subsidence and hinterland erosion. <i>American Journal of Science</i> . Vol. 254. Pg. 685-692

56	Upper Devonian	Guilin, South China	Tangjiawan and Yunghsien Formations	Platform Margins and Proximal Fore-Reef Slope	Shen, J., Teng, J. and Pedoja, K. 2005. Middle and Late Devonian microbial carbonates, reefs and mounds in Guilin, South China and their sequence stratigraphic, paleoenvironmental and paleoclimatic significance. <i>Science in China Series D: Earth Sciences</i> . Vol. 48. Pg. 1900-1912
57	Upper Devonian	Canning Basin, W Australia	Virgin Hills Formation	Proximal Fore-Reef Slope	Webb, G. 2001. Famennian mud-mounds in the proximal fore-reef slope, Canning Basin, Western Australia. <i>Sedimentary Geology</i> . Vol. 145. Pg. 295-315
58	Lower Carboniferous (Mississippian)	Kentucky, USA	Haney Limestone	Oolitic Shoal - Foreland Ramp	Al-Tawil, A. and Read, J. F. 2003. Late Mississippian (Late Meramecian-Chesterian), Glacio-Eustatic Sequence Development on an Active Foreland Ramp, Kentucky, U.S.A. In: Ahr, W. M., Harris, P. M., Morgan, W. A. and Somerville, I. D. (Eds.) <i>Permo-Carboniferous Carbonate Platforms And Reefs</i> . Society for Sedimentary Geology. Special Publication No. 78. And, The American Association of Petroleum Geologists. Memoir, 83. Pg. 35-55
59	Lower Carboniferous (Mississippian)	Nova Scotia	Windsor Group	?	Boehner, R. C. 1998. Carbonate buildups of Windsor Group Major Cycle 2: Maxner and Miller Limestones, Miller Creek Formation and Mosher Road Member, Elderbank Formation and B2 Limestone, Nova Scotia. In: Geldsetzer, H. H. J., James, N. P. and Tebbutt, G. E. (Eds.), <i>Reefs, Canada and Adjacent Area</i> . Canadian Society of Petroleum Geologists. Memoir 13. Pg. 600-608

60	Lower Carboniferous (Mississippian)	Central England	Milldale limestone Formation	Lower Ramp	Bridges, P. H. and Chapman, A. J. 1988. Anatomy of a deep water mud-mound complex to the southwest of the Dinantian platform in Derbyshire, UK. <i>Sedimentology</i> . Vol. 35. Pg. 139-162
61	Lower Carboniferous (Mississippian)	Indiana and Kentucky, USA	Ramp Creek and Harrodsburg limestone Formations	Ramp - Differing water depths	Brown M. A. and Dodd, J. R. 1990. Carbonate Mud Mounds in Middle Mississippian Strata of Southern Indiana and Northern Kentucky: End Members of a Middle Mississippian Mud Mound Spectrum? <i>Palaaios</i> . Vol. 5. Pg. 236-243
62	Lower Carboniferous (Mississippian)	Montana, USA	?	Fault Margin of Central Montana Trough	Cotter, E. 1966. Limestone Diagenesis and Dolomitization in Mississippian Carbonate Banks in Montana. <i>Journal of Sedimentary Research</i> . Vol. 36. Pg. 881-888
63	Lower Carboniferous (Mississippian)	Guadiato area, SW Spain	Sierra de la Estrella block	Variscan Orogeny? Ramp Setting	Cozar, P., Rodriguez-Martinez, M., Falces, S., Mas, R. and Rodriguez, S. 2003. Stratigraphic Setting in the Development of Microbial Mud Mounds of the Lower Carboniferous of the Guadiato Area (SW Spain). In: Ahr, W. M., Harris, P. M., Morgan, W. A. and Somerville, I. D. (Eds.) <i>Permo-Carboniferous Carbonate Platforms And Reefs</i> . Society for Sedimentary Geology. Special Publication No. 78. And, The American Association of Petroleum Geologists. Memoir, 83. Pg. 57-67

64	Lower Carboniferous (Mississippian)	Alberta, Peace River, Canada	Pekisko Formation	?	Davies, G. R., Edwards, D. E and Flach, P. 1998. Lower Carboniferous (Mississippian) Waulsortian reefs in the Seal area of North-Central Alberta. In: Geldsetzer, H. H. J., James, N. P. and Tebbutt, G. E. (Eds.), <i>Reefs, Canada and Adjacent Area</i> . Canadian Society of Petroleum Geologists. Memoir 13. Pg. 643-648
65	Lower Carboniferous (Mississippian)	Dinant Area, Southern Belgium	Freyrian Formation	Regression?	Dehantschutter, J. A. E. and Lees, A. 1996. Waulsortian buildups of Waulsort, Belgium. <i>Geological Journal</i> . Vol. 31. Pg. 123-142
66	Lower Carboniferous (Mississippian)	Western Ireland	Ballysteen Limestone	Transgression?	Devuyst, F-X. and Lees, A. 2001. The initiation of Waulsortian buildups in Western Ireland. <i>Sedimentology</i> . Vol. 48. Pg. 1121-1148
67	Lower Carboniferous (Mississippian)	Newfoundland	Codroy Group	Post Acadian Orogeny, Karstic Platform	Dix, G. R. and James, N. P. 1987. Late Mississippian bryozoan/microbial build-ups on a drowned karst terrain: Port au Port Peninsula, western Newfoundland. <i>Sedimentology</i> . Vol. 34. Pg. 779-793
68	Lower Carboniferous (Mississippian)	Central England	Eyam Monsal Dale Limestones	Hernancyan front?	Gutteridge, P. 1995. Late Dinantian (Brigantian) carbonate mud-mounds of the Derbyshire carbonate platform. In: Monty, C. L. V. Bosence, D. W. J. Bridges, P. H. and Pratt, B. R. (Eds.) <i>Carbonate Mud-Mounds Their Origin and Evolution</i> . International Association of Sedimentologists. Blackwell Science. Vol. 23. Pg. 289-307
69	Lower Carboniferous (Mississippian)	Sacramento Mountains, New Mexic, USA	Lake Valley Formation	Carbonate Ramp - Transgressive Phase	Jeffry, D. L. and Stanton Jr., J. R.. 1996. Growth history of Lower Mississippian Waulsortian mounds: Distribution, stratal patterns and geometries, New Mexico. <i>Facies</i> . Vol.

					35. Pg. 29-58
70	Lower Carboniferous (Mississippian)	Missouri, USA	Burlington Limestone	Kaskaskia Transgression	King Jr., D. T. 1986. Waulsortian - type buildups and resedimented (Carbonate-turbidite) facies, Early Mississippian Burlington Shelf, Central Missouri. <i>Journal of Sedimentary Petrology</i> . Vol. 56. Pg. 471-479
71	Lower Carboniferous (Mississippian)	Illinois, USA	Chouteau Limestone	Illinois Basin - Slowly subducting	Lasemi, Z., Norby, R. D., Utgaard, J. E., Ferry, W. R., Cuffey, R. J. and Dever, G. R. Jr. 2003. Mississippian Carbonate Buildups and Development of Cool-Water-Like Carbonate Platforms in the Illinois Basin, Midcontinent U.S.A. In: Ahr, W. M., Harris, P. M., Morgan, W. A. and Somerville, I. D. (Eds.) <i>Permo-Carboniferous Carbonate Platforms And Reefs</i> . Society for Sedimentary Geology. Special Publication No. 78. And, The American Association of Petroleum Geologists. Memoir, 83. Pg. 69-95
72	Lower Carboniferous (Mississippian)	Dinant Area, Southern Belgium	Freyrian Formation	Regression?	Lees, A. 1997. Biostratigraphy, sedimentology and palaeobathymetry of Waulsortian buildups and peri-Waulsortian rocks during the late Tournaisian regression, Dinant area, Belgium. <i>Geological Journal</i> . Vo. 32. Pg. 1-36
73	Lower Carboniferous (Mississippian)	Tennessee, USA	Fort Payne Formation	?	Macquown, W. C. and Perkins, J. H. 1982. Stratigraphy and petrology of petroleum-producing Waulsortian-type carbonate mounds in Fort Payne Formation (Lower Mississippian) of

					North-Central Tennessee. <i>American Association of Petroleum Geologists Bulletin</i> . Vol. 66. Pg. 1055-1075
74	Lower Carboniferous (Mississippian)	Algeria	Loucha and Kebir Formations	?	Madi, A., Savard, M. M., Bourque, P-A. and Chi, G. 2000. Hydrocarbon potential of the Mississippian carbonate platform, Bechar Basin, Algeria Sahara. <i>American Association of Petroleum Geologists Bulletin</i> . Vol. 84. Pg. 266-287
75	Lower Carboniferous (Mississippian)	Kentucky, USA	Fort Payne Formation	?	Meyer, D. L., Ausich, W. I., Bohl, D. T., Norris, W. A. and Potter, P. E. 1995. Carbonate mud-mounds in the Fort Payne Formation (lower Carboniferous), Cumberland Saddle region, Kentucky and Tennessee, USA. In: Monty, C. L. V. Bosence, D. W. J. Bridges, P. H. and Pratt, B. R. (Eds.) <i>Carbonate Mud-Mounds Their Origin and Evolution</i> . International Association of Sedimentologists. Blackwell Science. Vol. 23. Pg. 273-287
76	Lower Carboniferous (Mississippian)	Dakota, USA	Lodgepole Formation	?	Montgomery, S. L. 1996. Mississippian Lodgepole play, Williston Basin: A review. <i>American Association of Petroleum Geologists Bulletin</i> . Vol. 80. Pg. 796-810
77	Lower Carboniferous (Mississippian)	Harz Mountain, Germany	Iberg Formation	Foreland Basin?	Peckmann, J., Grischler, E., Oschmann, W. and Reitner, J. 2001. An Early Carboniferous seep community and hydrocarbon-derived carbonates from the Harz Mountains, Germany. <i>Geology</i> . Vol.. 29. Pg. 271-274

78	Lower Carboniferous (Mississippian)	Scotland	Midland Valley?	Topographic high - Shallow Water	Pickard, N. A. H. 1992. Depositional controls on Lower Carboniferous microbial buildups, eastern Midland Valley of Scotland. <i>Sedimentology</i> . Vol. 39. Pg. 1081-1100
79	Lower Carboniferous (Mississippian)	New Mexico, USA	?	Outer Shelf	Pray, L. C. 1958. Fenestrate Bryozoan Core Facies, Mississippian Bioherms, Southwestern United States. <i>Journal of Sedimentary Research</i> . Vol. 28. Pg. 261-273
80	Lower Carboniferous (Mississippian)	Sierra de la Estrella, SW Spain	Sierra de la Estrella succession	Middle-Ramp	Rodriguez-Martinez, M., Cozar, R., Mas, R. and Rodriguez, S. 2003. Upper Visean Saccaminopsis-Sponge Microbial Mud Mounds, Sierra de la Estrella, Southeastern Spain. In: Ahr, W. M., Harris, P. M., Morgan, W. A. and Somerville, I. D. (Eds.) <i>Permo-Carboniferous Carbonate Platforms And Reefs</i> . Society for Sedimentary Geology. Special Publication No. 78. And, The American Association of Petroleum Geologists. Memoir, 83. Pg. 189-200
81	Lower Carboniferous (Mississippian)	Williston Basin, Saskatchewan, Canada	Souris Valley Beds - (Lodgepole Formation Equiv.)	Williston Basin, Intracratonic	Sereda, R. D. and Kent, D. M. 1987. Waulsortian-type mounds in the Mississippian of the Williston Basin: New interpretation from old cores. In: Carlson, C. G. and Christopher, J. E. (Eds.), <i>Fifth International Williston Basin Symposium</i> . Saskatchewan Geological Society. Special Publication. No. 9. Pg. 98-106
82	Lower Carboniferous (Mississippian)	Guanqxi, South China	Tatang Formation	Passive Continental Margin (Fore-Reef Slope)	Shen, J-W. and Hairuo, Q 2010.. Mississippian (Early Carboniferous) stromatolite mounds in a fore-reef slope setting, Laibin, Guangxi, South China. <i>International Journal of Earth Science</i> . Vol 99. Pg. 443-458

83	Lower Carboniferous (Mississippian)	Montana, USA	Lodgepole Formation	?	Smith, D. L. 1977. Transition from deep- to shallow- water carbonates, Paine Member, Lodgepole Formation, Central Montana. In: Cook, H. E. and Enos, P. (Eds.), <i>Deep-Water Carbonate Environments</i> . Society for Sedimentary Research SEPM Special Publications. No. 25. Pg. 187-201
84	Lower Carboniferous (Mississippian)	Ireland (NE and SW)	?	Dublin Basin and Shannon Trough	Somerville, I. D. 2003. Review of Irish Lower Carboniferous (Mississippian) Mud Mounds: Depositional Setting, Biota, Facies, and Evolution. In: Ahr, W. M., Harris, P. M., Morgan, W. A. and Somerville, I. D. (Eds.) <i>Permo-Carboniferous Carbonate Platforms And Reefs</i> . Society for Sedimentary Geology. Special Publication No. 78. And, The American Association of Petroleum Geologists. Memoir, 83. Pg. 239-252
85	Lower Carboniferous (Mississippian)	Ireland	?	Dublin Basin	Somerville, I. D., Strogon, P. and Jones, G. Ll. 1992. Mid-Dinantian buildups in the Dublin Basin, Ireland. <i>Sedimentary Geology</i> . Vol. 79. Pg. 91-116
86	Lower Carboniferous (Mississippian)	Sacramento Mountains, New Mexic, USA	Lake Valley Formation	Carbonate Ramp - Transgressive Phase	Stanton, R. J., Jeffery, D. L. and Guillumette, R. N. 2000. Oxygen Minimum Zone and Internal Waves as Potential Controls on Location and Growth of Waulsortian Mounds (Mississippian, Sacramento Mountains, New Mexico. <i>Facies</i> . Vol. 42. Pg. 161-176
87	Lower Carboniferous (Mississippian)	Northwestern Ireland	Sligo Syncline	Transgression and Regression?	Warnke, K. 1994. Die unter-karbonischen Mud Mounds in den Counties Sligo und Leitrim, Nordwest- Ireland. <i>Facies</i> , Bildungsbedingungen und Diagenese.

					<i>Documenta naturae</i> . No. 88
88	Lower Carboniferous (Mississippian)	Sling, Ireland	Slingo Syncline	?	Warnke, K. and Meischner, D. 1995. Origin and depositional environment of lower Carboniferous mud mounds of Northwestern Ireland. In: Reitner, J. and Neuweiler, F. (Eds.), <i>Mud Mounds: A Polygenetic Spectrum of Fine-Grained Carbonate Buildups</i> . Facies. Vol. 32. Pg. 36-42
89	Lower Carboniferous (Mississippian)	Afghanistan	?	?	Webb, G. E. 1994. Non-Waulsortian Mississippian bioherms: A comparative analysis. In: Embry, A. F., Beauchamp, B. and Glass, D. J. (Eds.), <i>Pangea: Global Environments and Resources</i> . Canadian Society of Petroleum Geologists. Memoir 17. Pg. 701-713
90	Lower Carboniferous (Mississippian)	Eastern Anti-Atlas, Morocco	Zrigat Formation, Tafilalt Basin	?	Wendt, J., Kauffman, B. and Belka, Z. 2001. An exhumed Palaeozoic underwater scenery: the Visean mud mounds of the eastern Anti-Atlas (Morocco). <i>Sedimentary Geology</i> . Vol. 145. Pg. 215-233
91	Lower Carboniferous (Mississippian)	Sacramento Mountains, New Mexic, USA	Lake Valley Formation	Carbonate Ramp - Transgressive Phase	Wu, Y. and Chafetz, H. S. 2002. 13C-Enriched carbonate in Mississippian mud mounds: Alamogordo Member, Lake Valley Formation, Sacramento Mountains, New Mexico, U.S.A.. <i>Journal of Sedimentary Research</i> . Vol. 72. Pg. 138-145
92	Upper Carboniferous (Pennsylvanian)	Cantabrian Zone, Spain	Ponga Nappe Unit	Carbonate Platform Margin	Bahamonde, J. R., Colmenero, J. R. and Vera, C. 1997. Growth and demise of Late Carboniferous platforms in the eastern Cantabrian Zone, Asturias, northwestern Spain.

					<i>Sedimentary Geology</i> . Vol. 110. Pg. 99-122
93	Upper Carboniferous (Pennsylvanian)	Picos de Europa, N W Spain	Picos de Europa Formation	Carbonate Platform Margin	Bahamonde, J. R., Vera, C. and Colmenero, J. R. 2000. A steep-fronted Carboniferous carbonate platform: clinoformal geometry and lithofacies (Picos de Europa, NW Spain). <i>Sedimentology</i> . Vol. 47. Pg. 645-664
94	Upper Carboniferous (Pennsylvanian)	Canadian Arctic Islands	Otto Fiord and Hare Fiord Formations	Sverdrup Basin	Davies, G. R. and Nassichuk, W. W. 1990. Submarine cements and fabrics in Carboniferous to Lower Permian, reefal, shelf margin and slope carbonates, north-western Ellesmere Island, Canadian Arctic Archipelago. <i>Geological Survey of Canada Bulletin</i> . Vol. 399. Pg. 77
95	Upper Carboniferous (Pennsylvanian)	Canadian Arctic Islands	Otto Fiord and Hare Fiord Formations	Sverdrup Basin	Davies, G. R., Nassichuk, W. W. and Beuchamp, B. 1989. Upper Carboniferous 'Waulsortian' reefs, Canadian Arctic Archipelago. In: Geldsetzer, H. H. J., James, N. P. and Tebutt, G. E. (Eds.), <i>Reefs, Canada and Adjacent Areas</i> . Canadian Society of Petroleum Geologists. Memoir 13. Pg. 658-666
96	Upper Carboniferous (Pennsylvanian)	Alabama, USA	Bangor Limestone	Black Warrior Foreland Basin	Kopaska-Merkel, D. C. and Haywick, D. W. 2001b. A lone biotrital mound in the Chesterian (Carboniferous) of Alabama? <i>Sedimentary Geology</i> . Vol. 145. Pg. 253-268

97	Upper Carboniferous (Pennsylvanian)	Colorado Plateau, USA	Hermosa Formation	Paradox Basin - Extensional Basin	Peterson, J, A. 1966. <i>Genesis and Diagenesis of Paradox Basin Carbonate Mound Reservoirs. Symposium on Recently Developed Geologic Principles and Sedimentation of the Permo-Pennsylvanian of the Rocky Mountains</i> ; 20th Annual Conference. Pg. 67-86
98	Upper Carboniferous (Pennsylvanian)	Colorado Plateau, USA	Hermosa Formation	Paradox Basin - Extensional Basin	Peterson, J. A. 1966. <i>Genesis of Paradox Basin Carbonate Mound Reservoirs in Relation to Regional Pennsylvanian -Permian Sedimentation. Symposium on Recently Developed Geologic Principles and Sedimentation of the Permo-Pennsylvanian of the Rocky Mountains</i> ; 20th Annual Conference. Pg. 86a-86l
99	Upper Carboniferous (Pennsylvanian)	Colorado Plateau, USA	Hermosa Formation	Paradox Basin - Extensional Basin	Peterson, J. A. 1966. Stratigraphic Vs. Structural Controls on Carbonate-Mound Hydrocarbon Accumulation, Aneth Area, Paradox Basin. <i>Bulletin of the American Association of Petroleum Geologists</i> . Vol. 50. Pg. 2068-2081
100	Upper Carboniferous (Pennsylvanian)	Kansas, USA	Frisbie Limestone Member	?	Samankassou, E and West, R. R. 2002. Construction versus accumulation in phylloid algal mounds: an example of a small constructed mound in the Pennsylvanian of Kansas, USA. <i>Palaeogeography, Palaeoclimatology, Palaeoecology</i> . Vol. 185. Pg. 379-389

101	Upper Carboniferous (Pennsylvanian)	Cantabrian Mountains, Spain	San Emiliano Formation	Foreland Basin?	Samankassou, E. 2001. Internal structure and depositional environment of Late Carboniferous mounds from the San Emiliano Formation, Carmenes Syncline, Cantabrian Mountains, North Spain. <i>Sedimentary Geology</i> . Vol 145. Pg. 235-252
102	Upper Carboniferous (Pennsylvanian)	Carnic Alps, Austria-Italy	Auernig, Rattendorf and Trogkofel Groups	Variscan Orogenically formed basins	Samankassou, E. 2003. Upper Carboniferous-Lower Permian Buildups of the Carnic Alps, Austria-Italy. In: Ahr, W. M., Harris, P. M., Morgan, W. A. and Somerville, I. D. (Eds.) <i>Permo-Carboniferous Carbonate Platforms And Reefs</i> . Society for Sedimentary Geology. Special Publication No. 78. And, The American Association of Petroleum Geologists. Memoir, 83. Pg. 201-217
103	Upper Carboniferous (Pennsylvanian)	North Greenland	?	Basin, Tectonically Subsiding	Stemmerik, L. 2003. Controls on Localization and Morphology of Moskovian (Late Carboniferous) Carbonate Buildups, Southern Amstrup Land, North Greenland. In: Ahr, W. M., Harris, P. M., Morgan, W. A. and Somerville, I. D. (Eds.) <i>Permo-Carboniferous Carbonate Platforms And Reefs</i> . Society for Sedimentary Geology. Special Publication No. 78. And, The American Association of Petroleum Geologists. Memoir, 83. Pg. 253-265
104	Lower Permian	Ellesmere Island	Hauen Formation	?	Beauchamp, B. 1988a. Lower Permian (Artinskian) sponge - Bryozoan buildups, Southwestern Ellesmere Island, Canadian Arctic archipelago. In: Geldsetzer, H. H. J., James, N. P. and Tebutt, G. E. (Eds.), <i>Reefs, Canada and Adjacent Areas</i> . Canadian

					Society of Petroleum Geologists. Memoir 13. Pg. 575-584
105	Lower Permian	Ellesmere Island	Nansen Formation	?	Beauchamp, B. 1988b. Lower Permian (Sakmarian) Tubiphytes - Bryozoan buildup, Southwestern Ellesmere Island, Canadian Arctic archipelago. In: Geldsetzer, H. H. J., James, N. P. and Tebutt, G. E. (Eds.), <i>Reefs, Canada and Adjacent Areas</i> . Canadian Society of Petroleum Geologists. Memoir 13. Pg. 585-589
106	Lower Permian	Ellesmere Island	Mount Bayley and Tanquary Formations	Fault Related Subsidence - Evaporites - Glaciogenic	Beauchamp, B. and Olchoway, B. 2003. Early Permian Buildups (Tolkien Reefs) Associated with Subaqueous Evaporites, Canadian Arctic: A Record of Syn-Tectonic to Post-Tectonic Reciprocal Uplift and Subsidence. In: Ahr, W. M., Harris, P. M., Morgan, W. A. and Somerville, I. D. (Eds.) <i>Permo-Carboniferous Carbonate Platforms And Reefs</i> . Society for Sedimentary Geology. Special Publication No. 78. And, The American Association of Petroleum Geologists. Memoir, 83. Pg. 133-153
107	Lower Permian	Norway	Unnamed	?	Blendinger, W., Bowlin, B., Zijp, F. P., Darke, G. and Ekroll, M. 1997. Carbonate buildups flank deposits: an example from the Permian (Barents Sea, northern Norway) challenges classical facies models. <i>Sedimentary Geology</i> . Vol. 112. Pg. 89-103

108	Lower Permian	Carnic Alps, Austria/Italy	Trogkofel Limestone	Shallow marine platform	Krainer, K. 2007. Late Paleozoic reef mounds of the Carnic Alps (Austria/Italy). <i>Geobios</i> . Vol. 40. Pg. 625-643
109	Lower Permian	Japan	?	?	Sano, H., Horibo, K. and Kumamoto, Y. 1990. Tubiphytes- Archaeolithoporella-Girvanella reefal facies in Permian buildup, Mino Terrane, central Japan. <i>Sedimentary Geology</i> . Vpl. 68. Pg. 293-306
110	Lower Permian	New Mexico, USA	?	?	Thurmond, J. B., Drzewiecki, P. A. and Xu, X. 2005. Building simple multiscale visualisations of outcrops geology using virtual reality modeling language (VRML). <i>Computers and Geosciences</i> . Vol. 31. Pg. 913-919
111	Upper Permian	East Greenland	Wegener Halvo Formation	Jameson Land Basin?	Stemmerik, L. 1991. Reservoir evaluation of Upper Permian buildups in the Jameson Land Basin, East Greenland. <i>Geological Survey of Greenland</i> . Report 149
112	Upper Permian	Texas and New Mexico, USA	Capitan Reef	Rimmed Carbonate Shelf	Wood, R., Dickson, J. A. D. and Kirkland, B. L. 1996. New observations on the ecology of the Permian Capitan Reef, Texas and New Mexico. <i>Palaeontology</i> . Vol. 39. Pg. 733-762
113	Lower Triassic	West USA	Moenkopi Formation	End Permian Extinction...	Pruss, S. B. and Bottjer, D. J. 2004. Late Early Triassic microbial reefs of the western United States: a description and model for their deposition in the aftermath of the end- Permian mass extinction. <i>Palaeoecology, Palaeoclimatology, Palaeogeography</i> . Vol. 211. Pg. 127-137

114	Middle Triassic	Dolomites, Italy	Plattenkalke Formation	Contrin Carbonate Bank - Sinking into Anoxia	Gaetani, M., Fois, E., Jadoul, F. and Nicora, A. 1981. Nature and Evolution of Middle Triassic Carbonate Buildups in the Dolomites (Italy). <i>Marine Geology</i> . Vol. 44. Pg. 25-57
115	Middle Triassic	British Columbia, Canada	Liard Formation	Margin of Craton	Zonneveld, J-P. 2001. Middle Triassic biostromes from the Liard Formation, British Columbia, Canada: oldest examples from the Mesozoic of NW Pangea Zonneveld, J-P. 2001. Middle Triassic biostromes from the Liard Formation, British Columbia, Canada: oldest examples from the Mesozoic of NW Pangea. <i>Sedimentary Geology</i> . Vol. 145. Pg. 317-341
115b	Middle Triassic	Catalan, Spain	Muschelkalk	Carbonate ramp	Calvet, F. and Tucker, M. E. (1995) Mud-Mounds with Reefal Caps in the Upper Muschelkalk (Triassic), Eastern Spain. In; (eds) C. L. V. Monty, D. W. J. Bosence, P. H. Bridges and B. R. Pratt. Carbonate Mud-Mounds: Their Origin and Evolution. International Association of Sedimentologists. Blackwell Science. Vol. 23. Pg. 311-333
116	Upper Triassic	Styria, Austria	Aflenz Limestone	Marginal Platform	Nicol, S. A. 1987. A Down-slope Upper Triassic Reef Mound: Aflenz Limestone, Hochschwab Mountains, Northern Calcareous Alps. <i>Facies</i> . Vol. 16. Pg. 23-36
117	Lower Jurassic	High Atlas, Morocco	Idikel, Aberdouz and Ouchbis Formations	Atlas Rift (Inversion)	Chafiki, D., Canerot, J., Souhel, A., Hariri, K. E. and Eddine, K. T. 2004. The Sinemurian carbonate mud-mounds from central High Atlas (Morocco): stratigraphy, geometry, sedimentology and geodynamic patterns. <i>Journal of African Earth Sciences</i> . Vol. 39. Pg. 337-346

118	Lower Jurassic	Central High Atlas, Morocco	Liassic	Atlas Rift (Inversion)	Neuweiler, F., Mehdi, M., Wilmsen, O. and Wilsme, M. 2001. Facies of Liassic Sponge Mounds, Central High Atlas, Morocco. <i>Facies</i> . Vol. 44. Pg. 243-264
119	Lower Jurassic	Arzo, Switzerland	Broccatello Unit	Extentional (Syn-Sedimentary) Tectonics	Neuwieler, F. and Bernoulli, D. 2005. Mesozoic (Lower Jurassic) red stromatactis limestones from the Southern Alps (Arzo, Switzerland): calcite mineral authigenesis and syneresis-type deformation. <i>International Journal of Earth Science</i> . Vol. 94. Pg. 130-146
120	Middle Jurassic	Carpathians, Slovakia and Ukraine	Czorstyn Formation	Pannonian Basin	Aubrecht, R., Schlogl, J., Krobicki, M., Wierzbowski, H., Matyja, B. A. and Wierzbowski, A. 2009. Middle Jurassic stromatactis mud-mounds in the Pieniny Klippen Belt (Carpathians) - A possible clue to the origin of stromatactis. <i>Sedimentary Geology</i> . Vol. 213. Pg. 97-112
121	Middle Jurassic	Carpathians, Slovakia	Czorstyn Formation	Pannonian Basin	Aubrecht, R., Szulc, J., Michalik, J., Schlogl, J. and Wagreich, M. 2002. Middle Jurassic Stromatactis Mud-mound in the Pieniny Klippen Belt (Western Carpathians). <i>Facies</i> . Vol. 47. Pg. 113-126
122	Upper Jurassic	Germany	Swabian and Franconian Alb	Marine Transgression	Hammes, U. 1995. Development of small-scale sponge mud-mounds: Germany. In: Monty, C. L. V., Bosence, D. W. J., Bridges, P. H. and Pratt, B. R. (Eds.), <i>Carbonate Mud-Mounds Their Origin and Evolution</i> . International Association of Sedimentologists. Blackwell Science. Pg. 335-357

123	Upper Jurassic	SW Japan	Torinosu Group	?	Kano, A. 1988. Facies and Depositional Conditions of a Carbonate Mound (Tithonian-Berriasian, SW-Japan). <i>Facies</i> . Vol. 18. Pg. 27-48
124	Upper Jurassic	SW Germany	Western Molasse Basin?	Alpine Foreland (S Germany)	Meder, K. 1987. Dedolomitization of Upper Jurassic Carbonate Sediments of the TB-3 Saulgau Well (W-Molasse, SW-Germany). <i>Facies</i> . Vol. 17. Pg. 189-196
125	Upper Jurassic	S Germany, S Portugal, E Spain, Central Portugal	?	?	Schmid, D. U. Leinfelder, R. R. and Nose, M. 2001. Growth dynamics and ecology of Upper Jurassic mounds, with comparisons to Mid-Palaeozoic mounds. <i>Sedimentary Geology</i> . Vol. 145. Pg. 343-376
126	Lower Cretaceous	Canadian Arctic	Christopher Formation	Half Graben and Salt Diapir	Beauchamp, B. and Savard, M. 1992. Cretaceous Chemosynthetic Carbonate Mounds in the Canadian Arctic. <i>Palaios</i> . Vol. 7. Pg. 434-450
127	Lower Cretaceous	Soba, N Spain	Lunada-Soba	Platform-basin transition	Garcia-Mondejar, J. and Fernandez-Mendiola, P. A. 1995. Albian carbonate mounds: comparative study in the context of sea-level variations (Soba, northern Spain). In: Monty, C. L. V., Bosence, D. W. J., Bridges, P. H. and Pratt, B. R. (Eds.), <i>Carbonate Mud-Mounds Their Origin and Evolution</i> . International Association of Sedimentologists. Blackwell Science. Pg. 49-123
128	Lower Cretaceous	Mexico	Cupido Formation	Post-rift Carbonate Platform	Murillo-Muneton, G and Dorobek, S. L. 2003. Controls on the evolution of carbonate mud mounds in the Lower Cretaceous Cupido Formation, Northeastern Mexico. <i>Journal of Sedimentary Research</i> . Vol. 73. Pg. 869-886

129	Upper Cretaceous	Montana to New Mexico, USA	Pierre Shale	Eastern Front Rocky Mountains	Birgel, D., Peckmann, J., Klautzsch, S., Thiel, V. and Reitner, J. 2006. Anerobic and Aerobic Oxidation of Methane at Late Cretaceous Seeps in the Western Interior Seaway, USA. <i>Geomicrobiology Journal</i> . Vol. 23. Pg. 565-577
130	Upper Cretaceous	Algeria and Tunisia	Draa ez Zelma, Djebels Bireno and Mrhila	Carbonate Shelf	Camoin, G. F. 1995. Nature and origin of Late Cretaceous mud-mounds, north Africa. In: Monty, C. L. V., Bosence, D. W. J., Bridges, P. H. and Pratt, B. R. (Eds.), <i>Carbonate Mud-Mounds Their Origin and Evolution</i> . International Association of Sedimentologists. Blackwell Science. Pg. 385-400
131	Upper Cretaceous	Montana to New Mexico, USA	Pierre Shale	Eastern Front Rocky Mountains	Kauffman, E. G., Arthur, M. A., Howe, B. and Scholle, P. A. 1996. Widespread venting of methane-rich fluids in late Cretaceous (Campanian) submarine springs (Teepee Buttes) Western Interior seaway, USA. <i>Geology</i> . Vol. 24. No 9. Pg. 799-802
132	Upper Cretaceous	Tunisia	Annaba Formation?	Tectonically Unstable	Negra, M. H., Purser, B. H. and M'Rabet, A. 1995. Sedimentation, diagenesis and syntectonic erosion of Upper Cretaceous rudist mounds in central Tunisia. In: Monty, C. L. V., Bosence, D. W. J., Bridges, P. H. and Pratt, B. R. (Eds.), <i>Carbonate Mud-Mounds Their Origin and Evolution</i> . International Association of Sedimentologists. Blackwell Science. Pg. 401-419

133	Upper Cretaceous	Colorado, USA	Pierre Shale	Eastern Front Rocky Mountains	Shapiro, R. and Fricke, H. 2002. Tepee Buttes:Fossilized methane-seep ecosystems. In: Leonard, E. M., Hubbard, M. S., Kelley, S. A., Evanoff, E., Siddoway, C. S., Oviatt, C. G., Heizler, M. and Timmons, M. (Eds.) High Plains to Rio Grande Rift: Late Cenozoic Evolution of Central Colorado. <i>GSA Field Guides</i> . Pg. 59-93
134	Cenozoic	Porcupine Basin	?	Continental Margin	Bailey, W., Shannon, P. M., Walsh, J. J. and Unnithan, V. 2003. The spatial distributions of faults and deep sea carbonate mounds in the Porcupine Basin, offshore Ireland. <i>Marine and Petroleum Geology</i> . Vol. 20. Pg. 509-522
135	Cenozoic	South Rockall Trough	?	Continental Margin	de Hass, H., Mienis, F., Frank, N., Richter, T. O., Stienacher, R., de Stigter, H., van der Land, C. and van Weering, T. C. E. 2009. Morphology and sedimentology of (clustered) cold-water coral mounds at the south Rockall Trough margins, NE Atlantic Ocean. <i>Facies</i> . Vol. 55. Pg. 1-26
136	Cenozoic	Gulf of Cadiz (off Morocco)	?	Continental Margin	Foubert, A., Depreiter, D., Beck, T., Maignien, L., Pannemans, B., Frank, N., Blamart, D. and Henriët, J-P. 2008. Carbonate mounds in a mud volcano province off north-west Morocco: Key to processes and controls. <i>Marine Geology</i> . Vol. 248. Pg. 74-96
137	Cenozoic	Porcupine Basin	?	Continental Margin	Huvenne, V. A. I., Bailey, W. R., Shannon, P. M. Naeth, J., di Primo, R., Henriët, J. P., Horsfield, B., de Haas, H., Wheeler, A. and Olu-Le Roy, K. 2007. The Magellan mound

					province in the Porcupine Basin. <i>International Journal of Earth Science</i> . Vol. 96. Pg. 85-101
138	Cenozoic	Rockall Trough	?	Continental Margin	Kenyon, N. H., Akhmetzhanov, A. M., Wheeler, A. J., van Weering, T. C. E., de Haas, H. and Ivanov, M. K. 2003. <i>Marine Geology</i> . Vol. 195. Pg. 5-30
139	Cenozoic	South West Rockall Trough	?	Continental Margin	Mienis, F., van Weering, T., de Hass, H., de Stigter, H., Huvenne, V. and Wheeler, A. 2006. Carbonate mound development at the SW Rockall Trough margin based on high resolution TOBI and seismic recording. 2006. <i>Marine Geology</i> . Vol. 233. Pg. 1-19
140	Cenozoic	Porcupine Basin	?	Continental Margin	Naeth, J., di Primio, R., Horsfield, B., Schaefer, R. G. and Krooss, B. M. 2007. On the relationship between hydrocarbon migration pathways and carbonate mound occurrence in the Porcupine Basin. <i>International Journal of Earth Science</i> . Vol. 98. Pg. 199-200
141	Cenozoic	Porcupine Basin	?	Continental Margin	Naeth, J., di Primio, R., Horsfield, B., Schaefer, R. G., Shannon, P. M., Bailey, W. R. and Henriët, J. P. 2005. Hydrocarbon seepage and carbonate mound formation: a basin modelling study from the Porcupine Basin (offshore Ireland). <i>Journal of Petroleum Geology</i> . Vol. 28. Pg. 147-166
142	Cenozoic	Hatton Bank (N E Atlantic)	?	Continental Margin	Roberts, J. M., Henry, L-A., Long, D. and J. P. Hartley. 2008. Cold-water coral reef frameworks, megafaunal communities and evidence for coral carbonate mounds on the Hatton

					Bank, north east Atlantic. <i>Facies</i> . Vol. 54. Pg. 297-316
143	Cenozoic	Gulf of Mexico	?	Continental Margin	Sager, W. W., MacDonald, I. R. and Hou, R. 2003. Geophysical signatures of mud mounds at hydrocarbon seeps on the Louisiana continental slope, northern Gulf of Mexico. <i>Marine Geology</i> . Vol. 198. Pg. 97-132
144	Cenozoic	Rockall Trough (SW and SE)	?	Continental Margin	van Weering, T. C. E., de Haas, H., de Stiger, H. G., Lykke-Andersen, H. and Kouvaev, I. 2003. Structure and developmant of giant carbonate mounds at the SW and SE Rockall Trough margins, NE Atlantic Ocean. <i>Marine Geology</i> . Vol. 198. Pg. 67-81
145	Cenozoic	Rockall Bank	?	Continental Margin	Wienberg, C., Beuck, L., Heidkamp, S., Hebbeln, D., Freiwald, A., Pfannkuche, O. and Monteys, X. 2008. Franken Mound: facies and biocoenoses on a newly-discovered "carbonate mound" on the western Rockall Bank, NE Atlantic. <i>Facies</i> . Vol. 54. Pg. 1-24

SUBMISSION OF THESIS FOR A RESEARCH DEGREE**Part I. DECLARATION by the candidate for a research degree. To be bound in the thesis**

Degree for which thesis being submitted: Ph.D

Title of thesis: Pennsylvanian carbonate mud mounds from the sub-aerial to sub-marine transition along a tilted foreland basin, Cantabrian Mountains, Spain.

This thesis contains confidential information and is subject to the protocol set down for the submission and examination of such a thesis.

NO

Date of submission: 24/06/15

Original registration date: 19/10/09

(Date of submission must comply with Regulation 2D)

Name of candidate: Steven Leslie Rogers

Research Institute: EPSAM

Name of Lead Supervisor: Dr Michael Montenari

I certify that:

- (a) The thesis being submitted for examination is my own account of my own research
- (b) My research has been conducted ethically. Where relevant a letter from the approving body confirming that ethical approval has been given has been bound in the thesis as an Annex
- (c) The data and results presented are the genuine data and results actually obtained by me during the conduct of the research
- (d) Where I have drawn on the work, ideas and results of others this has been appropriately acknowledged in the thesis
- (e) Where any collaboration has taken place with one or more other researchers, I have included within an 'Acknowledgments' section in the thesis a clear statement of their contributions, in line with the relevant statement in the Code of Practice (see Note overleaf).
- (f) The greater portion of the work described in the thesis has been undertaken subsequent to my registration for the higher degree for which I am submitting for examination
- (g) Where part of the work described in the thesis has previously been incorporated in another thesis submitted by me for a higher degree (if any), this has been identified and acknowledged in the thesis
- (h) The thesis submitted is within the required word limit as specified in the Regulations

Total words in submitted thesis (including text and footnotes, but excluding references and appendices): 76,403

Signature of candidate



Date 22/07/15

Note

Extract from Code of Practice: If the research degree is set within a broader programme of work involving a group of investigators – particularly if this programme of work predates the candidate's registration – the candidate should provide an explicit statement (in an 'Acknowledgments' section) of the respective roles of the candidate and these other individuals in relevant aspects of the work reported in the thesis. For example, it should make clear, where relevant, the candidate's role in designing the study, developing data collection instruments, collecting primary data, analysing such data, and formulating conclusions from the analysis. Others involved in these aspects of the research should be named, and their contributions relative to that of the candidate should be specified (*this does not apply to the ordinary supervision, only if the supervisor or supervisory team has had greater than usual involvement*).